

NUREG/CR-5535  
INEL-95/0174  
Vol. 1

---

---

# **RELAP5/MOD3 Code Manual**

**Code Structure, System Models,  
and Solution Methods**

---

---

Manuscript Completed: June 1995  
Date Published: August 1995

Prepared by  
The RELAP5 Development Team

**Idaho National Engineering Laboratory  
Lockheed-Martin Idaho Technologies Company  
P.O. Box 1625  
Idaho Falls, ID 83415**

**Prepared for  
Division of Systems Technology  
Office of Nuclear Regulatory Research  
U.S. Nuclear Regulatory Commission  
Washington, DC 20555-0001  
NRC Job Code W6238**

**MASTER**

## AVAILABILITY NOTICE

### Availability of Reference Materials Cited in NRC Publications

Most documents cited in NRC publications will be available from one of the following sources:

1. The NRC Public Document Room, 2120 L Street, NW., Lower Level, Washington, DC 20555-0001
2. The Superintendent of Documents, U.S. Government Printing Office, P. O. Box 37082, Washington, DC 20402-9328
3. The National Technical Information Service, Springfield, VA 22161-0002

Although the listing that follows represents the majority of documents cited in NRC publications, it is not intended to be exhaustive.

Referenced documents available for inspection and copying for a fee from the NRC Public Document Room include NRC correspondence and internal NRC memoranda; NRC bulletins, circulars, information notices, inspection and investigation notices; licensee event reports; vendor reports and correspondence; Commission papers; and applicant and licensee documents and correspondence.

The following documents in the NUREG series are available for purchase from the Government Printing Office: formal NRC staff and contractor reports, NRC-sponsored conference proceedings, international agreement reports, grantee reports, and NRC booklets and brochures. Also available are regulatory guides, NRC regulations in the *Code of Federal Regulations*, and *Nuclear Regulatory Commission Issuances*.

Documents available from the National Technical Information Service include NUREG-series reports and technical reports prepared by other Federal agencies and reports prepared by the Atomic Energy Commission, forerunner agency to the Nuclear Regulatory Commission.

Documents available from public and special technical libraries include all open literature items, such as books, journal articles, and transactions. *Federal Register* notices, Federal and State legislation, and congressional reports can usually be obtained from these libraries.

Documents such as theses, dissertations, foreign reports and translations, and non-NRC conference proceedings are available for purchase from the organization sponsoring the publication cited.

Single copies of NRC draft reports are available free, to the extent of supply, upon written request to the Office of Administration, Distribution and Mail Services Section, U.S. Nuclear Regulatory Commission, Washington, DC 20555-0001.

Copies of industry codes and standards used in a substantive manner in the NRC regulatory process are maintained at the NRC Library, Two White Flint North, 11545 Rockville Pike, Rockville, MD 20852-2738, for use by the public. Codes and standards are usually copyrighted and may be purchased from the originating organization or, if they are American National Standards, from the American National Standards Institute, 1430 Broadway, New York, NY 10018-3308.

## DISCLAIMER NOTICE

This report was prepared as an account of work sponsored by an agency of the United States Government. Neither the United States Government nor any agency thereof, nor any of their employees, makes any warranty, expressed or implied, or assumes any legal liability or responsibility for any third party's use, or the results of such use, of any information, apparatus, product, or process disclosed in this report, or represents that its use by such third party would not infringe privately owned rights.

## **DISCLAIMER**

**Portions of this document may be illegible  
in electronic image products. Images are  
produced from the best available original  
document.**

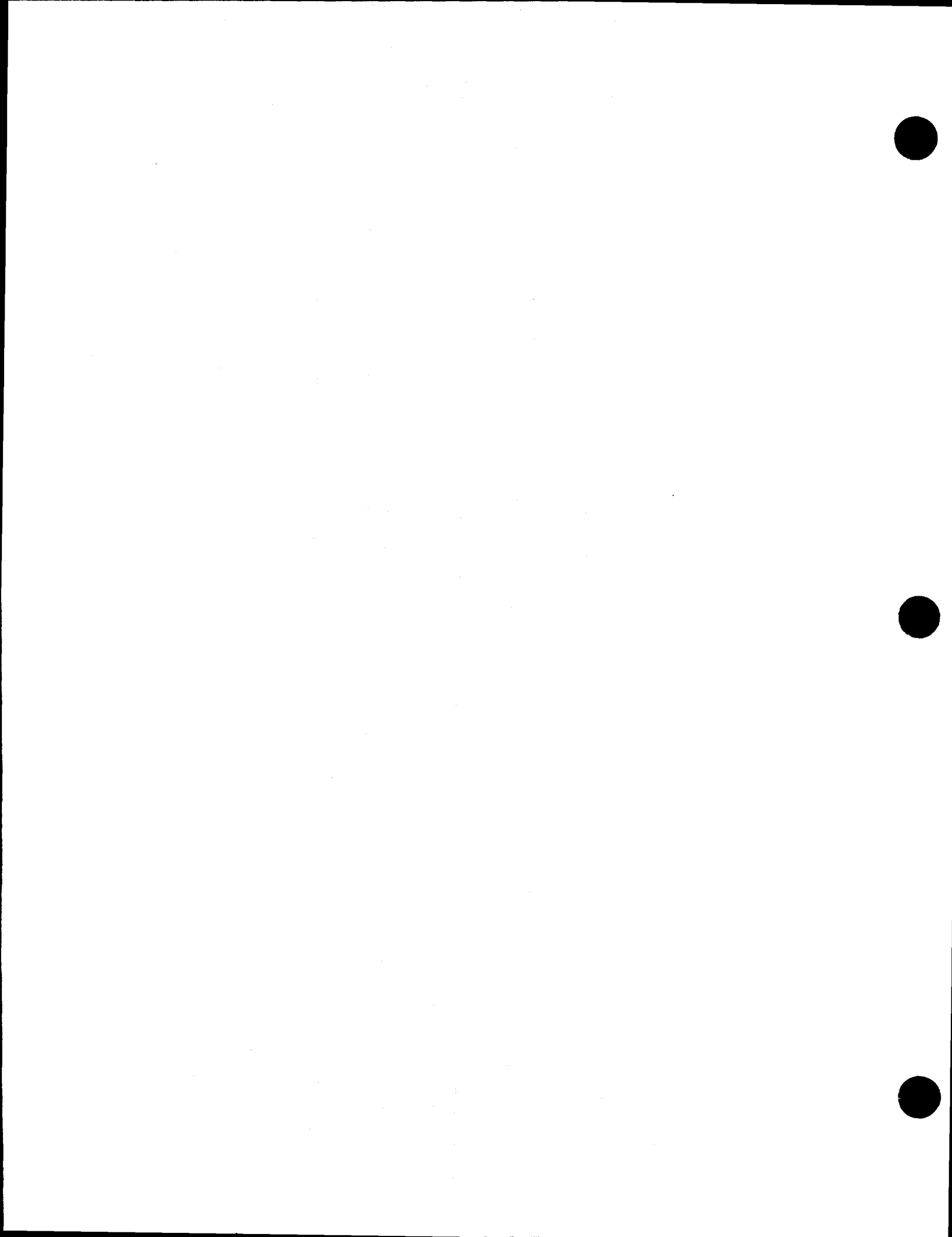
## ABSTRACT

The RELAP5 code has been developed for best-estimate transient simulation of light water reactor coolant systems during postulated accidents. The code models the coupled behavior of the reactor coolant system and the core for loss-of-coolant accidents and operational transients such as anticipated transient without scram, loss of offsite power, loss of feedwater, and loss of flow. A generic modeling approach is used that permits simulating a variety of thermal hydraulic systems. Control system and secondary system components are included to permit modeling of plant controls, turbines, condensers, and secondary feedwater systems.

RELAP5/MOD3 code documentation is divided into seven volumes: Volume I presents modeling theory and associated numerical schemes; Volume II details instructions for code application and input data preparation; Volume III presents the results of developmental assessment cases that demonstrate and verify the models used in the code; Volume IV discusses in detail RELAP5 models and correlations; Volume V presents guidelines that have evolved over the past several years through the use of the RELAP5 code; Volume VI discusses the numerical scheme used in RELAP5; and Volume VII presents a collection of independent assessment calculations.

## DISCLAIMER

This report was prepared as an account of work sponsored by an agency of the United States Government. Neither the United States Government nor any agency thereof, nor any of their employees, makes any warranty, express or implied, or assumes any legal liability or responsibility for the accuracy, completeness, or usefulness of any information, apparatus, product, or process disclosed, or represents that its use would not infringe privately owned rights. Reference herein to any specific commercial product, process, or service by trade name, trademark, manufacturer, or otherwise does not necessarily constitute or imply its endorsement, recommendation, or favoring by the United States Government or any agency thereof. The views and opinions of authors expressed herein do not necessarily state or reflect those of the United States Government or any agency thereof.



## CONTENTS

ABSTRACT .....	iii
CONTENTS .....	v
FIGURES.....	ix
TABLES.....	xiii
EXECUTIVE SUMMARY .....	xv
ACKNOWLEDGMENTS .....	xix
NOMENCLATURE.....	xxi
 1     INTRODUCTION .....	1-1
1.1    Development of RELAP5/MOD3 .....	1-1
1.1.1    References .....	1-3
1.2    Relationship to Previous Code Versions.....	1-3
1.2.1    References .....	1-3
1.3    Quality Assurance .....	1-4
 2     CODE ARCHITECTURE.....	2-1
2.1    Computer Adaptability .....	2-1
2.2    Top Level Organization .....	2-1
2.3    Input Processing Overview.....	2-2
2.4    Transient Overview .....	2-3
 3     HYDRODYNAMIC MODEL.....	3-1
3.0.1    References .....	3-2
3.1    Field Equations .....	3-3
3.1.1    Basic Differential Equations.....	3-3
3.1.2    Numerically Convenient Set of Differential Equations.....	3-15
3.1.3    Stratified Flow .....	3-19
3.1.4    Semi-Implicit Scheme Difference Equations .....	3-22
3.1.5    Time Advancement for the Semi-Implicit Scheme .....	3-31
3.1.6    Difference Equations and Time Advancement for the Nearly-Implicit Scheme .....	3-39
3.1.7    Volume-Average Velocities .....	3-46
3.1.8    Implicit Hydrodynamic and Heat Structure Coupling .....	3-52
3.1.9    Numerical Solution of Boron Transport Equation .....	3-55
3.1.10    References .....	3-58
3.2    State Relationships .....	3-61
3.2.1    State Equations .....	3-61
3.2.2    Single-Component, Two-Phase Mixture .....	3-62
3.2.3    Two-Component, Two-Phase Mixture .....	3-65

3.2.4	References .....	3-71
3.3	Constitutive Models.....	3-73
3.3.1	Vertical Volume Flow Regime Map .....	3-73
3.3.2	Horizontal Volume Flow Regime Map.....	3-78
3.3.3	High Mixing Volume Flow Regime Map.....	3-80
3.3.4	ECC Mixer Volume Flow Regime Map .....	3-80
3.3.5	Junction Flow Regime Map .....	3-84
3.3.6	Interphase Friction.....	3-85
3.3.7	Coefficient of Virtual Mass .....	3-107
3.3.8	Wall Friction .....	3-107
3.3.9	Wall Heat Transfer Models.....	3-116
3.3.10	Wall Heat Transfer Correlations .....	3-119
3.3.11	Interphase Mass Transfer.....	3-121
3.3.12	Direct Heating .....	3-136
3.3.13	References .....	3-136
3.4	Special Process Models .....	3-143
3.4.1	Choked Flow .....	3-143
3.4.2	Horizontal Stratification Entrainment Model.....	3-155
3.4.3	Abrupt Area Change.....	3-157
3.4.4	User-Specified Form Loss .....	3-166
3.4.5	Crossflow Junction .....	3-167
3.4.6	Water Packing Mitigation Scheme .....	3-170
3.4.7	Countercurrent Flow Limitation Model .....	3-172
3.4.8	Mixture Level Tracking Model .....	3-175
3.4.9	Thermal Stratification Model .....	3-191
3.4.10	Energy Conservation at an Abrupt Change .....	3-197
3.4.11	References .....	3-199
3.5	Component Models .....	3-203
3.5.1	Branch .....	3-203
3.5.2	Separator.....	3-206
3.5.3	Jet Mixer.....	3-217
3.5.4	Pump.....	3-223
3.5.5	Turbine.....	3-233
3.5.6	Valves .....	3-240
3.5.7	Accumulator .....	3-251
3.5.8	ECC Mixer .....	3-266
3.5.9	Annulus .....	3-282
3.5.10	References .....	3-282
4	HEAT STRUCTURE MODELS .....	4-1
4.1	Heat Conduction Numerical Technique .....	4-1
4.2	Mesh Point and Thermal Property Layout .....	4-2
4.3	Difference Approximation at Internal Mesh Points .....	4-4
4.4	Difference Approximation at Boundaries.....	4-7
4.5	Thermal Properties and Boundary Condition Parameters .....	4-8

4.6	RELAP5 Specific Boundary Conditions .....	4-8
4.6.1	Correlation Package Conditions .....	4-9
4.6.2	Insulated and Tabular Boundary Conditions .....	4-11
4.7	Solution of Simultaneous Equations .....	4-12
4.8	Computation of Heat Fluxes .....	4-13
4.9	Two-Dimensional Conduction Solution/Reflood .....	4-14
4.10	Fine Mesh Rezoning Scheme .....	4-17
4.10.1	Reference .....	4-19
4.11	Gap Conductance Model .....	4-20
4.11.1	References .....	4-28
4.12	Surface-to-Surface Radiation Model .....	4-28
4.12.1	References .....	4-30
4.13	Metal-Water Reaction Model .....	4-30
4.13.1	Reference .....	4-32
4.14	Cladding Deformation Model .....	4-32
4.14.1	References .....	4-37
5	TRIP SYSTEM .....	5-1
5.1	Variable Trips .....	5-1
5.2	Logical Trips .....	5-1
6	CONTROL SYSTEM .....	6-1
6.1	Arithmetic Control Components .....	6-1
6.1.1	Constant .....	6-1
6.1.2	Addition-Subtraction .....	6-1
6.1.3	Multiplication .....	6-1
6.1.4	Division .....	6-1
6.1.5	Exponentiation .....	6-2
6.1.6	Table Lookup Function .....	6-2
6.1.7	Standard Functions .....	6-2
6.1.8	Delay .....	6-2
6.1.9	Unit Trip .....	6-2
6.1.10	Trip Delay .....	6-3
6.2	Integration Control Component .....	6-3
6.3	Differentiation Control Components .....	6-4
6.4	Proportional-Integral Component .....	6-5
6.5	Lag Control Component .....	6-6
6.6	Lead-Lag Control Component .....	6-7
6.7	Shaft Component .....	6-8
7	POINT REACTOR KINETICS MODEL .....	7-1

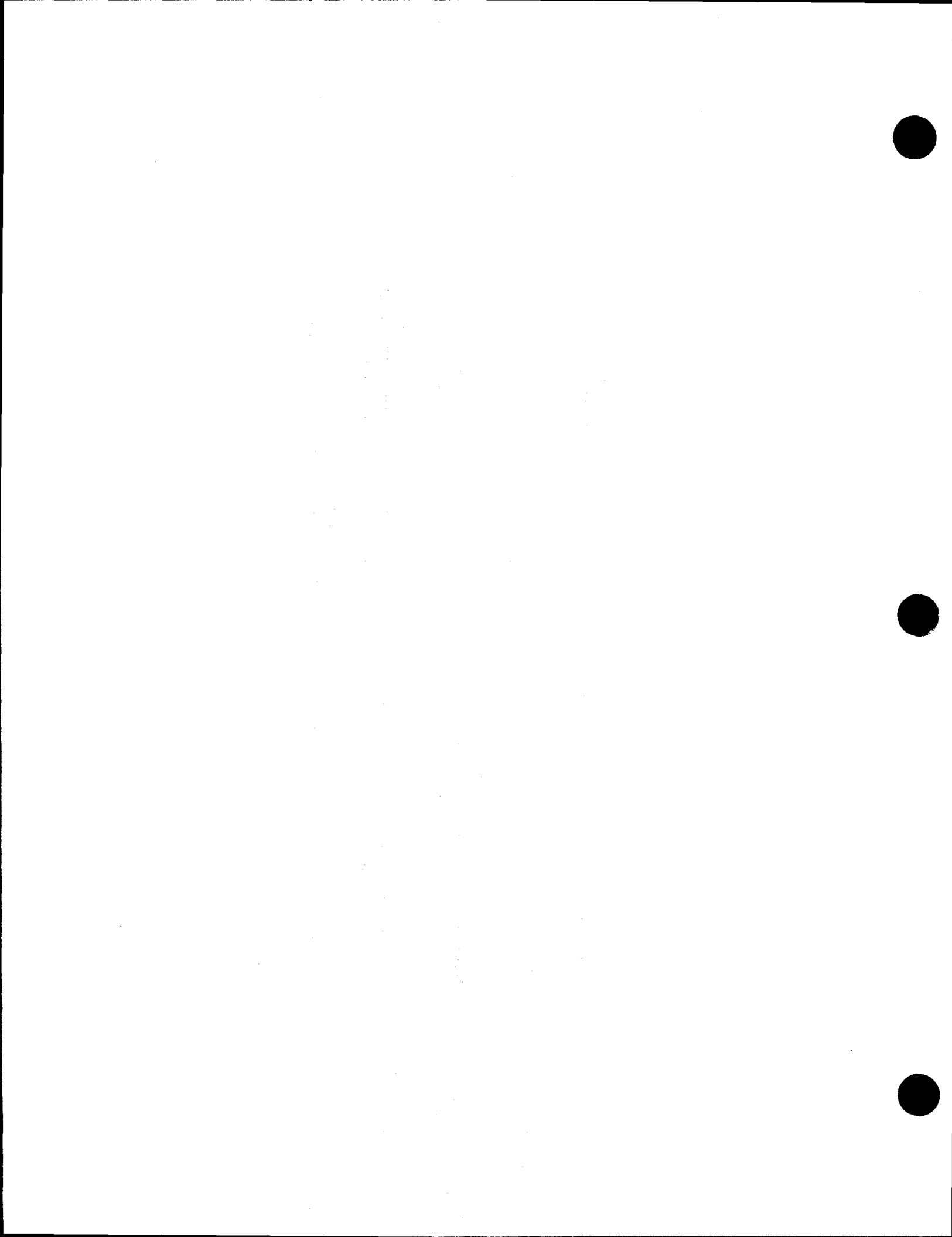
7.1	Point Reactor Kinetics Equations .....	7-1
7.2	Fission Product Decay Model .....	7-2
7.3	Actinide Decay Model.....	7-5
7.4	Transformation Of Equations For Solution .....	7-5
7.5	Initialization.....	7-7
7.6	Reactivity Feedback .....	7-8
7.6.1	Separable Feedback Model.....	7-9
7.6.2	Tabular Feedback Model .....	7-9
7.6.3	Reference.....	7-14
7.7	Reactor Kinetics Numerical Procedures.....	7-15
7.7.1	References .....	7-19
8	SPECIAL TECHNIQUES .....	8-1
8.1	Time Step Control .....	8-1
8.2	Mass/Energy Error Mitigation.....	8-2
8.3	Steady State .....	8-4
8.3.1	Fundamental Concepts for Detecting Hydrodynamic Steady-State During Transient Calculations.....	8-4
8.3.2	Calculational Precision and the Steady-State Convergence Criteria.....	8-7
8.3.3	Steady-State Testing Scheme, Time Interval Control, and Output.....	8-11
8.3.4	Heat Structure Heat Conductance Scheme for Steady-State .....	8-13
8.3.5	Interrelationship of Steady-State and Transient Restart/Plot Records .....	8-14
8.4	Self-Initialization .....	8-14
8.4.1	General Description.....	8-14
8.4.2	Required Plant Model Characteristics .....	8-15
8.4.3	Standard Suboptions .....	8-16
8.4.4	Inherent Model Incompatibilities .....	8-17
8.4.5	Description of Standard Controllers.....	8-18

## FIGURES

2.2-1.	RELAP5 top level structure.....	2-2
2.4-1.	Modular structures of transient calculations in RELAP5.....	2-3
2.4-2.	Transient (steady-state) block structure.....	2-4
3.1-1.	Interface heat transfer in the bulk and near the wall for subcooled boiling.....	3-8
3.1-2.	Relation of central angle $\theta$ to void fraction $\alpha_g$ .....	3-20
3.1-3.	Difference equation nodalization schematic.....	3-23
3.1-4.	Schematic of a volume cell showing multiple inlet and outlet junction mass flows.....	3-47
3.3-1.	Schematic of vertical flow regime map with hatchings indicating transitions.....	3-74
3.3-2.	Schematic of horizontal flow regime map with hatchings indicating transition regions.....	3-79
3.3-3.	Schematic of high mixing volume flow regime map.....	3-81
3.3-4.	Schematic of ECC mixer volume flow regime map (modified Tandon et al. <sup>3.3-18</sup> ).....	3-82
3.3-5.	Slug flow pattern.....	3-99
3.3-6.	Three vertical volumes with the middle volume being vertically stratified.....	3-102
3.3-7.	Flow regimes before and after the critical heat flux (CHF) transition.....	3-106
3.3-8.	RELAP5 boiling and condensing curves.....	3-117
3.3-9.	RELAP5 wall heat transfer flow chart.....	3-118
3.4-1.	Equilibrium speed of sound as a function of void fraction and virtual mass coefficient.....	3-147
3.4-2.	Coefficient of relative Mach number for thermal equilibrium flow as a function of void fraction and virtual mass coefficient.....	3-148
3.4-3.	Subcooled choking process.....	3-149
3.4-4.	Pressure distribution for choked flow through a converging-diverging nozzle.....	3-154
3.4-5.	Abrupt expansion.....	3-158
3.4-6.	Abrupt contraction.....	3-159
3.4-7.	Orifice at abrupt area change.....	3-160
3.4-8.	Schematic flow of two-phase mixture at abrupt area change.....	3-162
3.4-9.	Modeling of crossflows or leak.....	3-168
3.4-10.	Simplified tee crossflow.....	3-169
3.4-11.	Leak flow modeling.....	3-170
3.4-12.	Two vertical vapor/liquid volumes.....	3-172
3.4-13.	Pressure-drop characteristics near the boundary between countercurrent and cocurrent flow.....	3-173
3.4-14.	Plot of $H_g^{1/2}$ versus $H_f^{1/2}$ for a typical CCFL correlation.....	3-174
3.4-15.	Mixture level in normal void profile.....	3-177

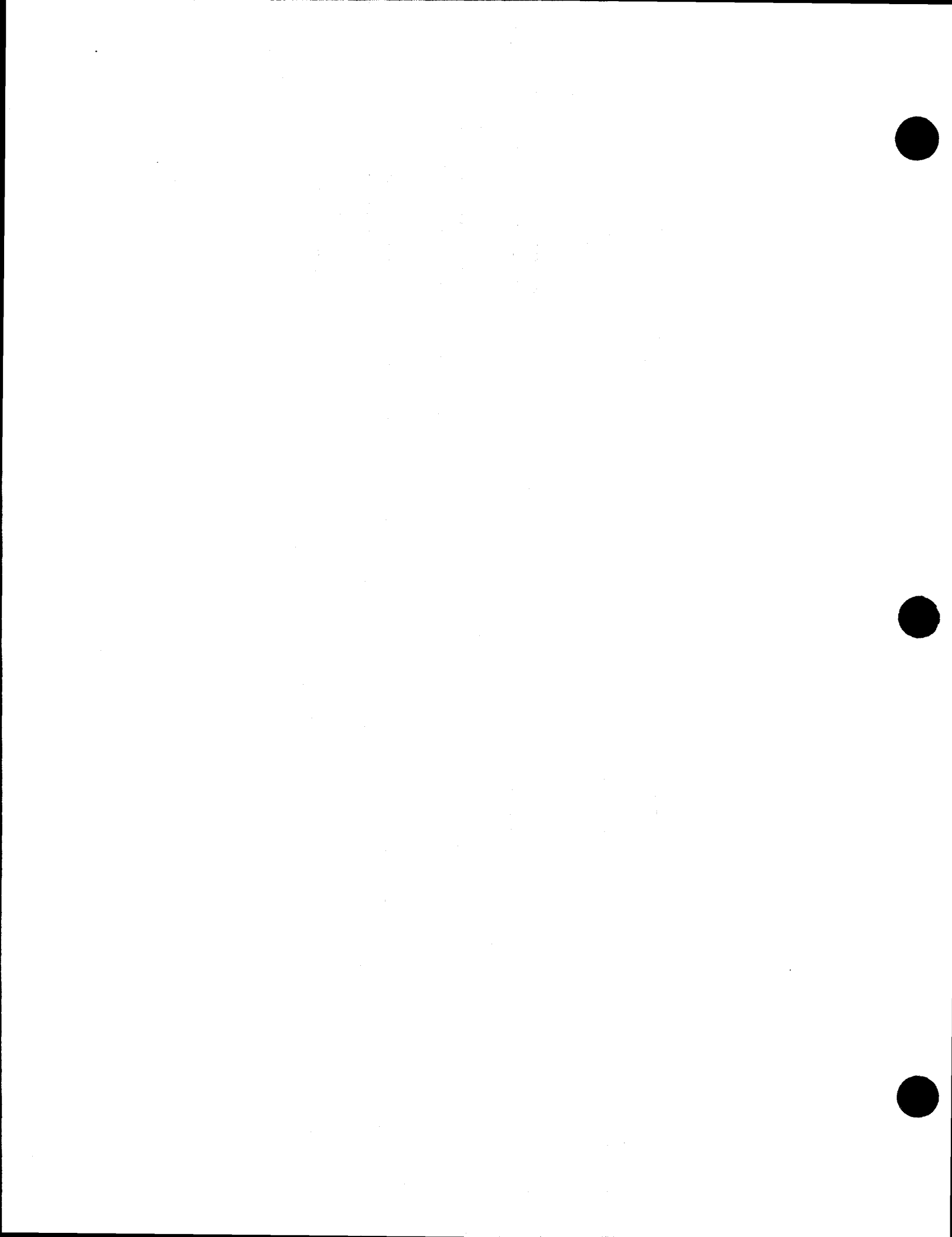
3.4-16.	Mixture level in a volume below a void fraction inversion.....	3-177
3.4-17.	Mixture level above a void fraction inversion.....	3-178
3.4-18.	Level detection logic diagram.....	3-179
3.4-19.	Level detection logic for volume L above an inverted profile.....	3-180
3.4-20.	Level detection logic diagram for volume L below an inverted profile.....	3-181
3.4-21.	Level detection logic diagram for a normal profile.....	3-182
3.4-22.	The control volume for momentum cell $j+1$ .....	3-188
3.4-23.	Mixture level rising through a control volume edge.....	3-189
3.4-24.	Hydrodynamic volume with heat structure.....	3-190
3.4-25.	Thermal front in a tank.....	3-192
3.4-26.	Thermal front detection logic diagram for volume L.....	3-194
3.4-27.	Computation of thermal front parameters logic diagram for volume L.....	3-196
3.4-28.	Hydrodynamic volume with thermal front.....	3-198
3.5-1.	One-dimensional branch.....	3-204
3.5-2.	Gravity effects on a tee.....	3-205
3.5-3.	Typical separator volume and junctions.....	3-206
3.5-4.	Donor junction voids for outflow.....	3-207
3.5-5.	Schematic of first stage of mechanistic separator.....	3-208
3.5-6.	Dryer capacity.....	3-217
3.5-7.	Schematic of mixing junctions.....	3-218
3.5-8.	Flow regimes and dividing streamline.....	3-222
3.5-9.	Typical pump characteristic four-quadrant curves.....	3-225
3.5-10.	Typical pump homologous head curves.....	3-226
3.5-11.	Typical pump homologous torque curves.....	3-227
3.5-12.	Single-phase homologous head curves for 1 1/2 loop MOD1 Semiscale pumps.....	3-228
3.5-13.	Fully degraded, two-phase homologous head curves for 1 1/2 loop MOD1 Semiscale pumps.....	3-229
3.5-14.	Torque versus speed, Type 93A pump motor (rated voltage).....	3-233
3.5-15.	A schematic of a stage group with idealized flow path between Points 1 and 2.....	3-234
3.5-16.	Schematic of lumped model for turbine stage group.....	3-240
3.5-17.	Diagram of inertial valve.....	3-243
3.5-18.	Two views of a partially open flapper valve.....	3-244
3.5-19.	Schematic of a typical relief valve in the closed position.....	3-247
3.5-20.	Schematic of a typical relief valve in the partially open position.....	3-248
3.5-21.	Schematic of a typical relief valve in the fully open position.....	3-249
3.5-22.	Typical cylindrical accumulator.....	3-252
3.5-23.	Typical spherical accumulator.....	3-253
3.5-24.	ECCMIX component.....	3-267

3.5-25.	Schematic cross section of stratified flow along the ECCMIX component, showing the length of interface, $L_m$ , and the jet length, $L_{jet}$ .....	3-270
3.5-26.	Schematic vertical cross section of the ECCMIX component, showing the width of liquid surface, $L_s$ , and the tending half-angle, $\theta$ .....	3-271
4.2-1.	Mesh point layout.....	4-2
4.2-2.	Typical mesh points.....	4-3
4.2-3.	Boundary mesh points.....	4-3
4.9-1.	Volume and surface elements around a mesh point (i,j).....	4-15
4.10-1.	An elementary heat structure unit for reflood.....	4-18
4.10-2.	An example of the fine mesh-rezoning process.....	4-19
4.11-1.	Segmentation at the fuel-cladding gap.....	4-20
4.14-1.	ORNL correlation of rupture temperature as a function of engineering hoop stress and temperature-ramp rate with data from internally heated zircaloy cladding in aqueous atmospheres.....	4-34
4.14-2.	Maximum circumferential strain as a function of rupture temperature for internally heated zircaloy cladding in aqueous atmospheres at heating rates less than or equal to 10 °C/s.....	4-36
4.14-3.	Maximum circumferential strain as a function of rupture temperature for internally heated zircaloy cladding in aqueous atmospheres at heating rates greater than or equal to 25 °C/s.....	4-36
4.14-4.	Reduction in PWR assembly flow area as a function of rupture temperature and ramp.....	4-37



## TABLES

3.2-1.	Values of $R_{ni}$ , $C_{o,ni}$ , $D_{o,ni}$ , and $U_{o,ni}$ for various noncondensable gases. ....	3-66
3.3-1.	List of flow regimes in the ECCMIX component.....	3-82
3.3-2.	Drift flux void fraction correlations for vertical bubbly-slug flow. ....	3-93
3.3-3.	Values of $K_{u,crit}$ .....	3-98
3.3-4.	RELAP5 interfacial mass transfer in bulk fluid.....	3-121
3.4-1.	Logic for determining donor void fraction. ....	3-187
3.4-2.	Logic for determining donor internal energy ( $v > 0 \leftrightarrow$ rising fluid) .....	3-197
3.5-1.	Summary of fitted parameters in a mechanistic separator model. ....	3-215
3.5-2.	SEMISCALE dimensionless head ratio difference data (single-phase minus two-phase).....	3-229
3.5-3.	Head multiplier and void fraction data. ....	3-231
3.5-4.	Contraction coefficient table. ....	3-245
4.11-1.	Constants used in gas thermal conductivity correlation. ....	4-25
4.11-2.	Radial thermal strain of zircaloy for $1083 \text{ K} < T < 1273 \text{ K}$ . ....	4-27
4.14-1.	Tabulation of cladding correlations. ....	4-34
8.4-1.	Independent/dependent data set suboptions.....	8-16



## EXECUTIVE SUMMARY

The light water reactor (LWR) transient analysis code, RELAP5, was developed at the Idaho National Engineering Laboratory (INEL) for the U.S. Nuclear Regulatory Commission (NRC). Code uses include analyses required to support rulemaking, licensing audit calculations, evaluation of accident mitigation strategies, evaluation of operator guidelines, and experiment planning analysis. RELAP5 has also been used as the basis for a nuclear plant analyzer. Specific applications have included simulations of transients in LWR systems such as loss of coolant, anticipated transients without scram (ATWS), and operational transients such as loss of feedwater, loss of offsite power, station blackout, and turbine trip. RELAP5 is a highly generic code that, in addition to calculating the behavior of a reactor coolant system during a transient, can be used for simulation of a wide variety of hydraulic and thermal transients in both nuclear and nonnuclear systems involving mixtures of steam, water, noncondensable, and solute.

The MOD3 version of RELAP5 has been developed jointly by the NRC and a consortium consisting of several countries and domestic organizations that were members of the International Code Assessment and Applications Program (ICAP) and its successor organization, Code Applications and Maintenance Program (CAMP). Credit also needs to be given to various Department of Energy sponsors, including the INEL laboratory-directed discretionary funding program. The mission of the RELAP5/MOD3 development program was to develop a code version suitable for the analysis of all transients and postulated accidents in LWR systems, including both large- and small-break loss-of-coolant accidents (LOCAs) as well as the full range of operational transients.

The RELAP5/MOD3 code is based on a nonhomogeneous and nonequilibrium model for the two-phase system that is solved by a fast, partially implicit numerical scheme to permit economical calculation of system transients. The objective of the RELAP5 development effort from the outset was to produce a code that included important first-order effects necessary for accurate prediction of system transients but that was sufficiently simple and cost effective so that parametric or sensitivity studies were possible.

The code includes many generic component models from which general systems can be simulated. The component models include pumps, valves, pipes, heat releasing or absorbing structures, reactor point kinetics, electric heaters, jet pumps, turbines, separators, accumulators, and control system components. In addition, special process models are included for effects such as form loss, flow at an abrupt area change, branching, choked flow, boron tracking, and noncondensable gas transport.

The system mathematical models are coupled into an efficient code structure. The code includes extensive input checking capability to help the user discover input errors and inconsistencies. Also included are free-format input, restart, renodalization, and variable output edit features. These user conveniences were developed in recognition that generally the major cost associated with the use of a system transient code is in the engineering labor and time involved in accumulating system data and developing system models, while the computer cost associated with generation of the final result is usually small.

The development of the models and code versions that constitute RELAP5 has spanned approximately 17 years from the early stages of RELAP5 numerical scheme development to the present. RELAP5 represents the aggregate accumulation of experience in modeling reactor core behavior during accidents, two-phase flow processes, and LWR systems. The code development has benefitted from extensive application and comparison to experimental data in the LOFT, PBF, Semiscale, ACRR, NRU, and other experimental programs.

Several new models, improvements to existing models, and user conveniences have been added to RELAP5/MOD3. The new models include

- The Bankoff counter-current flow limiting correlation that can be activated by the user at each junction in the system model
- The ECCMIX component for modeling of the mixing of subcooled emergency core cooling system (ECCS) liquid and the resulting interfacial condensation
- A zirconium-water reaction model to model the exothermic energy production on the surface of zirconium cladding material at high temperature
- A surface-to-surface radiation heat transfer model with multiple thermal radiation enclosures defined through user input
- A level tracking model
- A thermal stratification model.

Improvements to existing models include

- New correlations for interfacial friction for all types of geometry in the bubbly-slug flow regime in vertical flow passages
- Use of junction-based interphase drag
- An improved model for vapor pullthrough and liquid entrainment in horizontal pipes to obtain correct computation of the fluid state convected through a break
- A new critical heat flux correlation for rod bundles based on tabular data
- An improved horizontal stratification inception criterion for predicting the flow regime transition between horizontally stratified and dispersed flow
- A modified reflood heat transfer model
- Improved logic for vertical stratification inception to avoid excessive activation of the water packing model
- An improved boron transport model
- A mechanistic separator/dryer model
- An improved crossflow model
- An improved form loss model

- The addition of a simple plastic strain model with a clad burst criterion to the fuel mechanical model
- The addition of a radiation heat transfer term to the gap conductance model
- Modifications to the noncondensable gas model to eliminate erratic code behavior and failure
- Improvements to the downcomer penetration, ECCS bypass, and upper plenum deentrainment capabilities

Additional user conveniences include

- Code speedup through vectorization for the CRAY X-MP computer
- Computer portability through the conversion of the FORTRAN coding to adhere to the FORTRAN 77 standard
- Code execution and validation on a variety of systems. The code should be easily installed (i.e., the installation script is supplied with the transmittal) on the CRAY X-MP (UNICOS), DECstation 5000 (ULTRIX), DEC Alpha Workstation (OSF/1), IBM Workstation 6000 (UNIX), SUN Workstation (UNIX), and HP Workstation (UNIX). The code has been installed (although the installation script is not supplied with the transmittal) on the CDC Cyber (NOS/VE), IBM 3090 (MVS), and IBM-PC (DOS). The code can be installed easily on all 64-bit machines (integer and floating point operands) and any 32-bit machine that provides for 64-bit floating point.

The RELAP5/MOD3 code manual consists of seven separate volumes. The modeling theory and associated numerical schemes are described in Volume I, to acquaint the user with the modeling base and thus aid in effective use of the code. Volume II contains more detailed instructions for code application and specific instructions for input data preparation. Both Volumes I and II are expanded and revised versions of the RELAP5/MOD2 code manual<sup>a</sup> and Volumes I and III of the SCDAP/RELAP5/MOD2 code manual<sup>b</sup>.

Volume III<sup>c</sup> presents the results of developmental assessment cases run with RELAP5/MOD3 to demonstrate and validate the models used in the code. The assessment matrix contains phenomenological problems, separate-effects tests, and integral systems tests.

---

- a. V. H. Ransom et al., *RELAP5/MOD2 Code Manual, Volumes I and II*, NUREG/CR-4312, EGG-2396, August and December, 1985, revised April 1987.
- b. C. M. Allison and E. C. Johnson, Eds., *SCDAP/RELAP5/MOD2 Code Manual, Volume I: RELAP5 Code Structure, System Models, and Solution Methods, and Volume III: User's Guide and Input Requirements*, NUREG/CR-5273, EGG-2555, June 1989.
- c. To be published in 1996.

Volume IV contains a detailed discussion of the models and correlations used in RELAP5/MOD3. It presents the user with the underlying assumptions and simplifications used to generate and implement the base equations into the code so that an intelligent assessment of the applicability and accuracy of the resulting calculations can be made. Thus, the user can determine whether RELAP5/MOD3 is capable of modeling his or her particular application, whether the calculated results will be directly comparable to measurement or whether they must be interpreted in an average sense, and whether the results can be used to make quantitative decisions.

Volume V provides guidelines for users that have evolved over the past several years from applications of the RELAP5 code at the Idaho National Engineering Laboratory, at other national laboratories, and by users throughout the world.

Volume VI discusses the numerical scheme in RELAP5/MOD3, and Volume VII is a collection of independent assessment calculations.

## ACKNOWLEDGMENTS

Development of a complex computer code such as RELAP5 is the result of team effort and requires the diverse talents of a large number of people. Special acknowledgment is given to those who pioneered and continue to contribute to the RELAP5 code, in particular, V. H. Ransom, J. A. Trapp, and R. J. Wagner. A number of other people have made and continue to make significant contributions to the continuing development of the RELAP5 code. Recognition and gratitude is given to the other current members of the RELAP5 team:

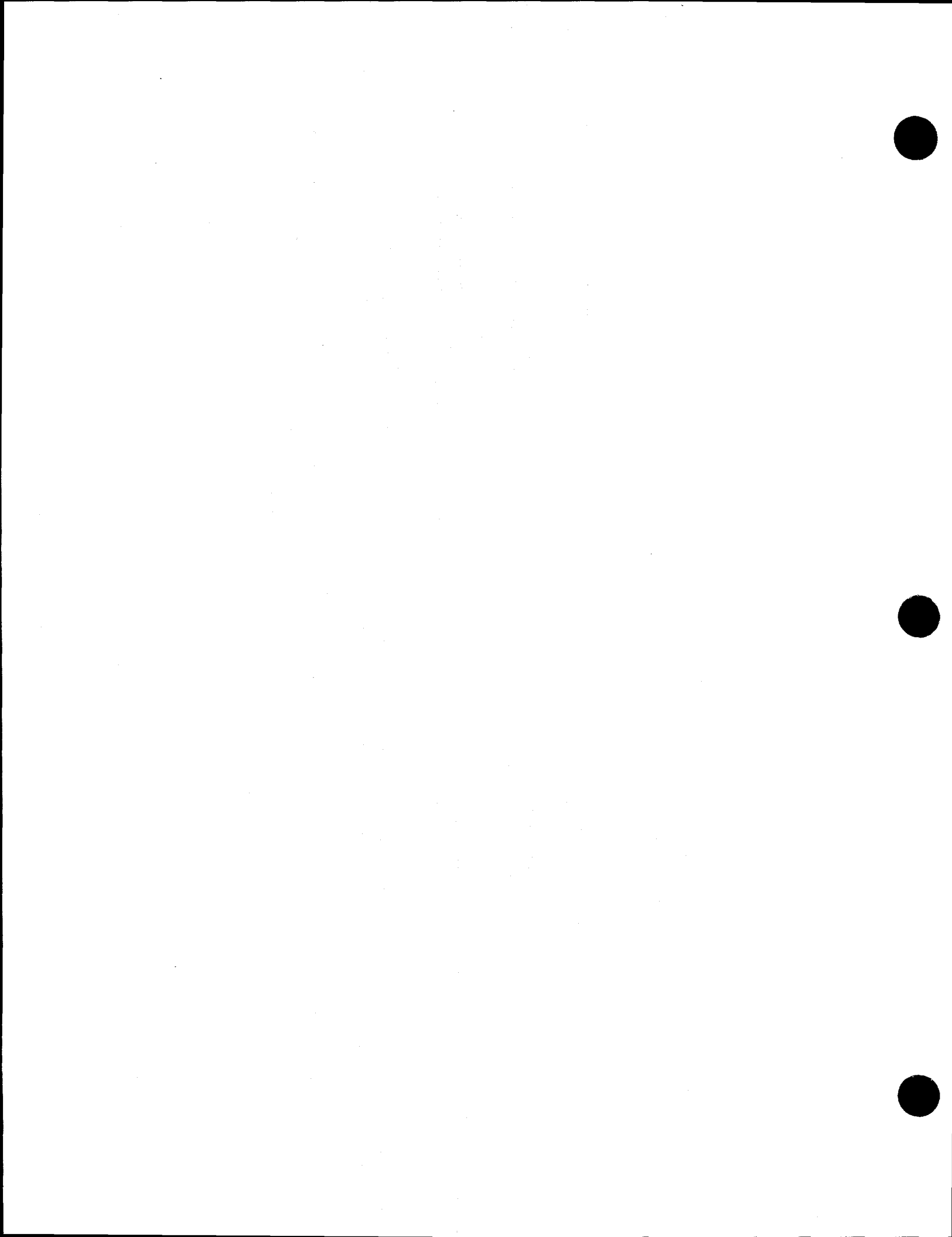
V. T. Berta	C. E. Lenglade	R. A. Riemke
K. E. Carlson	M. A. Lintner	R. R. Schultz
C. D. Fletcher	C. C. McKenzie	A. S-L. Shieh
E. E. Jenkins	G. L. Mesina	R. W. Shumway
E. C. Johnsen	C. S. Miller	C. E. Slater
G. W. Johnsen	G. A. Mortensen	S. M. Sloan
J. M. Kelly	P. E. Murray	M. Warnick
H-H. Kuo	R. B. Nielson	W. L. Weaver
N. S. Larson	S. Paik	G. E. Wilson

The list of contributors is incomplete, as many others have made significant contributions in the past. Rather than attempt to list them all and risk unknowingly omitting some who have contributed, we acknowledge them as a group and express our appreciation for their contributions to the success of the RELAP5 effort.

The RELAP5 Program is indebted to the technical monitors from the U. S. Nuclear Regulatory Commission and the Department of Energy-Idaho Operations Office for giving direction and management to the overall program. Those from the NRC include W. Lyon, Y. Chen, R. Lee, R. Landry, H. Scott, M. Rubin, and the current monitor D. E. Solberg. Those from DOE-ID include D. Majumdar, N. Bonicelli, C. Noble, and the current monitor, W. Rettig.

The technical editing of the RELAP5 manuals by D. Pack and E. May is greatly appreciated.

Finally, acknowledgment is made of all the code users who have been very helpful in stimulating timely correction of code deficiencies and suggesting improvements.



## NOMENCLATURE

A	cross-sectional area ( $m^2$ ), coefficient matrix in hydrodynamics, coefficient in pressure and velocity equations
$A_1$	coefficient in heat conduction equation at boundaries
$A_t$	throat area ( $m^2$ )
a	speed of sound (m/s), interfacial area per unit volume ( $m^{-1}$ ), coefficient in gap conductance, coefficient in heat conduction equation, absorption coefficient
B	coefficient matrix, drag coefficient, coefficient in pressure and velocity equations
$B_1$	coefficient in heat conduction equation at boundaries
b	coefficient in heat conduction equation, source vector in hydrodynamics
$B_x$	body force in x coordinate direction ( $m/s^2$ )
$B_y$	body force in y coordinate direction ( $m/s^2$ )
C	coefficient of virtual mass, general vector function, coefficient in pressure and velocity equations, delayed neutron precursors in reactor kinetics, concentration, pressure-dependent coefficient in Unal's correlation (1/K•s)
$C_o$	coefficient in noncondensable energy equation (J/kg•K)
$C_0, C_1$	constants in drift flux model
$C_d$	drag coefficient
$C_p$	specific heat at constant pressure (J/kg•K)
$C_v$	specific heat at constant volume (J/kg•K), valve flow coefficient
c	coefficient in heat conduction equation, coefficient in new time volume-average velocity equation, constant in CCFL model
D	coefficient of relative Mach number, diffusivity, diameter (m), heat conduction boundary condition matrix, coefficient in pressure and velocity equations
$D_o$	coefficient in noncondensable energy equation (J/kg•K <sup>2</sup> )
$D_1$	coefficient of heat conduction equation at boundaries
d	coefficient in heat conduction equation, droplet diameter (m)
DISS	energy dissipation function (W/m <sup>3</sup> )
E	total energy ( $U + v^2/2$ ) (J/kg), emissivity, Young's modulus, term in iterative heat conduction algorithm, coefficient in pressure equation
e	interfacial roughness
F	term in iterative heat conduction algorithm, gray-body factor with subscript, frictional loss coefficient, vertical stratification factor
FA	force per unit volume

FIF, FIG	interphase drag coefficients (liquid, vapor) ( $s^{-1}$ )
FI	interphase drag coefficient ( $m^3/kg \cdot s$ )
FWF, FWG	wall drag coefficients (liquid, vapor) ( $s^{-1}$ )
f	interphase friction factor, vector for liquid velocities in hydrodynamics
G	mass flux ( $kg/m^2 \cdot s$ ), shear stress, gradient, coefficient in heat conduction, vector quantity, fraction of delayed neutrons in reactor kinetics
GC	dynamic pressure for valve (Pa)
Gr	Grashof number
g	gravitational constant ( $m/s^2$ ), temperature jump distance (m), vector for vapor velocities in hydrodynamics
H	elevation (m), volumetric heat transfer coefficient ( $W/K \cdot m^3$ ), head (m)
HLOSSF, HLOSSG	form or frictional losses (liquid, vapor) (m/s)
h	specific enthalpy (J/kg), heat transfer coefficient ( $W/m^2 \cdot K$ ), energy transfer coefficient for $\Gamma_g$ , head ratio
$h_L$	dynamic head loss (m)
I	identity matrix, moment of inertia ( $N \cdot m \cdot s^2$ )
J	junction velocity (m/s)
j	superficial velocity
K	energy form loss coefficient
$K_s$	Spring constant
Ku	Kutateladze number
k	thermal conductivity ( $W/m \cdot K$ )
$k_B$	Boltzmann constant
L	length, limit function, Laplace capillary length
M	Mach number, molecular weight, pump two-phase multiplier, mass transfer rate, mass (kg)
m	constant in CCFL model
N	number of system nodes, number density ( $\#/m^3$ ), pump speed (rad/s), non-dimensional number
Nu	Nusselt number
n	unit vector, order of equation system
$P_{BP}$	valve closing back pressure (Pa)
P	pressure (Pa), reactor power (W), channel perimeter (m), turbine power (W)

$P_D$	nitrogen pressure in accumulator dome (Pa)
$P_f$	relates reactor power to heat generation rate in heat structures
$P_o$	atmospheric pressure (Pa)
$p$	wetted perimeter (m), particle probability function
PCV	specified pressure required to close a valve (Pa)
Pr	Prandtl number
$Q$	volumetric heat addition rate ( $\text{W}/\text{m}^3$ ), space dependent function, volumetric flow rate ( $\text{m}^3/\text{s}$ )
$Q_D$	total heat transfer rate to vapor dome (W)
$q$	heat transfer rate (W), heat flux ( $\text{W}/\text{m}^2$ )
$R$	radius (m), surface roughness in gap conductance, radiation resistance term, non-dimensional stratified level height
Re	Reynolds number
$Re_p$	the particle Reynolds number
$R_n, R_s$	gas constants (noncondensable, steam) ( $\text{N}\cdot\text{m}/\text{kg}\cdot\text{K}$ )
$r$	reaction fraction for turbine, radial position, ratio of volume centered boron density gradients
$S$	Chen's boiling suppression factor, stress gradient, specific entropy ( $\text{J}/\text{kg}\cdot\text{K}$ ), shape factor, real constant, source term in heat conduction or reactor kinetics (W)
$s$	surface, Laplace transform variable
$T$	temperature (K), trip
$T_c$	critical temperature (K)
$T_R$	reduced temperature (K)
$T_t$	specified time-dependent function in heat conduction
$t$	time (s)
$U$	specific internal energy ( $\text{J}/\text{kg}$ ), vector of dependent variables
$u$	radial displacement in gap conductance (m)
$V$	volume ( $\text{m}^3$ ), specific volume ( $\text{m}^3/\text{kg}$ ), control quantity
$V_D$	volume of noncondensable in accumulator dome ( $\text{m}^3$ )
VFDP, VGDP	coefficient for pressure change in momentum equations (liquid, vapor) ( $\text{m}/\text{s}\cdot\text{Pa}$ )
VIS	numerical viscosity terms in momentum equations ( $\text{m}^2/\text{s}^2$ )
VISF, VISG	numerical viscosity terms in momentum equations (liquid, vapor) ( $\text{m}^2/\text{s}^2$ )

VUNDER, VOVER	separator model parameters (liquid, vapor)
v	mixture velocity (m/s), phasic velocity (m/s), flow ratio, liquid surge line velocity (m/s)
$v_c$	choking velocity (m/s)
W	weight of valve disk, weighting function in reactor kinetics, relaxation parameter in heat conduction, shaft work per unit mass flow rate, mass flow rate
$W_{crit}$	critical Weber number
We	Weber number
w	humidity ratio
X	flow quality, static quality, mass fraction, conversion from MeV/s to watts
x	spatial coordinate (m), vector of hydrodynamic variables
Y	control variable
Z	two-phase friction correlation factor, function in reactor kinetics
$\Delta Z$	height of volume
z	elevation change coordinate (m)

## Symbols

$\alpha$	void fraction, subscripted volume fraction, angular acceleration ( $\text{rad/s}^2$ ), coefficient for least-squares fit, speed ratio
$\beta$	coefficient of isobaric thermal expansion ( $\text{K}^{-1}$ ), effective delayed neutron fraction in reactor kinetics
$\Gamma$	volumetric mass exchange rate ( $\text{kg/m}^3 \cdot \text{s}$ )
$\gamma$	exponential function in decay heat model
$\Delta P_f$	dynamic pressure loss (Pa)
$\Delta P_s$	increment in steam pressure (Pa)
$\Delta V_s$	increment in specific volume of steam ( $\text{m}^3/\text{kg}$ )
$\Delta t$	increment in time variable (s)
$\Delta t_c$	Courant time step (s)
$\Delta x$	increment in spatial variable (m)
$\delta$	area ratio, truncation error measure, film thickness (m), impulse function, Deryagin number
$\epsilon$	coefficient, strain function, emissivity, tabular function of area ratio, surface roughness, wall vapor generation/condensation flag
$\zeta$	diffusion coefficient, multiplier, or horizontal stratification terms

$\eta$	efficiency, bulk/saturation enthalpy flag
$\theta$	relaxation time in correlation for $\Gamma$ , angular position (rad), discontinuity detector function
$\kappa$	coefficient of isothermal compressibility ( $\text{Pa}^{-1}$ )
$\Lambda$	prompt neutron generation time, Baroczy dimensionless property index
$\lambda$	eigenvalue, interface velocity parameter, friction factor, decay constant in reactor kinetics
$\mu$	viscosity ( $\text{kg/m}\cdot\text{s}$ )
$\nu$	kinematic viscosity ( $\text{m}^2/\text{s}$ ), Poisson's ratio
$\xi$	exponential function, RMS precision
$\pi$	3.141592654
$\rho$	density ( $\text{kg/m}^3$ ), reactivity in reactor kinetics (dollars)
$\Sigma_f$	fission cross section
$\Sigma'$	depressurization rate ( $\text{Pa/s}$ )
$\sigma$	surface tension ( $\text{J/m}^2$ ), stress, flag used in heat conduction equations to indicate transient or steady-state
$\tau$	shear stresses (N), torque (N-m)
$v$	specific volume ( $\text{m}^3/\text{kg}$ )
$\phi$	donored property, Lockhart-Martinelli two-phase parameter, neutron flux in reactor kinetics, angle of inclination of valve assembly, velocity-dependent coefficient in Unal's correlation
$\Phi$	Roe's superbee gradient limiter
$\chi$	Lockhart-Martinelli function
$\Psi$	coefficient, fission rate (number/s)
$\omega$	angular velocity, constant in Gudanov solution scheme

## Subscripts

AM	annular-mist to mist flow regime transition
a	average value
ann	liquid film in annular mist flow regime
BS	bubbly to slug flow regime transition
b	bubble, boron
bulk	bulk fluid

CHF	value at critical heat flux condition
c	vena contract, continuous phase, cladding, critical property, cross-section, condensation
cm	cladding midpoint
co	carryover
core	vapor core in annular-mist flow regime
cr, crit	critical property or condition
cu	carryunder
D	drive line, vapor dome, discharge passage of mechanical separator
DE	value at lower end of slug to annular-mist flow regime transition
d	droplet, delay in control component
drp	droplet
e	thermodynamic equilibrium, equivalent quality in hydraulic volumes, value ring exit, elastic deformation, entrainment
ent	entrainment
F	wall friction, fuel
FB, FBB	film boiling, Bromley film boiling
f	liquid phase, flooding, film, flow
fg	phasic difference (i.e., vapor term-liquid term)
fp	onset of vapor pull-through
fr	frictional
front	value at thermal stratification front
g	vapor phase, gap
ge	incipient liquid entrainment
H	head
HE	homogeneous equilibrium
h, hy, hydro	hydraulic
I	interface
IAN	inverted annular flow regime
i	interface, index
in	volume inlets
iso	isothermal

j, j+1, j-1	spatial noding indices for junctions
K	spatial noding index for volumes
k	iteration index in choking model
L	spatial noding index for volume, laminar
lev, level	value at two-phase level
l	left boundary in heat conduction
M	rightmost boundary in heat conduction, spatial noding index for volume
m	mixture property, motor, mesh point
min	minimum value
NOZ	nozzle
n	noncondensable component of vapor phase
o	reference value
out	volume outlets
p	partial pressure of steam, particle, projected
pipe	cross section of flow channel
R	rated values
r	relative Mach number, right boundary in heat structure mesh
ref	reference value
rms	root mean square
S	suction region
SA	value at upper end of slug to annular-mist flow regime transition
s	steam component of vapor phase, superheated
sat	saturated quality
sb	small bubbles
sr	surface of heat structure
st	stratified
std	standard precision
T	point of minimum area, turbulent
TB	transition boiling
Tb	Taylor bubble
t	total pressure, turbulent, tangential, throat

up	upstream quantity
v	mass mean Mach number, vapor quantity, valve
w	wall, water
wall	wall
wg, wf	wall to vapor, wall to liquid
1	upstream station, multiple junction index, vector index
1 $\phi$	single-phase value
2	downstream station, multiple junction index, vector index
2 $\phi$	two-phase value
$\tau$	torque
$\mu$	viscosity
$\infty$	infinity
$\sim$	vector
$\approx$	Matrix

## Superscripts

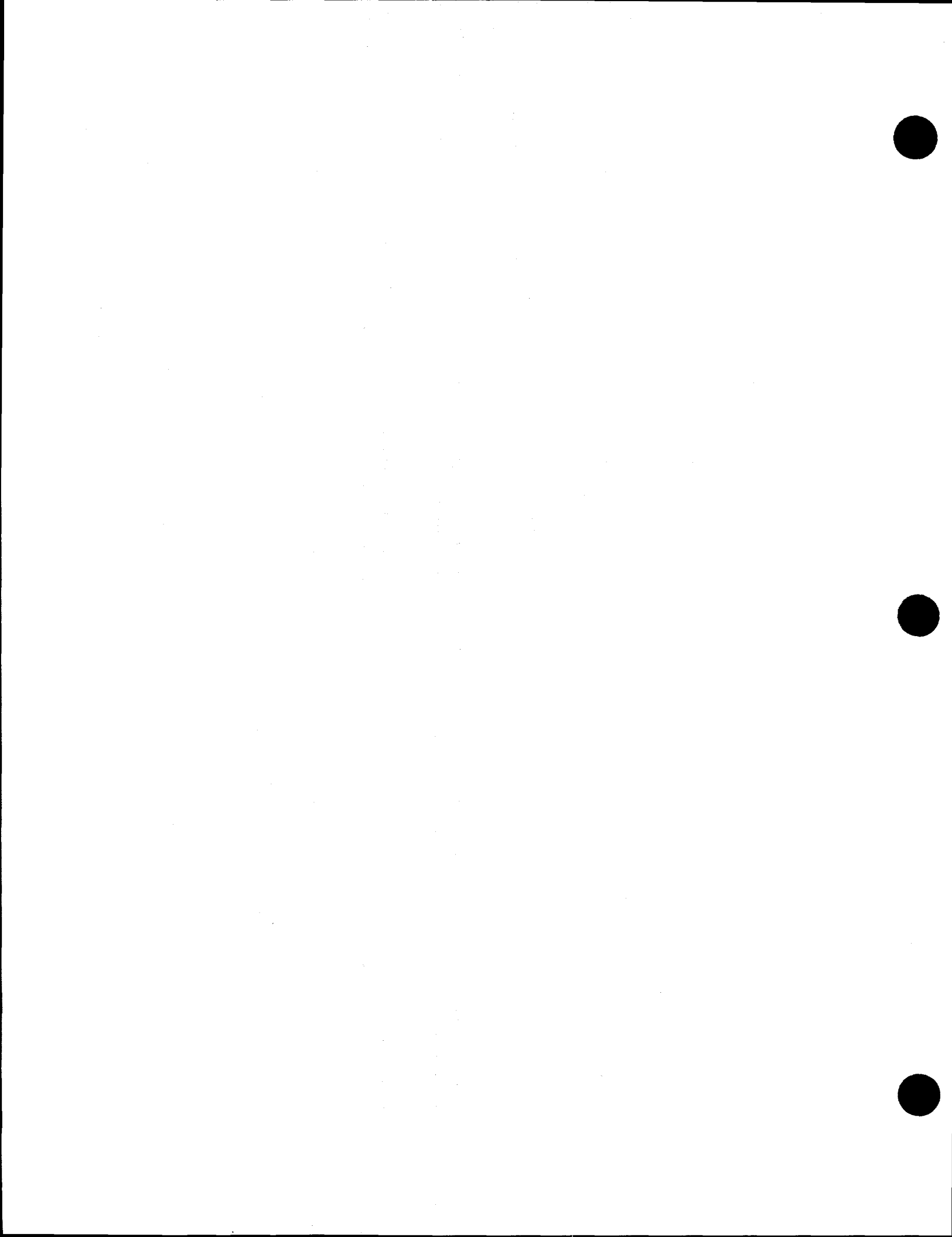
B	bulk liquid
b	boundary gradient weight factor in heat conduction, vector quantities
exp	old time terms in velocity equation, used to indicate explicit velocities in choking
m-1, m, m+1	mesh points in heat conduction finite difference equation or mean value
n, n+1	time level index
n+1/2	an average of quantities with superscripts n and n+1
o	initial value
R	real part of complex number, right boundary in heat conduction
s	saturation property, space gradient weight factor in heat conduction
v	volume gradient weight factor in heat conduction
W	wall
1	vector index, coefficient in velocity equation
2	vector index
*	total derivative of a saturation property with respect to pressure, local variable, bulk/saturation property
'	derivative

vector, average quantity

donored quantity

unit momentum for mass exchange, intermediate time variable

linearized quantity, quality based on total mixture mass



## 1 INTRODUCTION

The RELAP5 computer code is a light water reactor transient analysis code developed for the U.S. Nuclear Regulatory Commission (NRC) for use in rulemaking, licensing audit calculations, evaluation of operator guidelines, and as a basis for a nuclear plant analyzer. Specific applications of this capability have included simulations of transients in LWR systems, such as loss of coolant, anticipated transients without scram (ATWS), and operational transients such as loss of feedwater, loss of offsite power, station blackout, and turbine trip. RELAP5 is a highly generic code that, in addition to calculating the behavior of a reactor coolant system during a transient, can be used for simulation of a wide variety of hydraulic and thermal transients in both nuclear and nonnuclear systems involving mixtures of steam, water, noncondensable, and solute.

### 1.1 Development of RELAP5/MOD3

The MOD3 version of RELAP5 has been developed jointly by the NRC and a consortium consisting of several countries and domestic organizations that were members of the International Code Assessment and Applications Program (ICAP) and its successor organization, Code Applications and Maintenance Program (CAMP). In addition, improvements have been made on behalf of several Department of Energy sponsors. The mission of the RELAP5/MOD3 development program was to develop a code version suitable for the analysis of all transients and postulated accidents in LWR systems, including both large- and small-break loss-of-coolant accidents (LOCAs) as well as the full range of operational transients.

RELAP5/MOD3 was produced by improving and extending the modeling base that was established with the release of RELAP5/MOD2<sup>1.1-1,1.1-2,1.1-3</sup> in 1985. Code deficiencies identified by members of ICAP and CAMP through assessment calculations were noted, prioritized, and subsequently addressed. Consequently, several new models, improvements to existing models, and user conveniences have been added to RELAP5/MOD3. The new models include

- The Bankoff counter-current flow limiting correlation, that can be activated by the user at each junction in the system model
- The ECCMIX component for modeling of the mixing of subcooled emergency core cooling system (ECCS) liquid and the resulting interfacial condensation
- A zirconium-water reaction model to model the exothermic energy production on the surface of zirconium cladding material at high temperature
- A surface-to-surface radiation heat transfer model with multiple radiation enclosures defined through user input
- A level tracking model
- A thermal stratification model.

Improvements to existing models include

- New correlations for interfacial friction for all types of geometry in the bubbly-slug flow regime in vertical flow passages

- Use of junction-based interphase drag
- An improved model for vapor pullthrough and liquid entrainment in horizontal pipes to obtain correct computation of the fluid state convected through the break
- A new critical heat flux correlation for rod bundles based on tabular data
- An improved horizontal stratification inception criterion for predicting the flow regime transition between horizontally stratified and dispersed flow
- A modified reflood heat transfer model
- Improved vertical stratification inception logic to avoid excessive activation of the water packing model
- An improved boron transport model
- A mechanistic separator/dryer model
- An improved crossflow model
- An improved form loss model
- The addition of a simple plastic strain model with clad burst criterion to the fuel mechanical model
- The addition of a radiation heat transfer term to the gap conductance model
- Modifications to the noncondensable gas model to eliminate erratic code behavior and failure
- Improvements to the downcomer penetration, ECCS bypass, and upper plenum deentrainment capabilities

Additional user conveniences include

- Code speedup through vectorization for the CRAY X-MP computer
- Computer portability through the conversion of the FORTRAN coding to adhere to the FORTRAN 77 standard
- Code execution and validation on a variety of systems. The code should be easily installed (i.e., the installation script is supplied with the transmittal) on the CRAY X-MP (UNICOS), DECstation 5000 (ULTRIX), DEC Alpha Workstation (OSF/1), IBM Workstation 6000 (UNIX), SUN Workstation (UNIX), and HP Workstation (UNIX). The code has been installed (although the installation script is not supplied with the transmittal) on the CDC Cyber (NOS/VE), IBM 3090 (MVS), and IBM-PC (DOS). The code should be able to be installed on all 64-bit machines (integer and floating point operands) and any 32-bit machine that provides for 64-bit floating point operations.

### 1.1.1 References

- 1.1-1. V. H. Ransom et al., *RELAP5/MOD2 Code Manual, Volumes 1 and 2*, NUREG/CR-4312, EGG-2396, August 1985 and December 1985.
- 1.1-2. V. H. Ransom et al., *RELAP5/MOD2 Code Manual, Volume 3: Developmental Assessment Problems*, EGG-TFM-7952, December 1987.
- 1.1-3. R. A. Dimenna et al., *RELAP5/MOD2 Models and Correlations*, NUREG/CR-5194, EGG-2531, August 1988.

## 1.2 Relationship to Previous Code Versions

The series of RELAP codes began with RELAPSE (REactor Leak And Power Safety Excursion), which was released in 1966. Subsequent versions of this code are RELAP2,<sup>1.2-1</sup> RELAP3,<sup>1.2-2</sup> and RELAP4,<sup>1.2-3</sup> in which the original name was shortened to Reactor Excursion and Leak Analysis Program (RELAP). All of these codes were based on a homogeneous equilibrium model (HEM) of the two-phase flow process. The last code version of this series is RELAP4/MOD7,<sup>1.2-4</sup> which was released to the National Energy Software Center (NESC) in 1980.

In 1976, the development of a nonhomogeneous, nonequilibrium model was undertaken for RELAP4. It soon became apparent that a total rewrite of the code was required to efficiently accomplish this goal. The result of this effort was the beginning of the RELAP5 project.<sup>1.2-5</sup> As the name implies, this is the fifth in the series of computer codes that was designed to simulate the transient behavior of LWR systems under a wide variety of postulated accident conditions. RELAP5 follows the naming tradition of previous RELAP codes, i.e., the odd numbered series are complete rewrites of the program while the even numbered versions had extensive model changes, but used the architecture of the previous code. Each version of the code reflects the increased knowledge and new simulation requirements from both large- and small-scale experiments, theoretical research in two-phase flow, numerical solution methods, computer programming advances, and the increased capability of computers.

The principal new feature of the RELAP5 series was the use of a two-fluid, nonequilibrium, nonhomogeneous, hydrodynamic model for transient simulation of the two-phase system behavior. RELAP5/MOD2 employed a full nonequilibrium, six-equation, two-fluid model. The use of the two-fluid model eliminated the need for the RELAP4 submodels, such as the bubble rise and enthalpy transport models, which were necessary to overcome the limitations of the single-fluid model.

### 1.2.1 References

- 1.2-1. K. V. Moore and W. H. Rettig, *RELAP2 - A Digital Program for Reactor Blowdown and Power Excursion Analysis*, IDO-17263, March 1968.
- 1.2-2. W. H. Rettig et al., *RELAP3 - A Computer Program for Reactor Blowdown Analysis*, IN-1445, February 1971.
- 1.2-3. K. V. Moore and W. H. Rettig, *RELAP4 - A Computer Program for Transient Thermal-Hydraulic Analysis*, ANCR-1127, March 1975.

- 1.2-4. S. R. Behling et al., *RELAP4/MOD7 - A Best Estimate Computer Program to Calculate Thermal and Hydraulic Phenomena in a Nuclear Reactor or Related System*, NUREG/CR-1988, EGG-2089, August 1981.
- 1.2-5. V. H. Ransom et al., *RELAP5/MOD1 Code Manual, Volumes 1 and 2*, NUREG/CR-1826, EGG-2070, March 1982.

### **1.3 Quality Assurance**

RELAP5 is maintained under a strict code-configuration system that provides a historical record of the changes in the code. Changes are made using an update processor that allows separate identification of improvements made to each successive version of the code. Modifications and improvements to the coding are reviewed and checked as part of a formal quality program for software. In addition, the theory and implementation of code improvements are validated through assessment calculations that compare the code-predicted results to idealized test cases or experimental results.

## 2 CODE ARCHITECTURE

Modeling flexibility, user convenience, computer efficiency, and design for future growth were primary considerations in the selection of the basic architecture of the code. The following sections cover computer adaptability, code organization, input processing, and transient operation.

### 2.1 Computer Adaptability

RELAP5/MOD3 is written in FORTRAN 77 for a variety of 64-bit and 32-bit computers. Here, a 64-bit computer is one in which floating point, integer, and logical quantities use 64-bit words; a 32-bit machine uses 32-bit words for those same quantities but also allows 64-bit floating point operations. Examples of 64-bit computers are Cray, Cyber-NOS-VE, and DEC/Alpha machines. Examples of 32-bit computers include IBM mainframes, such as a 3090, workstations, including those from DEC, HP, IBM, SGI, and Sun, and even personal computers.

A common source is maintained for all computer versions. The common source is conditioned for a particular computer and operating system through the use of two precompilers maintained as part of RELAP5. The first precompiler processes compile time options such as machine and operating system dependencies. Through the use of standard Fortran and a widely used standard for bit operations, there is very little hardware dependence. The primary hardware dependence is in matrix factoring routines where details of the floating point characteristics are needed to monitor roundoff error. The program has been compiled and executed using Fortran-90; a future full conversion to that standard should remove all hardware dependencies. RELAP5 is developed and maintained at INEL on computers using the UNIX operating system. Some user convenient features have been incorporated into the code based on UNIX, but these are under compile time option, and the code does not depend on any particular operating system. The installation scripts distributed with the code are UNIX based, and control language to install and execute the code must be developed by the user for other operating systems. The source code appears to be written only for 64-bit machines. But the second precompiler converts the code for 32-bit computers by converting floating point variables to double precision, changing floating point literals to double precision, and adding an additional subscript to integer and logical arrays that are equivalenced to double precision floating point arrays such that they index as 64-bit quantities even though only 32-bit integer arithmetic and logical operations are used. As an example of the additional subscript, an integer statement would be changed from INTEGER IA(1000000) to INTEGER IA(2,1000000).

Transmittals of the code usually show the installation and execution of sample problems on several machines. The machines used depend on the machines currently available to the development staff.

### 2.2 Top Level Organization

RELAP5 is coded in a modular fashion using top-down structuring. The various models and procedures are isolated in separate subroutines. The top level structure is shown in **Figure 2.2-1** and consists of input (INPUT), transient/steady-state (TRNCTL), and stripping (STRIP) blocks.

The input block (INPUT) processes input, checks input data, and prepares required data blocks for all program options and is discussed in more detail in Section 2.3.

The transient/steady-state block (TRNCTL) handles both transient and the steady-state options. The steady-state option determines the steady-state conditions if a properly posed steady-state problem is presented. Steady state is obtained by running an accelerated transient until the time derivatives approach

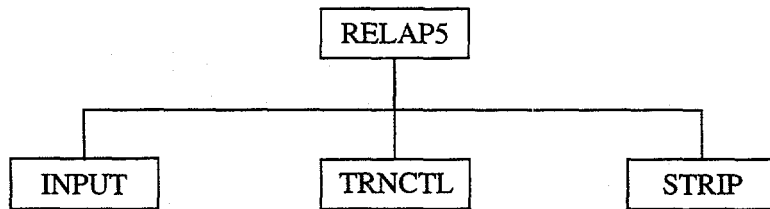


**Figure 2.2-1** RELAP5 top level structure.

zero. Thus, the steady-state option is very similar to the transient option but contains convergence testing algorithms to determine satisfactory steady state, divergence from steady state, or cyclic operation. If the transient technique alone were used, approach to steady state from an initial condition would be identical to a plant transient from that initial condition. Pressures, densities, and flow distributions would adjust quickly, but thermal effects would occur more slowly. To reduce the transient time required to reach steady-state, the steady-state option artificially accelerates heat conduction by reducing the thermal capacity of the conductors. The transient/steady-state block is discussed in more detail in Section 2.4.

The strip block (STRIP) extracts simulation data from a restart plot file for convenient passing of RELAP5 simulation results to other computer programs.

### 2.3 Input Processing Overview

RELAP5 provides detailed input checking for all system models using three input processing phases. The first phase reads all input data, checks for punctuation and typing errors (such as multiple decimal points and letters in numerical fields), and stores the data keyed by card number such that the data are easily retrieved. A list of the input data is provided, and punctuation errors are noted.

During the second phase, restart data from a previous simulation are read if the problem is a RESTART type, and all input data are processed. Some processed input is stored in fixed common blocks, but the majority of the data are stored in dynamic data blocks that are created only if needed by a problem and sized to the particular problem. In a NEW-type problem, dynamic blocks must be created. In RESTART problems, dynamic blocks may be created, deleted, added to, partially deleted, or modified as modeling features and components within models are added, deleted, or modified. Extensive input checking is done, but at this level, checking is limited to new data from the cards being processed. Relationships with other data cannot be checked because the latter may not yet be processed. As an illustration of this level of checking, junction data are checked to determine if they are within the appropriate range (such as positive, nonzero, or between zero and one) and volume connection codes are checked for proper format. No attempt is made at this point to check whether or not referenced volumes exist in the problem until all input data are processed.

The third phase of processing begins after all input data have been processed. Since all data have been placed in common or dynamic data blocks during the second phase, complete checking of interrelationships can proceed. Examples of cross-checking are existence of hydrodynamic volumes referenced in junctions and heat structure boundary conditions; entry or existence of material property data specified in heat structures; and validity of variables selected for minor edits, plotting, or used in trips and control systems. As the cross-checking proceeds, cross-linking of the data blocks is done so that it need not

be repeated at every time step. The initialization required to prepare the model for the start of the transient advancement is done at this level.

Input data editing and diagnostic messages can be generated during the second and/or third phases. Input processing for most models generates output and diagnostic messages during both phases. Thus, input editing for these models appears in two sections.

As errors are detected, various recovery procedures are used so that input processing can be continued and a maximum amount of diagnostic information can be furnished. Recovery procedures include supplying default or benign data, marking the data as erroneous so that other models do not attempt use of the data, or deleting the bad data. The recovery procedures sometimes generate additional diagnostic messages. Often after attempted correction of input, different diagnostic messages appear. These can be due to continued incorrect preparation of data, but the diagnostics may result from the more extensive testing permitted as previous errors are eliminated.

## 2.4 Transient Overview

**Figure 2.4-1** shows the functional modular structure for the transient calculations, while **Figure 2.4-2** shows the second-level structures for the transient/steady-state blocks or subroutines.

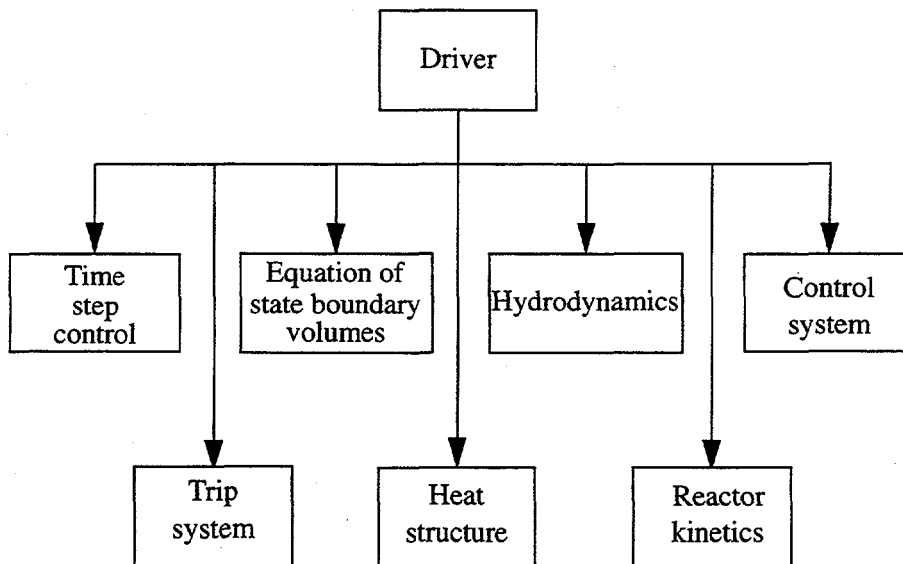


**Figure 2.4-1** Modular structures of transient calculations in RELAP5.

The subroutine TRNCTL shown in **Figure 2.4-2** consists only of the logic to call the next lower level routines. Subroutine TRNSET performs final cross-linking of information between data blocks, sets up arrays to control the sparse matrix solution, establishes scratch work space, and returns unneeded computer memory. Subroutine TRAN, the driver, controls the transient advancement of the solution. Nearly all the execution time is spent in this block, and this block is the most demanding of memory. Nearly all the dynamic data blocks must be in the central memory, and the memory required for instruction storage is high, since coding to advance all models resides in this block. When transient advances are terminated, the subroutine TRNFIN releases space for the dynamic data blocks that are no longer needed.

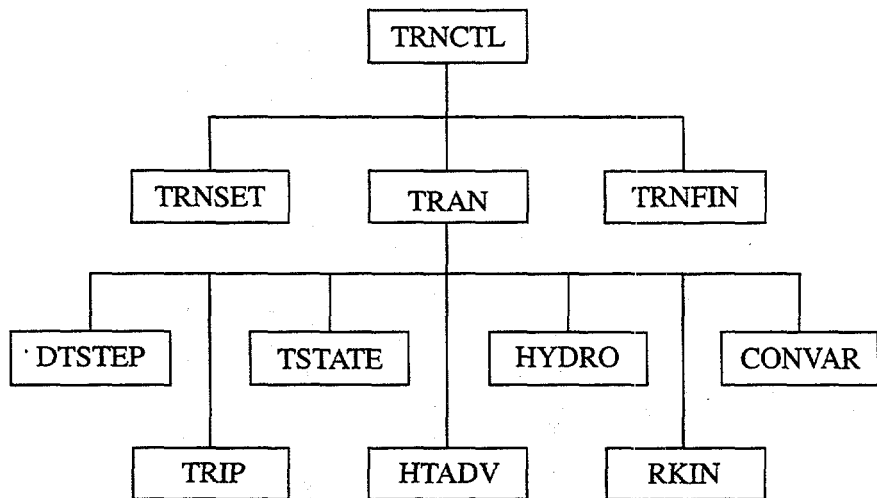


**Figure 2.4-2** Transient (steady-state) block structure.

A description is next presented of the functions of all of the modules (subroutines) driven by TRAN (see **Figure 2.4-2**).

The time step control module (DTSTEP) determines the time step size, controls output editing, and determines whether the transient advancements should be terminated. During program execution, this module displays such information as CPU time, problem time, time step size, and advancement number on the standard output, usually a terminal screen.

The trip system module (TRIP) evaluates logical statements. Each trip statement is a simple logical statement that has a true or false result. The decision of what action is needed resides within the components in other modules. For example, valve components are provided that open or close the valve based on trip values; pump components test trip status to determine whether a pump electrical breaker has tripped.

The equation of state boundary volume model (TSTATE) calculates the thermodynamic state of the fluid in each hydrodynamic boundary volume (time-dependent volume). This subroutine also computes velocities for the time-dependent junctions.

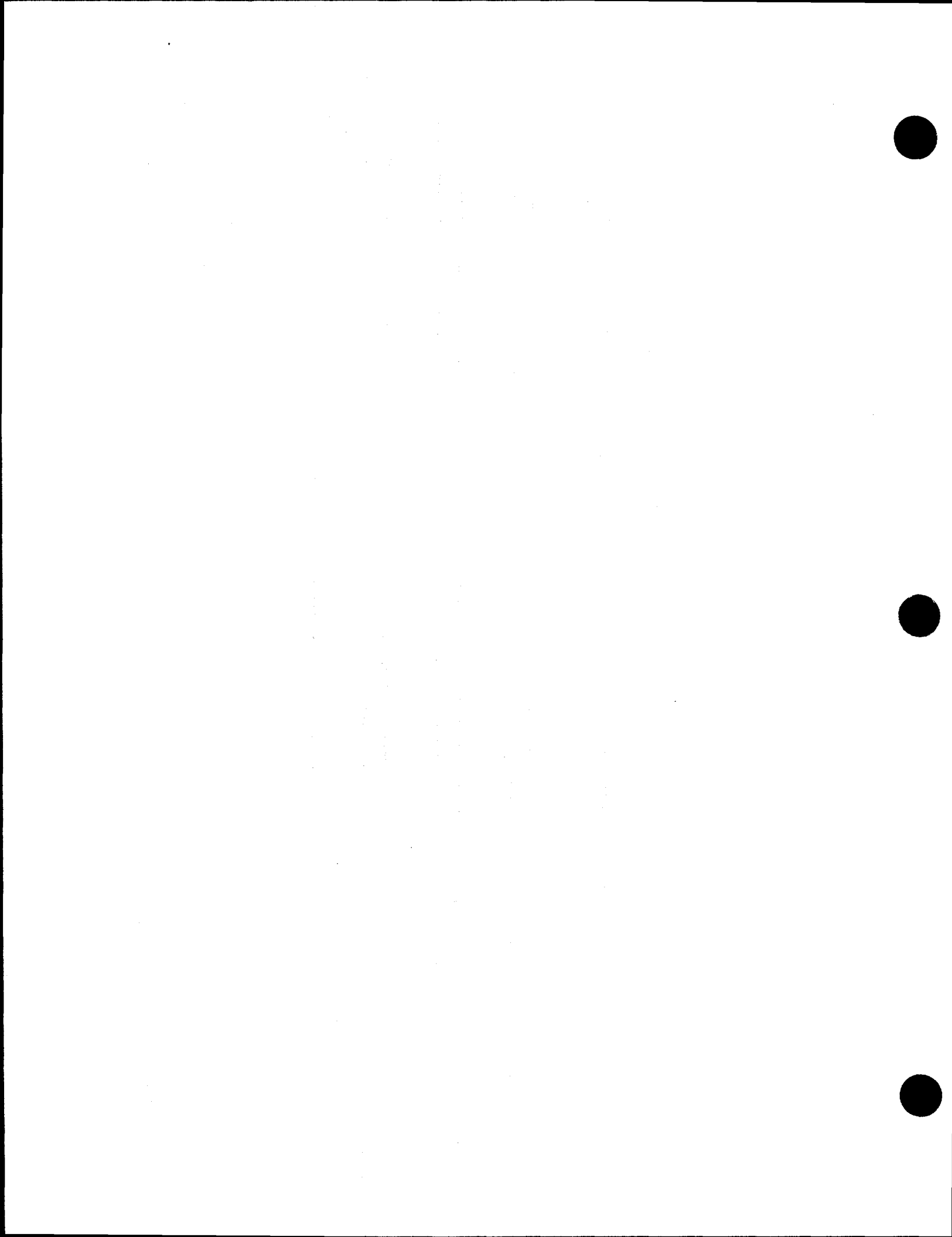
The heat structure model (HTADV) advances heat conduction/transfer solutions. It calculates heat transferred across solid boundaries of hydrodynamic volumes.

The hydrodynamics module (HYDRO) advances the hydrodynamic solution.

The reactor kinetics module (RKIN) advances the reactor kinetics of the code. It computes the power behavior in a nuclear reactor using the space-independent or point kinetics approximation, which assumes that power can be separated into space and time functions.

The control system module (CONVAR) provides the capability of simulating control systems typically used in hydrodynamic systems. It consists of several types of control components. Each component defines a control variable as a specific function of time advanced quantities. The time

advanced quantities include quantities from hydrodynamic volumes, junctions, pumps, valves, heat structures, reactor kinetics, trip quantities, and the control variables themselves. This permits control variables to be developed from components that perform simple, basic operations.



### 3 HYDRODYNAMIC MODEL

The RELAP5 hydrodynamic model is a one-dimensional, transient, two-fluid model for flow of a two-phase steam-water mixture that can contain noncondensable components in the steam phase and/or a soluble component in the water phase.

The RELAP5 hydrodynamic model contains several options for invoking simpler hydrodynamic models. These include homogeneous flow, thermal equilibrium, and frictionless flow models. These options can be used independently or in combination. The homogeneous and equilibrium models were included primarily to be able to compare code results with calculations from the older codes based on the homogeneous equilibrium model.

The two-fluid equations of motion that are used as the basis for the RELAP5 hydrodynamic model are formulated in terms of volume and time-averaged parameters of the flow. Phenomena that depend upon transverse gradients, such as friction and heat transfer, are formulated in terms of the bulk properties using empirical transfer coefficient formulations. In situations where transverse gradients cannot be represented within the framework of empirical transfer coefficients, such as subcooled boiling, additional models specially developed for the particular situation are employed. The system model is solved numerically using a semi-implicit finite-difference technique. The user can select an option for solving the system model using a nearly implicit finite-difference technique, which allows violation of the material Courant limit. This option is suitable for steady-state calculations and for slowly varying, quasi-steady transient calculations.

The basic two-fluid differential equations possess complex characteristic roots that give the system a partially elliptic character and thus constitute an ill-posed initial boundary value problem. In RELAP5, the numerical problem is rendered well-posed by the introduction of artificial viscosity terms in the difference equation formulation that damp the high frequency spatial components of the solution. The ill-posed character of the two-fluid model is a result of the spatial averaging process and neglect of higher-order physical effects in the momentum formulation. Ransom and Hicks<sup>3-0-1</sup> have studied several formulations in which two pressures (one for each fluid) are included in the model, and these models are totally hyperbolic and thus constitute well-posed problems. Limited numerical studies by Ransom and Scofield<sup>3-0-2</sup> have shown that solutions for the two-pressure model compare very well to that for the single-pressure model with damping. In general, the differences are significant only for short wavelength components of the solution where numerical truncation error is dominant. Thus, either approach provides a valid numerical simulation at solution component wavelengths of interest in most reactor safety problems. The simpler formulation of the single-pressure model favors using that approach.

The semi-implicit numerical solution scheme uses a direct sparse matrix solution technique for time step advancement. It is an efficient scheme and results in an overall grind time per node on the CRAY XMP/24 of ~0.00053 seconds, on the DEC Alpha 3000 of ~0.00057 seconds, and on the DECstation 5000 of ~0.00259 seconds. The method has a material Courant time step stability limit. However, this limit is implemented in such a way that single-node Courant violations are permitted without adverse stability effects. Thus, single small nodes embedded in a series of larger nodes will not adversely affect the time step and computing cost. The nearly implicit numerical solution scheme also uses a direct sparse matrix solution technique for time step advancement. This scheme has a grind time that is 25 to 60% greater than the semi-implicit scheme but allows violation of the material Courant limit for all nodes.

### 3.0.1 References

- 3.0-1. V. H. Ransom and D. L. Hicks, "Hyperbolic Two-Pressure Models for Two-Phase Flow," *Journal of Computational Physics*, 53, 1984, pp. 124-151.
- 3.0-2. V. H. Ransom and M. P. Scofield, *Two-Pressure Hydrodynamic Model for Two-Phase Separate Flow*, INEL Report SRD-50-76, 1976.

### 3.1 Field Equations

The RELAP5 thermal-hydraulic model solves eight field equations for eight primary dependent variables. The primary dependent variables are pressure (P), phasic specific internal energies ( $U_g$ ,  $U_f$ ), vapor volume fraction (void fraction) ( $\alpha_g$ ), phasic velocities ( $v_g$ ,  $v_f$ ), noncondensable quality ( $X_n$ ), and boron density ( $\rho_b$ ). The independent variables are time (t) and distance (x). Noncondensable quality is defined as the ratio of the noncondensable gas mass to the total gaseous phase mass, i.e.,  $X_n = M_n/(M_n + M_s)$ , where  $M_n$  is the mass of noncondensable in the gaseous phase and  $M_s$  is the mass of the steam in the gaseous phase. The secondary dependent variables used in the equations are phasic densities ( $\rho_g$ ,  $\rho_f$ ), phasic temperatures ( $T_g$ ,  $T_f$ ), saturation temperature ( $T^s$ ), and noncondensable mass fraction in noncondensable gas phase ( $X_{ni}$ ) for the i-th noncondensable species, i.e.,

$$X_{ni} = \frac{M_{ni}}{\sum_{i=1}^N M_{ni}} = \frac{M_{ni}}{M_n} \quad (3.1-1)$$

where  $M_{ni}$  is the mass of the i-th noncondensable in the gaseous phase, and  $M_n$  is the total mass of noncondensable gas in the gaseous phase.

The basic two-fluid differential equations that form the basis for the hydrodynamic model are next presented. This discussion will be followed by the development of a convenient form of the differential equations that is used as the basis for the numerical solution scheme. The modifications necessary to model horizontal stratified flow are also discussed. Subsequently, the semi-implicit scheme difference equations and the time advancement scheme are discussed. Next, the nearly-implicit scheme difference equations and the associated time advancement scheme are presented. Finally, the volume average velocity formulations, implicit hydrodynamic/heat structure coupling, and the boron transport equation numerical solution are presented.

#### 3.1.1 Basic Differential Equations

The differential form of the one-dimensional transient field equations is first presented for a one-component system. The modifications necessary to consider noncondensables as a component of the gaseous phase and boron as a nonvolatile solute component of the liquid phase are discussed separately.

**3.1.1.1 Vapor/Liquid System.** The basic field equations for the two-fluid nonequilibrium model consist of two phasic continuity equations, two phasic momentum equations, and two phasic energy equations. The equations are recorded in differential stream tube form with time and one space dimension as independent variables and in terms of time and volume-average dependent variables.<sup>a</sup> The development of such equations for the two-phase process has been recorded in several references<sup>3.1-1,3.1-2,3.1-3</sup> and is

a. In all the field equations shown herein, the correlation coefficients<sup>3.1-1</sup> are assumed to be unity so the average of a product of variables is equal to the product of the averaged variables.

not repeated here. The equations are cast in the basic form with discussion of those terms that may differ from other developments. Manipulations required to obtain the form of the equations from which the numerical scheme was developed are described in Section 3.1.2.

### Mass Continuity

The phasic continuity equations are

$$\frac{\partial}{\partial t}(\alpha_g \rho_g) + \frac{1}{A} \frac{\partial}{\partial x}(\alpha_g \rho_g v_g A) = \Gamma_g \quad (3.1-2)$$

$$\frac{\partial}{\partial t}(\alpha_f \rho_f) + \frac{1}{A} \frac{\partial}{\partial x}(\alpha_f \rho_f v_f A) = \Gamma_f \quad (3.1-3)$$

These equations come from the one-dimensional phasic mass equations [Equation (8.12)] in **Reference 3.1-1** as follows: Equation (8.12) can be written in area average notation wherein the term (L/V) has been reduced to (1/A). The vapor continuity Equation (3.1-2) then is the same as Equation (8.12) using k=g. The liquid continuity Equation (3.1-3) then is the same as Equation (8.12) using k=f. This derivation is discussed in Chapter 8 of **Reference 3.1-1**.

Generally, the flow does not include mass sources or sinks, and overall continuity consideration yields the requirement that the liquid generation term be the negative of the vapor generation, that is,

$$\Gamma_f = -\Gamma_g \quad (3.1-4)$$

The interfacial mass transfer model assumes that total mass transfer can be partitioned into mass transfer at the vapor/liquid interface in the bulk fluid ( $\Gamma_{ig}$ ) and mass transfer at the vapor/liquid interface in the boundary layer near the walls ( $\Gamma_w$ ); that is,

$$\Gamma_g = \Gamma_{ig} + \Gamma_w \quad (3.1-5)$$

The  $\Gamma_{ig}$  term will be developed in the following sections, and the  $\Gamma_w$  term is determined as part of the wall heat transfer computation (Section 3.3.10).

### Momentum Conservation

The phasic conservation of momentum equations are used, and recorded here, in an expanded form and in terms of momenta per unit volume using the phasic primitive variables  $v_g$  and  $v_f$ . The spatial variation of momentum term is expressed in terms of  $v_g^2$  and  $v_f^2$ . This form has the desirable feature that the momentum equation reduces to Bernoulli's equations for steady, incompressible, and frictionless flow. A guiding principle used in the development of the RELAP5 momentum formulation is that momentum effects are secondary to mass and energy conservation in reactor safety analysis and a less exact formulation (compared to mass and energy conservation) is acceptable especially since nuclear reactor

flows are dominated by large sources and sinks of momentum (i.e., pumps, abrupt area change). A primary reason for use of the expanded form is that is it more convenient for development of the numerical scheme. The momentum equation for the vapor phase is

$$\begin{aligned} \alpha_g \rho_g A \frac{\partial v_g}{\partial t} + \frac{1}{2} \alpha_g \rho_g A \frac{\partial v_g^2}{\partial x} = & - \alpha_g A \frac{\partial P}{\partial x} + \alpha_g \rho_g B_x A - (\alpha_g \rho_g A) FWG(v_g) \\ & + \Gamma_g A (v_{gI} - v_g) - (\alpha_g \rho_g A) FIG(v_g - v_f) \\ & - C \alpha_g \alpha_f \rho_m A \left[ \frac{\partial (v_g - v_f)}{\partial t} + v_f \frac{\partial v_g}{\partial x} - v_g \frac{\partial v_f}{\partial x} \right] \end{aligned} \quad (3.1-6)$$

and for the liquid phase is

$$\begin{aligned} \alpha_f \rho_f A \frac{\partial v_f}{\partial t} + \frac{1}{2} \alpha_f \rho_f A \frac{\partial v_f^2}{\partial x} = & - \alpha_f A \frac{\partial P}{\partial x} + \alpha_f \rho_f B_x A - (\alpha_f \rho_f A) FWF(v_f) \\ & - \Gamma_g A (v_{fI} - v_f) - (\alpha_f \rho_f A) FIF(v_f - v_g) \\ & - C \alpha_f \alpha_g \rho_m A \left[ \frac{\partial (v_f - v_g)}{\partial t} + v_g \frac{\partial v_f}{\partial x} - v_f \frac{\partial v_g}{\partial x} \right] . \end{aligned} \quad (3.1-7)$$

These equations come from the one-dimensional phasic momentum equations [Equation (8-13)] in **Reference 3.1-1** with the following simplifications: the Reynolds stresses are neglected, the phasic pressures are assumed equal, the interfacial pressures are assumed equal to the phasic pressures (except for stratified flow), the covariance terms are universally neglected (unity assumed for covariance multipliers), interfacial momentum storage is neglected, phasic viscous stresses are neglected, the interface force terms consist of both pressure and viscous stresses, and the normal wall forces are assumed adequately modeled by the variable area momentum flux formulation. The phasic continuity equations are multiplied by the corresponding phasic velocity, and are subtracted from the momentum equations. The vapor momentum Equation (3.1-6) is the same as the resulting vapor momentum equation using  $k = g$ ; the liquid momentum Equation (3.1-7) is the same as the resulting liquid momentum equation using  $k = f$ . This is discussed in Chapter 8 of **Reference 3.1-1**.

The force terms on the right sides of Equations (3.1-6) and (3.1-7) are, respectively, the pressure gradient, the body force (i.e., gravity and pump head), wall friction, momentum transfer due to interface mass transfer, interface frictional drag, and force due to virtual mass. The terms FWG and FWF are part of the wall frictional drag, which are linear in velocity, and are products of the friction coefficient, the frictional reference area per unit volume, and the magnitude of the fluid bulk velocity. The interfacial velocity in the interface momentum transfer term is the unit momentum with which phase appearance or disappearance occurs. The coefficients FIG and FIF are parts of the interface frictional drag, which is linear in relative velocity, and are products of the interface friction coefficients, the frictional reference area per unit volume, and the magnitude of interface relative velocity. The coefficient of virtual mass is the same as that used by Anderson<sup>3.1-4</sup> in the RISQUE code, where the value for C depends on the flow regime. A value of  $C > 1/2$  has been shown to be appropriate for bubbly or dispersed flows,<sup>3.1-5, 3.1-6</sup> while  $C = 0$  may be appropriate for a separated or stratified flow.

The virtual mass term listed in Equations (3.1-6) and (3.1-7) is the same objective formulation<sup>3.1-7, 3.1-8</sup> used in RELAP5/MOD1. In the RELAP5/MOD3 coding, however, this term is simplified. In particular, the spatial derivative portion of the term is neglected. The reason for this change is that inaccuracies in approximating spatial derivatives for the relatively coarse nodalizations used in system representations can lead to nonphysical characteristics in the numerical solution. The primary effect of the virtual mass term is on the mixture sound speed; thus, the simplified form is adequate, since critical flows are calculated in RELAP5 using an integral model<sup>3.1-9</sup> in which the sound speed is based on an objective formulation for the added mass terms.

Conservation of momentum at the interface requires that the force terms associated with interface mass and momentum exchange sum to zero, and is shown as

$$\begin{aligned} \Gamma_g A v_{gI} - (\alpha_g \rho_g A) FIG (v_g - v_f) - C \alpha_g \alpha_f \rho_m A \left[ \frac{\partial (v_g - v_f)}{\partial t} \right] \\ - \Gamma_g A v_{fI} - (\alpha_f \rho_f A) FIF (v_f - v_g) - C \alpha_f \alpha_g \rho_m A \left[ \frac{\partial (v_f - v_g)}{\partial t} \right] = 0 \end{aligned} \quad (3.1-8)$$

where the spatial derivatives have been eliminated as explained above.

This particular form for interface momentum balance results from consideration of the momentum equations in unexpanded form. The force terms associated with virtual mass acceleration in Equation (3.1-8) sum to zero identically as a result of the particular form chosen. In addition, it is usually assumed (although not required by any basic conservation principle) that the interface momentum transfer due to friction and due to mass transfer independently sum to zero, that is,

$$v_{gI} = v_{fI} = v_I \quad (3.1-9)$$

and

$$\alpha_g \rho_g FIG = \alpha_f \rho_f FIF = \alpha_g \alpha_f \rho_g \rho_f FI \quad (3.1-10)$$

These conditions are sufficient to ensure that Equation (3.1-8) is satisfied.

### Energy Conservation

The phasic thermal energy equations are

$$\begin{aligned} \frac{\partial}{\partial t} (\alpha_g \rho_g U_g) + \frac{1}{A} \frac{\partial}{\partial x} (\alpha_g \rho_g U_g v_g A) = -P \frac{\partial \alpha_g}{\partial t} - \frac{P}{A} \frac{\partial}{\partial x} (\alpha_g v_g A) \\ + Q_{wg} + Q_{ig} + \Gamma_{ig} h_g^* + \Gamma_w h_g + DISS_g \end{aligned} \quad (3.1-11)$$

$$\frac{\partial}{\partial t}(\alpha_f \rho_f U_f) + \frac{1}{A} \frac{\partial}{\partial x}(\alpha_f \rho_f U_f v_f A) = -P \frac{\partial \alpha_f}{\partial t} - \frac{P}{A} \frac{\partial}{\partial x}(\alpha_f v_f A) + Q_{wf} + Q_{if} - \Gamma_{ig} h_f^* - \Gamma_w h_f + DISS_f . \quad (3.1-12)$$

These equations come from the one-dimensional phasic thermal energy equations [Equation (8-16)] in **Reference 3.1-1** with the following simplifications: the Reynolds heat flux is neglected, the covariance terms are universally neglected (unity assumed for covariance multipliers), interfacial energy storage is neglected, and internal phasic heat transfer is neglected. The vapor thermal energy Equation (3.1-11) is the same as the resulting vapor thermal energy equation using  $k = g$ ; the liquid thermal energy Equation (3.1-12) is the same as the resulting liquid thermal energy equation using  $k = f$ . This derivation is discussed in Chapter 8 of **Reference 3.1-1**.

In the phasic energy equations,  $Q_{wg}$  and  $Q_{wf}$  are the phasic wall heat transfer rates per unit volume (see Section 3.3.9). These phasic wall heat transfer rates satisfy the equation

$$Q = Q_{wg} + Q_{wf} \quad (3.1-13)$$

where  $Q$  is the total wall heat transfer rate to the fluid per unit volume.

The phasic enthalpies ( $h_g^*$ ,  $h_f^*$ ) associated with bulk interface mass transfer in Equations (3.1-11) and (3.1-12) are defined in such a way that the interface energy jump conditions at the liquid-vapor interface are satisfied. In particular, the  $h_g^*$  and  $h_f^*$  are chosen to be  $h_g^s$  and  $h_f$ , respectively, for the case of vaporization and  $h_g$  and  $h_f^s$ , respectively, for the case of condensation. The same is true for the phasic enthalpies ( $h_g$ ,  $h_f$ ) associated with wall (thermal boundary layer) interface mass transfer. The logic for this choice will be further explained in the development of the mass transfer model.

### Vapor Generation

The vapor generation (or condensation) consists of two parts, vapor generation which results from energy exchange ( $\Gamma_{ig}$ ) and vapor generation due to wall heat transfer effects ( $\Gamma_w$ ) [see Equation (3.1-5)]. Each of the vapor generation (or condensation) processes involves interface heat transfer effects. The interface heat transfer terms ( $Q_{ig}$  and  $Q_{if}$ ) appearing in Equations (3.1-11) and (3.1-12) include heat transfer from the fluid states to the interface due to interface energy exchange in the bulk and near the wall. The vapor generation (or condensation) rates are established from energy balance considerations at the interface.

The summation of Equations (3.1-11) and (3.1-12) produces the mixture energy equation, from which it is required that the interface transfer terms sum to zero, that is,

$$Q_{ig} + Q_{if} + \Gamma_{ig} (h_g^* - h_f^*) + \Gamma_w (h_g - h_f) = 0 . \quad (3.1-14)$$

The interface heat transfer terms ( $Q_{ig}$  and  $Q_{if}$ ) consist of two parts, that is, interface heat transfer in the bulk ( $Q_{ig}^B$  and  $Q_{if}^B$ ) and interface heat transfer in the thermal boundary layer near the wall ( $Q_{ig}^W$  and  $Q_{if}^W$ ). This is one situation where the assumption of no transverse gradients needs to be supplemented by a special model. The interface heat transfer terms are shown in **Figure 3.1-1** for the case of subcooled boiling.

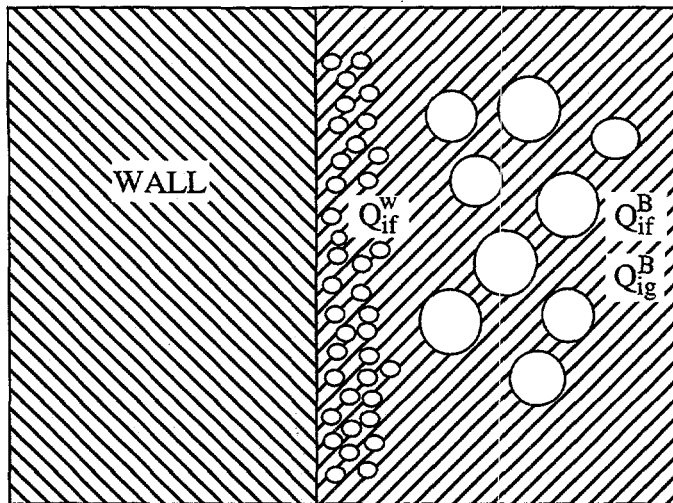


**Figure 3.1-1** Interface heat transfer in the bulk and near the wall for subcooled boiling.

The two parts are additive, that is,

$$Q_{ig} = Q_{ig}^B + Q_{ig}^W \quad (3.1-15)$$

and

$$Q_{if} = Q_{if}^B + Q_{if}^W \quad (3.1-16)$$

The bulk interface heat transfer is at the steam-liquid interface in the bulk. This represents thermal energy exchange between the fluid interface (at saturation temperature  $T^s$ ) and the bulk fluid state.

For gas, the bulk interface heat transfer is given by

$$Q_{ig}^B = H_{ig} (T^s - T_g) \quad (3.1-17)$$

where  $H_{ig}$  is the gas interface heat transfer coefficient per unit volume.

For liquid, the bulk interface heat transfer is given by

$$Q_{if}^B = H_{if} (T^s - T_f) \quad (3.1-18)$$

where  $H_{if}$  is the liquid interface heat transfer coefficient per unit volume.

The  $Q_{ig}^W$  and  $Q_{if}^W$  terms are the interface heat transfer rates near the wall and will be defined in terms of the wall vapor generation (or condensation) process. This is discussed in more detail in Volume IV. Inserting Equations (3.1-17) and (3.1-18) into Equations (3.1-15) and (3.1-16) gives

$$Q_{ig} = H_{ig} (T^s - T_g) + Q_{ig}^W \quad (3.1-19)$$

and

$$Q_{if} = H_{if} (T^s - T_f) + Q_{if}^W \quad (3.1-20)$$

Although it is not a fundamental requirement, it is assumed that Equation (3.1-14) will be satisfied by requiring that the bulk interface energy exchange terms and the near wall interface energy exchange terms each sum to zero independently. Thus,

$$H_{ig} (T^s - T_g) + H_{if} (T^s - T_f) + \Gamma_{ig} (h_g^* - h_f^*) = 0 \quad (3.1-21)$$

and

$$Q_{ig}^W + Q_{if}^W + \Gamma_w (h_g - h_f) = 0 \quad (3.1-22)$$

In addition, since it is assumed that vapor appears at saturation, it follows that  $Q_{ig}^W = 0$  for boiling processes in the boundary layer near the wall. Equation (3.1-22) can then be solved for the wall vaporization rate to give

$$\Gamma_w = \frac{-Q_{if}^W}{h_g - h_f} \quad (3.1-23)$$

for boiling in the boundary layer near the wall.

Similarly, since it is assumed that liquid appears at saturation, it follows that  $Q_{if}^w = 0$  for condensation processes in the boundary layer near the wall. Equation (3.1-22) can then be solved for the wall condensation rate to give

$$\Gamma_w = \frac{-Q_{ig}^w}{h_g' - h_f'} \quad (3.1-24)$$

for condensation in the boundary layer near the wall.

The interface energy transfer terms,  $Q_{ig}$  and  $Q_{if}$ , can thus be expressed in a general way as

$$Q_{ig} = H_{ig}(T^s - T_g) - \left(\frac{1-\varepsilon}{2}\right)\Gamma_w(h_g' - h_f') \quad (3.1-25)$$

and

$$Q_{if} = H_{if}(T^s - T_f) - \left(\frac{1+\varepsilon}{2}\right)\Gamma_w(h_g' - h_f') \quad (3.1-26)$$

where  $\varepsilon = 1$  for boiling in the boundary layer near the wall, and  $\varepsilon = -1$  for condensation in the boundary layer near the wall. Finally, Equation (3.1-14) can be used to define the interface vaporization (or condensation) rate:

$$\Gamma_{ig} = -\frac{Q_{ig} + Q_{if}}{h_g^* - h_f^*} - \Gamma_w \frac{(h_g' - h_f')}{h_g^* - h_f^*} \quad (3.1-27)$$

which, upon substitution of Equations (3.1-25) and (3.1-26), becomes

$$\Gamma_{ig} = -\frac{H_{ig}(T^s - T_g) + H_{if}(T^s - T_f)}{h_g^* - h_f^*} \quad (3.1-28)$$

The phase change process that occurs at the interface is envisioned as a process in which bulk fluid is heated or cooled to the saturation temperature and phase change occurs at the saturation state. The interface energy exchange process from each phase must be such that at least the sensible energy change to reach the saturation state occurs. Otherwise, it can be shown that the phase change process implies energy transfer from a lower temperature to a higher temperature. Such conditions can be avoided by the proper choice of the variables  $h_g^*$  and  $h_f^*$  for bulk interface mass transfer and  $h_g'$  and  $h_f'$  for near wall interface mass transfer. In particular, it can be shown that  $h_g^*$  and  $h_f^*$  should be

$$h_g^* = \frac{1}{2} [ (h_g^s + h_g) + \eta (h_g^s - h_g) ] \quad (3.1-29)$$

and

$$h_f^* = \frac{1}{2} [ (h_f^s + h_f) - \eta (h_f^s - h_f) ] \quad (3.1-30)$$

where

$$\eta = 1 \text{ for } \Gamma_{ig} \geq 0$$

$$\eta = -1 \text{ for } \Gamma_{ig} < 0.$$

It can also be shown that  $h_g'$  and  $h_f'$  should be

$$h_g' = \frac{1}{2} [ (h_g^s + h_g) + \varepsilon (h_g^s - h_g) ] \quad (3.1-31)$$

and

$$h_f' = \frac{1}{2} [ (h_f^s + h_f) - \varepsilon (h_f^s - h_f) ] \quad (3.1-32)$$

where

$$\varepsilon = 1 \text{ for } \Gamma_w \geq 0$$

$$\varepsilon = -1 \text{ for } \Gamma_w < 0.$$

Substituting Equation (3.1-28) into Equation (3.1-5) gives the final expression for the total interface mass transfer as

$$\Gamma_g = - \frac{H_{ig}(T^s - T_g) + H_{if}(T^s - T_f)}{h_g^* - h_f^*} + \Gamma_w \quad (3.1-33)$$

Volume IV of the manual discusses the energy partitioning in more detail.

#### Dissipation Terms

The phasic energy dissipation terms,  $DISS_g$  and  $DISS_f$ , are the sums of wall friction and pump effects. The dissipation effects due to interface mass transfer, interface friction, and virtual mass are neglected. This is a reasonable assumption since these terms are small in magnitude in the energy equation. In the mass and momentum equations, interface mass transfer, interface friction, and virtual mass are important and are not neglected. The wall friction dissipations are defined as

$$DISS_g = \alpha_g \rho_g FWG v_g^2 \quad (3.1-34)$$

and

$$DISS_f = \alpha_f \rho_f FWF v_f^2 \quad (3.1-35)$$

The phasic energy dissipation terms satisfy the relation

$$DISS = DISS_g + DISS_f \quad (3.1-36)$$

where  $DISS$  is the energy dissipation. When a pump component is present, the associated energy dissipation is also included in the dissipation terms (see Section 3.5.4).

**3.1.1.2 Noncondensables in the Gas Phase.** The basic, two-phase, single-component model just discussed can be extended to include a noncondensable component in the gas phase. The noncondensable component is assumed to be in mechanical and thermal equilibrium with the vapor phase, so that

$$v_n = v_g \quad (3.1-37)$$

and

$$T_n = T_g \quad (3.1-38)$$

where the subscript,  $n$ , is used to designate the noncondensable component.

The general approach for inclusion of the noncondensable component consists of assuming that all properties of the gas phase (subscript  $g$ ) are mixture properties of the steam/noncondensable mixture. The quality,  $X$ , is likewise defined as the mass fraction based on the mass of the gas phase. Thus, the two basic continuity equations [Equations (3.1-2) and (3.1-3)] are unchanged. However, it is necessary to add an additional mass conservation equation for the total noncondensable component, given by

$$\frac{\partial}{\partial t} (\alpha_g \rho_g X_n) + \frac{1}{A} \frac{\partial}{\partial x} (\alpha_g \rho_g X_n v_g A) = 0 \quad (3.1-39)$$

where

$X_n$  = total noncondensable mass fraction in the gas phase

$$= \frac{\sum_{i=1}^N M_{ni}}{\sum_{i=1}^N M_{ni} + M_s} = \frac{M_n}{M_n + M_s} \quad (3.1-40)$$

$M_{ni}$  = mass of i-th noncondensable gas

$M_s$  = mass of steam in the gas phase.

For each noncondensable specie, the mass conservation equation is

$$\frac{\partial}{\partial t} (\alpha_g \rho_g X_n X_{ni}) + \frac{1}{A} \frac{\partial}{\partial x} (\alpha_g \rho_g X_n X_{ni} v_g A) = 0 \quad (3.1-41)$$

where  $X_{ni}$  is defined in Equation (3.1-1). Only N-1 of the non-condensable gas specie equations need to be solved since the mass fraction of the N-th specie can be found as the difference between the total non-condensable gas mass fraction and the sum of the N-1 non-condensable gas specie mass fractions.

The energy equations are modified to include the sensible interface (direct) heating term  $Q_{gf}$ . This term is necessary because the interfacial terms use saturation temperature based on the bulk steam partial pressure rather than saturation temperature based on the local (interface) steam partial pressure. This is another situation in which the assumption of no transverse gradients in the one-dimensional formulation of the conservation equations needs to be supplemented by a special model. The energy field equations have the form

$$\begin{aligned} \frac{\partial}{\partial t} (\alpha_g \rho_g U_g) + \frac{1}{A} \frac{\partial}{\partial x} (\alpha_g \rho_g U_g v_g A) &= -P \frac{\partial \alpha_g}{\partial t} - P \frac{\partial}{\partial x} (\alpha_g v_g A) \\ &+ Q_{wg} + Q_{ig} + \Gamma_{ig} h_g^* + \Gamma_w h_g' - Q_{gf} + DISS_g \end{aligned} \quad (3.1-42)$$

$$\begin{aligned} \frac{\partial}{\partial t} (\alpha_f \rho_f U_f) + \frac{1}{A} \frac{\partial}{\partial x} (\alpha_f \rho_f U_f v_f A) &= -P \frac{\partial \alpha_f}{\partial t} - P \frac{\partial}{\partial x} (\alpha_f v_f A) \\ &+ Q_{wf} + Q_{if} - \Gamma_{ig} h_f^* - \Gamma_w h_f' + Q_{gf} + DISS_f . \end{aligned} \quad (3.1-43)$$

The term  $Q_{gf}$  in Equations (3.1-42) and (3.1-43) is the sensible heat transfer rate per unit volume. This is the heat transfer at the noncondensable gas-liquid interface, and it represents thermal energy exchange between the bulk fluid states themselves when noncondensable gas is present. This term is given by

$$Q_{gf} = \left( \frac{P - P_s}{P} \right) H_{gf} (T_g - T_f) = \frac{P_n}{P} H_{gf} (T_g - T_f) \quad (3.1-44)$$

where  $H_{gf}$  is the direct heat transfer coefficient per unit volume. This makes use of Dalton's law ( $P = P_s + P_n$ ), where  $P_n$  is the noncondensable gas partial pressure. This term is similar to the heat conduction term in the accumulator model (see Section 3.5.7.2). The multiplier based on the difference in the partial pressure of steam and the total pressure is an ad-hoc function used to turn off this term when there is no noncondensable gas in the volume. The value of the heat transfer coefficient depends upon the configuration of the interface between the liquid and the noncondensable gas just like the situation for the steam-liquid interface.

The interfacial heat transfer and mass transfer terms are also modified when noncondensables are present. The gas bulk interface heat transfer [Equation (3.1-17)] now has the form

$$Q_{ig}^B = \frac{P_s}{P} H_{ig} (T^s (P_s) - T_g) \quad (3.1-45)$$

Thus, the total gas interfacial heat transfer [Equation (3.1-19)] now has the form

$$Q_{ig} = \frac{P_s}{P} H_{ig} (T^s (P_s) - T_g) + Q_{ig}^W \quad (3.1-46)$$

The assumption that the bulk interface exchange terms sum to zero [Equation (3.1-21)], now has the form

$$\frac{P_s}{P} H_{ig} (T^s (P_s) - T_g) + H_{if} (T^s (P_s) - T_f) + \Gamma_{ig} (h_g^* - h_f^*) = 0 \quad (3.1-47)$$

Thus, the total gas interface energy transfer term [Equation (3.1-25)] is now expressed as

$$Q_{ig} = \frac{P_s}{P} H_{ig} (T^s (P_s) - T_g) - \left( \frac{1 - \epsilon}{2} \right) \Gamma_w (h_g' - h_f') \quad (3.1-48)$$

The bulk interface mass transfer rate [Equation (3.1-28)] now has the form

$$\Gamma_{ig} = - \frac{\frac{P_s}{P} H_{ig} (T^s (P_s) - T_g) + H_{if} (T^s (P_s) - T_f)}{h_g^* - h_f^*} \quad (3.1-49)$$

and the total interface mass transfer rate [Equation (3.1-33)] now has the form

$$\Gamma_g = -\frac{\frac{P}{P_s} H_{ig} (T^s (P_s) - T_g) + H_{if} (T^s (P_s) - T_f)}{h_g^* - h_f^*} + \Gamma_w \quad (3.1-50)$$

Volume IV of the manual discusses the energy partitioning in more detail.

The gas enthalpy  $h_g^*$ , which is used in the energy field equation and in the mass transfer  $\Gamma_g$ , is based on the partial pressure of steam instead of the total pressure when noncondensables are present.

The momentum field equations are unchanged when noncondensables are present. In all the equations, the vapor field properties are now evaluated for the steam/noncondensable mixture. The modifications appropriate to the state relationships are discussed in Section 3.2.3.

**3.1.1.3 Boron Concentration in the Liquid Field.** An Eulerian boron tracking model is used in RELAP5 that simulates the transport of a dissolved component in the liquid phase. The solution is assumed to be sufficiently dilute that the following assumptions are valid:

- Liquid properties are not altered by the presence of the solute
- Solute is transported only in the liquid phase and at the velocity of the liquid phase
- Energy transported by the solute is negligible
- Inertia of the solute is negligible.

Under these assumptions, only an additional field equation for the conservation of the solute is required. In differential form, the added equation is

$$\frac{\partial \rho_b}{\partial t} + \frac{1}{A} \frac{\partial (\alpha_f \rho_f C_b v_f A)}{\partial x} = 0 \quad (3.1-51)$$

where the concentration parameter,  $C_b$ , is defined as

$$C_b = \frac{\rho_b}{\rho_m (1 - X)} = \frac{\rho_b}{\alpha_f \rho_f} \quad (3.1-52)$$

$C_b$  is the concentration of dissolved solid in mass units per mass unit of liquid phase.

### 3.1.2 Numerically Convenient Set of Differential Equations

A more convenient set of differential equations upon which to base the numerical scheme is obtained from the basic density and energy differential equations by expanding the time derivative in each equation using the product rule. When the product rule is used to evaluate the time derivative, we will refer to this

form as the expanded form. The mass and momentum equations are used as sum and difference equations in the numerical scheme and are recorded here in that form. The reason for using this form is ease of degeneration of the model to the single-phase case.

A sum density equation is obtained by expanding the time derivative in the phasic density equations, Equations (3.1-2) and (3.1-3), adding these two new equations, and using the relation

$$\frac{\partial \alpha_f}{\partial t} = -\frac{\partial \alpha_g}{\partial t} . \quad (3.1-53)$$

This gives

$$\alpha_g \frac{\partial p_g}{\partial t} + \alpha_f \frac{\partial p_f}{\partial t} + (p_g - p_f) \frac{\partial \alpha_g}{\partial t} + \frac{1}{A} \frac{\partial}{\partial x} (\alpha_g \rho_g v_g A + \alpha_f \rho_f v_f A) = 0 . \quad (3.1-54)$$

A difference density equation is obtained by expanding the time derivative in the phasic density equations, Equations (3.1-2) and (3.1-3), subtracting these two new equations, again using the relation

$$\frac{\partial \alpha_f}{\partial t} = -\frac{\partial \alpha_g}{\partial t} \quad (3.1-55)$$

and substituting Equation (3.1-50) for  $\Gamma_g$ . This gives

$$\begin{aligned} \alpha_g \frac{\partial p_g}{\partial t} - \alpha_f \frac{\partial p_f}{\partial t} + (p_g + p_f) \frac{\partial \alpha_g}{\partial t} + \frac{1}{A} \frac{\partial}{\partial x} (\alpha_g \rho_g v_g A - \alpha_f \rho_f v_f A) \\ = -\frac{2 \left[ \frac{P_s}{P} H_{ig} (T^s - T_g) + H_{if} (T^s - T_f) \right]}{h_g^* - h_f^*} + 2\Gamma_w . \end{aligned} \quad (3.1-56)$$

The time derivative of the total noncondensable density equation, Equation (3.1-39), is expanded to give

$$\rho_g X_n \frac{\partial \alpha_g}{\partial t} + \alpha_g X_n \frac{\partial p_g}{\partial t} + \alpha_g \rho_g \frac{\partial X_n}{\partial t} + \frac{1}{A} \frac{\partial}{\partial x} (\alpha_g \rho_g X_n v_g A) = 0 . \quad (3.1-57)$$

The time derivative of the individual noncondensable density equation, Equation (3.1-41), is not expanded, since the individual noncondensable quality,  $X_{ni}$ , will be obtained from the unexpanded equation (Section 3.1.5.1).

The momentum equations are also rearranged into a sum and difference form. The sum momentum equation is obtained by direct summation of Equations (3.1-6) and (3.1-7) with the interface conditions

[Equations (3.1-8) through (3.1-10)] substituted where appropriate and the cross-sectional area canceled throughout. The resulting sum equation is

$$\alpha_g \rho_g \frac{\partial v_g}{\partial t} + \alpha_f \rho_f \frac{\partial v_f}{\partial t} + \frac{1}{2} \alpha_g \rho_g \frac{\partial v_g^2}{\partial x} + \frac{1}{2} \alpha_f \rho_f \frac{\partial v_f^2}{\partial x} = - \frac{\partial P}{\partial x} + \rho_m B_x \\ - \alpha_g \rho_g F W G v_g - \alpha_f \rho_f F W F v_f - \Gamma_g (v_g - v_f) \quad (3.1-58)$$

The difference of the phasic momentum equations is obtained by first dividing the vapor and liquid phasic momentum equations by  $\alpha_g \rho_g A$  and  $\alpha_f \rho_f A$ , respectively, and subtracting. Here again, the interface conditions are used, and the common area is divided out. As discussed, the virtual mass term is simplified by neglecting the spatial derivative portion. The resulting equation is

$$\frac{\partial v_g}{\partial t} - \frac{\partial v_f}{\partial t} + \frac{1}{2} \frac{\partial v_g^2}{\partial x} - \frac{1}{2} \frac{\partial v_f^2}{\partial x} = - \left( \frac{1}{\rho_g} - \frac{1}{\rho_f} \right) \frac{\partial P}{\partial x} \\ - F W G v_g + F W F v_f \\ + \Gamma_g [ \rho_m v_I - (\alpha_f \rho_f v_g + \alpha_g \rho_g v_f) ] / (\alpha_g \rho_g \alpha_f \rho_f) - \rho_m F I (v_g - v_f) \\ - C [ \rho_m^2 / (\rho_g \rho_f) ] \frac{\partial (v_g - v_f)}{\partial t} \quad (3.1-59)$$

where the interfacial velocity,  $v_I$ , is defined as

$$v_I = \lambda v_g + (1 - \lambda) v_f \quad (3.1-60)$$

This definition for  $v_I$  has the property that if  $\lambda = 1/2$  the interface momentum transfer process associated with mass transfer is reversible. This value leads to either an entropy sink or source, depending on the sign of  $\Gamma_g$ . However, if  $\lambda$  is chosen to be 0 for positive values of  $\Gamma_g$  and +1 for negative values of  $\Gamma_g$  (that is, a donor formulation), the mass exchange process is always dissipative. The latter model for  $v_I$  is the most realistic for the momentum exchange process and is used for the numerical scheme development.

To develop an expanded form of the vapor energy equation, the time derivative of the vapor energy Equation (3.1-42) is expanded,  $Q_{ig}$  Equation (3.1-48) and the  $\Gamma_{ig}$  Equation (3.1-49) are substituted, and the  $H_{ig}$ ,  $H_{if}$ ,  $\partial \alpha_g / \partial t$ , and convective terms are collected. This gives the desired form for the vapor energy equation

$$\begin{aligned}
 & (\rho_g U_g + P) \frac{\partial \alpha_g}{\partial t} + \alpha_g U_g \frac{\partial \rho_g}{\partial t} + \alpha_g \rho_g \frac{\partial U_g}{\partial t} + \frac{1}{A} \left[ \frac{\partial}{\partial x} (\alpha_g \rho_g U_g v_g A) + P \frac{\partial}{\partial x} (\alpha_g v_g A) \right] \\
 &= - \left( \frac{h_f^*}{h_g^* - h_f^*} \right) \frac{P_s}{P} H_{ig} (T^s - T_g) - \left( \frac{h_g^*}{h_g^* - h_f^*} \right) H_{if} (T^s - T_f) - \left( \frac{P - P_s}{P} \right) H_{gf} (T_g - T_f) \\
 & \quad + \left[ \left( \frac{1 + \varepsilon}{2} \right) h_g + \left( \frac{1 - \varepsilon}{2} \right) h_f \right] \Gamma_w + Q_{wg} + DISS_g .
 \end{aligned} \tag{3.1-61}$$

To develop an expanded form of the liquid energy equation, the time derivative of the liquid energy Equation (3.1-43) is expanded, the  $Q_{if}$  Equation (3.1-26) and the  $\Gamma_{ig}$  Equation (3.1-49) are substituted, and

$$\frac{\partial \alpha_f}{\partial t} = - \frac{\partial \alpha_g}{\partial t} \tag{3.1-62}$$

is used. Then the  $H_{ig}$ ,  $H_{if}$ ,  $\partial \alpha_g / \partial t$ , and convective terms are collected. This gives the desired form for the liquid energy equation:

$$\begin{aligned}
 & - (\rho_f U_f + P) \frac{\partial \alpha_g}{\partial t} + \alpha_f U_f \frac{\partial \rho_f}{\partial t} + \alpha_f \rho_f \frac{\partial U_f}{\partial t} + \frac{1}{A} \left[ \frac{\partial}{\partial x} (\alpha_f \rho_f U_f v_f A) + P \frac{\partial}{\partial x} (\alpha_f v_f A) \right] \\
 &= \left( \frac{h_f^*}{h_g^* - h_f^*} \right) \frac{P_s}{P} H_{ig} (T^s - T_g) + \left( \frac{h_g^*}{h_g^* - h_f^*} \right) H_{if} (T^s - T_f) + \left( \frac{P - P_s}{P} \right) H_{gf} (T_g - T_f) \\
 & \quad - \left[ \left( \frac{1 + \varepsilon}{2} \right) h_g + \left( \frac{1 - \varepsilon}{2} \right) h_f \right] \Gamma_w + Q_{wf} + DISS_f .
 \end{aligned} \tag{3.1-63}$$

The basic density and energy differential equations are, at times, used in nonexpanded form in the back substitution part of the numerical scheme. When the product rule is not used to evaluate the time derivative, we will refer to this form as the *unexpanded* form. There are situations after a phase has appeared in a volume, where unphysical energies are calculated by the expanded form of the energy equations. It was found that the nonexpanded form, when used in the back substitution step, gave more physical temperatures because there is no linearization error in the time derivative when using the unexpanded form of the energy equations.

The vapor, liquid, and noncondensable density equations, Equations (3.1-2), (3.1-3), and (3.1-39), are in nonexpanded form. The  $\Gamma_g$ , Equation (3.1-50), is not substituted into the vapor and liquid density equations. (The reason will be apparent in Section 3.1.5.) The vapor energy equation, Equation (3.1-42), is altered by substituting Equation (3.1-48) for  $Q_{ig}$ , substituting Equation (3.1-49) for  $\Gamma_{ig}$ , and collecting the  $H_{ig}$ ,  $H_{if}$ , and convective terms. This gives

$$\begin{aligned}
& \frac{\partial}{\partial t} (\alpha_g \rho_g U_g) + \frac{1}{A} \left[ \frac{\partial}{\partial x} (\alpha_g \rho_g U_g v_g A) + P \frac{\partial}{\partial x} (\alpha_g \rho_g A) \right] \\
& = -P \frac{\partial \alpha_g}{\partial t} - \left( \frac{h_f^*}{h_g^* - h_f^*} \right) \frac{P_s}{P} H_{ig} (T^s - T_g) - \left( \frac{h_g^*}{h_g^* - h_f^*} \right) H_{if} (T^s - T_f) - \left( \frac{P - P_s}{P} \right) H_{gf} (T_g - T_f) \\
& \quad + \left[ \left( \frac{1 + \epsilon}{2} \right) h_g' + \left( \frac{1 - \epsilon}{2} \right) h_f' \right] \Gamma_w + Q_{wg} + DISS_g .
\end{aligned} \tag{3.1-64}$$

The liquid energy equation, Equation (3.1-43), is also altered by substituting Equation (3.1-26) for  $Q_{if}$ , substituting Equation (3.1-49) for  $\Gamma_{ig}$ , using Equation (3.1-62), and collecting the  $H_{ig}$ ,  $H_{if}$ , and convective terms. This gives

$$\begin{aligned}
& \frac{\partial}{\partial t} (\alpha_f \rho_f U_f) + \frac{1}{A} \left[ \frac{\partial}{\partial x} (\alpha_f \rho_f U_f v_f A) + P \frac{\partial}{\partial x} (\alpha_f v_f A) \right] \\
& = P \frac{\partial \alpha_f}{\partial t} + \left( \frac{h_f^*}{h_g^* - h_f^*} \right) \frac{P_s}{P} H_{ig} (T^s - T_g) + \left( \frac{h_g^*}{h_g^* - h_f^*} \right) H_{if} (T^s - T_f) + \left( \frac{P - P_s}{P} \right) H_{gf} (T_g - T_f) \\
& \quad - \left[ \left( \frac{1 + \epsilon}{2} \right) h_g' + \left( \frac{1 - \epsilon}{2} \right) h_f' \right] \Gamma_w + Q_{wf} + DISS_f .
\end{aligned} \tag{3.1-65}$$

### 3.1.3 Stratified Flow

Flow at low velocity in a horizontal pipe can be stratified as a result of buoyancy forces caused by density differences between vapor and liquid. When the flow is stratified, the area average pressures are affected by nonuniform transverse distribution of the phases. Appropriate modifications to the basic field equations when stratified flow exists are obtained by considering separate area average pressures for the vapor and liquid phases and the interfacial pressure between them. Using this model, the pressure gradient force terms of Equations (3.1-6) and (3.1-7) become

$$-\alpha_g A \left[ \frac{\partial P}{\partial x} \right] \rightarrow -\alpha_g A \left[ \frac{\partial P_g}{\partial x} \right] + (P_I - P_g) A \left[ \frac{\partial \alpha_g}{\partial x} \right] \tag{3.1-66}$$

and

$$-\alpha_f A \left[ \frac{\partial P}{\partial x} \right] \rightarrow -\alpha_f A \left[ \frac{\partial P_f}{\partial x} \right] + (P_I - P_f) A \left[ \frac{\partial \alpha_f}{\partial x} \right] . \tag{3.1-67}$$

The area average pressure for the entire cross section of the flow is expressed in terms of the phasic area average pressures by

$$P = \alpha_g P_g + \alpha_f P_f . \tag{3.1-68}$$

With these definitions, the sum of the phasic momentum equations, written in terms of the cross-section average pressure [Equation (3.1-58)] remains unchanged. However, the difference of the phasic momentum equations [Equation (3.1-59)], contains the following additional terms on the right side

$$[\rho/(\alpha_g \alpha_f \rho_g \rho_f)] [-\alpha_f \partial(\alpha_g P_g)/\partial x + \alpha_g \partial(\alpha_f P_f)/\partial x + P_l(\partial \alpha_g/\partial x)] . \quad (3.1-69)$$

The interface and phasic cross-sectional average pressures,  $P_l$ ,  $P_g$ , and  $P_f$ , can be found by means of the assumption of a transverse hydrostatic pressure in a round pipe. For a pipe having diameter  $D$ , pressures  $P_l$ ,  $P_g$ , and  $P_f$  are given by

$$P_g = P_l - \rho_g B_y D [\sin^3 \theta / (3\pi \alpha_g) - (\cos \theta) / 2] \quad (3.1-70)$$

$$P_f = P_l - \rho_f B_y D [\sin^3 \theta / (3\pi \alpha_f) - (\cos \theta) / 2] \quad (3.1-71)$$

where  $B_y$  equals the transverse body force (ordinarily equal to  $-g$ ).

The angle,  $\theta$ , is defined by the void fraction, as illustrated in **Figure 3.1-2**. The algebraic relationship between  $\alpha_g$  and  $\theta$  is

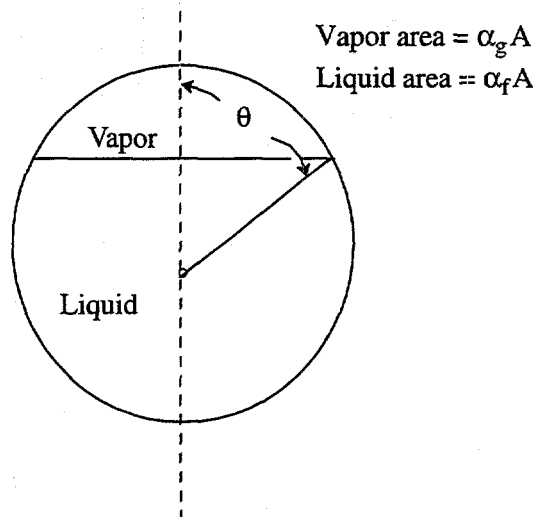


**Figure 3.1-2** Relation of central angle  $\theta$  to void fraction  $\alpha_g$ .

$$\alpha_g \pi = \theta - \sin \theta \cos \theta . \quad (3.1-72)$$

The additional term in the difference of the momentum equations [Equation (3.1-69)] can be simplified using Equations (3.1-70), (3.1-71), and (3.1-72) to obtain

$$- [\rho_m/(\rho_g \rho_f)] (\rho_f - \rho_g) [\pi D B_y / (4 \sin \theta)] (\partial \alpha_g / \partial x) \quad (3.1-73)$$

where  $\theta$  is related to the void fraction using Equation (3.1-72).

This equation can be rearranged to show more explicitly the dependence on the liquid level  $y$  as measured from the bottom of the pipe. Using Equation (3.1-72) along with

$$y = \frac{D}{2} (1 + \cos \theta), \quad (3.1-74)$$

term (3.1-73) becomes

$$[\rho/(\rho_g \rho_f)] (\rho_f - \rho_g) B_y (\partial y / \partial x). \quad (3.1-75)$$

For the phasic momentum Equations (3.1-6) and (3.1-7), the additional term takes the form

$$+ \left[ \frac{\alpha_g \alpha_f (\rho_f - \rho_g)}{\alpha_f \rho_f - \alpha_g \rho_g} \right] \rho_m B_y A \frac{\partial y}{\partial x} \quad (3.1-76)$$

for the gas momentum equation and

$$- \left[ \frac{\alpha_g \alpha_f (\rho_f - \rho_g)}{\alpha_f \rho_f - \alpha_g \rho_g} \right] \rho_m B_y A \frac{\partial y}{\partial x} \quad (3.1-77)$$

for the liquid momentum equation.

To model a pipe of varying diameter, the liquid level is measured with respect to the center of the pipe rather than the bottom of the pipe. Equations (3.1-75), (3.1-76), and (3.1-77) are still valid; however, Equation (3.1-74) is replaced by

$$y = \frac{D}{2} \cos \theta. \quad (3.1-78)$$

The additional force term that arises for a stratified flow geometry in horizontal pipes is added to the basic equation when the flow is established to be stratified from flow regime considerations. Note that the additional force term was derived assuming a round pipe. If the cross section is rectangular, this assumption is not valid.

A similar term is added when there is stratified flow in a series of cells defined as vertically oriented but are cross-connected in the horizontal direction. Equations (3.1-75), (3.1-76), and (3.1-77) are still used; however, Equation (3.1-74) is replaced with

$$y = \frac{1 - 2\alpha_g}{2} \Delta z \quad (3.1-79)$$

where  $\Delta z$  is the height of the volume.

In order to provide for a smooth transition between stratified and nonstratified flow situations, this term is activated in all flow regimes. Since this term is small compared to other terms in the momentum equation when the flow is nonstratified, this is a reasonable assumption.

### 3.1.4 Semi-Implicit Scheme Difference Equations

The semi-implicit numerical solution scheme is based on replacing the system of differential equations with a system of finite-difference equations partially implicit in time. The terms evaluated implicitly are identified as the scheme is developed. In all cases, the implicit terms are formulated to be linear in the dependent variables at new time. This results in a linear time-advancement matrix that is solved by direct inversion using a sparse matrix routine.<sup>3.1-10</sup> An additional feature of the scheme is that implicitness is selected such that the field equations can be reduced to a single difference equation per fluid control volume or mesh cell, which is in terms of the hydrodynamic pressure. Thus, only an  $N \times N$  system of equations must be solved simultaneously at each time step. ( $N$  is the total number of control volumes used to simulate the fluid system.)

It is well known<sup>3.1-4,3.1-11</sup> that the system of differential equations constitutes an ill-posed, initial-value problem. This fact is of little concern physically, since the addition of any second-order differential effect (regardless of how small), such as viscosity or surface tension, results in a well-posed problem.<sup>3.1-12</sup> However, the ill-posedness is of some concern numerically, since it is necessary that the numerical problem be well-posed. The approximations inherent in any numerical scheme modify the solution somewhat (truncation error); these effects can be either stabilizing or destabilizing. The resulting numerical scheme must be stable for mesh sizes of practical interest.

A well-posed and stable numerical algorithm results from employing several stabilizing techniques. These include the selective implicit evaluation of spatial gradient terms at the new time, donor formulations for the mass and energy flux terms, and use of a donor-like formulation for the momentum flux terms. Donor-like formulations for these flux terms are used because of the well-known instability of an explicit centered finite difference scheme. The term *donor-like* is used because the momentum flux formulation consists of a centered formulation for the spatial velocity gradient plus a numerical viscosity term. These two terms are similar to the form obtained when the momentum flux terms are donated with the unexpanded form of the momentum equations. The well-posedness of the final numerical scheme (as well as its accuracy) has been demonstrated for practical cell sizes by extensive numerical testing (see Volume VI).

The difference equations are based on the concept of a control volume (or mesh cell) in which mass and energy are conserved by equating accumulation to rate of influx through the cell boundaries. This model results in defining mass and energy volume average properties and requiring knowledge of velocities at the volume boundaries. The velocities at boundaries are most conveniently defined through use of momentum control volumes (cells) centered on the mass and energy cell boundaries. This approach results in a numerical scheme having a staggered spatial mesh. The scalar properties (pressure, energies, and void fraction) of the flow are defined at cell centers, and vector quantities (velocities) are defined on

the cell boundaries. The resulting one-dimensional spatial noding is illustrated in **Figure 3.1-3**. The term cell means an increment in the spatial variable,  $x$ , corresponding to the mass and energy control volume.

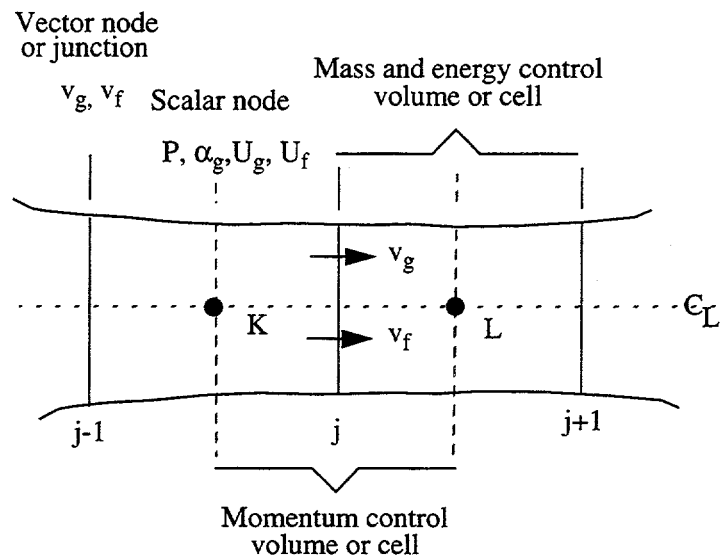


**Figure 3.1-3** Difference equation nodalization schematic.

The difference equations for each cell are obtained by integrating the mass and energy equations [Equations (3.1-54), (3.1-56), (3.1-57), (3.1-61), and (3.1-63)] with respect to the spatial variable,  $x$ , from the junction at  $x_j$  to  $x_{j+1}$ . The momentum equations [Equations (3.1-58) and (3.1-59)] are integrated with respect to the spatial variable from cell center to adjoining cell center ( $x_K$  to  $x_L$ , **Figure 3.1-3**). The equations are listed for the case of a pipe with no branching.

When the mass and energy equations [Equations (3.1-54), (3.1-56), (3.1-57), (3.1-61), and (3.1-63)] are integrated with respect to the spatial variable from junction  $j$  to  $j+1$ , differential equations in terms of cell-average properties and cell boundary fluxes are obtained. The subscripts and superscripts indicate integration limits for the enclosed quantity. The quantities not enclosed in parentheses are volume averages.

The sum density Equation (3.1-54) becomes

$$V \left[ \alpha_g \frac{\partial \rho_g}{\partial t} + \alpha_f \frac{\partial \rho_f}{\partial t} + (\rho_g - \rho_f) \frac{\partial \alpha_g}{\partial t} \right] + (\alpha_g \rho_g v_g A)_{x_j}^{x_{j+1}} + (\alpha_f \rho_f v_f A)_{x_j}^{x_{j+1}} = 0 \quad (3.1-80)$$

The difference density Equation (3.1-56) becomes

$$\begin{aligned}
 & V \left[ \alpha_g \frac{\partial \rho_g}{\partial t} - \alpha_f \frac{\partial \rho_f}{\partial t} + (\rho_g + \rho_f) \frac{\partial \alpha_g}{\partial t} \right] + (\alpha_g \rho_g v_g A)_{x_j}^{x_{j+1}} - (\alpha_f \rho_f v_f A)_{x_j}^{x_{j+1}} \\
 & = V \left\{ - \frac{2 \left[ \frac{P_s}{P} H_{ig} (T^s - T_g) + H_{if} (T^s - T_f) \right]}{h_g^* - h_f^*} + 2 \Gamma_w \right\} . \tag{3.1-81}
 \end{aligned}$$

The total noncondensable density Equation (3.1-57) becomes

$$V \left[ \rho_g X_n \frac{\partial \alpha_g}{\partial t} + \alpha_g X_n \frac{\partial \rho_g}{\partial t} + \alpha_g \rho_g \frac{\partial X_n}{\partial t} \right] + (\alpha_g \rho_g X_n v_g A)_{x_j}^{x_{j+1}} = 0 . \tag{3.1-82}$$

The vapor energy Equation (3.1-61) becomes

$$\begin{aligned}
 & V \left[ (\rho_g U_g + P) \frac{\partial \alpha_g}{\partial t} + \alpha_g U_g \frac{\partial \rho_g}{\partial t} + \alpha_g \rho_g \frac{\partial U_g}{\partial t} \right] + (\alpha_g \rho_g U_g v_g A)_{x_j}^{x_{j+1}} + P (\alpha_g v_g A)_{x_j}^{x_{j+1}} \\
 & = V \left\{ - \left( \frac{h_f^*}{h_g^* - h_f^*} \right) \frac{P_s}{P} H_{ig} (T^s - T_g) - \left( \frac{h_g^*}{h_g^* - h_f^*} \right) H_{if} (T^s - T_f) - \left( \frac{P - P_s}{P} \right) H_{gf} (T_g - T_f) \right. \\
 & \quad \left. + \left[ \left( \frac{1 + \epsilon}{2} \right) h_g' + \left( \frac{1 - \epsilon}{2} \right) h_f' \right] \Gamma_w + Q_{wg} + DISS_g \right\} . \tag{3.1-83}
 \end{aligned}$$

The liquid energy Equation (3.1-63) becomes

$$\begin{aligned}
 & V \left[ - (\rho_f U_f + P) \frac{\partial \alpha_g}{\partial t} + \alpha_f U_f \frac{\partial \rho_f}{\partial t} + \alpha_f \rho_f \frac{\partial U_f}{\partial t} \right] + (\alpha_f \rho_f U_f v_f A)_{x_j}^{x_{j+1}} + P (\alpha_f v_f A)_{x_j}^{x_{j+1}} \\
 & = V \left\{ \left( \frac{h_f^*}{h_g^* - h_f^*} \right) \frac{P_s}{P} H_{ig} (T^s - T_g) + \left( \frac{h_g^*}{h_g^* - h_f^*} \right) H_{if} (T^s - T_f) + \left( \frac{P - P_s}{P} \right) H_{gf} (T_g - T_f) \right. \\
 & \quad \left. - \left[ \left( \frac{1 + \epsilon}{2} \right) h_g' + \left( \frac{1 - \epsilon}{2} \right) h_f' \right] \Gamma_w + Q_{wf} + DISS_f \right\} . \tag{3.1-84}
 \end{aligned}$$

The sum and difference momentum equations [Equations (3.1-58) and (3.1-59)] are integrated from cell center to cell center to obtain

$$\begin{aligned}
 & \frac{V}{A} \left[ (\alpha_g \rho_g) \frac{\partial v_g}{\partial t} + (\alpha_f \rho_f) \frac{\partial v_f}{\partial t} \right] + \frac{1}{2} \alpha_g \rho_g (v_g^2)_{x_K}^{x_L} + \frac{1}{2} \alpha_f \rho_f (v_f^2)_{x_K}^{x_L} \\
 & = - (P)_{x_K}^{x_L} + \rho_m B_x (x_L - x_K) - (\alpha_g \rho_g F W G v_g + \alpha_f \rho_f F W F v_f) (x_L - x_K) \\
 & \quad - \Gamma_g (v_g - v_f) (x_L - x_K) \tag{3.1-85}
 \end{aligned}$$

and

$$\begin{aligned}
 \left(\frac{V}{A}\right) \left[ 1 + C \rho_m^2 / (\rho_g \rho_f) \right] \left( \frac{\partial v_g}{\partial t} - \frac{\partial v_f}{\partial t} \right) + \frac{1}{2} (v_g^2)_{x_K}^{x_L} - \frac{1}{2} (v_f^2)_{x_K}^{x_L} \\
 = - \left( \frac{1}{\rho_g} - \frac{1}{\rho_f} \right) (P)_{x_K}^{x_L} - (FWG v_g - FWF v_f) (x_L - x_K) \\
 + \{ \Gamma_g [\rho_m v_I - (\alpha_f \rho_f v_g + \alpha_g \rho_g v_f)] / (\alpha_g \rho_g \alpha_f \rho_f) \} (x_L - x_K) \\
 - \rho_m FI (v_g - v_f) (x_L - x_K) . \quad (3.1-86)
 \end{aligned}$$

Here, the common area term, A, has been factored from most terms. The quantities shown in brackets with limits are evaluated at the indicated limits, while the coefficients are averaged over the cell or integration interval. The indicated derivatives are now derivatives of cell average quantities. Since the integration interval is centered on the junction, the coefficient averages are approximated by the junction values. In all cases, the correlation coefficients for averaged products are taken as unity, so averaged products are replaced directly with products of averages.

Several general guidelines were followed in developing numerical approximations for Equations (3.1-80) through (3.1-86). These guidelines are summarized below.

- Mass and energy inventories are very important quantities in water reactor safety analysis. The numerical scheme should be consistent and conservative in these quantities. (A greater degree of approximation for momentum effects is considered acceptable.) Both mass and energy are convected from the same cell, and each is evaluated at the same time level; that is, mass density is evaluated at old time level, so energy density is also evaluated at old time.
- To achieve fast execution speed, implicit evaluation is used only for those terms responsible for the sonic wave propagation time step limit and those phenomena known to have small time constants. Thus, implicit evaluation is used for the velocity in the mass and energy transport terms, the pressure gradient in the momentum equations, and the interface mass and momentum exchange terms.
- To further increase computing speed, time-level evaluations are selected so the resulting implicit terms are linear in the new time variables. Where it is necessary to retain nonlinearities, Taylor series expansions about old time values are used to obtain a formulation linear in the new time variables. (Higher-order terms are neglected.) Linearity results in high computing speed by eliminating the need to iteratively solve systems of nonlinear equations.
- To allow easy degeneration to homogeneous, or single-phase, formulations, the momentum equations are used as a sum and a difference equation. The particular difference equation used is obtained by first dividing each of the phasic momentum equations by  $\alpha_g \rho_g$  and  $\alpha_f \rho_f$ , for the vapor and liquid phase equations, respectively, and then subtracting.

Using the above guidelines, the finite-difference equations for the mass and energy balances, corresponding to Equations (3.1-80) through (3.1-84), are listed below. Some of the terms are intermediate time variables, which are written with a tilde (~). The reason for their use is explained in Section 3.1.5.

The sum continuity equation is

$$V_L [\alpha_{g,L}^n (\tilde{\rho}_{g,L}^{n+1} - \rho_{g,L}^n) + \alpha_{f,L}^n (\tilde{\rho}_{f,L}^{n+1} - \rho_{f,L}^n) + (\rho_{g,L}^n - \rho_{f,L}^n) (\tilde{\alpha}_{g,L}^{n+1} - \alpha_{g,L}^n)] + \left( \dot{\alpha}_{g,j+1}^n \tilde{\rho}_{g,j+1}^n V_{g,j+1}^{n+1} A_{j+1} - \dot{\alpha}_{g,j}^n \tilde{\rho}_{g,j}^n V_{g,j}^{n+1} A_j \right) \Delta t + \left( \dot{\alpha}_{f,j+1}^n \tilde{\rho}_{f,j+1}^n V_{f,j+1}^{n+1} A_{j+1} - \dot{\alpha}_{f,j}^n \tilde{\rho}_{f,j}^n V_{f,j}^{n+1} A_j \right) \Delta t = 0 . \quad (3.1-87)$$

The difference continuity equation is

$$V_L [\alpha_{g,L}^n (\tilde{\rho}_{g,L}^{n+1} - \rho_{g,L}^n) - \alpha_{f,L}^n (\tilde{\rho}_{f,L}^{n+1} - \rho_{f,L}^n) + (\rho_{g,L}^n + \rho_{f,L}^n) (\tilde{\alpha}_{g,L}^{n+1} - \alpha_{g,L}^n)] + \left( \dot{\alpha}_{g,j+1}^n \tilde{\rho}_{g,j+1}^n V_{g,j+1}^{n+1} A_{j+1} - \dot{\alpha}_{g,j}^n \tilde{\rho}_{g,j}^n V_{g,j}^{n+1} A_j \right) \Delta t - \left( \dot{\alpha}_{f,j+1}^n \tilde{\rho}_{f,j+1}^n V_{f,j+1}^{n+1} A_{j+1} - \dot{\alpha}_{f,j}^n \tilde{\rho}_{f,j}^n V_{f,j}^{n+1} A_j \right) \Delta t = - \left( \frac{2}{h_g^* - h_f^*} \right)_L^n V_L \Delta t \left[ \frac{P_{s,L}^n}{P_L^n} H_{ig,L}^n \left( \tilde{T}_L^{s,n+1} - \tilde{T}_{g,L}^{n+1} \right) + H_{if,L}^n \left( \tilde{T}_L^{s,n+1} - \tilde{T}_{f,L}^{n+1} \right) \right] + 2 V_L \Delta t \Gamma_{w,L}^n . \quad (3.1-88)$$

The total noncondensable continuity equation is

$$V_L [\rho_{g,L}^n X_{n,L}^n (\tilde{\alpha}_{g,L}^{n+1} - \alpha_{g,L}^n) + \alpha_{g,L}^n X_{n,L}^n (\tilde{\rho}_{g,L}^{n+1} - \rho_{g,L}^n) + \alpha_{g,L}^n \rho_{g,L}^n (\tilde{X}_{n,L}^{n+1} - X_{n,L}^n)] + \left( \dot{\alpha}_{g,j+1}^n \tilde{\rho}_{g,j+1}^n X_{n,j+1}^{n+1} V_{g,j+1}^{n+1} A_{j+1} - \dot{\alpha}_{g,j}^n \tilde{\rho}_{g,j}^n X_{n,j}^{n+1} V_{g,j}^{n+1} A_j \right) \Delta t = 0 . \quad (3.1-89)$$

The vapor thermal energy equation is

$$V_L [(\rho_{g,L}^n U_{g,L}^n + P_L^n) (\tilde{\alpha}_{g,L}^{n+1} - \alpha_{g,L}^n) + \alpha_{g,L}^n U_{g,L}^n (\tilde{\rho}_{g,L}^{n+1} - \rho_{g,L}^n) + \alpha_{g,L}^n \rho_{g,L}^n (\tilde{U}_{g,L}^{n+1} - U_{g,L}^n)] + \left[ \dot{\alpha}_{g,j+1}^n \left( \tilde{\rho}_{g,j+1}^n U_{g,j+1}^n + P_L^n \right) V_{g,j+1}^{n+1} A_{j+1} - \dot{\alpha}_{g,j}^n \left( \tilde{\rho}_{g,j}^n U_{g,j}^n + P_L^n \right) V_{g,j}^{n+1} A_j \right] \Delta t = \left\{ - \left( \frac{h_f^*}{h_g^* - h_f^*} \right)_L^n \frac{P_{s,L}^n}{P_L^n} H_{ig,L}^n \left( \tilde{T}_L^{s,n+1} - \tilde{T}_{g,L}^{n+1} \right) - \left( \frac{h_g^*}{h_g^* - h_f^*} \right)_L^n H_{if,L}^n \left( \tilde{T}_L^{s,n+1} - \tilde{T}_{f,L}^{n+1} \right) \right\} \Delta t - \left( \frac{P_L^n - P_{s,L}^n}{P_L^n} \right) H_{gf,L}^n \left( \tilde{T}_{g,L}^{n+1} - \tilde{T}_{f,L}^{n+1} \right) + \left[ \left( \frac{1+\epsilon}{2} \right) h_{g,L}^{n+1} + \left( \frac{1-\epsilon}{2} \right) h_{f,L}^{n+1} \right] \Gamma_{w,L}^n + Q_{wg,L}^n + DISS_{g,L}^n \} V_L \Delta t . \quad (3.1-90)$$

The liquid thermal energy equation is

$$\begin{aligned}
& V_L [ -(\rho_{f,L}^n U_{f,L}^n + P_L^n) (\tilde{\alpha}_{g,L}^{n+1} - \alpha_{g,L}^n) + \alpha_{f,L}^n U_{f,L}^n (\tilde{\rho}_{f,L}^{n+1} - \rho_{f,L}^n) \\
& + \alpha_{f,L}^n \rho_{f,L}^n \left( \tilde{U}_{f,L}^{n+1} - U_{f,L}^n \right) ] + [ \dot{\alpha}_{f,j+1}^n \left( \dot{\rho}_{f,j+1}^n U_{f,j+1}^n + P_L^n \right) V_{f,j+1}^{n+1} A_{j+1} \\
& - \dot{\alpha}_{f,j}^n \left( \dot{\rho}_{f,j}^n U_{f,j}^n + P_L^n \right) V_{f,j}^{n+1} A_j ] \Delta t = \left\{ \left( \frac{h_f^*}{h_g^* - h_f^*} \right)_L^n \frac{P_{s,L}^n}{P_L^n} H_{ig,L}^n \left( \tilde{T}_{L}^{s,n+1} - \tilde{T}_{g,L}^{n+1} \right) \right. \\
& \left. + \left( \frac{h_g^*}{h_g^* - h_f^*} \right)_L^n H_{if,L}^n \left( \tilde{T}_L^{s,n+1} - \tilde{T}_{f,L}^{n+1} \right) + \left( \frac{P_L^n - P_{s,L}^n}{P_L^n} \right) H_{gf,L}^n \left( \tilde{T}_{g,L}^{n+1} - \tilde{T}_{f,L}^{n+1} \right) \right. \\
& \left. - \left[ \left( \frac{1+\varepsilon}{2} \right) h_{g,L}^{',n} + \left( \frac{1-\varepsilon}{2} \right) h_{f,L}^{',n} \right] \Gamma_{w,L}^n + Q_{wf,L}^n + DISS_{f,L}^n \right\} V_L \Delta t
\end{aligned} \tag{3.1-91}$$

The quantities having a dot overscore are donor quantities based on the junction velocities,  $v_{g,j}$  and  $v_{f,j}$ . The donor quantities are volume average scalar quantities defined analytically as

$$\dot{\phi}_j = \frac{1}{2} (\phi_K + \phi_L) + \frac{1}{2} \frac{|v_j|}{v_j} (\phi_K - \phi_L) \tag{3.1-92}$$

where  $\dot{\phi}_j$  is any of the donor properties, and  $v_j$  is the appropriate velocity (that is, vapor or liquid). This equation holds for the case  $v_j \neq 0$ . For the case  $v_j = 0$  and  $P_K > P_L$ ,

$$\dot{\phi}_j = \phi_K \tag{3.1-93}$$

For the case  $v_j = 0$  and  $P_K < P_L$ ,

$$\dot{\phi}_j = \phi_L \tag{3.1-94}$$

For the degenerate case of  $v_j = 0$  and  $P_K = P_L$ , a density-weighted average formulation is used,

$$\dot{\phi}_j = \frac{\rho_K \phi_K + \rho_L \phi_L}{\rho_K + \rho_L} \tag{3.1-95}$$

for all donor properties except for densities (which use a simple average). In this equation,  $\rho_K$  and  $\rho_L$  are the appropriate densities (e.g., vapor or liquid). Where donor values are not used at junctions, linear interpolations between neighboring cell values are used.

The provisional advanced time phasic densities used in Equations (3.1-87) through (3.1-91) are obtained by linearizing the phasic state relations about the old time values (see Section 3.2).

$$\tilde{\rho}_{g,L}^{n+1} = \rho_{g,L}^n + \left( \frac{\partial \rho_g}{\partial P} \right)_L^n (P_L^{n+1} - P_L^n) + \left( \frac{\partial \rho_g}{\partial X_n} \right)_L^n (\tilde{X}_{n,L}^{n+1} - X_{n,L}^n) + \left( \frac{\partial \rho_g}{\partial U_g} \right)_L^n (\tilde{U}_{g,L}^{n+1} - U_{g,L}^n) \quad (3.1-96)$$

$$\tilde{\rho}_{f,L}^{n+1} = \rho_{f,L}^n + \left( \frac{\partial \rho_f}{\partial P} \right)_L^n (P_L^{n+1} - P_L^n) + \left( \frac{\partial \rho_f}{\partial U_f} \right)_L^n (\tilde{U}_{f,L}^{n+1} - U_{f,L}^n) \quad (3.1-97)$$

The method of obtaining the state derivatives used in Equations (3.1-96) and (3.1-97) is also indicated in Section 3.2.

Provisional advanced time interface heat transfer rates can be written using the finite difference form of Equations (3.1-48) and (3.1-26) after evaluating the extrapolated temperature  $\tilde{T}^{n+1}$ .

$$\tilde{Q}_{ig,L}^{n+1} = \frac{P_{s,L}^n}{P_L^n} H_{ig,L}^n \left( \tilde{T}_L^{s,n+1} - \tilde{T}_{g,L}^{n+1} \right) - \left( \frac{1-\varepsilon}{2} \right) \Gamma_{w,L}^n (h_{g,L}^{',n} - h_{f,L}^{',n}) \quad (3.1-98)$$

$$\tilde{Q}_{if,L}^{n+1} = H_{if,L}^n \left( \tilde{T}_L^{s,n+1} - \tilde{T}_{f,L}^{n+1} \right) - \left( \frac{1+\varepsilon}{2} \right) \Gamma_{w,L}^n (h_{g,L}^{',n} - h_{f,L}^{',n}) \quad (3.1-99)$$

The provisional advanced time temperatures are obtained by linearizing the temperature relations about the old time values (see Section 3.2):

$$\tilde{T}_L^{s,n+1} = T_L^{s,n} + \left( \frac{\partial T^s}{\partial P} \right)_L^n (P_L^{n+1} - P_L^n) + \left( \frac{\partial T^s}{\partial X_n} \right)_L^n (\tilde{X}_{n,L}^{n+1} - X_{n,L}^n) + \left( \frac{\partial T^s}{\partial U_g} \right)_L^n (\tilde{U}_{g,L}^{n+1} - U_{g,L}^n) \quad (3.1-100)$$

$$\tilde{T}_{g,L}^{n+1} = T_{g,L}^n + \left( \frac{\partial T_g}{\partial P} \right)_L^n (P_L^{n+1} - P_L^n) + \left( \frac{\partial T_g}{\partial X_n} \right)_L^n (\tilde{X}_{n,L}^{n+1} - X_{n,L}^n) + \left( \frac{\partial T_g}{\partial U_g} \right)_L^n (\tilde{U}_{g,L}^{n+1} - U_{g,L}^n) \quad (3.1-101)$$

$$\tilde{T}_{f,L}^{n+1} = T_{f,L}^n + \left( \frac{\partial T_f}{\partial P} \right)_L^n (P_L^{n+1} - P_L^n) + \left( \frac{\partial T_f}{\partial U_f} \right)_L^n (\tilde{U}_{f,L}^{n+1} - U_{f,L}^n) \quad (3.1-102)$$

The method used in Equations (3.1-100) through (3.1-102) to obtain the temperature derivatives is also indicated in Section 3.2.

The previously stated guidelines are used to obtain the finite-difference form for the phasic momentum equations. In this case, volume-average properties for the momentum control volume are taken as junction properties (that is, linear interpolations between mass and energy control volume centers). The momentum flux terms are approximated using a donor-like formulation that results in a centered velocity gradient term and a viscous-like term (artificial viscosity). The difference equations for the sum and difference momentum equations, Equations (3.1-85) and (3.1-86), are

$$\begin{aligned}
& (\alpha_g \rho_g)_j^n (v_g^{n+1} - v_g^n)_j \Delta x_j + (\alpha_f \rho_f)_j^n (v_f^{n+1} - v_f^n)_j \Delta x_j \\
& + \frac{1}{2} (\dot{\alpha}_g \dot{\rho}_g)_j^n \left[ (v_g^2)_L^n - (v_g^2)_K^n \right] \Delta t + \frac{1}{2} (\dot{\alpha}_f \dot{\rho}_f)_j^n \left[ (v_f^2)_L^n - (v_f^2)_K^n \right] \Delta t \\
& - \frac{1}{2} \left[ (\dot{\alpha}_g \dot{\rho}_g)_j^n \text{VISG}_j^n + (\dot{\alpha}_f \dot{\rho}_f)_j^n \text{VISF}_j^n \right] \Delta t \\
& = - (P_L - P_K)^{n+1} \Delta t + \left[ (\rho_m)_j^n B_x - (\alpha_g \rho_g)_j^n \text{FWG}_j^n (v_g)_j^{n+1} \right. \\
& \quad \left. - (\alpha_f \rho_f)_j^n \text{FWF}_j^n (v_f)_j^{n+1} - (\Gamma_g)_j^n (v_g - v_f)_j^{n+1} \right] \Delta x_j \Delta t \\
& - \left[ (\dot{\alpha}_g \dot{\rho}_g)_j^n \text{HLOSSG}_j^n v_{g,j}^{n+1} + (\dot{\alpha}_f \dot{\rho}_f)_j^n \text{HLOSSF}_j^n v_{f,j}^{n+1} \right] \Delta t
\end{aligned} \tag{3.1-103}$$

and

$$\begin{aligned}
& [1 + C \rho_m^2 / (\rho_g \rho_f)]_j^n \left[ (v_g^{n+1} - v_g^n) - (v_f^{n+1} - v_f^n) \right]_j \Delta x_j \\
& + \frac{1}{2} \left[ (\dot{\alpha}_g \dot{\rho}_g) / (\alpha_g \rho_g) \right]_j^n \left[ (v_g^2)_L^n - (v_g^2)_K^n \right] \Delta t - \frac{1}{2} \left[ (\dot{\alpha}_g \dot{\rho}_g) / (\alpha_g \rho_g) \right]_j^n \text{VISG}_j^n \Delta t \\
& - \frac{1}{2} \left[ (\dot{\alpha}_f \dot{\rho}_f) / (\alpha_f \rho_f) \right]_j^n \left[ (v_f^2)_L^n - (v_f^2)_K^n \right] \Delta t + \frac{1}{2} \left[ (\dot{\alpha}_f \dot{\rho}_f) / (\alpha_f \rho_f) \right]_j^n \text{VISF}_j^n \Delta t \\
& = - \left[ (\rho_f - \rho_g) / (\rho_g \rho_f) \right]_j^n (P_L - P_K)^{n+1} \Delta t \\
& - \left\{ \text{FWG}_j^n (v_g)_j^{n+1} - \text{FWF}_j^n (v_f)_j^{n+1} \right. \\
& \quad \left. - [\Gamma_g^n (\rho_m v_L^{n+1} - \alpha_f^n \rho_f v_g^{n+1} - \alpha_g^n \rho_g v_f^{n+1}) / (\alpha_g \rho_g \alpha_f \rho_f)]_j^n \right. \\
& \quad \left. + (\rho_m \text{FI})_j^n (v_g^{n+1} - v_f^{n+1})_j \right\} \Delta x_j \Delta t - \left\{ [\dot{\alpha}_g \dot{\rho}_g / \alpha_g \rho_g]_j^n \text{HLOSSG}_j^n v_{g,j}^{n+1} \right. \\
& \quad \left. - [\dot{\alpha}_f \dot{\rho}_f / (\alpha_f \rho_f)]_j^n \text{HLOSSF}_j^n v_{f,j}^{n+1} \right\} \Delta t
\end{aligned} \tag{3.1-104}$$

where the so-called viscous terms are defined as

$$\text{VISG}_j^n = \frac{1}{2} \left\{ \left| v_{g,L}^n \right| \left[ (v_g^n)_{j+1} (A_{j+1}/A_j) - (v_g^n)_j \right] - \left| v_{g,K}^n \right| \left[ (v_g^n)_j - (v_g^n)_{j-1} (A_{j-1}/A_j) \right] \right\} \tag{3.1-105}$$

and

$$\text{VISF}_j^n = \frac{1}{2} \left\{ \left| v_{f,L}^n \right| \left[ (v_f^n)_{j+1} (A_{j+1}/A_j) - (v_f^n)_j \right] - \left| v_{f,K}^n \right| \left[ (v_f^n)_j - (v_f^n)_{j-1} (A_{j-1}/A_j) \right] \right\} \tag{3.1-106}$$

In momentum Equations (3.1-103) and (3.1-104), the scalar or thermodynamic variables needed at the junctions are either linear interpolations between the neighboring cell values or donated quantities.

Terms that are shown multiplied by  $\Delta x_j$  are interpolated between neighboring cell values based on the length of each half cell. The  $HLOSSG_j$  and  $HLOSSF_j$  terms contain both code-calculated abrupt area change loss terms (Section 3.4.3) and user-specified loss terms (Section 3.4.4). For the user-specified loss,  $HLOSSG_j^n = \frac{1}{2}K|v_{g,j}^n|$  and  $HLOSSF_j^n = \frac{1}{2}K|v_{f,j}^n|$ , where  $K$  is either the forward or reverse inputted user loss, depending on the phasic velocity direction.

Using the same averaging techniques, the nonexpanded form of the mass and energy equations [Equations (3.1-2), (3.1-3), (3.1-39), (3.1-41), (3.1-64), and (3.1-65)] are next presented in their final finite difference form.

The nonexpanded vapor density Equation (3.1-2) becomes

$$V_L \left[ (\alpha_g \rho_g)_L^{n+1} - (\alpha_g \rho_g)_L^n \right] + \left( \dot{\alpha}_{g,j+1}^n \dot{\rho}_{g,j+1}^n v_{g,j+1}^{n+1} A_{j+1} - \dot{\alpha}_{g,j}^n \dot{\rho}_{g,j}^n v_{g,j}^{n+1} A_j \right) \Delta t = \tilde{\Gamma}_{g,L}^{n+1} V_L \Delta t . \quad (3.1-107)$$

The provisional advancement time variable,  $\tilde{\Gamma}_{g,L}^{n+1}$ , is obtained using the finite difference form of Equation (3.1-50) and is written

$$\tilde{\Gamma}_{g,L}^{n+1} = - \frac{\frac{P_{s,L}^n}{P_L^n} H_{ig,L}^n \left( \tilde{T}_L^{s,n+1} - \tilde{T}_{g,L}^{n+1} \right) + H_{if,L}^n \left( \tilde{T}_L^{s,n+1} - \tilde{T}_{f,L}^{n+1} \right)}{h_{g,L}^{*,n} - h_{f,L}^{*,n}} + \Gamma_{w,L}^n . \quad (3.1-108)$$

The nonexpanded liquid density Equation (3.1-3) becomes

$$V_L \left[ (\alpha_f \rho_f)_L^{n+1} - (\alpha_f \rho_f)_L^n \right] + \left( \dot{\alpha}_{f,j+1}^n \dot{\rho}_{f,j+1}^n v_{f,j+1}^{n+1} A_{j+1} - \dot{\alpha}_{f,j}^n \dot{\rho}_{f,j}^n v_{f,j}^{n+1} A_j \right) \Delta t = -\tilde{\Gamma}_{g,L}^{n+1} V_L \Delta t . \quad (3.1-109)$$

The nonexpanded total noncondensable density Equation (3.1-39) becomes

$$V_L \left[ (\alpha_g \rho_g X_n)_L^{n+1} - (\alpha_g \rho_g X_n)_L^n \right] + \left( \dot{\alpha}_{g,j+1}^n \dot{\rho}_{g,j+1}^n \dot{X}_{n,j+1}^n v_{g,j+1}^{n+1} A_{j+1} - \dot{\alpha}_{g,j}^n \dot{\rho}_{g,j}^n \dot{X}_{n,j}^n v_{g,j}^{n+1} A_j \right) \Delta t . \quad (3.1-110)$$

The nonexpanded density equation for the  $i$ -th noncondensable species, Equation (3.1-41) becomes

$$V_L \left[ (\alpha_g \rho_g X_n X_{ni})_L^{n+1} - (\alpha_g \rho_g X_n X_{ni})_L^n \right] + \left( \dot{\alpha}_{g,j+1}^n \dot{\rho}_{g,j+1}^n \dot{X}_{n,j+1}^n \dot{X}_{ni,j+1}^{n+1} v_{g,j+1}^{n+1} A_{j+1} - \dot{\alpha}_{g,j}^n \dot{\rho}_{g,j}^n \dot{X}_{n,j}^n \dot{X}_{ni,j}^{n+1} v_{g,j}^{n+1} A_j \right) \Delta t = 0 . \quad (3.1-111)$$

The nonexpanded vapor energy Equation (3.1-64) becomes

$$\begin{aligned}
& V_L [ (\alpha_g \rho_g U_g)_L^{n+1} - (\alpha_g \rho_g U_g)_L^n ] + [ \dot{\alpha}_{g,j+1}^n ( \dot{\rho}_{g,j+1}^n U_{g,j+1}^n + P_L^n ) V_{g,j+1}^{n+1} A_{j+1} \\
& - \dot{\alpha}_{g,j}^n ( \dot{\rho}_{g,j}^n U_{g,j}^n + P_L^n ) V_{g,j}^{n+1} A_j ] \Delta t = - V_L P_L^n ( \tilde{\alpha}_{g,L}^{n+1} - \alpha_{g,L}^n ) \\
& + \left\{ - \left( \frac{h_f^*}{h_g^* - h_f^*} \right)_L^n \frac{P_{s,L}^n}{P_L^n} H_{ig,L}^n \left( \tilde{T}_L^{s,n+1} - \tilde{T}_{g,L}^{n+1} \right) - \left( \frac{h_g^*}{h_g^* - h_f^*} \right)_L^n H_{if,L}^n \left( \tilde{T}_L^{s,n+1} - \tilde{T}_{f,L}^{n+1} \right) \right\} \\
& - \left( \frac{P_L^n - P_{s,L}^n}{P_L^n} \right) H_{gf,L}^n \left( \tilde{T}_{g,L}^{n+1} - \tilde{T}_{f,L}^{n+1} \right) + \left[ \left( \frac{1+\varepsilon}{2} \right) h_{g,L}^{',n} + \left( \frac{1-\varepsilon}{2} \right) h_{f,L}^{',n} \right] \Gamma_{w,L}^n + Q_{wg,L}^n + DISS_{g,L}^n \} V_L \Delta t .
\end{aligned} \quad (3.1-112)$$

The variables  $\tilde{\alpha}_{g,L}^{n+1}$ ,  $\tilde{T}_L^{s,n+1}$ ,  $\tilde{T}_{g,L}^{n+1}$ , and  $\tilde{T}_{f,L}^{n+1}$  are written with a tilde (~) to indicate they are provisional advancement time variables. The nonexpanded liquid energy Equation (3.1-65) becomes

$$\begin{aligned}
& V_L [ (\alpha_f \rho_f U_f)_L^{n+1} - (\alpha_f \rho_f U_f)_L^n ] + [ \dot{\alpha}_{f,j+1}^n ( \dot{\rho}_{f,j+1}^n U_{f,j+1}^n + P_L^n ) V_{f,j+1}^{n+1} A_{j+1} \\
& - \dot{\alpha}_{f,j}^n ( \dot{\rho}_{f,j}^n U_{f,j}^n + P_L^n ) V_{f,j}^{n+1} A_j ] \Delta t = V_L P_L^n ( \tilde{\alpha}_{g,L}^{n+1} - \alpha_{g,L}^n ) \\
& + \{ \left( \frac{h_f^*}{h_g^* - h_f^*} \right)_L^n \frac{P_{s,L}^n}{P_L^n} H_{ig,L}^n \left( \tilde{T}_L^{s,n+1} - \tilde{T}_{g,L}^{n+1} \right) + \left( \frac{h_g^*}{h_g^* - h_f^*} \right)_L^n H_{if,L}^n \left( \tilde{T}_L^{s,n+1} - \tilde{T}_{f,L}^{n+1} \right) \} \\
& + \left( \frac{P_L^n - P_{s,L}^n}{P_L^n} \right) H_{gf,L}^n \left( \tilde{T}_{g,L}^{n+1} - \tilde{T}_{f,L}^{n+1} \right) - \left[ \left( \frac{1+\varepsilon}{2} \right) h_{g,L}^{',n} + \left( \frac{1-\varepsilon}{2} \right) h_{f,L}^{',n} \right] \Gamma_{w,L}^n + Q_{wf,L}^n + DISS_{f,L}^n \} V_L \Delta t .
\end{aligned} \quad (3.1-113)$$

### 3.1.5 Time Advancement for the Semi-Implicit Scheme

The solution scheme will be discussed with regard to the state of the fluid in a control volume for two successive time steps. There are four possible cases:

1. Two-phase to two-phase, where two-phase conditions exist at both old time (n) and new time (n+1).
2. One-phase to one-phase, where one-phase conditions (either pure gas or pure liquid) exist at both old time (n) and new time n+1.
3. Two-phase to one-phase (disappearance), where two-phase conditions exist at old time (n), and one-phase conditions exist at new time (n+1).
4. One-phase to two-phase (appearance), where one-phase conditions exist at old time (n), and two-phase conditions exist at new time n+1.

The solution scheme will first be presented for the two-phase to two-phase case, because it is the most general. Then, the solution scheme for the other three cases will be presented.

**3.1.5.1 Two-Phase To Two-Phase.** First, the density and temperature Equations (3.1-96), (3.1-97), (3.1-100), (3.1-101) and (3.1-102) are substituted into the five expanded density and energy difference Equations (3.1-87) through (3.1-91). The equations are then ordered so that the noncondensable density equation is first, the vapor energy equation is second, the liquid energy equation is third, the difference density equation is fourth, and the sum density equation is fifth. The five density and energy variables are expressed as differences, and the order is

$$(\tilde{X}_{n,L}^{n+1} - X_{n,L}^n), (\tilde{U}_{g,L}^{n+1} - U_{g,L}^n), (\tilde{U}_{f,L}^{n+1} - U_{f,L}^n), (\tilde{\alpha}_{g,L}^{n+1} - \alpha_{g,L}^n), \text{ and } (P_L^{n+1} - P_L^n) . \quad (3.1-114)$$

The tilde (~) is used for  $X_n$ ,  $U_g$ ,  $U_f$ , and  $\alpha_g$  to indicate that these are provisional new time variables and do not represent the final new time variables for the two-phase to two-phase case. The ordering of the variables and equations was selected so that a given equation is dominated by its corresponding variable (e.g., the vapor energy equation is second and the vapor energy variable  $U_g$  is also second). The noncondensable equation is placed first for ease of degeneration when a noncondensable component is not specified in the problem, and the pressure variable is placed last for numerical convenience in the pressure solution. The five equations are then each divided by the volume  $V_L$ . The system of equations has the following form, where the matrix  $\tilde{A}$  and the vectors  $\tilde{b}$ ,  $\tilde{g}^1$ ,  $\tilde{g}^2$ ,  $\tilde{f}^1$ ,  $\tilde{f}^2$  contain only old-time level variables (the subscript L and the superscript n has been dropped for the listing of the matrix and vectors):

$$\tilde{A}\tilde{x} = \tilde{b} + \tilde{g}^1 v_{g,j+1}^{n+1} + \tilde{g}^2 v_{g,j}^{n+1} + \tilde{f}^1 v_{f,j+1}^{n+1} + \tilde{f}^2 v_{f,j}^{n+1} \quad (3.1-115)$$

where

$$\tilde{A} = \begin{bmatrix} A_{11} & A_{12} & 0 & A_{14} & A_{15} \\ A_{21} & A_{22} & A_{23} & A_{24} & A_{25} \\ A_{31} & A_{32} & A_{33} & A_{34} & A_{35} \\ A_{41} & A_{42} & A_{43} & A_{44} & A_{45} \\ A_{51} & A_{52} & A_{53} & A_{54} & A_{55} \end{bmatrix} \quad \tilde{x} = \begin{bmatrix} \tilde{X}_{n,L}^{n+1} - X_{n,L}^n \\ \tilde{U}_{g,L}^{n+1} - U_{g,L}^n \\ \tilde{U}_{f,L}^{n+1} - U_{f,L}^n \\ \tilde{\alpha}_{g,L}^{n+1} - \alpha_{g,L}^n \\ P_L^{n+1} - P_L^n \end{bmatrix} \quad (3.1-116)$$

$$\tilde{b} = \begin{bmatrix} 0 \\ b_2 \\ b_3 \\ b_4 \\ 0 \end{bmatrix} \quad \tilde{g}^1 = \begin{bmatrix} g_1^1 \\ g_2^1 \\ 0 \\ g_4^1 \\ g_5^1 \end{bmatrix} \quad \tilde{g}^2 = \begin{bmatrix} g_1^2 \\ g_2^2 \\ 0 \\ g_4^2 \\ g_5^2 \end{bmatrix} \quad \tilde{f}^1 = \begin{bmatrix} 0 \\ 0 \\ f_3^1 \\ f_4^1 \\ f_5^1 \end{bmatrix} \quad \tilde{f}^2 = \begin{bmatrix} 0 \\ 0 \\ f_3^2 \\ f_4^2 \\ f_5^2 \end{bmatrix} \quad (3.1-117)$$

$$A_{11} = \alpha_g \left( X_n \frac{\partial \rho_g}{\partial X_n} + \rho_g \right) \quad (3.1-118)$$

$$A_{12} = \alpha_g X_n \frac{\partial \rho_g}{\partial U_g} \quad (3.1-119)$$

$$A_{14} = \rho_g X_n \quad (3.1-120)$$

$$A_{15} = \alpha_g X_n \frac{\partial \rho_g}{\partial P} \quad (3.1-121)$$

$$A_{21} = \alpha_g U_g \frac{\partial \rho_g}{\partial X_n} + \left( \frac{h_f^*}{h_g^* - h_f^*} \right) \Delta t \frac{P_s}{P} H_{ig} \left( \frac{\partial T^s}{\partial X_n} - \frac{\partial T_g}{\partial X_n} \right) + \left( \frac{h_g^*}{h_g^* - h_f^*} \right) \Delta t H_{if} \frac{\partial T^s}{\partial X_n} + \Delta t \frac{P - P_s}{P} H_{gf} \frac{\partial T_g}{\partial X_n} \quad (3.1-122)$$

$$A_{22} = \alpha_g \left( U_g \frac{\partial \rho_g}{\partial U_g} + \rho_g \right) + \left( \frac{h_f^*}{h_g^* - h_f^*} \right) \Delta t \frac{P_s}{P} H_{ig} \left( \frac{\partial T^s}{\partial U_g} - \frac{\partial T_g}{\partial U_g} \right) + \left( \frac{h_g^*}{h_g^* - h_f^*} \right) \Delta t H_{if} \frac{\partial T^s}{\partial U_g} + \Delta t \frac{P - P_s}{P} H_{gf} \frac{\partial T_g}{\partial U_g} \quad (3.1-123)$$

$$A_{23} = - \left( \frac{h_g^*}{h_g^* - h_f^*} \right) \Delta t H_{if} \frac{\partial T_f}{\partial U_f} - \Delta t \frac{P - P_s}{P} H_{gf} \frac{\partial T_f}{\partial U_f} \quad (3.1-124)$$

$$A_{24} = \rho_g U_g + P \quad (3.1-125)$$

$$A_{25} = \alpha_g U_g \frac{\partial \rho_g}{\partial P} + \left( \frac{h_f^*}{h_g^* - h_f^*} \right) \Delta t \frac{P_s}{P} H_{ig} \left( \frac{\partial T^s}{\partial P} - \frac{\partial T_g}{\partial P} \right) + \left( \frac{h_g^*}{h_g^* - h_f^*} \right) \Delta t H_{if} \left( \frac{\partial T^s}{\partial P} - \frac{\partial T_f}{\partial P} \right) + \Delta t \frac{P - P_s}{P} H_{gf} \left( \frac{\partial T_g}{\partial P} - \frac{\partial T_f}{\partial P} \right) \quad (3.1-126)$$

$$A_{31} = -\left(\frac{h_f^*}{h_g^* - h_f^*}\right) \Delta t \frac{P_s}{P} H_{ig} \left( \frac{\partial T^s}{\partial X_n} - \frac{\partial T_g}{\partial X_n} \right) - \left(\frac{h_g^*}{h_g^* - h_f^*}\right) \Delta t H_{if} \frac{\partial T^s}{\partial X_n} - \Delta t \frac{P - P_s}{P} H_{gf} \frac{\partial T_g}{\partial X_n} \quad (3.1-127)$$

$$A_{32} = -\left(\frac{h_f^*}{h_g^* - h_f^*}\right) \Delta t \frac{P_s}{P} H_{ig} \left( \frac{\partial T^s}{\partial U_g} - \frac{\partial T_g}{\partial U_g} \right) - \left(\frac{h_g^*}{h_g^* - h_f^*}\right) \Delta t H_{if} \frac{\partial T^s}{\partial U_g} - \Delta t \frac{P - P_s}{P} H_{gf} \frac{\partial T_g}{\partial U_g} \quad (3.1-128)$$

$$A_{33} = \alpha_f \left( U_f \frac{\partial \rho_f}{\partial U_f} + \rho_f \right) + \left(\frac{h_g^*}{h_g^* - h_f^*}\right) \Delta t H_{if} \frac{\partial T_f}{\partial U_f} + \Delta t \frac{P - P_s}{P} H_{gf} \frac{\partial T_f}{\partial U_f} \quad (3.1-129)$$

$$A_{34} = -\rho_f U_f - P \quad (3.1-130)$$

$$A_{35} = \alpha_f U_f \frac{\partial \rho_f}{\partial P} - \left(\frac{h_f^*}{h_g^* - h_f^*}\right) \Delta t \frac{P_s}{P} H_{ig} \left( \frac{\partial T^s}{\partial P} - \frac{\partial T_g}{\partial P} \right) - \left(\frac{h_g^*}{h_g^* - h_f^*}\right) \Delta t H_{if} \left( \frac{\partial T^s}{\partial P} - \frac{\partial T_f}{\partial P} \right) - \Delta t \frac{P - P_s}{P} H_{gf} \left[ \frac{\partial T_g}{\partial P} - \frac{\partial T_f}{\partial P} \right] \quad (3.1-131)$$

$$A_{41} = \alpha_g \frac{\partial \rho_g}{\partial X_n} + \left(\frac{2}{h_g^* - h_f^*}\right) \Delta t \frac{P_s}{P} H_{ig} \left( \frac{\partial T^s}{\partial X_n} - \frac{\partial T_g}{\partial X_n} \right) + \left(\frac{2}{h_g^* - h_f^*}\right) \Delta t H_{if} \frac{\partial T^s}{\partial X_n} \quad (3.1-132)$$

$$A_{42} = \alpha_g \frac{\partial \rho_g}{\partial U_g} + \left(\frac{2}{h_g^* - h_f^*}\right) \Delta t \frac{P_s}{P} H_{ig} \left( \frac{\partial T^s}{\partial U_g} - \frac{\partial T_g}{\partial U_g} \right) + \left(\frac{2}{h_g^* - h_f^*}\right) \Delta t H_{if} \frac{\partial T^s}{\partial U_g} \quad (3.1-133)$$

$$A_{43} = -\alpha_f \frac{\partial \rho_f}{\partial U_f} - \left(\frac{2}{h_g^* - h_f^*}\right) \Delta t H_{if} \frac{\partial T_f}{\partial U_f} \quad (3.1-134)$$

$$A_{44} = \rho_g + \rho_f \quad (3.1-135)$$

$$\begin{aligned}
 A_{45} &= \alpha_g \frac{\partial \rho_g}{\partial P} - \alpha_f \frac{\partial \rho_f}{\partial P} + \left( \frac{2}{h_g^* - h_f^*} \right) \Delta t \frac{P_s}{P} H_{ig} \left( \frac{\partial T^s}{\partial P} - \frac{\partial T_g}{\partial P} \right) \\
 &\quad + \left( \frac{2}{h_g^* - h_f^*} \right) \Delta t H_{if} \left( \frac{\partial T^s}{\partial P} - \frac{\partial T_f}{\partial P} \right) \tag{3.1-136}
 \end{aligned}$$

$$A_{51} = \alpha_g \frac{\partial \rho_g}{\partial X_n} \tag{3.1-137}$$

$$A_{52} = \alpha_g \frac{\partial \rho_g}{\partial U_g} \tag{3.1-138}$$

$$A_{53} = \alpha_f \frac{\partial \rho_f}{\partial U_f} \tag{3.1-139}$$

$$A_{54} = \rho_g - \rho_f \tag{3.1-140}$$

$$A_{55} = \alpha_g \frac{\partial \rho_g}{\partial P} + \alpha_f \frac{\partial \rho_f}{\partial P} \tag{3.1-141}$$

$$\begin{aligned}
 b_2 &= - \left( \frac{h_f^*}{h_g^* - h_f^*} \right) \Delta t \frac{P_s}{P} H_{ig} [T^s - T_g] - \left( \frac{h_g^*}{h_g^* - h_f^*} \right) \Delta t H_{if} (T^s - T_f) \\
 &\quad - \Delta t \frac{P - P_s}{P} H_{gf} (T_g - T_f) + \Delta t \Gamma_w \left[ \left( \frac{1 - \varepsilon}{2} \right) h_f' + \left( \frac{1 + \varepsilon}{2} \right) h_g' \right] + Q_{wg} \Delta t \\
 &\quad + DISS_g \Delta t \tag{3.1-142}
 \end{aligned}$$

$$\begin{aligned}
 b_3 &= \left( \frac{h_f^*}{h_g^* - h_f^*} \right) \Delta t \frac{P_s}{P} H_{ig} (T^s - T_g) + \left( \frac{h_g^*}{h_g^* - h_f^*} \right) \Delta t H_{if} (T^s - T_f) \\
 &\quad + \Delta t \frac{P - P_s}{P} H_{gf} [T_g - T_f] - \Delta t \Gamma_w \left[ \left( \frac{1 - \varepsilon}{2} \right) h_f' + \left( \frac{1 + \varepsilon}{2} \right) h_g' \right] + Q_{wf} \Delta t \\
 &\quad + DISS_f \Delta t \tag{3.1-143}
 \end{aligned}$$

$$b_4 = - \left( \frac{2}{h_g^* - h_f^*} \right) \Delta t \frac{P_s}{P} H_{ig} (T^s - T_g) - \left( \frac{2}{h_g^* - h_f^*} \right) \Delta t H_{if} (T^s - T_f) + 2 \Gamma_w \Delta t \tag{3.1-144}$$

$$g_1^1 = -(\dot{\alpha}_g \dot{\rho}_g \dot{X}_n A)_{j+1} \Delta t / V \quad (3.1-145)$$

$$g_2^1 = -[\dot{\alpha}_{g,j+1} (\dot{\rho}_{g,j+1} \dot{U}_{g,j+1} + P_L) A_{j+1}] \Delta t / V \quad (3.1-146)$$

$$g_4^1 = -(\dot{\alpha}_g \dot{\rho}_g A)_{j+1} \Delta t / V \quad (3.1-147)$$

$$g_5^1 = -(\dot{\alpha}_g \dot{\rho}_g A)_{j+1} \Delta t / V \quad (3.1-148)$$

$$g_1^2 = (\dot{\alpha}_g \dot{\rho}_g \dot{X}_n A)_j \Delta t / V \quad (3.1-149)$$

$$g_2^2 = [\dot{\alpha}_{g,j} (\dot{\rho}_{g,j} \dot{U}_{g,j} + P_L) A_j] \Delta t / V \quad (3.1-150)$$

$$g_4^2 = (\dot{\alpha}_g \dot{\rho}_g A)_j \Delta t / V \quad (3.1-151)$$

$$g_5^2 = (\dot{\alpha}_g \dot{\rho}_g A)_j \Delta t / V \quad (3.1-152)$$

$$f_3^1 = -[\dot{\alpha}_{f,j+1} (\dot{\rho}_{f,j+1} \dot{U}_{f,j+1} + P_L) A_{j+1}] \Delta t / V \quad (3.1-153)$$

$$f_4^1 = (\dot{\alpha}_f \dot{\rho}_f A)_{j+1} \Delta t / V \quad (3.1-154)$$

$$f_5^1 = -(\dot{\alpha}_f \dot{\rho}_f A)_{j+1} \Delta t / V \quad (3.1-155)$$

$$f_3^2 = [\dot{\alpha}_{f,j} (\dot{\rho}_{f,j} \dot{U}_{f,j} + P_L) A_j] \Delta t / V \quad (3.1-156)$$

$$f_4^2 = -(\dot{\alpha}_f \dot{\rho}_f A)_j \Delta t / V \quad (3.1-157)$$

$$f_5^2 = (\dot{\alpha}_f \dot{\rho}_f A)_j \Delta t / V \quad (3.1-158)$$

A solver<sup>a,3.1-13</sup> is used to obtain the bottom row of  $\mathbf{A}^{-1}$ . The solver uses LU factorization without pivoting and factors the matrix into upper and lower triangular matrices (LU factors) using triangular decomposition.

Multiplying Equation (3.1-115) by  $\mathbf{A}^{-1}$ , one can verify that just the bottom row of  $\mathbf{A}^{-1}$  is needed to obtain an equation that involves only the unknown variables  $(P_L^{n+1} - P_L^n)$ ,  $v_{g,j+1}^{n+1}$ ,  $v_{g,j}^{n+1}$ ,  $v_{f,j+1}^{n+1}$ , and  $v_{f,j}^{n+1}$ . Substituting the velocity equations [after solving momentum Equations (3.1-103) and (3.1-104) for  $v_{g,j}^{n+1}$  and  $v_{f,j}^{n+1}$ ] into this equation results in a single equation involving pressures. This is done for each volume, giving rise to an  $N \times N$  system of linear equations for the new time pressures in a system containing  $N$  volumes. Next, a sparse matrix solver<sup>3.1-10</sup> is used to obtain  $(P_L^{n+1} - P_L^n)$  for each volume. Then, the pressure differences  $(P_L^{n+1} - P_L^n)$  are substituted into the velocity equations to obtain the new time velocities.

Now, the new time velocities are substituted back into Equation (3.1-115) to obtain a single vector on the right side. The LU factors are used to obtain the provisional time variables  $\tilde{X}_{n,L}^{n+1}$ ,  $\tilde{U}_{g,L}^{n+1}$ ,  $\tilde{U}_{f,L}^{n+1}$ , and  $\tilde{\alpha}_{g,L}^{n+1}$ .

A mixture density,  $\rho_{m,L}^{n+1}$ , is then calculated from the unexpanded form of the mixture continuity equation which is numerically mass preserving. That density is compared with the mixture density,  $\rho_L^{n+1}$ , which is calculated from the state relations. The difference between these two mixture densities is used to provide a time step control based on truncation in the calculation of the mixture density. The mixture density  $\rho_{m,L}^{n+1}$  is calculated by adding the phasic density Equations, (3.1-2) and (3.1-3), to give the mixture continuity equation

$$\frac{\partial \rho_m}{\partial t} + \frac{1}{A} \frac{\partial}{\partial x} (\alpha_g \rho_g v_g A + \alpha_f \rho_f v_f A) = 0. \quad (3.1-159)$$

The mass-preserving finite difference approximation is

$$V_L [\rho_{m,L}^{n+1} - \rho_L^n] + \left( \dot{\alpha}_{g,j+1}^n \dot{\rho}_{g,j+1}^n v_{g,j+1}^{n+1} A_{j+1} - \dot{\alpha}_{g,j}^n \dot{\rho}_{g,j}^n v_{g,j}^{n+1} A_j \right) \Delta t + \left( \dot{\alpha}_{f,j+1}^n \dot{\rho}_{f,j+1}^n v_{f,j+1}^{n+1} A_{j+1} - \dot{\alpha}_{f,j}^n \dot{\rho}_{f,j}^n v_{f,j}^{n+1} A_j \right) \Delta t = 0 \quad (3.1-160)$$

from which  $\rho_{m,L}^{n+1}$  is obtained.

a. Private communication, E. S. Marwill to J. A. Trapp, EG&G Idaho, Inc., January 1983.

Next,  $\tilde{\Gamma}_{g,L}^{n+1}$  is calculated using Equation (3.1-108), where  $\tilde{T}_L^{s,n+1}$ ,  $\tilde{T}_{g,L}^{n+1}$ , and  $\tilde{T}_{f,L}^{n+1}$  are obtained from Equations (3.1-100) through (3.1-102) using the newly calculated variables  $P_L^{n+1}$ ,  $\tilde{U}_{g,L}^{n+1}$ ,  $\tilde{U}_{f,L}^{n+1}$ , and  $\tilde{X}_{n,L}^{n+1}$ .

To obtain the new time variables  $X_{n,L}^{n+1}$ ,  $X_{ni,L}^{n+1}$ ,  $U_{g,L}^{n+1}$ ,  $U_{f,L}^{n+1}$ , and  $\alpha_{g,L}^{n+1}$ , the unexpanded difference equations, Equations (3.1-107), (3.1-109), (3.1-110), (3.1-111), (3.1-112), and (3.1-113) are used. In the discussion introducing the unexpanded difference equations, motives were given for use of the unexpanded form. Extensive numerical testing has shown the benefits of the following procedures.

Using the phasic convective terms along with  $\tilde{\Gamma}_{g,L}^{n+1}$  from Equation (3.1-108), the unexpanded phasic density Equations (3.1-107) and (3.1-109) are used to obtain  $(\alpha_g \rho_g)_L^{n+1}$  and  $(\alpha_f \rho_f)_L^{n+1}$ .

Next, the unexpanded total noncondensable density Equation (3.1-110) is used to calculate  $(\alpha_g \rho_g X_n)_L^{n+1}$ , which is then divided by  $(\alpha_g \rho_g)_L^{n+1}$  to obtain  $X_{n,L}^{n+1}$ .

The nonexpanded individual noncondensable density Equation (3.1-111) is used to calculate  $(\alpha_g \rho_g X_n X_{ni})_L^{n+1}$ , which is divided by  $(\alpha_g \rho_g X_n)_L^{n+1}$  to obtain  $X_{ni,L}^{n+1}$ .

Following this, the unexpanded vapor energy Equation (3.1-112) is used with the vapor energy source and convective terms from the expanded equation as well as the provisional time variables  $\tilde{T}^{s,n+1}$ ,  $\tilde{T}_g^{n+1}$ , and  $\tilde{T}_f^{n+1}$  to obtain  $(\alpha_g \rho_g U_g)_L^{n+1}$ , which is divided by  $(\alpha_g \rho_g)_L^{n+1}$  to give  $U_{g,L}^{n+1}$ . Analogously, the unexpanded liquid energy Equation (3.1-113) is used to obtain  $(\alpha_f \rho_f U_f)_L^{n+1}$ , which is divided by  $(\alpha_f \rho_f)_L^{n+1}$  to give  $U_{f,L}^{n+1}$ .

Finally,  $\alpha_{g,L}^{n+1}$  is calculated from  $(\alpha_f \rho_f)_L^{n+1}$  using the equation

$$\alpha_{g,L}^{n+1} = 1 - \alpha_{f,L}^{n+1} = 1 - \frac{(\alpha_f \rho_f)_L^{n+1}}{\hat{\rho}_f^{n+1}} \quad (3.1-161)$$

where  $\hat{\rho}_f^{n+1}$  is obtained using a two term Taylor series expansion of the state Equation (3.1-97) and the new time variables  $P^{n+1}$  and  $U_f^{n+1}$ . The equation for  $\hat{\rho}_f^{n+1}$  has the formula

$$\hat{\rho}_{f,L}^{n+1} = \rho_{f,L}^n + \left( \frac{\partial \rho_f}{\partial P} \right)_L^n (P_L^{n+1} - P_L^n) + \left( \frac{\partial \rho_f}{\partial U_f} \right)_L^n (U_{f,L}^{n+1} - U_{f,L}^n) \quad (3.1-162)$$

The unexpanded equations are used in all two-phase to two-phase cases, except when the provisional void fraction  $\tilde{\alpha}_{g,L}^{n+1}$  is less than 0.001 and  $\tilde{\alpha}_{g,L}^{n+1} < \alpha_{g,L}^n$ . For this case, the provisional new time variables are taken to be the new time variables.

**3.1.5.2 One-Phase to One-Phase.** For this case, the pressure calculation remains the same as in the two-phase to two-phase case. For the densities and energies, however, the unexpanded equations are not used and the provisional new time variables obtained from the expanded equations are taken to be the new time variables. For the phase that is not present, the interfacial heat transfer coefficient for that phase is computed as if the void fraction was approximately  $10^{-5}$  instead of zero. This results in the internal energy of that phase being computed very close to saturation conditions. Slight numerical variations from saturation occur due to linearization; and the phasic energy, temperature, and density of the missing phase are reset to the saturation values in the state subroutine. This ensures agreement with saturation conditions. For the phase that is present, a value of 0.0 for the interfacial heat transfer coefficient is used, since there is no mass transfer occurring.

**3.1.5.3 Two-Phase to One-Phase (Disappearance).** For this case, the calculation is carried out in the same way as in the two-phase to two-phase case, where expanded calculations followed by unexpanded calculations are used (except for the case  $\tilde{\alpha}_{g,L}^{n+1} < 0.001$  and  $\tilde{\alpha}_{g,L}^{n+1} < \alpha_{g,L}^n$ ). Then, for the phase that disappears, the phasic energy, temperature, and density are reset to saturation values in the state subroutine, as is done with the one-phase to one-phase case.

**3.1.5.4 One-Phase to Two-Phase (Appearance).** Here, the calculation proceeds in the same way as in the one-phase to one-phase case. For the phase that is not present, the large interfacial heat transfer coefficient for that phase is computed as if the void fraction was approximately  $10^{-5}$  instead of zero. This results in the energy and temperature of that phase being computed very close to saturation conditions. Because the phase that is appearing is assumed to appear at saturation conditions, an error can be made if, in reality, the phase appeared by convection from a neighboring volume that was at a temperature different from saturation. The magnitude of the potential error is controlled by letting the phase appear at saturation but restricting the amount that can appear by time step control. If more than the limiting amount (amount determined through extensive testing) appears, an error is assumed to have occurred, and the time step is reduced and repeated.

### 3.1.6 Difference Equations and Time Advancement for the Nearly-Implicit Scheme

For problems where the flow is expected to change very slowly with time, it is possible to obtain adequate information from an approximate solution based on very large time steps. This would be advantageous if a reliable and efficient means could be found for solving difference equations treating all terms (i.e., phase exchanges, pressure propagation, and convection) by implicit differences. Unfortunately, the state of the art is less satisfactory here than in the case of semi-implicit (convection-explicit) schemes. For illustration, a fully implicit scheme for the six-equation model of a 100-cell problem would require the solution of 600 coupled algebraic equations. If these equations were linearized for a straight pipe, inversion of a block tri-diagonal, 600 x 600 matrix with 6 x 6 blocks would be required. This would yield a matrix of bandwidth 23 containing ~13,800 nonzero elements, resulting in an extremely costly time advancement scheme. Note that the tridiagonal shape is limited to a straight pipe problem.

To reduce the number of calculations required for solving fully implicit difference schemes, fractional step (sometimes called multiple step) methods have been tried. The equations can be split into fractional steps based upon physical phenomena. This is the basic idea in the nearly-implicit scheme. Fractional step methods for two-phase flow problems have been developed.<sup>3.1-14,3.1-15</sup> These earlier efforts have been used to guide the development of the present nearly-implicit scheme. The fractional step method described here<sup>3.1-16</sup> differs significantly from prior efforts in the reduced number of steps used to evaluate the momentum equations.

The nearly-implicit scheme consists of two steps. The first step solves all seven conservation equations, treating all interface exchange processes, the pressure propagation process, and the momentum convection process implicitly. These finite difference equations are exactly the expanded ones [Equations (3.1-87) through (3.1-91), (3.1-103), and (3.1-104)] solved in the semi-implicit scheme with one major change. The convective terms in the momentum Equations (3.1-103) and (3.1-104) are evaluated implicitly (in a linearized form) instead of in an explicit donor cell fashion as is done in the semi-implicit scheme. The second step consists of solving the unexpanded form of the mass and energy equations.

**3.1.6.1 First Step of the Nearly-Implicit Scheme.** The linearized implicit technique used for the convective terms in the first step is illustrated for the convective terms in the vapor part of the sum momentum Equation (3.1-85). An analogous result occurs for the liquid part as well as for the difference momentum Equation (3.1-86). The convective term is

$$\frac{1}{2} \alpha_g \rho_g (v_g^2)_{x_k}^{x_l} \quad (3.1-163)$$

In the nearly-implicit formulation, the VISF [Equation (3.1-106)] and VISG [Equation (3.1-105)] terms that result from the donor cell formulation are not used. Evaluating the velocities at new time gives the finite difference form as

$$\frac{1}{2} (\dot{\alpha}_g \dot{\rho}_g)_j^n \left[ (v_{g,L}^{n+1})^2 - (v_{g,K}^{n+1})^2 \right] \quad (3.1-164)$$

This term can be rewritten as

$$\begin{aligned} & \frac{1}{2} (\dot{\alpha}_g \dot{\rho}_g)_j^n \left[ (v_{g,L}^{n+1} - v_{g,L}^n)^2 + 2v_{g,L}^n (v_{g,L}^{n+1} - v_{g,L}^n) + (v_{g,L}^n)^2 \right. \\ & \left. - (v_{g,K}^{n+1} - v_{g,K}^n)^2 - 2v_{g,K}^n (v_{g,K}^{n+1} - v_{g,K}^n) - (v_{g,K}^n)^2 \right] \quad (3.1-165) \end{aligned}$$

Assuming that the leading quadratic term for L and K is small (small temporal changes in velocity) compared to the others results in the following form

$$\frac{1}{2} (\dot{\alpha}_g \dot{\rho}_g)_j^n \left[ 2v_{g,L}^n (v_{g,L}^{n+1} - v_{g,L}^n) + (v_{g,L}^n)^2 - 2v_{g,K}^n (v_{g,K}^{n+1} - v_{g,K}^n) - (v_{g,K}^n)^2 \right] \quad (3.1-166)$$

Using this linearized implicit form, the momentum flux terms in the sum momentum finite difference Equation (3.1-103) are replaced by

$$\begin{aligned} & \frac{1}{2} (\dot{\alpha}_g \dot{\rho}_g)_j^n [2v_{g,L}^n (v_{g,L}^{n+1} - v_{g,L}^n) + (v_{g,L}^n)^2 - 2v_{g,K}^n (v_{g,K}^{n+1} - v_{g,K}^n) - (v_{g,K}^n)^2] \Delta t \\ & + \frac{1}{2} (\dot{\alpha}_f \dot{\rho}_f)_j^n [2v_{f,L}^n (v_{f,L}^{n+1} - v_{f,L}^n) + (v_{f,L}^n)^2 - 2v_{f,K}^n (v_{f,K}^{n+1} - v_{f,K}^n) - (v_{f,K}^n)^2] \Delta t . \end{aligned} \quad (3.1-167)$$

Similarly, for the difference momentum finite difference Equation (3.1-104), the momentum flux terms become

$$\begin{aligned} & \frac{1}{2} [(\dot{\alpha}_g \dot{\rho}_g) / (\dot{\alpha}_g \dot{\rho}_g)]_j^n [2v_{g,L}^n (v_{g,L}^{n+1} - v_{g,L}^n) + (v_{g,L}^n)^2 - 2v_{g,K}^n (v_{g,K}^{n+1} - v_{g,K}^n) - (v_{g,K}^n)^2] \Delta t \\ & - \frac{1}{2} [(\dot{\alpha}_f \dot{\rho}_f) / (\dot{\alpha}_f \dot{\rho}_f)]_j^n [2v_{f,L}^n (v_{f,L}^{n+1} - v_{f,L}^n) + (v_{f,L}^n)^2 - 2v_{f,K}^n (v_{f,K}^{n+1} - v_{f,K}^n) - (v_{f,K}^n)^2] \Delta t . \end{aligned} \quad (3.1-168)$$

The volume-centered velocities are defined in terms of the velocities in the junctions attached to the volume (see Section 3.1.7). Thus, the new time volume-averaged velocities have the form

$$v_{f,L}^{n+1} = \sum_{j=1}^{J_{in}} c_{f,j}^n v_{f,j}^{n+1} + \sum_{j=1}^{J_{out}} c_{f,j}^n v_{f,j}^{n+1} \quad (3.1-169)$$

and

$$v_{g,L}^{n+1} = \sum_{j=1}^{J_{in}} c_{g,j}^n v_{g,j}^{n+1} + \sum_{j=1}^{J_{out}} c_{g,j}^n v_{g,j}^{n+1} \quad (3.1-170)$$

where  $c_{f,j}^n$  and  $c_{g,j}^n$  contain all old time quantities, and the equations have the same form as those in Section 3.1.7 except that the velocities are at new time values.

Although this additional implicitness involves only the momentum flux terms, it has a large impact on the algebraic solution algorithm in the first step of the multi-step method. In the semi-implicit scheme, Equations (3.1-87) through (3.1-91) are solved locally to give a single equation of the form

$$P_L^{n+1} = A v_{g,j+1}^{n+1} + B v_{g,j}^{n+1} + C v_{f,j+1}^{n+1} + D v_{f,j}^{n+1} + E \quad (3.1-171)$$

for pressure, where A, B, C, D, and E contain old time variables only (see Figure 3.1-3 for cell indexes). In the semi-implicit scheme, the momentum equations are also solved locally to obtain

$$v_{g,j}^{n+1} = A^1 (P_L^{n+1} - P_K^{n+1}) + C^1 \quad (3.1-172)$$

$$v_{f,j}^{n+1} = B^1 (P_L^{n+1} - P_K^{n+1}) + D^1 \quad (3.1-173)$$

where  $A^1$ ,  $B^1$ ,  $C^1$ , and  $D^1$  again contain only  $n$  time level variables. If the momentum Equations (3.1-172) and (3.1-173) are used to eliminate the  $n+1$  level velocities from Equation (3.1-171), we get the pressure equation used in the semi-implicit scheme to obtain all the  $n+1$  pressures. For the previous example of a 100-cell straight pipe problem, this results in a  $100 \times 100$  tri-diagonal matrix system to solve for all the  $P^{n+1}$ .

In the nearly-implicit scheme, because the momentum flux terms are implicit, the momentum Equations (3.1-103) and (3.1-104) [using the convective terms from Equations (3.1-167) and (3.1-168)] cannot be locally solved to get Equations (3.1-172) and (3.1-173). The new time convective terms bring in  $n+1$  level upstream and downstream velocities, e.g.,  $v_{f,j-1}^{n+1}$  and  $v_{f,j+1}^{n+1}$ . Equations (3.1-87) through (3.1-91) are still used to obtain Equation (3.1-171). In the nearly-implicit scheme, Equation (3.1-171) is used to eliminate the  $n+1$  level pressure terms from the sum and difference momentum Equations (3.1-103) and (3.1-104) [using the convective terms from Equations (3.1-167) and (3.1-168)], and a coupled pair of momentum equations involving only  $n+1$  level velocities is obtained. Because of the  $n+1$  level flux terms, this is a globally coupled system. For a straight pipe of 100 junctions, a  $200 \times 200$  matrix system is obtained. By partitioning the matrix into  $2 \times 2$  submatrices (or blocks), the matrix is in block tridiagonal form. This system is next preconditioned in order to enhance the diagonal dominance of the matrix.<sup>3.1-17</sup> This system of equations is then solved using a sparse matrix solution algorithm.<sup>3.1-10</sup> Once the  $v_f^{n+1}$  and  $v_g^{n+1}$  solution is obtained,  $P^{n+1}$  is obtained by substitution into Equation (3.1-171). Using Equations (3.1-87) through (3.1-91), provisional new time values for  $\alpha_g$ ,  $U_g$ ,  $U_f$ , and  $X_n$ , denoted by  $\tilde{\alpha}_g^{n+1}$ ,  $\tilde{U}_g^{n+1}$ ,  $\tilde{U}_f^{n+1}$ , and  $\tilde{X}_n^{n+1}$ , can also be obtained.

**3.1.6.2 Second Step of the Nearly-Implicit Scheme.** The second step in the nearly-implicit scheme is used to stabilize the convective terms in the mass and energy balance equations. This step uses the final  $n+1$  level velocities from the first step along with the interface exchange terms resulting from the provisional variables of the first step, i.e., the interface heat and mass exchanges for step two are calculated using  $P^{n+1}$ ,  $\tilde{U}_g^{n+1}$ ,  $\tilde{U}_f^{n+1}$ , and  $\tilde{X}_n^{n+1}$  from step one. The phasic continuity and energy equations in this second step have the convected variables evaluated at the  $n+1$  time level, i.e. implicitly, as compared to their explicit evaluation in the first step.

The vapor continuity equation is

$$V_L [(\alpha_g \rho_g)_L^{n+1} - (\alpha_g \rho_g)_L^n] + [(\dot{\alpha} \rho)_{g,j+1}^{n+1} v_{g,j+1}^{n+1} A_{j+1} - (\dot{\alpha} \rho)_{g,j}^{n+1} v_{g,j}^{n+1} A_j] \Delta t = \tilde{\Gamma}_{g,L}^{n+1} V_L \Delta t \quad (3.1-174)$$

The liquid continuity equation is

$$V_L [(\alpha_f \rho_f)_L^{n+1} - (\alpha_f \rho_f)_L^n] + [(\dot{\alpha} \rho)_{f,j+1}^{n+1} v_{f,j+1}^{n+1} A_{j+1} - (\dot{\alpha} \rho)_{f,j}^{n+1} v_{f,j}^{n+1} A_j] \Delta t = -\tilde{\Gamma}_{g,L}^{n+1} V_L \Delta t \quad (3.1-175)$$

In Equations (3.1-174) and (3.1-175), the interfacial mass exchange  $\tilde{\Gamma}_g^{n+1}$  is evaluated using the provisional values from the first step and is written

$$\tilde{\Gamma}_{g,L}^{n+1} = -\frac{\frac{P_{s,L}^n}{P_L^n} H_{ig,L}^n \left( \tilde{T}_L^{s,n+1} - \tilde{T}_{g,L}^{n+1} \right) + H_{if,L}^n \left( \tilde{T}_L^{s,n+1} - \tilde{T}_{f,L}^{n+1} \right)}{h_{g,L}^{*,n} - h_{f,L}^{*,n}} + \Gamma_{w,L}^n \quad (3.1-176)$$

where the provisional temperatures  $\tilde{T}^{n+1}$  are evaluated as functions of  $\tilde{U}_g^{n+1}$ ,  $\tilde{U}_f^{n+1}$ ,  $\tilde{X}_n^{n+1}$ , and  $P^{n+1}$  from the linearized state relationship [Equations (3.1-100), (3.1-101), and (3.1-102)].

The noncondensable continuity equation is

$$V_L [(\alpha_g \rho_g X_g)_L^{n+1} - (\alpha_g \rho_g X_g)_L^n] + [(\dot{\alpha}_g \rho_g X_g)_{j+1}^{n+1} v_{g,j+1}^{n+1} A_{j+1} - (\dot{\alpha}_g \rho_g X_g)_j^{n+1} v_{g,j}^{n+1} A_j] \Delta t = 0 \quad (3.1-177)$$

The vapor phase energy equation is given by

$$\begin{aligned} V_L [(\alpha_g \rho_g U_g)_L^{n+1} - (\alpha_g \rho_g U_g)_L^n] + [(\dot{\alpha} \rho U)_{g,j+1}^{n+1} v_{g,j+1}^{n+1} A_{j+1} - (\dot{\alpha} \rho U)_{g,j}^{n+1} v_{g,j}^{n+1} A_j] \Delta t \\ = -V_L P_L^n (\tilde{\alpha}_{g,L}^{n+1} - \alpha_{g,L}^n) - P_L^n \left( \dot{\alpha}_{g,j+1}^n v_{g,j+1}^{n+1} A_{j+1} - \dot{\alpha}_{g,j}^n v_{g,j}^{n+1} A_j \right) \Delta t \\ + \left\{ -\left( \frac{h_f^*}{h_g^* - h_f^*} \right)_L^n \frac{P_{s,L}^n}{P_L^n} H_{ig,L}^n \left( \tilde{T}_L^{s,n+1} - \tilde{T}_{g,L}^{n+1} \right) - \left( \frac{h_g^*}{h_g^* - h_f^*} \right)_L^n H_{if,L}^n \left( \tilde{T}_L^{s,n+1} - \tilde{T}_{f,L}^{n+1} \right) \right\} \Delta t \\ - \left( \frac{P_L^n - P_{s,L}^n}{P_L^n} \right) H_{gf,L}^n \left( \tilde{T}_{g,L}^{n+1} - \tilde{T}_{f,L}^{n+1} \right) + \left[ \left( \frac{1+\varepsilon}{2} \right) h_{g,L}^{*,n} + \left( \frac{1-\varepsilon}{2} \right) h_{f,L}^{*,n} \right] \Gamma_{w,L}^n + Q_{wg,L}^n + DISS_{g,L}^n \quad (3.1-178) \end{aligned}$$

The liquid phase energy equation is given by

$$\begin{aligned}
 & V_L \left[ (\alpha_f \rho_f U_f)_L^{n+1} - (\alpha_f \rho_f U_f)_L^n \right] + \left[ (\alpha \dot{\rho} U)_{f,j+1}^{n+1} v_{f,j+1}^{n+1} A_{j+1} - (\alpha \dot{\rho} U)_{f,j}^{n+1} v_{f,j}^{n+1} A_j \right] \Delta t \\
 & = V_L P_L^n \left( \tilde{\alpha}_{g,L}^{n+1} - \alpha_{g,L}^n \right) - P_L^n \left( \dot{\alpha}_{f,j+1}^n v_{f,j+1}^{n+1} A_{j+1} - \dot{\alpha}_{f,j}^n v_{f,j}^{n+1} A_j \right) \Delta t \\
 & + \left\{ \left( \frac{h_f^*}{h_g^* - h_f^*} \right)_L^n \frac{P_{s,L}^n}{P_L^n} H_{ig,L}^n \left( \tilde{T}_{L}^{s,n+1} - \tilde{T}_{g,L}^{n+1} \right) + \left( \frac{h_g^*}{h_g^* - h_f^*} \right)_L^n H_{if,L}^n \left( \tilde{T}_L^{s,n+1} - \tilde{T}_{f,L}^{n+1} \right) \right\} (3.1-179) \\
 & + \left( \frac{P_L^n - P_{s,L}^n}{P_L^n} \right) H_{gf,L}^n \left( \tilde{T}_{g,L}^{n+1} - \tilde{T}_{f,L}^{n+1} \right) - \left[ \left( \frac{1+\varepsilon}{2} \right) h_{g,L}^{',n} + \left( \frac{1-\varepsilon}{2} \right) h_{f,L}^{',n} \right] \Gamma_{w,L}^n + Q_{wf,L}^n + DISS_{f,L}^n \} V_L \Delta t .
 \end{aligned}$$

The second step uses the mass and energy balance equations. If the structure of Equations (3.1-174), (3.1-175), (3.1-177), (3.1-178), and (3.1-179) is examined, it is seen that each equation involves only one unknown variable:

- Vapor continuity Equation (3.1-174)  $(\alpha \rho)_g^{n+1}$
- Liquid continuity Equation (3.1-175)  $(\alpha \rho)_f^{n+1}$
- Noncondensable continuity Equation (3.1-177)  $(\alpha_g \rho_g X_n)^{n+1}$
- Vapor energy Equation (3.1-178)  $(\alpha \rho U)_g^{n+1}$
- Liquid energy Equation (3.1-179)  $(\alpha \rho U)_f^{n+1}$ .

This is because the new time velocities,  $v_g^{n+1}$  and  $v_f^{n+1}$ , are known from step one, and provisional  $n+1$  values from step one are used in the exchange terms. Hence, each equation is uncoupled from the others and can be solved independently. In addition, the three equations involving the gas phase, Equations (3.1-174), (3.1-177), and (3.1-178), have the same structural form for the convective terms, i.e., each equation convects with velocity  $v_g^{n+1}$ . The coefficient matrix generated by Equation (3.1-174) is inverted once, and then this inverse is used with different right sides to solve Equations (3.1-177) and (3.1-178). Hence, for the straight pipe problem of 100 cells, only one  $100 \times 100$  tri-diagonal system is inverted to obtain  $(\alpha \rho)_g^{n+1}$ ,  $(\alpha_g \rho_g X_n)^{n+1}$ , and  $(\alpha \rho U)_g^{n+1}$ . In like manner, the liquid phase Equations (3.1-175) and (3.1-179) have the same structure and require only one inversion to be carried out to solve both equation sets, giving  $(\alpha \rho)_f^{n+1}$  and  $(\alpha \rho U)_f^{n+1}$ .

With the above five new time variables known, we obtain  $X_n^{n+1}$ ,  $U_g^{n+1}$ , and  $U_f^{n+1}$  from

$$X_n^{n+1} = (\alpha_g \rho_g X_n)^{n+1} / (\alpha \rho)_g^{n+1} \quad (3.1-180)$$

$$U_g^{n+1} = (\alpha \rho U)_g^{n+1} / (\alpha \rho)_g^{n+1} \quad (3.1-181)$$

$$U_f^{n+1} = (\alpha \rho U)_f^{n+1} / (\alpha \rho)_f^{n+1} \quad (3.1-182)$$

The void fraction,  $\alpha_g^{n+1}$ , is obtained from

$$\alpha_g^{n+1} = \frac{\rho_m^{n+1} - \hat{\rho}_f^{n+1}}{\hat{\rho}_g^{n+1} - \hat{\rho}_f^{n+1}} = \frac{(\alpha \rho)_g^{n+1} + (\alpha \rho)_f^{n+1} - \hat{\rho}_f^{n+1}}{\hat{\rho}_g^{n+1} - \hat{\rho}_f^{n+1}} \quad (3.1-183)$$

where

$\rho_m^{n+1}$  = the overall mixture density

$\hat{\rho}_f^{n+1}$  = the liquid density, which is calculated from the linearized state relationship [Equation (3.1-97)] using  $U_f^{n+1}$  and  $P^{n+1}$

$\hat{\rho}_g^{n+1}$  = the vapor density, which is calculated from the linearized state relationship [Equation (3.1-96)] using  $U_g^{n+1}$ ,  $X_n^{n+1}$ , and  $P^{n+1}$ .

Up to this point of this section on the nearly-implicit scheme, the difference equations have been presented along with the time advancement for the case of two-phase to two-phase only. As indicated in Section 3.1.5, there are three other possible transition cases (one-phase to one-phase, two-phase to one-phase, and one-phase to two-phase). These three cases will now be described for the nearly-implicit scheme.

For the one-phase to one-phase case, both the first step and the second step are carried out as in the two-phase to two-phase case. For the phase that is not present, a large interfacial heat transfer coefficient consistent with the interfacial heat transfer coefficients computed from the correlation for a void fraction of  $10^{-5}$  is used. For the phase that is present, a value of 0.0 is used for the interfacial heat transfer coefficient. For the phase that is not present,  $\alpha$  is zero, and thus  $(\alpha \rho)^{n+1}$  equals zero for that phase. The provisional  $n+1$  value of the corresponding variable is used in order to avoid the division by zero in Equations (3.1-180) through (3.1-182). As with the semi-implicit time advancement, phasic energy, temperature, and density of the missing phase are reset to the saturation values in the state subroutine.

For the two-phase to one-phase case (disappearance), the calculation is carried out the same as in the two-phase to two-phase case. Then, for the phase that is missing, the phasic energy, temperature, and density of the missing phase are reset to saturation values in the state subroutine as is done with the one-phase to one-phase case. This is the same approach used in the semi-implicit scheme time advancement.

For the one-phase to two-phase case (appearance), the first step quantities are used for the appearing phase. A large interfacial heat transfer coefficient, consistent with the interfacial heat transfer coefficients from the correlations, as if the void fraction were  $10^{-5}$ , is used for the appearing phase, resulting in the energy and temperature of that phase being very close to saturation. Because the phase that is appearing is assumed to appear at saturation conditions, an error can be made if, in reality, the phase appeared by convection from a neighboring volume that was at a temperature different from saturation. The magnitude of the potential error is controlled by letting the phase appear at saturation but restricting the amount that can appear by time step control. If more than the limiting amount appears, an error is assumed to have occurred, and the time step is reduced and repeated. This is the same approach used in the semi-implicit scheme time advancement.

In summary, the second step stabilizes the convective terms in the mass and energy equations, and it does so with very little computational effort due to the fractional step nature of the scheme. As an example, if the nearly-implicit method is compared with the fully implicit method for a straight pipe problem of 100 cells, we have the following efficiency estimates. The fully implicit method requires the inversion of a banded block tri-diagonal  $600 \times 600$  matrix of bandwidth 23 containing 13,800 nonzero elements. The nearly-implicit method requires the inversion of one block tri-diagonal  $200 \times 200$  matrix with  $2 \times 2$  blocks and bandwidth 7 containing 1,400 nonzero elements plus two  $100 \times 100$  tri-diagonal matrices with 300 nonzero elements. The nearly-implicit method thus requires about 1/10 the number of storage locations required by the fully implicit method. If the computational efficiency is estimated by counting the number of multiplications in the forward part of a Gaussian elimination algorithm, then the fully implicit method for this problem requires about 450,000 multiplications, whereas the nearly-implicit method requires about 2,000 multiplications. Thus, the nearly-implicit method requires about 1/200 (based on the number of multiplications) of the computational time per time step needed for a fully implicit scheme.

### 3.1.7 Volume-Average Velocities

The previous development of the difference equations considered a pipe consisting of a series of singly connected volumes. In RELAP5/MOD3, each volume may have zero, one or more junctions attached to its inlet end, and, zero, one, or more junctions attached to its outlet end. Therefore, the flux terms at the inlet or outlet end of a volume consist of a summation over all of the junctions attached to that end of the volume.

Volume-average velocities are required for the momentum flux calculation, evaluation of the wall frictional forces, evaluation of the wall heat transfer, evaluation of the interfacial heat transfer, and the Courant time step limit. In a simple constant area passage, the arithmetic average between the inlet and outlet is a satisfactory approximation. However, at branch volumes with multiple inlets and/or outlets or for volumes with abrupt area change, use of the arithmetic average results in nonphysical behavior.

The liquid and vapor velocities in the volume cells are calculated by a method that averages the phasic mass flows over the volume cell inlet and outlet junctions. A cell volume is shown in **Figure 3.1-4**, where the rectangular box represents a cell volume. Each of the arrow vectors into or out of the box represents the liquid mass flow through an inlet or outlet junction, respectively. Jin is the number of inlet junctions, and Jout is the number of outlet junctions. This discussion will be for liquid velocity; the gas velocity derivation is the same.

At the inlet side of the volume, the total mass flow rate into the volume is given by

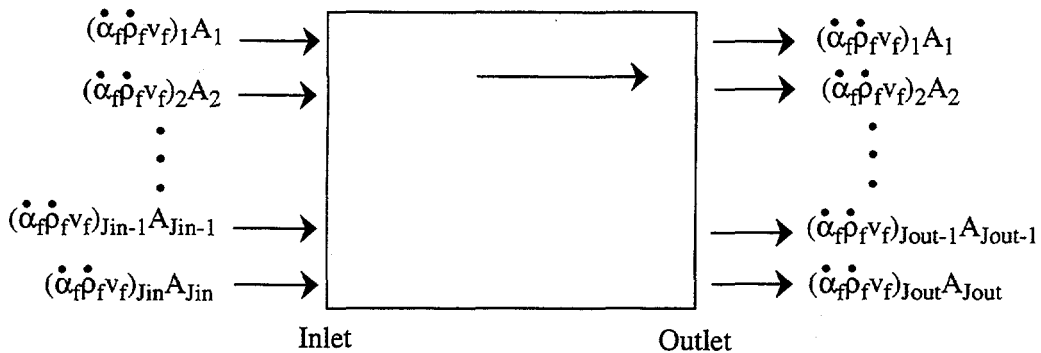


**Figure 3.1-4** Schematic of a volume cell showing multiple inlet and outlet junction mass flows.

$$M_{f,in} = \sum_{j=1}^{Jin} \dot{\alpha}_{f,j} \dot{\rho}_{f,j} v_{f,j} A_j \quad (3.1-184)$$

where  $M_{f,in}$  is the mass flow rate of liquid into the volume.

The average inlet liquid volume fraction can be defined as

$$\bar{\alpha}_{f,in} = \frac{\sum_{j=1}^{Jin} \dot{\alpha}_{f,j} A_j}{\sum_{j=1}^{Jin} A_j} \quad (3.1-185)$$

The average inlet liquid phase density can be defined as

$$\bar{\rho}_{f,in} = \frac{\sum_{j=1}^{Jin} \dot{\alpha}_{f,j} \dot{\rho}_{f,j} A_j}{\sum_{j=1}^{Jin} \dot{\alpha}_{f,j} A_j} \quad (3.1-186)$$

The average inlet phase velocity with respect to the total inlet junction cross-sectional area can be defined as

$$\bar{v}_{f,in} = \frac{\sum_{j=1}^{J_{in}} \dot{\alpha}_{f,j} \dot{\rho}_{f,j} v_{f,j} A_j}{\sum_{j=1}^{J_{in}} \dot{\alpha}_{f,j} \dot{\rho}_{f,j} A_j} \quad (3.1-187)$$

The total inlet junction cross-sectional area is

$$A_{in} = \sum_{j=1}^{J_{in}} A_j \quad (3.1-188)$$

Equation (3.1-184) can be expressed in terms of the average inlet conditions as

$$M_{f,in} = \sum_{j=1}^{J_{in}} \dot{\alpha}_{f,j} \dot{\rho}_{f,j} v_{f,j} A_j = \bar{\alpha}_{f,in} \bar{\rho}_{f,in} \bar{v}_{f,in} A_{in} \quad (3.1-189)$$

In terms of the volume cross-sectional area,  $A_L$ , the mass flow rate can be written as

$$M_{f,in} = \bar{\alpha}_{f,in} \bar{\rho}_{f,in} \bar{v}_{f,in}^L A_L \quad (3.1-190)$$

where  $\bar{v}_{f,in}^L$  is the liquid volume inlet velocity. By equating Equations (3.1-189) and (3.1-190), canceling terms and rearranging, the liquid volume inlet velocity can be expressed as

$$\bar{v}_{f,in}^L = \bar{v}_{f,in} \frac{A_{in}}{A_L} \quad (3.1-191)$$

Substituting Equations (3.1-187) and (3.1-188) into Equation (3.1-191) gives

$$\bar{v}_{f,in}^L = \frac{\sum_{j=1}^{J_{in}} \dot{\alpha}_{f,j} \dot{\rho}_{f,j} v_{f,j} A_j \sum_{j=1}^{J_{in}} A_j}{\sum_{j=1}^{J_{in}} \dot{\alpha}_{f,j} \dot{\rho}_{f,j} A_j} \quad (3.1-192)$$

Similarly, the volume outlet liquid velocity can be expressed as

$$\bar{v}_{f, out}^L = \frac{\sum_{j=1}^{J_{out}} \dot{\alpha}_{f,j} \dot{\rho}_{f,j} v_{f,j} A_j \sum_{j=1}^{J_{out}} A_j}{\sum_{j=1}^{J_{out}} \dot{\alpha}_{f,j} \dot{\rho}_{f,j} A_j} . \quad (3.1-193)$$

In RELAP5/MOD1, the total liquid momentum of the volume was expressed in terms of the momentum of the inlet and outlet halves of the volume as (assuming density changes are small)

$$\rho_{f,L} V_L v_{f,L} = \frac{1}{2} \rho_{f,L} V_L \bar{v}_{f,in}^L + \frac{1}{2} \rho_{f,L} V_L \bar{v}_{f,out}^L . \quad (3.1-194)$$

Thus,

$$v_{f,L} = \frac{1}{2} (\bar{v}_{f,in}^L + \bar{v}_{f,out}^L) . \quad (3.1-195)$$

Substitution of Equations (3.1-192) and (3.1-193) into Equation (3.1-195) yields

$$v_{f,L}^n = \frac{1}{2} \frac{\sum_{j=1}^{J_{in}} \dot{\alpha}_{f,j}^n \dot{\rho}_{f,j}^n v_{f,j}^n A_j \sum_{j=1}^{J_{in}} A_j}{\sum_{j=1}^{J_{in}} \dot{\alpha}_{f,j}^n \dot{\rho}_{f,j}^n A_j} + \frac{1}{2} \frac{\sum_{j=1}^{J_{out}} \dot{\alpha}_{f,j}^n \dot{\rho}_{f,j}^n v_{f,j}^n A_j \sum_{j=1}^{J_{out}} A_j}{\sum_{j=1}^{J_{out}} \dot{\alpha}_{f,j}^n \dot{\rho}_{f,j}^n A_j} . \quad (3.1-196)$$

where old time levels (n) are used for time varying quantities. This arithmetic average of the averaged inlet and averaged outlet velocities was used in RELAP5/MOD1. <sup>3.1-18</sup>

The use of the 1/2 factor in front of the inlet and outlet average velocities sometimes resulted in unphysical results in the convective term of the momentum equations (momentum flux), which uses the volume average velocities. One example occurred in a vertical pipe where both liquid and vapor were flowing upward. Sometimes the liquid velocity was calculated to be higher than the vapor velocity which is unphysical. Using the liquid and the inlets as an example, the 1/2 factor used in RELAP5/MOD1 was replaced in subsequent versions of RELAP5 by

$$\frac{\sum_{j=1}^{J_{in}} (\dot{\alpha}_f \dot{\rho}_f)_j^n A_j}{\sum_{j=1}^{J_{in}+J_{out}} (\dot{\alpha}_f \dot{\rho}_f)_j^n A_j} . \quad (3.1-197)$$

This is also done for the liquid outlets, as well as the vapor inlets and outlets. This approach resolves the above problem.

Using the modification discussed above, the RELAP5/MOD3 volume-average velocity formulas then have the form

$$(v_f)_L^n = \frac{\sum_{i=1}^{Jin} (\dot{\alpha}_f \dot{\rho}_f v_f)_j^n A_j \bullet \sum_{j=1}^{Jin} A_j}{A_L \sum_{j=1}^{Jin+Jout} (\dot{\alpha}_f \dot{\rho}_f)_j^n A_j} + \frac{\sum_{i=1}^{Jout} (\dot{\alpha}_f \dot{\rho}_f v_f)_j^n A_j \bullet \sum_{j=1}^{Jout} A_j}{A_L \sum_{j=1}^{Jin+Jout} (\dot{\alpha}_f \dot{\rho}_f)_j^n A_j} = \sum_{j=1}^{Jin} c_{f,j}^n v_{f,j}^n + \sum_{j=1}^{Jout} c_{f,j}^n v_{f,j}^n \quad (3.1-198)$$

and

$$(v_g)_L^n = \frac{\sum_{i=1}^{Jin} (\dot{\alpha}_g \dot{\rho}_g v_g)_j^n A_j \bullet \sum_{j=1}^{Jin} A_j}{A_L \sum_{j=1}^{Jin+Jout} (\dot{\alpha}_g \dot{\rho}_g)_j^n A_j} + \frac{\sum_{i=1}^{Jout} (\dot{\alpha}_g \dot{\rho}_g v_g)_j^n A_j \bullet \sum_{j=1}^{Jout} A_j}{A_L \sum_{j=1}^{Jin+Jout} (\dot{\alpha}_g \dot{\rho}_g)_j^n A_j} = \sum_{j=1}^{Jin} c_{g,j}^n v_{g,j}^n + \sum_{j=1}^{Jout} c_{g,j}^n v_{g,j}^n \quad (3.1-199)$$

where  $c_{f,j}^n$  and  $c_{g,j}^n$  contain only old time quantities (no velocities).

Equations (3.1-198) and (3.1-199) are used for the momentum flux calculation, evaluation of the interfacial heat transfer, and the Courant time step limit. For the evaluation of the wall frictional forces and the wall heat transfer, different formulas are used.

For the evaluation of the wall frictional forces, the magnitude of the volume velocities is needed. An obvious way to compute this magnitude is to take just the absolute value of the result from Equations (3.1-198) and (3.1-199). A problem can occur when the magnitude is zero because the inlet velocity is equal and opposite to the outlet velocity. To avoid this case, the calculation of the magnitude of the volume velocities used in the wall friction uses the same form as Equations (3.1-198) and (3.1-199), with the magnitude of the junction velocities used in the formulas. Thus, the equations used in the wall friction evaluation are

$$|v_f|_L^n = \frac{\sum_{i=1}^{Jin} (\dot{\alpha}_f \dot{\rho}_f |v_f|)_j^n A_j \bullet \sum_{j=1}^{Jin} A_j}{A_L \sum_{j=1}^{Jin+Jout} (\dot{\alpha}_f \dot{\rho}_f)_j^n A_j} + \frac{\sum_{i=1}^{Jout} (\dot{\alpha}_f \dot{\rho}_f |v_f|)_j^n A_j \bullet \sum_{j=1}^{Jout} A_j}{A_L \sum_{j=1}^{Jin+Jout} (\dot{\alpha}_f \dot{\rho}_f)_j^n A_j} \quad (3.1-200)$$

$$|v_g|_L^n = \frac{\sum_{i=1}^{J_{in}} (\dot{\alpha}_g \dot{\rho}_g |v_g|_j^n A_j \cdot \sum_{j=1}^{J_{in}} A_j) + \sum_{i=1}^{J_{out}} (\dot{\alpha}_g \dot{\rho}_g |v_g|_j^n A_j \cdot \sum_{j=1}^{J_{out}} A_j)}{A_L \sum_{j=1}^{J_{in}+J_{out}} (\dot{\alpha}_g \dot{\rho}_g)_j^n A_j} \quad (3.1-201)$$

For the evaluation of the wall heat transfer rate, a simpler version of Equations (3.1-198) and (3.1-199) is used for the volume average velocities. This arose during the implementation of the Groeneveld CHF (see Volume IV) correlation into RELAP5/MOD3, where it was observed that the total volume mass flux  $G_L$ , which is based on the volume velocities, was not well behaved for the purpose of wall heat transfer. The mass flux  $G_L$  is given by

$$G_L = (\alpha_g \rho_g v_g)_L + (\alpha_f \rho_f v_f)_L \quad (3.1-202)$$

It was found that the volume mass flux using Equations (3.1-198) and (3.1-199) for  $v_{gL}$  and  $v_{fL}$  was as much as 30% below the volumes' inlet mass flux and outlet mass flux in RELAP5 simulations of Bennett's CHF experiments (steady state boiling of water in a heated tube). This Bennett experiment is discussed in Volume 3 of this manual. As a result of the problem exhibited in Bennett's problem, a simpler version of the volume velocities is used instead for wall heat transfer.

Here, the average inlet phase velocity with respect to the total inlet junction cross-sectional area is

$$\bar{v}_{f,in} = \frac{\sum_{i=1}^{J_{in}} \dot{\alpha}_{f,j} \dot{\rho}_{f,j} v_{f,j} A_j}{\alpha_{f,L} \rho_{f,L} \sum_{j=1}^{J_{in}} A_j} \quad (3.1-203)$$

Substitution into Equation (3.1-191) yields for the volume inlet liquid velocity

$$\bar{v}_{f,in}^L = \frac{\sum_{i=1}^{J_{in}} \dot{\alpha}_{f,j} \dot{\rho}_{f,j} v_{f,j} A_j}{\alpha_{f,L} \rho_{f,L} A_L} \quad (3.1-204)$$

Similarly, the volume outlet liquid velocity is given by

$$\bar{v}_{f,out}^L = \frac{\sum_{i=1}^{J_{out}} \dot{\alpha}_{f,j} \dot{\rho}_{f,j} v_{f,j} A_j}{\alpha_{f,L} \rho_{f,L} A_L} \quad (3.1-205)$$

Thus, using Equation (3.1-195), the volume liquid velocity used in the wall heat transfer rate calculation is

$$v_{f,L}^n = \frac{\frac{1}{2} \sum_{j=1}^{J_{in}} (\dot{\alpha}_f \dot{\rho}_f v_f)_j^n A_j + \frac{1}{2} \sum_{j=1}^{J_{out}} (\dot{\alpha}_f \dot{\rho}_f v_f)_j^n A_j}{\alpha_{f,L}^n \rho_{f,L}^n A_L} \quad (3.1-206)$$

Similarly, the volume gas velocity used in the wall heat transfer is

$$v_{g,L}^n = \frac{\frac{1}{2} \sum_{j=1}^{J_{in}} (\dot{\alpha}_g \dot{\rho}_g v_g)_j^n A_j + \frac{1}{2} \sum_{j=1}^{J_{out}} (\dot{\alpha}_g \dot{\rho}_g v_g)_j^n A_j}{\alpha_{g,L}^n \rho_{g,L}^n A_L} \quad (3.1-207)$$

These forms of the volume average velocity produce the same mass flux at steady state for the volume as well as for its inlet and outlet junctions, which is the desired result.

### 3.1.8 Implicit Hydrodynamic and Heat Structure Coupling

An option exists to implicitly couple the time advancement of the hydrodynamic and heat structure models. Heat structures represent the solid structures bounding hydrodynamic volumes (i.e., pipe walls) or structures internal to the volumes (fuel pins). One dimensional heat conduction is used to compute temperature distributions within heat structures. Hydrodynamic and heat structure conditions are coupled through heat structure boundary conditions. The solution matrix for the set of simultaneous equations resulting from the implicit coupling of hydrodynamic and heat structure advancement contains the same number of nonzero elements as discussed in the previous sections but with some of the elements having additional terms. In addition, the total set of simultaneous equations includes an equation from each mesh point of each heat structure attached to the hydrodynamic volumes. The heat conduction equations have additional terms related to fluid temperatures introduced in the boundary conditions. However, this larger set of simultaneous equations is solved with only a modest increase in computations compared to the explicit coupling. This implicit coupling can be used with either the semi-implicit or nearly-implicit advancement.

The purpose of the implicit coupling of hydrodynamic and heat structure time advancement is to more accurately model the exchange of energy between the structures and fluid in the volumes, to avoid numerical instabilities due to explicit coupling, and to achieve reduction of computing time through larger time steps.

The purpose of the remainder of this section is to show the additional terms added to the hydrodynamic equations because of the implicit coupling. A complete understanding of the implicit coupling requires information from Section 4 describing numerical techniques for heat structures, information from Section 3.3.10 describing heat transfer correlations, and information from Volume IV, describing relationships between heat transfer from structures, heat added to volumes, and mass transfer associated with wall heat transfer. Equations (3.1-211) through (3.1-214) follow directly from the material in Volume IV.

In previous subsections [see Equations (3.1-4) and (3.1-5)], the quantities,  $\Gamma_w$ ,  $Q_{wg}$ , and  $Q_{wf}$ , which are related to heat and mass transfer at and near the wall surface, were introduced. These were discussed as if only one wall surface could be attached to a volume. Similarly to the possibility of multiple junctions being connected to the ends of a volume, multiple wall surfaces representing quite different heat transfer situations can be attached to a volume. Thus the  $\Gamma_w$ ,  $Q_{wg}$ , and  $Q_{wf}$  quantities involve summations over the surfaces attached to a volume. Details of the summations are shown in Volume IV.

The previous section combined boiling and condensation in the  $\Gamma_w$  quantity, but showed a difference in the two situations through the factor  $\epsilon$  [Equations (3.1-31) and (3.1-32)]. That notation is correct for one heat structure connected to a volume and relies on the wall surface possibly boiling, or condensing, but not both simultaneously. With multiple heat structures, some might be boiling and others could be condensing. Accordingly, boiling mass transfer,  $\Gamma_w$ , and condensing mass transfer,  $\Gamma_c$ , are separated. Thus, the total mass transfer consists of mass transfer in the bulk fluid ( $\Gamma_{ig}$ ) and mass transfer in the boundary layers near the walls ( $\Gamma_w$  and  $\Gamma_c$ ); that is,

$$\Gamma_g = \Gamma_{ig} + \Gamma_w + \Gamma_c . \quad (3.1-208)$$

With implicit hydrodynamic and heat structure coupling, some source terms in the mass and energy equations for the semi-implicit and nearly-implicit scheme become implicit. In the continuity equations,  $\Gamma_w$  becomes  $\tilde{\Gamma}_{w,L}^{n+1} + \tilde{\Gamma}_{c,L}^{n+1}$ . In the vapor energy equations, terms involving  $\Gamma_w$  and  $Q_{wg}$  becomes

$$\tilde{\Gamma}_{w,L}^{n+1} h_{g,L}^{s,n} + \tilde{\Gamma}_{c,L}^{n+1} h_{f,L}^{s,n} + \tilde{Q}_{wg,L}^{n+1} . \quad (3.1-209)$$

In the liquid energy equations, terms involving  $\Gamma_w$  and  $Q_{wf}$  becomes

$$-\tilde{\Gamma}_{w,L}^{n+1} h_{g,L}^{s,n} - \tilde{\Gamma}_{c,L}^{n+1} h_{f,L}^{s,n} + \tilde{Q}_{wf,L}^{n+1} . \quad (3.1-210)$$

Volume IV discusses multiple heat structures connected to hydrodynamic volumes. Summations over the multiple heat structures that can be connected to hydrodynamic volumes are discussed. After applying the summations discussed in Volume IV, the wall heat transfer and mass transfer terms can be written as

$$\begin{aligned} \tilde{Q}_{wf}^{n+1} = & Q_{wf0}^n + Q_{wff}^n \left( \tilde{T}_f^{n+1} - T_f^n \right) + Q_{wfg}^n \left( \tilde{T}_g^{n+1} - T_g^n \right) + Q_{wft}^n \left( \tilde{T}_t^{s,n+1} - T_t^{s,n} \right) \\ & + Q_{wfp}^n \left( \tilde{T}^{s,n+1} - T^{s,n} \right) \end{aligned} \quad (3.1-211)$$

$$\begin{aligned} \tilde{Q}_{wg}^{n+1} = & Q_{wg0}^n + Q_{wgf}^n \left( \tilde{T}_f^{n+1} - T_f^n \right) + Q_{wgg}^n \left( \tilde{T}_g^{n+1} - T_g^n \right) + Q_{wgt}^n \left( \tilde{T}_t^{s,n+1} - T_t^{s,n} \right) \\ & + Q_{wgp}^n \left( \tilde{T}^{s,n+1} - T^{s,n} \right) \end{aligned} \quad (3.1-212)$$

$$\tilde{\Gamma}_w^{n+1} = \tilde{\Gamma}_{wf}^{n+1} = \Gamma_{wf0}^n + \Gamma_{wff}^n \left( \tilde{T}_f^{n+1} - T_f^n \right) + \Gamma_{wfg}^n \left( \tilde{T}_g^{n+1} - T_g^n \right) + \Gamma_{wft}^n \left( \tilde{T}_t^{s,n+1} - T_t^{s,n} \right) + \Gamma_{wfp}^n \left( \tilde{T}^{s,n+1} - T^{s,n} \right) \quad (3.1-213)$$

$$\tilde{\Gamma}_c^{n+1} = \tilde{\Gamma}_{wg}^{n+1} = \Gamma_{wg0}^n + \Gamma_{wgf}^n \left( \tilde{T}_f^{n+1} - T_f^n \right) + \Gamma_{wgg}^n \left( \tilde{T}_g^{n+1} - T_g^n \right) + \Gamma_{wgt}^n \left( \tilde{T}_t^{s,n+1} - T_t^{s,n} \right) + \Gamma_{wgp}^n \left( \tilde{T}^{s,n+1} - T^{s,n} \right) \quad (3.1-214)$$

The variables  $\tilde{T}^{s,n+1}$ ,  $\tilde{T}_g^{n+1}$ , and  $\tilde{T}_f^{n+1}$  are given by Equations (3.1-100) through (3.1-102), where  $T^s$  is the saturation temperature. When noncondensables are present, this  $T^s$  is based on the partial pressure of steam [ $T^s(P_s)$ ]. Some of the heat transfer terms, when noncondensables are present, use the saturation temperature based on the total pressure  $P (= P_s + P_n)$ . In Equations (3.1-211) through (3.1-214), the saturation temperature based on  $P_s$  is denoted by  $T^s(P_s)$  and the saturation temperature based on  $P$  is denoted by  $T^s(P)$ . Thus,  $\tilde{T}_L^{s,n+1}(P)$  is given by

$$\tilde{T}_L^{s,n+1}(P) = T_L^s(P^n) + \left( \frac{dT^s}{dP} \right)_L^n (P_L^{n+1} - P_L^n) \quad (3.1-215)$$

When the implicit coupling of the hydrodynamics and the heat slabs is used, additional terms are added to some of the terms of the  $\mathbf{A}$  matrix. For example see Equation (3.1-115). These additional terms are next shown as additions to the  $\mathbf{A}$  matrix elements listed in Equations (3.1-118) through (3.1-141).

$$A_{21} = A_{21} - \Delta t [Q_{wgg} + \Gamma_{wfg} h_g^s + \Gamma_{wgg} h_f^s] \frac{\partial T_g}{\partial X_n} - \Delta t [Q_{wgp} + \Gamma_{wfp} h_g^s + \Gamma_{wgp} h_f^s] \frac{\partial T^s}{\partial X_n} \quad (3.1-216)$$

$$A_{22} = A_{22} - \Delta t [Q_{wgg} + \Gamma_{wfg} h_g^s + \Gamma_{wgg} h_f^s] \frac{\partial T_g}{\partial U_g} - \Delta t [Q_{wgp} + \Gamma_{wfp} h_g^s + \Gamma_{wgp} h_f^s] \frac{\partial T^s}{\partial U_g} \quad (3.1-217)$$

$$A_{23} = A_{23} - \Delta t [Q_{wgf} + \Gamma_{wff} h_g^s + \Gamma_{wgf} h_f^s] \frac{\partial T_f}{\partial U_f} \quad (3.1-218)$$

$$A_{25} = A_{25} - \Delta t [Q_{wgf} + \Gamma_{wff} h_g^s + \Gamma_{wgf} h_f^s] \frac{\partial T_f}{\partial P} - \Delta t [Q_{wgg} + \Gamma_{wfg} h_g^s + \Gamma_{wgg} h_f^s] \frac{\partial T_g}{\partial P} - \Delta t [Q_{wgp} + \Gamma_{wfp} h_g^s + \Gamma_{wgp} h_f^s] \frac{\partial T^s}{\partial P} \Big|_{P_s} - \Delta t [Q_{wgt} + \Gamma_{wft} h_g^s + \Gamma_{wgt} h_f^s] \frac{\partial T^s}{\partial P} \Big|_P \quad (3.1-219)$$

$$A_{31} = A_{31} - \Delta t [Q_{wfg} - \Gamma_{wfg} h_g^s - \Gamma_{wgg} h_f^s] \frac{\partial T_g}{\partial X_n} - \Delta t [Q_{wfp} - \Gamma_{wfp} h_g^s - \Gamma_{wgp} h_f^s] \frac{\partial T_g^s}{\partial X_n} \quad (3.1-220)$$

$$A_{32} = A_{32} - \Delta t [Q_{wfg} - \Gamma_{wfg} h_g^s - \Gamma_{wgg} h_f^s] \frac{\partial T_g}{\partial U_g} - \Delta t [Q_{wfp} - \Gamma_{wfp} h_g^s - \Gamma_{wgp} h_f^s] \frac{\partial T_g^s}{\partial U_g} \quad (3.1-221)$$

$$A_{33} = A_{33} - \Delta t [Q_{wff} - \Gamma_{wff} h_g^s - \Gamma_{wgf} h_f^s] \frac{\partial T_f}{\partial U_f} \quad (3.1-222)$$

$$A_{35} = A_{35} - \Delta t [Q_{wff} - \Gamma_{wff} h_g^s - \Gamma_{wgf} h_f^s] \frac{\partial T_f}{\partial P} - \Delta t [Q_{wfg} - \Gamma_{wfg} h_g^s + \Gamma_{wgg} h_f^s] \frac{\partial T_g}{\partial P} \\ - \Delta t [Q_{wfp} - \Gamma_{wfp} h_g^s - \Gamma_{wgp} h_f^s] \frac{\partial T_g^s}{\partial P} \Big|_{P_s} - \Delta t [Q_{wft} - \Gamma_{wft} h_g^s - \Gamma_{wgt} h_f^s] \frac{\partial T_g^s}{\partial P} \Big|_P \quad (3.1-223)$$

$$A_{41} = A_{41} - 2\Delta t [\Gamma_{wfg} + \Gamma_{wgg}] \frac{\partial T_g}{\partial X_n} - 2\Delta t [\Gamma_{wfp} + \Gamma_{wgp}] \frac{\partial T_g^s}{\partial X_n} \quad (3.1-224)$$

$$A_{42} = A_{42} - 2\Delta t [\Gamma_{wfg} + \Gamma_{wgg}] \frac{\partial T_g}{\partial U_g} - 2\Delta t [\Gamma_{wfp} + \Gamma_{wgp}] \frac{\partial T_g^s}{\partial U_g} \quad (3.1-225)$$

$$A_{43} = A_{43} - 2\Delta t [\Gamma_{wff} + \Gamma_{wgf}] \frac{\partial T_f}{\partial U_f} \quad (3.1-226)$$

$$A_{45} = A_{45} - 2\Delta t [\Gamma_{wff} + \Gamma_{wgf}] \frac{\partial T_f}{\partial P} - 2\Delta t [\Gamma_{wfg} + \Gamma_{wgg}] \frac{\partial T_g}{\partial P} \\ - 2\Delta t [\Gamma_{wfp} + \Gamma_{wgp}] \frac{\partial T_g^s}{\partial P} \Big|_{P_s} - 2\Delta t [\Gamma_{wft} + \Gamma_{wgt}] \frac{\partial T_g^s}{\partial P} \Big|_P \quad (3.1-227)$$

### 3.1.9 Numerical Solution of Boron Transport Equation

The boron field and its attendant modeling assumptions were discussed in Section 3.1.1.3. Accurate calculation of the boron field is required to simulate the coupled hydrodynamics and neutron behavior of a reactor. Recent advances in shock-capturing schemes or the TVD schemes (the oscillation-suppression strategy of the total-variation diminishing scheme) achieve impressive results for the numerical solution of the advective transport equations.<sup>3.1-19,3.1-20,3.1-21</sup> These schemes use locally varying positive artificial diffusion or viscosity (first order upwind) to suppress oscillations combined with local negative viscosity (such as first order downwinding) to compress or steepen the front. Rider and Woodruff<sup>3.1-22</sup> reported that an algorithm using a second-order accurate Godunov method with a highly compressive limiter can

adequately solve the advective transport equation for solute tracking. This method is chosen to solve the boron transport Equation (3.1-51) because it is consistent with RELAP5 numerics and is applicable to complex geometry.

A second-order accurate Godunov method to solve the boron transport equation was implemented in RELAP5/MOD3. The new method significantly improves the results as compared with that using the highly diffusive first-order upwind difference previously used.

The equation governing boron transport, Equation (3.1-51), can be rewritten in a control volume ( $V$ ) with surface area  $A$  as:

$$\int_V \frac{\partial \rho_b}{\partial t} dV + \int_A \rho_b v_f \cdot dA = 0 . \quad (3.1-228)$$

The use of the second-order accurate Godunov method to solve Equation (3.1-228) is well documented by Rider and Woodruff. The essential numerics are summarized below.

The numerical solution of Equation (3.1-228) can be written as

$$\rho_{b,L}^{n+1} = \rho_{b,L}^n + \frac{\Delta t}{V_L} A_j F_j^n - \frac{\Delta t}{V_L} A_{j+1} F_{j+1}^n . \quad (3.1-229)$$

The flux  $F$  is expressed by

$$F_{j+1}^n = \frac{1}{2} \left( v_{f_{j+1}}^{n+\frac{1}{2}} (\rho_{b,j+1}^n + \rho_{b,j+1}^n) + \left| v_{f_{j+1}}^{n+\frac{1}{2}} \right| (\rho_{b,j+1}^n - \rho_{b,j+1}^n) \right) , \quad (3.1-230)$$

$$v_{f_{j+1}}^{n+\frac{1}{2}} = v = \frac{1}{2} \left( v_{f_{j+1}}^{n+1} + v_{f_{j+1}}^n \right) , \quad (3.1-231)$$

$$\rho_{b,j+1}^n = \rho_{b,L}^n + \left( \frac{1}{2} \Delta x_L \right) \left( 1 - \frac{v \Delta t}{\Delta x_L} \right) \bar{S}_L \quad (3.1-232)$$

and

$$\rho_{b,j+1}^n = \rho_{b,M}^n - \left( \frac{1}{2} \Delta x_M \right) \left( 1 + \frac{v \Delta t}{\Delta x_M} \right) \bar{S}_M . \quad (3.1-233)$$

The cell-centered limited gradient  $\bar{S}_L$  is given as

$$S_L = (1 + \theta_L \omega_L) \Phi(r, 1) S_{j+1} = (1 + \theta_L \omega_L) \Phi(r, 1) \left( \frac{\rho_{b,M}^n - \rho_{b,L}^n}{\Delta x_{j+1}} \right) . \quad (3.1-234)$$

Note that both the superbee limiter of Roe<sup>3.1-23</sup>  $\Phi(r, 1)$  and artificial compression<sup>3.1-24</sup>  $(1 + \theta_L \omega_L)$  are introduced. This step is necessary because the number of grid points in modeling the reactor system tend to be relatively small. It also ensures that the method is a TVD scheme.<sup>3.1-21</sup> The superbee limiter is defined as

$$\Phi(r, 1) = \max(0, \min(2r, 1), \min(r, 2)) \quad (3.1-235)$$

where

$$r = \frac{S_j}{S_{j+1}} \quad (3.1-236)$$

$$S_j = \frac{\rho_{b,L}^n - \rho_{b,K}^n}{\Delta x_j} \quad (3.1-237)$$

and

$$S_{j+1} = \frac{\rho_{b,M}^n - \rho_{b,L}^n}{\Delta x_{j+1}} \quad (3.1-238)$$

In the artificial compression  $(1 + \theta_L \omega_L)$ , the discontinuity detector  $\theta_L$  is given as

$$\theta_L = \frac{|1 - r|}{1 + |r|} . \quad (3.1-239)$$

The parameter  $\omega_L$  is chosen to be a function of the local Courant number  $v_L = \frac{v_L \Delta t}{\Delta x_L}$ ,

$$\omega_L = \min(v_L, 1 - v_L) . \quad (3.1-240)$$

In modeling a reactor system, there are components containing volumes to which multiple junctions are connected to form a multi-dimensional flow network. The cell-centered limited gradient  $\bar{S}_L$  is set to zero in these volumes and the Godunov scheme reverts to the upwind difference scheme for these

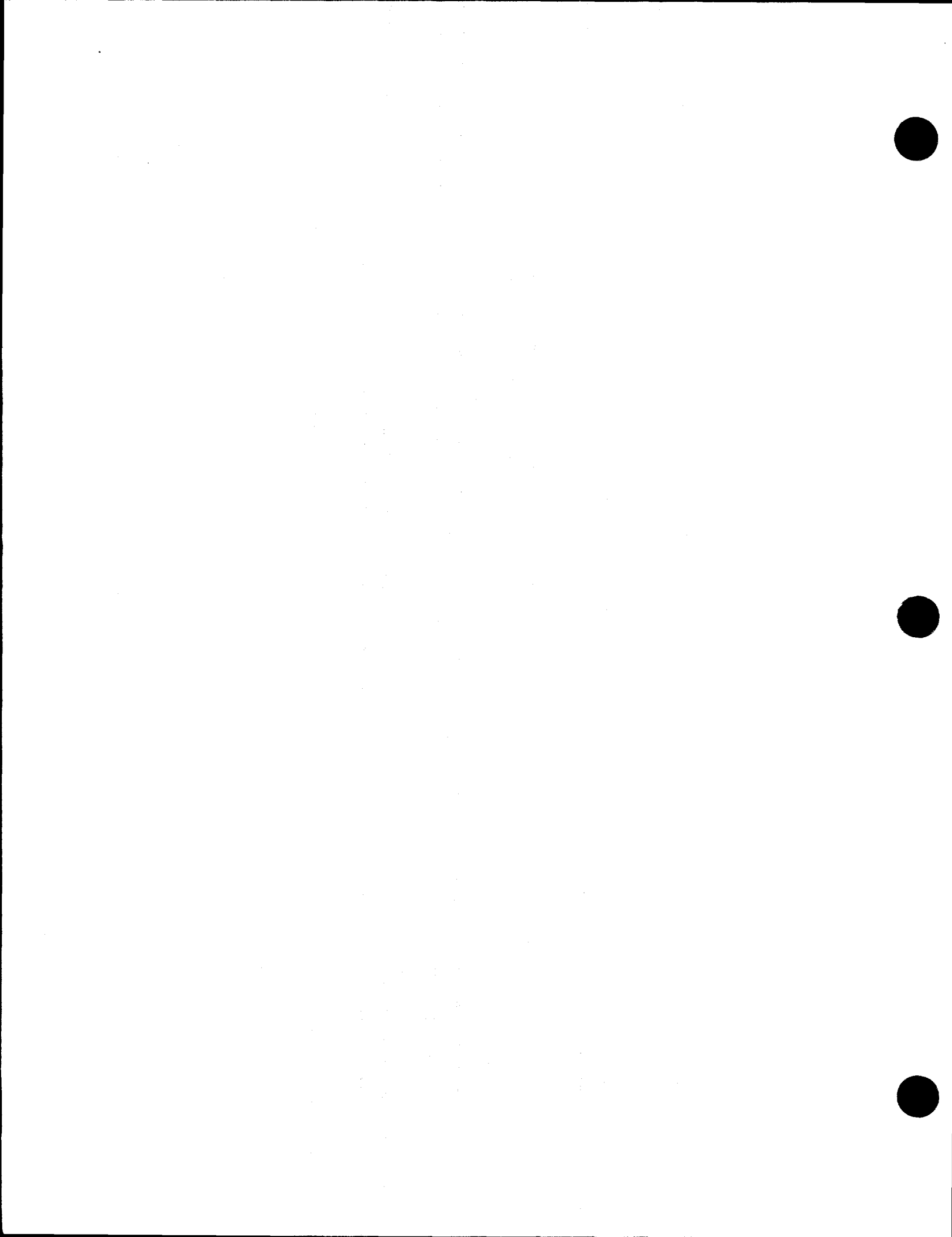
volumes. The default model for solute tracking is the upwind difference model but the Godunov scheme can be activated by the user in his input deck.

The above numerical solution is used when the semi-implicit scheme is chosen to solve the field equations. If the nearly-implicit scheme is employed to solve the field equations, the time-step used in the scheme may be greater than the material Courant limit. A subcycling calculation of the boron transport is implemented for the nearly-implicit scheme. In the method, the boron transport is integrated within each large time step taken by the advancement of the field equations. The time step used in the boron calculation is limited by the Courant condition. The fluid velocity used in the boron calculation is interpolated from the results of the field equations. The boron transport is calculated in such a fashion such that solutions of the field equations and boron transport are synchronized in the same large time step.

### 3.1.10 References

- 3.1-1. V. H. Ransom, *Course A--Numerical Modeling of Two-Phase Flows for Presentation at Ecole d'Ete d'Analyse Numerique*, EGG-EAST-8546, May 1989.
- 3.1-2. M. Ishii, *Thermo-Fluid Dynamic Theory of Two-Phase Flow*, Collection de la Direction des Etudes d'Recherches of Electricite de France, 1975.
- 3.1-3. F. H. Harlow and A. A. Amsden, "Flow of Interpenetrating Material Phases," *Journal of Computational Physics*, 18, 1975, pp. 440-464.
- 3.1-4. P. S. Anderson, P. Astrup, L. Eget, and O. Rathman, "Numerical Experience with the Two-Fluid Model RISQUE," *Proceedings from Topical Meeting on Thermal Reactor Safety, Sun Valley, ID, July 31-August 4, 1977*.
- 3.1-5. N. Zuber, "On the Dispersed Two-Phase Flow in the Laminar Flow Regime," *Chemical Engineering Science*, 19, 1964, pp. 897-917.
- 3.1-6. L. Van Wijngaarden, "Hydrodynamic Interaction between Gas and Bubbles in Liquid," *Journal of Fluid Mechanics*, 77, 1, 1976, pp. 27-44.
- 3.1-7. R. T. Lahey, Jr., "RPI Two-Phase Flow Modeling Program," *Fifth Water Reactor Safety Research Information Meeting, Washington, D.C., November 7-11, 1977*.
- 3.1-8. D. A. Drew, L. Y. Cheng, and R. T. Lahey, Jr., "The Analysis of Virtual Mass Effects in Two-Phase Flow," *International Journal of Multiphase Flow*, 5, 1979, pp. 233-242.
- 3.1-9. J. A. Trapp and V. H. Ransom, "A Choked-Flow Calculation Criterion for Nonhomogeneous, Nonequilibrium Two-Phase Flows," *International Journal of Multiphase Flow*, 8, 6, 1982, pp. 669-681.
- 3.1-10. A. R. Curtis and J. K. Reid, *FORTRAN Subroutines for the Solution of Sparse Sets of Linear Equations*, AERE-R6844, 1971.

- 3.1-11. D. Gidaspow (Chairman), "Modeling of Two-Phase Flow," *Proceedings of Round Table Discussion RT-1-2 at the Fifth International Heat Transfer Conference, Tokyo, Japan, September 3-7, 1974, also in ASME Journal of Heat Transfer, 3, 1974.*
- 3.1-12. J. D. Ramshaw and J. A. Trapp, "Characteristics, Stability, and Short-Wavelength Phenomena in Two-Phase Flow Equation Systems," *Nuclear Science and Engineering, 66, 1978, pp. 93-102.*
- 3.1-13. J. J. Dongarra, C. B. Moler, J. R. Bunch, and G. W. Stewart, *LINPACK User's Guide*, SIAM, Philadelphia, PA, 1979.
- 3.1-14. H. B. Stewart, "Fractional Step Methods for Thermodynamic Calculations," *Journal of Computational Physics, 40, 1981, pp. 77-90.*
- 3.1-15. J. H. Mahaffy, "A Stability-Enhancing Two-Step Method for Fluid Flow Calculations," *Journal of Computational Physics, 46, 1982, pp. 329-341.*
- 3.1-16. J. A. Trapp and R. A. Riemke, "A Nearly-Implicit Hydrodynamic Numerical Scheme for Two-Phase Flows," *Journal of Computational Physics, 66, 1986, pp. 62-68.*
- 3.1-17. A. S. Shieh and R. A. Riemke, "Diagonally Dominant Enhancement Methods for Matrix Solvers in RELAP5," *Nuclear Science and Engineering, 105, 1990, pp. 404-408.*
- 3.1-18. V. H. Ransom et al., *RELAP5/MOD1 Code Manual*, NUREG/CR-1826, EGG-2070, March 1982.
- 3.1-19. H. C. Yee, *Upwind and Symmetric Shock-Capturing Schemes*, NASA Technical Memorandum 1000916, Ames Research Center, 1987.
- 3.1-20. B. P. Leonard, *Universal Limiter for Transient Interpolation Modeling of the Advective Transport Equation: The ULTIMATE Conservative Difference Scheme*, NASA Technical Memorandum 1000916, Ames Research Center, 1988.
- 3.1-21. W. J. Rider, *Design of High Resolution Upwind Shock-Capturing Methods*, LA-12327-T, Los Alamos National Laboratory, 1992.
- 3.1-22. W. J. Rider and S. B. Woodruff, *High-Order Solute Tracking in Two-Phase Thermal Hydraulics*, LA-UR-91-2263, Los Alamos National Laboratory, 1991.
- 3.1-23. P. L. Roe, "Some Contributions to the Modeling of Discontinuous Flow," *Lectures in Applied Mathematics, Vol. 22, Part 2, pp. 163-193, 1975.*
- 3.1-24. H. C. Yee, and R. F. Warming, "Implicit Total Variation Diminishing (TVD) Schemes for Steady-State Calculations," *Journal of Computational Physics, Vol. 57, pp. 327-360, 1985.*



## 3.2 State Relationships

The six-equation model uses five independent state variables with an additional equation for the noncondensable gas component. The independent variables are chosen to be  $P$ ,  $\alpha_g$ ,  $U_g$ ,  $U_f$ , and  $X_n$ . All the remaining thermodynamic variables (temperatures, densities, partial pressures, qualities, etc.) are expressed as functions of these five independent variables. In addition to these variables, several state derivatives are needed for some of the linearizations used in the numerical scheme. This section contains three parts. The first discusses the state property derivatives needed in the numerical scheme. The second section develops the appropriate derivative formulas for the single component case. The third section does the same for the two-phase, two-component case.

### 3.2.1 State Equations

To expand the time derivatives of the phasic densities in terms of these independent state variables using two-term Taylor series expansions, the following derivatives of the phasic densities are needed:

$$\left(\frac{\partial \rho_g}{\partial P}\right)_{U_g, X_n}, \left(\frac{\partial \rho_g}{\partial U_g}\right)_{P, X_n}, \left(\frac{\partial \rho_g}{\partial X_n}\right)_{P, U_g}, \left(\frac{\partial \rho_f}{\partial P}\right)_{U_f}, \left(\frac{\partial \rho_f}{\partial U_f}\right)_P.$$

The interphase mass and heat transfer models use an implicit (linearized) evaluation of the interphase temperature potentials  $T_f - T_I$  and  $T_g - T_I$ . The quantity  $T_I$  is the temperature that exists at the phase interface. For a single-component mixture, we have

$$T_I = T^s(P) \quad (3.2-1)$$

where the superscript  $s$  denotes a saturation value. In the presence of a noncondensable mixed with the steam, we assume<sup>3.2-1</sup>

$$T_I = T^s(P_s) \quad (3.2-2)$$

where  $P_s$  is the partial pressure of the steam in the gaseous phase. The gaseous phase properties for a two-component mixture can be described with three independent properties.<sup>3.2-2</sup> In particular, the steam partial pressure,  $P_s$ , can be expressed as

$$P_s = P_s(P, X_n, U_g) \quad (3.2-3)$$

Substituting Equation (3.2-3) into Equation (3.2-2) gives the interface temperature,  $T_I$ , as the desired function of  $P$ ,  $X_n$ , and  $U_g$ .<sup>a</sup> The implicit evaluation of the temperature potential in the numerical scheme requires the following derivatives of the phasic and interface temperatures:

$$\left(\frac{\partial T_g}{\partial P}\right)_{U_g, X_n}, \left(\frac{\partial T_g}{\partial U_g}\right)_{P, X_n}, \left(\frac{\partial T_g}{\partial X_n}\right)_{P, U_g}, \left(\frac{\partial T_f}{\partial P}\right)_{U_f}, \left(\frac{\partial T_f}{\partial U_f}\right)_P, \left(\frac{\partial T^s}{\partial P}\right)_{U_g, X_n}, \left(\frac{\partial T^s}{\partial U_g}\right)_{P, X_n}, \left(\frac{\partial T^s}{\partial X_n}\right)_{P, U_g}.$$

If we have a single component, the  $X_n$  derivatives are zero and

$$\left(\frac{\partial T^s}{\partial U_g}\right)_P = 0 \quad (3.2-4)$$

since  $T^s$  is only a function of  $P$  for this case.

In addition to these derivatives, the basic phasic properties as functions of  $P$ ,  $U_g$ ,  $U_f$ , and  $X_n$  are needed, along with the homogeneous equilibrium sound speed for the critical flow model.

The basic properties are calculated from thermodynamic tables<sup>3.2-3</sup> that tabulate saturation properties as a function of temperature, saturation properties as a function of pressure, and single-phase properties as a function of pressure and temperature. The properties and derivatives in the tables are saturation pressure, saturation temperature, specific volume ( $v$ ), specific internal energy, and three phasic derivatives, the isobaric thermal expansion coefficient ( $\beta$ ), the isothermal compressibility ( $\kappa$ ), and the specific heat at constant pressure ( $C_p$ ).

### 3.2.2 Single-Component, Two-Phase Mixture

For the purposes of this manual, a single-component, two-phase mixture is referred to as Case 1. Case 1 is straightforward. Liquid properties are obtained from the steam tables, given  $P$  and  $U_f$ . All the desired density and temperature derivatives can then be obtained from  $\kappa_f$ ,  $\beta_f$ , and  $C_{pf}$ .<sup>3.2-4</sup> The desired derivatives are given as

$$\left(\frac{\partial \rho_f}{\partial U_f}\right)_P = -\left(\frac{v_f \beta_f}{C_{pf} - v_f \beta_f P}\right) / v_f^2 \quad (3.2-5)$$

$$\left(\frac{\partial T_f}{\partial U_f}\right)_P = \left(\frac{1}{C_{pf} - v_f \beta_f P}\right) \quad (3.2-6)$$

a. The properties  $\rho_g$  and  $T_g$  could have initially been written with  $P_s$ ,  $X_n$ ,  $U_g$  as the independent arguments.

Equation (3.2-3) would then be used to write  $\rho_g$  and  $T_g$ , with  $P$ ,  $X_n$ , and  $U_g$  as the independent variables.

$$\left(\frac{\partial \rho_f}{\partial P}\right)_{U_f} = \left[ \frac{C_{pf}v_f\kappa_f - T_f(v_f\beta_f)^2}{C_{pf} - v_f\beta_f P} \right] / v_f^2 \quad (3.2-7)$$

$$\left(\frac{\partial T_f}{\partial P}\right)_{U_f} = -\left( \frac{Pv_f\kappa_f - T v_f \beta_f}{C_{pf} - v_f \beta_f P} \right) \quad (3.2-8)$$

Parallel formulae hold for the vapor phase, with  $P$  and  $U_g$  as the independent variables.

The only nonstandard feature involved in the evaluation of the formulae in Equations (3.2-5) through (3.2-8) is the calculation of  $v$ ,  $T$ ,  $\kappa$ ,  $\beta$ , and  $C_p$  if the steam is subcooled or the liquid is superheated, i.e., metastable states. A constant pressure extrapolation from the saturation state is used for the temperature and specific volume for metastable states. Using the first two terms of a Taylor series, this gives

$$T \approx T^s(P) + \frac{1}{C_p^s(P) - Pv^s(P)\beta^s(P)} [U - U^s(P)] \quad (3.2-9)$$

$$v \approx v^s(P) + v^s(P)\beta^s(P) [T - T^s(P)] \quad (3.2-10)$$

In these Equations, (3.2-9) and (3.2-10), the argument  $P$  indicates a saturation value.

To obtain the properties  $\beta$ ,  $\kappa$ , and  $C_p$  corresponding to the extrapolated  $v$  and  $T$ , the extrapolation formulas are differentiated. Taking definitions and the appropriate derivatives of Equation (3.2-9) and (3.2-10) gives

$$C_p(P, T) \Delta \left(\frac{\partial h}{\partial T}\right)_P = \left(\frac{\partial U}{\partial T}\right)_P + P \left(\frac{\partial v}{\partial T}\right)_P = C_p(P) \quad (3.2-11)$$

$$\beta(P, T) \Delta \frac{1}{v} \left(\frac{\partial v}{\partial T}\right)_P = \frac{v(P)\beta(P)}{v(P, T)} \quad (3.2-12)$$

$$\kappa(P, T) \Delta -\frac{1}{v} \left(\frac{\partial v}{\partial P}\right)_T = \{v(P) + [T - T(P)]v(P)\beta(P)\} \frac{\kappa(P)}{v(P, T)} - [T - T(P)]v(P) \left[ \frac{d\beta(P)}{dP} + \beta^2(P) \frac{dT(P)}{dP} \right] / v(P, T) \quad (3.2-13)$$

Equation (3.2-11) shows that the extrapolated  $C_p$  is equal to the saturation value  $C_p(P)$ . Equation (3.2-12) gives the extrapolated  $\beta$  as a function of the saturation properties and the extrapolated  $v$ . Equation (3.2-13) gives the extrapolated  $\kappa$  as a function of the extrapolated properties and saturation properties. The extrapolated  $\kappa$  in Equation (3.2-13) involves a change of saturation properties along the saturation line. In

particular,  $\frac{d\beta(P)}{dP}$  involves a second derivative of specific volume. Since no second-order derivatives are

available from the steam property tables, this term was approximated for the vapor phase by assuming that the fluid behaves as an ideal gas. With this assumption, the last term in Equation (3.2-13) vanishes and the appropriate formula for the vapor phase  $\kappa$  is

$$\kappa_g(P, T_g) = \kappa_g(P) \quad (3.2-14)$$

where Equation (3.2-10) has been used to simplify the results.

For the liquid phase extrapolation (superheated liquid), only the specific volume correction factor in Equation (3.2-13) was retained, i.e.,

$$\kappa_f(P, T_f) = \frac{v_f(P) \kappa_f(P)}{v_f(P, T_f)} \quad (3.2-15)$$

The homogeneous equilibrium sound speed (a) for a two-phase mixture is calculated from standard formulas (see Volume IV) using the appropriate saturation values for  $T$ ,  $v$ ,  $\kappa$ ,  $\beta$  and  $C_p$ . The sound speed formula

$$a^2 = v^2 \left( \frac{dP^s}{dT} \right)^2 / \left( X_e \left[ \frac{C_{pg}^s}{T^s} + v_g^s \frac{dP^s}{dT} \left( \kappa_g^s \frac{dP^s}{dT} - 2\beta_g^s \right) \right] + (1 - X_e) \left[ \frac{C_{pf}^s}{T^s} + v_f^s \frac{dP^s}{dT} \left( \kappa_f^s \frac{dP^s}{dT} - 2\beta_f^s \right) \right] \right) \quad (3.2-16)$$

is used, where from Clapeyron's equation

$$\frac{dP^s}{dT} = \frac{h_g^s - h_f^s}{T^s (v_g^s - v_f^s)}, \quad (3.2-17)$$

$$v = X_e v_g^s + (1 - X_e) v_f^s \quad (3.2-18)$$

and  $X_e$  is the equilibrium quality, which is given by

$$X_e = \frac{(\alpha_g \rho_g U_g + \alpha_f \rho_f U_f) - U_f^s}{U_g^s - U_f^s} \quad (3.2-19)$$

The sound speed,  $a$ , for both single-phase liquid and single-phase vapor is given by

$$a = v \left\{ \frac{\left( \frac{C_p}{T v \beta} \right)}{v \left[ \kappa \left( \frac{C_p}{T v \beta} \right) - \beta \right]} \right\}^{1/2} \quad (3.2-20)$$

and the thermodynamic variables are either liquid or vapor quantities, depending on the phase present.

### 3.2.3 Two-Component, Two-Phase Mixture

This case is referred to as Case 2. The liquid phasic properties and derivatives are calculated in exactly the same manner as described in Case 1 (see Section 3.2.2); we assume that the noncondensable component is present only in the gaseous phase.

The properties for the gaseous phase are calculated assuming a modified Gibbs-Dalton mixture of steam (real gas from steam table data) and an ideal noncondensable gas. The modified Gibbs-Dalton mixture is based upon the following assumptions:

$$P_n = \sum_{i=1}^N P_{ni} \quad (3.2-21)$$

$$P = P_n + P_s \quad (3.2-22)$$

$$U_g = X_n U_n + (1 - X_n) U_s \quad (3.2-23)$$

$$v_g = X_n v_n = (1 - X_n) v_s \quad (3.2-24)$$

where  $P_s$  and  $P_{ni}$  are the partial pressures of the steam and the individual noncondensable components, respectively. The internal energies,  $U_s$ ,  $U_n$ , and the specific volumes,  $v_s$ ,  $v_n$ , are evaluated at the gas temperature and the respective partial pressures. The vapor properties are obtained from the steam tables, and the noncondensable state equations are

$$P_n v_n = R_n T_g \quad (3.2-25)$$

and

$$U_n = \begin{cases} C_o T_g + U_o & T_g < T_o \\ C_o T_g + \frac{1}{2} D_o (T_g - T_o)^2 + U_o & T_g \geq T_o \end{cases} \quad (3.2-26)$$

where

$$R_n = \sum_{i=1}^N R_{ni} X_{ni} \quad (3.2-27)$$

$$C_o = \sum_{i=1}^N C_{o,ni} X_{ni} \quad (3.2-28)$$

$$D_o = \sum_{i=1}^N D_{o,ni} X_{ni} \quad (3.2-29)$$

$$U_o = \sum_{i=1}^N U_{o,ni} X_{ni} \quad (3.2-30)$$

$$T_o = 250 \text{ K.} \quad (3.2-31)$$

**Table 3.2-1** lists the values used by the code for  $R_{ni}$ ,  $C_{o,ni}$ ,  $D_{o,ni}$ , and  $U_{o,ni}$  in SI units. The values for  $R_{ni}$  are given as the universal gas constant 8314.3 J/kmole-K divided by the molecular weight (Kmole-kg).  $C_{o,ni}$  is the ideal specific heat at constant volume, i.e.,  $C_{o,ni} = 1.5 R_{ni}$  for a monatomic gas, and  $C_{o,ni} = 2.5 R_{ni}$  for a diatomic gas. The temperature  $T_o$  is the upper limit at which the ideal specific heat is no longer applicable, and the higher order effects have to be taken into account. The values of  $D_{o,ni}$  and  $U_{o,ni}$  are obtained by least-squares fitting to the data reported by Reynolds<sup>3.2-5</sup> for 250 K to 700 K.

**Table 3.2-1** Values of  $R_{ni}$ ,  $C_{o,ni}$ ,  $D_{o,ni}$ , and  $U_{o,ni}$  for various noncondensable gases.

Noncondensable Gas	$R_{ni}$ (J/kg•K)	$C_{o,ni}$ (J/kg•K)	$D_{o,ni}$ (J/kg•K <sup>2</sup> )	$U_{o,ni}$ (J/kg)
Helium	8314.3/ 4.002598	3115.839	0.003455924	13256.44
Hydrogen	8314.3/2.01593	10310.75	0.522573	182783.4
Nitrogen	8314.3/ 28.01403	741.9764	0.1184518	145725.884
Krypton	8314.3/ 83.800	148.824	0.0035	122666.5
Xenon	8314.3/ 131.300	94.9084	0.0035	122666.5
Air	8314.3/28.963	715.0	0.10329037	158990.52
Argon	8314.3/39.948	312.192	0.003517	122666.5

Given  $P$ ,  $U_g$ , and  $X_n$ , we must solve Equations (3.2-21) through (3.2-24) implicitly to find the state of the gaseous phase. If Equation (3.2-22) is used to eliminate  $P_n$ , and Equation (3.2-25) is used for  $v_n$ , Equations (3.2-23) and (3.2-24) can be written as

$$(1 - X_n)U_s + X_nU_n [T_g(U_s, P_s)] - U_g = 0 \quad (3.2-32)$$

and

$$(1 - X_n) \left[ \frac{v_s(U_s, P_s) P_s}{T_s(U_s, P_s)} \right] (P - P_s) - X_n R_n P_s = 0 \quad (3.2-33)$$

If  $P$ ,  $U_g$ , and  $X_n$  are known, Equations (3.2-32) and (3.2-33) implicitly determine  $U_s$  and  $P_s$ . [Equation (3.2-24) was divided by the temperature and multiplied by the partial pressures to obtain Equation (3.2-33).]

To obtain the derivatives needed in the numerical scheme, we must evaluate the derivatives of  $U_s$  and  $P_s$  with respect to  $P$ ,  $U_g$ , and  $X_n$ . These derivatives can be obtained from Equations (3.2-32) and (3.2-33) by the use of the chain rule and implicit differentiation. For example, taking the derivative of Equations (3.2-32) and (3.2-33) with respect to  $P$  [recall that  $P_s = P_s(P, U_g, X_n)$  and  $U_s = U_s(P, U_g, X_n)$ ], we obtain

$$\begin{bmatrix} X_n \left( \frac{dU_n}{dT_g} \right) \left( \frac{\partial T_g}{\partial P_s} \right)_{U_s} & 1 - X_n + X_n \left( \frac{dU_n}{dT_g} \right) \left( \frac{\partial T_g}{\partial U_s} \right)_{P_s} \\ - X_n R_n - (1 - X_n) R_s & \text{TERM2} \\ + \text{TERM1} & \end{bmatrix} \times \begin{bmatrix} \left( \frac{\partial P_s}{\partial P} \right)_{U_g, X_n} \\ \left( \frac{\partial U_s}{\partial P} \right)_{U_g, X_n} \end{bmatrix} = \begin{bmatrix} 0 \\ -(1 - X_n) R_s \end{bmatrix} \quad (3.2-34)$$

as a linear system of two equations determining

$$\left( \frac{\partial P_s}{\partial P} \right)_{U_g, X_n} \text{ and } \left( \frac{\partial U_s}{\partial P} \right)_{U_g, X_n}.$$

In Equation (3.2-34),

$$R_s = \frac{P_s v_s}{T_g} \quad (3.2-35)$$

is the equivalent gas constant for the steam vapor,

$$\text{TERM1} = (1 - X_n) P_n R_s \left[ \frac{1}{P_s} + \frac{1}{v_s} \left( \frac{\partial v_s}{\partial P_s} \right)_{U_s} - \frac{1}{T_g} \left( \frac{\partial T_g}{\partial P_s} \right)_{U_s} \right] \quad (3.2-36)$$

and

$$\text{TERM2} = (1 - X_n) P_n R_s \left[ \frac{1}{v_s} \left( \frac{\partial v_s}{\partial U_s} \right)_{P_s} - \frac{1}{T_g} \left( \frac{\partial T_g}{\partial U_s} \right)_{P_s} \right] \quad (3.2-37)$$

To obtain the derivatives of  $P_s$  and  $U_s$  with respect to  $U_g$  and  $X_n$ , we repeat the above development taking derivatives of Equations (3.2-32) and (3.2-33) with respect to  $U_g$  and  $X_n$ . In each case, linear equations parallel to those in Equation (3.2-34) are obtained. In fact, the left side matrix is exactly the same, and the right side vector changes.

Having obtained all the derivatives of  $P_s$  and  $U_s$ , it is relatively easy to obtain the derivatives needed for the gaseous phase. From the chain rule, we have

$$\left( \frac{\partial T_g}{\partial P} \right)_{U_g, X_n} = \left( \frac{\partial T_g}{\partial P_s} \right)_{U_s} \left( \frac{\partial P_s}{\partial P} \right)_{U_g, X_n} + \left( \frac{\partial T_g}{\partial U_s} \right)_{P_s} \left( \frac{\partial U_s}{\partial P} \right)_{U_g, X_n} \quad (3.2-38)$$

$$\left( \frac{\partial T_g}{\partial U_g} \right)_{P, X_n} = \left( \frac{\partial T_g}{\partial P_s} \right)_{U_s} \left( \frac{\partial P_s}{\partial U_g} \right)_{P, X_n} + \left( \frac{\partial T_g}{\partial U_s} \right)_{P_s} \left( \frac{\partial U_s}{\partial U_g} \right)_{P, X_n} \quad (3.2-39)$$

$$\left( \frac{\partial T_g}{\partial X_n} \right)_{P, U_g} = \left( \frac{\partial T_g}{\partial P_s} \right)_{U_s} \left( \frac{\partial P_s}{\partial X_n} \right)_{P, U_g} + \left( \frac{\partial T_g}{\partial U_s} \right)_{P_s} \left( \frac{\partial U_s}{\partial X_n} \right)_{P, U_g} \quad (3.2-40)$$

where

$$\left( \frac{\partial T_g}{\partial P_s} \right)_{U_s} \text{ and } \left( \frac{\partial T_g}{\partial U_s} \right)_{P_s}$$

are the standard phasic derivatives for the vapor phase. Equations (3.2-38) through (3.2-40) give all the desired gaseous temperature derivatives. The interface temperature derivatives are obtained from Clapeyron's equation and the known  $P_s$  derivatives, i.e.,

$$\left( \frac{\partial T_I}{\partial P} \right)_{U_g, X_n} = \frac{dT_I}{dP_s} \left( \frac{\partial P_s}{\partial P} \right)_{U_g, X_n} \quad (3.2-41)$$

$$\left( \frac{\partial T_I}{\partial U_g} \right)_{P, X_n} = \frac{dT_I}{dP_s} \left( \frac{\partial P_s}{\partial U_g} \right)_{P, X_n} \quad (3.2-42)$$

$$\left(\frac{\partial T_I}{\partial X_n}\right)_{P, U_g} = \frac{dT_I}{dP_s} \left(\frac{\partial P_s}{\partial X_n}\right)_{P, U_g} \quad (3.2-43)$$

where  $dT_I/dP_s$  is given by the reciprocal of Equation (3.2-17).

The derivatives of the densities can be obtained from  $v_g = X_n v_n$  or  $v_g = (1 - X_n) v_s$ , as these two formulae for the gaseous specific volume are equivalent [see Equation (3.2-24)]. A symmetric formula can be obtained by eliminating  $X_n$  from the above two formulae, giving

$$v_g = \frac{v_s v_n}{v_s + v_n} \quad (3.2-44)$$

Using Equation (3.2-44), we have for the derivatives of  $\rho_g$  with respect to  $P$

$$\left(\frac{\partial \rho_g}{\partial P}\right)_{U_g, X_n} = -\frac{1}{v_n^2} \left(\frac{\partial v_n}{\partial P}\right)_{U_g, X_n} - \frac{1}{v_s^2} \left(\frac{\partial v_s}{\partial P}\right)_{U_g, X_n} \quad (3.2-45)$$

Similar formulas are obtained when either  $U_g$  or  $X_n$  is the independent variable. The partial derivatives on the right side of Equation (3.2-45) are obtained from formulae exactly parallel to those in Equations (3.2-38) through (3.2-40) with  $T_g$  replaced by  $v_s$  or  $v_n$ . When taking the derivatives of  $v_n$ , remember that

$$v_n = \frac{R_n T_g (P_s, v_s)}{P - P_s} \quad (3.2-46)$$

Hence, an additional term appears in Equation (3.2-38) due to the direct dependence of  $v_n$  on  $P$ .

The homogeneous equilibrium sound speed (a) for a noncondensable-steam-water mixture is<sup>3.2-2</sup> taken from

$$a^2 = \frac{v^2}{-\left(\frac{\partial v}{\partial P}\right)_{s, \dot{x}_n}} \quad (3.2-47)$$

where

$$\begin{aligned} \left( \frac{\partial v}{\partial P} \right)_{s, \hat{x}_n} = & (1 - \hat{X}_f) \{ X_n^2 v_n \left[ \left( \beta_n \frac{1}{P'_s} + \kappa_n \right) \left( \frac{\partial P_s}{\partial P} \right)_{s, \hat{x}_n} - \kappa_n \right] + X_s^2 v_s \left( \beta_s \frac{1}{P'_s} - \kappa_s \right) \left( \frac{\partial P_s}{\partial P} \right)_{s, \hat{x}_n} \} \\ & + \hat{X}_f v_f \left[ \beta_f \frac{1}{P'_s} \left( \frac{\partial P_s}{\partial P} \right)_{s, \hat{x}_n} - \kappa_f \right] + (v_g - v_f) \left( \frac{\partial \hat{X}_s}{\partial P} \right)_{s, \hat{x}_n} \end{aligned} \quad (3.2-48)$$

$$P'_s = \frac{dP^s}{dT} = \frac{h_s^s - h_f^s}{T^s (v_s^s - v_f^s)} = \frac{S_s^s - S_f^s}{v_s^s - v_f^s} \quad (3.2-49)$$

Equation (3.2-48) is similar to Equation (18) in **Reference 3.2-2**, where the relation

$$\left( \frac{\partial T}{\partial P} \right)_{s, x_n} = \frac{1}{P'_s} \left( \frac{\partial P_s}{\partial P} \right)_{s, x_n} \quad (3.2-50)$$

is used. Equation (3.2-49) is the inverse of Equation (22) (Clausius-Clapeyron relation) in **Reference 3.2-2**. The quantities  $\left( \frac{\partial P_s}{\partial P} \right)_{s, \hat{x}_n}$  and  $\left( \frac{\partial \hat{X}_s}{\partial P} \right)_{s, \hat{x}_n}$  in Equation (3.2-48) are obtained from the following matrix equation

$$\begin{bmatrix} \hat{X}_n v_n \beta_n - \hat{X}_s v_s \beta_s & S_s - S_f \\ \frac{1}{P'_s} \left[ (\hat{X}_n C_{pn} + \hat{X}_s C_{ps}) \frac{1}{T_g} + \hat{X}_f C_{pf} \frac{1}{T_f} \right] & \end{bmatrix} \cdot \begin{bmatrix} \left( \frac{\partial P_s}{\partial P} \right)_{s, \hat{x}_n} \\ \left( \frac{\partial \hat{X}_s}{\partial P} \right)_{s, \hat{x}_n} \end{bmatrix} = \begin{bmatrix} \hat{X}_n v_n \beta_n + \hat{X}_f v_f \beta_f \\ \hat{X}_n v_n \kappa_n \end{bmatrix} \quad (3.2-51)$$

Equation (3.2-51) is from the first and third equations in Equation (19) in **Reference 3.2-2**, where Equation (3.2-50) is used as well as

$$\hat{X}_n v_n = \hat{X}_s v_s = \hat{X}_g v_g \quad (3.2-52)$$

In the above formulae,  $\hat{X}_s$ ,  $\hat{X}_n$ ,  $\hat{X}_g$ , and  $\hat{X}_f$  are, respectively, mass qualities for steam, noncondensable, gas, and liquid based on the total mixture mass;  $X_s$  and  $X_n$  are the mass qualities for steam and noncondensable based on the gas mixture mass. Thus, their definitions are

$$\hat{X}_s = \frac{M_s}{M_s + M_n + M_f} \quad (3.2-53)$$

$$\hat{X}_n = \frac{M_n}{M_s + M_n + M_f} \quad (3.2-54)$$

$$\hat{X}_g = X = \frac{M_s + M_n}{M_s + M_n + M_f} = \frac{M_g}{M_g + M_f} \quad (3.2-55)$$

$$\hat{X}_f = \frac{M_f}{M_s + M_n + M_f} = \frac{M_f}{M_g + M_f} \quad (3.2-56)$$

$$X_s = \frac{M_s}{M_s + M_n} \quad (3.2-57)$$

The liquid properties and derivatives are obtained as above for Case 1. To obtain the gaseous properties, Equations (3.2-32) and (3.2-33) must be solved iteratively. A global Newton iteration in two variables is used.<sup>3.2-6</sup> The iteration variables are  $P_s$  and  $U_s$ . The steam table subroutine is called once during each iteration to obtain all the needed steam vapor properties, and Equations (3.2-25) and (3.2-26) are used to obtain the air properties. Once the iteration has converged, the gaseous properties are determined from the formulas in this section.

The transport properties phasic viscosities  $\mu_g$ ,  $\mu_f$ , phasic thermal conductivities  $k_g$ ,  $k_f$ , and surface tension  $\sigma$  are evaluated as functions of the local thermodynamic properties. Correlations from ASME<sup>3.2-3</sup> and Schmidt<sup>3.2-7</sup> are used for steam and liquid water. The presence of noncondensables in the vapor phase are accounted for by using Wilke's semi-empirical formula<sup>3.2-8</sup> for  $\mu_g$ , and by using Mason and Saxena's analogous method<sup>3.2-9</sup> (with approved modification by Bird, Stewart, and Lightfoot<sup>3.2-10</sup>) for  $k_g$ .

Evaluation of the sound speed formulas at the saturated equilibrium state requires a second iteration. To avoid this extra iteration, the sound speed formulas were evaluated using the nonequilibrium state properties.

### 3.2.4 References

- 3.2-1. J. G. Collier, *Convective Boiling and Condensation*, 2nd Edition, New York: McGraw-Hill, 1981.
- 3.2-2. V. H. Ransom and J. A. Trapp, "Sound Speed Models for a Noncondensable Gas-Steam-Water Mixture," *Proceedings Japan-U.S. Seminar on Two-Phase Flow Dynamics*, Lake Placid, NY, July 29-August 3, 1984.
- 3.2-3. American Society of Mechanical Engineers, *Thermodynamic and Transport Properties of Steam*, United Engineering Center, 345 East 45th Street, New York, NY, 1967.

- 3.2-4. P. W. Bridgman, *Thermodynamics of Electrical Phenomena in Metals and a Condensed Collection of Thermodynamic Formulas*, New York: Dover Publications, 1961.
- 3.2-5. W. C. Reynolds, *Thermodynamic Properties in SI*, Stanford University, 1979.
- 3.2-6. J. Dennis and R. Schnabel, *Quasi-Newton Methods for Unconstrained Nonlinear Problems*, Prentice-Hall, 1983.
- 3.2-7. E. Schmidt, *Properties of Water and Steam in SI Units*, New York: Springer-Verlag, 1969.
- 3.2-8. C. R. Wilke, "A Viscosity Equation for Gas Mixtures," *J. Chem Physics*, 18, 1950, pp. 517-519.
- 3.2-9. E. A. Mason and S. C. Saxena, "Approximate Formula for the Thermal Conductivity of Gas Mixtures," *The Physics of Fluid*, 1, 1958, pp. 361-369.
- 3.2-10. R. B. Bird, W. E. Stewart, and E. N. Lightfoot, *Transport Properties*, New York: Wiley and Sons, 1960.

### 3.3 Constitutive Models

The constitutive relations include models for defining flow regimes and flow-regime-related models for interphase drag and shear, the coefficient of virtual mass, wall friction, wall heat transfer, and interphase heat and mass transfer. Heat transfer regimes are defined and used for wall heat transfer. For the virtual mass, a formula based on the void fraction is used.

In RELAP5/MOD2, all constitutive relations were evaluated using volume-centered conditions; junction parameters, such as interfacial friction coefficients, were obtained as volume-weighted averages of the volume-centered values in the volumes on either side of a junction. The procedure for obtaining junction parameters as averages of volume parameters was adequate when the volumes on either side of a junction were in the same flow regime and the volume parameters were obtained using the same flow regime map (i.e., both volumes were horizontal volumes or both volumes were vertical volumes). Problems were encountered when connecting horizontal volumes to vertical volumes.

These problems have been eliminated in RELAP5/MOD3 by computing the junction interfacial friction coefficient using junction properties so that the interfacial friction coefficient would be consistent with the state of the fluid being transported through the junction. The approach has been used successfully in the TRAC-B code.<sup>3.3-1,3.3-2</sup> The independent variables in the flow regime maps for the volumes and junctions are somewhat different as a result of the finite-difference scheme and staggered mesh used in the numerical scheme.

The volume and junction flow regime maps will be discussed separately, followed by a discussion of the interphase drag and shear, coefficient of virtual mass, wall friction, wall heat transfer models, and interphase heat and mass transfer.

The volume map is based on volume quantities. It is used for interphase heat and mass transfer, wall friction, and wall heat transfer. The constitutive relations, in general, include flow regime effects for which simplified mapping techniques have been developed to control the use of constitutive relation correlations. The flow regime maps are based on the work of Taitel and Dukler<sup>3.3-3,3.3-4</sup> and Ishii.<sup>3.3-5,3.3-6,3.3-7</sup>

Taitel and Dukler have simplified flow regime classifications and developed semi-empirical relations to describe flow regime transitions. However, some of their transition criteria are quite complex, and further simplification has been carried out in order to efficiently apply these criteria in RELAP5. In addition, post-critical heat flux (CHF) regimes as suggested by Ishii<sup>3.3-5</sup> are included.

Four flow regime maps are used: a horizontal map for flow in pipes, a vertical map for flow in pipes and bundles, a high mixing map for flow in pumps, and an ECC mixer map.

#### 3.3.1 Vertical Volume Flow Regime Map

The vertical flow regime map (for both up and down flow) is for volumes whose elevation angle  $\phi$  is such that  $45 < |\phi| \leq 90$  degrees. This map is modeled as nine regimes--four for pre-CHF heat transfer, four for post-CHF heat transfer, and one for vertical stratification. For pre-CHF heat transfer, the regimes modeled are the bubbly, slug, annular mist, and mist-pre-CHF regimes. Formulations for the first three regimes were utilized by Vince and Lahey<sup>3.3-8</sup> to analyze their data. The mist-pre-CHF regime was added for smoothness. For post-CHF heat transfer, the bubbly, slug, and annular mist regimes are transformed to the inverted annular, inverted slug, and mist regimes, respectively, as suggested by Ishii.<sup>3.3-5</sup> The mist-

post-CHF regime was added for symmetry with the mist-pre-CHF regime. The mist flow regimes consist of pure droplet flow where all of the available liquid is assumed to be entrained and there is no liquid film on the wall. Unheated components are also modeled, utilizing the pre-CHF map. A schematic representing the pre-CHF, post-CHF, and transition regimes of the vertical flow regime map is shown in Figure 3.3-1. The schematic is three-dimensional, to illustrate flow regime transitions as functions of void fraction  $\alpha_g$ , average mixture velocity  $v_m$ , and boiling regime (pre-CHF, transition, and post-dryout) where

$$v_m = \frac{G_m}{\rho_m} \quad (3.3-1)$$

$$G_m = \alpha_g \rho_g |v_g| + \alpha_f \rho_f |v_f| \quad (3.3-2)$$

$$\rho_m = \alpha_g \rho_g + \alpha_f \rho_f \quad (3.3-3)$$

The map consists of bubbly, slug, annular mist, and dispersed (droplet or mist) flows in the pre-CHF regime; inverted annular, inverted slug, and dispersed (droplet or mist) flows in post-dryout; and vertically stratified for sufficiently low mixture velocity  $v_m$ . Transition regions provided in the code are shown. The flow regime identifiers which appear in the printed output is shown for each of the regimes. The criteria for defining the boundaries for transition from one regime to another are given by the following correlations.

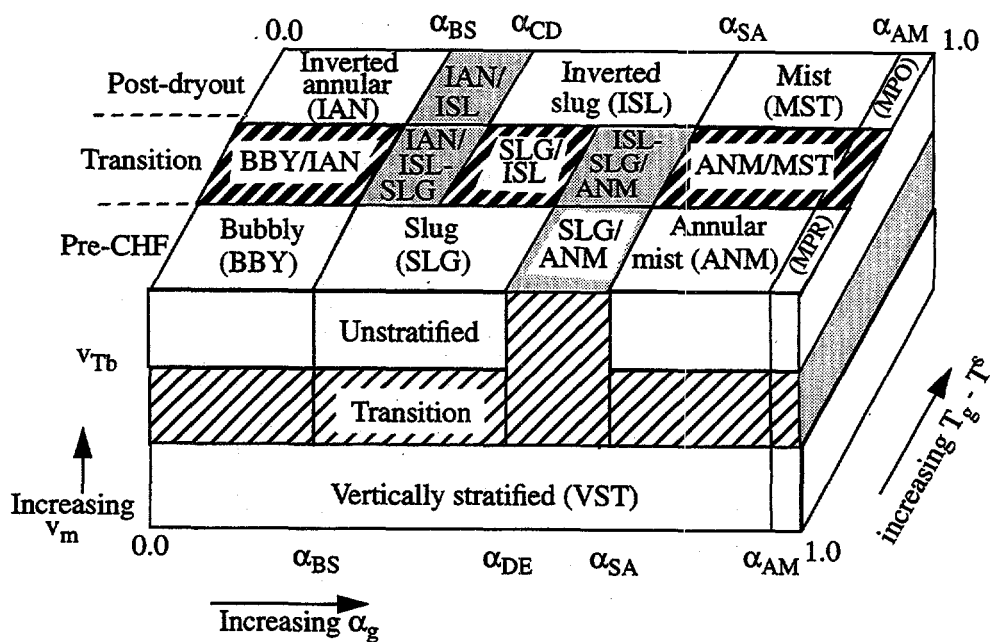


Figure 3.3-1 Schematic of vertical flow regime map with hatchings indicating transitions.

For the bubbly to slug transition, Taitel and Dukler<sup>3.3-3,3.3-4</sup> suggested that bubbly flow may not exist in tubes of small diameter where the rise velocity of small bubbles exceeds that of Taylor bubbles. The small bubble rise velocity is given by the correlation<sup>3.3-4</sup>

$$v_{sb} = 1.53 \left[ \frac{D^* \sigma}{D \rho_f} \right]^{1/2} = 1.53 \left[ \frac{g (\rho_f - \rho_g) \sigma}{\rho_f^2} \right]^{1/4} \quad (3.3-4)$$

and the Taylor bubble rise velocity is given by the correlation<sup>3.3-9</sup>

$$v_{Tb} = 0.35 D^* \left[ \frac{\sigma}{D \rho_f} \right]^{1/2} = 0.35 \left[ \frac{g D (\rho_f - \rho_g)}{\rho_f} \right]^{1/2} \quad (3.3-5)$$

(Note: in Reference 3.3-4,  $\rho_f - \rho_g$  is approximated as  $\rho_f$ ; see also Reference 3.3-6 and Reference 3.3-10.) Accordingly, the limiting tube diameter allowing the presence of bubbly flow is

$$D^* \geq 19.11 \quad (3.3-6)$$

where  $D^*$  is the dimensionless tube diameter,

$$D^* = D [g(\rho_f - \rho_g)/\sigma]^{1/2} \quad (3.3-7)$$

In the coding, 19.11 has been modified to 22.22 where this value was chosen based on comparisons with data during the developmental assessment of RELAP5/MOD2.<sup>3.3-11</sup> This is discussed further in Volume IV of this manual.

Equation (3.3-7) is the dimensionless ratio of tube diameter to film thickness times the Deryagin number, where the Deryagin number is the ratio of film thickness to capillary length. Also, in the limit, as the fluid properties approach the thermodynamic critical pressure,  $D^* = D$ .

For tubes with diameters satisfying the condition of Equation (3.3-6), the bubble-slug transition occurs at a void fraction  $\alpha_g = 0.25$  for low mass fluxes of  $G \leq 2000 \text{ kg/m}^2\text{s}$ . By combining this void criterion with Equation (3.3-6) and using 22.22 instead of 19.11, the bubble-slug transition criterion can be defined such that

$$\alpha_L = 0.25 \min [1.0, (D^* / 22.22)^8] \quad (3.3-8)$$

Hence, if the local void fraction,  $\alpha_g$ , exceeds the criterion of Equation (3.3-8), then bubbly flow cannot exist, since the rise velocity of small bubbles exceeds that of Taylor bubbles. The exponential power of 8 is used to provide a smooth variation of  $\alpha_L$  as  $D^*$  decreases.

At high mass fluxes of  $G_m \geq 3000 \text{ kg/m}^2 \cdot \text{s}$ , bubbly flow with finely dispersed bubbles can exist up to a void fraction,  $\alpha_g$ , of 0.5. Then, if the criterion is linearly interpolated between the upper and lower void limits, the bubbly-slug transition criterion can be written as

$$\alpha_{BS} = \alpha_L \quad (3.3-9)$$

for mass fluxes of  $G_m \leq 2000 \text{ kg/m}^2 \text{ s}$ ,

$$\alpha_{BS} = \alpha_L + 0.001 (G_m - 2000) (0.5 - \alpha_L) \quad (3.3-10)$$

for mass fluxes of  $2000 < G_m < 3000 \text{ kg/m}^2 \text{ s}$ , and

$$\alpha_{BS} = 0.5 \quad (3.3-11)$$

for mass fluxes of  $G_m \geq 3000 \text{ kg/m}^2 \text{ s}$ . The flow regime can therefore be said to be in the bubbly regime if  $\alpha_g < \alpha_{BS}$  and in the slug regime if  $\alpha_g \geq \alpha_{BS}$ .

The bubble-slug transition defined by Equations (3.3-9) to (3.3-11) is similar to that given by Taitel and Dukler,<sup>3.3-4</sup> except that their void fraction relation is converted into a form based on liquid and vapor superficial velocities, and finely dispersed bubbles are also distinguished from ordinary bubbles.

For the slug to annular transition, Taitel et al.<sup>3.3-4</sup> and Mishima and Ishii<sup>3.3-12</sup> indicate that the annular flow transition for upflow is principally governed by criteria of the form

$$j_g^* = \frac{\alpha_g v_g}{\left[ gD \frac{(\rho_f - \rho_g)}{\rho_g} \right]^{1/2}} \geq j_{g, crit}^* \quad (3.3-12)$$

and

$$Ku_g = \frac{\alpha_g v_g}{\left[ g\sigma \frac{(\rho_f - \rho_g)}{\rho_g^2} \right]^{1/4}} \geq Ku_{g, crit} \quad (3.3-13)$$

with the first criterion (flow reversal) controlling the transition in small tubes and the second criterion (droplet entrainment) applying in large tubes. McQuillan and Whalley<sup>3.3-13,3.3-14</sup> considered the above criteria using

$$j_{g,crit}^* = 1 \quad (3.3-14)$$

and

$$Ku_{g,crit} = 3.2 \quad (3.3-15)$$

and obtained good predictions of the annular flow boundary in each case. Putney<sup>3.3-15</sup> has found that better agreement can be obtained if annular flow occurs when either criterion is satisfied. In terms of the slug-to-annular transition void fraction  $\alpha_{SA}$ , Putney indicates that these criteria take on the form

$$\alpha_{SA} = \min [\alpha_{crit}^f, \alpha_{crit}^e] \quad (3.3-16)$$

where

$$\alpha_{crit}^f = \frac{1}{v_g} \left[ \frac{gD(\rho_f - \rho_g)}{\rho_g} \right]^{1/2} \text{ for upflow} \quad (3.3-17)$$

$$\alpha_{crit}^f = 0.75 \text{ for downflow and countercurrent flow} \quad (3.3-18)$$

and

$$\alpha_{crit}^e = \frac{3.2}{v_g} \left[ \frac{g\sigma(\rho_f - \rho_g)}{\rho_g^2} \right]^{1/4} \quad (3.3-19)$$

where the void fraction for flow reversal,  $\alpha_{crit}^f$ , is found by combining Equations (3.3-12) and (3.3-14) and the void fraction for droplet entrainment,  $\alpha_{crit}^f$ , is found by combining Equations (3.3-13) and (3.3-15).

The transition region between the slug flow and annular-mist flow regimes is defined by  $\alpha_{DE}$  and  $\alpha_{SA}$  where

$$\alpha_{DE} = \max (\alpha_{BS}, \alpha_{SA} - 0.05) \quad (3.3-20)$$

The minimum void fraction for annular-mist flow,  $\alpha_{SA}$ , is constrained to lie between 0.5 and 0.9. The flow regime is said to be in the slug regime if  $\alpha_g \leq \alpha_{SA}$  and in the annular-mist regime if  $\alpha_g > \alpha_{SA}$ . For the transition between annular-mist and mist-pre-CHF (regime MPR in Figure 3.3-1), the value of  $\alpha_{AM}$  is

$$\alpha_{AM} = 0.9999 \quad (3.3-21)$$

where all of the available liquid is assumed to be in the form of droplets in the mist regimes.

If the hydrodynamic volume has heat flux from a surrounding wall to the vapor or the reflood model is turned on for that wall, and the vapor temperature is more than 1°K superheated, then the flow regime is a post-CHF regime. For post-CHF heat transfer, the above formulations are also used to define the regimes. Equations (3.3-9) through (3.3-11) define the inverted-annular to inverted-slug regime transition, Equation (3.3-16) defines the inverted-slug-to-mist regime transition, and Equation (3.3-21) defines the mist-to-mist-post-CHF regime transition.

At low mass fluxes, the possibility exists for vertically stratified conditions. In RELAP5, vertical flow in a volume cell is considered to be stratified if the following criteria are met:

- The void fraction for the volume above is  $> 0.7$ , and the difference between the void fractions in the volume in question and the void fraction in the volume above or below is  $> 0.2$ . This criterion is the same as the level detection logic for a normal profile from TRAC-B<sup>3.3-1,3.3-2</sup>
- The magnitude of the volume average mixture mass flux is less than the Taylor bubble rise velocity mass flux. The Taylor bubble criterion is based on the Taylor bubble velocity given by Equation (3.3-5) such that

$$G_m < \rho_m v_{Tb} \quad (3.3-22)$$

where  $v_{Tb}$  is the Taylor bubble velocity. Hence, if Equation (3.3-22) is true, then transition to vertical stratification exists; and if Equation (3.3-22) is false, then transition to vertical stratification does not exist. Fixed numbers are not shown on Figure 3.3-1 for the mass flux limits for the vertical stratification region because these depend on  $v_{Tb}$ . The vertical stratification model does not calculate a mixture level position and is not intended to be a mixture level model. A more mechanistic level tracking model is described in Section 3.4.8.

The transition region between inverted slug flow and inverted annular flow regimes is defined by  $\alpha_{BS}$  and  $\alpha_{CD}$  where

$$\alpha_{CD} = \alpha_{BS} + 0.2 \quad (3.3-23)$$

### 3.3.2 Horizontal Volume Flow Regime Map

The horizontal flow regime map is for volumes whose elevation angle  $\phi$  is such that  $0 \leq |\phi| \leq 45$  degrees. This map is similar to the vertical flow regime map except that the post-CHF regimes are not included, and a horizontally stratified regime replaces the vertically stratified regime. The horizontal flow regime map therefore consists of horizontally stratified, bubbly, slug, annular mist, and mist-pre-CHF regimes. A schematic for the horizontal flow regime map is shown in Figure 3.3-2. The criteria for the

bubbly-to-slug and the slug to annular mist regimes are also similar to those for the vertical map, except that the bubbly to slug transition criterion is a constant.

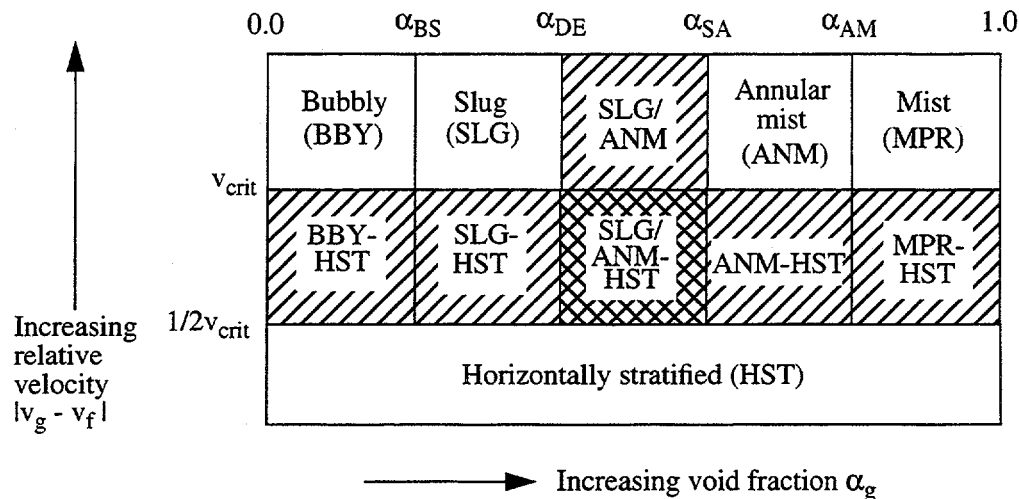


**Figure 3.3-2** Schematic of horizontal flow regime map with hatchings indicating transition regions.

$$\alpha_{BS} = 0.25 \quad G_m \leq 2000 \text{ kg/m}^2\text{-s} \quad (3.3-24)$$

$$= 0.25 + 0.00025 (G_m - 2000) \quad 2000 < G_m < 3000 \text{ kg/m}^2\text{-s}$$

$$= 0.5 \quad G_m \geq 3000 \text{ kg/m}^2\text{-s}$$

and the minimum void fraction for annular-mist flow,  $\alpha_{SA}$ , is a constant

$$\alpha_{SA} = 0.8 \quad (3.3-25)$$

and the transition region between slug flow and annular-mist flow regimes is defined by  $\alpha_{DE}$  and  $\alpha_{SA}$  where

$$\alpha_{DE} = 0.75 \quad (3.3-27)$$

The annular-mist to mist pre-CHF transition criterion is

$$\alpha_{AM} = 0.9999 \quad (3.3-28)$$

The criterion defining the horizontally stratified regime is based on the one developed by Taitel and Dukler.<sup>3.3-3</sup> According to Taitel and Dukler, the flow field is horizontally stratified if the vapor velocity satisfies the condition

$$|v_g| < v_{crit} \quad (3.3-29)$$

where  $v_{crit}$  is the gas velocity above which waves on the horizontal interface will begin to grow and is given by

$$v_{crit} = \frac{1}{2} \left[ \frac{(\rho_f - \rho_g) g \alpha_g A}{\rho_g D \sin \theta} \right]^{\frac{1}{2}} (1 - \cos \theta) \quad (3.3-30)$$

where  $\theta$  is given by the solution of Equation (3.1-73).

This condition is modified in the code to handle situations where the flow is stratified but the liquid is not stagnant as was assumed by Taitel and Dukler.<sup>3.3-3</sup> The flow is horizontally stratified if the phasic velocity difference satisfies the condition

$$|v_g - v_f| < v_{crit} \quad (3.3-31)$$

and the mass flux satisfies the condition

$$G_m < 3000 \text{ kg/m}^2\text{-s} \quad (3.3-32)$$

and the angle  $\theta$  (see Figure 3.1-2) is related to the liquid level with respect to the bottom of the volume.

If the horizontal stratification conditions of Equations (3.3-31) and (3.3-32) are met, then the flow field undergoes a transition to the horizontally stratified flow regime. If the conditions of Equations (3.3-31) and (3.3-32) are not met, then the flow field undergoes a transition to the bubbly, slug, annular mist, or mist-pre-CHF flow regime.

### 3.3.3 High Mixing Volume Flow Regime Map

The high mixing flow regime map (used in pumps) is based on vapor void fraction,  $\alpha_g$ , and consists of a bubbly regime for  $\alpha_g \leq 0.5$ , a mist regime for  $\alpha_g \geq 0.95$ , and a transition regime for  $0.5 < \alpha_g < 0.95$ . The transition regime is modeled as a mixture of bubbles dispersed in liquid and droplets dispersed in vapor. A schematic for the high mixing flow regime map is shown in Figure 3.3-3.

### 3.3.4 ECC Mixer Volume Flow Regime Map

Prior to the introduction of the ECCMIX component into RELAP5/MOD3, RELAP5 included three flow regime maps, as described in the RELAP5/MOD2 manual<sup>3.3-16</sup> and in the RELAP5/MOD2 models

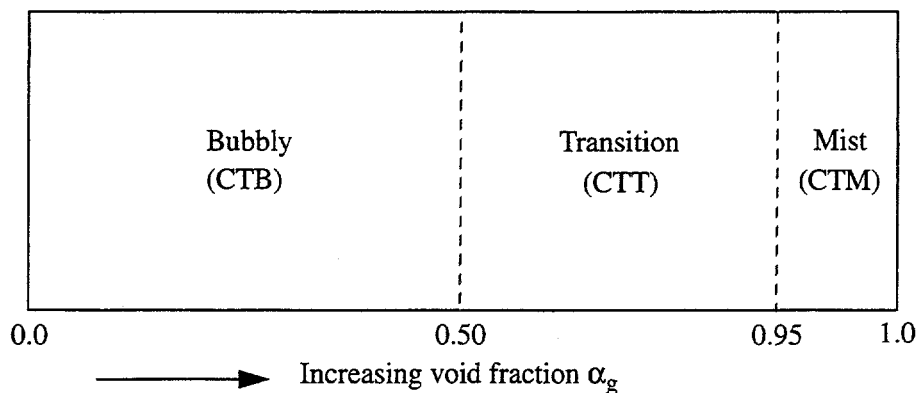


**Figure 3.3-3** Schematic of high mixing volume flow regime map.

and correlations report.<sup>3.3-17</sup> However, none of those would applied specifically to the condensation process in a horizontal pipe near the emergency core coolant (ECC) injection port. A flow regime map for condensation inside horizontal tubes is reported by Tandon et al.,<sup>3.3-18</sup> and it was considered a more suitable basis for interfacial heat transfer calculation in condensation for this geometry. According to **Reference 3.3-18**, the two-phase flow patterns during condensation inside a horizontal pipe may be identified in terms of the local volumetric ratio of liquid and vapor,  $(1 - \alpha)/\alpha$ , and the nondimensional vapor velocity,  $v_g^*$ , where

$$v_g^* = X_f G / [g D \rho_g (\rho_f - \rho_g)]^{1/2}$$

$$X_f = (\alpha_g \rho_g v_g) / (\alpha_g \rho_g v_g + \alpha_f \rho_f v_f)$$

$$G = \alpha_g \rho_g v_g + \alpha_f \rho_f v_f.$$

Although, the condensation flow regime map of Tandon et al.,<sup>3.3-18</sup> does not include any zone for bubbly flow; the existence of a bubbly flow regime at very low void fractions cannot be logically excluded, particularly in a highly turbulent liquid flow. For this reason, a region of bubbly flow was included for void fractions less than 20% ( $\alpha_g \leq 0.2$ ). Furthermore, to protect against failure of the numerical solution, it is necessary to specify some reasonable flow pattern for every combination of the volumetric ratio and  $v_g^*$  and to include transition zones around some of the boundaries between different flow patterns. The transition zones are needed for interpolation between the calculated values of the correlations for the interfacial heat transfer and friction that apply for the different flow patterns. These interpolations prevent discontinuities that would otherwise exist and that could make the numerical solutions very difficult. With these considerations, the flow regime map of **Reference 3.3-18** was modified, as shown in **Figure 3.3-4**. The modified condensation flow regime map comprises eleven different zones that include six basic patterns and five interpolation zones. **Table 3.3-1** shows a list of the basic flow patterns and the interpolation zones for the ECCMIX component, with their acronyms and flow regime numbers, that are printed out in the RELAP5/MOD3 output.

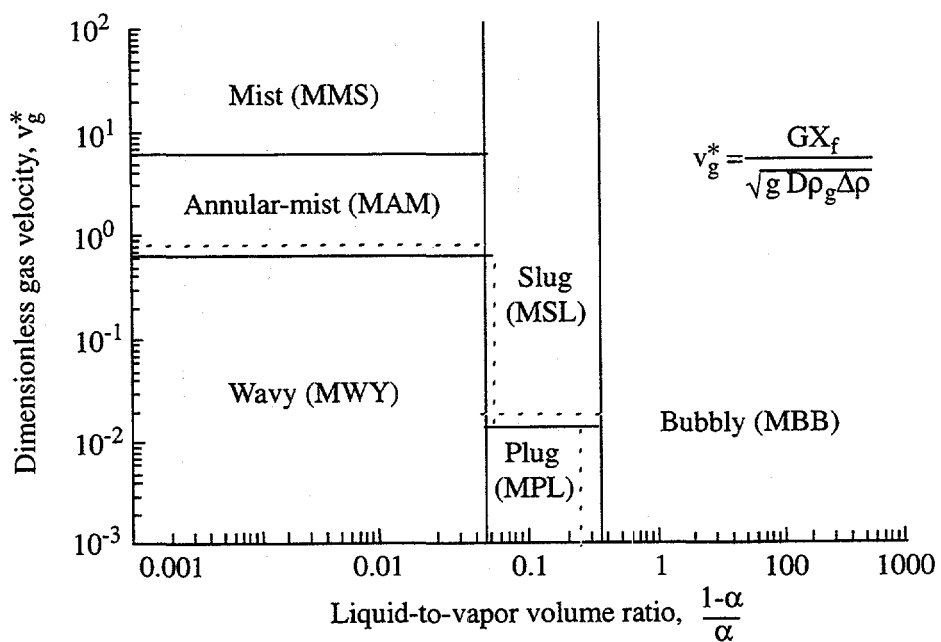


Figure 3.3-4 Schematic of ECC mixer volume flow regime map (modified Tandon et al.<sup>3.3-18</sup>).

Table 3.3-1 List of flow regimes in the ECCMIX component.

Flow Regime Number <sup>a</sup>	Flow Regime	Acronym	Remarks
14 <sup>a</sup>	Wavy	MWY	Basic pattern
15	Wavy/annular-mist	MWA	Transition between wavy and annular-mist flows
16	Annular-mist	MAM	Basic pattern
17	Mist	MMS	Basic pattern
18	Wavy/slug	MWS	Transition between wavy and slug flows
19	Wavy/plug/slug	MWP	Transition between wavy, plug, and slug flows

**Table 3.3-1** List of flow regimes in the ECCMIX component. (Continued)

Flow Regime Number <sup>a</sup>	Flow Regime	Acronym	Remarks
20	Plug	MPL	Basic pattern
21	Plug/slug	MPS	Transition between plug and slug flows
22	Slug	MSL	Basic pattern
23	Plug/bubbly	MPB	Transition between plug and bubbly flows
24	Bubbly	MBB	Basic pattern

a. Flow regime numbers 1 through 13 are used in RELAP5 for flow patterns in other components.

The variable names that are used in the coding for the coordinates of the condensation flow regime map are

$$\text{voider} = (1.0 - \alpha)/\alpha \quad (3.3-33)$$

$$\text{stargj} = v_g^* = X_f G / [g D \rho_g (\rho_f - \rho_g)]^{1/2} \quad (3.3-34)$$

In terms of these variables, the different zones of the flow regime map are:

If  $\text{voider} > 4.0$ , bubbly flow, MBB.

If  $3.0 < \text{voider} \leq 4.0$  and  $\text{stargj} < 0.01$ , transition, MPB.

If  $0.5 < \text{voider} \leq 4.0$  and  $\text{stargj} > 0.0125$ , slug flow, MSL.

If  $0.625 < \text{voider} \leq 4.0$ , and  $0.01 < \text{stargj} \leq 0.0125$ , transition, MPS.

If  $0.5 < \text{voider} \leq 3.0$ , and  $\text{stargj} \leq 0.01$ , plug flow, MPL.

If  $0.5 < \text{voider} \leq 0.625$ , and  $0.01 < \text{stargj} \leq 0.0125$ , transition, MWP.

If  $0.5 < \text{voider} \leq 0.625$ , and  $0.0125 < \text{stargj} \leq 1.0$ , transition, MWS.

If  $\text{voider} \leq 0.5$  and  $\text{stargj} \leq 1.0$ , wavy flow, MWY.

If voider  $\leq 0.5$ , and  $1.0 < \text{stargj} \leq 1.125$ , transition, MWA.

If voider  $\leq 0.5$ , and  $1.125 < \text{stargj} < 6.0$ , annular-mist, MAM.

If voider  $\leq 0.5$ , and  $\text{stargj} > 6.0$ , mist flow, MMS.

In the coding, each one of these regions is identified by a flow pattern identification flag, MFLAG, whose value varies from 1 for wavy flow to 11 for bubbly flow.

In addition to the transition zones that are shown on **Figure 3.3-4** and listed in **Table 3.3-1**, there are two other transitions, namely:

- Transition between wavy and plug flows
- Transition between annular-mist and mist (or droplet) flows.

Interpolations between the interfacial friction, interfacial heat transfer, and the wall friction rates for these transitions are performed through the gradual changes in the interfacial area in the first case and the droplet entrainment fraction in the second case. Hence, there was no need for specifying transition zones for these on the flow regime map.

### 3.3.5 Junction Flow Regime Map

The junction map is based on both junction and volume quantities. It is used for the interphase drag and shear, as well as the coefficient of virtual mass. The flow regime maps used for junctions are the same as used for the volumes and are based on the work of Taitel and Dukler,<sup>3.3-3,3.3-19</sup> Ishii,<sup>3.3-7</sup> and Tandon et al.<sup>3.3-18</sup>

Junction quantities used in the map decisions are junction phasic velocities, donor (based on phasic velocities) phasic densities, and donor (based on superficial mixture velocity) surface tension.

The junction void fraction,  $\alpha_{g,j}^*$ , is calculated from either of the volume void fractions of the neighboring volumes,  $\alpha_{g,K}$  or  $\alpha_{g,L}$ , using a donor direction based on the mixture superficial velocity,  $j_m$ . A cubic spline weighting function is used to smooth the void fraction discontinuity across the junction when  $|j_m| < 0.465$  m/s. The purpose of this method is to use a void fraction that is representative of the real junction void fraction. This is assumed to have the form

$$\alpha_{g,j}^* = w_j \cdot \alpha_{g,K} + (1 - w_j) \cdot \alpha_{g,L} \quad (3.3-35)$$

where

$$w_j = 1.0 \quad \text{when } j_m > 0.465 \text{ m/s} \quad (3.3-36)$$

$$w_j = x_1^2 (3 - 2x_1) \quad \text{when } -0.465 \text{ m/s} \leq j_m \leq 0.465 \text{ m/s} \quad (3.3-37)$$

$$w_j = 0 \quad \text{when } j_m < -0.465 \text{ m/s} \quad (3.3-38)$$

$$x_1 = \frac{j_m + 0.465}{0.93} \quad (3.3-39)$$

$$j_m = \dot{\alpha}_{g,j} v_{g,j} + \dot{\alpha}_{f,j} v_{f,j} \quad (3.3-40)$$

For horizontal stratified flow, the void fraction from the entrainment/pullthrough (or offtake) model is used (see Section 3.4.2). The case of vertical stratified flow will be discussed in Section 3.3.6.7. The junction mass flux is determined from

$$G_j = \dot{\alpha}_{g,j} \dot{\rho}_{g,j} |v_{g,j}| + \dot{\alpha}_{f,j} \dot{\rho}_{f,j} |v_{f,j}| \quad (3.3-41)$$

The methods for calculating  $\dot{\alpha}_{g,j}^*$  and  $G_j$  are the same ones that are used in TRAC-B.<sup>3.3-1,3.3-2</sup>

As with the volumes, four junction flow regime maps are used. They are a horizontal map for flow in pipes; a vertical map for flow in pipes/bundles; a high mixing map for flow in pumps; and an ECC mixer map. These will not be discussed in any detail because they are similar to the volumes flow regime maps. The decision of whether a junction is in the horizontal or vertical junction flow regime is done differently than for a volume. The junction angle is determined from either of the volume vertical inclination angles,  $\phi_K$  or  $\phi_L$ , input by the user using a donor direction based on the mixture superficial velocity,  $j_m$ . The formula used is similar to that used for the junction void fraction; however, it uses the sine of the angle. It is given by

$$\sin \phi_j = w_j \sin \phi_k + (1 - w_j) \sin \phi_L \quad (3.3-42)$$

The vertical flow regime map is for junctions whose elevation angle  $\phi_j$  is such that  $60 \leq |\phi_j| \leq 90$  degrees. The horizontal flow regime map is for junctions whose elevation angle  $\phi_j$  is such that  $0 \leq |\phi_j| \leq 30$  degrees. An interpolation region between vertical and horizontal flow regimes is used for junctions whose elevation angle  $\phi_j$  is such that  $30 < |\phi_j| < 60$  degrees.

### 3.3.6 Interphase Friction

The interface friction per unit volume in the phasic momentum equations [Equations (3.1-6) and (3.1-7)] is expressed in terms of a phasic interfacial friction coefficients as,

$$F_{ig} = \alpha_g \rho_g FIG (v_g - v_f) \quad (3.3-43)$$

and

$$F_{if} = \alpha_f \rho_f FIF (v_g - v_f) \quad (3.3-44)$$

where  $F_{ig}$  is the magnitude of the interfacial friction force on the vapor and  $F_{if}$  is the magnitude of the interfacial friction force on the liquid. The magnitude of the interfacial drag force per unit volume on the liquid is assumed to be equal to the magnitude of the interfacial drag on the vapor phase. This assumption leads to the condition

$$\alpha_g \rho_g FIG = \alpha_f \rho_f FIF = \alpha_g \rho_g \alpha_f \rho_f FI \quad (3.3-45)$$

where a global interfacial friction coefficient  $FI$  is defined in terms of the phasic interfacial friction coefficients.

The interfacial friction force term in the difference momentum equation is given by,

$$\frac{F_{ig}}{\alpha_g \rho_g} + \frac{F_{if}}{\alpha_f \rho_f} = (FIG + FIF) (v_g - v_f) \quad (3.3-46)$$

which becomes,

$$\frac{F_{ig}}{\alpha_g \rho_g} + \frac{F_{if}}{\alpha_f \rho_f} = \rho_m FI (v_g - v_f) \quad (3.3-47)$$

when the phasic interfacial drag coefficients are represented in terms of the global interfacial drag coefficient. This relation can be rearranged to give a constitutive relation for the global interfacial friction coefficient

$$FI = \frac{\left( \frac{F_{ig}}{\alpha_g \rho_g} + \frac{F_{if}}{\alpha_f \rho_f} \right)}{\rho_m (v_g - v_f)} \quad (3.3-48)$$

Once the interfacial friction forces have been computed, the global interfacial friction coefficient  $FI$  can be determined.

RELAP5/MOD3 uses two different models for the phasic interfacial friction force computation, the drift flux method and the drag coefficient method. The basis of each of these methods will be described in the following sections. Once the two methods have been explained, the final form of the difference momentum equation incorporating a framework within which both methods have been implemented will be presented. Finally, the drift flux and drag coefficient correlations used in the several flow regimes will be presented.

**3.3.6.1 Drift Flux Method.** The drift flux approach is used in the bubbly and slug flow regimes for vertical flow. The drift flux model specifies the distribution coefficient and the vapor drift velocity. These two quantities must be converted into a constitutive relation for the interfacial frictional force per unit volume in order to compute the global interfacial friction coefficient  $FI$ . This conversion is accomplished

in two steps. The first step considers the effect of the phasic wall frictional force on the relative velocity between the phases and the second step computes the interfacial friction force per unit volume from the drift flux parameters.

The first step begins by writing the steady state phasic momentum equations in symbolic form and neglecting the virtual mass force and the momentum flux terms. The simplified equations are,

$$0 = -\alpha_g \frac{dP}{dx} - F_{ig} - F_{wg} - \alpha_g \rho_g g \quad (3.3-49)$$

$$0 = -\alpha_f \frac{dP}{dx} + F_{if} - F_{wf} - \alpha_f \rho_f g .$$

If we multiply the first equation by  $\alpha_g$  and the second by  $\alpha_f$  and subtract the second equation from the first, the pressure gradient term is eliminated. The resulting equation can be rearrange to give,

$$\alpha_f F_{ig} + \alpha_g F_{if} = \alpha_f \alpha_g (\rho_f - \rho_g) g - \alpha_f F_{wg} + \alpha_g F_{wf} \quad (3.3-50)$$

which can be simplified by remembering that the magnitudes of the interfacial force on the two phases are equal to give

$$F_i = \alpha_f \alpha_g (\rho_f - \rho_g) g - \alpha_f F_{wg} + \alpha_g F_{wf} \quad (3.3-51)$$

where

$$F_{ig} = F_{if} = F_i .$$

Equation (3.3-51) states that the interfacial frictional force is balanced by buoyancy and wall friction. Because the drift flux correlations already contain the effect of the wall friction in the distribution parameter, we need to remove the wall friction terms from Equation (3.3-51) before proceeding. This can be accomplished by partitioning the wall frictional force between the phases based on the phasic void fractions (also see Anderson<sup>3.3-20</sup> and Ishii<sup>3.3-21, 3.3-22</sup>) rather than by the use of the Chisholm model (see Section 3.3.8). That is we want,

$$\begin{aligned} F_{wg} &= \alpha_g F_{wt} \\ F_{wf} &= \alpha_f F_{wt} \end{aligned} \quad (3.3-52)$$

where  $F_{wt}$  is the total wall frictional force on the two-phase mixture.

Substitution of Equation (3.3-52) into Equation (3.3-51) gives

$$F_i = \alpha_f \alpha_g (\rho_f - \rho_g) g \quad (3.3-53)$$

where the interfacial frictional force is balance by the buoyancy force. Recalling that the total wall frictional force on the two-phase mixture is given by

$$F_{wt} = \alpha_f \rho_f FWFv_f + \alpha_g \rho_g FWGv_g \quad (3.3-54)$$

the desired wall frictional force on the phases is given by

$$\begin{aligned} F_{wf} &= \alpha_f (\alpha_f \rho_f FWFv_f + \alpha_g \rho_g FWGv_g) \\ F_{wg} &= \alpha_g (\alpha_f \rho_f FWFv_f + \alpha_g \rho_g FWGv_g) \end{aligned} \quad (3.3-55)$$

Comparing these phasic wall frictional force terms to the wall friction terms already included in the phasic momentum equations shows that additional terms must be added to the phasic momentum equations to effect the changing of the partitioning of the wall frictional force. These extra terms are

$$\alpha_g \alpha_f \rho_f FWFv_f - \alpha_f \alpha_g \rho_g FWGv_g \quad (3.3-56)$$

for the liquid momentum equation and

$$-\alpha_g \alpha_f \rho_f FWFv_f + \alpha_f \alpha_g \rho_g FWGv_g \quad (3.3-57)$$

for the vapor momentum equation. These terms can be simplified by defining,

$$\begin{aligned} f_{wg} &= \alpha_f \alpha_g \rho_g FWG \\ f_{wf} &= \alpha_g \alpha_f \rho_f FWF \end{aligned} \quad (3.3-58)$$

so that the extra terms in the liquid momentum equations can be written as,

$$f_{wf}v_f - f_{wg}v_g \quad (3.3-59)$$

and for the vapor momentum equations as,

$$f_{wg}v_g - f_{wf}v_f \quad (3.3-60)$$

A means of removing the extra terms when the interfacial frictional force model is not being determined from the drift flux correlations has been implemented by multiplying the extra terms by a parameter  $f_x$  which is defined as  $f_x = 1$  when the drift flux model is being used to determine the interfacial

friction force and is defined as  $f_x = 0$  when the drag coefficient model is being to determine the interfacial friction force. This parameter is interpolated from one to zero in the interpolation region between flow regimes using the drift flux model and those using the two-fluid model for the determination of the interfacial force term.

The interfacial force relation specified by Equation (3.3-53) does not constitute a constitutive relation for the interfacial force since it does not provide a relationship between the interfacial force and the relative velocity. Such a relation can be found by assuming that the interfacial force is given by,

$$F_i = C_i |v_R| v_R \quad (3.3-61)$$

where  $C_i$  is a unknown coefficient and  $v_R$  is the relative velocity between the phases. Within the context of the drift flux model, the relative velocity between the phases in not the difference between the phasic velocities but is a weighted difference between the phase velocities given by,

$$v_R = C_1 v_g - C_0 v_f \quad (3.3-62)$$

where  $C_0$  is given by the drift flux correlation and  $C_1$  is given by

$$C_1 = \frac{1 - \alpha_g C_0}{1 - \alpha_g} \quad (3.3-63)$$

Substituting these relations into Equation (3.3-61) gives the interfacial force in terms of the phasic velocities

$$F_i = C_i |C_1 v_g - C_0 v_f| (C_1 v_g - C_0 v_f) \quad (3.3-64)$$

with the coefficient  $C_i$  undetermined as yet. The drift flux model also specifies that the relative velocity  $v_R$  can be written as the ratio of the vapor drift velocity and the void fraction as

$$v_R = \frac{v_{gj}}{\alpha_g} \quad (3.3-65)$$

where the vapor drift velocity  $v_{gj}$  is given by the drift flux correlations. Substituting this value of the relative velocity into Equation (3.3-61) and combining the resulting equation with Equation (3.3-53) allows the coefficient  $C_i$  to be determined from

$$C_i = \frac{\alpha_f \alpha_g^3 (\rho_f - \rho_g) g}{v_{gj}^2} \quad (3.3-66)$$

We are now in a position to determine the global interfacial friction coefficient  $FI$  from Equation (3.3-48) taking into account the different definition of the relative velocity in the drift flux model,

$$FI = \frac{\left( \frac{F_{ig}}{\alpha_g \rho_g} + \frac{F_{if}}{\alpha_f \rho_f} \right)}{\rho_m (C_1 v_g - C_0 v_f)} \quad (3.3-67)$$

and modifying the definition of the relative velocity in the interfacial friction term in the difference momentum equation accordingly.

**3.3.6.2 Drag Coefficient Method.** The drag coefficient method is used in all flow regimes except for bubbly and slug flows in vertical components. The model uses correlations for drag coefficients and for the computation of the interfacial area density and is the model used by previous versions of RELAP5 for all flow regimes.

The constitutive relation for the frictional force on a body moving relative to a fluid is given by

$$F = \frac{1}{2} \rho v^2 C_d A \quad (3.3-68)$$

where

$F$	=	drag force
$\rho$	=	fluid density
$v$	=	velocity of body relative to the fluid
$C_d$	=	drag coefficient,
$A$	=	projected area of the body.

Expressing the frictional force for a group of bodies moving relative to a fluid (e.g. bubbles moving through liquid or droplets moving through vapor) in terms of the frictional force for each body leads to the following constitutive relation for the frictional force per unit volume of fluid

$$F_i = \frac{1}{8} \rho_c |v_g - v_f| (v_g - v_f) C_d S_F a_{gf} \quad (3.3-69)$$

where

$$F_i = \text{force per unit volume of fluid}$$

$\rho_c$	=	density of continuous phase
$a_{gf}$	=	interfacial area per unit volume
$S_F$	=	shape factor.

The additional factor of 1/4 comes from the conversion of the projected area of spherical particles (i.e.  $\pi r^2$ ) into the interfacial area (i.e.  $4\pi r^2$ ) and the shape factor is included to account for non-spherical particles. The drag coefficient model for the global interfacial friction coefficient has been reduced to the specification of the continuous density, drag coefficient, interfacial area density, and shape factor for the several flow regimes. Once these quantities have been computed, the interfacial force per unit volume is computed from Equation (3.3-69) from which the global interfacial friction coefficient can be computed using Equation (3.3-48).

**3.3.6.3 Difference Momentum Equation.** The difference momentum equation must be modified to incorporate a framework under which the additional wall friction terms which appear when the drift flux model is used for the computation of the interfacial friction force can be included as well as accommodate the drift flux definition of the relative velocity. This framework uses a parameter  $f_x$  which is used to select either the drift flux model or the drag coefficient model for the interfacial friction force. The value of this parameter is selected on the basis of the flow regime in a junction. The drift flux model is used for bubbly and slug flows in vertical components and the drag coefficient model is used for all other flow regimes. The finite difference form of the difference momentum equation [Equation (3.1-104)] becomes,

$$\begin{aligned}
 & [1 + C\rho_m^2 / (\rho_g \rho_f)]_j^n [(v_g^{n+1} - v_g^n) - (v_f^{n+1} - v_f^n)]_j \Delta x_j \\
 & + \frac{1}{2} [(\dot{\alpha}_g \dot{\rho}_g) / (\alpha_g \rho_g)]_j^n [(v_g^2)_L^n - (v_g^2)_K^n] \Delta t - \frac{1}{2} [(\dot{\alpha}_g \dot{\rho}_g) / (\alpha_g \rho_g)]_j^n VISMG_j^n \Delta t \\
 & - \frac{1}{2} [(\dot{\alpha}_f \dot{\rho}_f) / (\alpha_f \rho_f)]_j^n [(v_f^2)_L^n - (v_f^2)_K^n] \Delta t + \frac{1}{2} [(\dot{\alpha}_f \dot{\rho}_f) / (\alpha_f \rho_f)]_j^n VISF_j^n \Delta t \\
 & = -[(\rho_f - \rho_g) / (\rho_g \rho_f)]_j^n (P_L - P_K)^{n+1} \Delta t \\
 & - \left\{ FWG_j^n (v_g)_j^{n+1} - FWF_j^n (v_f)_j^{n+1} \right. \\
 & - (f_x)_j^n \left( \frac{1}{\alpha_g \rho_g} + \frac{1}{\alpha_f \rho_f} \right)_j^n [(f_{wg})_j^n (v_g)_j^{n+1} - (f_{wf})_j^n (v_f)_j^{n+1}] \\
 & - [\Gamma_g^n (\rho_m^n v_I^{n+1} - \alpha_f^n \rho_f^n v_g^{n+1} - \alpha_g^n \rho_g^n v_f^{n+1}) / (\alpha_g \rho_g \alpha_f \rho_f)]_j^n \\
 & + (\rho_m FI)_j^n \left( [1 + f_x (C_1 - 1)]_j^n (v_g)_j^{n+1} - [1 + f_x (C_0 - 1)]_j^n (v_f)_j^{n+1} \right) \} \Delta x_j \Delta t \\
 & - \left\{ [(\dot{\alpha}_g \dot{\rho}_g) / (\alpha_g \rho_g)]_j^n HLOSSG_j^n (v_g)_j^{n+1} - [(\dot{\alpha}_f \dot{\rho}_f) / (\alpha_f \rho_f)]_j^n HLOSSF_j^n (v_f)_j^{n+1} \right\} \Delta t
 \end{aligned} \tag{3.3-70}$$

**3.3.6.4 Dispersed Flow.** The bubbly, mist, mist-pre-CHF, and mist-post-CHF flow regimes are considered as dispersed flow. For non-vertical bubbly flow and all droplet flow situations, the drag coefficient model is used for which  $f_x = 0$ .

According to Wallis<sup>3.3-23</sup> and Shapiro,<sup>3.3-24</sup> the dispersed bubbles or droplets can be assumed to be spherical particles with a size distribution of the Nukiyama-Tanasawa<sup>3.3-23</sup> form. The Nukiyama-Tanasawa distribution function in nondimensional form is

$$p^* = 4d^{*2} e^{-2d^*} \quad (3.3-71)$$

where  $d^* = d/d'$ ,  $d'$  is the most probable particle diameter, and  $p^*$  is the probability of particles with nondimensional diameter  $d^*$ . With this distribution, it can be shown that the average particle diameter  $d_o = 1.5 d'$ , and the surface area per unit volume is

$$a_{gf} = \frac{6\bar{\alpha}}{d'} - \frac{\int d^{*2} p^* dd^*}{\int d^{*3} p^* dd^*} = \frac{2.4\bar{\alpha}}{d'} \quad (3.3-72)$$

where  $\bar{\alpha} = \alpha_g$  for bubbles and  $\bar{\alpha} = \alpha_f$  for droplets. In terms of the average diameter,  $d_o$ , the interfacial area per unit volume,  $a_{gf}$ , is

$$a_{gf} = 3.6\bar{\alpha}/d_o \quad (3.3-73)$$

The average diameter  $d_o$  is obtained by assuming that  $d_o = (1/2)d_{max}$ . The maximum diameter,  $d_{max}$ , is related to the critical Weber number,  $We$ , by

$$We = d_{max} \rho_c (v_g - v_f)^2 / \sigma \quad (3.3-74)$$

where  $\sigma$  is the surface tension. The values for  $We$  are presently taken as  $We = 10.0$  for bubbly flow,  $We = 3.0$  for mist-pre-CHF flow, and  $We = 12.0$  for mist and mist-post-CHF flow.

The drag coefficient to be used in non-vertical bubbly flow and all droplet flow situations is given by Ishii and Chawla<sup>3.3-6</sup> for the viscous regime as

$$C_D = 24 (1.0 + 0.1 Re_p^{0.75}) / Re_p \quad (3.3-75)$$

where the particle Reynolds number,  $Re_p$ , is defined as

$$Re_p = |v_g - v_f| d_o \rho_c / \mu_m \quad (3.3-76)$$

The density,  $\rho_c$ , is for the continuous phase, and is given by  $\rho_f$  for bubbles and  $\rho_g$  for drops. The mixture viscosity,  $\mu_m$ , is for the continuous phase, and is given by  $\mu_m = \mu_f/\alpha_f$  for bubbles and  $\mu_m = \mu_g/(\alpha_g)^{2.5}$  for droplets. This is from Ishii and Chawla.<sup>3.3-6</sup>

For vertical bubbly flow, the drift flux model is used for which  $f_x = 1$ . The drift flux parameters are calculated using drift flux correlations from the literature based on Putney's work.<sup>3.3-25,3.3-26,3.3-27,3.3-28,3.3-29</sup> Table 3.3-2 indicates which correlations are used for different geometry and flow conditions. The number in parenthesis is the value of the minor edit/plot variable IREGJ, the vertical bubbly/slug flow junction flow regime number. The name in parenthesis is the subroutine used to calculate the correlation.

Table 3.3-2 Drift flux void fraction correlations for vertical bubbly-slug flow.<sup>a</sup>

Flow Rates	Rod Bundles	Small Pipes $D \leq 0.018m$	Intermediate Pipes $0.018m < D \leq 0.08m$	Large Pipes $0.08m < D$
High upflow rates $G > 100$ $kg/m^2 \cdot s$	EPRI (2) (eprij)	EPRI (3) (eprij)	EPRI (9) (eprij)	Churn-Turbulent Bubbly Flow (14) Transition (15) Kataoka-Ishii (16) (katokj)
Low up, down, and countercurrent flow rates $G < 50$ $kg/m^2 \cdot s$		Transition (5)	Transition (13)	
$G > -50$ $kg/m^2 \cdot s$		Zuber-Findlay Slug Flow (4) (zfslgj)	Churn-Turbulent Bubbly Flow (10) Transition (11) Kataoka-Ishii (12) (katokj)	
High downflow rates $G < -100$ $kg/m^2 \cdot s$		Transition (5)	Transition (13)	
		EPRI (3) (eprij)	EPRI (9) (eprij)	

a. Interpolation is applied between different flow regions in pipes.

The correlation labeled EPRI is by Chexal and Lellouche.<sup>3.3-30</sup> The correlation has been recently modified<sup>3.3-31</sup> and the changes have been incorporated into RELAP5/MOD3. The distribution coefficient  $C_o$  is calculated from

$$C_o = \frac{L(\alpha_g, P)}{[K_o + (1 - K_o)(\alpha_g)^r]} \quad (3.3-77)$$

where

$$L(\alpha_g, P) = \frac{1 - \exp(-C_1 \alpha_g)}{1 - \exp(-C_1)} \quad (3.3-78)$$

$$C_1 = \left| \frac{4P_{crit}^2}{P(P_{crit} - P)} \right| \quad (3.3-79)$$

$P_{crit}$  = critical pressure

$$K_0 = B_1 + (1 - B_1) \left( \frac{\rho_g}{\rho_f} \right)^{1/4} \quad (3.3-80)$$

$$B_1 = \min(0.8, A_1) \quad (3.3-81)$$

$$A_1 = \frac{1}{[1 + \exp(-Re/60,000)]} \quad (3.3-82)$$

$$Re = Re_g \quad \text{if } Re_g > Re_f \text{ or } Re_g < 0 \quad (3.3-83)$$

$$Re_f \quad \text{otherwise} \quad (3.3-84)$$

$Re_f$  = local liquid superficial Reynolds number

$$= \frac{\rho_f j_f D_h}{\mu_f} \quad (3.3-85)$$

$Re_g$  = local vapor superficial Reynolds number

$$= \frac{\rho_g j_g D_h}{\mu_g} \quad (3.3-86)$$

$$r = \frac{1 + 1.57 \left[ \frac{\rho_g}{\rho_f} \right]}{1 - B_1} \quad (3.3-87)$$

The sign of  $j_k$  is positive if phase  $k$  flows upwards and negative if it flows downwards. This convention determines the sign of  $Re_g$ ,  $Re_f$ , and  $Re$ .

The vapor drift velocity,  $v_{gj}$ , for the Chexal-Lellouche correlation is calculated from

$$v_{gj} = 1.41 \left[ \frac{(\rho_f - \rho_g) \sigma g}{\rho_f^2} \right]^{1/4} C_2 C_3 C_4 C_9 \quad (3.3-88)$$

where

$$C_2 = 1 \quad \text{if } C_5 \geq 1 \quad (3.3-89)$$

$$= \frac{1}{1 - \exp(-C_6)} \quad \text{if } C_5 < 1 \quad (3.3-90)$$

$$C_5 = \left[ 150 \left( \frac{\rho_g}{\rho_f} \right) \right]^{1/2} \quad (3.3-91)$$

$$C_6 = \frac{C_5}{1 - C_5} \quad (3.3-92)$$

$$C_4 = 1 \quad \text{if } C_7 \geq 1 \quad (3.3-93)$$

$$= \frac{1}{1 - \exp(-C_8)} \quad \text{if } C_7 < 1 \quad (3.3-94)$$

$$C_7 = \left( \frac{D_2}{D} \right)^{0.6} \quad (3.3-95)$$

$$D_2 = 0.09144 \text{ m (normalizing diameter)}$$

$$C_8 = \frac{C_7}{1 - C_7} \quad (3.3-96)$$

$$C_9 = (1 - \alpha_g) B_1 \quad \text{if } Re_g \geq 0 \quad (3.3-97)$$

$$= \min [0.7, (1 - \alpha_g)^{0.65}] \quad \text{if } Re_g < 0. \quad (3.3-98)$$

The parameter  $C_3$  depends on the directions of the vapor and liquid flows:

Upflow (both  $j_g$  and  $j_f$  are positive)

$$C_3 = \max [0.50, 2 \exp(-|Re_f|/60,000)] \quad (3.3-99)$$

Downflow (both  $j_g$  and  $j_f$  are negative)

$$C_3 = \left( \frac{C_{10}}{2} \right)^{B_2} \quad (3.3-100)$$

$$B_2 = \frac{1}{1 + 0.05 \left| \frac{Re_f}{35,000} \right|^{0.4}} \quad (3.3-101)$$

$$C_{10} = 2 \exp \left[ \left( \frac{|Re_f|}{350,000} \right)^{0.4} \right] - 1.75 |Re_f|^{0.03} \exp \left[ \frac{-|Re_f|}{50,000} \left( \frac{D_1}{D} \right)^2 \right] + \left( \frac{D_1}{D} \right)^{0.25} |Re_f|^{0.001} \quad (3.3-102)$$

$$D_1 = 0.0381 \text{ m (normalizing diameter).} \quad (3.3-103)$$

Countercurrent Flow ( $j_g$  is positive,  $j_f$  is negative)

$$C_3 = \left( \frac{C_{10}}{2} \right)^{B_2} \quad (3.3-104)$$

$$B_2 = \frac{1}{1 + 0.05 \left| \frac{Re_f}{35,000} \right|^{0.4}} \quad (3.3-105)$$

$$C_{10} = 2 \exp \left[ \left( \frac{|Re_f|}{350,000} \right)^{0.4} \right] - 1.75 |Re_f|^{0.03} \exp \left[ \frac{-|Re_f|}{50,000} \left( \frac{D_1}{D} \right)^2 \right] + \left( \frac{D_1}{D} \right)^{0.25} |Re_f|^{0.001} \quad (3.3-106)$$

$$D_1 = 0.0381 \text{ (normalizing diameter).} \quad (3.3-107)$$

The parameters  $C_2, C_3, C_4, \dots, C_{10}$  are from the Chexal-Lellouche correlation.<sup>3.3-30, 3.3-31</sup>

The correlation labeled Zuber-Findlay Slug Flow is by Zuber and Findlay.<sup>3.3-32, 3.3-33</sup> The distribution parameter is given by

$$C_0 = 1.2 \quad (3.3-108)$$

and the drift velocity is given by

$$v_{gj} = 0.35 \left[ \frac{(\rho_f - \rho_g) g D}{\rho_f} \right]^{1/2} \quad (3.3-109)$$

The correlation labeled Kataoka-Ishii is by Kataoka and Ishii.<sup>3.3-34</sup> The distribution parameter is given by the modified Rouhani correlation<sup>3.3-35</sup> used in TRAC-BF1,<sup>3.3-36</sup>

$$C_o = C_\infty - (C_\infty - 1)(\rho_g/\rho_f)^{1/2} \quad (3.3-110)$$

$$C_\infty = 1 + 0.2 [\rho_f(gD)^{1/2}/(|G| + 0.001)]^{1/2} \quad (3.3-111)$$

and the drift velocity is given by

$$v_{gj} = 0.0019 (D^*)^{0.809} \left( \frac{\rho_g}{\rho_f} \right)^{-0.157} N_{\mu f}^{-0.562} \left[ \frac{\sigma g (\rho_f - \rho_g)}{\rho_f^2} \right]^{1/4} \text{ for } D^* \leq 30 \quad (3.3-112)$$

$$v_{gj} = 0.030 \left( \frac{\rho_g}{\rho_f} \right)^{-0.157} N_{\mu f}^{-0.562} \left[ \frac{\sigma g (\rho_f - \rho_g)}{\rho_f^2} \right]^{1/4} \text{ for } D^* > 30 \quad (3.3-113)$$

where  $D^*$  is the Bond number given by Equation (3.3-7) and the viscosity number,  $N_{\mu f}$ , is given by

$$N_{\mu f} = \frac{\mu_f}{\{\rho_f \sigma \left[ \frac{\sigma}{g(\rho_f - \rho_g)} \right]^{1/2}\}^{1/2}} \quad (3.3-114)$$

The correlation labeled Churn Turbulent Bubbly Flow is by Zuber and Findlay.<sup>3.3-32,3.3-33</sup> The distribution parameter is given by the modified Rouhani correlation<sup>3.3-35</sup> used in TRAC-BF1,<sup>3.3-36</sup> Equations (3.3-110) and (3.3-111) and the drift velocity is given by

$$v_{gj} = 1.41 \left[ \frac{\sigma g (\rho_f - \rho_g)}{\rho_f^2} \right]^{1/4} \quad (3.3-115)$$

For intermediate pipes (for low up, down, and countercurrent flow rates) and large pipes (all cases), the churn turbulent bubbly flow correlation is applied when

$$j_g^+ = \frac{j_g}{\left[ \frac{\sigma g (\rho_f - \rho_g)}{\rho_f^2} \right]^{1/4}} \leq j_{g1}^+ = 0.5$$

The Kataoka-Ishii correlation is applied when

$$j_g^+ \geq j_{g2}^+ \quad (3.3-116)$$

where  $j_{g2}^+ = 1.768$ . Linear interpolation is used between the two correlations.

Putney has also placed a countercurrent flow limitation (CCFL) on the drift flux parameters. The limitation is based on the Kutateladze condition (see Section 3.4.7)

$$|Ku_g|^{1/2} + m|Ku_f|^{1/2} = Ku_{crit}^{1/2} \quad (3.3-117)$$

where

$$Ku_g = \frac{\alpha_g v_g \rho_g^{\frac{1}{2}}}{[\sigma g (\rho_f - \rho_g)]^{\frac{1}{4}}} \quad (3.3-118)$$

$$Ku_f = \frac{\alpha_f v_f \rho_f^{\frac{1}{2}}}{[\sigma g (\rho_f - \rho_g)]^{\frac{1}{4}}} \quad (3.3-119)$$

$$m = 1 \quad (3.3-120)$$

and  $Ku_{crit}$  (using linear interpolation) is given by Table 3.3-3. This table for  $Ku_{crit}$  as a function of  $D^*$  is from Wallis and Makkenchey.<sup>3.3-37</sup> This has been used successfully in the RELAP-UK code.<sup>3.3-38</sup> The value of  $m = 1$  was also used in the RELAP-UK code.

**Table 3.3-3** Values of  $Ku_{crit}$ .

$D^*$	$Ku_{crit}$
$\leq 2$	0
4	1.0
10	2.1
14	2.5
20	2.8
28	3.0
$\geq 50$	3.2

On the flooding curve, the drift flux parameters satisfy the relationship

$$v_{gj} = \frac{(1 - \alpha_g C_o) C_o K u_{crit} \left[ \frac{(\rho_f - \rho_g) g \sigma}{\rho_f^2} \right]^{1/4}}{\alpha_g C_o \left( \frac{\rho_g}{\rho_f} \right)^{1/2} + m^2 (1 - \alpha_g C_o)} \quad (3.3-121)$$

This flooding limit for  $v_{gj}$  is applied for mass fluxes ( $G$ ) larger than  $100 \text{ kg/m}^2\text{s}$  and for  $\alpha_g \geq 0.5$ . Linear interpolation is used down to a mass flux of  $50 \text{ kg/m}^2\text{s}$  and to  $\alpha_g = 0.3$ , at which point the normal drift flux correlations are used.

**3.3.6.5 Slug Flow.** Slug flow for non-vertical geometry is modeled as a series of Taylor bubbles separated by liquid slugs containing small bubbles. A sketch of a slug flow pattern is shown in Figure 3.3-5. The Taylor bubble has a diameter nearly equal to the pipe diameter and a length varying from 1 to 100 pipe diameters.

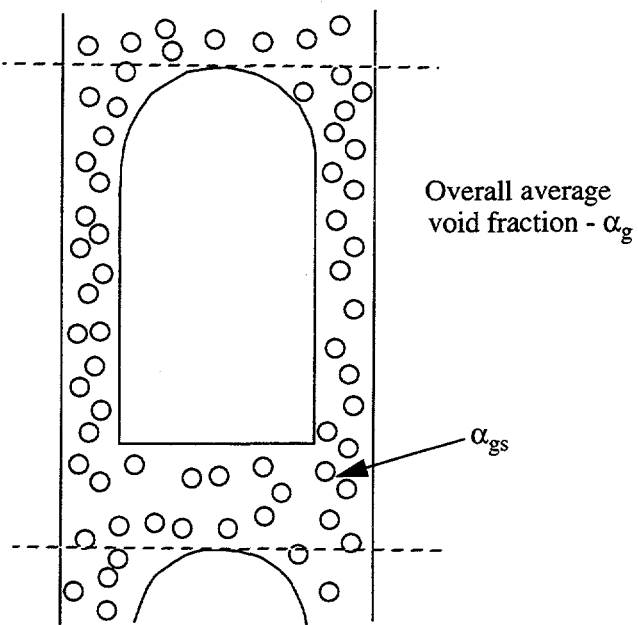


Figure 3.3-5 Slug flow pattern.

Let  $\alpha_{gs}$  be the average void fraction in the liquid film and slug region. The void fraction of a single Taylor bubble,  $\alpha_b$ , in the total mixture is then

$$\alpha_b = (\alpha_g - \alpha_{gs}) / (1 - \alpha_{gs}) \quad (3.3-122)$$

The Taylor bubble frontal area per unit volume is  $a_b/L$ , where  $L$  is the cell length. Consequently, the interfacial area per unit volume,  $a_{gf}$ , for slug flow is

$$a_{gf} = (\alpha_b/L) + (3.6 \alpha_{gs}/d_o)(1 - \alpha_b) \quad (3.3-123)$$

To provide a smooth transition into and out of slug flow,  $\alpha_{gs}$  in Equation (3.3-122) is considered as a free parameter varying from  $\alpha_{BS}$  at the bubbly-to-slug flow regime transition to nearly zero at the slug-to-annular-mist flow regime transition. The variation is represented by the exponential expression

$$\alpha_{gs} = \alpha_{BS} \exp[-8(\alpha_g - \alpha_{BS})/(\alpha_{SA} - \alpha_{BS})] \quad (3.3-124)$$

The drag coefficient for Taylor bubbles in non-vertical slug flow is given by Ishii and Chawla<sup>3.3-6</sup> as

$$C_D = 10.9 (D'/D) (1 - \alpha_b)^3 \quad (3.3-125)$$

where  $D'$  is the Taylor bubble diameter and  $\alpha_b$  is given by combining Equations (3.3-122) and (3.3-124).

The drag coefficient for small bubbles in non-vertical slug flow is given by Ishii and Chawla<sup>3.3-6</sup> by Equation (3.3-75).

For vertical slug flow, the interphase drag and shear terms are calculated using the same drift flux correlations that are used in vertical bubbly flow.

**3.3.6.6 Annular Mist Flow.** Annular mist flow is characterized by a liquid film along the wall and a vapor core containing entrained liquid droplets. Let  $\alpha_{ff}$  be the average liquid volume fraction of the liquid film along the wall. Then, from simple geometric considerations, the interfacial area per unit volume can be shown to be

$$a_{gf} = (4C_{ann}/D)(1 - \alpha_{ff})^{1/2} + (3.6\alpha_{fd}/d_o)(1 - \alpha_{ff}) \quad (3.3-126)$$

where  $C_{ann}$  is a roughness parameter introduced to account for waves in the liquid wall film,  $\alpha_{fd}$  is the average liquid volume fraction in the vapor core, for which

$$\alpha_{fd} = (\alpha_f - \alpha_{ff})/(1 - \alpha_{ff}) \quad (3.3-127)$$

and  $d_o$  is the average diameter of the drops. For an annulus component, all the liquid is in the film and there are no drops. Thus,  $\alpha_{ff} = \alpha_f$  and  $\alpha_{fd} = 0$  are used for an annulus.

A simple relation based on the flow regime transition criterion and liquid Reynolds number is used to correlate the average liquid film volume fraction. For vertical flow regimes, the entrainment relation is

$$\alpha_{ff} = \alpha_f C_f \exp[-7.5 \times 10^{-5} (\alpha_g v_g / u_c)^6] \quad (3.3-128)$$

where  $u_c$  is the critical entrainment superficial velocity given by the combination of Equations (3.3-13) and (3.3-15).

For horizontal flow regimes, the entrainment relation is

$$\alpha_{ff} = \alpha_f C_f \exp[-4.0 \times 10^{-5} (|v_g - v_f|/v_{gL})^6] \quad (3.3-129)$$

where  $v_{gL}$  is the horizontal stratification critical velocity given by Equation (3.3-30). The term  $C_f$  is expressed as

$$C_f = 1.0 - 10^{-4} \left( \alpha_f \rho_f |v_f| \frac{D}{\mu_f} \right)^{0.25} \quad (3.3-130)$$

The interfacial friction factor,  $f_i$ , for the liquid film takes the place of  $C_D$  in Equation (3.3-69), and is described by a standard correlation in the laminar region and is based on Wallis' correlation in the turbulent region.<sup>3.3-23</sup> In the turbulent region, the Wallis correlation was modified to use the factor 0.02 rather than 0.005. This is the value used in RELAP5/MOD1,<sup>3.3-39</sup> and it was selected because of the MOD1 assessment. It is based on the vapor Reynolds number defined as

$$Re_g = \frac{\rho_g |v_g - v_f| D_g}{\mu_g} \quad (3.3-131)$$

where

$$D_g = \alpha_g^{1/2} D \text{ is the equivalent wetted diameter} \quad (3.3-132)$$

$$\mu_g = \text{viscosity of the vapor phase.} \quad (3.3-133)$$

The values of  $f_i$  are

$$\begin{aligned} f_i &= \frac{64}{Re_g} \quad \text{for } Re_g \leq 500 \\ &= \left( \frac{1500 - Re_g}{1000} \right) \frac{64}{Re_g} + \left( \frac{Re_g - 500}{1000} \right) 0.02 \{ 1 + 150 [1 - (1 - \alpha_{ff})^{1/2}] \}, \\ &\quad \text{for } 500 < Re_g < 1500 \\ &= 0.02 \{ 1 + 150 [1 - (1 - \alpha_{ff})^{1/2}] \} \text{ for } Re_g \geq 1500. \end{aligned} \quad (3.3-134)$$

The interfacial drag coefficient  $C_D$  for the drops is given by Ishii and Chawla<sup>3.3-6</sup> from Equation (3.3-75).

**3.3.6.7 Vertical Stratified Flow.** For the junction above the vertically stratified volume (junction  $j$  in Figure 3.3-6), the interphase drag is based on the void fraction in the volume above (volume  $L$ ). This is consistent with the junction-based interphase drag. This is obtained as follows: The void fraction  $\alpha_{g,j}^*$  used in the junction  $j$  for the junction-based interphase drag is given by

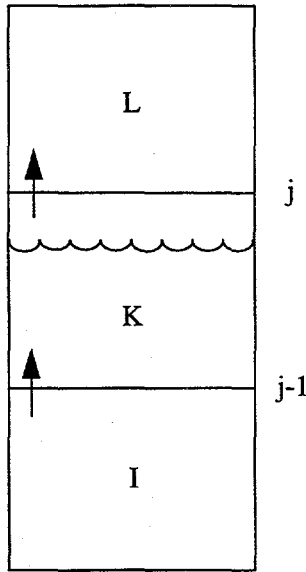


**Figure 3.3-6** Three vertical volumes with the middle volume being vertically stratified.

$$\alpha_{g,j}^* = w_j \cdot \alpha_{g,K}^* + (1 - w_j) \cdot \alpha_{g,L} \quad (3.3-135)$$

and is similar to Equation (3.3-35) except that  $\alpha_{g,K}$  is replaced by  $\alpha_{g,K}^*$ . This void fraction is given by

$$\alpha_{g,K}^* = \text{strat} \cdot \alpha_{g,L} + (1 - \text{strat}) \cdot \alpha_{g,K} \quad (3.3-136)$$

where strat takes on values from 0 to 1. For a vertically stratified volume, strat = 1,  $\alpha_{g,K}^* = \alpha_{g,L}$  and  $\alpha_{g,j}^* = \alpha_{g,L}$ . For a non-vertically stratified volume, strat = 0,  $\alpha_{g,K}^* = \alpha_{g,K}$ , and  $\alpha_{g,j}^*$  is given by Equation (3.3-35). The smoothing parameter strat is given by

$$\text{strat} = \text{strat1} \cdot \text{strat2} \quad (3.3-137)$$

where

$$\text{strat1} = 1 - e^{-0.5\alpha_{f,L}} \quad (3.3-138)$$

$$\text{strat2} = 2(1 - v_m/v_{Tb}). \quad (3.3-139)$$

Both strat1 and strat2 are limited to values between 0 and 1. Equation (3.3-138) for strat1 is a modification of the approach used in RELAP5/MOD2. The variable strat1 exponentially turns off the stratification effect when the volume above (volume L) becomes empty of liquid. When  $\alpha_{f,L} = 0.01$ , strat1 = 0.005. For strat2, the variables  $v_m$  and  $v_{Tb}$  are the mixture velocity based on the volume centered velocities and Taylor bubble rise velocity given by Equation (3.3-5).

A different method is used at junction j-1 below the vertically stratified volume. Equations (3.3-135), (3.3-136), (3.3-137), and (3.3-139) are used, however, strat1 is given by

$$\text{strat1} = 20(\alpha_{\text{level}} - 0.05) \quad (3.3-140)$$

where

$$\alpha_{\text{level}} = \frac{\alpha_{g,L} - \alpha_{g,K}}{\alpha_{g,L} - \alpha_{g,I}}. \quad (3.3-141)$$

The variable  $\alpha_{\text{level}}$  is an implied non-dimensional mixture level position within volume K. The coding is generalized to handle the case where the volumes and junctions are oriented downward. The vertical stratification model is not intended to be a mixture level model, and a more mechanistic level tracking model is described in Section 3.4.8.

**3.3.6.8 Horizontal Stratified Flow.** By simple geometric consideration, one can show that the interfacial area per unit volume is

$$a_{gf} = 4C_{st} \sin\theta/(\pi D) \quad (3.3-142)$$

where  $C_{st}$  is a roughness parameter introduced to account for surface waves and is set to 1 at the present time. (See Figure 3.1-2 for the definition of angle  $\theta$ ).

The interface Reynolds number is defined with the vapor properties and regarding liquid as the continuous phase for which

$$Re_i = D_i \rho_g |v_g - v_f| / \mu_g \quad (3.3-143)$$

where the equivalent wetted diameter,  $D_i$ , for the interface is

$$D_i = \alpha_g \pi D / (\theta + \sin\theta) \quad (3.3-144)$$

The interfacial friction factor,  $f_i$ , replaces  $C_D$  in Equation (3.3-69) and is obtained by assuming typical friction factor relationships for which

$$f_i = \max \left[ \frac{64}{Re_i}, 0.3164/Re_i^{0.25} \right] . \quad (3.3-145)$$

**3.3.6.9 Inverted Flow Regimes.** These regimes arise when there is hot vapor in the cell and either hot walls or the reflood model is on. The interphase drag relationships for post-CHF inverted flow regimes are treated in a similar fashion to the corresponding pre-CHF flow regimes, except that the roles of vapor and liquid are interchanged.

**3.3.6.9.1 Inverted Annular Flow**--Immediately downstream of a quench front or CHF position, there may be an inverted annular flow region if the combination of liquid flow and subcooling are high enough. The physical concept in the model is the presence of vapor bubbles in the liquid core (just as there are liquid drops in the vapor core region for annular mist flow) and an annular gas layer between the walls and the core. The drag term [ $f_{gf}$  in Equation (3.3-69)] is the sum of the drag between the bubbles and the liquid in the core and the drag between the vapor annulus and the outer surface of the core.

The drag coefficient for the bubbles is the Ishii-Chawla correlation given by Equation (3.3-75), and the interfacial area is:

$$\alpha_{gb} = (3.6 \alpha_{gb}/d_o)(1 - \alpha_B) \quad (3.3-146)$$

where:

$\alpha_{gb}$  = the gas void fraction in the liquid core

$d_o$  = the bubble diameter

$\alpha_B$  = the fraction of the total area occupied by the steam annulus.

The Weber number used to solve for the bubble diameter is 10. The annulus gas void fraction is an exponential function of the total gas void fraction, similar to Equation (3.3-124), and is presented in Volume IV of the RELAP5/MOD3 manuals. The core gas void fraction is:

$$\alpha_{gb} = \frac{V_{gas, core}}{V_{core}} = \frac{V_{gas, tot} - V_{gas, ann}}{V_{tot} - V_{gas, ann}} = \frac{\alpha_g - \alpha_B}{1 - \alpha_B} \quad (3.3-147)$$

where

$V_{core}$  = volume of the liquid core including bubbles

$$V_{\text{tot}} = \text{volume of control volume.}$$

The annular shear force uses the Bharathan et al.<sup>3.3-40</sup> equation for the drag coefficient:

$$C_D = 4[0.005 + A(\delta^*)^B] \quad (3.3-148)$$

where

$$\log_{10} A = -0.56 + 9.07/D^* \quad (3.3-149)$$

$$B = 1.63 + 4.74/D^* \quad (3.3-150)$$

$$\delta^* = \delta \left[ \frac{(\rho_f - \rho_g) g}{\sigma} \right]^{1/2} \quad (3.3-151)$$

The term  $\delta^*$  is the liquid wall film Deryagin number for which  $\delta$  is the film thickness, and  $D^*$  is the dimensionless diameter Bond number given by Equation (3.3-7).

The interfacial area of the gas annular film per unit length in a pipe is

$$a_{g_f, \text{ann}} = \frac{\pi D'}{\frac{\pi D^2}{4}} = \frac{4D'}{D^2} \quad (3.3-152)$$

where

$$D' = \text{inner diameter of annulus}$$

$$D = \text{diameter of pipe}$$

$$\frac{V_{\text{core}}}{V_{\text{tot}}} = \frac{(\pi/4) D'^2}{(\pi/4) D^2} = \frac{D'^2}{D^2} = (1 - \alpha_B) \quad (3.3-153)$$

where

$$V_{\text{core}} = \text{idealized volume of the gas core per unit length}$$

$$V_{\text{tot}} = \text{volume of control volume per unit length.}$$

Solving for the ratio  $D'/D$  from Equation (3.3-153) and putting it into Equation (3.3-152) yields:

$$a_{gf, ann} = \frac{4}{D} (1 - \alpha_B)^{1/2} \quad (3.3-154)$$

**3.3.6.9.2 Inverted Slug Flow**—The inverted slug flow regime as envisioned by DeJarlais and Ishii<sup>3.3-41</sup> consists of bubble-impregnated liquid droplets (see Figure 3.3-7). The coded interfacial friction coefficients recognize the liquid droplets, vapor blanket, and liquid slugs, but not the presence of bubbles in the slugs. Contributions to the interfacial friction are recognized then, as coming from two sources: (a) the liquid droplet interfaces in the vapor annulus and (b) the liquid slug/annulus interface. It is assumed that the liquid slugs are so long that any contributions to interfacial friction at their ends are negligible.

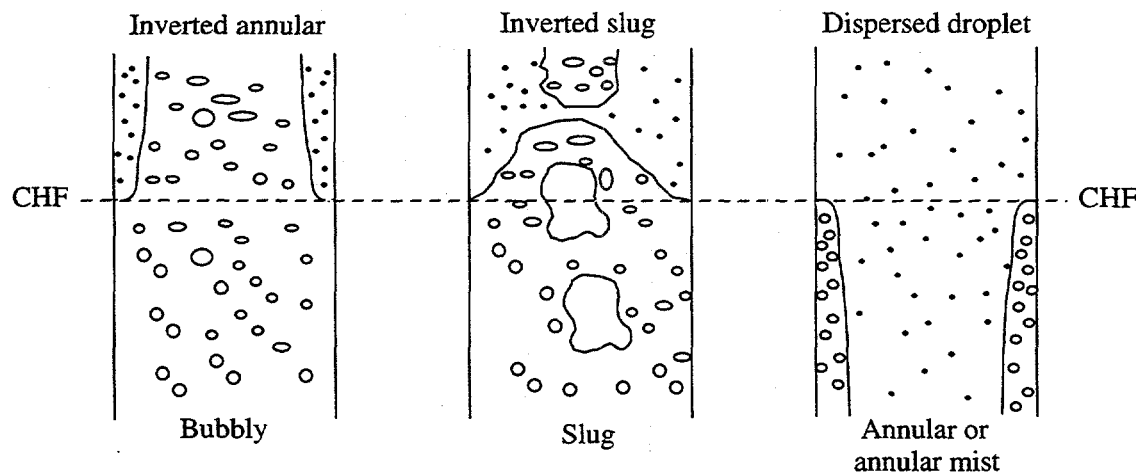


Figure 3.3-7 Flow regimes before and after the critical heat flux (CHF) transition.

The interfacial areas for the annulus/droplet portion and the slug/annulus portion are derived analogously to those for nonvertical slug flow (Section 3.3.6.5). The void fraction of the liquid slug,  $\alpha_B$ , is analogous to that for a Taylor bubble,  $\alpha_{Tb}$ , and the average droplet void in the vapor blanket,  $\alpha_{drp}$ , is analogous to the average void,  $\alpha_{gs}$ , in the liquid annulus for slug flow. That is, the interfacial areas are computed for inverted slug flow by simply reversing the liquid and vapor phases from slug flow. The droplet void,  $\alpha_{drp}$ , in the vapor annulus is an expression that exponentially increases the portion of  $\alpha_f$  due to droplets as  $\alpha_g$  increases until the transition void,  $\alpha_{SA}$ , is reached, at which point all of the liquid is appropriately assumed to be in droplet form. The value for the Weber number used is 12.0.

The drag coefficients for the annulus/droplet portion and the slug/annulus portion are analogous to those for non-vertical slug flow, except that the liquid and vapor phases are reversed.

**3.3.6.9.3 Mist Flow**—The mist flow regime is discussed in Section 3.3.6.4, Dispersed Flow. For mist-pre-CHF,  $We = 3.0$ , and for mist and mist-post-CHF,  $We = 12.0$ .

### 3.3.7 Coefficient of Virtual Mass

The coefficient of virtual mass is determined based on the junction flow regime map. The calculation of the drag due to the virtual mass effect (dynamic drag) is based on an objective and symmetric formulation of the relative acceleration.<sup>3.3-42</sup> The inertial drag force per unit volume in the phasic momentum equations is written as

$$FA_{gf} = -C\alpha_g(1 - \alpha_g)\rho \left[ \frac{\partial}{\partial t} (v_g - v_f) \right] \quad (3.3-155)$$

where

$$\rho = \alpha_g \rho_g + (1 - \alpha_g) \rho_f \quad (3.3-156)$$

$$FA_{gf} = \text{force per unit volume due to dynamic drag.}$$

The factor,  $C\alpha_g(1 - \alpha_g)\rho$ , is chosen to ensure a smooth transition between  $\alpha_g = 0$  and  $\alpha_g = 1.0$ . This factor also gives the proper limit,  $C\alpha_g\rho_f$  in the thinly dispersed bubbly flow, and  $C(1 - \alpha_g)\rho_g$  in the dispersed droplet flow. The virtual mass coefficient,  $C$ , is given<sup>3.3-43</sup> as

$$C = \frac{1}{2} \frac{(1 + 2\alpha_g)}{(1 - \alpha_g)} \text{ for } 0 \leq \alpha_g \leq 1/2 \quad (3.3-157)$$

$$C = \frac{1}{2} \frac{(3 - 2\alpha_g)}{\alpha_g} \text{ for } 1/2 \leq \alpha_g \leq 1 \quad (3.3-158)$$

It may be appropriate to assume that  $C = 0$  should be used for separated or stratified flow. At present, the value of  $C$  defined by Equations (3.3-157) and (3.3-158) is used without regard to the flow regime.

### 3.3.8 Wall Friction

The wall friction is determined based on the volume flow regime map. The wall friction force terms include only wall shear effects. Losses due to abrupt area change are calculated using mechanistic form-loss models. Other losses due to elbows or complicated flow passage geometry are modeled using energy-loss coefficients that must be input by the user.

Emphasis was placed on obtaining reasonable values for wall friction in all flow regimes in the development of the wall friction model. The flow regime models are discussed in Section 3.3.1 through Section 3.3.4.

The wall friction model is based on a two-phase multiplier approach in which the two-phase multiplier is calculated from the Heat Transfer and Fluid Flow Service (HTFS)-modified Baroczy correlation.<sup>3.3-44</sup> The individual phasic wall friction components are calculated by apportioning the two-

phase friction between the phases using a technique derived by Chisholm<sup>3.3-45</sup> from the Lockhart-Martinelli<sup>3.3-46</sup> model. The partitioning model is based on the assumption that the frictional pressure drop may be calculated using a quasi-steady form of the momentum equation.

**3.3.8.1 The Two-Phase Friction Multiplier Approach.** The Lockhart-Martinelli model computes the overall friction pressure drop in terms of the liquid-alone wall friction pressure drop

$$\left(\frac{dP}{dx}\right)_{2\phi} = \phi_f^2 \left(\frac{dP}{dx}\right)_f \quad (3.3-159)$$

or the vapor-alone wall friction pressure drop

$$\left(\frac{dP}{dx}\right)_{2\phi} = \phi_g^2 \left(\frac{dP}{dx}\right)_g \quad (3.3-160)$$

where  $\phi_f$  and  $\phi_g$  are the liquid-alone and vapor-alone two-phase Darcy-Weisbach friction multipliers, respectively. The phasic wall friction pressure gradients are expressed as

$$\left(\frac{dP}{dx}\right)_f = \frac{\lambda_f' (Re_f') M_f^2}{2D\rho_f A^2} \quad (3.3-161)$$

for the liquid alone, and

$$\left(\frac{dP}{dx}\right)_g = \frac{\lambda_g' (Re_g') M_g^2}{2D\rho_g A^2} \quad (3.3-162)$$

for the vapor alone, where the prime indicates the liquid and vapor-alone Darcy-Weisbach friction factors, respectively, calculated at the respective Reynolds numbers

$$Re_f' = \frac{M_f D}{\mu_f A} \quad (3.3-163)$$

and

$$Re_g' = \frac{M_g D}{\mu_g A} \quad (3.3-164)$$

The liquid and vapor mass flow rates, respectively, are defined as

$$M_f = \alpha_f \rho_f v_f A \quad (3.3-165)$$

and

$$M_g = \alpha_g \rho_g v_g A \quad (3.3-166)$$

Throughout the current literature, the overall two-phase friction pressure gradient is calculated using two-phase friction multiplier correlations. However, regardless of the correlation used, the multipliers may be interrelated using Equations (3.3-159) through (3.3-162) and the Lockhart-Martinelli<sup>3.3-46</sup> ratio defined as

$$\chi^2 = \frac{\left(\frac{dP}{dx}\right)_f}{\left(\frac{dP}{dx}\right)_g} = \frac{\phi_g^2}{\phi_f^2} \quad (3.3-167)$$

**3.3.8.2 The HTFS Two-Phase Friction Multiplier Correlation.** The HTFS correlation<sup>3.3-44</sup> is used to calculate the two-phase friction multipliers. This correlation was chosen because it is correlated to empirical data over very broad ranges of phasic volume fractions, phasic flow rates and phasic flow regimes. The correlation has also been shown to give good agreement with empirical data.

The HTFS correlation for the two-phase friction multiplier<sup>3.3-44</sup> is expressed as

$$\phi_f^2 = 1 + \frac{C}{\chi} + \frac{1}{\chi^2} \quad (3.3-168)$$

for the liquid-alone multiplier, or

$$\phi_g^2 = \chi^2 + C\chi + 1 \quad (3.3-169)$$

for the vapor-alone multiplier, where C is the correlation coefficient and  $\chi$  is the Lockhart-Martinelli ratio given by Equation (3.3-167). The correlation term is expressed in terms of scalar mass flux, G, and the Baroczy dimensionless property index,  $\Lambda$ , such that

$$2 \leq C = -2 + f_1(G) T_1(\Lambda, G) \quad (3.3-170)$$

where

$$f_1(G) = 28 - 0.3 \sqrt{G} \quad (3.3-171)$$

$$T_1(\Lambda, G) = \exp \left[ \frac{(\log_{10}\Lambda + 2.5)^2}{2.4 - G(10^{-4})} \right] \quad (3.3-172)$$

$$\Lambda = \frac{\rho_g \left( \frac{\mu_f}{\mu_g} \right)^{0.2}}{\rho_f} \quad (3.3-173)$$

The terms  $\rho$ ,  $\mu$ ,  $\alpha$  and  $v$  denote the density, viscosity, volume fraction and velocity, respectively.

If the HTFS correlation is combined with the wall friction formulations by combining Equations (3.3-159) through (3.3-162), (3.3-165) through (3.3-167), (3.3-169), and (3.3-170), then

$$\left( \frac{dP}{dx} \right)_{2\phi} = \phi_f^2 \left( \frac{dP}{dx} \right)_f = \phi_g^2 \left( \frac{dP}{dx} \right)_g = \frac{1}{2D} \{ \lambda'_f \rho_f (\alpha_f v_f)^2 + C [ \lambda'_f \rho_f (\alpha_f v_f)^2 \lambda'_g \rho_g (\alpha_g v_g)^2 ]^{1/2} + \lambda'_g \rho_g (\alpha_g v_g)^2 \} \quad (3.3-174)$$

**3.3.8.3 Partitioning of Wall Friction.** Two-phase friction can be modeled in terms of two-phase friction multipliers and known friction factors using the method developed by Lockhart-Martinelli.<sup>3.3-46</sup> Chisholm<sup>3.3-45</sup> also developed a theoretical basis for the Lockhart-Martinelli model that provides a rationale for partitioning the overall wall friction between the phases which is independent of the model for interfacial friction.

From the theoretical basis developed by Chisholm, the phasic momentum equations can be expressed in scalar form as

$$\alpha_f A \left( \frac{dP}{dx} \right)_{2\phi} - \tau_f p_f + S_{FI} = 0 \quad (3.3-175)$$

for the liquid, and

$$\alpha_g A \left( \frac{dP}{dx} \right)_{2\phi} - \tau_g p_g - S_{FI} = 0 \quad (3.3-176)$$

for the vapor, where  $\tau_f$  and  $\tau_g$  are the liquid and vapor wall shear stresses, respectively,  $p_f$  and  $p_g$  are the liquid and vapor wetted perimeters, respectively, and  $S_{FI}$  is a stress gradient due to interphase friction. Eliminating the overall pressure gradient between these two equations determines the interfacial friction term in terms of the ratio of the phasic shear stresses and phasic wetted perimeters.

$$\frac{1 + S_R \left( \frac{\alpha_g}{\alpha_f} \right)}{(1 - S_R)} = \frac{(\tau_f p_f) / \alpha_f}{(\tau_g p_g) / \alpha_g} = Z^2 \quad (3.3-177)$$

where the interphase friction term,  $S_R$ , is defined as

$$S_R = \frac{S_{FI}}{\alpha_g A \left( \frac{dP}{dx} \right)_{2\phi}} \quad (3.3-178)$$

Equation (3.3-177) can be rearranged to give a relation for the interfacial shear stress gradient in terms of the ratio of the phasic wall shear forces. This relation can then be substituted into the quasi-static momentum balances to give a relation for the individual phasic wall shear force gradients in terms of the overall wall friction and the ratio of the phasic wall shear stresses.

$$\tau_f p_f = \alpha_f \frac{dP}{dx} \Big|_{2\phi} \left( \frac{Z^2}{\alpha_g + \alpha_f Z^2} \right) \quad (3.3-179)$$

and

$$\tau_g p_g = \alpha_g \frac{dP}{dx} \Big|_{2\phi} \left( \frac{1}{\alpha_g + \alpha_f Z^2} \right) \quad (3.3-180)$$

These relations are nothing more than a rearrangement of the quasi-static momentum equations and have only eliminated one unknown, the interfacial shear stress in terms of another unknown,  $Z^2$ , the ratio of the phasic wall friction gradients. Chisholm postulated that the phasic wall shear stress could be determined using Darcy-Weisbach friction factors computed from Reynolds numbers based on phasic properties as

$$\tau_f = \lambda (Re_f) \frac{\rho_f v_f^2}{2} \quad (3.3-181)$$

where

$$\lambda(Re_f) = \text{liquid Darcy friction factor} \quad (3.3-182)$$

$$Re_f = \text{liquid Reynolds number} \quad (3.3-183)$$

$$= \frac{\rho_f v_f D_f}{\mu_f} \quad (3.3-184)$$

$$D_f = \text{liquid hydraulic diameter} \quad (3.3-185)$$

$$= \frac{4A_f}{p_f} \quad (3.3-186)$$

$$A_f = \text{liquid flow area} \quad (3.3-187)$$

$$= \alpha_f A \quad (3.3-188)$$

$$p_f = \text{liquid wetted perimeter} \quad (3.3-189)$$

$$= \alpha_{fw} p \quad (3.3-190)$$

where  $\alpha_{fw}$  is the liquid fraction on the wall, and the vapor shear stress is defined in an analogous manner based on vapor properties. Substituting the liquid shear stress from Equation (3.3-181) and the liquid wetted perimeter from Equation (3.3-190) and the analogous expressions for the vapor friction factor and wetted perimeter, defines the unknown parameter  $Z^2$

$$Z^2 = \frac{\lambda_f (Re_f) \rho_f v_f^2 \frac{\alpha_{fw}}{\alpha_f}}{\lambda_g (Re_g) \rho_g v_g^2 \frac{\alpha_{gw}}{\alpha_g}} \quad (3.3-191)$$

Substituting Equation (3.3-191) into the relations for the phasic wall friction forces Equations (3.3-179) and (3.3-180) yields equations which determine the magnitude of the phasic wall friction force in terms of the overall wall friction force and the ratio of the phasic wall frictional forces, independent of the formulation for the interfacial shear forces and independent of the particular model for the overall wall frictional force.

It should be noted that the calculation of the phasic friction factors using the Reynolds numbers defined above and the assumption that two-phase flows behave similarly to single-phase flows in the laminar, transition, and turbulent regimes provides the rationale relating Equations (3.3-179) and (3.3-180) to empirical data. It is this same rationale that allows the correlating term  $Z^2$  to be expressed in terms of friction factors that are independent of interphase friction as given by Equation (3.3-177). It is this equation that forms the basis for apportioning the overall two-phase wall friction between the phases.

**3.3.8.4 RELAP5 Wall Friction Coefficients.** The RELAP5 phasic momentum equations, Equations (3.1-6) and (3.1-7) can be written in a quasi-static form similar to Equations (3.3-175) and (3.3-176), except that the wall friction terms are in terms of the RELAP5 wall friction coefficients instead of phasic wall shear stresses. Comparison of these two forms of the momentum equations provides a definition of the RELAP5 phasic wall friction coefficients as

$$FWF(\alpha_f p_f v_f) A = \tau_f p_f A = \alpha_f \left( \frac{dP}{dx} \right) \Big|_{2\phi} \left( \frac{Z^2}{\alpha_g + \alpha_f Z^2} \right) A \quad (3.3-192)$$

and

$$FWG(\alpha_g p_g v_g) A = \tau_g p_g A = \alpha_g \left( \frac{dP}{dx} \right) \Big|_{2\phi} \left( \frac{1}{\alpha_g + \alpha_f Z^2} \right) A \quad (3.3-193)$$

Taking the sum of these two equations gives the overall quasi-static, two-phase wall friction pressure gradient as

$$FWF(\alpha_f p_f v_f) A + FWG(\alpha_g p_g v_g) A = \left( \frac{dP}{dx} \right) \Big|_{2\phi} A \quad (3.3-194)$$

**3.3.8.5 Flow Regime Factors for Phasic Wall Friction.** Phasic wall friction is expressed in terms of wall shear stress, which, in turn, requires knowledge of the surface area wetted by each phase. From the flow regime model discussed in Section 3.3.1 through Section 3.3.4 expressions for the wall film phasic volume fractions can be derived. Using these expressions, the phasic wall friction factor that appears in Equations (3.3-181) may then be computed.

In the flow regime map, eight flow regimes are modeled, which are: for pre-CHF heat transfer, the bubbly, slug, and annular mist; for post-CHF heat transfer, the inverted-annular, inverted-slug and mist; and for stratified flow, the vertically and horizontally stratified. For the transition regime between pre- and post-CHF heat transfer, an interpolation scheme is also implemented in the code.

To implement flow regime effects in the two-phase wall friction model, first consider the wall liquid and vapor volume fractions. These terms are

$$\frac{p_f}{p} = \alpha_{fw} \quad (3.3-195)$$

which represents the liquid volume fraction in the wall film, and

$$\frac{p_g}{p} = \alpha_{gw} \quad (3.3-196)$$

which represents the vapor volume fraction in the wall film, where the terms  $p_f$ ,  $p_g$ , and  $p$  are the perimeters wetted by the liquid, vapor, and mixture, respectively. Then, from the flow regime model, these are formulated for all of the flow regimes as follows:

For the bubbly regime,

$$\alpha_{fw} = \alpha_f \text{ and } \alpha_{gw} = \alpha_g \quad (3.3-197)$$

where  $\alpha_f$ ,  $\alpha_g$  are the overall liquid and vapor volume fractions, respectively.

For the slug regime,

$$\alpha_{fw} = 1 - \alpha_{gs} \text{ and } \alpha_{gw} = \alpha_{gs} \quad (3.3-198)$$

where  $\alpha_{gs}$  is given by Equation (3.3-124).

For the annular-mist regime,

$$\alpha_{fw} = (\alpha_{ff})^{1/4} \text{ and } \alpha_{gw} = 1 - (\alpha_{ff})^{1/4} \quad (3.3-199)$$

where  $\alpha_{ff}$  is given by Equation (3.3-129).

For the inverted-annular regime,

$$\alpha_{fw} = 1 - (\alpha_{gg})^{1/4} \text{ and } \alpha_{gw} = (\alpha_{gg})^{1/4} \quad (3.3-200)$$

where  $\alpha_{gg}$  is the inverted form of Equation (3.3-129).

For the inverted-slug regime,

$$\alpha_{fw} = \alpha_{fs} \text{ and } \alpha_{gw} = 1 - \alpha_{fs} \quad (3.3-201)$$

where  $\alpha_{fs}$  is the inverted form of Equation (3.3-124).

For the mist regime,

$$\alpha_{fw} = \alpha_f \text{ and } \alpha_{gw} = \alpha_g \quad (3.3-202)$$

similar to the bubbly regime.

For the vertically stratified regime,

$$\alpha_{fw} = \alpha_f \text{ and } \alpha_{gw} = \alpha_g \quad (3.3-203)$$

For the horizontally stratified regime,

$$\alpha_{fw} = 1 - \frac{\theta}{\pi} \text{ and } \alpha_{gw} = \frac{\theta}{\pi} \quad (3.3-204)$$

where  $\theta$  results from the solution of Equation (3.1-73).

**3.3.8.6 The Friction Factor Model.** In RELAP5 the Darcy-Weisbach friction factor is computed from correlations for laminar and turbulent flows with interpolation in the transition regime. There are two turbulent flow friction factor models. The first model computes the turbulent friction factor using an engineering approximation to the Colebrook-White correlation,<sup>3.3-47</sup> while the second model uses an exponential function with users' input coefficients.

The friction factor model is simply an interpolation scheme linking the laminar, laminar-turbulent transition, and turbulent flow regimes. The laminar friction factor is calculated as

$$\lambda_L = \frac{64}{Re\Phi_s}, \quad 0 \leq Re \leq 2200 \quad (3.3-205)$$

where  $Re$  is the Reynolds number and  $\Phi_s$  is a user input shape factor for noncircular flow channels. The friction factor in the transition region between laminar and turbulent flows is computed by linear interpolation as

$$\lambda_{L,T} = \left( \frac{Re - 2200}{3000 - 2200} \right) (\lambda_{T,3000} - \lambda_{L,2200}) + \lambda_{L,2200} \quad \text{for } 2200 < Re < 3000 \quad (3.3-206)$$

where  $\lambda_{L,2200}$  is the laminar factor at a Reynolds number of 2200,  $\lambda_{T,3000}$  is the turbulent friction factor at a Reynolds number of 3000, and the interpolation factor is defined to lie between zero and one.

The turbulent friction factor is given by the Zigrang-Sylvester approximation<sup>3.3-48</sup> to the Colebrook-White correlation<sup>3.3-47</sup> as,

$$\frac{1}{\sqrt{\lambda_T}} = -2\log_{10} \left\{ \frac{\varepsilon/D}{3.7} + \frac{2.51}{Re} \left[ 1.14 - 2\log_{10} \left( \frac{\varepsilon}{D} - \frac{21.25}{Re^{0.9}} \right) \right] \right\} \quad (3.3-207)$$

where  $\varepsilon$  is the surface roughness, and the other variables have been defined previously. The Zigrang-Sylvester equation, Equation (3.3-207), has the advantage that it is an explicit relation for the friction factor, while the Colebrook-White correlation is a transcendental function requiring iteration for the determination of the friction factor. Reference 3.3-48 incorrectly uses 1.114 rather than the correct value 1.14.

**3.3.8.7 Heated Wall Effect.** The friction model as described above applies to unheated surfaces. The user may correct the isothermal friction factor for the variation of the fluid viscosity near a heated surface using the relationship used in the VIPRE code.<sup>3.3-49</sup> This relation is given by

$$\frac{f}{f_{iso}} = 1 + \frac{P_H}{P_W} \left( \left( \frac{\mu_{wall}}{\mu_{bulk}} \right)^D - 1 \right) \quad (3.3-208)$$

where  $f_{iso}$  is the friction factor evaluated with properties at the bulk fluid temperature,  $P_H$  is the heated perimeter of the surface,  $P_W$  is the wetter perimeter of the surface,  $\mu_{wall}$  is the viscosity evaluated at the surface temperature,  $\mu_{bulk}$  is the viscosity evaluated at the bulk fluid temperature, and the exponent D is a user input constant (viscosity ratio exponent).

### 3.3.9 Wall Heat Transfer Models

In RELAP5/MOD3.2 the total wall heat flux ( $q''$ ) is the heat flux to vapor plus the heat flux to liquid:

$$q'' = h_g (T_w - T_{refg}) + h_f (T_w - T_{reff}) \quad (3.3-209)$$

where

$h_g$  = heat transfer coefficient to gas,

$h_f$  = heat transfer coefficient to liquid,

$T_w$  = wall temperature,

$T_{refg}$  = gas reference temperature,

$T_{reff}$  = liquid reference temperature.

The reference temperatures can be the local gas or liquid temperature or the saturation temperature, depending on the heat transfer coefficient correlation being used.

A code user may flag a heat transfer structure as a reflood structure. Structures flagged as reflood structures employ axial conduction. RELAP5/MOD3.2 uses the same wall heat transfer logic for reflood flagged surfaces as it does for other surfaces.

A boiling curve is used in RELAP5 to govern the selection of the wall heat transfer correlations when the wall surface temperature is above the saturation temperature (superheated relative to the saturation temperature based on total pressure). When a hydraulic volume is voided and the adjacent surface temperature is subcooled, steam condensation on the surface is predicted. If noncondensable gases are present, the phenomena is more complex because while boiling is a function of the wall superheat based on the total pressure, condensation is based on the partial pressure of steam. When the wall temperature is less than the saturation temperature based on total pressure, but greater than the saturation temperature based on steam partial pressure, a convection condition exists. **Figure 3.3-8** illustrates these three regions.

There are many factors to consider when deciding which convective heat transfer coefficient correlation to use. Relative factors that are addressed by the MOD3.2 logic are: (a) is the pressure above

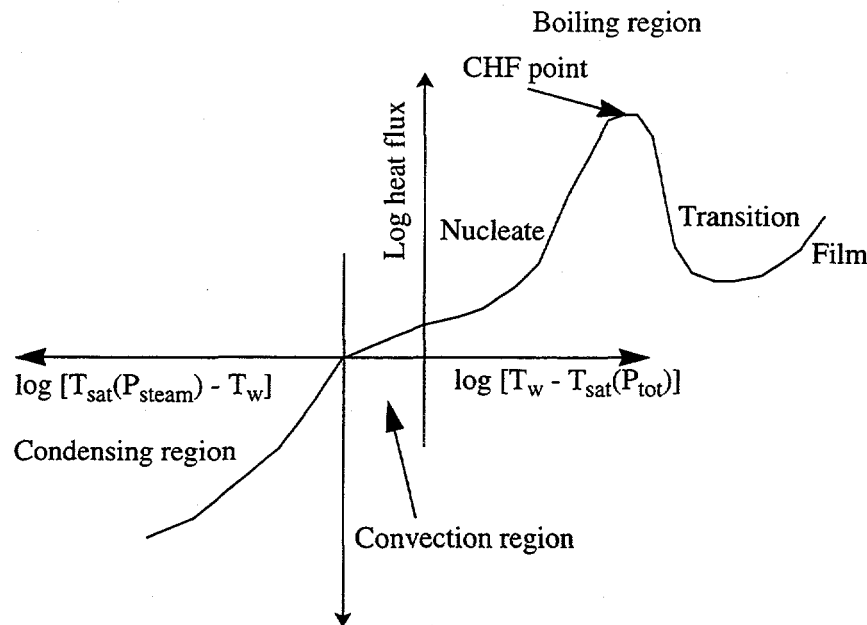
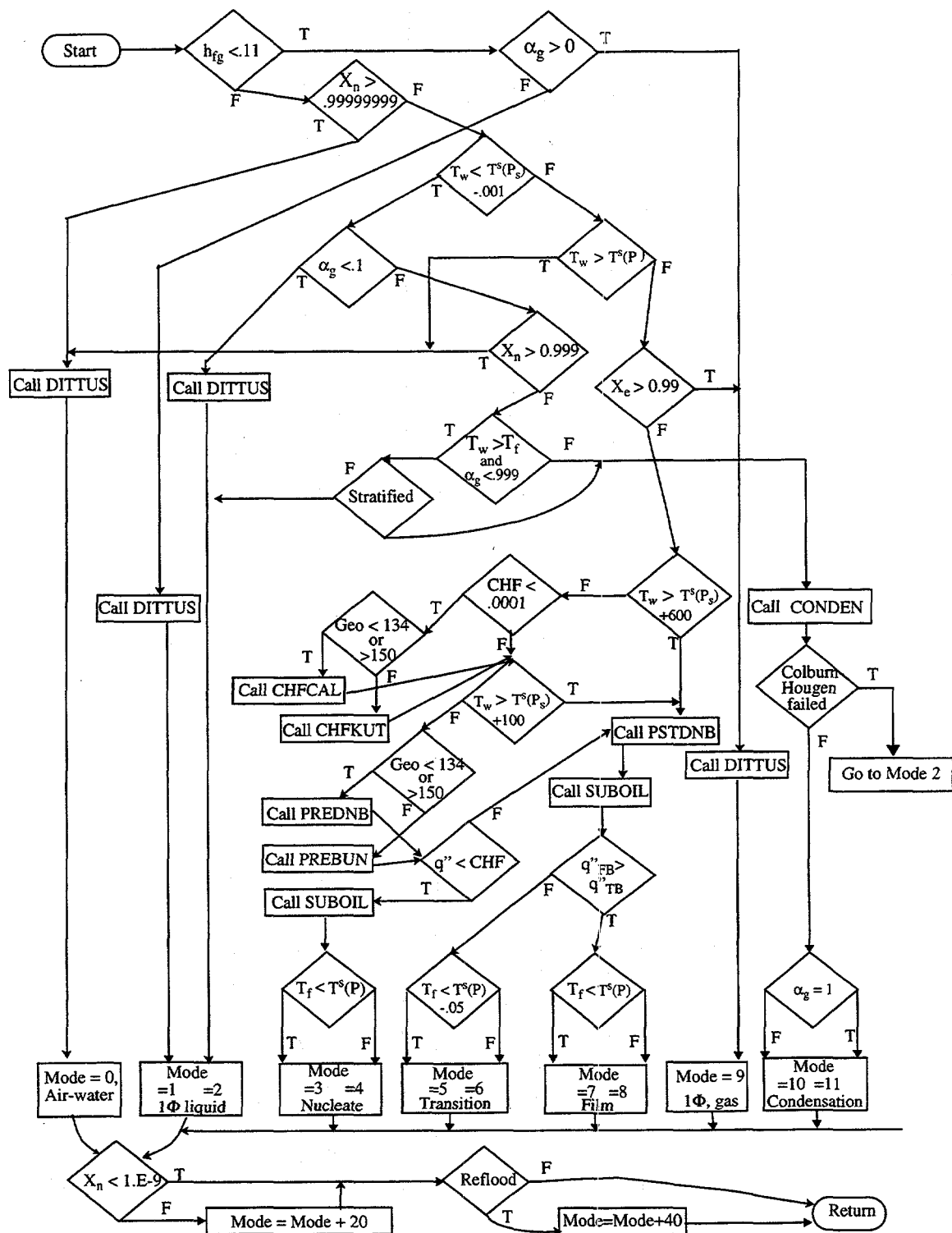


Figure 3.3-8 RELAP5 boiling and condensing curves.

the critical pressure, (b) is the wall temperature above the saturation temperature, (c) is a noncondensable gas present, (d) is the fluid liquid, two-phase, or vapor, (e) is the heat flux above the critical heat flux (CHF), and (f) is the film boiling heat flux greater than the transition boiling heat flux? The decision logic in RELAP5 leads to the selection of the appropriate correlation for the heat transfer coefficient that is used to find the heat flux.

The heat transfer mode number is a code output parameter used to inform users of the heat transfer regime or correlation selected by the code. Twelve mode numbers from 0 to 11 are possible, as shown in Figure 3.3-9, where

T	=	TRUE
F	=	FALSE
$h_{fg}$	=	saturated enthalpy difference between steam and liquid
$X_n$	=	noncondensable mass quality
$X_e$	=	equilibrium quality
$\alpha_g$	=	gas void fraction
$T_w$	=	wall temperature



**Figure 3.3-9** RELAP5 wall heat transfer flow chart.

$T^s(P)$	=	steam saturation temperature based on total pressure
$T^s(P_s)$	=	steam saturation temperature based on steam partial pressure
$T_f$	=	liquid temperature
CHF	=	critical heat flux
$q''$	=	heat flux
$q''_{FB}$	=	film boiling heat flux
$q''_{TB}$	=	transition boiling heat flux
Geom	=	type of hydraulic cell
$1\Phi$	=	single phase.

If a noncondensable gas is present, 20 is added to the mode number; and another 40 is added if the surface is a reflood surface. Most of this logic is built into the HTFC1 subroutine. The heat transfer coefficients are determined in one of five subroutines: DITTUS, PREDNB, PREBUN, PSTDNB, and CONDEN. Subroutine CONDEN calculates the coefficients when the wall temperature is below the saturation temperature based on the partial pressure of steam. DITTUS is called for single-phase liquid or vapor conditions. PREDNB contains the nucleate boiling correlations for all surfaces except horizontal bundles and PREBUN is used for the outer surface of horizontal bundles of rods or tubes. PSTDNB has the transition and film boiling correlations. Subroutine CHFKUT calculates CHF for horizontal bundles and CHFCAL determines the CHF for all other surfaces using a table lookup method. Subroutine SUBOIL calculates the vapor generation rate in the superheated liquid next to a superheated wall.

RELAP5 wall heat transfer correlations are based mainly on internal flow in pipes. Additional geometries considered in the logic are vertical and horizontal tube bundles and horizontal flat plates.

### 3.3.10 Wall Heat Transfer Correlations

The boiling curve uses the Chen<sup>3.3-50</sup> boiling correlation up to the critical heat flux point. A table lookup method<sup>3.3-51</sup> developed by Groeneveld-Cheng-Doan is used for the prediction of the critical heat flux. When the wall superheat exceeds the critical value, the heat flux for both the transition boiling and the film boiling regimes are calculated and the maximum value is used. This eliminates the need for a prediction of a minimum film boiling temperature. The Chen-Sundaram-Ozkaynak correlation<sup>3.3-52</sup> is used for transition boiling and a modified Bromley correlation<sup>3.3-53</sup> is used for film boiling.

To obtain the fraction of the boiling heat flux which causes steam generation near a superheated wall, the Lahey method<sup>3.3-54</sup> is used. The expression for mass transfer rate per unit volume, gamma, is

$$\Gamma_w = \frac{q'' A_w}{V (h_g - h_f)} \text{Mul} \quad (3.3-210)$$

where

$q''$  = total wall heat flux

$A_w$  = wall surface area

$V$  = cell volume

$\text{Mul}$  = multiplier.

The multiplier is defined as:

$$\text{Mul} = \frac{h_f - h_{cr}}{(h_f^s - h_{cr}) (1 + \varepsilon)} \quad (3.3-211)$$

where

$h_{cr}$  = critical enthalpy for net voids calculated using the Saha-Zuber<sup>3.3-55</sup> correlation (see Section 4 of Volume IV)

$\varepsilon$  = a term named the pumping term

$$\varepsilon = \frac{\rho_f [h_f - \min (h_p, h_f^s)]}{\rho_g h_{fg}} \quad (3.3-212)$$

Convection mode calculations rely on evaluating forced convection, laminar convection, and natural convection and selecting the maximum of these three. The correlations are by Dittus-Boelter,<sup>3.3-56</sup> Kays,<sup>3.3-57</sup> and Churchill-Chu,<sup>3.3-58</sup> respectively.

RELAP5 treats vertical bundles differently than pipes. The turbulent convection coefficient is multiplied by the tube pitch-to-diameter ratio as suggested by Inayatov.<sup>3.3-59</sup>

Horizontal bundles in RELAP5 differ from pipes only in their nucleate boiling and critical heat flux prediction methods. Nucleate boiling predictions follow the Polley-Ralston-Grant method<sup>3.3-60</sup> and prediction of critical heat flux uses the Folkin-Goldberg method.<sup>3.3-61</sup>

The heat transfer coefficient in the condensation mode for all geometries uses the maximum of Nusselt<sup>3.3-62</sup> and Shah.<sup>3.3-63</sup> When noncondensable gases are present the Colburn-Hougen<sup>3.3-64</sup> iteration

method is used to solve for the interface temperature between the steam and liquid and uses this value in the heat flux calculation.

Details of heat transfer coefficient correlations and implementation are given in Volume IV.

### 3.3.11 Interphase Mass Transfer

The interphase mass transfer is modeled according to the volume flow regime discussed in Section 3.3.1 through Section 3.3.4. It is used to determine the phasic interfacial area and to select the interphase heat transfer correlation for superheated liquid (SHL), subcooled liquid (SCL), superheated gas (SHG), and subcooled gas (SCG).

The mass transfer model is formulated so that the net interfacial mass transfer rate is composed of two components; the mass transfer rate in the bulk fluid, and the mass transfer rate near the wall. It is expressed as

$$\Gamma_g = \Gamma_{ig} + \Gamma_w \quad (3.3-213)$$

where  $\Gamma_{ig}$  is given by Equation (3.1-49) and  $\Gamma_w$  is presented in Volume IV.

For components not modeling wall heat transfer and for the general bulk mass transfer processes, the interfacial mass transfer model in the bulk fluid depends on the volume flow regime. In the bubbly flow regime for a condition of superheated liquid, interfacial mass transfer is the larger of either the model for bubble growth developed by Plesset and Zwick<sup>3.3-65</sup> or the model for convective heat transfer for a spherical bubble (modified Lee and Ryley).<sup>3.3-66</sup> For the bubbly flow regime with a condition of superheated vapor, an interphase heat transfer coefficient is assumed that is high enough that the vapor temperature will relax toward the equilibrium (saturation) condition. Analogously, in the mist flow regime for the condition of superheated vapor, a convective heat transfer model for a spherical droplet<sup>3.3-66</sup> is used for the interphase heat transfer coefficient. For mist flow with superheated liquid, an interphase heat transfer coefficient is assumed that is high enough that the liquid temperature will relax toward the equilibrium (saturation) condition. In the bubbly flow regime for the subcooled liquid condition, the interfacial mass transfer is calculated by the modified Unal bubble collapse model<sup>3.3-67,3.3-68</sup> and the Lahey model.<sup>3.3-54</sup> In the annular mist flow regime for the subcooled liquid condition, the interfacial mass transfer is calculated by the modified Brown droplet model<sup>3.3-69</sup> for the drops and the modified Theofanous interfacial condensation model<sup>3.3-70</sup> for the film. Correlations used to calculate the coefficients in the interfacial mass transfer in the bulk fluid are summarized in Table 3.3-4. For bubbles and drops, the critical Weber number shown is reduced by 50% in the coded value to reflect the fact that the code uses the Weber to calculate a particle size that is half the maximum size. Volume IV of this manual (Models and Correlations), from which this table was extracted and simplified, contains a more detailed description of the correlations used in each flow regime.

Table 3.3-4 RELAP5 interfacial mass transfer in bulk fluid.

#### Bubbly Flow

SHL (superheated liquid,  $\Delta T_{sf} < 0$ )

$$H_{if} = \max \left[ \begin{array}{l} -\frac{k_f}{d_b} \frac{12}{\pi} \Delta T_{sf} \frac{\rho_f C_{pf} \beta}{\rho_g h_{fg}} \\ \frac{k_f}{d_b} (2.0 + 0.74 Re_b^{0.5}) \end{array} \right] a_{gf} \quad \begin{array}{l} \text{(Plessent-Zwick)} \\ \text{(modified Lee-Ryley)} \end{array}$$

where

$$\Delta T_{sf} = T^s - T_f$$

$$Re_b = \frac{We \sigma (1 - \alpha_{bub})}{\mu_f (v_{fg}^2)^{1/2}}$$

$$We = \rho_f d_b v_{fg}^2 / \sigma = 5$$

$$d_b = \text{average bubble diameter } (= 1/2 d_{max})$$

$$\beta = 1.0 \text{ for bubbly flow}$$

$$a_{gf} = \text{interfacial area per unit volume}$$

$$= 3.6 \alpha_{bub} / d_b$$

$$\alpha_{bub} = \max (\alpha_g, 10^{-5})$$

$$v_{fg} = v_g - v_f$$

SCL (subcooled liquid,  $\Delta T_{sf} > 0$ )

$$H_{if} = \frac{F_5 h_{fg} \rho_g \rho_f \alpha_g}{\rho_f - \rho_g} \quad \begin{array}{l} \text{(modified Unal)} \\ \text{(Lahey)} \end{array}$$

where

$$F_5 = 0.075 \quad \alpha_{bub} \geq 0.25$$

$$= 1.8 \phi C \exp(-45\alpha_{bub}) + 0.075 \quad \alpha_{bub} < 0.25$$

$$C = 65.0 - 5.69 \times 10^{-5} (P - 1.0 \times 10^5) \frac{1}{K \cdot s} \quad P \leq 1.1272 \times 10^6 \text{ Pa}$$

$$= 2.5 \times 10^9 / P^{1.418} \frac{1}{K \cdot s} \quad P > 1.1272 \times 10^6 \text{ Pa}$$

P = pressure (Pa)

$\phi = 1.0 \quad |v_f| \leq 0.61 \text{ m/s}$

$$= [1.639344|v_f|]^{0.47} \quad |v_f| > 0.61 \text{ m/s.}$$

**SHG** (superheated gas,  $\Delta T_{sg} < 0$ )

$$H_{ig} = h_{ig} a_{gf}$$

where

$$h_{ig} = 10^4 \text{ W/m}^2\text{-K}$$

$a_{gf}$  is as for bubbly SHL.

**SCG** (subcooled gas,  $\Delta T_{sg} > 0$ )

$H_{ig}$  is as for bubbly SHG

### Slug Flow

**SHL** ( $\Delta T_{sf} < 0$ )

$$H_{if} = H_{if,Tb} + H_{if,bub}$$

where

$$H_{if,Tb} = 3 \times 10^6 a_{gf,Tb}^* \alpha_{Tb}$$

where

$a_{gf,Tb}^*$  = volumetric interfacial area =  $[4.5/D] (2)$ , where 2 is a roughness factor

$\alpha_{Tb}$  = Taylor bubble void fraction =  $(\alpha_g - \alpha_{gs}) / (1 - \alpha_{gs})$

= Taylor bubble volume/total volume

$\alpha_{gs}$  = the average void fraction in the liquid film and slug region

$$\begin{aligned}
 &= \alpha_{BS} F_9 \\
 F_9 &= \exp \left[ -8 \left( \frac{\alpha_g - \alpha_{BS}}{\alpha_{SA} - \alpha_{BS}} \right) \right] \\
 \alpha_{BS} &= \alpha_g \text{ for bubbly-slug transition (see Section 3.3.1)} \\
 \alpha_{SA} &= \alpha_g \text{ for slug-annular mist transition (see Section 3.3.1)}
 \end{aligned}$$

and

$H_{if,bub}$  is as for  $H_{if}$  for bubbly SHL with the following modifications:

$$\begin{aligned}
 \alpha_{bub} &= \alpha_{AB} F_9 \\
 v_{fg} &= (v_g - v_f) F_9^2 \\
 a_{gf,bub} &= (a_{gf})_{bub} (1 - \alpha_{Tb}) F_9 \\
 \beta &= F_9.
 \end{aligned}$$

**SCL** ( $\Delta T_{sf} > 0$ )

$$H_{if} = H_{if,Tb} + H_{if,bub}$$

where

$$H_{if,Tb} = 1.18942 \text{Re}_f^{0.5} \text{Pr}_f^{0.5} \frac{k_f}{D} a_{gf,Tb}^* \alpha_{Tb}$$

where

$\alpha_{Tb}$  and  $a_{gf,Tb}^*$  are as for slug SHL

$$\begin{aligned}
 \text{Pr}_f &= C_{pf} \mu_f / k_f \\
 \text{Re}_f &= \rho_f D |v_f - v_g| / \mu_f
 \end{aligned}$$

and

$H_{if,bub}$  is as for bubbly SCL.

**SHG** ( $\Delta T_{sg} < 0$ )

$$H_{ig} = H_{ig,Tb} + H_{ig,bub}$$

where

$$H_{ig,Tb} = (2.2 + 0.82 Re_g^{0.5}) \frac{k_g}{D} a_{gf,Tb}^* \alpha_{Tb}$$

where

$a_{gf,Tb}^*$  and  $\alpha_{Tb}$  are as for slug SHL

$$Re_g = \rho_g |v_f - v_g| D / \mu_g$$

and

$$H_{ig,bub} = h_{ig} (1 - \alpha_{Tb}) a_{gf,bub}$$

where

$\alpha_{Tb}$  and  $a_{gf,bub}$  are as for slug SHL

and

$h_{ig}$  is as for bubbly SHG.

**SCG** ( $\Delta T_{sg} > 0$ )

$$H_{ig} = H_{ig,Tb} + H_{ig,bub}$$

where

$$H_{ig,Tb} = h_{ig} \alpha_{Tb} a_{gf,Tb}^*$$

where  $\alpha_{Tb}$  and  $a_{gf,Tb}^*$  are as for slug SHL

$h_{ig}$  is as for bubbly SHG

and

$H_{ig,bub}$  is as for slug SHG.

### Annular Mist Flow

**SHL** ( $\Delta T_{sf} < 0$ )

$$H_{if} = H_{if,ann} + H_{if,drp}$$

where

$$H_{if,ann} = 3.0 \times 10^6 a_{gf,ann}$$

where

$$a_{gf,ann} = (4C_{ann}/D)(1 - \alpha_{ff})^{1/2}$$

$$C_{ann} = (30\alpha_{ff})^{1/8} (2.5), 2.5 \text{ is a roughness factor}$$

$$\alpha_{ff} = \alpha_f F_{11}$$

$$F_{11} = (1 - G^*) \exp(-C_e \times 10^{-5} \lambda^6)$$

$$C_e = 4.0 \text{ horizontal}$$

$$= 7.5 \text{ vertical}$$

$$\lambda = |v_g - v_f|/v_{crit} \text{ horizontal flow}$$

$$= \alpha_g v_g / v_{crit} \text{ vertical flow}$$

$$v_{crit} (\text{horizontal}) = 0.5 \left[ \frac{(\rho_f - \rho_g) g \alpha_g A_{\text{pipe}}}{\rho_g D \sin \theta} \right]^{1/2} (1 - \cos \theta), [\text{see Equation (3.3-30)}]$$

$$v_{crit} (\text{vertical}) = 3.2 [\sigma g (\rho_f - \rho_g)]^{1/4} / \rho_g^{1/2} [\text{see Equation (3.3-19)}]$$

$$G^* = 10^{-4} Re_f^{0.25}$$

$$Re_f = \alpha_f \rho_f |v_f| D / \mu_f$$

$$H_{if,drp} = \frac{k_f}{d_d} F_{13} a_{gf,drp}$$

$$d_d = \frac{We \sigma}{\rho_g v_{fg}^2}, We = 1.5, We \sigma = \max(We \sigma, 10^{-10})$$

$$v_{fg} = v_g - v_f$$

$$\alpha_{fd} = \max \left[ \frac{\alpha_f - \alpha_{ff}}{1 - \alpha_{ff}}, (1 - \alpha_{AM}) \right]$$

$$F_{13} = 2.0 + 7.0 \min \left[ 1.0 + \frac{C_{pf} \max (1.0, \Delta T_{sf})}{h_{fg}}, 8.0 \right]$$

$$a_{gf,drp} = \frac{3.6 \alpha_{fd}}{d_d} (1 - \alpha_{ff}).$$

For an annulus component,  $\alpha_{ff} = \alpha_f$  and  $\alpha_{fd} = 0$ .

**SCL** ( $\Delta T_{sf} > 0$ )

$$H_{if} = H_{if,ann} + H_{if,drp}$$

where

$$H_{if,ann} = 10^{-3} \rho_f C_{pf} |v_f| a_{gf,ann} \quad (\text{modified Theofanous})$$

where

$a_{gf,ann}$  is as for annular mist SHL

and

$$H_{if,drp} = \frac{k_f}{d_d} F_{13} a_{gf,drp} \quad (\text{modified Brown})$$

where

$a_{gf,drp}$ ,  $F_{13}$ , and  $d_d$  are as for annular mist SHL.

For an annulus component,  $\alpha_{ff} = \alpha_f$  and  $\alpha_{fd} = 0$ .

**SHG** ( $\Delta T_{sg} < 0$ )

$$H_{ig} = H_{ig,ann} + H_{ig,drp}$$

where

$$H_{ig,ann} = \frac{k_g}{D} 0.023 Re_g^{0.8} a_{gf,ann}$$

where

$$Re_g = \rho_g |v_g - v_f| D \alpha_g / \mu_g$$

$a_{gf,ann}$  is as for annular mist SHL, and

$$H_{ig,drp} = \frac{k_g}{d_d} (2.0 + 0.5 Re_d^{0.5}) a_{gf,drp} \text{ (Lee-Riley)}$$

where

$d_d$  is as for annular mist SHL

$$Re_d = \frac{We \sigma (1 - \alpha_{drp})^3}{\mu_g [v_{fg}^2 (1 - \alpha_{drp})]^{1/2}}, \text{ where } We = 1.5$$

$a_{gf,drp}$ ,  $\alpha_{drp}$ , and  $v_{fg}^2$  are as for annular mist SHL.

For an annulus component,  $\alpha_{ff} = \alpha_f$  and  $\alpha_{fd} = 0$ .

SCG ( $\Delta T_{sg} > 0$ )

$$H_{ig} = H_{ig,ann} + H_{ig,drp}$$

where

$$H_{ig,ann} = h_{ig} a_{gf,ann}$$

where  $h_{ig}$  is as for bubbly SHG and  $a_{gf,ann}$  is as for annular mist SHL

and

$$H_{ig,drp} = h_{ig} a_{gf,drp}$$

where

$h_{ig}$  is as for bubbly SHG and

$a_{gf,drp}$  is as for annular mist SHG.

For an annulus component,  $\alpha_{ff} = \alpha_f$  and  $\alpha_{fd} = 0$ .

### Inverted Annular Flow

**SHL ( $\Delta T_{sf} < 0$ )**

$$H_{if} = H_{if,bub} + H_{if,ann}$$

where

$H_{if,bub}$  is as for  $H_{if}$  for bubbly with the following modifications:

$$v_{fg} = (v_g - v_f) F_{16}^2$$

where

$$F_{16} = 1 - F_{17}$$

$$F_{17} = \exp \left[ \frac{-8(\alpha_{BS} - \alpha_{IAN})}{\alpha_{BS}} \right]$$

$$\alpha_{IAN} = \alpha_g \text{ inverted annular}$$

$$= \alpha_{AB} \text{ IAN/ISL transition (see Figure 3.3-1)}$$

$$\beta = F_{16}$$

$$\alpha_g = \alpha_{bub}$$

$$\alpha_{bub} = \frac{(\alpha_{IAN} - \alpha_B)}{(1 - \alpha_B)}$$

$$\alpha_B = F_{17} \alpha_{IAN}$$

$$a_{gf,bub} = \frac{3.6 \alpha_{bub}}{d_b} (1 - \alpha_B) F_{16}$$

and

$$H_{if,ann} = 3 \times 10^6 a_{gf,ann}$$

where

$$a_{gf,ann} = \frac{4}{D} F_{15} (2.5), \text{ where 2.5 is a roughness factor}$$

$$F_{15} = (1 - \alpha_B)^{1/2}.$$

SCL ( $\Delta T_{sf} > 0$ )

$$H_{if} = H_{if,bub} + H_{if,ann}$$

where

$H_{if,bub}$  is as for bubbly SCL

and

$$H_{if,ann} = \frac{k_f}{D} 0.023 Re_{IAN}^{0.8} a_{gf,ann}$$

where

$$Re_{IAN} = \rho_f |v_f - v_g| (1 - \alpha_{IAN}) / \mu_f$$

$a_{gf,ann}$  and  $\alpha_{IAN}$  are as for inverted annular SHL.

SHG ( $\Delta T_{sg} < 0$ )

$$H_{ig} = H_{ig,bub} + H_{ig,ann}$$

where

$$H_{ig,bub} = h_{ig} a_{gf,bub}$$

where

$h_{ig}$  is as for bubbly SHG and  $a_{gf,bub}$  is as for inverted annular SHL

and

$$H_{ig,ann} = \frac{k_g}{D} a_{gf,ann}$$

where

$a_{gf,ann}$  is as for inverted annular SHL.

SCG ( $\Delta T_{sg} > 0$ )

$H_{ig}$  is as for inverted annular SHG.

### Inverted Slug Flow

SHL ( $\Delta T_{sf} < 0$ )

$$H_{if} = H_{if,ann} + H_{if,drp}$$

where

$$H_{if,ann} = \frac{k_f}{D} F_{13} a_{gf,ann}$$

where

$$a_{gf,ann} = \frac{4.5}{D} \alpha_B (2.5), \text{ where 2.5 is a roughness factor}$$

$$\alpha_B = (\alpha_f - \alpha_{drp}) / (1 - \alpha_{drp})$$

$$\alpha_{drp} = (1 - \alpha_{AM}) F_{21}$$

$$F_{21} = \exp \left[ - \frac{(\alpha_{AM} - \alpha_g)}{(\alpha_{AM} - \alpha_{BS})} \right]$$

and

$$H_{if,drp} = \frac{k_f}{d_d} F_{13} a_{gf,drp}$$

where

$$a_{gf,drp} = (3.6 \alpha_{drp} / d_d) (1 - \alpha_B)$$

$d_d$  = characteristic droplet diameter

$$= \frac{We \sigma}{\rho_g V_{fg}^2}, \text{ where } We = 6.0$$

$$V_{fg} = (v_g - v_f) F_{21}^2$$

SCL ( $\Delta T_{sf} > 0$ )

$$H_{if} = H_{if,ann} + H_{if,drp}$$

where

$$H_{if,ann} = \frac{k_f}{D} F_{13} a_{gf,ann}$$

where

$F_{13}$  is as for annular mist SCL

$a_{gf,ann}$  is as for inverted slug SHL

and

$$H_{if,drp} = \frac{k_f}{d_d} F_{13} a_{gf,drp}$$

where

$a_{gf,drp}$  is as for inverted slug SHL.

SHG ( $\Delta T_{sg} < 0$ )

$$H_{ig} = H_{ig,ann} + H_{ig,drp}$$

where

$$H_{ig,ann} = \frac{k_g}{D} a_{gf,ann}$$

where

$a_{gf,ann}$  is as for inverted slug SHL

and

$$H_{ig,drp} = \frac{k_g}{d_d} (2.0 + 0.5 Re_{drp}^{0.5}) a_{gf,drp}$$

where

$d_d$  and  $a_{gf,drp}$  are as for inverted slug SHL

and

$$Re_{drp} = \frac{\rho_g v_{fg} d_d}{\mu_g}$$

**SCG** ( $\Delta T_{sg} > 0$ )

$H_{ig}$  is as for inverted slug SHG.

### Dispersed (Droplet) Flow

**SHL** ( $\Delta T_{sf} < 0$ )

$$H_{if} = \frac{k_f}{d_d} F_{13} a_{gf}$$

where

$$a_{gf} = 3.6 \alpha_f / d_d$$

$$d_d = \frac{We \sigma}{\rho_g v_{fg}^2}, \text{ where } We = 1.5 \text{ for pre-CHF and } 6.0 \text{ for post-CHF}$$

$$v_{fg} = v_g - v_f$$

**SCL** ( $\Delta T_{sf} > 0$ )

$$H_{if} = \frac{k_f}{d_d} a_{gf}$$

where

$F_{13}$  is as for annular mist SCL

$a_{gf}$  is as for dispersed SHL.

**SHG** ( $\Delta T_{sg} < 0$ )

$$H_{ig} = \frac{k_g}{d_d} (2.0 + 0.5 Re_{drp}^{0.5}) a_{gf}$$

where  $d_d$ , and  $a_{gf}$  are as for dispersed SHL.

**SCG** ( $\Delta T_{sg} > 0$ )

$$H_{ig} = h_{ig} a_{gf}$$

where

$h_{ig}$  is as for bubbly SHG and

$a_{gf}$  is as for dispersed SHG.

### Horizontally Stratified Flow

$H_{if} = 0$  unless  $\alpha_g > 0$  or  $\Delta T_{sf} < -1$  K

$H_{ig} = 0$  unless  $\alpha_f > 0$  or  $\Delta T_{sg} > 0.2$  K

otherwise:

**SHL** ( $\Delta T_{sf} < 0$ )

$$H_{if} = \frac{k_f}{D_{hf}} \left[ 0.023 Re_f^{0.8} - 3.81972 \frac{\Delta T_{sf} \rho_f C_{pf}}{\rho_g h_{fg} \max(4\alpha_g, 1)} \right] a_{gf}$$

where

$$\begin{aligned} D_{hf} &= \text{liquid phase hydraulic diameter} \\ &= \pi \alpha_f D / (\pi - \theta + \sin \theta) \quad (\text{see Figure 3.1-2 for definition of } \theta) \\ Re_f &= \alpha_f \rho_f D |v_g - v_f| / \mu_f \\ a_{gf} &= (4 \sin \theta / \pi D) F_{27} \\ F_{27} &= 1 + \left| \frac{v_g - v_f}{v_{crit}} \right| \end{aligned}$$

**SCL** ( $\Delta T_{sf} > 0$ )

$$H_{if} = \frac{k_f}{D_{hf}} (0.023 Re_f^{0.8}) a_{gf}$$

where

$D_{hf}$ ,  $Re_f$  and  $a_{gf}$  are as for horizontally stratified SHL.

**SHG ( $\Delta T_{sg} < 0$ )**

$$H_{ig} = \frac{k_g}{D_{hg}} [0.023 Re_g^{0.8} + h_{ig} (4) \max (0.0, 0.25 - \alpha_g) ] a_{gf}$$

where

$D_{hg}$  = vapor phase hydraulic diameter

$$= \pi \alpha_g D / (\theta + \sin \theta)$$

$$Re_g = \alpha_g \rho_g D |v_g - v_f| / \mu_g$$

$h_{ig}$  is as for bubbly SHG, and  $a_{gf}$  is as for horizontally stratified SHL.

**SCG ( $\Delta T_{sg} > 0$ )**

$$H_{ig} = h_{ig} a_{gf}$$

where

$h_{ig}$  is as for bubbly SHG and

$a_{gf}$  is as for horizontally stratified SHL.

**Vertically Stratified Flow****SHL ( $\Delta T_{sf} < 0$ )**

$$H_{if} = H_{if,REG}$$

where

REG = flow regime of flow when not vertically stratified, which can be BBY, SLG, SLG/ANM, ANM, MPR, IAN, IAN/ISL, ISL, MST, MPO, IAN/ISL - SLG, ISL-SLG/ANM, ANM/MST, BBY/IAN, SLG/ISL (see flow regime map, **Figure 3.3-1**).

**SCL ( $\Delta T_{sf} > 0$ )**

$$H_{if} = Nu (k_f/D) a_{gf} \quad (\text{McAdams})$$

where

$$a_{gf} = \frac{A}{V} = \frac{A}{AL} = \frac{1}{L}$$

$L$  = length of volume cell

$$Nu = 0.27 (GrPr)^{0.25}$$

SHG ( $\Delta T_{sg} < 0$ )

$$H_{ig} = Nu (k_g/D) a_{gf}$$

where

$$Nu = 0.27 (GrPr)^{0.25}$$

$$a_{gf} = \frac{A}{V} = \frac{A}{AL} = \frac{1}{L}$$

$a_{gf}$  is as for vertically stratified SHL.

SCG ( $\Delta T_{sg} > 0$ )

$$H_{ig} = H_{ig,REG}$$

### 3.3.12 Direct Heating

The direct heating between the gas and liquid becomes important when there is noncondensable present. This occurs when  $P_s < P$ . The value used for the direct heat transfer coefficient is  $H_{gf} = 10^4 \text{ W/m}^3 \cdot \text{K}$ .

### 3.3.13 References

- 3.3-1. W. L. Weaver et al., *TRAC-BF1 Manual: Extensions to TRAC-BD1/MOD1*, NUREG/CR-4391, EGG-2417, August 1986.
- 3.3-2. D. D. Taylor et al., *TRAC-BD1/MOD1: An Advanced Best Estimate Computer Program for Boiling Water Reactor Transient Analysis, Volume I: Model Description*, NUREG/CR-3633, EGG-2294, April 1984.
- 3.3-3. Y. Taitel and A. E. Dukler, "A Model of Predicting Flow Regime Transitions in Horizontal and Near Horizontal Gas-Liquid Flow," *AIChE Journal*, 22, 1976, pp. 47-55.
- 3.3-4. Y. Taitel, D. Bornea, and A. E. Dukler, "Modeling Flow Pattern Transitions for Steady Upward Gas-Liquid Flow in Vertical Tubes," *AIChE Journal*, 26, 1980, pp. 345-354.

- 3.3-5. M. Ishii and G. De Jarlais, "Inverted Annular Flow Modeling," *Advanced Code Review Group Meeting, Idaho Falls, ID, July 27, 1982*.
- 3.3-6. M. Ishii and T. C. Chawla, *Local Drag Laws in Dispersed Two-Phase Flow*, NUREG/CR-1230, ANL-79-105, 1979.
- 3.3-7. M. Ishii and K. Mishima, *Study of Two-Fluid Model and Interfacial Area*, NUREG/CR-1873, ANL-80-111, 1980.
- 3.3-8. M. A. Vince and R. T. Lahey, Jr., "On the Development of An Objective Flow Regime Indicator," *International Journal of Multiphase Flow*, 8, 1982, pp. 93-124.
- 3.3-9. M. Ishii, *Thermo-Fluid Dynamic Theory of Two-Phase Flow*, Collection de la Direction des Etudes d'Recherches of Electricute de France, 1975.
- 3.3-10. D. T. Dumitrescu, "Stomung an einer Luftblase in senkrechten Rohr," *Z. Angel Math. Mech.* 23, 1943, p. 139.
- 3.3-11. V. H. Ransom et. al., *RELAP5/MOD2 Code Manual, Volume 3; Developmental Assessment Problems*, EGG-TFM-7952, Idaho National Engineering Laboratory, December, 1987.
- 3.3-12. K. Mishima and M. Ishii, "Flow Regime Transition Criteria for Upward Two-Phase Flow in Vertical Tubes," *International Journal of Heat and Mass Transfer*, 27, 1984, pp. 723-737.
- 3.3-13. K. W. McQuillan and P. B. Whalley, *Flow Patterns in Vertical Two-Phase Flow*, AERE-R 11032, 1983.
- 3.3-14. K. W. McQuillan and P. B. Whalley, "Flow Patterns in Vertical Two-Phase Flow," *International Journal of Multiphase Flow*, 11, 1985, pp. 161-175.
- 3.3-15. J. M. Putney, *An Assessment of the Annular Flow Transition Criteria and Interphase Friction Models in RELAP5/MOD2*, CERL Report RD/L/3451/R89, PWR/HTWG/P(88)653, February 1989.
- 3.3-16. V. H. Ransom et al., *RELAP5/MOD2 Code Manual*, NUREG/CR-4312, EGG-2396, August 1985.
- 3.3-17. R. A. Dimenna et al., *RELAP5/MOD2 Models and Correlations*, NUREG/CR-5194, August 1988.
- 3.3-18. T. N. Tandon, H. K. Varma, and C. P. Gupta, "A New Flow Regime Map for Condensation Inside Horizontal Tubes," *Journal of Heat Transfer*, 104, November 1982, pp. 763-768.
- 3.3-19. Y. Taitel, N. Lee, and A. E. Dukler, "Transient Gas-Liquid Flow in Horizontal Pipes: Modeling Flow Pattern Transitions," *AICHE Journal*, 24, 5, 1978, pp. 920-934.

3.3-20. J. G. M. Anderson and K. H. Chu, *BWR Refill-Reflood Program Task 4.7--Constitutive Correlations for Shear and Heat Transfer for the BWR Version of TRAC*, NUREG/CR-2134, EPRI NP-1582, 1981.

3.3-21. M. Ishii, T. Chawla, and N. Zuber, "Constitutive Equation for Vapor Drift Velocity in Two Phase Annular Flow, *AIChE Journal*, 22, 1976, pp. 283-289.

3.3-22. M. Ishii, *One-Dimensional Drift-Flux Model and Constitutive Equations for Relative Motion Between Phases in Various Two-Phase Flow Regimes*, ANL-77-47, 1977.

3.3-23. G. B. Wallis, *One-Dimensional Two-Phase Flow*, New York: McGraw-Hill Book Company, 1969.

3.3-24. A. H. Shapiro and A. J. Erickson, *Transactions of ASME*, 79, 1957, p. 775.

3.3-25. J. M. Putney, *Proposals for Improving Interphase Drag Modeling for the Bubbly and Slug Regimes in RELAP5*, CERL Report RD/L/3306/R88, PWR/HTWG/P(88)622, June 1988.

3.3-26. J. M. Putney, *Implementation of a New Bubbly-Slug Interphase Drag Model in RELAP5/MOD2*, CERL Report RD/L/3369/R88, PWR/HTWG/P(88)597, November 1988.

3.3-27. J. M. Putney, *Equations for Calculating Interfacial Drag and Shear from Void Fraction Correlations*, CERL Report RD/L/3429/R88, PWR/HTWG/P(88)630, December 1988.

3.3-28. J. M. Putney, *Development of a New Bubbly-Slug Interfacial Friction Model for RELAP5--Final Report*, National Power Report ESTD/L/0075/R89, PWR/HTWG/P(89)722, October 1989.

3.3-29. J. M. Putney, Development of a New Bubbly-Slug Interfacial Friction Model for RELAP5, *Nuclear Engineering and Design*, 131, 1991, pp. 223-240.

3.3-30. B. Chexal and G. Lellouche, *A Full-Range Drift-Flux Correlation for Vertical Flows (Revision 1)*, EPRI NP-3989-SR, September 1986.

3.3-31. B. Chexal et al., *The Chexal-Lellouche Void Fraction Correlation for Generalized Applications*, NSAC-139, April 1991.

3.3-32. N. Zuber and J. Findlay, "Average Volumetric Concentrations in Two-Phase Flow Systems," *Journal of Heat Transfer*, 87, 1965, pp. 453-568.

3.3-33. N. Zuber et al., *Steady-State and Transient Void Fraction in Two-Phase Flow Systems*, GEAP-5417, 1967.

3.3-34. I. Kataoka and M. Ishii, "Drift Flux Model for Large Diameter Pipe and New Correlation for Pool Void Fraction," *International Journal of Heat Mass Transfer*, 30, 1987, pp. 1927-1939.

- 3.3-35. S. Rouhani, *Modified Correlations for Void and Pressure Drop*, AB Atomenergi, Sweden, Internal Report AE-RTC 841, March 1969.
- 3.3-36. S. Rouhani et al., *TRAC-BF1 Models and Correlations*, NUREG/CR-4391, EGG-2680, August 1992.
- 3.3-37. G. B. Wallis and S. Makkenchey, "The Hanging Film Phenomenon in Vertical Annular Two-Phase Flow", *Transactions ASME, Series I*, 96, 1974, p. 297.
- 3.3-38. J. A. Holmes, "Description of the Drift Flux Model in the LOCA Code RELAP-UK," *I. Mech. E.*, C206/77, 1977.
- 3.3-39. V. H. Ransom et al., *RELAP5/MOD1 Code Manual*, NUREG/CR-1826, EGG-2070, March 1982.
- 3.3-40. D. Bharathan, G. B. Wallis, and H. J. Richter, *Air-Water Counter-Current Annular Flow*, EPRI/NP-1165, 1979.
- 3.3-41. G. DeJarlais and M. Ishii, *Inverted Annular Flow Experimental Study*, NUREG/CR-4277, ANL-85-31, April 1985.
- 3.3-42. N. Zuber, "On the Dispersed Two-Phase Flow in the Laminar Flow Regime," *Chemical Engineering Science*, 19, 1964, pp. 897-917.
- 3.3-43. D. A. Drew, L. Y. Cheng, and R. T. Lahey, Jr., "The Analysis of Virtual Mass Effects in Two-Phase Flow," *International Journal of Multiphase Flow*, 5, 1979, pp. 233-242.
- 3.3-44. K. T. Chaxton, J. G. Collier, and J. A. Ward, *H.T.F.S. Correlation for Two-Phase Pressure Drop and Void Fraction in Tubes*, AERE-R7162, 1972.
- 3.3-45. D. Chisholm, "A Theoretical Basis for the Lockhart-Martinelli Correlation for Two-Phase Flow," *Journal of Heat-Mass Transfer*, 10, 1967, pp. 1767-1778.
- 3.3-46. R. W. Lockhart and R. C. Martinelli, "Proposed Correlation of Data for Isothermal Two-Phase, Two-Component Flow in Pipes," *Chemical Engineering Progress*, 45, 1, 1949, pp. 39-48.
- 3.3-47. C. F. Colebrook, "Turbulent Flow in Pipes with Particular Reference to the Transition Region Between Smooth and Rough Pipe Laws," *Journal of Institute of Civil Engineers*, 11, 1939, pp. 133-156.
- 3.3-48. D. J. Zigrang and N. D. Sylvester, "A Review of Explicit Friction Factor Equations," *Transactions of ASME, Journal of Energy Resources Technology*, 107, 1985, pp. 280-283.
- 3.3-49. C. W. Stewart et al., *VIPRE-01: A Thermal-Hydraulic Code for Reactor Cores*, EPRI NP-2511-CCM, July 1985.

3.3-50. J. C. Chen, "A Correlation for Boiling Heat Transfer to Saturated Fluids in Convective Flow," *Process Design and Development*, 5, 1966, pp. 322-327.

3.3-51. D. C. Groeneveld, S. C. Cheng, and T. Doan, "1986 AECL-UO Critical Heat Flux Lookup Table," *Heat Transfer Engineering*, 7, 1-2, 1986, pp. 46-62.

3.3-52. J. C. Chen, R. K. Sundaram, and F. T. Ozkaynak, *A Phenomenological Correlation for Post-CHF Heat Transfer*, NUREG-0237, June 1977.

3.3-53. L. A. Bromley, "Heat Transfer in Stable Film Boiling," *Chemical Engineering Progress*, 46, 1950, pp. 221-227.

3.3-54. R. T. Lahey, "A Mechanistic Subcooled Boiling Model," *Proceedings Sixth International Heat Transfer Conference, Toronto, Canada*, 1978, Volume 1, pp. 293-297.

3.3-55. P. Saha and N. Zuber, "Point of Net Vapor Generation and Vapor Void Fraction in Subcooled Boiling," *Proceedings Fifth International Heat Transfer Conference*, 1974, Volume 4, pp. 175-179.

3.3-56. F. W. Dittus and L. M. K. Boelter, "Heat Transfer in Automobile Radiators of the Tubular Type," *Publications in Engineering*, 2, University of California, Berkeley, 1930, pp. 443-461.

3.3-57. W. M. Kays, "Numerical Solution for Laminar Flow Heat Transfer in Circular Tubes," *Transactions, American Society of Mechanical Engineers*, 77, 1955, pp. 1265-1274.

3.3-58. S. W. Churchill and H. H. S. Chu, "Correlating Equations for Laminar and Turbulent Free Convection From a Vertical Plate," *International Journal of Heat and Mass Transfer*, 18, 1975, pp. 1323-1329.

3.3-59. A. Y. Inayatov, "Correlation of Data on Heat Transfer Flow Parallel to Tube Bundles at Relative Tube Pitches of  $1.1 < s/d < 1.6$ ," *Heat Transfer-Soviet Research*, 7, 3, May-June 1975.

3.3-60. G. T. Polley, T. Ralston, and I. D. R. Grant, "Forced Crossflow Boiling in an Ideal In-line Tube Bundle," *ASME 80-HT-46*, 1981.

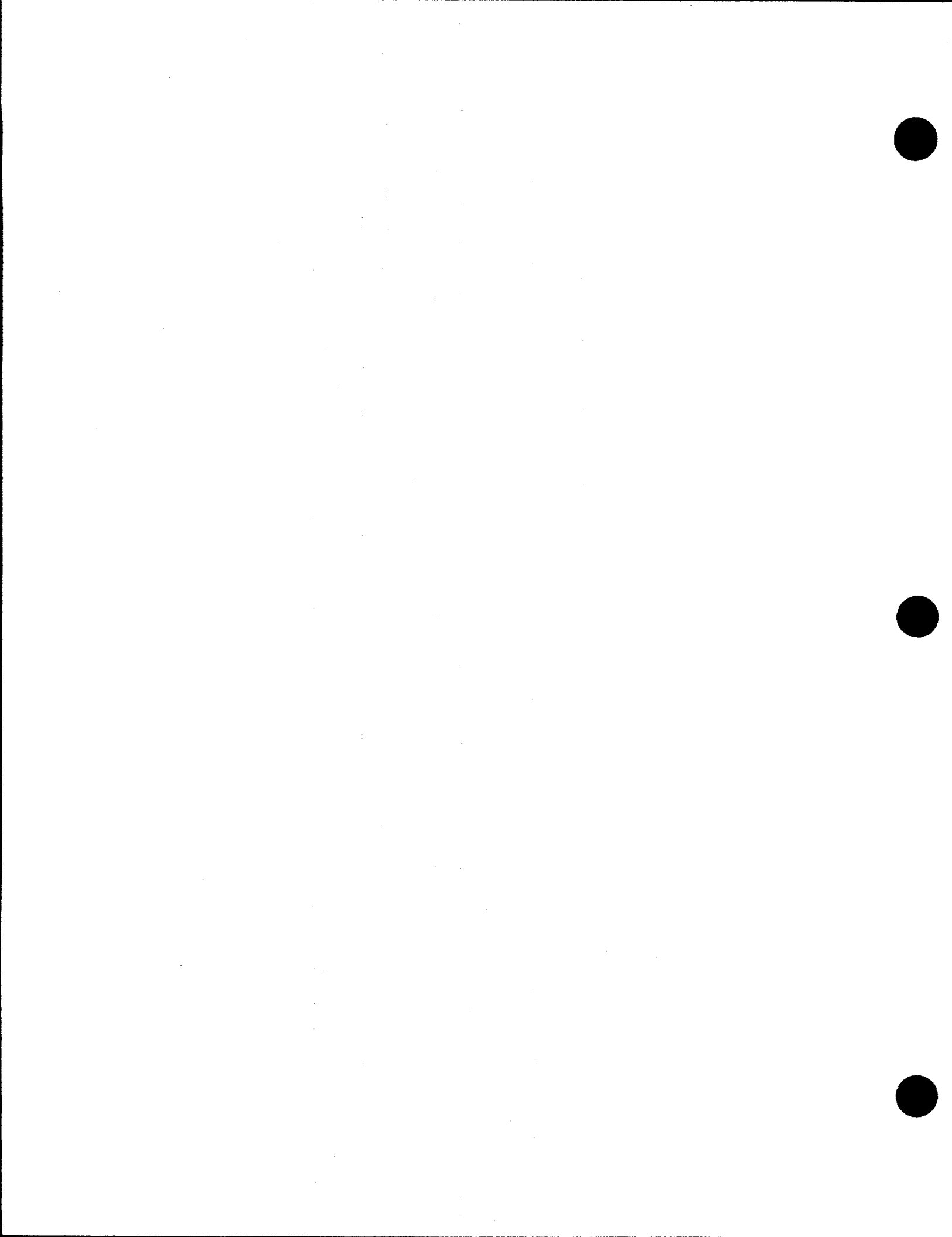
3.3-61. B. S. Folkin and Y. N. Goldberg, "Simulation of Free Convection Boiling Crisis In Vapor Blanketing of a Horizontal Tube Bundle," *Heat Transfer Soviet Research*, 12, 3, 1980, pp. 77-81.

3.3-62. W. Nusselt, "Die Oberflachenkondensation des Wasserdampfes," *Ver. deutsch. Ing.*, 60, 1916, p. 541

3.3-63. M. M. Shah, "A General Correlation for Heat Transfer during Film Condensation Inside Pipes," *International Journal of Heat and Mass Transfer*, 22, 1979, pp. 547-556.

3.3-64. A. P. Colburn and O. A. Hougen, "Design of Cooler Condensers for Mixtures of Vapors with Non-Condensing Gases," *Industrial and Engineering Chemistry* 26, 1934, pp. 1178-1182.

- 3.3-65. M. S. Plesset and S. A. Zwick, "Growth of Vapor Bubbles in Superheated Liquids," *Journal of Applied Physics*, 25, 4, 1954, pp. 493-500.
- 3.3-66. K. Lee and D. J. Ryley, "The Evaporation of Water Droplets in Superheated Steam," *Journal of Heat Transfer, ASME*, November 1968, pp. 445-456.
- 3.3-67. H. C. Unal, "Maximum Bubble Diameter, Maximum Bubble-Growth Time and Bubble-Growth Rate During the Subcooled Nucleate Flow Boiling of Water Up to 17.MN/m<sup>2</sup>," *International Journal of Heat Mass Transfer*, 19, 1976, pp. 643-649.
- 3.3-68. R. A. Riemke, "Modification to Unal's Subcooled Flow Boiling Bubble Model," *Nuclear Technology*, 102, 1993, pp. 416-417.
- 3.3-69. G. Brown, "Heat Transmission by Condensation of Steam on a Spray of Water Drops," *Institute of Mechanical Engineers*, 1951, pp. 49-52.
- 3.3-70. T. G. Theofanous, "Modeling of Basic Condensation Processes," *The Water Reactor Safety Research Workshop on Condensation, Silver Springs, MD, May 24-25, 1979*.



### 3.4 Special Process Models

Certain models in RELAP5 have been developed to simulate special processes. These models are described in the following subsections.

#### 3.4.1 Choked Flow

A choked-flow model developed by Ransom and Trapp<sup>3.4-1,3.4-2</sup> is included primarily for calculation of the mass discharge from the system at a pipe break or a nozzle. Generally, the flow at the break or nozzle is choked until the system pressure nears the containment pressure. The choked-flow model is used to predict if the flow is choked at a break or nozzle and, if it is, to establish the discharge boundary condition. In addition, the choked-flow model can be used to predict existence of and calculate choked flow at internal points in the system.

Choking is defined as the condition wherein the mass flow rate becomes independent of the downstream conditions (that point at which further reduction in the downstream pressure does not change the mass flow rate). The fundamental reason that choking occurs is that acoustic signals can no longer propagate upstream. This occurs when the fluid velocity equals or exceeds the propagation velocity. The choked-flow model is based on a definition that is established by a characteristic analysis using time-dependent differential equations.

Consider a system of  $n$  first-order, quasi-linear, partial differential equations of the form

$$A(U) (\partial U / \partial t) + B(U) (\partial U / \partial x) + C(U) = 0 . \quad (3.4-1)$$

The characteristic directions (or characteristic velocities) of the system are defined<sup>3.4-3,3.4-4</sup> as the roots,  $\lambda_j$  ( $j \leq n$ ), of the characteristic polynomial

$$(A\lambda - B) = 0 . \quad (3.4-2)$$

The real part of any root,  $\lambda_j$ , gives the velocity of signal propagation along the corresponding characteristic path in the space/time plane. The imaginary part of any complex root,  $\lambda_j$ , gives the rate of growth or decay of the signal propagating along the respective path. For a hyperbolic system in which all the roots of Equation (3.4-2) are real and nonzero, the number of boundary conditions required at any boundary point equals the number of characteristic lines entering the solution region as time increases. If we consider the system [Equation (3.4-1)] for a particular region  $0 \leq x \leq L$  and examine the boundary conditions at  $x = L$ , as long as any  $\lambda_j$  are less than zero, we must supply some boundary information to obtain the solution. If all  $\lambda_j$  are greater than or equal to zero, no boundary conditions are needed at  $x = L$ ; and the interior solution is unaffected by conditions beyond this boundary.

A choked condition exists when no information can propagate into the solution region from the exterior. Such a condition exists at the boundary point,  $x = L$ , when

$$\lambda_j \geq 0 \text{ for all } j \leq n . \quad (3.4-3)$$

These are the mathematical conditions satisfied by the equations of motion for a flowing fluid when reduction in downstream pressure ceases to result in increased flow rate. It is well known<sup>3.4-5</sup> that the choked condition for single-phase flow occurs when the fluid velocity just equals the local sound speed. For this case, one of the  $\lambda_j$ 's is just equal to zero. For the two-phase case, it is possible for all  $\lambda_j$ 's to be greater than zero under special conditions which can exist during discharge of a subcooled liquid.

Extensive investigation was carried out to determine a two-phase choked-flow criterion under two assumed conditions:<sup>a</sup> (a) thermal equilibrium between phases, and (b) adiabatic phases without phase change (frozen).<sup>3.4-6</sup> The frozen assumption was in poor agreement with data compared to the thermal equilibrium assumption. Therefore, the thermal equilibrium assumption with slip is used as the basis for the RELAP5 choked-flow criterion when two conditions exist.

**3.4.1.1 Choking Criterion for Nonhomogeneous, Equilibrium Two-Phase Flow.** The two-fluid model for the conditions of thermal equilibrium (equilibrium interphase mass transfer) is described by the overall mass continuity equation, two-phasic momentum equations, and the mixture entropy equation. This system of equations is

$$\partial(\alpha_g \rho_g + \alpha_f \rho_f) / \partial t + \partial(\alpha_g \rho_g v_g + \alpha_f \rho_f v_f) / (\partial x) = 0 \quad (3.4-4)$$

$$\begin{aligned} & \alpha_g \rho_g [\partial v_g / \partial t + v_g (\partial v_g / \partial x)] + \alpha_g (\partial P / \partial x) \\ & + C \alpha_g \alpha_f \rho [\partial v_g / \partial t + v_f (\partial v_g / \partial x) - \partial v_f / \partial t - v_g (\partial v_f / \partial x)] = 0 \end{aligned} \quad (3.4-5)$$

$$\begin{aligned} & \alpha_f \rho_f [\partial v_f / \partial t + v_f (\partial v_f / \partial x)] + \alpha_f (\partial P / \partial x) \\ & + C \alpha_f \alpha_g \rho [\partial v_f / \partial t + v_g (\partial v_f / \partial x) - \partial v_g / \partial t - v_f (\partial v_g / \partial x)] = 0 \end{aligned} \quad (3.4-6)$$

$$\partial(\alpha_g \rho_g S_g + \alpha_f \rho_f S_f) / \partial t + \partial(\alpha_g \rho_g S_g v_g + \alpha_f \rho_f S_f v_f) / (\partial x) = 0 \quad (3.4-7)$$

The momentum equations include the interphase force terms due to relative acceleration.<sup>3.4-7</sup> These force terms have a significant effect on wave propagation velocity and consequently on the choked flow velocity. The particular form chosen is frame invariant and symmetrical; and the coefficient of virtual mass,  $C \alpha_g \alpha_f \rho$ , is chosen to ensure a smooth transition between pure vapor and pure liquid. For a dispersed flow, the constant, C, has a theoretical value of 0.5; whereas for a separated flow, the value may approach zero. The energy equation is written in terms of mixture entropy, which is constant for adiabatic flow. (The energy dissipation associated with interphase mass transfer and relative phase acceleration is neglected.)

---

a. The hydrodynamic model is not based on either of these assumptions. However, the purpose of this analysis is simply to establish a criterion for a choked flow; thus, there is no conflict with the basic hydrodynamic model.

The nondifferential source terms,  $C(U)$ , in Equation (3.4-1) do not enter into the characteristic analysis or affect the propagation velocities. For this reason, the source terms associated with wall friction, interphase drag, and heat transfer are omitted for brevity in Equations (3.4-4) through (3.4-7).

In the thermal equilibrium case,  $\rho_g$ ,  $\rho_f$ ,  $S_g$ , and  $S_f$  are known functions of the pressure only (the vapor and liquid values along the saturation curve). The derivatives of these variables are designated by an asterisk as follows

$$\rho_f^* = d\rho_f^s/dP, \rho_g^* = d\rho_g^s/dP \quad (3.4-8)$$

$$S_f^* = dS_f^s/dP, S_g^* = dS_g^s/dP \quad (3.4-9)$$

The system of governing equations [Equations (3.4-4) through (3.4-7)] can be written in terms of the four dependent variables,  $\alpha_g$ ,  $P$ ,  $v_g$ , and  $v_f$ , by application of the chain rule and the property derivatives [Equations (3.4-8) and (3.4-9)]. Thus, the system of equations can be written in the form of Equation (3.4-1) where the  $A$  and  $B$  are fourth-order square coefficient matrices.

The characteristic polynomial that results is fourth-order in  $\lambda$ , and factorization can only be carried out approximately to obtain the roots for  $\lambda$  and establish the choking criterion. The first two roots are

$$\lambda_{1,2} = \frac{\left\{ \alpha_f \rho_g + \rho C/2 \pm [(\rho C/2)^2 - \alpha_g \alpha_f \rho_g \rho_f]^{1/2} \right\} v_g}{(\alpha_f \rho_g + \rho C/2) + (\alpha_g \rho_f + \rho C/2)} + \frac{\left\{ \alpha_g \rho_f + \rho C/2 + [(\rho C/2)^2 - \alpha_g \alpha_f \rho_g \rho_f]^{1/2} v_f \right\}}{(\alpha_f \rho_g + \rho C/2) + (\alpha_g \rho_f + \rho C/2)} \quad (3.4-10)$$

These two roots are obtained by neglecting the fourth-order factors relative to the second-order factors in  $(\lambda - v_g)$  and  $(\lambda - v_f)$ . There are no first- or third-order factors. Inspection of Equation (3.4-10) shows that  $\lambda_{1,2}$  have values between  $v_g$  and  $v_f$ ; thus, the fourth-order factors,  $(\lambda - v_g)$  and  $(\lambda - v_f)$ , are small (i.e., neglecting these terms is justified). The values for  $\lambda_{1,2}$  may be real or complex depending on the sign of the quantity  $[(\rho C/2)^2 - \alpha_g \alpha_f \rho_g \rho_f]$ .

The remaining two roots are obtained by dividing out the quadratic factor containing  $\lambda_{1,2}$ , neglecting the remainder, and factoring the remaining quadratic terms. [This procedure can be shown to be analogous to neglecting the second- and higher-order terms in the relative velocity,  $(v_g - v_f)$ .] The remaining roots are

$$\lambda_{3,4} = v + D(v_g - v_f) \pm a \quad (3.4-11)$$

where

$$v = (\alpha_g \rho_g v_g + \alpha_f \rho_f v_f) / \rho \quad (3.4-12)$$

$$a = a_{HE} \{ [C\rho^2 + \rho(\alpha_g\rho_f + \alpha_f\rho_g)] / (C\rho^2 + \rho_g\rho_f) \}^{1/2} \quad (3.4-13)$$

and

$$D = 0.5 \left[ \frac{(\alpha_g\rho_f - \alpha_f\rho_g)}{(\rho C + \alpha_f\rho_g + \alpha_g\rho_f)} + \frac{\rho_g\rho_f(\alpha_f\rho_f - \alpha_g\rho_g)}{\rho(\rho_g\rho_f + C\rho^2)} - a_{HE}^2 \frac{\rho(\alpha_g\rho_g^2 S_g^* + \alpha_f\rho_f^2 S_f^*)}{\rho_g\rho_f(S_g - S_f)} \right] \quad (3.4-14)$$

The quantity,  $a_{HE}$ , is the homogeneous equilibrium speed of sound. The roots,  $\lambda_{3,4}$ , have only real values.

The general nature and significance of these roots is revealed by applying the characteristic considerations. The speed of propagation of small disturbances is related to the values of the characteristic roots. In general, the velocity of propagation corresponds to the real part of a root, and the growth or attenuation is associated with the complex part of the root. Choking will occur when the signal, which propagates with the largest velocity relative to the fluid, is just stationary, i.e.,

$$\lambda^R = 0 \text{ for } j \leq 4 \quad (3.4-15)$$

and

$$\lambda^R \geq 0 \text{ for all } i \neq j \quad (3.4-16)$$

The existence of complex roots for  $\lambda_{1,2}$  makes the initial boundary value problem ill-posed. This problem has been discussed by many investigators,<sup>3.4-8,3.4-9</sup> and the addition of any small, second-order viscous effects renders the problem well-posed.<sup>3.4-8,3.4-10</sup> The whole phenomenon of systems with mixed orders of derivatives and a first-order system with the addition of a small, second-order term has been discussed and analyzed by Whitham.<sup>3.4-4</sup> He has shown that the second-order viscous terms give infinite characteristic velocities. However, very little information is propagated along these characteristic lines; and the bulk of the information is propagated along characteristic lines defined by the first-order system. We conclude that the ill-posed nature of Equations (3.4-4) through (3.4-7) can be removed by the addition of small, second-order viscous terms that have little effect upon the propagation of information. Therefore, the choking criterion for the two-phase flow system analyzed here is established from Equation (3.4-15).

The explicit character of the choking criterion for the two-phase flow model defined by Equations (3.4-4) through (3.4-7) is examined. Since the two roots,  $\lambda_{1,2}$ , are between the phase velocities,  $v_f$  and  $v_g$ , the choking criterion is established from the roots,  $\lambda_{3,4}$ , and Equation (3.4-15). The choking criterion is

$$v + D(v_g - v_f) = \pm a \quad (3.4-17)$$

The choking criterion can be rewritten in terms of the mass mean and relative Mach numbers

$$M_v = v/a, M_r = (v_g - v_f)/a \quad (3.4-18)$$

as

$$M_v + DM_r = \pm 1 \quad (3.4-19)$$

This relation is similar to the choking criterion for single-phase flow where only the mass average Mach number appears and choking corresponds to a Mach number of unity.

The choking criterion [Equation (3.4-19)] is a function of the two parameters, D and a. In **Figure 3.4-1**, a is plotted as a function of the void fraction,  $\alpha_g$ , for a typical steam/water system at 7.5 MPa, with C equal to zero (the stratified equilibrium sound speed), C equal to 0.5 (the typical value for a dispersed flow model), and in the limiting case when C becomes infinite (homogeneous equilibrium sound speed). From **Figure 3.4-1**, it is evident that the virtual mass coefficient has a significant effect upon the choked-flow dynamics in two-phase flow.<sup>3.4-11</sup>

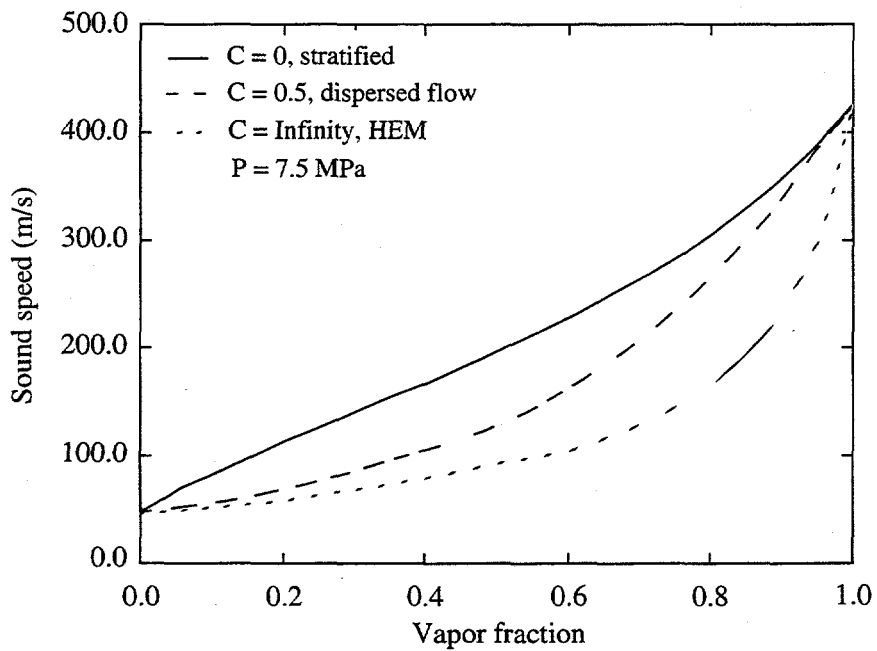


**Figure 3.4-1** Equilibrium speed of sound as a function of void fraction and virtual mass coefficient.

To establish the actual choked-flow rate for two-phase flow with slip, the relative velocity term in Equation (3.4-19) must also be considered. The relative Mach number coefficient, D, is shown plotted in **Figure 3.4-2** for values of C equal to 0, 0.5, and infinity. It is evident from these results that the choked-flow velocity can differ appreciably from the mass mean velocity when slip occurs. It is significant that the variation of the choked-flow criterion from the homogeneous result is entirely due to velocity nonequilibrium, since these results have been obtained under the assumption of thermal equilibrium. The particular values of these parameters used in the model are further discussed later in this section.

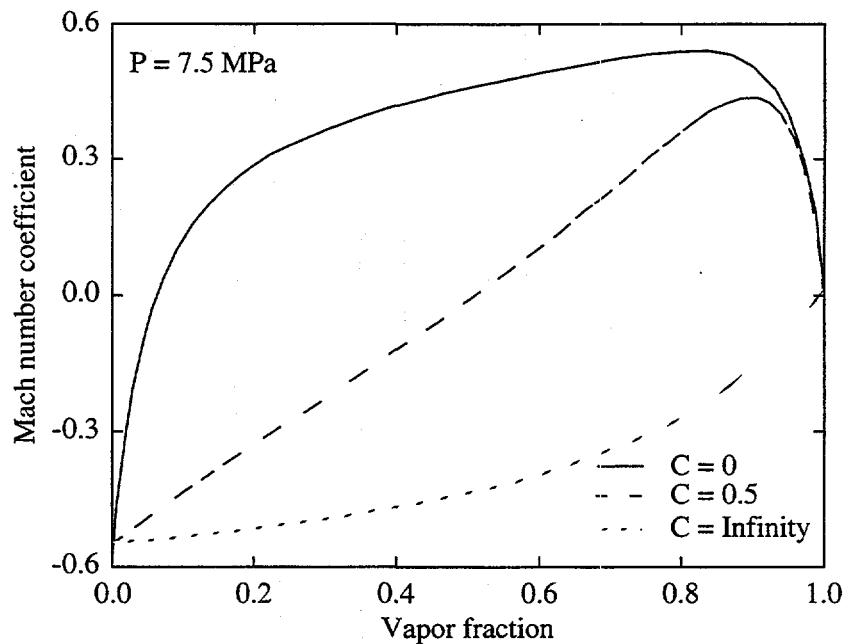


**Figure 3.4-2** Coefficient of relative Mach number for thermal equilibrium flow as a function of void fraction and virtual mass coefficient.

**3.4.1.2 Subcooled Choking Criterion.** The previous analysis assumes two-phase conditions exist throughout the break flow process. However, initially and in the early phase of blowdown, the flow approaching the break or break nozzle will be subcooled liquid. Under most conditions of interest in LWR systems, the fluid undergoes a phase change at the break. The transition from single- to two-phase flow is accompanied by a discontinuous change in the fluid bulk modulus. This is especially true for the liquid-to-liquid/vapor transition. For example, at 600 KPa, the ratio of the single- to two-phase sound speed at the liquid boundary is 339.4. Thus, considerable care must be exercised when analyzing a flow having transitions to or from a pure phase. (A discontinuity is also present at the vapor boundary, but the ratio is only 1.069.)

To understand the physical process that occurs for subcooled upstream conditions, consider the flow through a converging/diverging nozzle connected to an upstream plenum with subcooled water at a high pressure. For a downstream pressure only slightly lower than the upstream pressure, subcooled liquid flow will exist throughout the nozzle. Under these conditions, the flow can be analyzed using Bernoulli's equation, which predicts a minimum pressure,  $P_t$ , at the throat.<sup>a</sup> As the downstream pressure is lowered further, a point is reached where the throat pressure equals the local saturation pressure,  $P_{sat}$ . If the downstream pressure is lowered further, vaporization will take place at the throat.<sup>b</sup> When this happens, the fluid sound speed lowers drastically; but continuity considerations dictate that the velocity,  $v_t$ , of the two-phase mixture (at the point of minuscule void fraction) just equals the velocity of the subcooled water

a. For all practical cases of choking, the subcooled water can be considered incompressible with infinite sound speed.

slightly upstream of the throat. When this occurs,  $v_t$  in the subcooled region is less than the water sound speed; but in the two-phase region,  $v_t$  can be greater than the two-phase sound speed. Hence, the subcooled water has a Mach number ( $M$ )  $< 1$ , whereas the two-phase mixture at the throat has a Mach number  $> 1$ . Under these conditions (Mach numbers  $> 1$  in the two-phase region), downstream pressure effects are not propagated upstream and the flow is choked. In particular, the supersonic two-phase fluid at the throat must increase in velocity and the pressure must drop as it expands in the diverging section.<sup>a</sup> (Transition back to subsonic flow can occur in the nozzle as a result of a shock wave.) This choked condition is shown as case (a) in **Figure 3.4-3**. Contrary to the usual single-phase choked flow in a converging/diverging nozzle, there is no point in the flow field where  $M = 1$ . This is because in the homogeneous equilibrium model the fluid undergoes a discontinuous change in sound speed from single-phase subcooled conditions to two-phase conditions, although the fluid properties are continuous through the transition point.

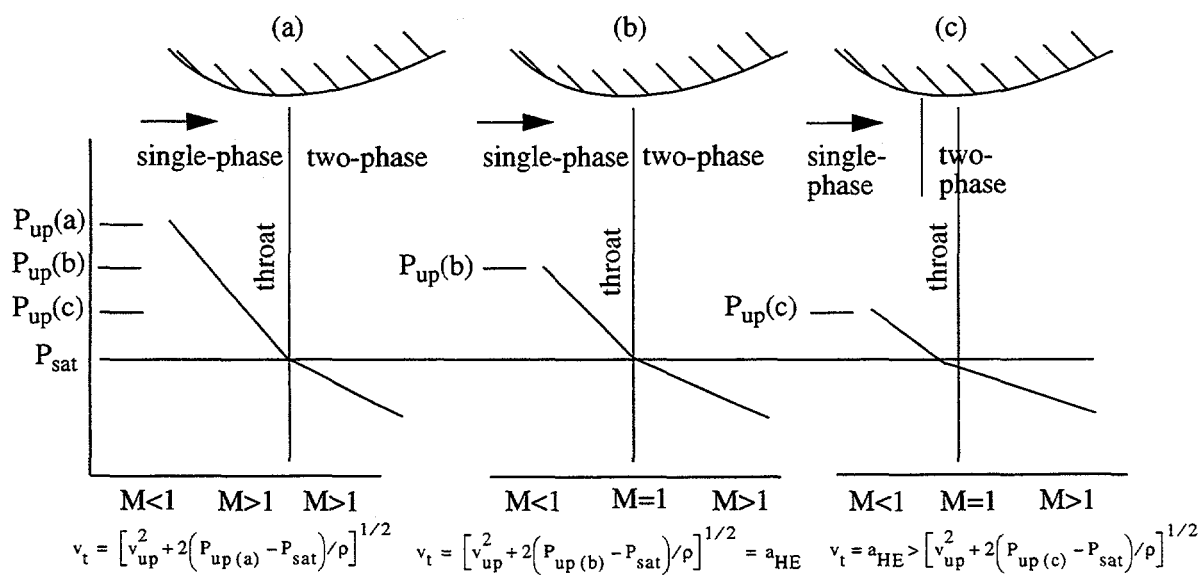


**Figure 3.4-3** Subcooled choking process.

When this condition prevails, the flow rate can be established from application of Bernoulli's equation  $[1/2\rho(v_t^2 - v_{up}^2) = P_{up} - P_{sat}]$ . For further decrease in the downstream pressure, no further increase in upstream fluid velocity will occur as long as the upstream conditions are maintained constant.

Now consider the process where a subcooled choked flow, as described above, initially exists (with a very low downstream pressure) and the upstream pressure is lowered as shown in cases (b) and (c) in **Figure 3.4-3**. As the upstream pressure decreases, the pressure at the throat will remain at  $P_{sat}$ , and Bernoulli's equation will give a smaller subcooled water velocity ( $v_t$ ) at the throat. As  $P_{up}$  is lowered

b. An idealized one-dimensional homogeneous equilibrium model is assumed.

a. In a supersonic flow, a diverging nozzle implies an increase in velocity.

further, a point is reached where  $v_t = a_{HE}$  and  $M = 1$  on the two-phase side of the throat. (The Mach number in the subcooled portion upstream of the throat is much less than 1.) This situation is shown schematically in **Figure 3.4-3** as case (b).

As the upstream pressure is lowered further, the point where the pressure reaches  $P_{sat}$  must move upstream of the throat. This is shown as case (c) in **Figure 3.4-3**. The subcooled water velocity at the  $P_{sat}$  location is smaller than the two-phase sound speed, and the flow is subsonic. In the two-phase region between the point at which  $P_{sat}$  is reached and the throat, the Mach number is less than 1 but increases to  $M = 1$  at the throat; that is, the two-phase sonic velocity is reached at the throat (as in the case of choked flow having a continuous variation of sound speed with pressure). As  $P_{up}$  is lowered still further, the  $P_{sat}$  point moves upstream until the flow becomes completely two-phase.

The homogeneous assumption applied in the above subcooled choking description is very close to the real situation when vapor is first formed. However, nonequilibrium can result in a superheated liquid state at a throat pressure,  $P_t$ , much lower than the saturation pressure,  $P_{sat}$ . The onset of vaporization occurs at  $P_t$  instead of  $P_{sat}$ .

The pressure undershoot,  $P_{sat} - P_t$ , can be described by the Alamgir-Lienhard-Jones correlation<sup>3.4-12,3.4-13,3.4-14</sup>

$$P_{sat} - P_t = \max (\Delta P, 0) \quad (3.4-20)$$

with

$$\Delta P = 0.258 \sigma^{3/2} T_R^{13.76} (1 + 13.25 R \Sigma'^{0.8})^{1/2} / [(k_B T_c)^{1/2} (1 - V_f/V_g)] - 0.07 (A_t/A)^2 [\rho v_c^2] . \quad (3.4-21)$$

The first term in  $\Delta P$  represents the static depressurization effect and is derived by Alamgir and Lienhard<sup>3.4-13</sup> based on classical nucleation theory. For a steady flow in a nozzle, the depressurization rate,  $\Sigma'$ , can be shown to be

$$\Sigma' = [\rho v_c^3 / A_t] (dA/dx)_t . \quad (3.4-22)$$

Note that in Equation (3.4-21),  $\Sigma'$  is in units of  $\text{Matm/s}$ , but in Equation (3.4-22),  $\Sigma'$  is in units of  $\text{Pa/s}$ . Here,  $(dA/dx)_t$  is the variation of area with respect to axial length and is to be evaluated between the center of the upstream volume and the throat. The second term in  $\Delta P$  [Equation (3.4-22)] represents the turbulence effect and is developed by Jones.<sup>3.4-14</sup>

The choking velocity, based upon the process shown in **Figure 3.4-3**, can be obtained in the following manner. The subcooled critical flow model is based on the assumption that flashing occurs at the throat of the nozzle or upstream of the throat. This assumption implies that critical flow of subcooled liquid must be accompanied by a minimum pressure drop, which we denote by  $\Delta P_{min}$ . In this case  $\Delta P_{min} = P_{up} - P_t$ , where  $P_{up}$  is the pressure in the upstream volume and  $P_t$  is the throat pressure obtained from the Alamgir-Lienhard-Jones correlation. This leads to a condition on the fluid velocity at the throat, which is

obtained from the Bernoulli equation. Assuming the fluid is incompressible and that frictional and gravitational forces are negligible, the Bernoulli equation is given by  $\Delta P = (1/2) \rho (v_t^2 - v_{up}^2)$ , where  $\Delta P$  is the pressure drop from the upstream volume to the throat,  $v_t$  is the velocity at the throat, and  $v_{up}$  is the velocity in the upstream volume. Thus we obtain the condition  $v_t > v_c$ , where

$$v_c = [v_{up}^2 + 2 ( (P_{up} - P_t) / \rho )]^{1/2} \quad (3.4-23)$$

and  $P_t$  is to be computed from Equation (3.4-20).

For the process shown in **Figure 3.4-3** case (a), the choking velocity is given by Equation (3.4-23), and for the process shown in **Figure 3.4-3** case (b) and **Figure 3.4-3** case (c), the two-phase choking criterion applies and

$$v_c = a_{HE} \quad (3.4-24)$$

where  $a_{HE}$  is the equilibrium sound speed of a two-phase mixture.

To determine which of the above situations exists, both  $v_c$ 's are calculated and the larger is used as the choking velocity to be imposed at the throat. This velocity is imposed numerically in exactly the same way as the choking criterion used for the two-phase condition described previously.

The equilibrium sound speed,  $a_{HE}$ , is calculated using thermodynamic conditions at the throat. Momentum and mechanical energy balances are used to calculate the pressure and internal energy at the throat and use the water property tables to obtain the thermodynamic properties of a saturated liquid-vapor mixture at this pressure and internal energy. This method is consistent with the process of subcooled critical flow described in this section, and allows for the presence of a two-phase mixture at the throat. The precise equations used to determine the hydrodynamic conditions at the throat are presented in Volume IV of the RELAP5 Code Manual. Note that in an earlier version of RELAP5, the quality of the two-phase mixture at the throat was not determined. Instead the throat was assumed to contain saturated liquid at the temperature of the subcooled liquid upstream. However, this assumption led to an abrupt change of the computed flowrate at the single-phase to two-phase transition.

The subcooled choking model is very similar in concept to the model proposed by Burnell<sup>3.4-15</sup> in that both models assume a Bernoulli expansion to the point of vapor inception at the choke plane. The criterion for transition from subcooled choking to two-phase choking is now better understood and is in agreement with the physics of two-phase flow. The model here is also in agreement with cavitating venturi experience (experimentally confirmed behavior)<sup>3.4-12</sup>. The RELAP5 subcooled choking model is somewhat different than the model proposed by Moody<sup>3.4-16</sup> in that the Moody model assumes that an isentropic process occurs to the choke plane.

**3.4.1.3 Implementation of Choked Flow Model.** Ideally, the two-phase choking criterion [Equation (3.4-17)] can be used as a boundary condition for obtaining flow solutions. However, the applicability of Equation (3.4-17) has not been fully explored. Instead, an approximate criterion

$$(\alpha_g \rho_f v_g + \alpha_f \rho_g v_f) / (\alpha_g \rho_f + \alpha_f \rho_g) = \pm a_{HE} \quad (3.4-25)$$

has been applied extensively and has produced good code/data comparisons. Equation (3.4-25) can be obtained from Equation (3.4-17) in the following manner. Neglecting the third term in D, we obtain

$$\begin{aligned} \frac{\alpha_g \rho_g v_g + \alpha_f \rho_f v_f}{\rho} + 0.5 \left[ \frac{(\alpha_g \rho_f - \alpha_f \rho_g)}{(\rho C + \alpha_f \rho_g + \alpha_g \rho_f)} + \frac{\rho_g \rho_f (\alpha_f \rho_f - \alpha_g \rho_g)}{\rho (\rho_g \rho_f + C \rho^2)} \right] (v_g - v_f) \\ = \pm a_{HE} \left[ \frac{C \rho^2 + \rho (\alpha_g \rho_f - \alpha_f \rho_g)}{C \rho^2 + \rho_g \rho_f} \right]^{0.5} . \end{aligned} \quad (3.4-26)$$

Then setting  $C = 0$  (stratified) on the left side of Equation (3.4-26) and  $C = \infty$  (homogeneous) on the right side of Equation (3.4-26) and computing the limits, we obtain the approximate criterion given by Equation (3.4-25). Because of the extensive experience with this approximate model, Equation (3.4-25) is currently used in RELAP5 choked flow calculations.

In the RELAP5 critical flow model, choking is assumed to occur at the narrowest part of the flow channel. This location is called the throat. Under critical flow conditions, the fluid velocity at the throat is equal to the two-phase speed of sound. The critical flow model includes two separate tests to determine if critical flow occurs: a choking test to determine if the hydrodynamic conditions lead to critical flow, and an unchoking test to determine if the hydrodynamic conditions can maintain critical flow. In the choking test [Equation (3.4-25)], the fluid velocity is compared to the local speed of sound, which is based on the hydrodynamic conditions at the throat. In the unchoking test, a momentum balance from the upstream volume center to the throat is used to determine whether the pressure drop is large enough to sustain choked flow. Ideally, choked flow occurs only if the fluid velocity exceeds the local speed of sound and the minimum pressure drop condition is satisfied. In the current implementation of the critical flow model, however, these conditions are relaxed in order to prevent the computed solution from oscillating at the threshold between sonic and subsonic flow. The precise logic used to determine critical flow and a flowchart of the algorithm is presented in Volume IV of the RELAP5 Code Manual.

At each time step and at each flow junction where two-phase cocurrent flow exists, the choking criterion [Equation (3.4-25)] is checked using explicitly calculated values. When choking occurs, Equation (3.4-25) is solved semi-implicitly with the upstream vapor and liquid momentum equations for  $v_g$ ,  $v_f$ , and  $P_t$ , throat pressure, at the point of flow choking (upstream with reference to  $v_g$  and  $v_f$ ). As  $P_t$  is not needed in system calculations, we can eliminate  $\partial P / \partial x$  from the vapor and liquid momentum equations to obtain

$$\begin{aligned} \rho_g (\partial v_g / \partial t + 1/2 \partial v_g^2 / \partial x) - \rho_f (\partial v_f / \partial t + 1/2 \partial v_f^2 / \partial x) \\ = (\rho_g - \rho_f) B_x + \Gamma_g (v_I - \alpha_f v_g - \alpha_g v_f) / (\alpha_f \alpha_g) \\ - \rho_g v_g FWG + \rho_f v_f FWF - \rho_f \rho_g (v_g - v_f) FI - C \rho \partial (v_g - v_f) / \partial t . \end{aligned} \quad (3.4-27)$$

The finite-difference form of this equation is obtained by integrating with respect to the spatial variable from the upstream volume center to the junction. In this finite-difference equation, all junction velocities are evaluated implicitly;<sup>3.4-17</sup>  $a_{He,j}^{n+1}$  is approximated by

$$a_{HEj}^{n+1} = a_{HEj}^n + (\partial a_{HE}/\partial P)_j^n (P_K^{n+1} - P_K^n) \quad (3.4-28)$$

where  $P_K$  is the upstream volume pressure. The finite-difference equations corresponding to Equations (3.4-25) and (3.4-27) can be solved for  $v_{g,j}^{n+1}$  and  $v_{f,j}^{n+1}$  in terms of  $P_K^{n+1}$  and old time values.

The unchoking test may be explained by reference to **Figure 3.4-4**, which illustrates the effect of downstream pressure on choked flow through a typical converging-diverging nozzle. In this case, a necessary condition for choked flow is  $P_t < P_K$ , where  $P_t$  is the pressure at the throat and  $P_K$  is the pressure in the upstream volume. However, we may have  $P_t > P_L$  or  $P_t < P_L$ , where  $P_L$  is the pressure in the downstream volume. In some cases, shocks may occur in the diverging portion of the nozzle in order that the pressure of the fluid leaving the nozzle matches the downstream pressure. We also require  $P_K - P_L > \Delta P_{min}$ , where  $\Delta P_{min}$  is the minimum pressure difference needed to maintain choked flow. The quantity  $\Delta P_{min}$  is calculated from a momentum balance which includes the effects of the variation of flow area, wall friction, and form loss. In particular, the calculation includes the following sequence of steps: (1) use momentum and energy balances from the upstream volume center to the throat in order to obtain  $P_t$  and  $U_t$ , (2) use the water property tables to determine the thermodynamic state at the throat from which the two-phase sound speed is obtained, (3) assuming the fluid velocity at the throat is equal to the two-phase sound speed, use a momentum balance from the upstream volume center to the downstream volume center in order to obtain the pressure drop due to a change in flow area, wall friction, and form loss downstream of the expansion. This is the minimum pressure drop needed to sustain choked flow. We note that the static pressure increases in the diverging section of the nozzle because the fluid decelerates, but the total pressure decreases due to friction and form losses, (4) test for unchoking by comparing the actual pressure drop to the minimum pressure drop. We can justify this test by observing that for choked flow an increase in the downstream pressure eventually leads to unchoking, and the critical value of downstream pressure is  $P_K - \Delta P_{min}$ . This test is especially important for critical flow of subcooled liquid through an abrupt area change. Since an abrupt area change is accompanied by form loss downstream of the throat, the pressure drop must be large enough to accelerate the liquid to sonic velocity at the throat and overcome the form loss downstream of the throat. Note that the minimum pressure drop condition had not been strictly enforced in an earlier version of RELAP5, and this led to a discontinuous prediction of mass flow rate at the transition from sonic to subsonic flow.

In general, there is a large drop in critical velocity when the fluid changes from a subcooled to a two-phase state. This sudden change often leads to unrealistic velocity oscillations and causes the time step to be reduced considerably. To provide a smooth transition from subcooled to two-phase, a transition region is inserted between subcooled choking ( $\dot{\alpha}_g < 10^{-5}$ ) and two-phase choking ( $\dot{\alpha}_g > 0.10$ ) in which the sound speed is interpolated between the subcooled choking sound speed and the two-phase sound speed, based on the donor value of the junction void fraction,  $\dot{\alpha}_g$ . The subcooled sound speed is computed from Equation (3.4-23), and the two-phase sound speed is computed from thermodynamic relations using a void fraction of 10%. A void fraction of 10% was chosen so that it would require several time steps to traverse the interpolation region based on typical time step sizes and typical rates to change of void fraction per time step. To provide additional smoothing of the transition between subcooled and two-phase choking, the phase velocities obtained from the choking computation [i.e., the simultaneous solution of Equation (3.4-25) and the finite difference form of Equation (3.4-27)] are relaxed with the values from the previous time step, using a variable relaxation factor.

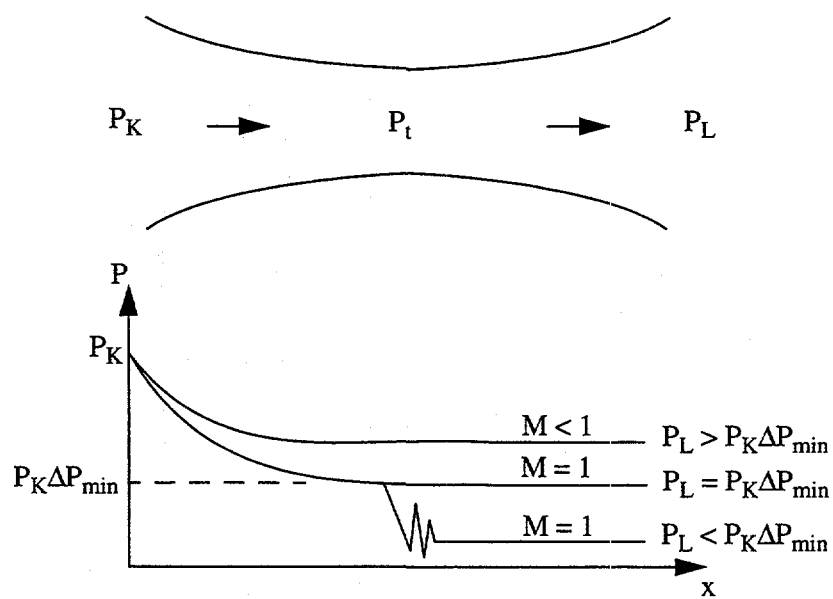


Figure 3.4-4 Pressure distribution for choked flow through a converging-diverging nozzle.

$$v_{g,j}^{n+1} = v_{g,j}^n + R (v_{g,j}^{n+1} - v_{g,j}^n) \quad (3.4-29)$$

$$v_{f,j}^{n+1} = v_{f,j}^n + R (v_{g,j}^{n+1} - v_{f,j}^n) \quad (3.4-30)$$

where

$$R = 0.1 \text{ for } \dot{\alpha}_{g,j} \leq 0.10$$

$$1.0 \text{ for } \dot{\alpha}_{g,j} \geq 0.15 \quad (3.4-31)$$

and the relaxation factor is interpolated between the two values of the junction void fraction. A variable relaxation factor is used to reduce the numerical noise that would result from an abrupt switch from the heavy under-relaxation in the transition region to no under-relaxation outside the transition region.

In the implementation of the RELAPS critical flow model, an accurate prediction of critical flow through a nozzle or a break in a pipe requires an accurate determination of the hydrodynamic conditions at the throat. Three important variables are the velocity, pressure, and density at the throat. However, the pressure at the throat depends on the velocity at the throat: for a large area contraction, the pressure drop  $P_K - P_t$  is primarily affected by the convective acceleration  $\rho_K v_K^2 - \rho_t v_t^2$ . Moreover, the density ratio  $\rho_K/\rho_t$  depends on the thermodynamic conditions at the throat. Therefore a simultaneous determination of  $P_t$ ,  $v_t$  and  $\rho_t$  may be required. Because of the nonlinear relation between these variables, iteration is used to obtain the sonic velocity. But excessive use of iteration may increase the execution time of RELAPS.

Thus, various methods were tested to detect the need for iteration and the following criterion was developed: if either of the following is true,

$$\dot{\alpha}_g \left| \frac{v_g^{k+1} - v_g^k}{v_g^{k+1}} \right| + \dot{\alpha}_f \left| \frac{v_f^{k+1} - v_f^k}{v_f^{k+1}} \right| > \epsilon, \quad (3.4-32)$$

$$\left| \frac{(\rho_K/\rho_t)^{k+1} - (\rho_K/\rho_t)^k}{(\rho_K/\rho_t)^{k+1}} \right| > \epsilon, \quad (3.4-33)$$

then calculate the sonic velocity again. In this test,  $\epsilon$  is a tolerance which is currently set to 0.01, and  $k$  is the iteration number. Therefore, iteration is only activated if the junction velocity or density ratio change more than 1% during a time step. The values of  $v_g$ ,  $v_f$ , and  $\rho_K/\rho_t$  used in this test are calculated and updated at each iteration, and the values of  $\dot{\alpha}_g$  and  $\dot{\alpha}_f$  are obtained from the previous time step. The number of iterations is currently limited to 10. In case the time step size is small, the variables in Equations (3.4-32) and (3.4-33) do not change much during a time step and so iteration is usually activated only at the onset of choked flow.

Iteration was not used in an earlier version of RELAP5. Instead, the junction velocity and density ratio at the previous time step were used to estimate  $P_t$ . This approximation eliminates the need for iteration and is adequate during most of the transient. At the onset of critical flow, however, this approximation may result in an overestimation of the sonic velocity. This overestimation is severe in case the flowrate changes abruptly; for example, a valve opening instantaneously or a sudden break in a pipe. Moreover, it was observed that after the onset of critical flow, the computed mass flowrate approached a steady-state value and the rate of relaxation was independent of the time step size. This observation suggests that a fixed number of time steps are required to obtain consistent values of the variables. If iteration is used, then the initial overestimation of the mass flowrate is significantly reduced.

### 3.4.2 Horizontal Stratification Entrainment Model

Under stratified conditions in horizontal components, the void fraction flowing through a junction may be different from the upstream volume void fraction. Consequently, the regular donor scheme for junction void fraction is no longer appropriate because vapor may be pulled through the junction and liquid may also be entrained and pulled through the junction. A model for this process of vapor pullthrough and liquid entrainment for various conditions was developed by Ardon and Bryce<sup>3.4-18</sup> and implemented by Bryce.<sup>3.4-19</sup> The correlation for the onset of pullthrough or entrainment is given by

$$h_b = \frac{K W_k^{0.4}}{(g \rho_k \Delta \rho)^{0.2}} \quad (3.4-34)$$

where

$h_b$  = the distance between the stratified liquid level and the junction at which pullthrough or entrainment first begins (i.e., the inception height) (m)

$W_k$  = mass flow rate of the continuous phase in the branch

and  $K$  is a constant defined as follows: for a vertically upward branch,  $K = 1.67$ ; for a vertically downward branch,  $K = 1.50$ ; for gas pullthrough in a horizontal side branch,  $K = 0.75$ ; and for liquid entrainment in a horizontal side branch,  $K = 0.69$ .

Once the liquid level is closer to the junction than the inception height, the flow quality through the junction is given by the following set of correlations:

For a vertically upward branch,

$$X = R^{3.25(1-R)^2} \quad (3.4-35)$$

where

$$R = h/h_b$$

$h$  = distance from the stratified liquid level to the junction.

For a vertically downward branch,

$$X = X_o^{2.5R} [1 - 0.5R(1+R)X_o^{(1-R)}]^{0.5} \quad (3.4-36)$$

where

$$X_o = \frac{1.15}{1 + \left(\frac{\rho_f}{\rho_g}\right)^{1/2}} \quad (3.4-37)$$

For a horizontal side branch,

$$X = X_o^{1+CR} [1 - 0.5R(1+R)X_o^{(1-R)}]^{0.5} \quad (3.4-38)$$

where  $C = 1.09$  for gas pullthrough,  $C = 1.00$  for liquid entrainment, and  $X_o$  is given by Equation (3.4-37). The flow quality is converted into a junction void fraction using the slip ratio in the junction from the previous time step.

The calculation of the junction void fraction is subject to several limitations to handle special situations (e.g., inception height greater than pipe radius for side branch or greater than pipe diameter for vertical branches) and to eliminate oscillations that would cause the time step to be reduced, thereby increasing code run time. The details of the implementation of the horizontal stratification entrainment model can be found in Volume IV of this manual, in Ardon and Bryce,<sup>3.4-18</sup> and in Bryce.<sup>3.4-19</sup>

### 3.4.3 Abrupt Area Change

The general reactor system contains piping networks with many sudden area changes and orifices. To apply the RELAP5 hydrodynamic model to such systems, analytical models for these components have been developed.<sup>3.4-20</sup> The basic hydrodynamic model is formulated for slowly varying (continuous) flow area variations; therefore, special models are not required for this case.

The abrupt area change model, discussed here and developed in detail in Reference 3.4-20, is based on the Bourda-Carnot<sup>3.4-21</sup> formulation for a sudden enlargement and standard pipe flow relations, including the vena-contracta effect for a sudden contraction or an orifice or both. Quasi-steady continuity and momentum balances are employed at points of abrupt area change. The numerical implementation of these balances is such that hydrodynamic losses are independent of upstream and downstream nodalization. In effect, the quasi-steady balances are employed as jump conditions that couple fluid components having abrupt changes in cross-sectional area. This coupling process is achieved without change to the basic linear semi-implicit and nearly-implicit numerical time-advancement schemes.

**3.4.3.1 Abrupt Area Change Modeling Assumptions.** The basic assumption used for the transient calculation of two-phase flow in flow passages with points of abrupt area change is: the transient flow process can be approximated as a quasi-steady flow process that is instantaneously satisfied by the upstream and downstream conditions (that is, transient inertia, mass, and energy storage are neglected at abrupt area changes). However, the upstream and downstream flows are treated as fully transient flows.

There are several bases for the above assumption. A primary consideration is that available loss correlations are based on data taken during steady flow processes; however, transient investigations<sup>3.4-22</sup> have verified the adequacy of the quasi-steady assumption. The volume of fluid and associated mass, energy, and inertia at points of abrupt area change is generally small compared with the volume of upstream and downstream fluid components. The transient mass, energy, and inertia effects are approximated by lumping them into upstream and downstream flow volumes. Finally, the quasi-steady approach is consistent with modeling of other important phenomena in transient codes (that is, heat transfer, pumps, and valves).

**3.4.3.2 Review of Single-Phase Abrupt Area Change Models.** The modeling techniques used for dynamic pressure losses associated with abrupt area change in single-phase flow are reviewed briefly before discussing the extension of these methods to two-phase flows. In a steady incompressible flow, losses at an area change are modeled by the inclusion of an appropriate dynamic head loss term,  $h_L$ , in the one-dimensional modified Bernoulli equation

$$(v^2/2 + P/\rho)_1 = (v^2/2 + P/\rho)_2 + h_L . \quad (3.4-39)$$

The particular form of the dynamic head loss is obtained by employing the Bourda-Carnot<sup>3.4-21</sup> assumption for calculating losses associated with the expansion part of the flow process at points of abrupt area change.

**3.4.3.2.1 Expansion**--Consider a steady and incompressible flow undergoing a sudden increase in cross-sectional area (expansion) as shown in **Figure 3.4-5**. Here the flow is assumed to be from left to right with the upstream conditions denoted by the subscript 1 and the downstream condition by 2. Here the upstream and downstream conditions are assumed to be far enough removed from the point of area change that flow is one-dimensional, i.e., none of the two-dimensional effects of the abrupt area change exist. These locations can range from several diameters upstream to as many as 30 diameters downstream. However, for purposes of modeling the overall dynamic pressure loss, the entire process is assumed to occur as a discontinuous jump in flow condition at the point of abrupt area change. In this context, the stations 1 and 2 refer to locations immediately upstream and downstream of the abrupt area change.

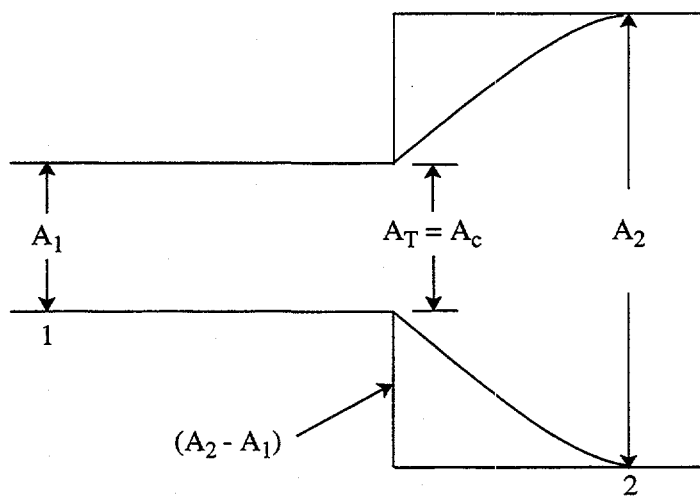


**Figure 3.4-5** Abrupt expansion.

The dynamic head loss for the abrupt expansion shown in **Figure 3.4-5** can be obtained using the Bourda-Carnot<sup>3.4-21</sup> assumption, i.e., the pressure acting on the "washer shaped" area,  $A_2 - A_1$ , is the upstream pressure,  $P_1$ . When this assumption is employed in an overall momentum balance, the head loss is

$$h_L = \frac{1}{2} \left( 1 - \frac{A_2}{A_1} \right)^2 v_2^2 \quad (3.4-40)$$

By defining  $\varepsilon = A_2/A_1$  as the expansion area ratio, the loss in the dynamic pressure associated with the area change is related to the head by

$$\Delta P_L = \rho h_L = \frac{1}{2} \rho (1 - \epsilon)^2 v_2^2 \quad (3.4-41)$$

**3.4.3.2.2 Contraction**—The flow process at a point of abrupt reduction in flow area (contraction) is idealized in much the same manner as for the expansion, except that an additional process must be considered. The flow continues to contract beyond the point of abrupt area reduction and forms a vena contracta, see Figure 3.4-6. The point of vena contracta is designated by c. The far-upstream and far-downstream conditions are designated by 1 and 2, respectively.

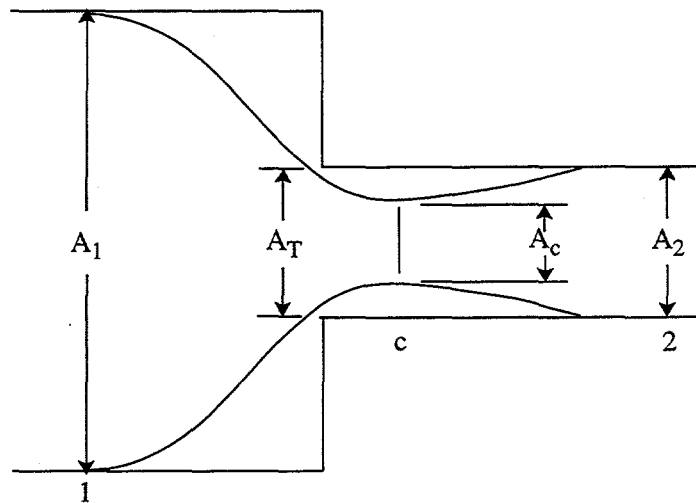


Figure 3.4-6 Abrupt contraction.

Consider a sudden contraction in a steady incompressible flow. The loss in dynamic pressure from the upstream station to the vena contracta is usually neglected. Measurements indicate that the contracting flow experiences a loss no larger than  $\Delta P_L \sim 0.05 (1/2 \rho v_c^2)$ ,<sup>3.4-21</sup> where  $v_c$  is the velocity at the contracta. The dynamic pressure loss associated with the new expansion from the area at vena contracta to the downstream area is modeled using the Bourda-Carnot assumption with the condition at vena contracta as the upstream condition, that is

$$\Delta P_L = \frac{1}{2} \rho (1 - A_c/A_2)^2 v_c^2, \quad (3.4-42)$$

where from continuity considerations for incompressible flow

$$v_c = \frac{A_2 v_2}{A_c} . \quad (3.4-43)$$

The contraction ratio  $A_c/A_2$ , is an empirical function of  $A_2/A_1$ . The function is  $A_c/A_2 = 0.62 + 0.38(A_2/A_1)^3$  (see Reference 3.4-21). Combining Equations (3.4-42) and (3.4-43) leads to

$$\Delta P_L = \frac{1}{2}\rho \left(1 - \frac{A_2}{A_c}\right)^2 v_2^2 \quad (3.4-44)$$

as the dynamic pressure loss for a contraction.<sup>3.4-21</sup>

**3.4.3.2.3 Abrupt Area Change With an Orifice**--The most general case of an abrupt area change is a contraction with an orifice at the point of contraction. Such a configuration is shown in Figure 3.4-7. In this case, an additional flow area, the orifice flow area, must be specified. Conditions at the orifice throat station will be designated by a subscript T. Three area ratios are used throughout this development. The first is the contraction area ratio at the vena-contracta relative to the minimum physical area,  $\epsilon_c = A_c/A_T$ . The second is the ratio of the minimum physical area to the upstream flow area,  $\epsilon_T = A_T/A_1$ . The third is the ratio of the downstream to upstream area,  $\epsilon = A_2/A_1$ .

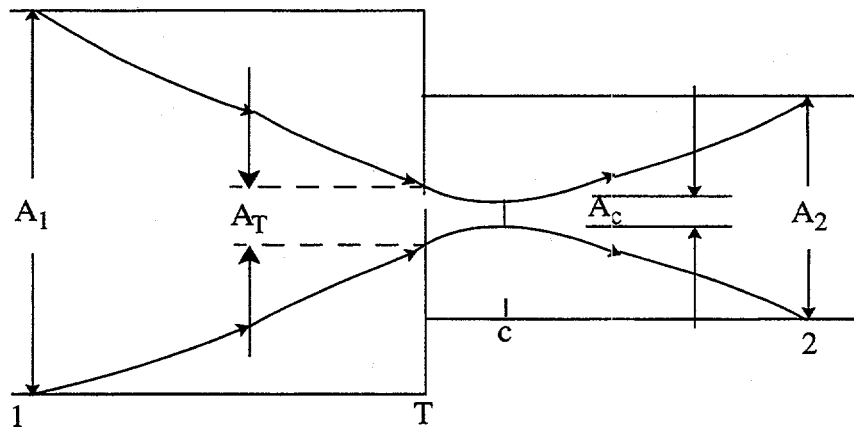


Figure 3.4-7 Orifice at abrupt area change.

The dynamic pressure loss for an abrupt area contraction combined with an orifice is analyzed in a manner parallel to that for a simple contraction. The loss associated with the contracting fluid stream from Station 1 to c (the point of vena-contracta) is neglected. The dynamic pressure loss associated with the expansion from the vena-contracta to the downstream section is given by

$$\Delta P_L = \frac{1}{2}\rho \left(1 - \frac{A_c}{A_2}\right)^2 v_c^2 \quad (3.4-45)$$

The contraction ratio,  $\varepsilon_c = A_c/A_T$ , is an empirical function of  $\varepsilon_T = A_T/A_1$ . The function is  $\varepsilon_c = 0.62 + 0.38(\varepsilon_T)^3$  (see Reference 3.4-21). Using the continuity equations,  $v_c = \frac{A_T v_T}{A_c} = v_T \varepsilon_c$  and  $v_T = \frac{A_2 v_2}{A_T} = \frac{\varepsilon}{\varepsilon_T} v_2$ , Equation (3.4-45) can be written as

$$\Delta P_L = \frac{1}{2} \rho \left( 1 - \frac{\varepsilon}{\varepsilon_c \varepsilon_T} \right)^2 v_2^2 \quad (3.4-46)$$

Equation (3.4-46) is a generalization applicable to all the cases previously treated. For a pure expansion,  $\varepsilon_T = 1$ ,  $\varepsilon_c = 1$ , and  $\varepsilon > 1$ ; for a contraction,  $\varepsilon_T = \varepsilon < 1$  and  $\varepsilon_c < 1$ . Each of these is a special case of Equation (3.4-46). The two-phase dynamic pressure loss model is based on an adaptation of the general single-phase head loss given by Equation (3.4-46).

**3.4.3.3 Two-Phase Abrupt Area Change Model.** The two-phase flow through an abrupt area change is modeled in a manner very similar to that for single-phase flow by defining phasic flow areas. The two phases are coupled through the interphase drag, a common pressure gradient, and the requirement that the phases coexist in the flow passage.

The one-dimensional phasic stream-tube momentum equations are given in Section 3.1.1. The flow at points of abrupt area change is assumed to be quasi-steady and incompressible. In addition, the terms in the momentum equations due to body force, wall friction, and mass transfer are assumed to be small in the region affected by the area change. The interphase drag terms are retained, since the gradient in relative velocity can be large at points of abrupt area changes.

Equations (3.1-7) and (3.1-8) can be integrated approximately for a steady incompressible, smoothly varying flow to obtain modified Bernoulli-type equations for each phase

$$\left( \frac{1}{2} \rho_f v_f^2 + P \right)_1 = \left( \frac{1}{2} \rho_f v_f^2 + P \right)_2 + \left( \frac{FI'}{\alpha_f} \right)_1 (v_{f1} - v_{g1}) L_1 + \left( \frac{FI'}{\alpha_f} \right)_2 (v_{f2} - v_{g2}) L_2 \quad (3.4-47)$$

and

$$\left( \frac{1}{2} \rho_g v_g^2 + P \right)_1 = \left( \frac{1}{2} \rho_g v_g^2 + P \right)_2 + \left( \frac{FI'}{\alpha_g} \right)_1 (v_{g1} - v_{f1}) L_1 + \left( \frac{FI'}{\alpha_g} \right)_2 (v_{g2} - v_{f2}) L_2 \quad (3.4-48)$$

where  $L_1$  and  $L_2$  are the lengths from the upstream condition to the throat and from the throat to the downstream condition respectively and where  $FI' = \alpha_f \alpha_g \rho_f \rho_g FI$ .  $FI$  is determined from Equation (3.3-45). The interphase drag is divided into two parts associated with the upstream and downstream parts of the flow affected by the area change.

**3.4.3.4 General Model.** Consider the application of Equations (3.4-47) and (3.4-48) to the flow of a two-phase fluid through a passage having a generalized abrupt area change (the flow passage shown in Figure 3.4-8.<sup>a</sup>) Here, the area  $A_T$  is the throat or minimum area associated with an orifice located at the point of the abrupt area change. Since each phase is governed by a modified Bernoulli-type equation, it is reasonable to assume that losses associated with changes in the phasic flow area can be modeled by separate dynamic pressure loss terms for both the liquid and gas phases. Hence, we assume that the liquid sustains a loss as if it alone (except for interphase drag) were experiencing an area change from  $\alpha_{f1} A_1$  to  $\alpha_{fT} A_T$  to  $\alpha_{f2} A_2$ ; and the gas phase experiences a loss as if it alone were flowing through an area change from  $\alpha_{g1} A_1$  to  $\alpha_{gT} A_T$  to  $\alpha_{g2} A_2$ . The area changes for each phase are the phasic area changes (see Figure 3.4-8). When the losses for these respective area changes [based on the Bourda-Carnot model and given by Equation (3.4-46)] are added to Equations (3.4-47) and (3.4-48), the following phasic momentum equations are obtained:

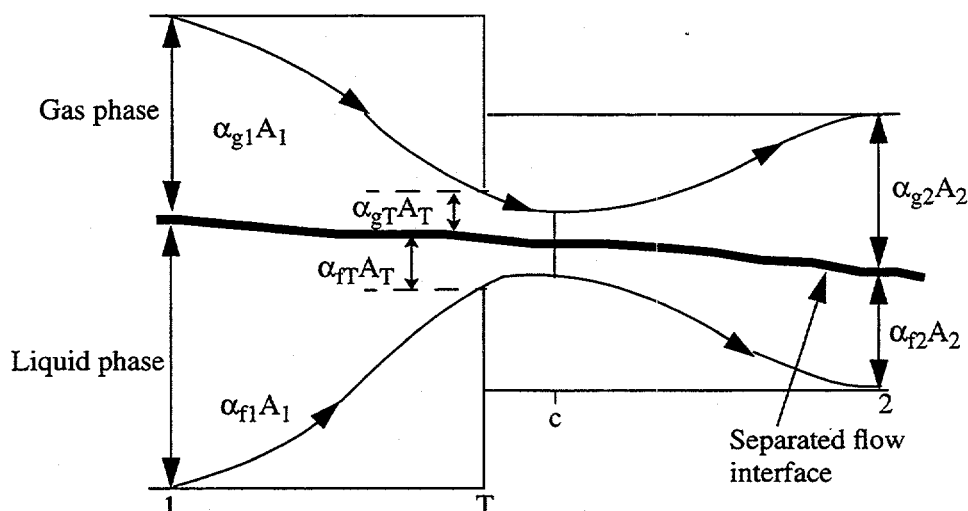


Figure 3.4-8 Schematic flow of two-phase mixture at abrupt area change.

a. In Figure 3.4-8, the flow is shown as a separated flow for clarity. The models developed are equally applicable to separated and dispersed flow regimes, as evidenced by the calculations performed when the abrupt area change model was incorporated into RELAP5.<sup>3.4-20</sup> The model was verified on single phase expansions, contractions, and orifices. Three two-phase problems were also run: (1) expansion case with the interphase drag equal to zero, which simulates separated flow, (2) expansion case with the interphase drag appropriate for dispersed flow, and (3) contraction case with the interphase drag appropriate for dispersed flow.

$$\left( \frac{1}{2} \rho_f v_f^2 + P \right)_1 = \left( \frac{1}{2} \rho_f v_f^2 + P \right)_2 + \frac{1}{2} \rho_f \left( 1 - \frac{\alpha_{f2} \varepsilon}{\alpha_{fT} \varepsilon_{fc} \varepsilon_T} \right)^2 (v_{f2})^2 + \left( \frac{FI'}{\alpha_f} \right)_1 (v_{f1} - v_{g1}) L_1 + \left( \frac{FI'}{\alpha_f} \right)_2 (v_{f2} - v_{g2}) L_2 \quad (3.4-49)$$

and

$$\left( \frac{1}{2} \rho_g v_g^2 + P \right)_1 = \left( \frac{1}{2} \rho_g v_g^2 + P \right)_2 + \frac{1}{2} \rho_g \left( 1 - \frac{\alpha_{g2} \varepsilon}{\alpha_{gT} \varepsilon_{gc} \varepsilon_T} \right)^2 (v_{g2})^2 + \left( \frac{FI'}{\alpha_g} \right)_1 (v_{g1} - v_{f1}) L_1 + \left( \frac{FI'}{\alpha_g} \right)_2 (v_{g2} - v_{f2}) L_2 \quad (3.4-50)$$

These phasic momentum equations are used across an abrupt area change. In Equations (3.4-49) and (3.4-50),  $\varepsilon_{fc}$  and  $\varepsilon_{gc}$  are the same tabular function of area ratio as in the single-phase case, except the area ratios used are the phasic area ratios

$$\varepsilon_{fT} = (\alpha_{fT}/\alpha_{f1}) \varepsilon_T \quad (3.4-51)$$

and

$$\varepsilon_{gT} = (\alpha_{gT}/\alpha_{g1}) \varepsilon_T \quad (3.4-52)$$

respectively. The area ratios,  $\varepsilon = A_2/A_1$  and  $\varepsilon_T = A_T/A_1$ , are the same as for single-phase flow.

The interphase drag effects in Equations (3.4-49) and (3.4-50) are important. These terms govern the amount of slip induced by an abrupt area change; and, if they are omitted, the model will always predict a slip at the area change appropriate to a completely separated flow situation and give erroneous results for a dispersed flow.

**3.4.3.5 Model Application.** A few remarks concerning the way Equations (3.4-49) and (3.4-50) are applied to expansions and contractions, both with and without an orifice, are necessary. In a single-phase, steady flow situation and given the upstream conditions  $v_1$  and  $P_1$ , one can solve for  $v_2$  and  $P_2$  by using the continuity equation ( $v_1 A_1 = v_2 A_2$ ) and Equation (3.4-39). Equations (3.4-49) and (3.4-50), along with the two phasic continuity equations, can be used in a similar manner except that now the downstream void fraction is an additional unknown which must be determined.

**3.4.3.5.1 Expansion**--For the purpose of explanation, consider the case of an expansion ( $\alpha_{fT} = \alpha_{f1}$ ,  $\alpha_{gT} = \alpha_{g1}$ ,  $\varepsilon > 1$ ,  $\varepsilon_T = 1$ ,  $\varepsilon_{fc} = \varepsilon_{gc} = 1$ ,  $FI_1 = 0$ ,  $L_1 = 0$ ) for which Equations (3.4-49) and (3.4-50) reduce to

$$\left(\frac{1}{2} \rho_f v_f^2 + P\right)_1 = \left(\frac{1}{2} \rho_f v_f^2 + P\right)_2 + \frac{1}{2} \rho_f \left(1 - \frac{\alpha_{f2}\epsilon}{\alpha_{f1}}\right)^2 (v_{f2})^2 + \left(\frac{FI}{\alpha_f}\right)_2 (v_{f2} - v_{g2}) L_2 \quad (3.4-53)$$

and

$$\left(\frac{1}{2} \rho_g v_g^2 + P\right)_1 = \left(\frac{1}{2} \rho_g v_g^2 + P\right)_2 + \frac{1}{2} \rho_g \left(1 - \frac{\alpha_{g2}\epsilon}{\alpha_{g1}}\right)^2 (v_{g2})^2 + \left(\frac{FI}{\alpha_g}\right)_2 (v_{g2} - v_{f2}) L_2 \quad (3.4-54)$$

These two equations with the incompressible continuity equations

$$\alpha_{f1} v_{f1} A_1 = \alpha_{f2} v_{f2} A_2 \quad (3.4-55)$$

and

$$\alpha_{g1} v_{g1} A_1 = \alpha_{g2} v_{g2} A_2 \quad (3.4-56)$$

are a system of four equations having four unknowns,  $\alpha_{f2}$  ( $\alpha_{g2} = 1 - \alpha_{f2}$ ),  $v_{f2}$ ,  $v_{g2}$ , and  $P_2$ , given the upstream conditions,  $\alpha_{f1}$  ( $\alpha_{g1} = 1 - \alpha_{f1}$ ),  $v_{f1}$ ,  $v_{g1}$ , and  $P_1$ . (The interphase drag,  $FI$ , is a known function of the flow properties.) It is important to note that the downstream value of the liquid fraction ( $\alpha_{f2}$ ) is an additional unknown compared with the single-phase case and is determined (with the downstream velocities and pressure) by simultaneous solution of Equations (3.4-53) through (3.4-56) without additional assumptions. It is reassuring that by taking a proper linear combination of Equations (3.4-49) and (3.4-50), the usual overall momentum balance obtained using the Bourda-Carnot<sup>3.4-21</sup> assumption can be obtained.<sup>3.4-23,3.4-24</sup>

If, as in the cited literature,<sup>3.4-23,3.4-24,3.4-25,3.4-26</sup> only the overall momentum balance is used at an expansion, there will be an insufficient number of equations to determine all the downstream flow parameters,  $\alpha_{f2}$ ,  $v_{f2}$ ,  $v_{g2}$ , and  $P_2$ . The indeterminacy has been overcome in cited works by means of several different assumptions concerning the downstream void fraction.<sup>a</sup> In the model developed here [Equations (3.4-53) and (3.4-54)], division of the overall loss into liquid and gas parts, respectively, results in sufficient conditions to determine all downstream flow variables, including  $\alpha_{f2}$ . In addition, the present model includes force terms due to interphase drag in Equations (3.4-53) and (3.4-54), which are necessary to predict the proper amount of slip and void redistribution that occurs at points of area change.

**3.4.3.5.2 Contraction**--Consider the application of Equations (3.4-49) and (3.4-50) to a contraction. To determine both the downstream conditions and throat conditions from the upstream values

---

a. J. G. Collier<sup>3.4-23</sup> mentions three different assumptions that have been used: (1)  $\alpha_{f2} = \alpha_{f1}$ , (2)  $\alpha_{f2}$  is given by a homogeneous model, and (3)  $\alpha_{f2}$  is given by the Hughmark void fraction correlation.

of  $\alpha_{f1}(\alpha_{g1})$ ,  $v_{f1}$ ,  $v_{g1}$ , and  $P_1$ , an additional consideration needs to be made. To obtain the throat values, apply the momentum equations valid for the contracting section of flow. (Here, the  $L_1$  portion of the interphase force is associated with the contraction.)

$$\left(\frac{1}{2} \rho_f v_f^2 + P\right)_1 = \left(\frac{1}{2} \rho_f v_f^2 + P\right)_T + \left(\frac{FI}{\alpha_f}\right)_1 (v_{f1} - v_{g1}) L_1 \quad (3.4-57)$$

$$\left(\frac{1}{2} \rho_g v_g^2 + P\right)_1 = \left(\frac{1}{2} \rho_g v_g^2 + P\right)_T + \left(\frac{FI}{\alpha_g}\right)_1 (v_{g1} - v_{f1}) L_1 \quad (3.4-58)$$

$$\alpha_{f1} v_{f1} A_1 = \alpha_{fT} v_{fT} A_T \quad (3.4-59)$$

$$\alpha_{g1} v_{g1} A_1 = \alpha_{gT} v_{gT} A_T \quad (3.4-60)$$

These four equations are solved simultaneously for the values of  $\alpha_{fT}(\alpha_{gT})$ ,  $v_{fT}$ ,  $v_{gT}$ ,  $P_T$  at the throat section (the minimum physical area). No additional or special assumptions are made concerning the throat conditions, since they follow as a direct consequence of the unique head loss models for each phase. After the throat values have been obtained, the conditions, at the point of vena-contracta are established, assuming the void fraction is the same as at the throat. Thus,  $\varepsilon_{fc}$  and  $\varepsilon_{gc}$  are established using the tabular function in Appendix A of Reference 3.4-20 and the throat area ratios,  $\varepsilon_{fT}$  and  $\varepsilon_{gT}$ , defined by Equations (3.4-51) and (3.4-52). The functions are  $\varepsilon_{fc} = 0.62 + 0.38(\varepsilon_{ft})^3$  and  $\varepsilon_{gc} = 0.62 + 0.38(\varepsilon_{gt})^3$ . To determine the downstream values, Equations (3.4-49) and (3.4-50) can be applied directly from Stations 1 to 2 with the throat values known, or the expansion loss equations can be used from the throat section to Station 2. Both approaches produce identical downstream solutions. As in the case of an expansion, because the proper upstream and downstream interphase drag is included, this modeling approach establishes the phase slip and resulting void redistribution. An orifice at an abrupt area change is treated exactly as the contraction explained above (that is, with two separate calculations to establish first the throat and then the downstream flow variables).

**3.4.3.5.3 Countercurrent Flow**--The preceding development implicitly assumed a cocurrent flow. For countercurrent flow, Equations (3.4-49) and (3.4-50) are applied exactly as in cocurrent flow except that the upstream sections for the respective phases are located on different sides of the abrupt area change. The difference appears in how the throat and downstream voids are determined. To determine the throat properties, equations similar to Equations (3.4-57) through (3.4-60) are used with the upstream values appropriate for each phase. These four equations are then solved for  $\alpha_{fT}(\alpha_{gT})$ ,  $v_{fT}$ ,  $v_{gT}$ , and  $P_T$ . To determine the downstream values for each phase, only the head loss terms are needed for the downstream voids. (The downstream  $v_f$ ,  $v_g$ , and  $P$  do not appear.) For countercurrent flow, these voids are set such that the downstream void of each phase plus the upstream void of the opposite phase adds to 1. (Both phases together must fill the flow channel.) With the throat and downstream voids now known, Equations (3.4-49) and (3.4-50) can be used directly to determine the total loss for each phase at the abrupt area change.

### 3.4.4 User-Specified Form Loss

In the calculation of the total form loss, partitioning of the form friction losses between the liquid and the vapor phases are implemented based on the phasic void fractions. However, there are many practical situations for the users of using flow condition dependent form loss coefficients in order to represent the friction loss close to experimental values. This section documents the implementation of the general user-specified form loss coefficients.

The  $HLOSSG_j^n$  and  $HLOSSF_j^n$  terms in Section 3.1.4 momentum Equations (3.1-103) and (3.1-104) contain either the code-calculated abrupt area change loss term or the user-specified loss term. There are code variables  $HLOSSG$  and  $HLOSSF$ , which are different than the variables  $HLOSSG_j^n$  and  $HLOSSF_j^n$  in the finite difference equations. The code variables  $HLOSSG$  and  $HLOSSF$  are

$$HLOSSG = \left( \frac{\dot{\alpha}_g \dot{\rho}_g}{\alpha_g \rho_g} \right)_j^n HLOSSG_j^n = \left( \frac{\dot{\alpha}_g \dot{\rho}_g}{\alpha_g \rho_g} \right)_j^n \frac{1}{2} K |v_{g,j}^n + 0.01 \text{ atroat}| \quad (3.4-61)$$

$$HLOSSF = \left( \frac{\dot{\alpha}_f \dot{\rho}_f}{\alpha_f \rho_f} \right)_j^n HLOSSF_j^n = \left( \frac{\dot{\alpha}_f \dot{\rho}_f}{\alpha_f \rho_f} \right)_j^n \frac{1}{2} K |v_{f,j}^n + 0.01 \text{ atroat}| \quad (3.4-62)$$

where  $K$  is the code-calculated or user specified loss and the term 0.01 atroat prevents the form loss becoming zero when the velocity is zero.

In many cases the form loss coefficient is a function of the Reynolds number. Thus it is suggested that the form loss coefficients can be generally expressed as

$$K_f = A_f + B_f Re^{-C_f} \quad (3.4-63)$$

$$K_r = A_r + B_r Re^{-C_r} \quad (3.4-64)$$

where  $K_f$  and  $K_r$  are the forward and reverse form loss coefficients;  $A_f$ ,  $A_r$ ,  $B_f$ ,  $B_r$ ,  $C_f$ , and  $C_r$  are the constants that are user-specified and  $Re$  is the Reynolds number based on mixture fluid properties. There are several different ways of defining the mixture Reynolds number based on the way the mixture viscosity is computed.<sup>3.4-27</sup> In RELAP5, the mixture viscosity  $\mu_m$  defined by Cicchitti<sup>3.4-28</sup> is implemented for calculating the mixture Reynolds number

$$\mu_m = X_f \mu_g + (1 - X_f) \mu_f \quad (3.4-65)$$

### 3.4.5 Crossflow Junction

The RELAP5 numerical scheme is generally formulated using one-dimensional elements. However, there are several applications where an approximate treatment of crossflow provides an improved physical simulation. Three different applications for a crossflow formulation are described in the following paragraphs.

The first application concerns a small crossflow between two essentially axial flow streams. This situation is typical of regions such as a reactor core or a steam generator, because the component geometry provides a large resistance (i.e., small flow rate) to crossflow and a small resistance (i.e., large flow rate) to axial flow. Hence, simplified crossflow momentum equations can be used to couple a hot flow channel to a bulk flow channel.

The second application of a crossflow junction is to provide a tee model. In this case, the momentum flux in the side branch is assumed to be perpendicular to the main stream; thus, the main stream momentum flux does not contribute to the crossflow momentum formulation.

The third application is modeling of leak flow paths. In this case, the flow is small and governed primarily by pressure differential, gravity, and flow resistance. Thus, the momentum flux terms can be neglected.

The vapor momentum finite difference equation used in the basic numerical scheme is

$$\begin{aligned}
 & (\alpha_g \rho_g)_j^n (v_g^{n+1} - v_g^n)_j \Delta x_j + \frac{1}{2} (\dot{\alpha}_g \dot{\rho}_g)_j^n [(v_g^2)_L^n - (v_g^2)_K^n] \Delta t + \text{VISCOUS TERMS} \\
 & = -\alpha_{g,j}^n (P_L^{n+1} - P_K^{n+1}) \Delta t - (\alpha_g \rho_g)_j^n (FWG_j^n \Delta x_j + HLOSSG_j^n) v_{g,j}^{n+1} \Delta t \\
 & \quad - (\alpha_g \rho_g)_j^n FIG_j^n (v_{g,j}^{n+1} - v_{f,j}^{n+1}) \Delta x_j \Delta t + (\alpha_g \rho_g)_j^n B_x \Delta x_j \Delta t \\
 & \quad + \text{ADDED MASS} + \text{MASS TRANSFER MOMENTUM} \\
 & \quad + \text{STRATIFIED PRESSURE GRADIENT EFFECT}
 \end{aligned} \tag{3.4-66}$$

where

$$\Delta x_j = \frac{1}{2} (\Delta x_K + \Delta x_L) \tag{3.4-67}$$

A parallel equation holds for the liquid phase. It should be noted that the momentum Equation (3.4-66) is in reality the sum of half the K cell momentum plus half the L cell momentum. This is the reason for Equation (3.4-67).

In crossflow junctions, just as in the normal junctions, the transverse momentum advection terms are neglected, i.e., there is no transport of x-direction momentum due to the flow in the transverse direction.

For the case of a small crossflow junction between two axial flow streams (J<sub>2</sub> in **Figure 3.4-9**) all the geometric input (area, length, elevation change) for both of the volumes relates to the axial flow direction, as do the wall drag and code-calculated form losses.

The crossflow area and the length scale can be either user-specified or code-calculated values. When code-calculated values are used, the volume geometries are defaulted for the case of a cylindrical pipe, and the appropriate length scale and flow area are used in the code. When user-specified values are used, the user should provide the representative crossflow area and length scale in the input deck. The length scale can be calculated as the volume divided by the crossflow area.

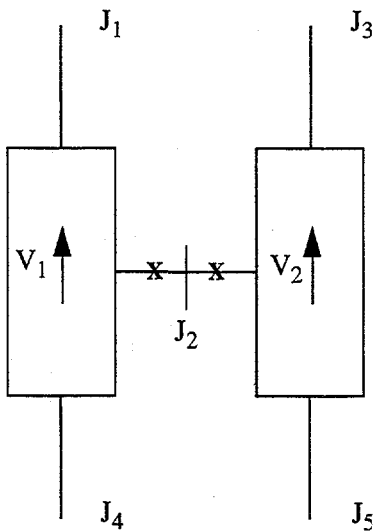


**Figure 3.4-9** Modeling of crossflows or leak.

Since the connecting K and L volumes are assumed to be predominantly axial flow volumes, the crossflow junction momentum flux (related to the axial volume velocity in K and L) can be neglected (by using a junction flag) along with the associated numerical viscous term.

The resulting vapor momentum finite difference equation (when the momentum flux is neglected) for a crossflow junction between two axial flow streams is

$$\begin{aligned}
 (\alpha_g \rho_g)_j^n (v_g^{n+1} - v_g^n)_j \Delta x_j &= -\alpha_{g,j}^n (P_L - P_K)^{n+1} \Delta t - (\alpha_g \rho_g)_j^n HLOSSG_g^n v_{g,j}^{n+1} \Delta t \\
 &\quad - (\alpha_g \rho_g)_j^n FIG_j^n (v_{g,j}^{n+1} - v_{f,j}^{n+1}) \Delta x_j \Delta t + (\alpha_g \rho_g)_j^n B_x \Delta x_j \Delta t \\
 &\quad + \text{ADDED MASS} + \text{MASS TRANSFER MOMENTUM} \\
 &\quad + \text{STRATIFIED PRESSURE GRADIENT EFFECT} .
 \end{aligned} \tag{3.4-68}$$

A similar equation can be written for the liquid phase. The  $\Delta x_j$  term that is used to estimate the inertial length associated with crossflow is defined using the diameters of volumes K and L,

$$\Delta x_j = \frac{1}{2} [D(K) + D(L)] \tag{3.4-69}$$

if the default is used. If user-specified lengths are input, they are used instead of D(K) and D(L).

The crossflow option can be used with the crossflow junction perpendicular to the axial flow in volume L (or K) but parallel to the axial flow in volume K (or L) (see **Figure 3.4-10**). Here, the situation regarding the half cell momentum contribution in volume L is the same as described above. The half cell momentum contribution associated with volume K is the same as for a normal junction. This type of crossflow modeling can be used for a 90-degree tee simulation.

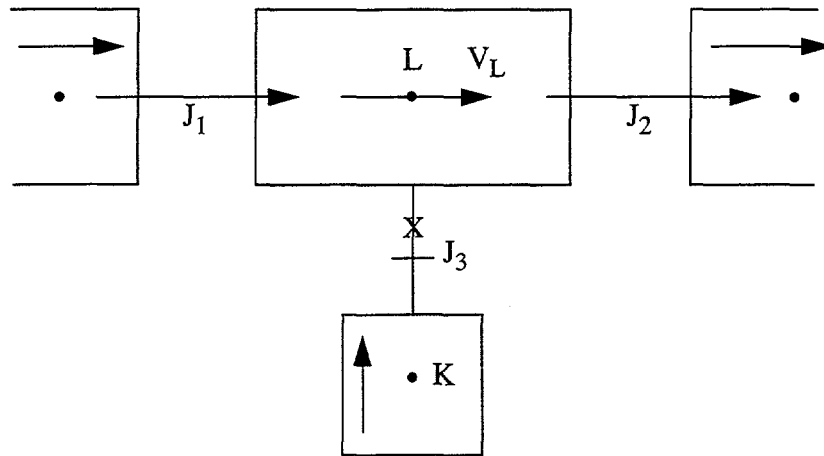


**Figure 3.4-10** Simplified tee crossflow.

The resulting vapor momentum finite difference equation for a crossflow junction perpendicular to the axial flow in volume L but parallel to the axial flow in volume K is

$$\begin{aligned}
 & (\alpha_g \rho_g)_j^n (v_g^{n+1} - v_g^n)_j \Delta x_j + \frac{1}{2} (\dot{\alpha}_g \dot{\rho}_g)_j^n [-(v_g^2)_K^n] \Delta t + (\text{VISCOSITY TERM})_K \\
 & = -\alpha_{g,j}^n (P_L^{n+1} - P_K^{n+1}) \Delta t - (\alpha_g \rho_g)_j^n \left[ \text{FWG}_K \frac{1}{2} \Delta x_K + \text{HLOSS}_j^n \right] v_{g,j}^{n+1} \Delta t \\
 & \quad - (\alpha_g \rho_g)_j^n \text{FIG}_j^n (v_{g,j}^{n+1} - v_{f,j}^{n+1}) \Delta x_j \Delta t + (\alpha_g \rho_g)_j^n B_x \Delta x_j \Delta t \\
 & \quad + \text{ADDED MASS} + \text{MASS TRANSFER MOMENTUM} \\
 & \quad + \text{STRATIFIED PRESSURE GRADIENT EFFECT}
 \end{aligned} \tag{3.4-70}$$

where the momentum flux in volume L is neglected by using a junction flag.

A similar equation can be written for the liquid phase. The  $\Delta x_j$  term has the form

$$\Delta x_j = \frac{1}{2} [\Delta x_K + D(L)] \tag{3.4-71}$$

if the default is used. If a user-specified length is input for the L volume, it is used instead of D(L).

For leak flows and minor flow paths, the modeling approach shown in **Figure 3.4-11** is recommended. Here,  $J_3$  is the normal flow path, whereas junction  $J_1$ , volume  $M$ , and junction  $J_2$  represent the leak flow path. Junctions  $J_1$  and  $J_2$  should be modeled as tee junctions described above. The only reason for using volume  $M$  is to obtain a correct representation of the gravity head from  $K$  to  $L$ . If a crossflow junction were modeled directly between volumes  $K$  and  $L$ , then there would be no gravity head in the leak flow junction equation. Leak paths may also be modeled using a crossflow junction that is perpendicular to both the  $K$  and  $L$  volumes when the leak flow is between volumes having the same volume center elevation.

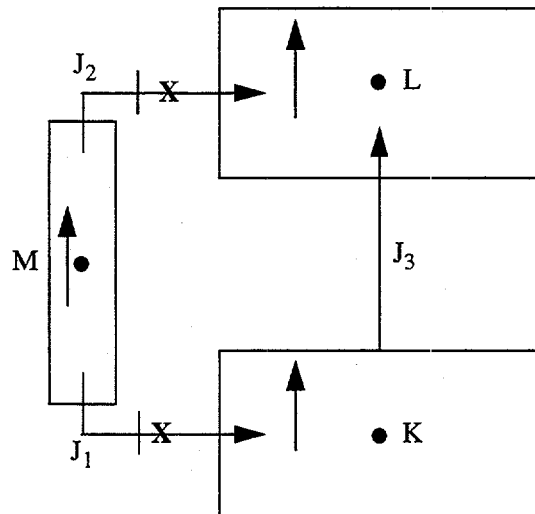


**Figure 3.4-11** Leak flow modeling.

### 3.4.6 Water Packing Mitigation Scheme

Large pressure spikes that cannot be explained by known physical phenomena are at times encountered when Eulerian-type codes are used to analyze integral systems tests or reactor accidents. These fictitious pressure spikes are sometimes calculated when steam is disappearing from, and water is about to fill, a control volume. The situation is often referred to as water packing.

The cause of the anomalous pressure spikes is the discontinuous change in compressibility between a two-phase mixture of small void fraction and a pure liquid phase, and approximations inherent in the discrete momentum equations. The same problems are seen using a two-fluid model or the homogeneous equilibrium model. Consider the homogeneous equilibrium case and a cell that is nearly full of liquid with a net influx of mass. The density-pressure relationship used to calculate the new time pressure is based upon the beginning of time step values for the state properties and derivatives. The compressibility of this low void fraction cell is dominated by the mass transfer. The equivalent mixture corresponds to a highly compressible fluid, i.e., significant volume changes can easily occur with very little change in pressure. This high compressibility can allow significant continuing influx of liquid with very little pressure rise. In fact, in some cases the net volume influx of liquid during the time step can be larger than the initial vapor volume in the cell. This filling of the cell is accompanied by only slight pressure changes. This small change in pressure may do little to slow down or reverse the liquid influx momentum. If this is the case, the following time step will be taken with a liquid full cell and large liquid influx momentum existing at

the beginning of the time step. Because the liquid is nearly incompressible, this large influx of liquid momentum will cause a large increase in pressure during this following time step.

In the neighborhood of these spurious numerical pressure spikes, the calculated phasic velocities may increase substantially, and smaller time-step sizes are needed to satisfy the material Courant stability limit. Thus, the computational efficiency is greatly reduced by the presence of water packing. Of course, the computed pressure spikes are unphysical. Furthermore, water packing may severely distort the transient solution by changing the void distribution or driving the liquid completely out of an open system.

A water packing scheme has been installed to mitigate these spikes. The water packing scheme closely follows the method used in the TRAC code.<sup>3.4-29,3.4-30</sup> It involves a detection scheme to determine when a pressure change occurs in a volume containing mostly liquid. It then imposes changes to the momentum equations, followed by a recalculation of the pressure solution using the sparse matrix solver.

The detection logic used in the water packing scheme evolved from experience gained in running a vertical fill problem.<sup>3.4-31</sup> The detection logic requires the following formula for the pressure:

$$P_K^{n+1} \geq P_K^n + 0.0023 P_K^n \quad (3.4-72)$$

where volume K is the volume that water packs and volume L is the next volume (see **Figure 3.4-12**). In volume K, the detection scheme also requires a void fraction ( $\alpha_g$ )  $\leq 0.12$ , the liquid temperature ( $T_f$ ) to be less than the saturation temperature ( $T^s$ ), the volume to be flagged as vertically stratified, and the next volume above to be highly voided. Thus, a legitimate water hammer situation would not be eliminated by the water packing scheme.

The next part of the scheme involves altering the liquid momentum equation so that only small pressure changes will occur when the volume fills with water. The scheme involves modifying the coefficient that multiplies the pressure change in the filling volume. The modification multiplies this coefficient by a large number and is discussed in more detail in the next paragraph. Since the pressure solution is rejected when water packing occurs, the pressure calculation is repeated using the sparse matrix solver.

The finite difference form of the liquid momentum equation used can be written

$$v_{f,j}^{n+1} = v_{f,j}^{n,exp} - (VFDP)_j^n [ (P_L^{n+1} - P_L^n) - (P_K^{n+1} - P_K^n) ] \quad (3.4-73)$$

where  $v_{f,j}^{n,exp}$  contains all the old time terms and  $(VFDP)_j^n$  contains all the terms that multiply the pressure change. Consider the filling example in **Figure 3.4-12**, where volume K is full of liquid and volume L is full of steam. The first change to the liquid momentum equation is to set  $v_{f,j}^{n,exp}$  to 0.01 m/s to insure the explicit liquid velocity is going from the K volume to the L volume. The second change to the liquid momentum equation is to multiply the  $(P_K^{n+1} - P_K^n)$  terms by a large number (FACTOR), which

forces  $P_K^{n+1}$  to be approximately the same as  $P_K^n$ . Thus, the water-filled K volume will not show a pressure spike. The K liquid momentum equation then has the form

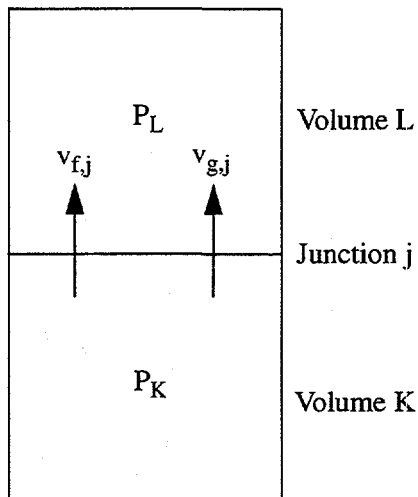


**Figure 3.4-12** Two vertical vapor/liquid volumes.

$$v_{f,j}^{n+1} = 0.01 - (\text{VFDP})_j^n (P_L^{n+1} - P_L^n) + (\text{VFDP})_j^n (\text{FACTOR}) (P_K^{n+1} - P_K^n) \quad (3.4-74)$$

The term FACTOR is pressure dependent because the density is pressure dependent. A pressure-dependent linear ramp is used that begins ramping FACTOR from a highest value of  $10^6$  at 1,500 psia ( $10.342 \times 10^6$  Pa) to a lowest value of  $10^4$  at 1,250 psia ( $8.618 \times 10^6$  Pa).

### 3.4.7 Countercurrent Flow Limitation Model

There are several structures internal to RCSs where gravity drainage of liquid can be impeded by upward flowing vapor. These include the upper core tie plate, downcomer annulus, steam generator tube support plates, and the entrance to the tube sheet in the steam generator inlet plenum. A completely mechanistic approach to determine the onset of flow limiting for all structural configurations is impractical. Both the Wallis and Kutateladze forms of the general flooding limit equation have been found to provide acceptable results when constants applicable to specific geometries are used in conjunction with them. Wallis<sup>3.4-27</sup> discusses the phenomenon of flooding, which can occur when liquid is falling in a vertical structure and gas is moving upward. For a specified liquid downflow rate, there is a certain gas upward flow rate at which very large waves appear on the interface, the flow becomes chaotic, gas pressure drop increases, and liquid flows upward. Figure 3.4-13 is a reproduction of Wallis' Figure 11.11 and shows this phenomena. Wallis points out that the flooding point is not approached as the limit of a continuous process (which occurs in drops or bubbles), but it is the result of a marked instability.

A general countercurrent flow limitation (CCFL) model is implemented<sup>3.4-32</sup> that allows the user to select the Wallis form, the Kutateladze form, or a form in between the Wallis and Kutateladze forms. This

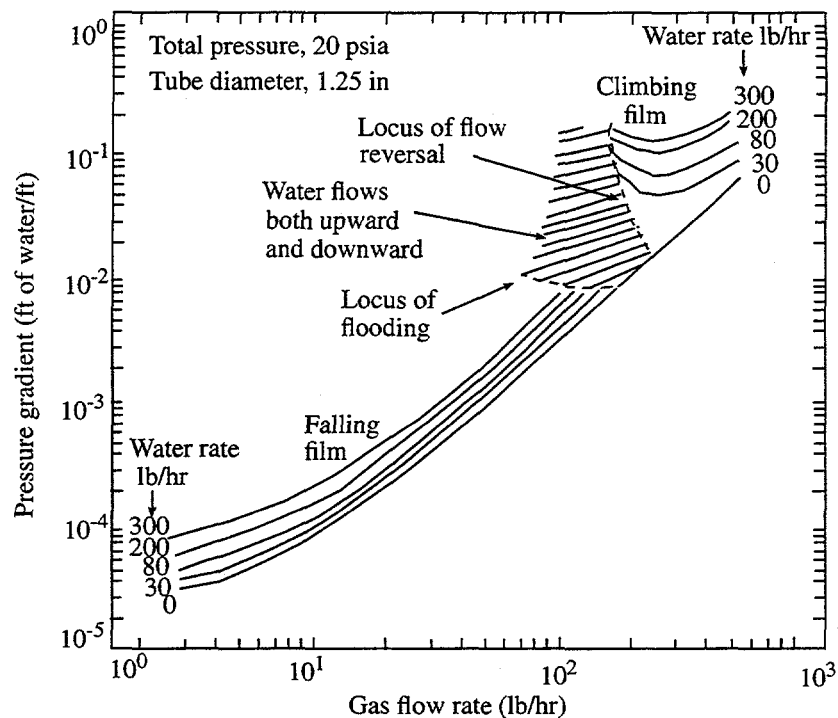


**Figure 3.4-13** Pressure-drop characteristics near the boundary between countercurrent and cocurrent flow.

general form was proposed by Bankoff et al.<sup>3.4-33</sup> and is used in the TRAC-PF1 code.<sup>3.4-34</sup> It has the structure

$$H_g^{1/2} + m H_f^{1/2} = c \quad (3.4-75)$$

where  $H_g$  is the dimensionless gas flux,  $H_f$  is the dimensionless liquid flux,  $c$  is the gas intercept (value of  $H_g^{1/2}$  when  $H_f = 0$ , i.e., complete flooding), and  $m$  is the “slope”, that is the gas intercept divided by the liquid intercept (the value of  $H_f^{1/2}$  when  $H_g = 0$ ). A typical plot of  $H_g^{1/2}$  versus  $H_f^{1/2}$  is shown in Figure 3.4-14. Quotes are used around the word “slope” because in a strict mathematical sense, the slope is negative for Equation (3.4-75) and  $m = -\text{slope}$ . The constant  $m$  will be called the slope in this section of the manual and in the input cards and output edit, but one should think of this as the negative of the true slope. The dimensionless fluxes have the form

$$H_g = j_g \left[ \frac{\rho_g}{g w (\rho_f - \rho_g)} \right]^{1/2} \quad (3.4-76)$$

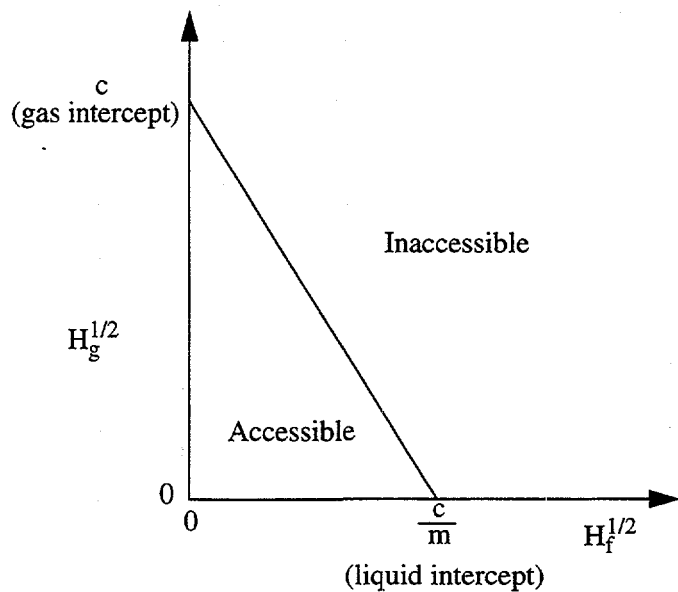


Figure 3.4-14 Plot of  $H_g^{1/2}$  versus  $H_f^{1/2}$  for a typical CCFL correlation.

$$H_f = j_f \left[ \frac{\rho_f}{g w (\rho_f - \rho_g)} \right]^{1/2} \quad (3.4-77)$$

where  $j_g$  is the gas superficial velocity ( $\alpha_g v_g$ ),  $j_f$  is the liquid superficial velocity ( $\alpha_f v_f$ ),  $\rho_g$  is the gas density,  $\rho_f$  is the liquid density,  $\alpha_g$  is the gas volume fraction,  $\alpha_f$  is the liquid volume fraction,  $g$  is the gravitational acceleration, and  $w$  is the length scale and is given by the expression

$$w = D_j^{1-\beta} L^\beta \quad (3.4-78)$$

where  $\beta$  is a user input constant.

In Equation (3.4-78),  $D_j$  is the junction hydraulic diameter and  $L$  is the Laplace capillary constant, given by

$$L = \left[ \frac{\sigma}{g (\rho_f - \rho_g)} \right]^{1/2} \quad (3.4-79)$$

In Equation (3.4-78),  $\beta$  can be a number from 0 to 1. For  $\beta = 0$ , the Wallis form of the CCFL equation is obtained; and for  $\beta = 1$ , the Kutateladze form of the CCFL equation is obtained. For  $0 < \beta < 1$ , a form in between the Wallis and Kutateladze forms is obtained; and Bankoff<sup>3.4-33</sup> suggests that  $\beta$  be

correlated to data for the particular geometry of interest. He has included a possible function for  $\beta$ , although it is somewhat restrictive. The form of Equations (3.4-75) through (3.4-79) is general enough to allow the Wallis or Kutateladze form to appear at either small or large diameters. Other approaches (e.g., Tien, et. al.<sup>3.4-35</sup>) appear to be more restrictive by defaulting to the Wallis form at small diameters and the Kutateladze form at large diameters.

With regard to the solution method, if the CCFL model is requested by the user, the coding checks if countercurrent flow exists and if the liquid downflow exceeds the limit imposed by Equation (3.4-75). If this is true, the sum momentum equation [Equation (3.1-103)] and the flooding limit equation are applied. This approach was suggested by Trapp,<sup>a</sup> who observed that the CCFL model is similar to the choking model in that both place limits on the momentum equations. He observed that since the flooding phenomenon can be incorporated by altering the interphase friction (as is done in TRAC-PF1), it can also be incorporated by replacing the code's difference momentum equation [Equation (3.1-104)] with the flooding limit equation. The difference equation contains the interphase friction, whereas the sum equation does not. (In the choking model, the sum momentum equation is replaced with the choking limit equation.) This method is advantageous in that the phasic velocities still must satisfy the sum momentum equation, which contains gravity and pressure terms. The numerical form of Equation (3.4-75) needed by the code is obtained by letting  $c_g = H_g/v_g$  and  $c_f = H_f/v_f$ , solving for  $mH_f^{1/2}$ , and squaring the equation, which results in

$$m^2 c_{f,j}^n v_{f,j}^{n+1} = c^2 - 2c (c_{g,j}^n)^{1/2} (v_{g,j}^{n+1})^{1/2} + c_{g,j}^n v_{g,j}^{n+1} . \quad (3.4-80)$$

Linearization of  $(v_{g,j}^{n+1})^{1/2}$  gives

$$(v_{g,j}^{n+1})^{1/2} = (v_{g,j}^n)^{1/2} + (1/2) (v_{g,j}^n)^{-1/2} (v_{g,j}^{n+1} - v_{g,j}^n) \quad (3.4-81)$$

and substitution into Equation (3.4-80) gives

$$m^2 c_{f,j}^n v_{f,j}^{n+1} + [c (c_{g,j}^n)^{1/2} (v_{g,j}^n)^{-1/2} - c_{g,j}^n] v_{g,j}^{n+1} = c^2 - c (c_{g,j}^n)^{1/2} (v_{g,j}^n)^{1/2} . \quad (3.4-82)$$

### 3.4.8 Mixture Level Tracking Model

Accurate tracking of liquid levels is essential for modeling gravity-driven cooling systems. In modeling a reactor system using RELAP5, a set of large hydrodynamic volumes are used to model the various components. Because the discretization of the governing equations uses mean void fractions in each control volume, a fine nodalization is required to resolve a large change in void fraction, such as is associated with a liquid level. Even that may not be adequate to model the phenomena because RELAP5 uses a highly diffusive upwind difference scheme to discretize the advection terms. To compensate for the

---

a. Personal communication, J. A. Trapp, January 1987.

inherent limitation of the finite-difference scheme used in RELAP5 and to allow a coarser nodalization to reduce the computational cost, a mixture level tracking model is implemented in RELAP5/MOD3.

The mixture level tracking model implemented in RELAP5/MOD3 is based on TRAC-BF1/MOD1.<sup>3.4-36,3.4-37</sup> The mixture level is defined as the location where a sharp change of the void fraction distribution exists. This sharp change is associated with the change in flow regime. The model consists of four parts.

1. Detection of the mixture level appearance and disappearance.
2. Calculation of mixture level parameters that are necessary to describe a mixture level, such as the position and velocity of the level, and the void fractions above and below the level.
3. Modification of the field equations of RELAP5 to accurately convect void fractions above and below the mixture level.
4. Modification of the heat transfer calculation according to the mixture level.

The details of the model and its implementation in RELAP5 are presented in the next subsections.

**3.4.8.1 Detection of Level Appearance and Disappearance.** The mixture level is the location of an abrupt change in void fraction that is associated with a change in flow regime. There are two types of mixture levels, normal and inverted. With a normal mixture level (void profile), the void fraction increases in the upward axial direction, while with an inverted void profile, the void fraction decreases in the upward axial direction. These situations are illustrated in **Figure 3.4-15**, **Figure 3.4-16**, and **Figure 3.4-17**. Two situations that give rise to a normal void profile are heating along a vertical flow path and depressurization in a vertical column. Inverted void profiles typically arise as the result of liquid pooling in the upper and lower tie plates of a BWR pressure vessel.

The logic for the detection of a mixture level appearance and disappearance in a computational cell is based on BWR experimental data and numerical experiments.<sup>3.4-37,3.4-38,3.4-39</sup> The logic for detecting a mixture level is different for the two different kinds of mixture levels.

The level detection logic for a normal void profile, **Figure 3.4-15**, is

$$\alpha_M - \alpha_L > \delta\alpha_c \text{ (default = 0.2)} \quad (3.4-83)$$

or

$$\alpha_L - \alpha_K > \delta\alpha_c \text{ (default = 0.2)} \quad (3.4-84)$$

and

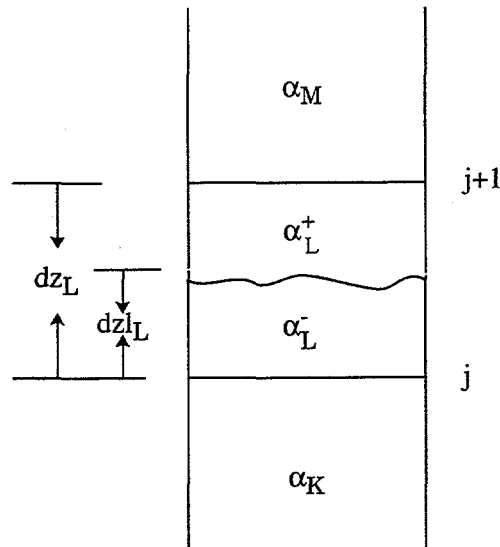


Figure 3.4-15 Mixture level in normal void profile.

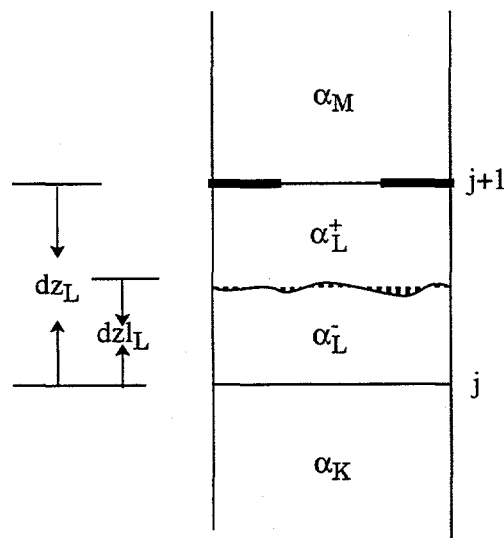
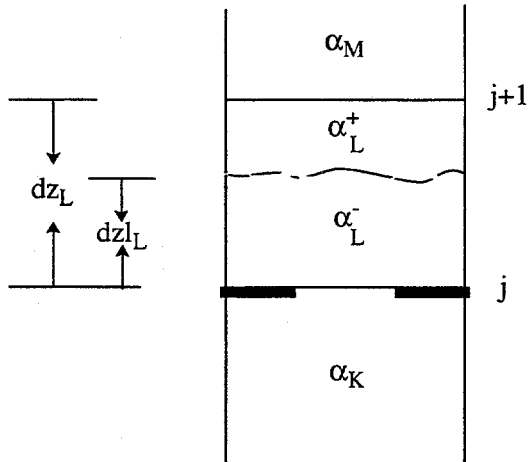


Figure 3.4-16 Mixture level in a volume below a void fraction inversion.



**Figure 3.4-17** Mixture level above a void fraction inversion.

$$\alpha_M > \alpha_c \text{ (default} = 0.7\text{)} \quad (3.4-85)$$

provided that no level exists in cell M or cell K. Here,  $\alpha_c$  is the minimum allowable void fraction in the cell above a normal mixture level, and  $\delta\alpha_c$  is the smallest change that signals the presence of a normal mixture level. The values in parentheses are the default values to be used in RELAP5/MOD3 and are recommended by Cheung et al.<sup>3.4-38</sup> The notation  $\alpha$  or  $\alpha_g$  is used for vapor void fraction.

The logic for an inverted void profile depends on whether a particular cell is above or below a void inversion. A mixture level is defined as being below a void profile inversion **Figure 3.4-16** if

$$\alpha_L - \alpha_M > \delta\alpha_j \text{ (default} = 0.1\text{)} \quad (3.4-86)$$

If a mixture level is above a void profile inversion (**Figure 3.4-17**), the criteria becomes

$$\alpha_K - \alpha_L > \delta\alpha_j \text{ (default} = 0.1\text{)} \quad (3.4-87)$$

The void inversion logic is activated if there is an orifice at the junction. The level detection logic is summarized in block diagrams as shown in **Figure 3.4-18**, **Figure 3.4-19**, **Figure 3.4-20**, and **Figure 3.4-21**.

**3.4.8.2 Calculation of Level Parameters.** The parameters that describe the mixture level are:

1. The void fraction above and below the level  $\alpha_L^+$  and  $\alpha_L^-$

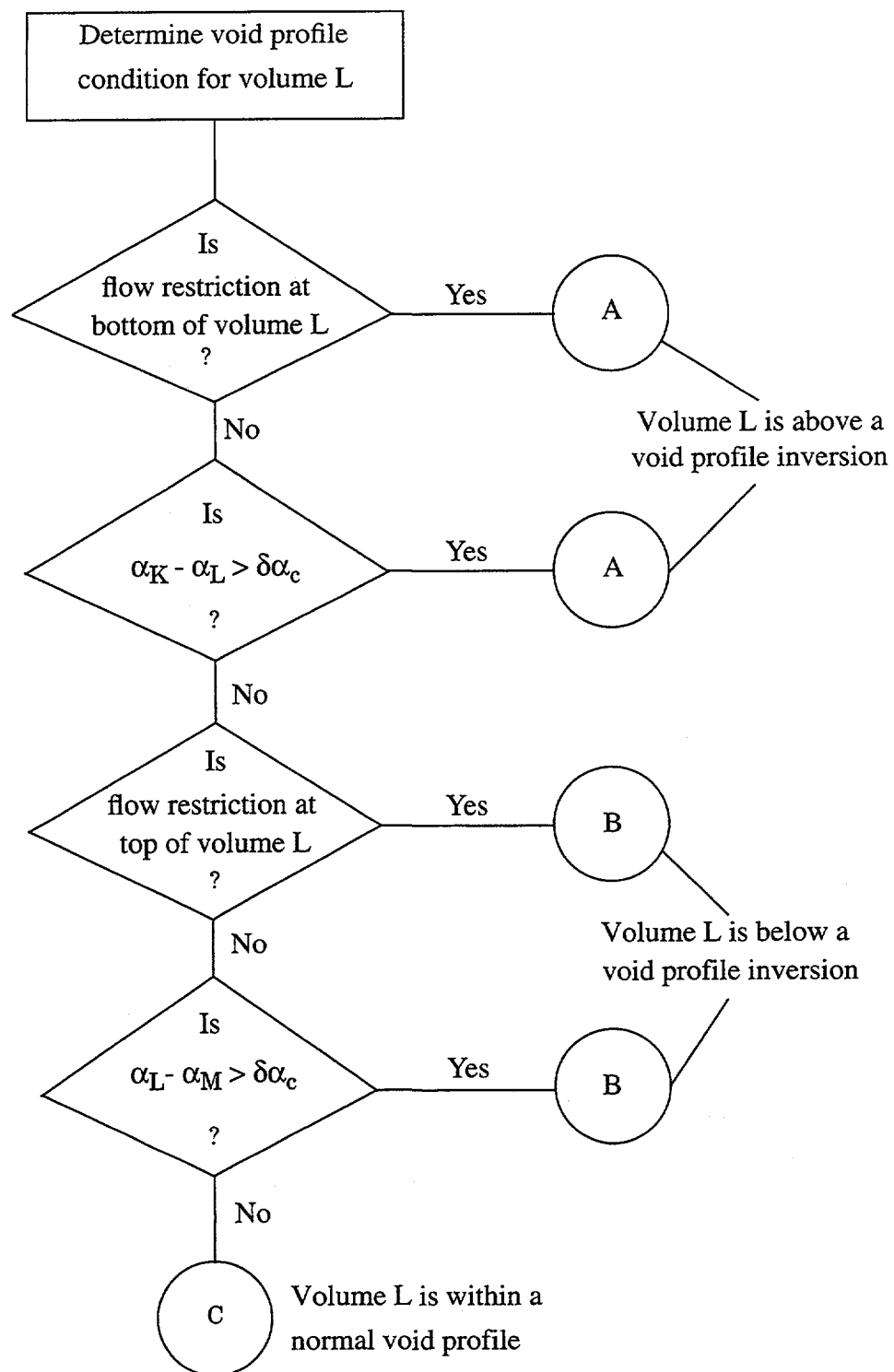


Figure 3.4-18 Level detection logic diagram.

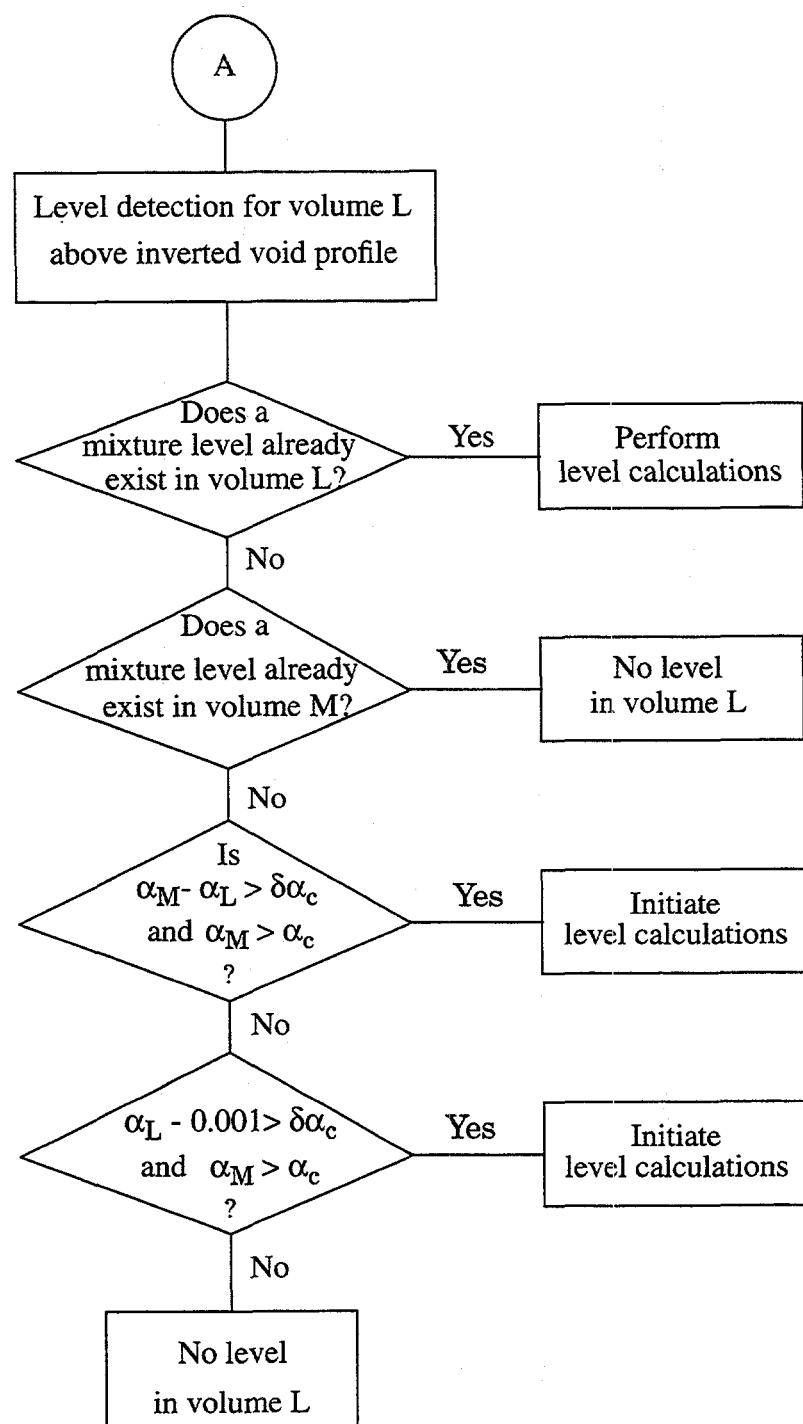


Figure 3.4-19 Level detection logic for volume L above an inverted profile.

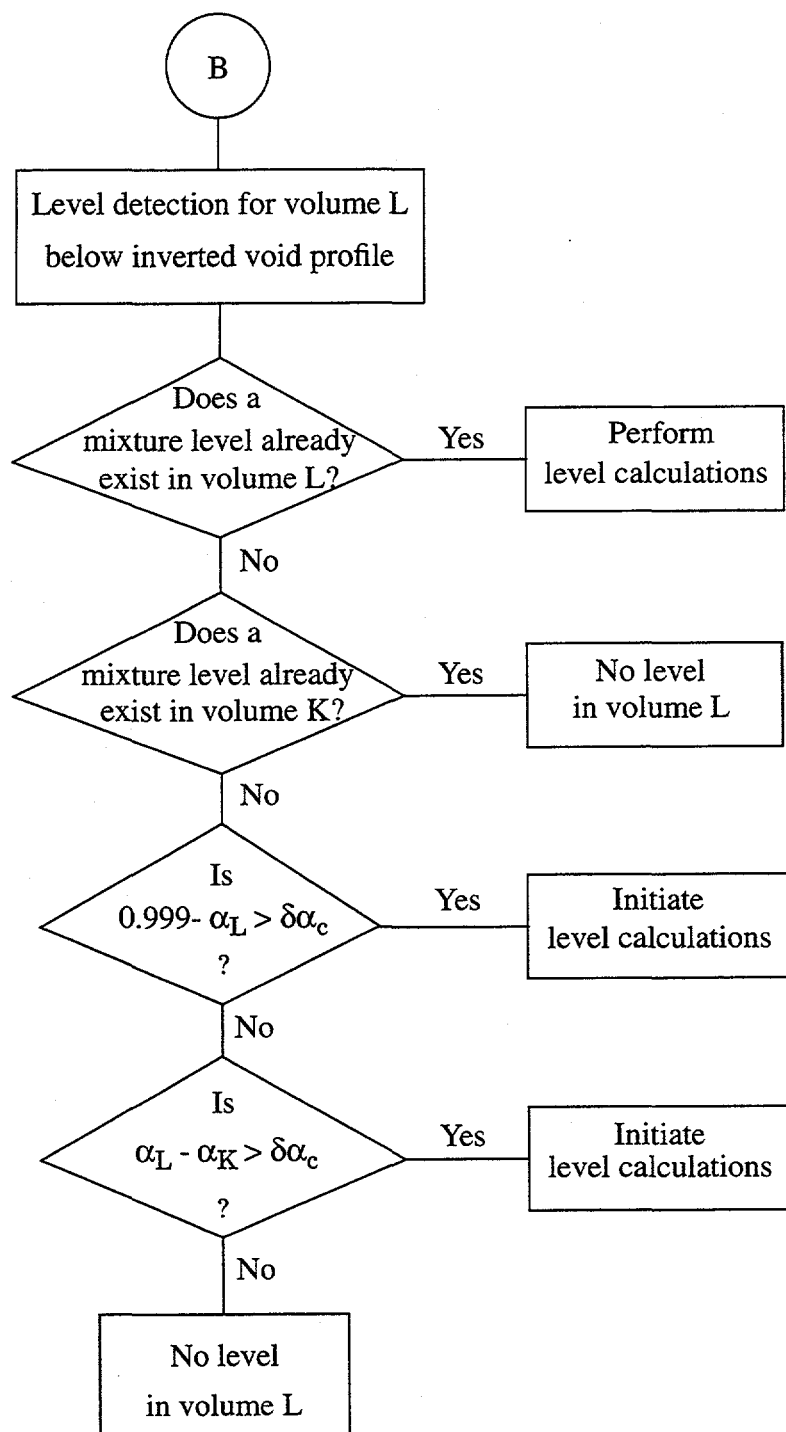


Figure 3.4-20 Level detection logic diagram for volume L below an inverted profile.

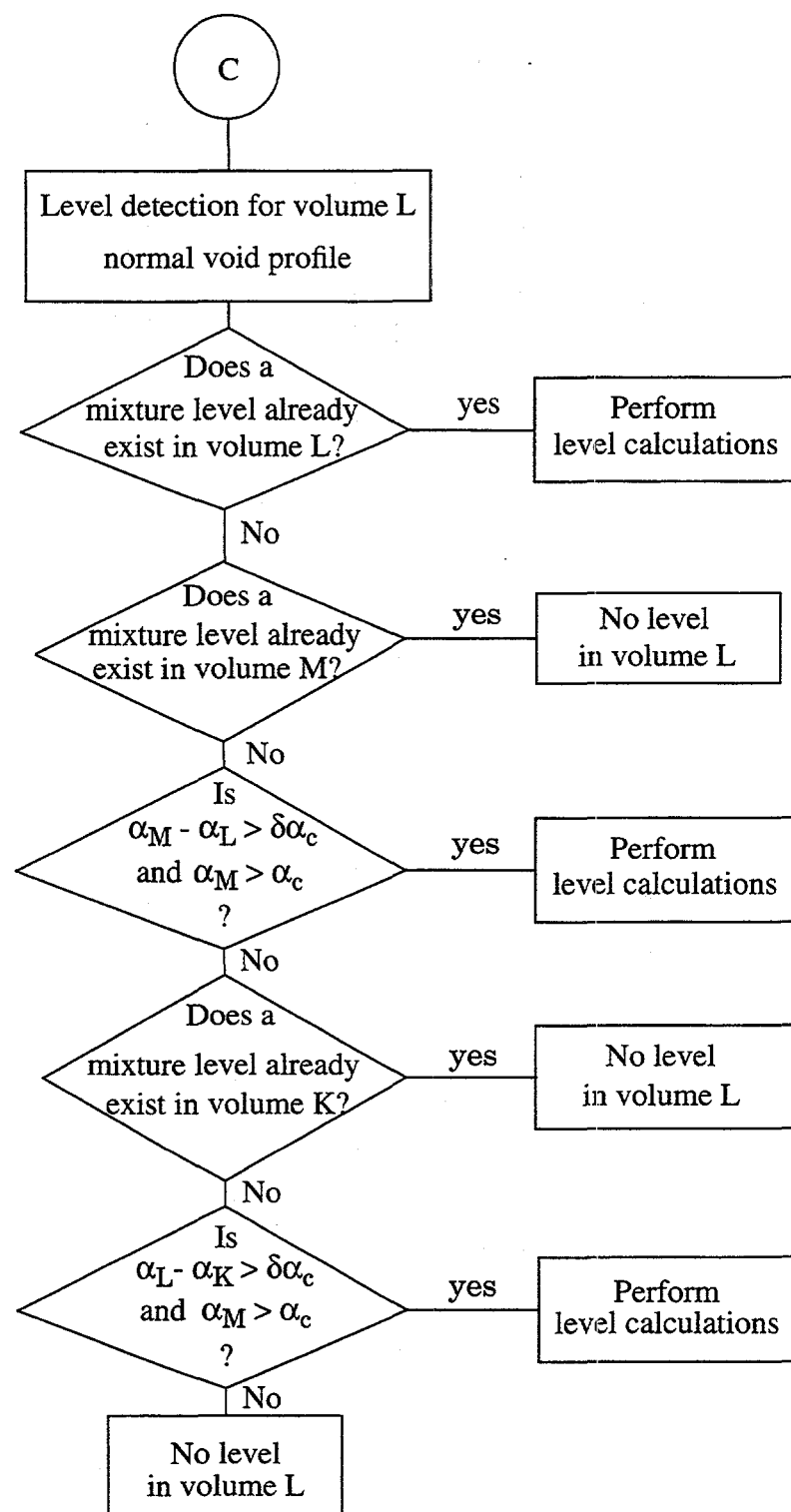


Figure 3.4-21 Level detection logic diagram for a normal profile.

2. The location of the level (dzl)
3. The mixture level velocity ( $v_{lev}$ ).

**3.4.8.2.1 Determination of the Void Fraction Above and Below the Level**--The correlations to calculate the void fraction above and below the level  $\alpha_L^+$  and  $\alpha_L^-$ , respectively, are given below for the three cases:

1. Normal profile
2. Void inversion above volume L or flow restriction at the top of volume L
3. Void inversion below volume L or flow restriction at the bottom of volume L.

**Case 1: Normal Void Profile.**

For a normal void profile, the void fraction below the level is assumed to equal the void fraction in volume K:

$$\alpha_L^- = \alpha_K \quad . \quad (3.4-88)$$

In the absence of entrainment of liquid from below the level, the void fraction above the level is given by:

$$\alpha_L^+ = \alpha_M \quad . \quad (3.4-89)$$

If the velocity at the cell junction is upward, the void fraction  $\alpha_L^+$  is derived from the correlation of the entrainment liquid mass flux ( $G_{lent}$ ) developed by Rosen<sup>3.4-40</sup> as

$$\alpha_L^+ = 1 - \frac{G_{lent}}{\rho_f v_f} \quad (3.4-90)$$

and

$$v_f = v_{f,j+1} \left( \frac{A_{j+1}}{A_L} \right) \quad (3.4-91)$$

where

$$v_{f,j+1} = \text{the junction liquid velocity}$$

$A_{j+1}$  = the junction area  
 $A_L$  = the average area of the control volume.

The entrainment liquid mass flux ( $G_{\text{ent}}$ ) is expressed by

$$G_{\text{ent}} = \left( 3.0 \times 10^{-5} (CK^{0.5} + 530 \cdot CK^{2.1}) \left( \frac{\rho_f - \rho_g}{\rho_g} \right)^{0.5} \right) j_g \rho_g \quad (3.4-92)$$

where

$$CK = \frac{2.0 \cdot DMAX \cdot L_g}{\left( VCRIT \cdot g \cdot \left( \frac{\sigma}{\rho_g - \rho_g} \right)^{0.5} \right)} \quad (3.4-93)$$

$$VCRIT = 2.0 \left( \frac{\sigma g (\rho_f - \rho_g)}{\rho_g^2} \right)^{0.25} \quad (3.4-94)$$

$$DMAX = 0.3375 \left( \frac{\rho_g v_g^2}{g (\rho_f - \rho_g)} \right). \quad (3.4-95)$$

In the above expression,  $G_{\text{ent}}$  is calculated using donor cell-averaged values for  $\rho_f$ ,  $\rho_g$ , and  $\sigma$  at cell L. The value of  $L_g$  is set equal to (for positive  $v_f$ )

$$j_g = \alpha_M v_g \quad (3.4-96)$$

and

$$v_g = v_{g,j+1} \left( \frac{A_{j+1}}{A_L} \right) \quad (3.4-97)$$

where  $v_{g,j+1}$  is the junction vapor phasic velocity.

If either  $v_{f,j+1}$  or  $v_{g,j+1}$  is negative,  $\alpha_L^+$  is given by

$$\alpha_L^+ = \alpha_M \quad (3.4-98)$$

**Case 2: Void Inversion Above Volume L or Flow Restriction at the Top of Volume L.**

The calculation of the void fraction above and below the level ( $\alpha_L^+$  and  $\alpha_L^-$ ) is similar to Case 1 except with the following modification.

The volumetric vapor flux used in Equations (3.4-92) and (3.4-93) becomes

$$j_g = 0.999 v_g . \quad (3.4-99)$$

If  $v_{g,j+1}$  is negative, then

$$\alpha_L^+ = 0.999 . \quad (3.4-100)$$

**Case 3: Void Inversion Below Volume L or Flow Restriction at the Bottom of Volume L.**

For a cell mixture level occurring above a void fraction inversion or bottom cell area reduction, the void fraction below the level  $\alpha_L^-$  is calculated using the drift flux approximation

$$\alpha_L^- = \frac{j_g}{C_o j^- + v_{gj}} \quad (3.4-101)$$

where

$$v_{gj} = 1.41 \left( \frac{\Delta \rho g \sigma}{\rho_f^2} \right)^{\frac{1}{4}} \quad (3.4-102)$$

$$C_o = C_\infty - (C_\infty - 1) \sqrt{\frac{\rho_g}{\rho_f}} \quad (3.4-103)$$

$$C_\infty = 1.0 + 0.2 \left( \frac{\rho_f (g D_h)^{\frac{1}{2}}}{|v_g \alpha_g \rho_g| + |v_f \alpha_f \rho_f|} \right)^{\frac{1}{2}} . \quad (3.4-104)$$

Rouhani's<sup>3.4-41</sup> correlation is used for  $C_\infty$ . The parameters used in calculating  $C_\infty$  are based on cell-centered quantities. The volumetric fluxes  $L_g^-$  and  $j^-$  are calculated using junction-donored velocities from

bottom cell  $j$  and void fractions of either  $\alpha_K$  or  $\alpha_L^-$ , depending on whether or not the phasic velocities are positive or negative, respectively.

$$j_g^- = \frac{1}{2} v'_{g,j} ((\alpha_{g,K} + \alpha_L^-) + \text{sgn}(v'_{g,j}) (\alpha_{g,K} - \alpha_L^-)) \quad (3.4-105)$$

$$j_f^- = \frac{1}{2} v'_{f,j} ((\alpha_{f,K} + (1 - \alpha_L^-)) + \text{sgn}(v'_{f,j}) (\alpha_{f,K} - (1 - \alpha_L^-))) \quad (3.4-106)$$

$$j^- = j_f^- + j_g^- \quad (3.4-107)$$

where

$$v'_{f,j} = v_{f,j} \left( \frac{A_j}{A_L} \right) \quad (3.4-108)$$

$$v'_{g,j} = v_{g,j} \left( \frac{A_j}{A_L} \right) . \quad (3.4-109)$$

The logic and correlations used to calculate  $\alpha_L^+$  are the same as for the normal void profile scheme.

**3.4.8.2.2 Location of the Mixture Level**--Once the presence of a level is determined in a particular volume, a level flag is set and the level parameters are calculated. The position of the level ( $dzl_L$ ) of a cell with length  $dz_L$  is given by

$$dzl_L = dz_L \left( \frac{\alpha_L^+ - \alpha_L^-}{\alpha_L^+ - \alpha_L^-} \right) \quad (3.4-110)$$

where the above and below mixture level void fractions are given above.

**3.4.8.2.3 Velocity of Level Movement**--The level velocity  $v_{lev}$  is obtained by forming a difference approximation to the time derivative of Equation (3.4-110) as:

$$v_{lev} = \frac{dzl_L^n - dzl_L^{n-1}}{\Delta t} \quad (3.4-111)$$

**3.4.8.3 Modification of RELAP5 Field Equations for Level Tracking.** The following modifications will be made in solving the field equations in RELAP5:

1. The donor cell void fraction based on the void fraction above and below the mixture level will be used in the momentum equations and mass and energy convective terms.
2. The hydrostatic pressure will be modified according to the location of the mixture level.
3. When the mixture level crosses the cell boundary, the level model will be turned off.

**3.4.8.3.1 Donor Cell Void Formulation--**The donor void fraction to be used at junctions  $j+1$  and  $j$  in the momentum equations and convective terms of the mass and energy equations are given in Table 3.4-1<sup>a</sup>.

**Table 3.4-1** Logic for determining donor void fraction.

Junction	$v_g$	$\dot{\alpha}_g$	$v_f$	$\dot{\alpha}_f$
$j + 1$ above level	$>0$	$\alpha_L^+$	$>0$	$1 - \alpha_L^+$
$j + 1$ above level	$<0$	$\alpha_M$	$<0$	$1 - \alpha_M$
$j$ below level	$>0$	$\alpha_K$	$>0$	$1 - \alpha_K$
$j$ below level	$<0$	$\alpha_L^-$	$<0$	$1 - \alpha_L^-$

The determination of the donor void fraction is to ensure that the level is maintained as a sharp interface in RELAPS.

**3.4.8.3.2 Hydrostatic Pressure Calculation--**The pressure drop terms in the momentum equations are modified to include the effect of a two-mixture level on the gravity head. The pressure drop is calculated as:

$$\Delta P = P_M - P_L - \Delta P_{\text{hydro}} \quad (3.4-112)$$

When the mixture level exists below junction  $j+1$  in volume  $L$ , the hydrostatic pressure is calculated as **Figure 3.4-22-A**:

Case A-1: for  $dz_L > \frac{dz_L}{2}$ :

a. Personal communication with K. E. Carlson 1993.

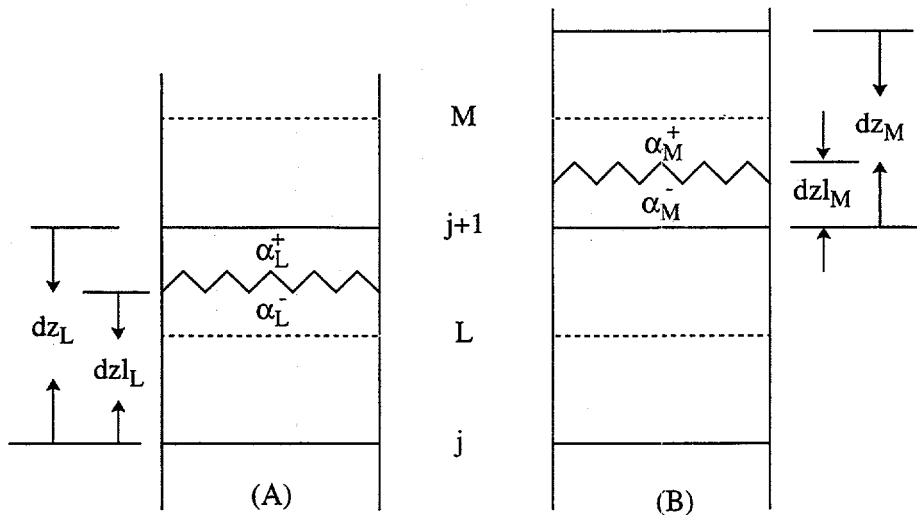


Figure 3.4-22 The control volume for momentum cell  $j+1$ .

$$\begin{aligned}\Delta P_{\text{hydro}} = & (dz_L - dz_L/2) g [\alpha_L^- \rho_{g,L} + (1 - \alpha_L^-) \rho_{f,L}] \\ & + (dz_L - dz_L) g [\alpha_L^+ \rho_{g,L} + (1 - \alpha_L^+) \rho_{f,L}] \\ & + (dz_M/2) g (\alpha_{g,M} \rho_{g,M} + \alpha_{f,M} \rho_{f,M}) .\end{aligned}\quad (3.4-113)$$

Case A-2: for  $dz_L < \frac{dz_L}{2}$ :

$$\begin{aligned}\Delta P_{\text{hydro}} = & (dz_L/2) g [(\alpha_L^+ \rho_{g,L} + (1 - \alpha_L^+) \rho_{f,L})] \\ & + (dz_M/2) g (\alpha_{g,M} \rho_{g,M} + \alpha_{f,M} \rho_{f,M}) .\end{aligned}\quad (3.4-114)$$

When the mixture level exists above junction  $j+1$  in volume  $M$ , the hydrostatic pressure is calculated as Figure 3.4-22-B:

Case B-1: for  $dz_M > \frac{dz_M}{2}$ :

$$\begin{aligned}\Delta P_{\text{hydro}} = & (dz_M/2) g [\alpha_M^- \rho_{g,M} + (1 - \alpha_M^-) \rho_{f,M}] \\ & + (dz_L/2) g (\alpha_{g,L} \rho_{g,L} + \alpha_{f,L} \rho_{f,L}) .\end{aligned}\quad (3.4-115)$$

Case B-2: for  $dzl_M < \frac{dz_M}{2}$ :

$$\begin{aligned}\Delta P_{\text{hydro}} = & (dzl_M/2 - dzl_M) g [\alpha_M^+ \rho_{g,M} + (1 - \alpha_M^+) \rho_{f,M}] \\ & + (dzl_M) g [\alpha_M^- \rho_{g,M} + (1 - \alpha_M^-) \rho_{f,M}] \\ & + (dz_L/2) g [\alpha_{g,L} \rho_{g,L} + \alpha_{f,L} \rho_{f,L}]\end{aligned}\quad (3.4-116)$$

**3.4.8.3.3 Criterion for the Level Crossing Cell Boundary**—Two criteria are used to determine if a level will cross a cell boundary (Figure 3.4-23). The first criteria is:

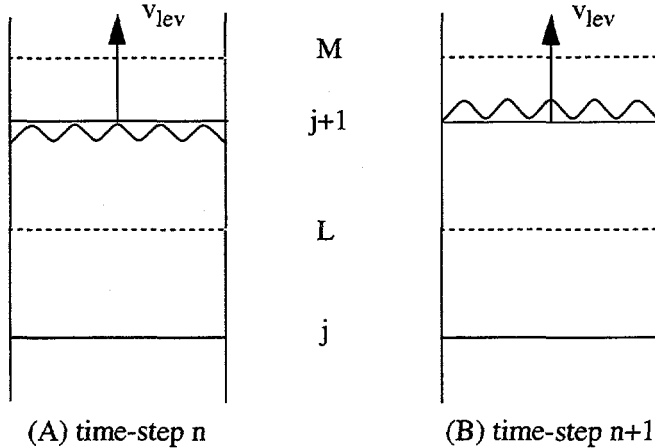


Figure 3.4-23 Mixture level rising through a control volume edge.

For a rising level,  $v_{\text{lev}} > 0$ ,

$$|\alpha_L - \alpha_L^-| < \epsilon \alpha_c \text{ (default = 0.02)} \quad (3.4-117)$$

or

$$\frac{dzl_L}{dz_L} \geq 0.98 \quad (3.4-118)$$

This is the case when the level is near the top of volume L and the void fraction  $\alpha_L$  and  $\alpha_L^-$  are very close.

For a falling level,  $v_{lev} < 0$

$$|\alpha_L^+ - \alpha_L^-| < \varepsilon \alpha_c \text{ (default} = 0.02\text{)} \quad (3.4-119)$$

or

$$\frac{dz_L}{dz_L} \leq 0.02 \quad (3.4-120)$$

This is the case when the level is near the bottom of volume L and the void fraction  $\alpha_L$  and  $\alpha_L^+$  are very close. The values in the parentheses are default values to be used in RELAP5/MOD3.

When the level crosses the boundary, the normal numerics of RELAP5 are used in all of the calculations.

**3.4.8.4 Modification of Heat Transfer Calculation.** When a heat structure is associated with a hydrodynamic volume where a mixture level exists, the heat transfer will be partitioned according the level location (Figure 3.4-24). The heat transfers from wall to liquid and gas phase ( $q_{wf}$  and  $q_{wg}$ ) are calculated as:

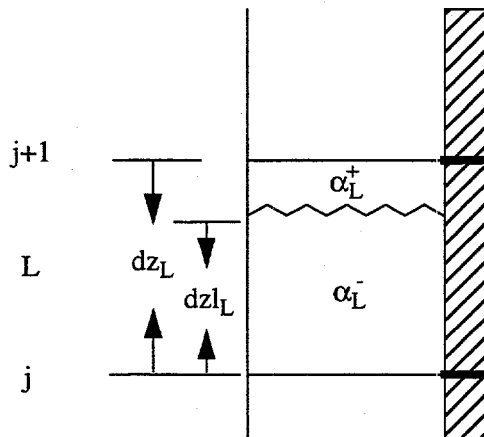


Figure 3.4-24 Hydrodynamic volume with heat structure.

$$q_{wg} = htcg (T_w - T_g) \left( 1 - \frac{dz_L}{dz_L} \right) \quad (3.4-121)$$

$$q_{wf} = h_{cf}(T_w - T_f) \left( \frac{dz_L}{dz_L} \right) \quad (3.4-122)$$

where the heat transfer coefficient to gas and liquid ( $h_{cg}$  and  $h_{cf}$ ), wall temperature ( $T_w$ ), and gas and liquid temperature ( $T_g$  and  $T_f$ ) are the same as described in Section 3.3.9.

### 3.4.9 Thermal Stratification Model

A thermal stratification model is included to improve the accuracy of solutions when there is warm fluid appearing above cold fluid in a vertical stack of cells. In this case, there is a sharp thermal front between the two fluids because of the density differences between them. Because RELAP5 uses a first-order upwind differencing scheme that has considerable numerical diffusion, there is significant artificial mixing of the hot and cold fluids. This has an unfavorable effect on the accuracy of the solution. Therefore, a model is included with the following features:

1. A sharp temperature profile is maintained which separates the hot fluid from the cold fluid whenever thermal stratification occurs
2. Correct donorizing of liquid internal energy at the junctions for the cell where the thermal stratification occurs
3. Only the hot fluid in a cell which contains the thermal front is allowed to flash.

In addition, the model is compatible with the mixture level model and when used in conjunction with the level model, it allows the code to predict the stratified behavior in a tank with considerable accuracy.

There are essentially two good choices to meet the requirements stated above. One possibility is to use a Godunov-type scheme with artificial compression method to sharpen the temperature profile at the edge of the cell. The second approach is to use Harten's subcell resolution scheme,<sup>3.4-42</sup> to track the front in the interior of the cell. The problem with the first approach is that the front is tracked at the edge of the cell, whereas the front spends most of its time in the interior of the cell. Among other things, criteria 2 and 3 of the above may never be satisfied. This is not a serious problem for CFD codes where cell size tends to be fairly small. For engineering codes that use coarse nodalization, Harten's approach is the best approach if it is applicable to the problems in question.

It should be emphasized that although the proposed model can be viewed as an extension of Harten's method to the liquid internal energy for two-phase flow problems, the implementation of the model draws heavily from that of the mixture level model. Still, to have a deeper understanding of the range of applicability of the method, the reader is strongly encouraged to read Harten's paper. In the thermal model, the solution locally near the front is assumed to have a very simple profile. It is piecewise constant with the larger positive value appearing on top of a smaller value. Because RELAP5 uses a simple first-order scheme with positive coefficients, it is therefore possible to determine the position of the front accurately using a simple calculation given in Section 3.4.9.3 below.

**3.4.9.1 Overview of Software Design for the Thermal Stratification Model.** The thermal front is defined as the location where a sharp change in the temperature of the fluid occurs. The thermal-front tracking model implemented in RELAP5/MOD3 is analogous to the mixture-level tracking model

currently in RELAP5/MOD3 (see Section 3.4.8), both in its methodology and in its implementation. The model consists of four parts:

1. Detection of the thermal front appearance and disappearance
2. Calculation of thermal front parameters that are necessary to describe a thermal front such as the position and velocity of the front, and the temperatures above and below the front
3. Modification of the liquid internal energy at the junctions to accurately convect the liquid internal energy above and below the front
4. Modification of the heat transfer calculation and vapor generation rate according to the position of the thermal front and temperature of the hot fluid in the cell that contains the thermal front.

**3.4.9.2 Detection of Thermal Front Appearance and Disappearance.** The thermal front is the location of an abrupt change in the fluid temperature. The logic for the detection of a thermal front appearance and disappearance in a computational cell is based on experimental data and numerical experiments. The density difference between the hot and cold fluid typically exceeds 3%. The thermal front detection logic for cell  $j$  in **Figure 3.4-25** is:

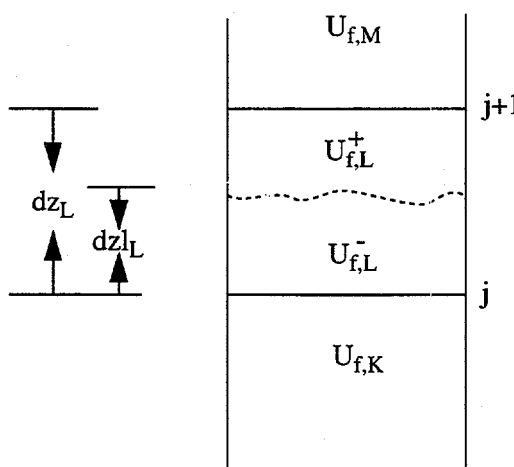


**Figure 3.4-25** Thermal front in a tank.

$$\frac{|\rho_M - \rho_L|}{\rho_L} > 0.01 \quad (3.4-123)$$

or

$$\frac{|\rho_K - \rho_L|}{\rho_L} > 0.01 \quad (3.4-124)$$

provided that no thermal front exists in cell M or cell K and the liquid in the cells K, L, and M is stably stratified, or in other words, the internal energy of the liquid is a monotonically increasing function of  $j$  in the three cells in question. This is both a physical and mathematical necessity, since the computed  $dz_1$  at cell  $j$  according to Equation (3.4-123) should be a positive number less than  $dz$ . See Figure 3.4-26 for the logic diagram for front detection.

**3.4.9.3 Calculation of Front Parameters.** The front parameters that describe the thermal front are:

1. The internal energy of the fluid above and below the front ( $U_{fL}^+$  and  $U_{fL}^-$ )
2. The location of the front ( $dz_1$ )
3. the thermal front velocity ( $v_{front}$ ).

**3.4.9.3.1 Determination of the Internal Energy Above and Below the Front**--The internal energy of the fluid below the front is set equal to the internal energy of the fluid in volume K

$$U_{fL}^- = U_{f, K} \quad (3.4-125)$$

while the internal energy of the fluid above the front is set equal to the internal energy of the fluid in volume M

$$U_{fL}^+ = U_{f, M} \quad (3.4-126)$$

**3.4.9.3.2 Location of the Thermal Front.** Once the presence of a thermal front is determined in a particular volume, a flag is set and the front parameters are calculated. The position of the front ( $dz_1_L$ ) of a volume with length  $dz_L$  is given by

$$dz_1_L = dz_L \left( \frac{U_{fL}^+ - U_{fL}^-}{U_{fL}^+ - U_{fL}^-} \right) \quad (3.4-127)$$

where the  $U_{fL}^+$  and  $U_{fL}^-$  are given in Section 3.4.9.3.1. It is emphasized that this computation is performed only when  $U_{fL}^+ > U_{fL}^- > U_{fL}^-$ . This ensures that  $dz_1_L$  is a positive number less than  $dz_L$ .

**3.4.9.3.3 Velocity of the Thermal Front**--The velocity of the thermal front is computed from:

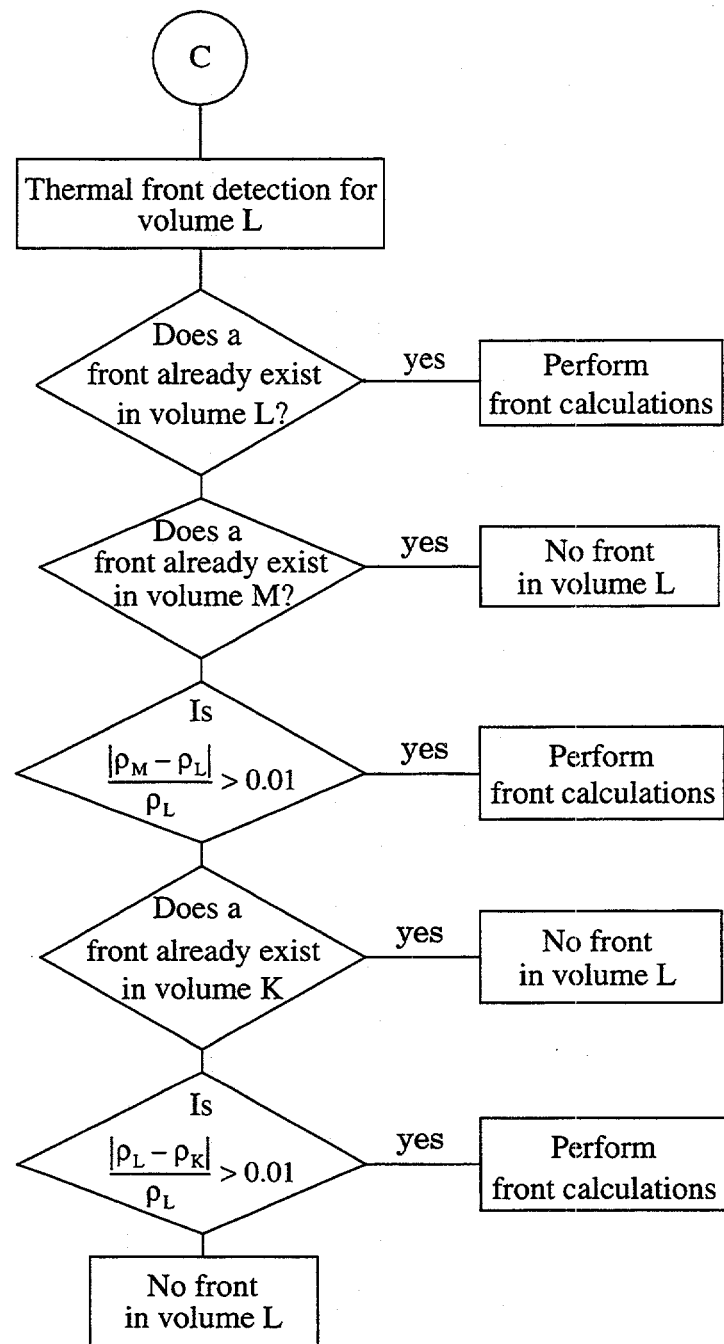


Figure 3.4-26 Thermal front detection logic diagram for volume L.

$$v_{\text{front}} = \frac{dz1_L^n - dz1_L^{n-1}}{\Delta t} \quad (3.4-128)$$

**3.4.9.3.4 Modifications for Front Crossing**--The criteria to determine if a thermal front will cross a cell boundary area

1. For a rising front,  $v_{\text{front}} > 0$ ,

$$\frac{|\rho_L^+ - \rho_L^-|}{\rho_L} < 0.001 \quad (3.4-129)$$

or

$$\frac{dz1_L}{dz_L} \geq 0.98 \quad (3.4-130)$$

This is the case when the thermal front is near the top of volume L and the densities  $\rho_L$  and  $\rho_L^+$  are very close.

2. For a falling front,  $v_{\text{front}} < 0$

$$\frac{|\rho_L^+ - \rho_L^-|}{\rho_L} < 0.001 \quad (3.4-131)$$

or

$$\frac{dz1_L}{dz_L} \leq 0.02 \quad (3.4-132)$$

This is the case when the thermal front is near the bottom of volume L and the densities  $\rho_L$  and  $\rho_L^+$  are very close. **Figure 3.4-27** shows the logic diagram for the computation of thermal front parameters with modifications for front crossing.

**3.4.9.4 Modification of RELAP5 Field Equations for Front Tracking.** The following modifications were made in solving the field equations in RELAP5:

1. The donor cell liquid internal energy based on the liquid internal energy above and below the thermal front will be used in the field equations

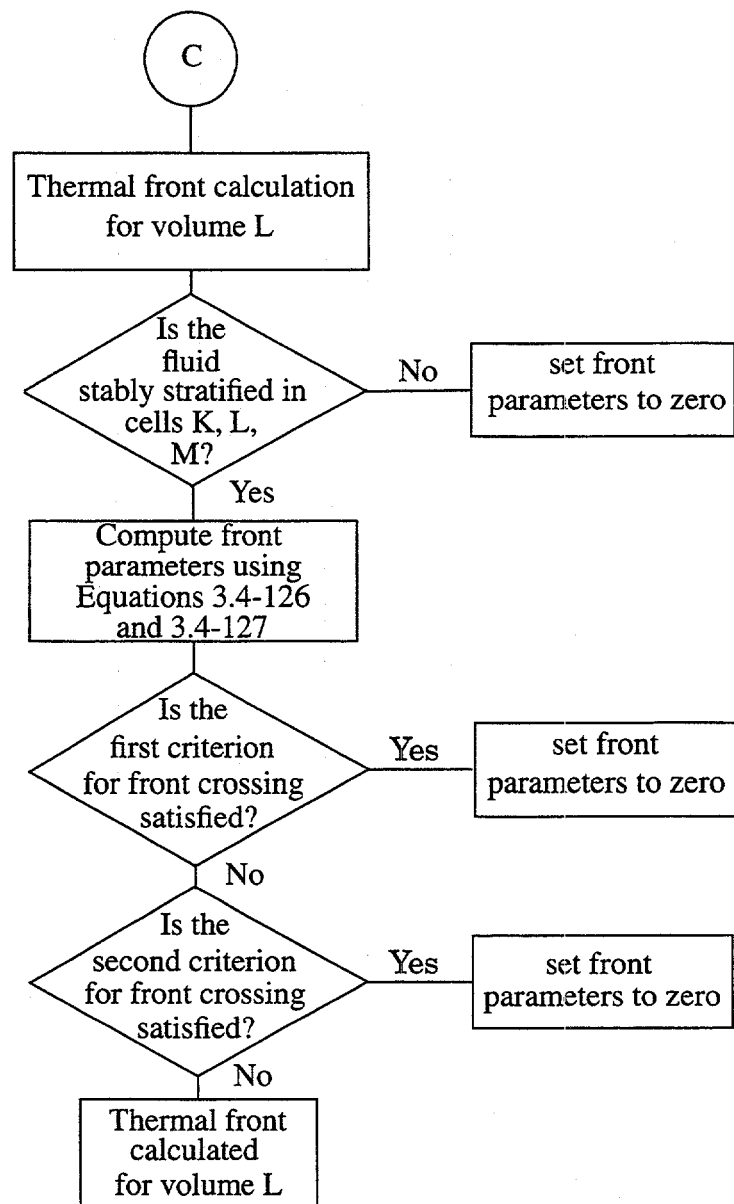


Figure 3.4-27 Computation of thermal front parameters logic diagram for volume L.

2. The liquid temperature in the cell that contains the thermal front is modified in the computation of mass and energy transfer to indicate that only the hot fluid in the cell can undergo phase change, (i.e., flash to vapor)
3. The interphase heat transfer coefficient in the cell that contains the thermal front is modified to indicate that only the hot fluid in the cell can flash.

**3.4.9.4.1 Donor Cell Internal Energy Formulation**—The donor internal energies to be used at junctions  $j+1$  and  $j$  in the field equations are given in **Table 3.4-2**.

**Table 3.4-2 Logic for determining donor internal energy ( $v > 0 \leftrightarrow$  rising fluid)** .

Junction	$v_g$	$\dot{U}_g$	$v_f$	$\dot{U}_f$
$j+1$ above front	$> 0$	$u_{g,L}$	$> 0$	$u_{f,M}$
$j+1$ above front	$< 0$	$u_{g,M}$	$< 0$	$u_{f,M}$
$j$ below front	$> 0$	$u_{g,K}$	$> 0$	$u_{f,K}$
$j$ below front	$< 0$	$u_{g,L}$	$< 0$	$u_{f,K}$

**3.4.9.4.2 Modifications of Mass and Energy Transfer Calculation**—Because only hot fluid in the cell that contains the thermal front can flash, the interfacial heat transfer coefficients need to be recalculated to reflect this. If the thermal front occurs at cell  $L$ , then  $H_{if}$  will be recomputed as

$$H_{if}^{new} = H_{if} \left( 1 - \frac{dz_L}{dz_L} \right) . \quad (3.4-133)$$

The contribution to the vapor generation by the term  $H_{if} (T_s - T_{fL})$  is then modified to be

$$H_{if}^{new} (T_s - T_f (U_{f,L}^+)) \quad (3.4-134)$$

where  $T_f (U_{f,L}^+)$  is the temperature of the hot fluid in the cell that contains the front (**Figure 3.4-28**).

### 3.4.10 Energy Conservation at an Abrupt Change

In special situations involving abrupt changes in either flow geometry (i.e., area changes) or flow conditions (i.e., shocks), predictions using the default RELAP5 models do not conserve total energy. The situation usually involves significant pressure drops between RELAP5 volumes. The primary interest in this is the simulation of the discharge at a break in the piping at a nuclear plant into the containment vessel. When the containment is modeled using normal RELAP5 volumes (not time-dependent volumes), the lack of total energy conservation can result in the containment temperature being significantly under-predicted (by approximately 100°F).<sup>a</sup>

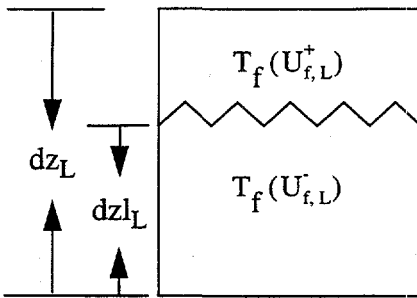


Figure 3.4-28 Hydrodynamic volume with thermal front.

The thermal (internal) energy Equations (3.1-11) and (3.1-12) are equivalent to the total energy equations (i.e., energy is conserved) in the differential sense. This will not be true in the finite difference implementation because thermal energy equations cannot be expressed in so-called conservation law form as is possible for the total energy equations. Although the total energy equations can be implemented in the conservation form, there are some difficulties in the numerical implementation. These include the energy storage, energy flux, interfacial energy, and kinetic energy terms. The method used in RELAP5/MOD3 is to allow the user to correct the energy flux terms at points where they are known to be in error. This is done through a user junction input flag. The method used will next be described.

The vapor thermal energy equation will be used to describe the method. The liquid thermal energy equation is similar. The nonexpanded vapor thermal energy Equation (3.1-112) is of the finite difference form

$$V_L [ (\alpha_g \rho_g U_g)_L^{n+1} - (\alpha_g \rho_g U_g)_L^n ] + (\dot{\alpha}_{g,j+1}^n (\dot{\rho}_{g,j+1}^n \dot{U}_{g,j+1}^n + P_L^n) V_{g,j+1}^{n+1} A_{j+1} - \dot{\alpha}_{g,j}^n (\dot{\rho}_{g,j}^n \dot{U}_{g,j}^n + P_L^n) V_{g,j}^{n+1} A_j] \Delta t = RHS \quad (3.4-135)$$

where RHS is the right-hand side terms. If the vapor velocity is positive through junctions  $j$  and  $j+1$ , the pressure used in the energy flux term for junction  $j$  is  $P_K^n$  rather than  $P_L^n$ . Thus, Equation (3.4-135) becomes

$$V_L [ (\alpha_g \rho_g U_g)_L^{n+1} - (\alpha_g \rho_g U_g)_L^n ] + (\dot{\alpha}_{g,j+1}^n (\dot{\rho}_{g,j+1}^n \dot{U}_{g,j+1}^n + P_L^n) V_{g,j+1}^{n+1} A_{j+1} - \dot{\alpha}_{g,j}^n (\dot{\rho}_{g,j}^n \dot{U}_{g,j}^n + P_K^n) V_{g,j}^{n+1} A_j] \Delta t = RHS \quad (3.4-136)$$

a. Personal communication, M. Van Haltern, Northeast Utilities, November 1991.

For positive vapor velocity in junction j, the donor density  $\dot{\rho}_{g,j}$  and the donor energy  $\dot{U}_{g,j}$ , will also be from volume K. Thus, the energy flux term for junction j is really the enthalpy from volume K. This modification results in using internal energy in the time derivative and enthalpy in the convective terms. This is the approach used in the containment code CONTAIN.<sup>3.4-43</sup> In the CONTAIN code, the total energy equation is the starting equation, but the kinetic energy is then ignored in the time derivative and convective terms because typical containment volumes are quite large. The resultant time derivative and convective terms are the same as shown in Equation (3.4-136). Using CONTAIN and the RELAP5 modification to the energy flux give results that correctly match the containment temperature.

### 3.4.11 References

- 3.4-1. V. H. Ransom and J. A. Trapp, "The RELAP5 Choked Flow Model and Application to a Large Scale Flow Test," *Proceedings of the ANS/ASME/NRC International Topical Meeting on Nuclear Reactor Thermal-Hydraulics, Saratoga Springs, New York, October 5-8, 1980*, pp. 799-819.
- 3.4-2. J. A. Trapp and V. H. Ransom, "A Choked-Flow Calculation Criterion for Nonhomogeneous, Nonequilibrium Two-Phase Flows", *International Journal of Multiphase Flow*, 8, 6, 1982, pp. 669-681.
- 3.4-3. P. R. Garabedian, *Partial Differential Equations*, New York: John Wiley and Sons, 1964.
- 3.4-4. G. B. Whitham, *Linear and Nonlinear Waves*, New York: John Wiley and Sons, 1974.
- 3.4-5. A. H. Shapiro, *The Dynamics and Thermodynamics of Compressible Fluid Flow, II*, New York: Ronald, 1954.
- 3.4-6. V. H. Ransom and J. A. Trapp, *RELAP5 Progress Summary Analytical Choking Criterion for Two-Phase Flow*, CDAP-TR-013, 1978.
- 3.4-7. D. A. Drew, L. Y. Cheng, and R. T. Lahey, Jr., "The Analysis of Virtual Mass Effects in Two-Phase Flow," *International Journal of Multiphase Flow*, 5, 1979, pp. 233-242.
- 3.4-8. P. S. Anderson, P. Astrup, L. Eget, and O. Rathman, "Numerical Experience with the Two-Fluid Model RISQUE," *Proceedings from Topical Meeting on Thermal Reactor Safety, Sun Valley, ID, July 31-August 4, 1977*.
- 3.4-9. D. Gidaspow (Chairman), "Modeling of Two-Phase Flow," *Proceedings of Round Table Discussion RT-1-2 at the Fifth International Heat Transfer Conference, Tokyo, Japan, September 3-7, 1974*, also in *ASME Journal of Heat Transfer*, 3, 1974.
- 3.4-10. J. D. Ramshaw and J. A. Trapp, "Characteristics, Stability, and Short-Wavelength Phenomena in Two-Phase Flow Equation Systems," *Nuclear Science and Engineering*, 66, 1978, pp. 93-102.
- 3.4-11. N. Zuber, "On the Dispersed Two-Phase Flow in the Laminar Flow Regime," *Chemical Engineering Science*, 19, 1964, pp. 897-917.

- 3.4-12. N. Abuaf, O. C. Jones, Jr., and B. J. C. Wu, *Critical Flashing Flow in Nozzles with Subcooled Inlet Conditions*, BNL-NUREG-27512, 1980.
- 3.4-13. M. D. Alamgir and J. H. Lienhard, "Correlation of Pressure Undershoot During Hot Water Depressurization," *ASME Journal of Heat Transfer*, 103, 1981, pp. 52-73.
- 3.4-14. O. C. Jones, Jr., "Flashing Inception in Flowing Liquids," *ASME Journal of Heat Transfer*, 102, 1980, pp. 439-444.
- 3.4-15. J. W. Burnell, "Flow of Boiling Water through Nozzles, Orifices, and Pipes," *Engineering*, 1947, pp. 572-576.
- 3.4-16. F. J. Moody, "Maximum Flow Rate of a Single Component, Two-Phase Mixture," *Transactions of the American Society of Mechanical Engineers*, February 1965, pp. 136-143.
- 3.4-17. W. M. Bryce, *Improvements to the RELAP5/MOD1/014 LOCA Code: The RELAP5/MOD1/ WIN001 Code*, AEEW-R-1649, May 1983, pp. 64-65.
- 3.4-18. K. H. Ardron and W. M. Bryce, *Assessment of Horizontal Stratification Entrainment Model in RELAP5/MOD3*, AEEW-R 2345, April 1988.
- 3.4-19. W. M. Bryce, *Numerics and Implementation of the UK Horizontal Stratification Entrainment Off-Take Model into RELAP5/MOD3*, AEA-TRS-1050, AEEW-R 2501, March 1991.
- 3.4-20. J. A. Trapp and V. H. Ransom, *RELAP5 Hydrodynamic Model Progress Summary--Abrupt Area Changes and Parallel Branching*, PG-R-77-92, November 1977.
- 3.4-21. J. K. Vennard, *Elementary Fluid Mechanics*, 4th Edition, New York: John Wiley and Sons, 1965.
- 3.4-22. J. Weisman, T. Ake, and R. Knott, "Two-Phase Pressure Drop Across Abrupt Area Changes in Oscillatory Flow," *Nuclear Science and Engineering*, 61, 1976, pp. 297-309.
- 3.4-23. J. G. Collier, "Advanced Study Institute on Two-Phase Flows and Heat Transfer," *ASI Proceedings, Istanbul, Turkey, August 1976*.
- 3.4-24. M. M. El-Wakil, *Nuclear Heat Transport*, Scranton: International Textbook Company, 1971.
- 3.4-25. B. Harsch, A. Hussain, and J. Weisman, *Two-Phase Pressure Drop Across Restrictions and Other Abrupt Area Changes*, NUREG-0062, April 1976.
- 3.4-26. P. A. Lottes, "Expansion Losses in Two-Phase Flows," *Nuclear Science and Energy*, 9, 1961, pp. 26-31.
- 3.4-27. G. B. Wallis, *One-Dimensional Two-Phase Flow*, New York: McGraw-Hill Book Company, 1969, pp. 336-341.

- 3.4-28. A. Cicchitti et al., "Two-Phase Cooling Experiments-Pressure Drop, Heat Transfer, and Burnout Measurements," *Energi Nucl.*, 7, 1960, pp. 407-425.
- 3.4-29. D. R. Liles et al., *TRAC-PFI/MOD1: Correlations and Models*, NUREG/CR-5069, LA-11208-MS, December 1988.
- 3.4-30. J. H. Mahaffy and D. R. Liles, "Numerically Induced Pressure Excursions in Two-Phase Flow Calculations," *2nd International Topical Meeting on Nuclear Reactor Thermal Hydraulics, Santa Barbara, CA, January 11-14, 1983*.
- 3.4-31. V. H. Ransom et al., *RELAP5/MOD0 Code Description*, Volume 2, Code Development Update and Sample Problems, CDAP-TR-057, May 1979.
- 3.4-32. R. Riemke "Countercurrent Flow Limitation Model for RELAP5/MOD3," *Nuclear Technology*, 93, 1991, pp. 166-173.
- 3.4-33. S. G. Bankoff, R. S. Tankin, M. C. Yuen, and C. L. Hsieh, "Countercurrent Flow of Air/Water and Steam/Water Through a Horizontal Perforated Plate," *International Journal of Heat and Mass Transfer*, 14, 1981, pp. 1381-1385.
- 3.4-34. M. W. Cappiello, *A Description of the TRAC-PFI/MOD1 CCFL Model*, LA-UR-87-294, 1987.
- 3.4-35. C. L. Tien, K. S. Chung, and C. P. Liu, *Flooding in Two-Phase Countercurrent Flows*, EPRI NP-984, February 1979.
- 3.4-36. B. Aktas, *Improvements to the Two-Phase Water Level Modeling of a Transient Reactor Analysis Code*, MS Dissertation, Pennsylvania State University.
- 3.4-37. J. A. Borkowski, et al., *TRAC-BFI/MOD1 Models and Correlations*, NUREG/CR-4391, EGG-2680, 1992.
- 3.4-38. Y. K. Cheung, V. Parameswaran, and J. C. Shaug, *BWR Refill-Reflood Program Task 4.7 Model Development TRAC-BWR Component Models*, NUREG/CR-2574, EPRI NP-2376, GEAP-22052.
- 3.4-39. D. D. Taylor, *1-D Level Tracking Model*, IS-NSMD-83-011, April 1983.
- 3.4-40. A. Rosen et al., *Teploenergetika*, 1976, Vol. 11, p. 59
- 3.4-41. S. Z. Rouhani, *Modified Correlations for Void and Pressure Drop*, AB Atomenergi, Sweden, Internal Report No. AE-RTV 841, March 1969.
- 3.4-42. A. Harten, "End Schemes with Subcell Resolution," *Journal of Computational Physics*, 83, 1989, pp. 148-184.

3.4-43. K. W. Washington et al., *Reference Manual for the CONTAIN 1.1 Code for Containment Severe Accident Analysis*, NUREG/CR-5715, SAND91-0835, May 1991.

## 3.5 Component Models

RELAP5 consists of a variety of generic models that are used to build system models. These include the pipe, annulus, branch, single volume, single junction, etc., and will be discussed in more detail in Volume II of this manual. The general philosophy has been to avoid system component models such as steam generator and core. However, certain subsystem components are unavoidable due to unique processes or performance. RELAP5 contains models for subsystem components such as a branch, separator, jet mixer, pump, turbine, valve, accumulator, ECC mixer, and annulus. A brief summary of each of these models is included here.

### 3.5.1 Branch

The branch component is a model designed for convenient interconnection of hydrodynamic components. The identical result can be obtained by using a single-volume component and several single-junction components. Thus, the branch is a separate component only in the input processing scheme.

The crossflow junction has been added in which the junction velocities are assumed to be normal to the one-dimensional flow path of the hydrodynamic volume. Thus, the branch component can include multiple connections at the inlet, outlet, or in the crossflow direction.

Specialized modeling considerations are applied to any volume having multiple junctions connected at either volume end. (The ends of a hydrodynamic volume are the inlet and outlet, as defined in Section 3.1.1.)

These special calculations include both the method for calculating the volume average velocities and the method for partitioning the volume cross-sectional area between the multiple inlet or multiple outlet junctions. The partitioned volume areas are used both in the abrupt area change model, to calculate junction kinetic loss factors, and in the momentum equations, to simulate the stream-tube area.

In applications, the multiple junction and crossflow models are used in three distinct ways to model branching flows. These are a one-dimensional branch, a tee branch, and a crossflow branch. A combination of the three basic branches may also occur. Each of the three basic models will be discussed in turn.

**3.5.1.1 One-Dimensional Branch.** This basic branch model is consistent with the one-dimensional approximation for a piping network and assumes that multidimensional effects at branches are small compared to system interaction effects. In the case of branched flows that occur in headers or plena, the model gives an accurate physical description of the flow division or merging process; and the one-dimensional branch model is intended primarily for use in modeling such branched flows. Examples of such situations in LWR systems are flow division at the core inlet if parallel flow paths through the core are modeled, steam generator inlet and outlet plena when several parallel tube groups are modeled (for the effect of tube height and length), or at a wye connection.

The one-dimensional branch is illustrated in **Figure 3.5-1** for a volume having two inlet junctions and one outlet junction. The junctions  $J_1$  and  $J_2$  are the inlet junctions, and junction  $J_3$  is the outlet junction. The multiple flows are assumed to merge in such a way that they come to the common velocity equal to the inlet volume average velocity for volume  $V_1$ . The volume cross-sectional area is then divided in proportion to the volume flow of the respective inlet junctions. This method of apportioning volume

cross-sectional area satisfies continuity but does not conserve momentum, particularly for high velocity differences between the merging streams. (For flow splitting, however, the method does preserve momentum.) For this reason, the special jet mixer component was developed for merging flows having high relative velocities, such as in a jet pump. The jet mixer can be used for one-dimensional mixing but is limited to two inlet streams and a single outlet stream. (See Section 3.5.3 for a description of the jet mixer model.) The volume partitioned areas are calculated as follows:

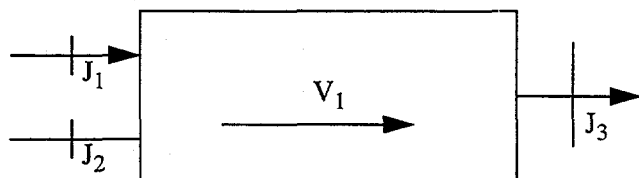


Figure 3.5-1 One-dimensional branch.

$$(A_K)_j = \frac{\left[ \sum_{i=J_1}^{J_N} \left[ (\dot{\alpha}_f)_i^n (v_f)_i^n + (\dot{\alpha}_g)_i^n (v_g)_i^n \right] A_i \right] A_j A_K}{\sum_{i=J_1}^{J_N} \left[ (\dot{\alpha}_f)_i^n (v_f)_i^n + (\dot{\alpha}_g)_i^n (v_g)_i^n \right] A_i} \quad (3.5-1)$$

The apportioned volume areas for each junction are used with the abrupt area change model, Section 3.4.3, to calculate energy loss coefficients for the liquid and vapor streams at each junction.

**3.5.1.2 Tee Branch.** The crossflow junction (see Section 3.4.5) is used to form a 90-degree tee, as shown in Figure 3.4-10. In this particular application, the side connection to the tee is modeled using a junction in which one-half of the junction momentum equation has the crossflow form. (The half of junction  $J_3$  associated with volume  $V_L$  is a crossflow junction and is designated by an X, see Figure 3.4-10.)

No special component is provided to accomplish the input associated with a model, such as illustrated in Figure 3.4-10. The volume,  $V_L$ , may be specified as a branch with the associated junctions or as a single volume with single junctions used to specify the connecting junctions. In either case, junctions  $J_1$  and  $J_2$  should be specified as smooth unless actual abrupt changes in area occur at either junction. Junction  $J_3$  should be specified as smooth with a user-specified form loss factor to account for the turning and entrance losses. In addition, junction  $J_3$  must be specified so that the half of the junction associated with volume  $V_L$  is modeled as a crossflow junction and the half associated with volume  $V_K$  is a normal junction. These options are specified through input of junction control flags.

It is also possible to model a 90-degree tee without using a crossflow junction; however, unphysical numerical results have been obtained at times for reasons that are not fully understood. Thus, the 90-degree tee model using the crossflow junction is recommended and is a closer approximation to the actual fluid momentum interaction that occurs at a tee.

In some branching situations where the throughflow is small or where the flow is constrained by the geometry, body force effects may be significant. Examples that occur in PWR systems are the cold leg connections to the inlet annulus and downcomer and the hot leg connection to the upper plenum and core. This type of branched flow is modeled as shown in **Figure 3.5-2**. Here the vertical direction is modeled as the throughflow direction (indicated by the volume orientation arrows). The cold or hot leg connections are modeled by crossflow junctions. The throughflow direction of volume  $V_3$  is chosen to correspond to the major flow path. In the case of a PWR inlet annulus, throughflow in the horizontal direction is inhibited by the annular structure; in the case of the upper-plenum-to-core connection, the area for flow in the vertical direction is large compared to the flow area in the horizontal direction. Some judgment is required to select the orientation. However, the crossflow branch connection will permit throughflow in the horizontal direction, but with some accompanying pressure rise and drop associated with the fact that the momentum flux terms can be neglected in the crossflow part of the junction.

The model illustrated in **Figure 3.5-2** has the additional advantage that the effect of vertical void gradients in the flow out of the horizontal connections may be more sharply defined as a result of the central volume,  $V_3$ , which has a vertical height equal to the diameter of branch volumes  $V_1$  and  $V_4$ .

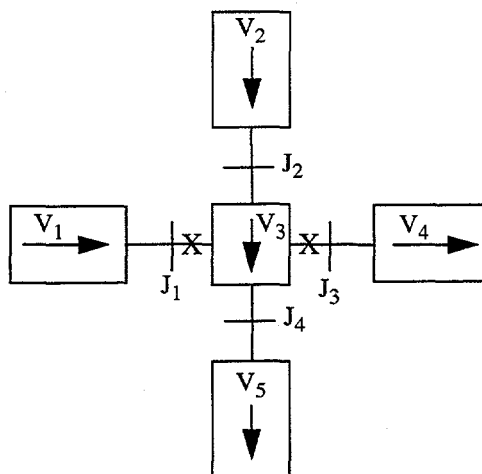


**Figure 3.5-2** Gravity effects on a tee.

No special component model is provided for modeling the vertical tee, and either a branch or a single volume may be used for volume  $V_3$ . The branch component is more convenient, since all junctions connecting to volume  $V_3$  can be specified with the branch component.

**3.5.1.3 Crossflow Branch.** A third type of branched flow path can be created by the use of a crossflow junction to couple two volumes. This type of branch is used to model crossflow between parallel core channels and leak paths between volumes having centers at the same vertical elevation. The application of the crossflow junction for crossflow or leak path modeling is illustrated in **Figure 3.4-9**. The default length scale associated with the crossflow junction is one half the diameter of the K volume plus one half the diameter of the L volume. This length is only used for modeling the fluid inertia terms in the momentum equation. The user has the option to input the length for a crossflow junction.

The pure crossflow branch is most easily modeled using a single-junction component for the crossflow junction. However, either volume  $V_1$  or  $V_2$  in **Figure 3.4-9** can be modeled using the branch component and specifying the coupling junctions with that component.

### 3.5.2 Separator

The separator component model has two options, the simple separator model which was implemented in previous versions of RELAP5 and a mechanistic separator model intended to model the centrifugal separators and chevron dryers in BWR reactors. The separator model determines the convected void fractions in the liquid fall back junction and the vapor outlet junction.

**3.5.2.1 Simple Separator.** The model is a nonmechanistic or black-box model consisting of a special volume with junction flows, as pictured in **Figure 3.5-3**. A steam-water inflowing mixture is separated by defining the quality of the outflow streams using empirical functions. No attempt is made to model the actual separation process from first principles.

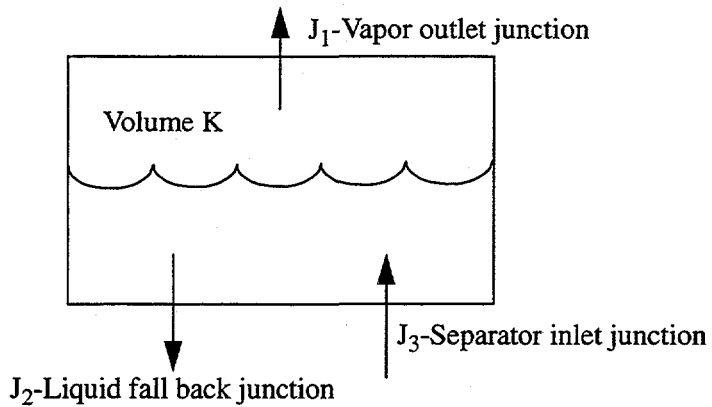


**Figure 3.5-3** Typical separator volume and junctions.

The separator vapor outlet performance is defined by means of a special function for the vapor void fraction at  $J_1$ . The donor junction vapor void fraction used to flux mass through the steam outlet is related to the vapor void fraction in the separator volume using the curve in **Figure 3.5-4**. For separator volume void fractions above the value of VOVER (an input parameter), a perfect separation is assumed and pure vapor is fluxed out junction  $J_1$ . For separator volume void fractions less than VOVER, a two-phase mixture is fluxed out. The VOVER parameter governs the vapor void fraction of the outflow. If VOVER is small, the vapor outflow corresponds to an ideal separator. If VOVER equals 1.0, the vapor outlet junction behaves as a normal junction; and the vapor outlet junction void fraction is equal to the separator volume average void fraction. A limit is placed on the vapor void fraction of the outflow, in that at most 90% of the vapor present in the separator volume can be fluxed out junction  $J_1$ . This limit is used to prevent over extraction of vapor.

The flow of the separator liquid drain junction is modeled in a manner similar to the steam outlet except that pure liquid outflow is assumed when the volume liquid void fraction is greater than the value of

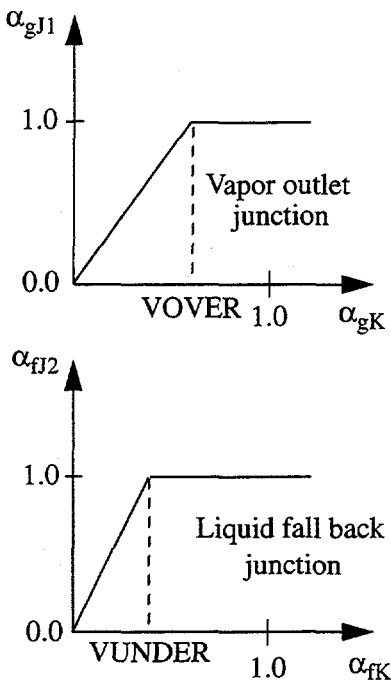


**Figure 3.5-4** Donor junction voids for outflow.

VUNDER (see **Figure 3.5-4**). As with the steam outlet, a 90% extraction limit is placed on the liquid drain. Normal donor fluxes are used for the separator inlet junction. Although the void fractions used to flux mass and energy from the separator volumes are modified, the normal junction momentum equations are used to calculate the flow velocities.

**3.5.2.2 Mechanistic Separator.** The mechanistic separator component model is intended to model the centrifugal separators and chevron dryers in BWR reactors. Like the simple separator, the mechanistic separator consists of a special volume with three junction flows, as pictured in **Figure 3.5-3**. A steam-water inflowing mixture is separated by defining the quality of the outflow streams using mechanistic models of the separating process in the separator and dryer components.

**3.5.2.2.1 Centrifugal Separator Model.** The model for the centrifugal separator was taken from the TRAC-BWR computer code and was developed by the General Electric Company as part of the joint USNRC-EPRI-General Electric Company sponsored BWR Refill-Reflood Program. Separators are made up of either two or three stages connected in series. The separator model determines the separating efficiency of a single stage, feeding the output of one stage to the input of the next stage. The primary measures of separator performance are carryover of entrained liquid in the steam leaving the separator, carryunder of steam in the liquid leaving the discharge passage of the separator, and the separator pressure drop. A mechanistic model has been developed to calculate the carryover, carryunder, and separator pressure drop. The separator component volume as shown in **Figure 3.5-3** represents the physical volume in the separator barrel and discharge passages. The inlet junction  $J_3$  represents the flow from the separator standpipe through the swirl vanes to the separator barrel. The vapor outlet junction  $J_1$  represents the flow out of the top of the separating barrel from the last separating stage and the liquid outlet junction  $J_2$

represents the combined discharge passages of all of the stages. The following description of the mechanistic separator model is adapted from Reference 3.5-1.

A separator component consists of three regions, a standpipe, the separator barrel, and the discharge passage. **Figure 3.5-5** shows a schematic of the first stage of a separator component. A two-phase mixture enters the separator barrel from the standpipe, passing through a set of stationary swirl vanes attached to the separator hub which acts as a bladed nozzle. These vanes produce a high rotational velocity component in the fluid flowing through the separator barrel. The resultant centrifugal force separates the steam-water mixture into a water vortex on the inner wall of the separating barrel and a steam vortex core. Separation is accomplished by directing the water layer on the wall into the discharge passage through pick-off rings at the exit of the separator barrel.

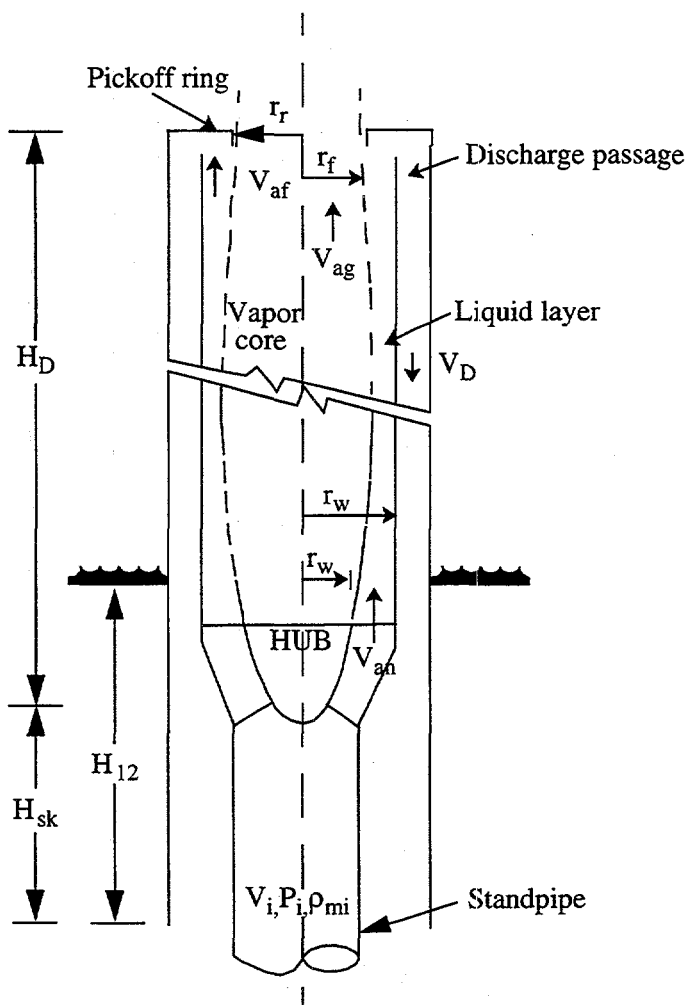


**Figure 3.5-5** Schematic of first stage of mechanistic separator.

**3.5.2.2.2 Assumptions and Model Equations**--In this model, the following assumptions are made for the axial location near the pick-off ring:

1. There is one uniform axial velocity in each of the flow regions, i.e.

$$0 \leq r \leq r_f : V_a = V_{ag} , \text{ uniform in vapor core} \quad (3.5-2)$$

$$r_f \leq r \leq r_w : V_a = V_{af} , \text{ uniform in water layer} \quad (3.5-3)$$

where  $r_f$  is the inner radius of the water layer.

2. The tangential velocity in each region is proportional to  $C$  which is related to the vortex strength, and is a function of  $r$  as follows:

$$0 \leq r \leq r_f : V_t = \frac{rC}{r_f^{3/2}} \quad (3.5-4)$$

$$r_f \leq r \leq r_w : V_t = \frac{C}{\sqrt{r}} \quad (3.5-5)$$

3. The void profiles are assumed as follows:

$$0 \leq r \leq r_f : \alpha = 1 - b \frac{r}{r_w} \quad (3.5-6)$$

$$r_f \leq r \leq r_w : \alpha = a \left( \frac{r_w}{r} - 1 \right) \quad (3.5-7)$$

and

$$a = AA \left( \frac{\sqrt{gr_w^2}}{C} \right)^{0.5} X_i^2 \quad \text{for } X_i < 0.15 \quad (3.5-8)$$

$$a = AA \left( \frac{\sqrt{gr_w^2}}{C} \right)^{0.5} (0.09335) X_i^{0.75}, \quad \text{for } X_i > 0.15 \quad (3.5-9)$$

$$b = BB \left( \frac{\sqrt{gr_w}}{C} \right)^{0.5} (1 - X_i)^3 \quad (3.5-10)$$

where  $X_i$  is the inlet flow quality, and AA and BB are parameters to be fitted with data

4. The pressure in the vapor core ( $P_o$ ) is assumed to be uniform radially and axially, and the pressure at the separator wall ( $P_w$ ) is related to  $P_o$  by centrifugal force across the water layer.

For the first stage of the separator, a total of six unknowns are introduced in this model. These are  $V_{ag}$ ,  $V_{af}$ ,  $C$ ,  $r_f$ ,  $P_o$ , and  $P_w$ . The required equations are formulated from conservation of water mass, vapor mass, axial momentum, and angular momentum entering and leaving the separating barrel, from centrifugal pressure drop across the water layer and from pressure drop in the discharge passage. The above unknowns can now be solved from given conditions of pressure,  $P_i$ , total flow rate,  $W_i$ , and flow quality at the swirl vane inlet,  $X_i$ .

The mass and momentum conservation equations for flows entering and leaving the separating barrel are:

#### Water mass

$$(1 - X_i) W_i = 2\pi \int (1 - \alpha) \rho_f V_a r dr = 2\pi V_{ag} \rho_f \left( \frac{1}{3} \frac{r_f b}{r_w} \right) r_f^2 + 2\pi \rho_f V_{af} \left[ \left( \frac{1 + a}{2} \right) (r_w^2 - r_f^2) - a (r_w - r_f) \right] \quad (3.5-11)$$

#### Vapor Mass

$$X_i W_i = 2\pi \int_0^{r_w} \alpha \rho_g V_g r dr = 2\pi \rho_g V_{ag} \left( \frac{1}{2} - \frac{1}{3} b \frac{r_f}{r_w} \right) r_f^2 + 2\pi \rho_g V_{af} a \frac{1}{2} (r_w - r_f)^2 \quad (3.5-12)$$

#### Angular Momentum

$$\int_{r_h}^{r_w} V_{tn} r (2\pi r \rho_{mi} V_{an}) dr = \int_0^{r_w} V_t r (2\pi r \rho V_a) dr + F_t r_w \quad (3.5-13)$$

#### Axial Momentum

$$\pi r_h^2 P_o = 2\pi \int_0^{r_w} (\rho_{mi} V_{an}^2 + P_n) r dr = 2\pi \int_0^{r_w} (\rho V_a^2 + P) r dr + F_a \quad (3.5-14)$$

Assuming that the flow through the swirl vane passages is homogeneous and that the swirl vane passages act as a nozzle, the pressure and velocity entering the separating barrel are related to the conditions in the standpipe as follows:

$$W_i = \rho_{mi} V_i A_i = \rho_{mi} V_{an} A_n \quad (3.5-15)$$

$$P_i + \frac{1}{2} \rho_{mi} V_i^2 = P_n + \frac{1}{2} \rho_{mi} (V_{an}^2 + V_{tn}^2) (1 + C_{NOZ}) \quad (3.5-16)$$

$$\frac{V_{an}}{V_{tn}} = \tan \theta \quad (3.5-17)$$

where  $\theta$  is the angle between the swirl vanes and the horizontal plane,  $\rho_{mi}$  is the inlet mixture density, and  $C_{NOZ}$  is the contraction loss coefficient defined as:

$$C_{NOZ} = 0.5 \left( 1 - \frac{A_n}{A_i} \right) \quad (3.5-18)$$

where  $A_n$  is the swirl vane flow area and  $A_i$  is the standpipe flow area.

$F_a$  and  $F_t$  in Equations (3.5-13) and (3.5-14) are the axial and tangential components of the frictional force on the swirling water layer,

$$F_a = F_f \left( \frac{V_{af}}{V_w} \right) \quad (3.5-19)$$

$$F_t = F_f \left( \frac{V_{tw}}{V_w} \right) \quad (3.5-20)$$

where  $V_{tw}$  is the tangential velocity on the wall,

$$V_{tw} = \frac{C}{\sqrt{r_w}} \quad (3.5-21)$$

and  $V_w$  is the resultant swirling velocity on the wall,

$$V_w = \sqrt{V_{tw}^2 + V_{af}^2} \quad (3.5-22)$$

$F_f$  is the resultant frictional force,

$$F_f = \frac{1}{2} \rho_f C_F V_w^2 (2\pi r_w) H_D \quad (3.5-23)$$

Assuming that the liquid film is thin with respect to the radius of curvature of the separator barrel, the flow can be considered to be film flow over a flat plate. For turbulent flow over a flat plate,

$$C_F = \frac{0.455}{(\log Re_L)^{2.58}} \quad (3.5-24)$$

where  $Re_L$  is defined as

$$Re_L = \frac{\rho V_w H_D V_w}{\mu} \quad (3.5-25)$$

The radial pressure drop across the water layer due to centrifugal force is

$$\int_{P_0}^{P_w} dP = \int_{r_f}^{r_w} \rho \frac{V_t^2}{r} dr \quad (3.5-26)$$

or

$$P_o = P_w - [\rho_f + a(\rho_f - \rho_g)] C^2 \left( \frac{1}{r_f} - \frac{1}{r_w} \right) + a(\rho_f - \rho_g) C^2 \left( \frac{r_w}{r_f r_r} - \frac{1}{r_w} \right) \quad (3.5-27)$$

The pressure drop in the discharge passage is

$$\int_{r_f}^{r_w} \left( \frac{1}{2} \rho V_a^2 + P \right) dA / \int_{r_f}^{r_w} dA = \frac{1}{2} \rho_{M,D} V_D^2 \left[ 1 + 2C_F \left( \frac{H_D}{D_D} + EFLD \right) + C_K \right] + (P_o + \rho_f g H_{12} - \rho_D g (H_D + H_{sk})) \quad (3.5-28)$$

where  $\rho_{M,D}$  and  $V_D$  are the mixture density and velocity in the discharge passage,  $H_D$  and  $D_D$  are the length of the separator barrel and hydraulic diameter of the discharge passage,  $EFFLD$  is the effective L/D coefficient at the pick-off ring,  $C_K$  is the total loss coefficient in the discharge passage,  $H_{12}$  is the height of the liquid pool surrounding the separator relative to the bottom of the discharge passage, and  $H_{sk}$  is the axial distance between the separator hub and the bottom of the discharge passage.

For the discharge passage,

$$C_F = \frac{0.079}{Re^{0.25}} . \quad (3.5-29)$$

The steam and water flows discharged through the discharge passage are calculated as follows:

$$W_{g, cu} = 2\pi \int_{r_f}^{r_w} \alpha \rho_g V_a r dr \quad (3.5-30)$$

$$W_{f, cu} = \int_{r_f}^{r_w} (1 - \alpha) \rho_f V_a r dr .$$

For a water layer thicker than the gap between the pick-off ring and the separator barrel, i.e.,  $r_f < r_r$ , the steam and water flows through the discharge passage are

$$W_{g, cu} = \pi \rho_g V_{af} a (r_w - r_f)^2 \quad (3.5-31)$$

$$W_{f, cu} = \pi \rho_f V_{af} [(r_w^2 - r_f^2) - a (r_w - r_f)^2] .$$

For a water layer thinner than the gap between the pick-off ring and the separator barrel wall, i.e.,  $r_f < r_r$ , the liquid and vapor flow rates in the discharge passage are

$$W_{g, cu} = X_i W_i - 2\pi \rho_g V_{ag} \left( \frac{1}{2} - \frac{1}{3} b \frac{r_r}{r_w} \right) r_r^2 \quad (3.5-32)$$

$$W_{f, cu} = (1 - X_i) W_i - 2\pi \rho_f V_{ag} r_r^2 \left( \frac{1}{2} \right) b \frac{r_r}{r_w} .$$

The steam and water flows leaving the present stage and entering the next stage are

$$W_{g, co} = (\text{steam flow})_{in} - W_{g, cu} \quad (3.5-33)$$

$$W_{f, co} = (\text{water flow})_{in} - W_{f, cu} .$$

The total discharge flow is

$$W_D = W_{g,cu} + W_{f,cu} \quad (3.5-34)$$

Assuming homogeneous flow in the discharge passage, the mean void fraction is

$$\alpha_{cu} = \frac{W_{g,cu}}{W_{g,cu} + W_{f,cu}} \frac{\rho_g}{\rho_f}, \quad (3.5-35)$$

the mixture density in the discharge passage is

$$\rho_{M,D} = \alpha_{cu}\rho_g + (1 - \alpha_{cu})\rho_f \quad (3.5-36)$$

and the velocity in the discharge passage is

$$V_D = \frac{W_D}{\rho_{M,D} A_D} \quad (3.5-37)$$

In summary, for given swirl vane inlet conditions,  $P_i$ ,  $X_i$ , and  $W_i$ , the unknowns  $V_{ag}$ ,  $V_{af}$ ,  $C$ ,  $r_f$ ,  $P_o$ , and  $P_w$  are calculated by solving Equations (3.5-11) to (3.5-28) simultaneously.

Similar equations can be written for the second and third stages. Since it is assumed that  $P_o$  is uniform axially, i.e., the vapor core pressure drop in the axial direction is small, the axial momentum equation can be neglected in the solution for the upper stages. For these stages, the unknowns are reduced to  $V_{ag}$ ,  $V_{af}$ ,  $C$ ,  $r_f$ , and  $P_w$ , and the equations are the conservation of water mass, vapor mass, angular momentum, the pressure drop across the water layer, and the pressure drop in the discharge passage.

The right hand sides of Equations (3.5-11), (3.5-12), and (3.5-13) represent the water flow, vapor flow, and angular momentum entering the separator barrel. For the second and third stages, these terms are modified as follows:

$$\begin{aligned} (\text{Water flow})_{in} &= (W_{f,co})_{\text{previous stage}} \\ (\text{Steam flow})_{in} &= (W_{g,co})_{\text{previous stage}} \\ (\text{Angular momentum})_{in} &= \left[ \int_{r_o}^{r_f} V_t r (2\pi \rho V_a) r dr \right]_{\text{previous stage}} \end{aligned} \quad (3.5-38)$$

**3.5.2.2.3 Carryover and Carryunder.** The total vapor flow that is carried under consists of two parts; i.e., the steam flow through the first discharge passage which discharges its fluid below the liquid

level and the steam entrained by the water discharged from higher stages. The exits of the discharge passages of the higher stages are located above the liquid level. It is assumed that the entrainment is proportional to the square of the total water flow discharged from the higher stages, i.e.,

$$(W_{g,cu})_{\text{total}} = (W_{g,cu})_1 + CC \left( \sum_{i=2}^N (W_{g,cu})_i \right) \quad (3.5-39)$$

where

$$\begin{aligned} N &= 2 \text{ for a two-stage separator, and} \\ &= 3 \text{ for a three-stage separator} \end{aligned}$$

and CC is a constant to be fitted with data.

The total water that is carried over consists of two parts, the water flow through the last stage and the water flow entrained by the steam discharged from the higher stages through their discharge passages. Similarly, the second part is assumed to be proportional to the square of the total steam flow discharged from the higher stages, i.e.,

$$(W_{f,co})_{\text{total}} = (W_{f,co})_N + DD \left( \sum_{i=2}^N (W_{g,cu})_i \right) \quad (3.5-40)$$

where DD is a constant to be fitted with data.

The carryunder and carryover are defined as

$$\begin{aligned} CU &= \frac{(W_{g,cu})_{\text{total}}}{\text{Total downward water flow}} \\ CO &= \frac{(W_{f,co})_{\text{total}}}{\text{Total upward steam flow}} \end{aligned} \quad (3.5-41)$$

The parameters AA, BB, CC, and DD were tuned to fit the available test data<sup>3.5-2,3.5-3,3.5-4</sup> for two- and three-stage separators. **Table 3.5-1** summarizes the values for these parameters.

**Table 3.5-1** Summary of fitted parameters in a mechanistic separator model.

Parameter	2-Stage Separator		3-Stage Separator		
	1 <sup>st</sup> Stage	2 <sup>nd</sup> Stage	1 <sup>st</sup> Stage	2 <sup>nd</sup> Stage	3 <sup>rd</sup> Stage
AA	110.	20.	110.	20.	20.

**Table 3.5-1** Summary of fitted parameters in a mechanistic separator model. (Continued)

Parameter	2-Stage Separator		3-Stage Separator		
	1 <sup>st</sup> Stage	2 <sup>nd</sup> Stage	1 <sup>st</sup> Stage	2 <sup>nd</sup> Stage	3 <sup>rd</sup> Stage
BB	0.5	0.25	0.5	0.25	0.55
CC	0.0004	---	0.0004	---	---
DD	0.009	---	0.11	---	---

**3.5.2.2.4 Chevron Dryer Model.** The steam dryer uses chevron vanes to remove the moisture which is discharged from the steam separators. The vanes provide a curved path which the liquid droplets must follow if they are to flow through the dryer. If the interfacial force is too low, it cannot drag the liquid droplets along the curved path due to their inertial and they hit the vanes, are de-entrained, and the resultant liquid film flows down the vanes under the force of gravity into collecting trays and then back to the liquid pool surrounding the separators. If the vapor velocity is high, it exerts a larger interfacial force on the droplets and more of the entrained liquid gets through the dryer vanes. Thus the dryer efficiency depends on the steam velocity and the moisture content of the steam flow entering the dryer. For a given steam inlet velocity, there is a critical dryer inlet moisture. Good moisture separation is achieved if the inlet moisture is lower than the critical value. If the inlet moisture is above the critical value, the dryer separating capacity is exceeded and the moisture can pass through the dryer.

The dryer capacity is simulated by a capacity factor GDRY which is defined in the following way. For a given steam velocity V at the inlet to the dryer, the critical dryer inlet moisture CDIM is calculated as

$$\begin{aligned}
 \text{CDIM} &= 1; \quad V < \text{VDRY1} \\
 \text{CDIM} &= 1 - \frac{V - \text{VDRY1}}{\text{VDRY2} - \text{VDRY1}}; \quad \text{VDRY1} < V < \text{VDRY2} \\
 \text{CDIM} &= 0.; \quad \text{VDRY2} < V
 \end{aligned} \tag{3.5-42}$$

where CDIM is the critical inlet moisture, VDRY1 is the vapor velocity below which any amount of moisture is assumed to be separated from the vapor stream, and VDRY2 is the vapor velocity above which no amount of moisture, however small, can be separated from the vapor stream. (3.5-43)

The dryer inlet moisture (DIM) is computed assuming homogeneous flow as

$$\text{DIM} = 1 - \frac{\alpha_g}{\alpha_g + (1 - \alpha_g) \frac{\rho_f}{\rho_g}} \tag{3.5-44}$$

where  $\alpha_g$ ,  $\rho_f$ , and  $\rho_g$  are the vapor void fraction, liquid density, and the vapor density in the dryer.

The capacity factor GDRY is defined as

$$\begin{aligned}
 \text{GDRY} &= 1.; \quad \text{DIM} < \text{CDIM} \\
 \text{GDRY} &= 1. + \frac{\text{CDIM} - \text{DIM}}{\text{DELDIM}}; \quad \text{CDIM} < \text{DIM} < (\text{CDIM} + \text{DELDIM}) \\
 \text{GDRY} &= 0.; \quad (\text{CDIM} + \text{DELDIM}) < \text{DIM}
 \end{aligned} \tag{3.5-45}$$

where DELDIM is the range of inlet moisture over which the dryer capacity goes from one to zero for a fixed vapor inlet velocity. These relations are shown schematically in **Figure 3.5-6**.

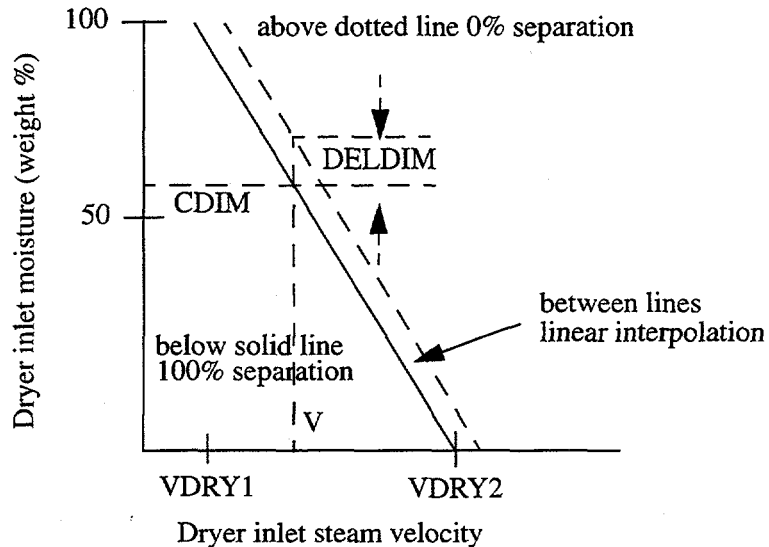


**Figure 3.5-6** Dryer capacity.

The capacity factor GDRY is used to modify the void fraction in the dryer outlet junction such that if the dryer capacity is one, the donor void fraction is one; if the dryer capacity is zero, the regular donor void fraction is used, and if the dryer capacity is between zero and one, the void fraction is interpolated between the values for the capacities of zero and one.

### 3.5.3 Jet Mixer

There are several components in a typical reactor plant where the momentum effects due to the mixing of two parallel streams of fluid at different velocities may be important. An example of this is the jet pump in a BWR. In this component, the pumping action is caused by the momentum transfer between the two fluid streams. Momentum effects may also be important for mixing at ECC injection points or for the aspirators present in some steam generators. The JETMIXER component was developed for these cases.

**3.5.3.1 Basic Jet Mixing Model.** The basic approach for modeling the jet mixing process is to superimpose a quasi-steady model for the mixing process on the normal volume-junction flow path representation used in RELAPS. To derive the momentum equations needed to model a jet mixing situation, consider the schematic shown in **Figure 3.5-7**, which illustrates a mixing volume connected to a

drive and a suction volume.<sup>a</sup> The suction junction (with velocity  $v_S$  and area  $A_S$ ) connects the last upstream suction region volume,  $K_S$ , to the mixing volume,  $L$ . The drive junction (with velocity  $v_D$  and area  $A_D$ ) connects the last upstream drive line volume,  $K_D$ , to the mixing volume,  $L$ . Figure 3.5-7 shows the drive junction as a smooth junction and the suction junction as abrupt. The user can model either junction either way if the appropriate loss factors are included (see input guidelines in Volume II of this manual). Void fractions and densities subscripted by a D or S are denoted values; a subscript a indicates an average value.

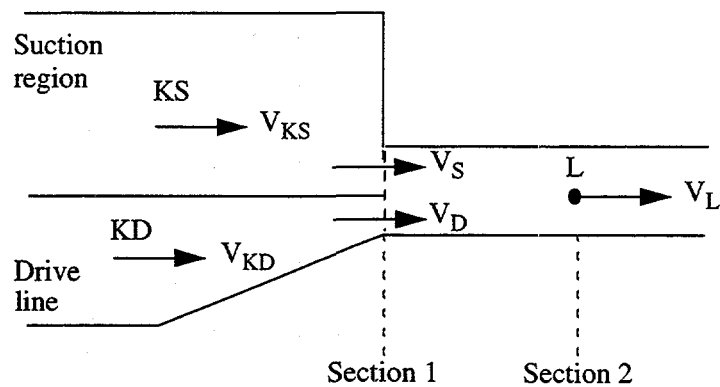


Figure 3.5-7 Schematic of mixing junctions.

The mixing of the drive and suction flows between cross section 1 and 2 requires a reevaluation of the momentum flux terms. The wall drag, interphase drag, temporal acceleration, momentum exchange due to mass transfer, and gravity head terms for the drive and suction junctions are treated exactly as they are at any other junction. Only the pressure and momentum flux terms will be examined in the following momentum equation development.

Consider a control volume in the mixing region between cross sections 1 and 2 and assume the following: (a) steady single-phase flow; (b) one-dimensional flow at cross sections 1 and 2; (c) equal pressures at junctions D and S; and (d) constant area in the mixing region. If we apply the conservation of momentum principle for this control volume with these assumptions, the momentum equation becomes

$$(P_L - P_1) A_L + \rho_L v_L^2 A_L - \rho_S v_S^2 A_S - \rho_D v_D^2 A_D = 0 \quad (3.5-46)$$

Conservation of mass applied with these same assumptions gives

$$\rho_L v_L A_L - \rho_S v_S A_S - \rho_D v_D A_D = 0 \quad (3.5-47)$$

a. The drive and suction junctions should be the high-speed and low-speed junctions respectively when the JETMIXER component is used for other than jet pump applications.

Equation (3.5-47) can be used to write Equation (3.5-46) in an expanded form, obtaining

$$(P_L - P_1) + \rho_S v_S A_S (v_L - v_S) / A_L + \rho_D v_D A_D (v_L - v_D) / A = 0 . \quad (3.5-48)$$

Equation (3.5-48) gives the momentum equation (pressure and flux terms) for the upstream half of the mixing volume. To develop the momentum equation for the suction junction, a normal RELAP5 half-cell momentum equation is written from KS to cross section 1, i.e.,

$$(P_1 - P_{KS}) + 1/2 \rho_{KS} (v_S^2 - v_{KS}^2) = 0 . \quad (3.5-49)$$

Adding this to the half cell momentum Equation (3.5-48) for cross sections 1 to L (Section 2) gives

$$P_L - P_{KS} + 1/2 \rho_{KS} (v_S^2 - v_{KS}^2) + \rho_S v_S A_S (v_L - v_S) / A_L + \rho_D v_D A_D (v_L - v_D) / A_L = 0 . \quad (3.5-50)$$

This equation shows how the pressure and momentum flux terms should be calculated for the suction junction equation.

If the suction junction were a normal junction, its momentum equation (pressure and flux terms) would be

$$(P_L - P_{KS}) + 1/2 \rho_S (v_L^2 - v_{KS}^2) = 0 . \quad (3.5-51)$$

The velocity terms in Equation (3.5-51) must be replaced by the velocity terms in Equation (3.5-50) to correctly model the momentum equation at the suction junction. Similar equations for the drive junction can be obtained.

**3.5.3.2 Jet Mixing in Two-Phase Flows.** If a derivation similar to the previous section is carried out for the pressure and momentum flux terms in the two-phase case, the following equations are obtained for the liquid phase in the mixing region:

Conservation of momentum (from cross-section 1 to L),

$$\alpha_{fL} A_L (P_L - P_1) + \alpha_{fL} \rho_{fL} v_{fL}^2 A_L - \alpha_{fs} \rho_{fs} v_{fs}^2 A_S - \alpha_{fd} \rho_{fd} v_{fd}^2 A_D = 0 . \quad (3.5-52)$$

Conservation of mass (from cross section 1 to L),

$$\alpha_{fL} \rho_L v_{fL} A_L - \alpha_{fs} \rho_{fs} v_{fs} A_{fS} - \alpha_{fd} \rho_{fd} v_{fd} A_D = 0 . \quad (3.5-53)$$

Using Equation (3.5-53) in Equation (3.5-52) and rewriting Equation (3.5-46) in expanded form yields

$$\alpha_{fL}(P_L - P_1) + \alpha_{fs}\rho_{fs}v_{fs}A_S(v_{fL} - v_{fs})/A_L + \alpha_{fD}\rho_{fD}v_{fD}A_D(v_{fL} - v_{fD})/A_L = 0 \quad (3.5-54)$$

Equation (3.5-54) can now be combined with the appropriate half-cell momentum equation for the upstream volume to obtain the final momentum equation for the liquid flow at the suction junction. A parallel development gives the gas-phase momentum equation at the suction junction.

The momentum equations used consist of the sum of the phasic momentum equations and the difference of the phasic momentum equations. To derive the sum momentum equation (pressure and flux terms only) for the suction junction, Equation (3.5-54) for the liquid phase is added to a similar equation for the gas phase to obtain

$$(P_L - P_1) + \alpha_{fs}\rho_{fs}v_{fs}A_S(v_{fL} - v_{fs})/A_L + \alpha_{fD}\rho_{fD}v_{fD}A_D(v_{fL} - v_{fD})/A_L + \alpha_{gs}\rho_{gs}v_{gs}A_S(v_{gL} - v_{gs})/A_L + \alpha_{gD}\rho_{gD}v_{gD}A_D(v_{gL} - v_{gD})/A_L = 0 \quad (3.5-55)$$

The normal half-cell sum momentum equation (pressure and flux terms only) for the upstream suction volume can then be added to Equation (3.5-55) to give

$$(P_L - P_{KS}) + \alpha_{fs}\rho_{fs}v_{fs}A_S(v_{fL} - v_{fs})/A_L + \alpha_{fD}\rho_{fD}v_{fD}A_D(v_{fL} - v_{fD})/A_L + \alpha_{gs}\rho_{gs}v_{gs}A_S(v_{gL} - v_{gs})/A_L + \alpha_{gD}\rho_{gD}v_{gD}A_D(v_{gL} - v_{gD})/A_L + 1/2\alpha_{fKS}\rho_{fKS}(v_{fs}^2 - v_{fKS}^2) + 1/2\alpha_{gKS}\rho_{gKS}(v_{gs}^2 - v_{gKS}^2) = 0 \quad (3.5-56)$$

as the final form for the pressure and momentum flux terms in the new sum momentum equation for the suction junction. The pressure term in this equation has exactly the same form as the pressure term in the normal sum momentum equation. A parallel equation holds for the drive junction. Hence, at the drive and suction mixing junctions, the normal momentum flux terms in the sum momentum equation must be replaced by those in Equation (3.5-56).

The difference momentum equation for the suction junction is derived by dividing the liquid momentum mixing Equation (3.5-54) by  $\alpha_{fL}$  and adding it to the half-cell liquid momentum equation for the upstream suction volume (also divided by the appropriate void fraction,  $\alpha_{fKS}$ ) to obtain

$$(P_L - P_{KS}) + \alpha_{fs}\rho_{fs}v_{fs}A_S(v_{fL} - v_{fs})/\alpha_{fL}A_L + \alpha_{fD}\rho_{fD}v_{fD}A_D(v_{fL} - v_{fD})/\alpha_{fL}A_L + 1/2\rho_{fKS}(v_{fs}^2 - v_{fKS}^2) = 0 \quad (3.5-57)$$

Next, Equation (3.5-57) is divided by the average junction liquid density,  $\rho_{fa}$ , and subtracted from the corresponding gas equation to obtain

$$\begin{aligned}
 & \left( \frac{\rho_f - \rho_g}{\rho_f \rho_g} \right)_a (P_L - P_{KS}) + \alpha_{gS} \rho_{gS} v_{gS} A_S (v_{gL} - v_{gS}) / \alpha_{gL} \rho_{ga} A_L \\
 & + \alpha_{gD} \rho_{gD} v_{gD} A_D (v_{gL} - v_{gD}) / \alpha_{gL} \rho_{ga} A_L + \frac{1}{2} \rho_{gKS} (v_{gS}^2 - v_{gKS}^2) \rho_{ga} \\
 & - \alpha_{fS} \rho_{fS} v_{fS} A_S (v_{fL} - v_{fS}) / \alpha_{fL} \rho_{fa} A_L - \alpha_{fD} \rho_{fD} v_{fD} A_D (v_{fL} - v_{fD}) / \alpha_{fL} \rho_{fa} A_L \\
 & - \frac{1}{2} \rho_{fKS} (v_{fS}^2 - v_{fKS}^2) / \rho_{fa} = 0
 \end{aligned} \tag{3.5-58}$$

as the final difference momentum equation to be used at Junction S. A parallel equation must be used at the drive junction. The pressure term in Equation (3.5-58) has exactly the same form as the pressure term in the normal difference momentum equation. Hence, at the drive and suction mixing junctions the normal momentum flux terms in the difference momentum equation must be replaced by those in Equation (3.5-58).

**3.5.3.3 Associated Flow Losses.** The flow in the *mixing* region of volume L can in reality be either a true jet mixing or a flow split (for reverse flow). The flow split case is governed by different physics than the jet-mixing case considered in the previous discussions. The redistribution that occurs when the flow splits is primarily determined by the effective resistances downstream of the separation point in the suction and drive flow paths. The mixing terms derived above do not apply. For this reason, the additional mixing terms are applied only for the positive-drive flow regimes. The normal momentum flux calculations are used for the negative-drive flow regimes.

The junctions associated with the JETMIXER component can be modeled as smooth or abrupt. If the junctions are input as smooth, then the appropriate flow resistances should be calculated in a standard fashion and input as form loss coefficients at the appropriate junctions by the user.

If the junctions in the JETMIXER component are input as abrupt area changes, then the code will calculate form loss coefficients as usual except that (a) the forward loss coefficients at the drive and suction junctions are set to zero and (b) the reverse loss coefficients for the suction and drive junctions are those associated with the expansions from the junction areas to the suction or drive volume areas. The forward losses at these junctions are actually associated with the expansion from the *vena-contracta* to the downstream mixing volume flow area. For parallel mixing streams, this loss is no longer appropriate. The losses associated with any contraction from the mixing volume to the suction or drive junctions are neglected for the same reason.

If the above normal flow losses are used when the suction flow reverses, it will be found that jet pump performance (head ratio) in this regime is significantly below the experimental data. The reverse flow loss coefficient applied in the suction junction has a significant effect on the jet pump performance in this flow situation. This loss coefficient (in addition to the normal loss coefficient associated with the expansion from  $A_S$  to area  $A_{KS}$ ) represents all the irreversible losses associated with the turning and expansion of the flow from the drive junction. Because this flow regime is an important regime in the accident analysis of a BWR, it was decided to include an approximation for this flow-dependent loss in the jet mixing model.

This reverse suction flow loss was based upon the expansion losses experienced by the flow as it moves from the drive to the suction junction. Two flow situations with reversed suction flow and positive

drive flow are possible, depending upon the flow direction in the mixing section (Figure 3.5-8). In the first situation, the expansion loss associated with the area change  $A_D$  to  $A_S$ , i.e.,

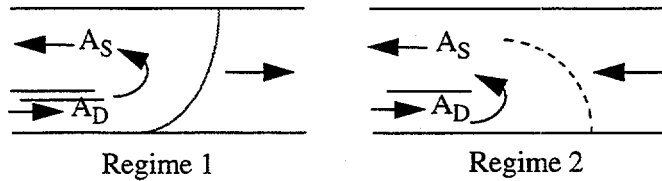


Figure 3.5-8 Flow regimes and dividing streamline.

$$K = (A_S/A_D - 1)^2 \quad (3.5-59)$$

is added to the user-specified reverse loss coefficient (or the standard abrupt area change loss factor if the junction is input as abrupt) for the suction junction. In the second situation, the effective area for the suction flow that comes from the drive junction is less than  $A_S$  because the discharge flow is reversed. In this situation, the effective areas for the expansion loss are  $A_D$  and  $A_S|W_D/W_S|$ . Hence, for the second situation, the loss coefficient

$$K + \left( \frac{A_S|W_D/W_S|}{A_D} - 1 \right)^2 \quad (3.5-60)$$

is added to the user-specified reverse loss coefficient (or the abrupt area loss factor if the junction is input as abrupt) at the suction junction only if  $A_S|W_D/W_S|$  is  $> A_D$ . If  $A_S|W_D/W_S|$  is  $< A_D$ , the drive-to-suction flow is effectively a contraction, and the additional loss coefficient is set to zero.

Since the jet mixing and effective resistances are modeled by special terms in the suction and drive junction momentum equations, the normal losses associated with the partitioning of volume  $L$  are not included in these junction equations. However, the normal losses associated with the area ratios experienced by the flow upstream of the suction and drive junctions are retained in the junction momentum equations.

**3.5.3.4 Numerical Implementation.** The basic numerical algorithm used to evaluate the new momentum flux terms in Equations (3.5-56) and (3.5-58) is similar to the numerical evaluation of the normal momentum flux terms. The normal momentum flux terms are calculated explicitly at the  $n$ -th time level. The new momentum flux terms in Equations (3.5-56) and (3.5-58) are also explicitly evaluated, and the spatial location of each variable is indicated by its subscript.

### 3.5.4 Pump

The RELAP5/MOD3 pump model is almost identical to the RELAP5/MOD1 pump model,<sup>3.5-5</sup> which was originally adapted from the RELAP4 pump model.<sup>3.5-6</sup> The only significant difference is that in RELAP5/MOD3, there is the added capability of linking the pump to a shaft component. The pump can be linked to a shaft component, and thus can be driven by either a motor or a turbine. The RELAP5/MOD1 options for a motor-driven pump were retained so that input changes to an existing plant model using the pump are not required unless it is desired to make use of the shaft coupling.

The basic approach to pump modeling is to superimpose a quasi-static model for pump performance on the RELAP5 volume-junction flow path representation. The pump is a volume-oriented component, and the head developed by the pump is apportioned equally between the suction and discharge junctions that connect the pump volume to the system. The pump model is interfaced with the two-fluid hydrodynamic model by assuming the head developed by the pump is similar to a body force. Thus, the head term appears in the mixture momentum equation; but, like the gravity body force, it does not appear in the difference momentum equation used in RELAP5. The term that is added to the mixture momentum equation is  $1/2 \rho g H$ , where  $H$  is the total head rise of the pump (m),  $\rho$  is the volume fluid density ( $\text{kg/m}^3$ ), and  $g$  is the acceleration due to gravity ( $\text{m/s}^2$ ). The factor  $1/2$  is needed because the term is applied at both the suction and discharge junctions.

In both the semi-implicit and nearly-implicit numerical schemes, the pump head is coupled implicitly to the velocities through its dependence on the volumetric flow rate,  $Q$ . The volumetric flow rate is defined as the volume mass flow rate divided by the volume density. It is assumed that the head depends on the volumetric flow rate, and can be approximated by a two-term Taylor series expansion,

$$H^{n+1} = H^n + \left( \frac{dH}{dQ} \right)^n (Q^{n+1} - Q^n) . \quad (3.5-61)$$

Thus, the numerical equivalent of the term  $\rho g H$  in both schemes is

$$\frac{1}{2} \rho^n g H^n \Delta t + \frac{1}{2} \rho^n g \left( \frac{dH}{dQ} \right)^n (Q^{n+1} - Q^n) \Delta t . \quad (3.5-62)$$

This term is added to the right side of the mixture momentum Equation (3.1-103). For the semi-implicit scheme, only one of the junction velocities is made implicit (the junction for which the new time velocity is calculated). For the nearly-implicit scheme, both junction velocities are made implicit simultaneously.

The pump dissipation is calculated for the pump volume as

$$\tau \omega - gH (\alpha_f \rho_f v_f + \alpha_g \rho_g v_g) A \quad (3.5-63)$$

where  $\tau$  is the pump torque and  $\omega$  is the pump angular rotation speed.

This term is evaluated explicitly in both the semi-implicit and nearly-implicit schemes, and it is partitioned between the liquid and vapor thermal energy equations in such a way that the rise in temperature due to dissipation is equal in each phase. (The details of the dissipation mechanism in a two-phase system are unknown, so the assumption is made that the mechanism acts in such a way that thermal equilibrium between the phases is maintained without phase change.) Thus, the terms that are added to the right sides of the liquid and vapor thermal energy equations, Equations (3.1-90) and (3.1-91), are

$$\frac{[\tau^n \omega^n - g H^n (\alpha_f^n \rho_f^n \bar{v}_f^n + \alpha_g^n \rho_g^n \bar{v}_g^n) A] \Delta t (\alpha_f^n \rho_f^n C_{pf}^n)}{(\alpha_f^n \rho_f^n C_{pf}^n + \alpha_g^n \rho_g^n C_{pg}^n)} \quad (3.5-64)$$

and

$$\frac{[\tau^n \omega^n - g H^n (\alpha_f^n \rho_f^n \bar{v}_f^n + \alpha_g^n \rho_g^n \bar{v}_g^n) A] \Delta t (\alpha_g^n \rho_g^n C_{pg}^n)}{(\alpha_f^n \rho_f^n C_{pf}^n + \alpha_g^n \rho_g^n C_{pg}^n)} \quad (3.5-65)$$

respectively.

The pump head,  $H$ , and torque,  $\tau$ , are defined by means of an empirical homologous pump performance model, and the pump speed,  $\omega$ , is defined by a pump drive model. The derivative of the pump head with respect to the volumetric flow rate,  $dH/dQ$ , is obtained from the empirical steady-state homologous pump performance model, using the assumption that the pump speed is constant.

**3.5.4.1 Centrifugal Pump Performance Model.** The basic pump performance data must be generated experimentally. Analytical programs have been developed that are reasonably successful in predicting near-design pump performance for single-phase fluids. However, for off-design operation or for operation with a two-phase fluid, the problems of analytical pump performance prediction are nearly insurmountable. The basic parameters that characterize the pump performance are the rotational speed,  $\omega$  or  $N$ , the volumetric flow,  $Q$ , the head rise,  $H$ , and the shaft torque,  $\tau$ . The relationship between these four parameters can be uniquely displayed by a four-quadrant representation of such data. A typical four-quadrant curve is shown in **Figure 3.5-9**. Both positive and negative values for each of the four parameters are represented. The disadvantages in using such a data map for numerical purposes are the need for two-dimensional interpolation, the large number of points needed to define the entire range, and the fact that the map is infinite in extent. These objections can be largely overcome by use of a homologous transformation based on the centrifugal pump similarity relationships. Such a transformation collapses the four-quadrant data onto a single, bounded, dimensionless curve having eight octants. Typical homologous curves for the head and torque are illustrated in **Figure 3.5-10** and **Figure 3.5-11**, respectively, where  $\omega_R$ ,  $Q_R$ ,  $H_R$ , and  $\tau_R$  are the rated values for the pump speed, volumetric flow rate, head, and torque, respectively. Details on generating the homologous curves are presented in Volumes II and IV. The homologous transformation is not unique, and not all points of **Figure 3.5-9** lie on the curves of **Figure 3.5-10** and **Figure 3.5-11**. However, the data are closely grouped, and the single curve is a good approximation for pump performance. The pump model allows the user the option of accounting for two-phase degradation effects on pump performance.

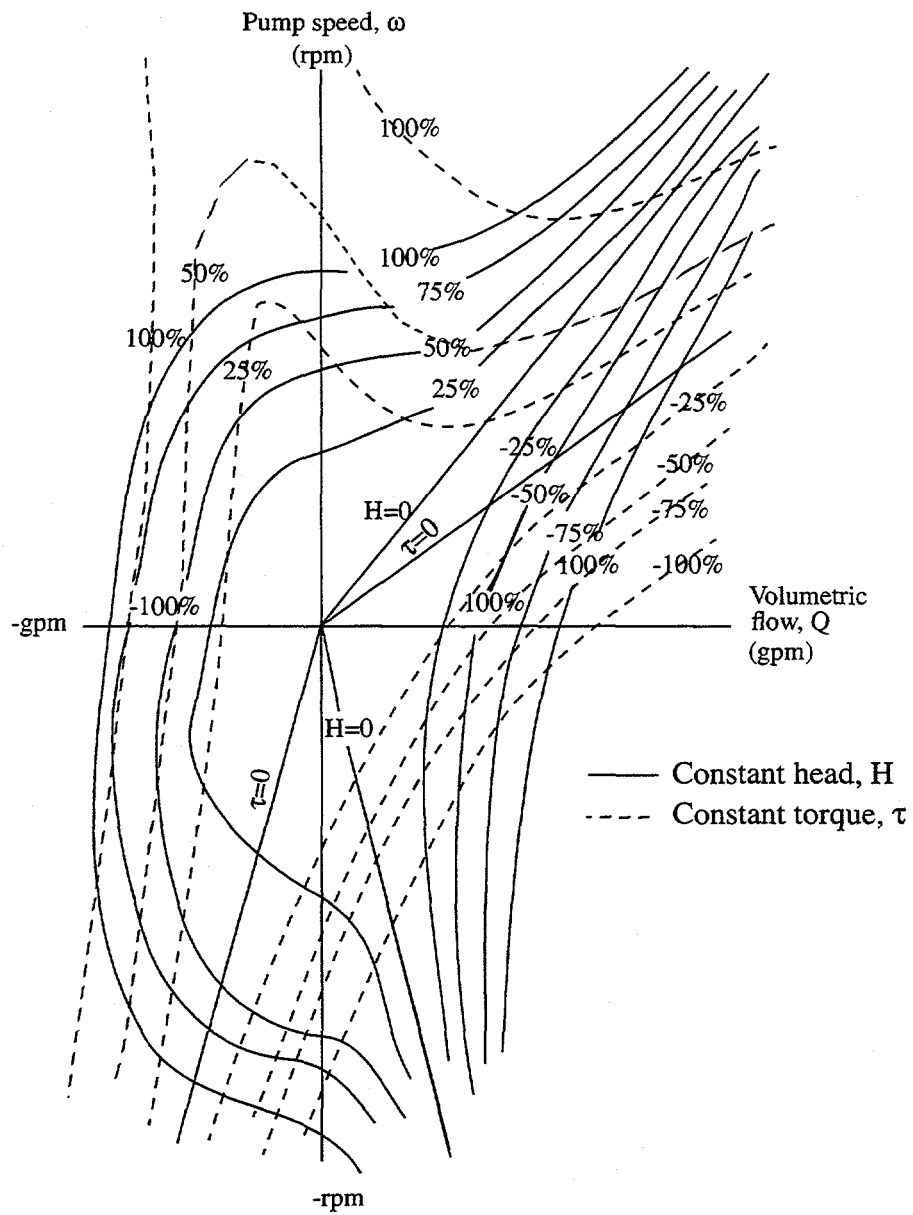


**Figure 3.5-9** Typical pump characteristic four-quadrant curves.

The two-phase degradation model is based on experimental data. Available pump data from the 1-1/2 Loop Model Semiscale and Westinghouse Canada Limited (WCL) experiments were used in developing the two-phase pump model. The single-phase pump head (dimensionless) curve for the Semiscale pump is shown in **Figure 3.5-12**, and the fully degraded two-phase pump head curves are shown in **Figure 3.5-13**. These represent complete pump characteristics (except for the reverse pump fully degraded region) for the Semiscale pump operating under two-phase conditions, with the average of the void fractions of the pump

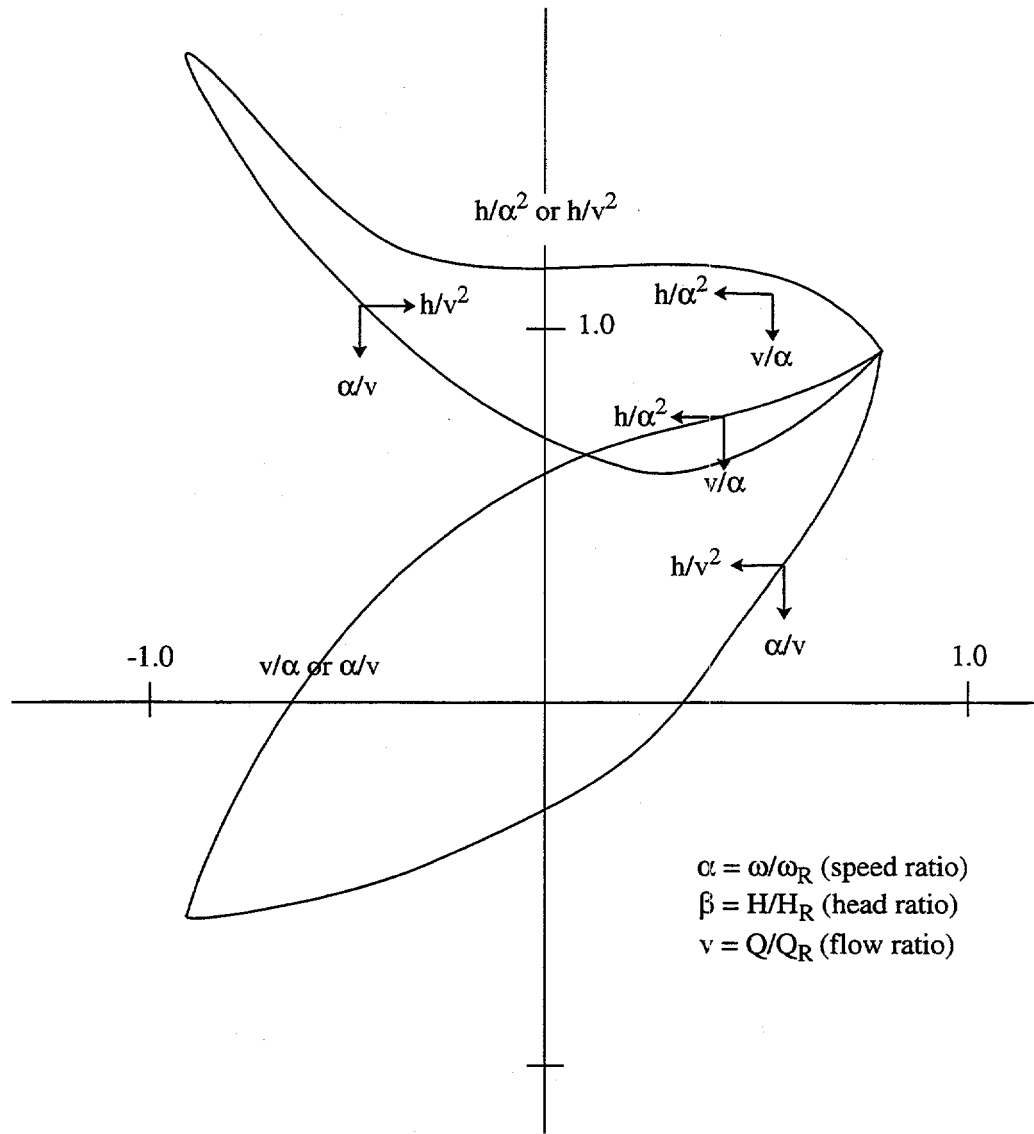


**Figure 3.5-10** Typical pump homologous head curves.

inlet and outlet mixtures between 0.2 and 0.9. The lines drawn through the data were determined by least-squares polynomial fits to the data using known constraints.

A comparison of the two-phase data in **Figure 3.5-13** with the single-phase data in **Figure 3.5-12** shows that the two-phase dimensionless head ratio ( $h/v^2$  or  $h/\alpha^2$ ) is significantly less than the single-phase dimensionless head ratio for the normal pump operation region (HAN and HVN). For negative ratios of  $v/\alpha$ , such as those that occur in the HAD region, the pump flow becomes negative. When the pump flow is negative, the two-phase dimensionless head ratio is greater than the single-phase dimensionless head ratio. Two-phase flow friction losses are generally greater than single-phase losses, and friction is controlling in

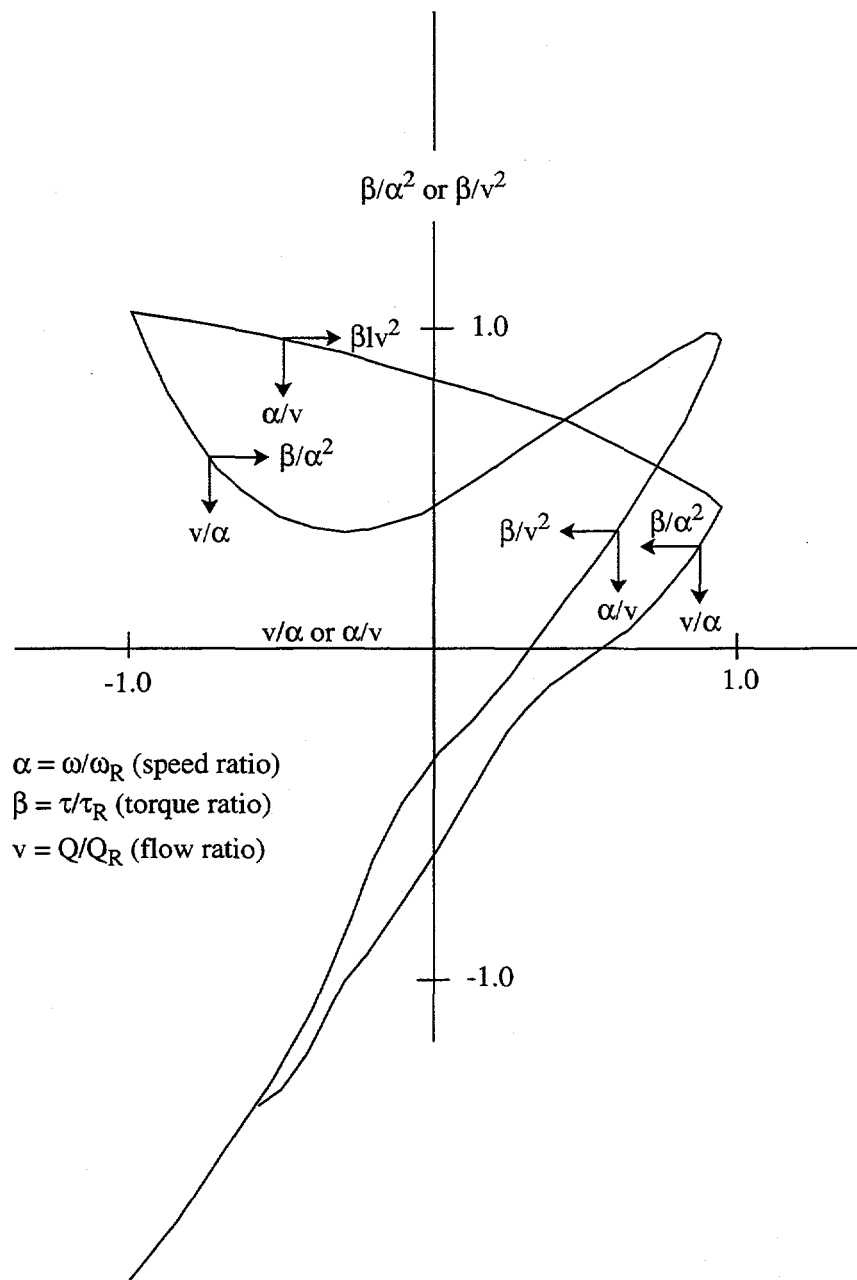


Figure 3.5-11 Typical pump homologous torque curves.

Normal pump	(+ Q, + $\alpha$ )	{ $\frac{H}{H_N}$
Energy dissipation	(- Q, + $\alpha$ )	{ $\frac{H}{H_D}$
Normal turbine	(- Q, - $\alpha$ )	{ $\frac{H}{H_T}$
Reverse pump	(+ Q, - $\alpha$ )	{ $\frac{H}{H_R}$

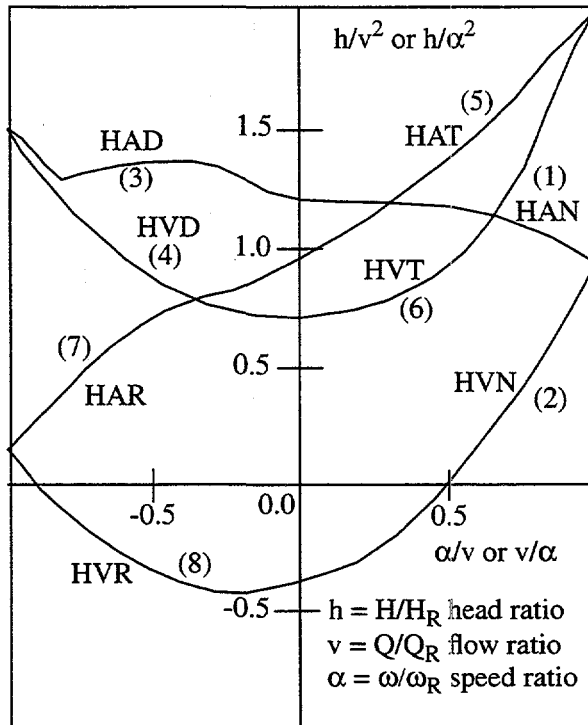


Figure 3.5-12 Single-phase homologous head curves for 1 1/2 loop MOD1 Semiscale pumps.

this energy dissipation region (HAD). The other regions of two-phase dimensionless head ratio data show similar deviations from single-phase data.

Table 3.5-2 presents the difference between the single and two-phase dimensionless head ratio data as a function of  $v/\alpha$  and  $\alpha/v$  for the various pumping regions shown in Figure 3.5-12 and Figure 3.5-13 where

$$x = \frac{v}{\alpha} \text{ or } \frac{\alpha}{v}$$

$$y = \left( \frac{h}{\alpha^2} \Big|_{1\phi} - \frac{h}{\alpha^2} \Big|_{2\phi} \right) \text{ or } \left( \frac{h}{v^2} \Big|_{1\phi} - \frac{h}{v^2} \Big|_{2\phi} \right) \quad (3.5-66)$$

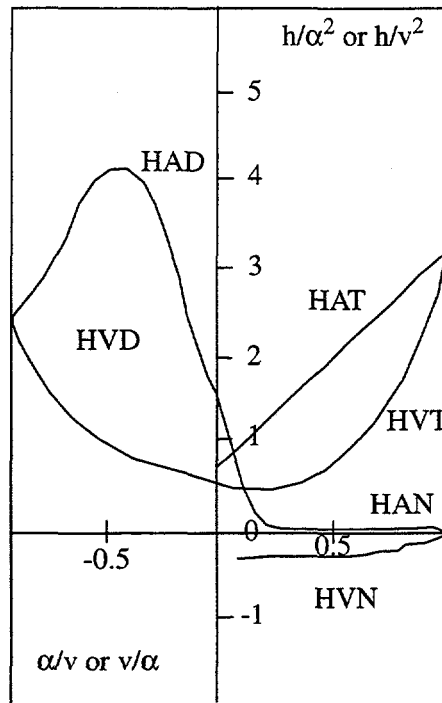


**Figure 3.5-13** Fully degraded, two-phase homologous head curves for 1 1/2 loop MOD1 Semiscale pumps.

The differences shown in **Table 3.5-2** are for the eight curve types used for determining pump head.

**Table 3.5-2** SEMISCALE dimensionless head ratio difference data (single-phase minus two-phase).

Curve Type	x	y	Curve Type	x	y
1 (HAN)	0.00	0.00	4 (HVD)	-1.00	-1.16
	0.10	0.83		-0.90	-0.78
	0.20	1.09		-0.80	-0.50
	0.50	1.02		-0.70	-0.31
	0.70	1.01		-0.60	-0.17
	0.90	0.94		-0.50	-0.08
	1.00	1.00		-0.35	0.00
				-0.20	0.05
2 (HVN)	0.00	0.00		-0.10	0.08

**Table 3.5-2 SEMISCALE dimensionless head ratio difference data (single-phase minus two-phase).**

Curve Type	x	y	Curve Type	x	y
	0.10	-0.04		0.00	0.11
	0.20	0.00			
	0.30	0.10	5 (HAT)	0.00	0.00
	0.40	0.21		0.20	-0.34
	0.80	0.67		0.40	-0.65
	0.90	0.80		0.60	-0.95
	1.00	1.00		0.80	-1.19
				1.00	-1.47
3 (HAD)	-1.00	-1.16			
	-0.90	-1.24	6 (HVT)	0.00	0.11
	-0.80	-1.77		0.10	0.13
	-0.70	-2.36		0.25	0.15
	-0.60	-2.79		0.40	0.13
	-0.50	-2.91		0.50	0.07
	-0.40	-2.67		0.60	-0.04
	-0.25	-1.69		0.70	-0.23
	-0.10	-0.50		0.80	-0.51
	0.00	0.00		0.90	-0.91
				1.00	-1.47
			7 (HAR)	-1.00	0.00
				0.00	0.00
			8 (HVR)	-1.00	0.00
				0.00	0.00

The head multiplier,  $M_H(\alpha_g)$ , and void fraction data shown in **Table 3.5-3** were obtained in the following manner. The Semiscale and WCL pump data<sup>3.5-6</sup> were converted to dimensionless head ratios of  $h/\alpha^2$  or  $h/v^2$ . Values of the dimensionless head ratios were obtained for pump speeds and volumetric flow rates within 50% of the rated speed and flow rate for the pumps. The difference between the single- and

two-phase dimensionless ratios was developed as a function of the average void fractions for the pump inlet and outlet mixtures. The difference between the single- and two-phase dimensionless ratios was then normalized to a value between 0 and 1.0. The normalized result was tabulated as a function of the void fraction.

**Table 3.5-3** Head multiplier and void fraction data.

$\alpha_g$	$M_H(\alpha_g)$
0.000	0.00
0.070	0.00
0.080	0.74
0.165	1.00
0.900	1.00
1.000	0.00

If the two-phase option is selected, the pump head and torque are calculated from

$$H = H_{1\phi} - M_H(\alpha_g) (H_{1\phi} - H_{2\phi}) \quad (3.5-67)$$

$$\tau = \tau_{1\phi} - M_\tau(\alpha_g) (\tau_{1\phi} - \tau_{2\phi}) \quad (3.5-68)$$

where

$1\phi$  = single-phase value

$2\phi$  = two-phase, fully degraded value,  $0.2 < \alpha_g < 0.9$

$M$  = multiplier on difference curve as a function of  $\alpha_g$ .

Assumptions inherent in the pump model for two-phase flow include:

- The head multiplier,  $M_H(\alpha_g)$ , determined empirically for the normal operating region of the pump, is also valid as an interpolating factor in all other operating regions.
- The relationship of the two-phase to the single-phase behavior of the Semiscale pump is applicable to large reactor pumps. This assumes that the pump model of two-phase flow is independent of pump specific speed.

**3.5.4.2 Centrifugal Pump Drive Model.** The pump torque is used to calculate the pump speed after the pump has been shut off by the input trip signal. The speed is calculated by the deceleration equation

$$I \frac{d\omega}{dt} = \tau \quad . \quad (3.5-69)$$

The finite difference approximation of this equation is

$$\omega_{t+\Delta t} = \omega_t + \frac{\tau \Delta t}{I} \quad (3.5-70)$$

where

$\tau$  = net torque

$I$  = moment of inertia

$t$  = time

$\Delta t$  = time step

$\omega$  = angular velocity.

The rate of energy addition to the pump system is given by  $\tau\omega$  and has been used in Equation (3.5-63) to calculate the pump dissipation.

The total pump torque is calculated by considering the hydraulic torque from the homologous curves and the pump frictional torque. The net torque with the drive motor shut off is

$$\tau = \tau_{hy} + \tau_{fr} \quad (3.5-71)$$

where

$\tau_{hy}$  = hydraulic torque

$\tau_{fr}$  = frictional torque.

The frictional torque is in the form of a cubic equation. The value of the frictional torque is also dependent on the sign of the pump speed. An option is available to specify whether reverse rotation of the pump is allowed.

The electric drive motor will affect the speed behavior of the pump while the motor remains connected to its power source. The net torque with the drive motor on is incorporated into the pump model by adding the value of motor torque,  $\tau_m$ , to the torque summation

$$\tau = \tau_{hy} + \tau_{fr} - \tau_m \quad (3.5-72)$$

where the sign of the motor torque is the same as that of the hydraulic and frictional torque for steady operating conditions, that is, zero net torque.

Induction motors are used to drive primary coolant pumps. At constant voltage, the motor torque is an explicit function of speed. This torque/speed relationship is normally available from the motor manufacturer.

Motor torque is supplied to the pump model as a tabular function of torque versus speed as given by the manufacturer's data. A typical torque/speed curve for an induction motor is shown in **Figure 3.5-14**.

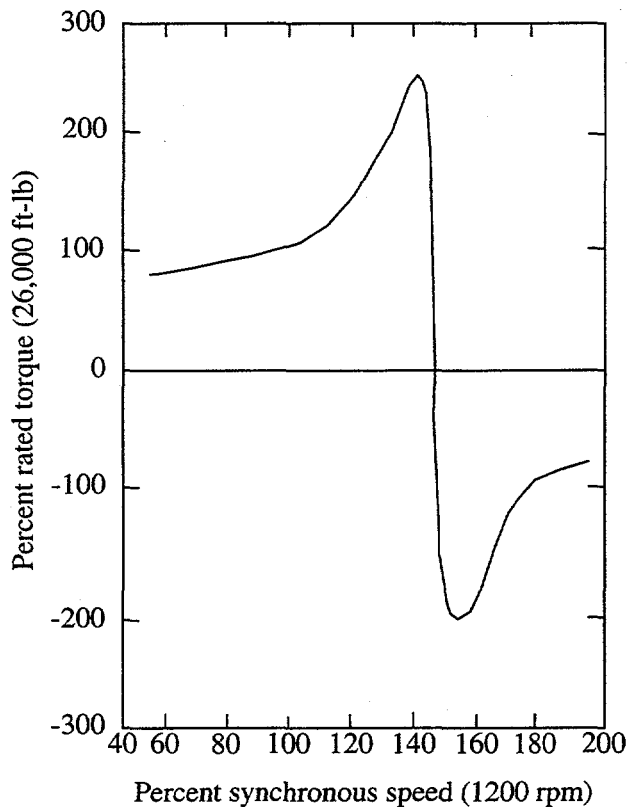


**Figure 3.5-14** Torque versus speed, Type 93A pump motor (rated voltage).

The capability to simulate a locked-rotor condition of the pump is included in RELAP5. This option provides for simulation of the pump rotor lockup as a function of input elapsed time, maximum forward speed, or maximum reverse speed. At the time the rotor locks (and at all times thereafter), the pump speed is set equal to zero.

### 3.5.5 Turbine

A steam turbine is a device that converts thermal energy contained in high-pressure, high-temperature steam to mechanical work. The complicated configuration of a steam turbine precludes a complete first-principles model, at least for the purpose of system transient calculations. A lumped-

parameter turbine model is used in RELAP5 wherein a sequence of turbine stages (henceforth referred to as a stage group) is treated as a single junction and volume. The stage group is then represented using modified energy, continuity, and momentum equations. An efficiency factor based upon simple momentum and energy considerations is used to represent the nonideal internal processes.

A turbine can be modeled using a single stage group, i.e., a single volume and junction, or several stage groups depending upon the resolution required. If turbine steam is extracted to preheat the feedwater, then several stage groups may be needed to obtain the correct steam properties at the feedwater heating bleed points. All such steam bleed points are modeled as crossflow junctions in the RELAP5 model.

**3.5.5.1 Model Design.** The normal unmodified volume continuity equations are used for the stage group, with a representative nozzle throat area for the inlet junction and the last stator nozzle throat discharge area as the outlet junction area. It is important to use the same representative nozzle area at both junctions.

Unlike the continuity equations, the momentum equations are modified by the work extracted in the rotating blade system of each stage group. To develop the general form for the momentum equations, we first consider a steady-state total energy balance for a homogeneous fluid passing through a stage group (**Figure 3.5-15**). We will subsequently extend this general form to that used for the two-fluid system.

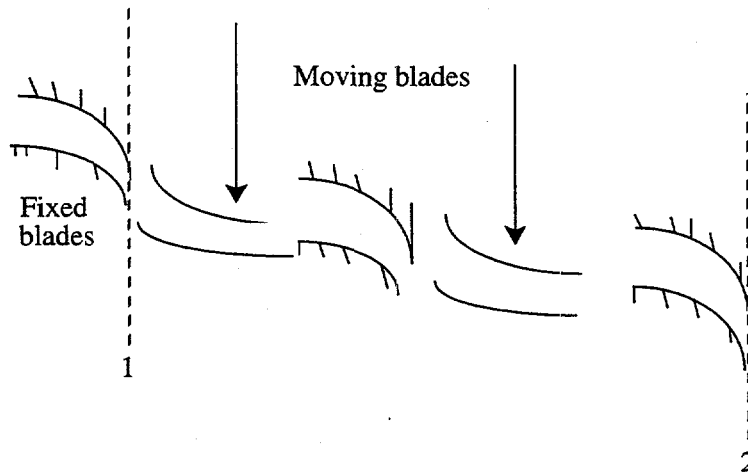


**Figure 3.5-15** A schematic of a stage group with idealized flow path between Points 1 and 2.

Although the fluid particles follow a tortuous path through the turbine, we can still write a total energy balance between cross sections 1 and 2 (**Figure 3.5-15**). For a steady-state situation, this gives

$$\left[ \rho v A \left( \frac{1}{2} v^2 + h \right) \right]_1 = \left[ \rho v A \left( \frac{1}{2} v^2 + h \right) \right]_2 + (\rho v A)_1 W \quad (3.5-73)$$

where

$\rho$	=	the density
$v$	=	the velocity
$h$	=	the enthalpy
$A$	=	the cross-sectional area.

The term  $W$  represents the shaft work per mass flow rate extracted from the fluid. Heat loss is neglected in this ideal analysis. From continuity considerations,  $\rho v A$  is constant. Dividing Equation (3.5-73) by  $\rho v A$ , we obtain

$$\frac{1}{2}v_2^2 - \frac{1}{2}v_1^2 = - (h_2 - h_1) - W \quad (3.5-74)$$

In this way, the energy balance is converted into an equivalent force balance (power = force x velocity).

In this idealized process where external heat loss and internal dissipation are neglected, the process is isentropic and

$$dh = \frac{1}{\rho} dP \quad (3.5-75)$$

Integrating Equation (3.5-75) approximately (assuming constant density) between points 1 and 2 gives

$$h_2 - h_1 = \frac{1}{\rho} (P_2 - P_1) \quad (3.5-76)$$

where  $\rho$  is an average density.

The actual work,  $W$ , produced by the fluid on the rotating blades as its momentum is changed, is usually written as an efficiency factor times the isentropic enthalpy change across the stage and becomes

$$W = -\eta \int_{S=\text{const}} dh = -\eta \int_{S=\text{const}} \frac{1}{\rho} dP \quad (3.5-77)$$

If a constant efficiency and density for the stage group is assumed, Equation (3.5-77) can be approximated as

$$W = -\eta \frac{1}{\rho} (P_2 - P_1) \quad (3.5-78)$$

When Equations (3.5-76) and (3.5-78) are substituted into Equation (3.5-74), we obtain

$$\frac{1}{2}v_2^2 - \frac{1}{2}v_1^2 = -\frac{(1-\eta)}{\rho} (P_2 - P_1) \quad (3.5-79)$$

as the momentum equation for this steady-state case. Equation (3.5-79) shows that only a small fraction,  $(1 - \eta)$ , of the pressure gradient contributes to changes in the kinetic energy of the fluid. The larger fraction,  $\eta$ , of the pressure gradient results in turbine work [Equation (3.5-78)].

Using Equation (3.5-79) as a prototype, the full two-fluid momentum equations which are used in the turbine model are (in differential form)

$$(\alpha_g \rho_g) \left( \frac{\partial v_g}{\partial t} + v_g \frac{\partial v_g}{\partial x} \right) = -\alpha_g (1 - \eta) \frac{\partial P}{\partial x} - \alpha_g \rho_g \text{HLOSSG } v_g - \alpha_g \rho_g \text{FIG } (v_g - v_f) \quad (3.5-80)$$

$$(\alpha_f \rho_f) \left( \frac{\partial v_f}{\partial t} + v_f \frac{\partial v_f}{\partial x} \right) = -\alpha_f (1 - \eta) \frac{\partial P}{\partial x} - \alpha_f \rho_f \text{HLOSSF } v_f - \alpha_f \rho_f \text{FIF } (v_f - v_g) \quad (3.5-81)$$

The application guidelines will be summarized in Volume II of this report, but it seems appropriate at this point to mention three guidelines that are related to the momentum equation development:

1. In practice, a steam turbine does not usually contain significant liquid water, and the tortuous path precludes accurate modeling of the interphase drag. Therefore, it is recommended that the homogeneous option be used at all axial turbine junctions. The effect of condensation could be included in the efficiency factor, if desired. At present, it is not included, as the effect is usually small.
2. The fluid path through the turbine volume is very tortuous. This, coupled with the large number of blades, makes the standard wall friction calculation meaningless. For this reason, the wall friction terms have not been shown in Equations (3.5-80) and (3.5-81). It is recommended that the turbine volume wall friction flag be set to use the zero wall friction option. If the user wants to include any momentum effects due to frictional or form losses, it should be done with an appropriate user-specified form loss.
3. The area changes in a turbine are gradual, so the smooth junction option should be used.

The inefficiency of the turbine gives rise to some dissipation that is a source of internal energy. The dissipation is assumed to be a small effect and is neglected in the present turbine model formulation.

The only equations that are modified as a result of the turbine model are the momentum equations, in which the pressure gradient terms are multiplied by the coefficient  $(1 - \eta)$ .

**3.5.5.2 Efficiency Formulas.** The basic efficiency formulas can be derived from velocity diagrams with assumed nozzle and blade efficiency factors. The derivations are fairly straightforward and

are found in standard texts. The efficiency formulas recorded here were obtained from **Reference 3.5-7**. The efficiency factors for three turbine designs are described in the following paragraph.

**3.5.5.2.1 Single-Stage Turbine**--The first model considered is the most general. We consider a single-row fixed-blade system followed by a single-row rotating-blade system. Let  $r$  be the reaction fraction, i.e., the fraction of the stage energy released (enthalpy change) in the moving-blade system. If  $r$  is zero, we have a pure impulse stage with no pressure drop in the moving-blade system, i.e., the moving blades only change the fluid flow direction. A turbine stage with nonzero  $r$  at design conditions is commonly called a reaction stage. A value of  $r = 0.5$  is a common design.

If all blading angles are ideal and all nozzle losses are zero, the ideal efficiency, as given in **Reference 3.5-7**, is

$$\eta = \left\{ (vb - v_t) + \left[ (vb - v_t)^2 + rv^2 \right]^{1/2} \right\} \left( \frac{2v_t}{v^2} \right) \quad (3.5-82)$$

where  $v$  is the fluid velocity at the nozzle exit,  $v_t$  is the tangential or rim velocity of the moving blades, and

$$b = (1 - r)^{1/2} \quad (3.5-83)$$

In general, due to nozzle losses, entrance effects, and nonideal blading angles, the efficiency is less than that given by Equation (3.5-82). The maximum efficiency ( $\eta = 1.0$ ) given by Equation (3.5-82) can be found by differentiation to occur when

$$\frac{v_t}{v} = \frac{0.5}{(1 - r)^{1/2}} \quad (3.5-84)$$

For an impulse stage, the maximum efficiency occurs at  $v_t/v = 0.50$ . For a reaction turbine designed with  $r = 0.5$ , the maximum efficiency occurs at  $v_t/v = 0.707$ .

In general, the actual efficiency is less than the ideal value derived above. A first approximation to the actual efficiency (see **Reference 3.5-7**) is to include a constant factor,  $\eta_o$ , in Equation (3.5-82) that represents the actual efficiency at the maximum point, i.e.,

$$\eta = \eta_o \frac{2v_t}{v^2} \left\{ (vb - v_t) + \left[ (vb - v_t)^2 + rv^2 \right]^{1/2} \right\} \quad (3.5-85)$$

Equation (3.5-85) is the general efficiency formula that is applied to a single-row impulse or reaction turbine. This formula is applied to a stage group that may consist of a single-blade passage or multiple-blade passages. If the stage group contains multiple-blade passages, the efficiency represents some average value.

**3.5.5.2.2 Two-Stage Impulse Turbine**--The second turbine design considered is a two-row impulse stage, i.e., a nozzle, a moving constant-area blade passage, a fixed constant-area stationary passage, and a final constant-area moving blade passage. This blading system is modeled as a single-stage group. This type of stage design is sometimes used as the first stage in a turbine for governing purposes. Reference 3.5-7 records the efficiency formula for this design as

$$\eta = \eta_0 \frac{8v_t}{v^2} (v - 2v_t) \quad (3.5-86)$$

**3.5.5.2.3 Constant Efficiency**--The final efficiency option that is included is a constant efficiency independent of the reaction, nozzle fluid velocity, and rim speed, i.e.,

$$\eta = \eta_0 \quad (3.5-87)$$

It should be noted that a turbine stage, designed to operate with a given reaction fraction  $r$  at design conditions, will have a different reaction fraction for off-design conditions. The change in reaction fraction with  $v_t/v$  can be calculated [Reference 3.5-7, p. 207, Equation (14)]. For reaction stages, the change is small. In all cases, this change in  $r$  is neglected in the above efficiency formulas.

**3.5.5.2.4 Power/Torque Output of Turbine**--In general, the relationship between power and torque for a rotating shaft is

$$P = \tau \omega \quad (3.5-88)$$

The power extracted from the fluid per mass flow rate for a given stage group is

$$\eta \int_{S=\text{const}} dh \quad (3.5-89)$$

so we have for the torque

$$\tau = (\rho v A) \frac{\eta}{\rho} (P_2 - P_1) / \omega \quad (3.5-90)$$

or

$$\tau = (\rho v A) \frac{\eta}{\rho} (P_2 - P_1) \frac{R}{v_t} \quad (3.5-91)$$

where  $R$  is the mean stage radius at the nozzle and the approximation in Equation (3.5-78) has been used.

Equation (3.5-91) gives the torque that is extracted from a given stage group in terms of the stage efficiency, mean stage radius  $R$ , mean blade tangential velocity  $v_t$ , and pressure drop. This is the torque that is applied by the turbine component when it is coupled to the shaft component.

**3.5.5.2.5 Numerical Implementation**--As noted in the model design section, a stage group is modeled as a single junction (j) and volume (L) (see **Figure 3.5-16**).

The continuity and internal energy equations in Section 3.1 are unchanged from their standard form. The normal finite difference form of the momentum equations for junction j is modified in two ways:

1. The pressure gradient term in the sum and difference numerical equations is multiplied by  $(1 - \eta)$ .
2. The numerical differencing of the convective terms has been modified. At a normal junction, the convective terms are approximated as

$$v \frac{\partial v}{\partial x} = \left( \frac{1}{2} v_L^2 - \frac{1}{2} v_K^2 \right) / \Delta x + \frac{1}{2} VIS / \Delta x \quad (3.5-92)$$

The small viscous term VIS is numerically calculated so as to give a damped formulation of the momentum flux term in a straight pipe. For a variable-area channel, it is formulated so that it vanishes for a variable-area channel with a constant density fluid. In a turbine, the area is slowly varying; but the fluid experiences large pressure changes (due to the work extraction), hence large density changes. A numerical simulation with the above convective terms used at the turbine junctions resulted in a viscous term that is larger than the kinetic energy terms. The normal viscous terms for a variable area channel are inaccurate in the turbine situation with large density changes and dominate the physical kinetic energy change. An alternative form of the convective terms which is sufficiently accurate and stable for the variable area turbine model is

$$v \frac{\partial v}{\partial x} = v_j (v_j - v_{j-1}) / (\Delta x) \quad (3.5-93)$$

when the flow is from left to right in **Figure 3.5-16**.

This difference form is used for all turbine junctions. If the  $v_j$  multiplying the numerical gradient is assumed to be approximately equal to  $\frac{1}{2} (v_j + v_{j-1})$ , then Equation (3.5-93) yields

$$v \frac{\partial v}{\partial x} = \frac{1}{2} (v_j^2 - v_{j-1}^2) / (\Delta x) \quad (3.5-94)$$

and a reasonable approximation to the kinetic energy change between j-1 and j results.

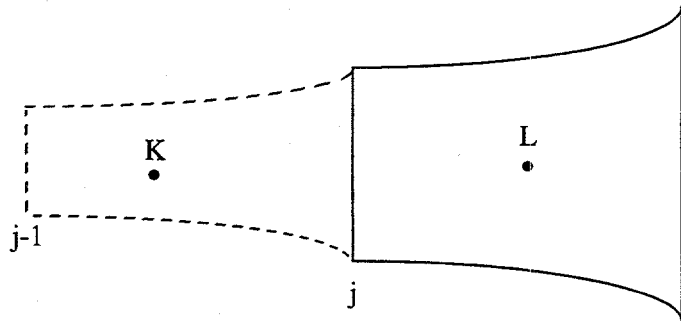


**Figure 3.5-16** Schematic of lumped model for turbine stage group.

The algebraic efficiency formulas in Equations (3.5-85) through (3.5-87) are coded with  $v$ ,  $\eta_0$ ,  $r$ ,  $\omega$ , and  $R$  (where  $v_t = R\omega$ ) as arguments. The type of the turbine stage group is fixed at input time.

The stage torque that is applied to the shaft is calculated from Equation (3.5-91). The torques from each stage group are added using the SHAFT component that integrates the angular momentum equation. The power is calculated from Equation (3.5-88). This variable is not needed in the integration scheme but is printed in the major edits.

### 3.5.6 Valves

Valves are quasi-steady models that are used either to specify an option in a system model or to simulate control mechanisms in a hydrodynamic system. The valve models can be classified into two categories: valves that open or close instantly and valves that open or close gradually. Either type can be operated by control systems or by flow dynamics.

Valves in the first category are trip valves and check valves. The model for these valves does not include valve inertia or momentum effects. If the valve is used as a junction with an abrupt area change, then the abrupt area change model is used to calculate kinetic loss factors when the valve is open.

Valves in the second category are the inertial swing check valve, the motor valve, the servo valve, and the relief valve. The inertial valve and relief valve behavior is modeled using Newton's second law of motion. The abrupt area change model controls losses through these valves as the cross-sectional flow area varies with valve assembly movement. The motor and servo valve use differential equations to control valve movement. These two valves include the options to use the abrupt area change model to calculate losses across the valve or to use flow coefficients ( $C_v$ ) specified by the user. The  $C_v$ 's are converted to energy loss coefficients within the numerical scheme [see Equation (3.5-108)].

Valves are modeled as junction components. The types of valves are defined as follows.

**3.5.6.1 Trip Valve.** The operation of a trip valve is solely dependent on the trip selected. With an appropriate trip, an abrupt full opening or full closing of the valve will occur. A latch option is also included for latching the valve in the open or closed position.

**3.5.6.2 Check Valve.** The operation of a check valve can be specified to open or close by static differential pressure, to open by static differential pressure and close by flow reversal, or to open by static differential pressure and close by dynamic differential pressure.

All of the check valves will be opened based on static differential pressure across the junction according to

$$(P_K - \Delta P_{K_g}) - (P_L + \Delta P_{L_g}) - PCV > 0, \text{ valve opens} \quad (3.5-95)$$

where

$P_K, P_L$  = junction *from* and *to* volume thermodynamic pressures

$\Delta P_{K_g}, \Delta P_{L_g}$  = static pressure head due to gravity

PCV = back pressure required to close the valve (user input).

For a *static pressure* controlled check valve, the valve will open if Equation (3.5-95) becomes positive and will close if Equation (3.5-95) becomes negative. If Equation (3.5-95) is zero, the valve will remain as previously defined.

For a *flow controlled* check valve, the valve will open if Equation (3.5-95) is positive and will close only if a flow reversal occurs such that

$$GC < 0 \quad (3.5-96)$$

where GC is the dynamic pressure given as

$$GC = \frac{1}{2} (|\bar{\rho} \bar{v}| \bar{v})_j = \frac{1}{2} [\alpha_f \rho_f v_f + \alpha_g \rho_g v_g]_j (\alpha_f v_f + \alpha_g v_g)_j \quad (3.5-97)$$

For a *dynamic pressure* controlled check valve, the valve opens if Equation (3.5-95) is greater than zero. Once the valve is open, the forces due to pressure differential and momentum hold the valve open until

$$(P_K - \Delta P_{K_g}) - (P_L + \Delta P_{L_g}) + GC - PCV < 0, \text{ valve closes,} \quad (3.5-98)$$

$= 0$ , remains as previously defined.

The terms  $\alpha_f$  and  $\alpha_g$  are the junction liquid and vapor volume fractions, respectively;  $\rho_f$  and  $\rho_g$  are the junction liquid and vapor densities, respectively; and  $v_f$  and  $v_g$  are the junction liquid and vapor velocities, respectively.

*Flow and dynamic pressure* controlled valves exhibit a hysteresis effect with respect to the forces opening and closing the valve. The *static pressure* controlled valve, however, has no hysteresis effect.

All check valves may be initialized as either open or closed. Leakage is also allowed if the valve is closed, and the abrupt area change model is used to calculate the valve form losses.

**3.5.6.3 Inertial Valve.** This valve models the motion of the valve flapper assembly in an inertial-type check valve. The abrupt area change model is used to calculate kinetic form losses, assuming that the area between the flapper and the valve seat behaves as an orifice whose area changes in time as a function of the inertial valve geometry.

The motion of the flapper about the shaft axis is given by Newton's second law (angular version) as

$$\Sigma T = I\dot{\omega} \quad (3.5-99)$$

where

$T$  = torque

$I$  = moment of inertia

$\dot{\omega}$  = angular acceleration

$\omega$  = angular velocity =  $\dot{\theta}$ , counter-clockwise motion is positive

$\theta$  = disc angular position,  $\theta = 0$  is fully closed.

Torque is defined as  $r \times F$ ; the cross product of a force  $F$  and the distance from the hinge pivot point,  $r$ , to the force. Each particle of a rotating body has kinetic energy. Kinetic energy is defined as  $0.5mV^2$  where  $m$  is the mass and  $V$  is the velocity. Since  $V=r\omega$  where  $r$  is the distance to the particle and  $\omega$  is the angular velocity, the kinetic energy of the particle is  $0.5mr^2\omega^2$ . The total kinetic energy of a rotating body is the sum of the kinetic energy of all of its particles. Since the angular velocity of all particles is the same,  $\omega$  can be factored out to give:

$$\text{Kinetic Energy} = 0.5 (\sum m_i r_i^2) \omega^2 \quad (3.5-100)$$

The term in parentheses is known as the moment of inertia,  $I$ .

A diagram of an inertial valve is shown in **Figure 3.5-17**. The valve flapper disc resides in a pipe and swings on a hinge pin. The valve is used to prevent backflow. The flapper position depends on factors such as: flapper mass, gravity vector, moment of inertia, distance from the hinge pin to the center of mass, flapper area, pressure difference across the valve, viscous and Coulomb friction between the flapper and

the pin and lift and drag forces on the flapper. Only torque due to differential pressure,  $T_{DP}$ , Coulomb friction,  $T_F$ , and weight,  $T_W$ , are included in this model:

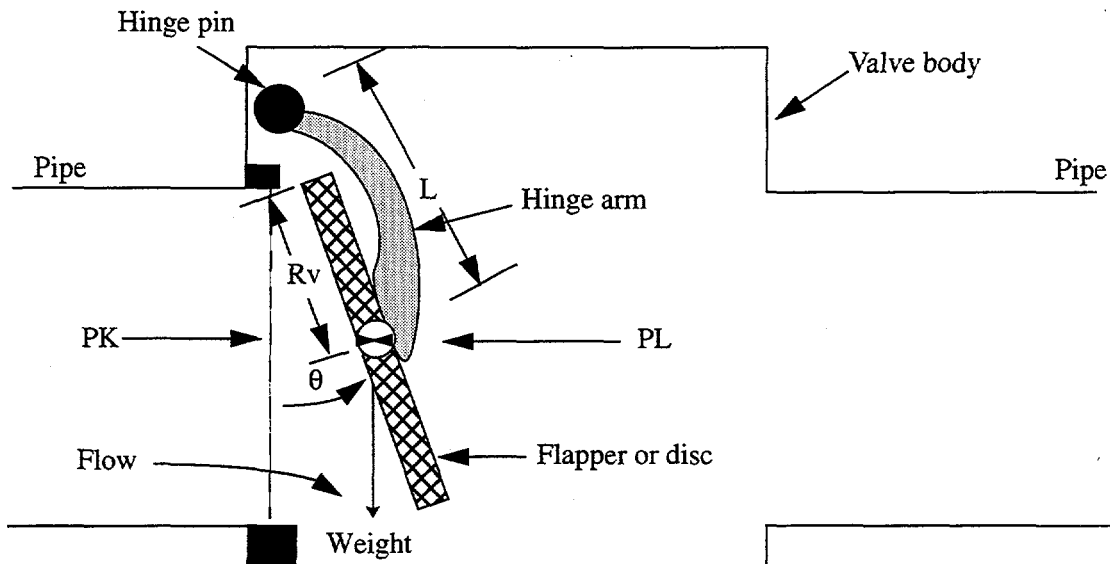


Figure 3.5-17 Diagram of inertial valve.

$$T_{DP} = (P_K - P_L) A_p L \quad (3.5-101)$$

$$T_F = \Delta P_F A_R L \quad (3.5-102)$$

$$T_W = -Mg L \sin \theta \quad (3.5-103)$$

where

$P_K$  = pressure in the hydraulic cell on the left

$P_L$  = pressure in the hydraulic cell on the right

$A_p$  = projected area of the disc

$L$  = user input flapper moment arm length from the hinge to the center of inertia

$$A_R = \text{area of disc} = \pi R_v^2$$

$$R_v = \text{user input disc radius}$$

$$\Delta P_F = \text{user input value of minimum pressure difference across the valve required to initiate motion (cracking pressure)}$$

$$g = \text{acceleration due to gravity}$$

$$M = \text{mass of the flapper.}$$

The differential pressure across the flapper faces decreases as the valve flapper swings into hydraulic cell on the right. To approximate this decrease, the projected area is used in the  $T_{DP}$  term (see **Figure 3.5-18**). The projected area of a circle is an ellipse with an area of  $\pi R_v b$ . Since  $b = R_v \sin(\phi)$  where  $\phi$  is  $90-\theta$ ;



**Figure 3.5-18** Two views of a partially open flapper valve.

$$A_P = \pi R_v^2 \sin(90-\theta) = \pi R_v^2 \cos \theta . \quad (3.5-104)$$

The angular acceleration is solved from Equation (3.5-99):

$$\dot{\omega}^n = \frac{\sum T}{I} \quad (3.5-105)$$

and the new time flapper velocity and angle are:

$$\omega^n = \omega^{n-1} + \dot{\omega}^n \Delta t . \quad (3.5-106)$$

The new time angle is calculated from the angle at the previous time step and the average velocity during the time step.

$$\theta^n = \theta^{n-1} + 0.5(\omega^{n-1} + \omega^n) \Delta t \quad (3.5-107)$$

where superscript n stands for new time and n-1 indicates the previous time step value.

In order to obtain the correct velocity to compare with the sonic speed at the valve the vena-contracta is considered. The effective flow area is  $C_c$  times the actual open area.

$C_c$  = contraction coefficient, effective area/actual open area.

**Table 3.5-4** gives the table of contraction coefficients<sup>3.5-8</sup>.  $C_c$  is less than one and has the effect of increasing the code calculated velocity in the valve opening. also shown is the loss coefficient which the abrupt area change model should automatically calculate for the code users.

**Table 3.5-4** Contraction coefficient table.

Area Fraction Open	0.0	0.1	0.2	0.3	0.4	0.5	0.6	0.7	0.8	0.9	1.0
$C_c$	0.617	0.624	0.632	0.643	0.659	0.681	0.712	0.755	0.813	0.892	1.0
$K_{Loss}$	0.5	0.46	0.41	0.36	0.30	0.24	0.18	0.12	0.06	0.02	0.0

Several options are allowed with the use of this valve, such as specifying minimum and maximum flapper angular positions when the valve is closed, specifying latch or no latch options, and specifying leakage area.

**3.5.6.4 Motor Valve.** This valve model has the capability of controlling the junction flow area between two control volumes as a function of time. The operation of the valve is controlled by two trips; one for opening the valve and a second for closing the valve. A constant rate parameter controls the speed at which valve area changes. The motor valve area variation can also be specified using a general table. When the general table is specified, the constant rate parameter controls the valve stem position and the general table relates the stem position to the valve flow area. Conversely, when the general table is not specified, the constant rate parameter controls the rate of change in valve area.

The abrupt area change model is used to calculate kinetic form losses with respect to the valve area. However, if the normalized valve flow area has a value less than  $1.0 \times 10^{-10}$ , the valve is assumed to be closed.

A second option allowed for the motor valve is the specification of valve flow coefficients,  $C_v$ . These coefficients may be specified using a general table of  $C_v$  versus normalized stem position and the smooth junction option must be specified. The conversion of  $C_v$  to an energy loss coefficient,  $K$ , is done in the numerical scheme using the formula

$$K = 2 \frac{A_{\text{valve}}^2}{C_v^2 \rho_0} \quad (3.5-108)$$

where  $\rho_0$  is the density of water at 288.71 K (630.0°F). Provisions also exist for applying multipliers to both stem position and  $C_v$ .

**3.5.6.5 Servo Valve.** The servo valve operation is similar to that for the motor valve. However, the valve area or stem position is controlled by a control variable rather than by a specified rate parameter. The servo valve also has the same options as the motor valve.

**3.5.6.6 Relief Valve.** For thermal-hydraulic analysis of overpressure transients, it is necessary to simulate the effects of relief valves. In particular, it is desirable to model the valve dynamic behavior, including simulation of valve flutter and hysteresis effects.

To assist in understanding the relief valve model, three schematics of a typical relief valve are shown in **Figure 3.5-19**, **Figure 3.5-20**, and **Figure 3.5-21**. The three schematics represent the valve in the closed (**Figure 3.5-19**), partially open (**Figure 3.5-20**), and fully open (**Figure 3.5-21**) modes, respectively. In the schematics, the seven main components of a relief valve are shown, which are the valve housing, inlet, outlet, piston, rod assembly, spring, bellows, and valve adjusting ring assembly.

The numerical model of the valve simply approximates the fluid forces acting on the valve piston and the valve reaction to these forces. The model of the fluid forces is based on a quasi-steady-state form of the impulse momentum principle, and the valve reaction force is based on Newton's Second Law of motion.

A qualitative understanding of the operation of the relief valve can be gained by referring again to **Figure 3.5-19**, **Figure 3.5-20**, and **Figure 3.5-21**. If the valve inlet pressure is low the valve is closed, as shown in **Figure 3.5-19**. As the inlet pressure increases, the valve piston will remain closed until the force of the upstream pressure on the valve exceeds the set point forces. The set point forces are the combined forces of the piston and rod assembly weight, the valve spring, the atmospheric pressure inside the bellows, and the downstream back pressure around the outside of the bellows. Once the set point forces are exceeded, the valve piston will begin to lift. Upon opening, the upstream fluid will begin to expand through the opening into the valve ring region. This initial expansion occurs through the angle  $\alpha_0$ , and the flow changes direction through an average angle  $\theta_0$ , as shown in **Figure 3.5-19**. As the flow accelerates, the momentum effects of the expansion and change in flow direction exert a thrust on the valve piston, causing the valve to open further. As the valve partially opens, the angle of expansion decreases to  $\alpha_1$  and the change in flow direction increases to  $\theta_1$ , as shown in **Figure 3.5-20**. This effect, in turn, further increases the thrust on the valve piston, causing it to fully open, as shown in **Figure 3.5-21**. As these processes occur, the valve reaction forces and fluid momentum forces vary in such a manner that the valve will not close until the upstream pressure decreases significantly below the valve set point pressure. In this respect, a hysteresis effect is observed that is characteristic of relief valves.

The relief valve model consists of a set of equations designed to approximate the behavior described above. In implementing the model, the dynamic behavior of the fluid is calculated at each time step by the RELAP5 hydrodynamic solution scheme. The resultant phasic velocities and thermodynamic properties are then used to solve a quasi-steady equation approximating the fluid forces on the valve piston. The

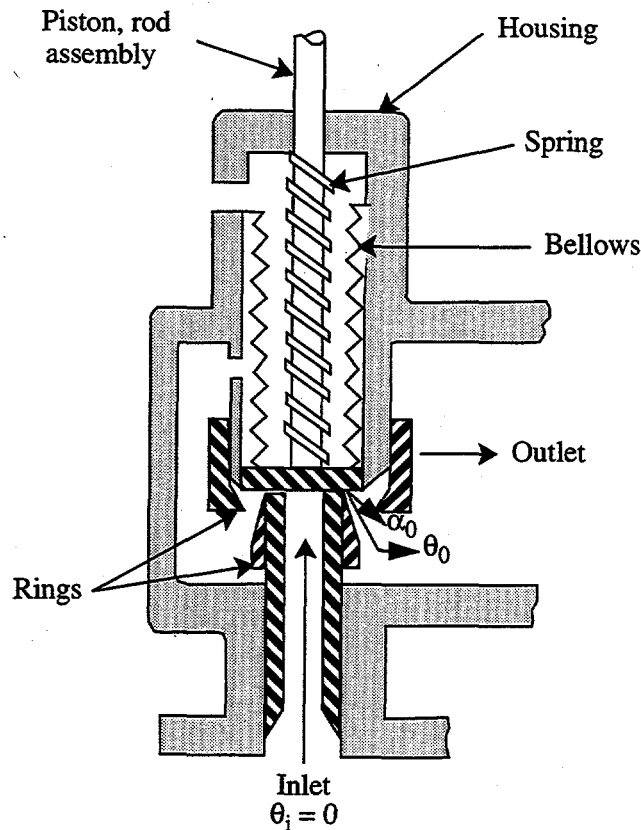


**Figure 3.5-19** Schematic of a typical relief valve in the closed position.

valve dynamic reaction forces are then calculated, and the new time valve piston speed and position are estimated.

The relief valve model is formulated, applying D'Alembert's principle in which the forces acting on the face of the valve piston are balanced, for which the valve reaction forces can be written as

$$(\text{reaction forces}) = F_R = m_v a_{v,x} + B (v_{v,x} - v_{\text{housing}}) + K_s x \quad (3.5-109)$$

where

$m_v$  = mass of the valve mechanism that is in motion (i.e. the valve piston, rod assembly combined with the spring and bellows)

$a_{v,x}$  = valve assembly acceleration in the x direction

$B$  = damping coefficient

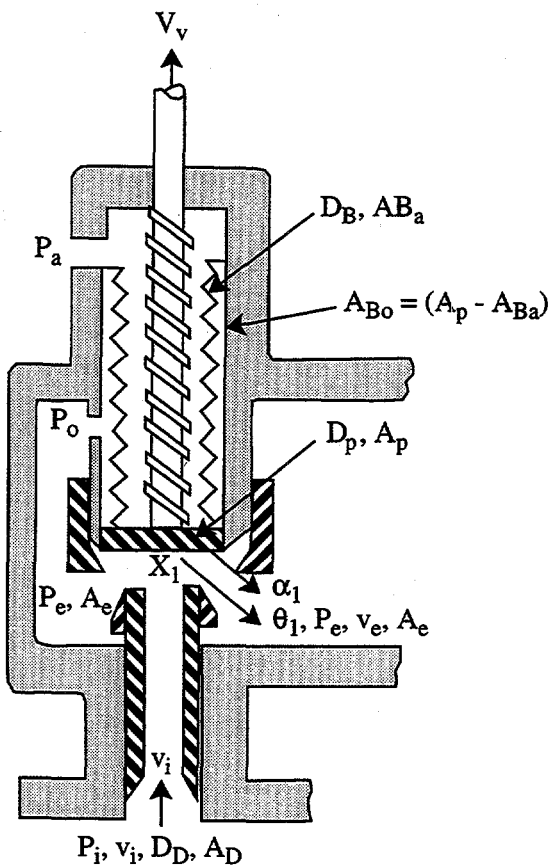


**Figure 3.5-20** Schematic of a typical relief valve in the partially open position.

$v_{v,x}$  = velocity of the valve mechanism in the x direction

$v_{\text{housing}}$  = velocity of the valve housing = 0

$K_s$  = spring constant

$x$  = piston position (i.e., x coordinate).

The positive x direction is assumed to be in the direction of fluid flow at the valve inlet. The fluid forces,  $F_F$ , can be formulated by summing the forces acting over the surfaces of the fluid flow channel such that

$$F_F = (P_i A_D)_x - (P_a A_{B_a})_x - (P_o A_{B_o}) - (P_e A_e)_x - F_R \quad (3.5-110)$$

where

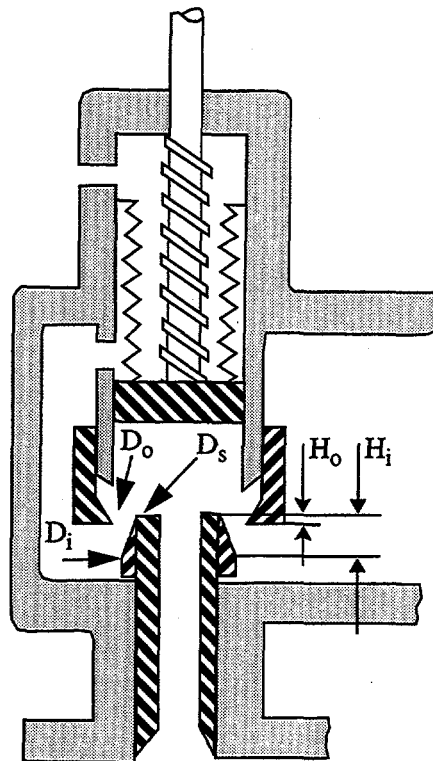


**Figure 3.5-21** Schematic of a typical relief valve in the fully open position.

$F_R$  = reaction forces

$P_i$  = valve inlet pressure

$A_D$  = valve piston face area exposed to the inlet flow stream

$P_a$  = atmospheric pressure inside the bellows

$A_{Ba}$  = valve piston area inside the bellows

$P_o$  = valve back pressure outside the bellows

$A_{Bo}$  = valve piston area outside the bellows

$A_e$  = valve ring exit area

$P_e$  = valve ring exit pressure

and where the subscript x denotes that the force component is in the x direction. Since the fluid is flowing through a channel that both expands and changes direction, the fluid undergoes a change in momentum expressed by the impulse momentum principle as

$$F_F = \Delta(mv) = \dot{m}_F (v_{e,x} - v_{i,x}) \quad (3.5-111)$$

where

$\dot{m}_F$  = mass flow rate of the fluid through the valve

$v_{e,x}$  = fluid velocity exiting through the rings

$v_{i,x}$  = fluid velocity entering the valve inlet.

Balancing the forces by combining Equations (3.5-109) through (3.5-111) gives

$$m_v a_{v,x} + B v_{v,x} + K_s x = - (P_a A_{Ba}) - (P_o A_{Bo}) - (P_e A_e) \cos \theta - \dot{m}_f (v_e \cos \theta - v_i) + P_i A_D \quad (3.5-112)$$

The valve acceleration can be expressed in terms of the valve velocity as

$$a_{v,x} = \frac{dv_{v,x}}{dt} + g \quad (3.5-113)$$

where g is the acceleration of gravity.

Combining Equations (3.5-112) and (3.5-113), treating the velocity damping term and spring force position terms implicitly, and integrating over the time step gives

$$m_v (v_{v,x}^{n+1} - v_{v,x}^n) + B v_{v,x}^{n+1} dt + K_s x^{n+1} dt + m_v g dt = [ (P_i^n A_D) - (P_a A_{Ba}) - (P_o A_{Bo}) ] - (P_e^n A_e) \cos \theta_e^n - \dot{m}_f^n (v_e^n \cos \theta_e^n - v_i^n) dt \quad (3.5-114)$$

where n and n+1 represent the old and new time terms, respectively.

The position term,  $x^{n+1}$ , can be written in terms of the valve velocity by considering that

$$v_{v,x} = \frac{dx}{dt} \quad (3.5-115)$$

If Equation (3.5-115) is integrated over the time step, then

$$x^{n+1} = x^n + v_{v,x}^{n+1} dt \quad (3.5-116)$$

If the valve set point pressure is equated to  $K_s x_o$ , then combining Equations (3.5-114) and (3.5-116) and both adding and subtracting the term  $K_s x_o$  gives the numerical form of the relief valve model,

$$\begin{aligned} & m_v (v_{v,x}^{n+1} - v_{v,x}^n) + [ (B + K_s dt) v_{v,x}^{n+1} + K_s (x^n - x_o) + m_v g ] dt \\ & = -K_s x_o dt + [ (P_i^n A_D) - (P_a A_{Ba}) - (P_o^n A_{Bo}) - (P_e^n A_e) \cos \theta_e^n - \dot{m}_F^n (v_e^n \cos \theta_e^n - v_i^n) ] dt \end{aligned} \quad (3.5-117)$$

where the sign of the gravity term,  $g$ , is dependent on the valve orientation. For example, if the valve is oriented upward (i.e.,  $+x$  is upward), then the gravity term is expressed as  $g = -|g|$ .

In the numerical scheme, Equation (3.5-117) is solved for the new time valve piston velocity,  $v_{v,x}^{n+1}$ , in terms of the current time terms with superscript  $n$ . The terms required to model the valve geometry and the valve damping, spring, and back pressure forces are input to the code as described in Volume II, Appendix A, of this report.

The characteristic relief valve hysteresis effects are inherent in the formulation of Equation (3.5-117). For example, if the valve is closed, then all velocity terms are zero and  $x = x_o$ . Therefore, acceleration of the valve piston in the positive  $x$  direction cannot occur until the upstream force  $P_i A_D$  exceeds the spring set point and valve weight. Once the valve opens and the fluid accelerates, the forces due to the change in fluid momentum aid in holding the valve open. Therefore, the valve cannot close until the combined fluid pressure and momentum terms decrease significantly below the set point forces. Hence, the desired hysteresis is incorporated in the model.

### 3.5.7 Accumulator

An accumulator model is included that features mechanistic relationships for the hydrodynamics, heat transfer from the tank wall and water surface, condensation in the vapor dome, and vaporization from the water surface to the vapor dome. The geometry of the tank may be cylindrical or spherical.

**3.5.7.1 Hydrodynamic Model.** An accumulator is modeled in RELAP5 as a lumped-parameter component. This model was chosen for two reasons; the spatial gradients in the accumulator tank are expected to be small, and a simple ideal gas equation of state can be used.

The accumulator model and associated notations are shown in **Figure 3.5-22** for the case of a cylindrical tank, and **Figure 3.5-23** for the case of a spherical tank. The basic model assumptions are:

- Heat transfer from the accumulator walls and heat and mass transfer from the liquid are modeled using natural convection correlations, assuming similarity between heat and mass transfer from the liquid surface.
- The gas in the gas dome is modeled as a closed expanding system composed of an ideal gas with constant specific heat. The steam in the dome exists at a very low partial

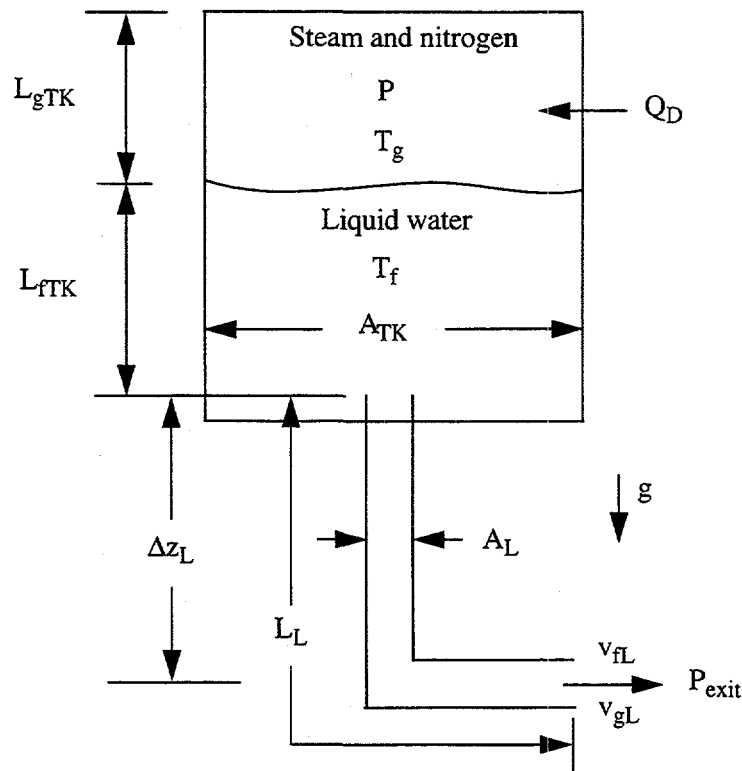


Figure 3.5-22 Typical cylindrical accumulator.

pressure; hence, its effect on the nitrogen state is neglected. However, energy transport to the gas dome as a result of vaporization/condensation is included.

- Because of the high heat capacity and large mass of water below the interface, the water is modeled as an isothermal system.
- The model for liquid flow includes inertia, wall friction, form loss, and gravity effects.

Using these assumptions, the basic equations governing the thermal-hydraulics of the tank and discharge line are as follows:

The conservation of mass for the nitrogen dome is

$$M_n = \text{constant} = \rho_n V_D \quad (3.5-118)$$

where

$$M_n = \text{gas mass}$$

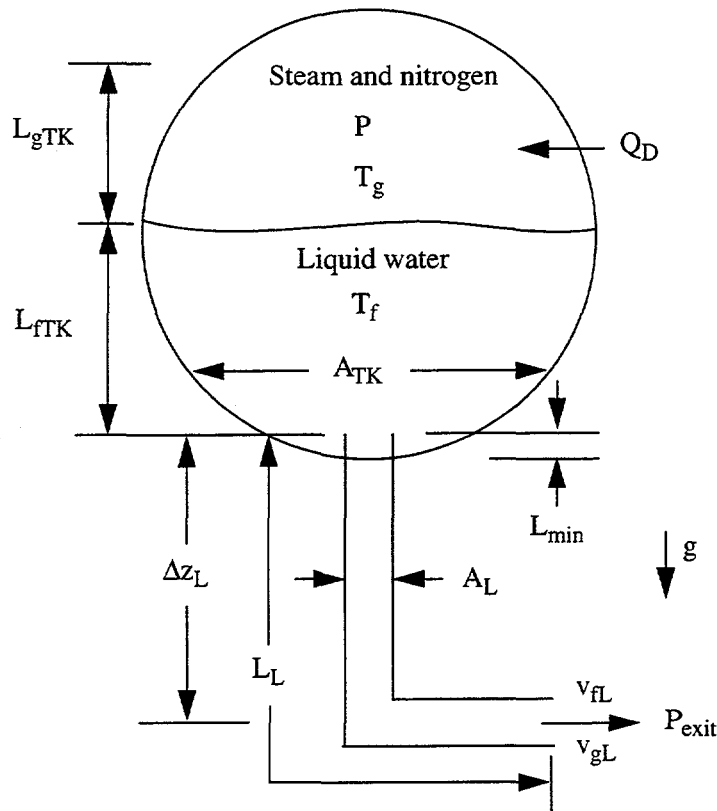


Figure 3.5-23 Typical spherical accumulator.

$\rho_n$  = noncondensable gas density

$V_D$  = gas dome volume.

The conservation of energy for the nitrogen dome is

$$M_n \left( \frac{dU_n}{dt} \right) = -P_D \left( \frac{dV_D}{dt} \right) + \dot{Q}_D \quad (3.5-119)$$

where

$U_n$  = nitrogen internal energy

$P$  = vapor dome pressure

$\dot{Q}_D$  = net heat transfer rate to the gas dome from all sources.

The conservation of energy for the tank wall is

$$M_{wall} C_{v,wall} \frac{dT_{wall}}{dt} = -\dot{Q}_{wall} \quad (3.5-120)$$

where

$M_{wall}$  = metal mass in the tank wall

$C_{v,wall}$  = metal specific heat

$T_{wall}$  = mean metal temperature

$\dot{Q}_{wall}$  = heat transfer rate to the wall.

The conservation of momentum,<sup>a</sup> for the accumulator tank and surge line is

$$\rho A \left( L \frac{dv}{dt} + \frac{1}{2} v^2 \right) + Fv = -A(P - P_{exit}) + A\Delta P_z \quad (3.5-121)$$

where

$A$  = flow channel cross-sectional area

$L$  = discharge line flow channel length

$v$  = velocity in discharge line

$F$  = frictional loss coefficient

$P_{exit}$  = pressure at exit of surge line

$\Delta P_z$  = elevation pressure differential between discharge line entrance and liquid surface.

The equations of state for the non-condensable gas in the dome are,

$$PV_D = M_n R_n T_g \quad (3.5-122)$$

---

a. Equation (3.5-121) is the combined tank and discharge line momentum equation. The wall drag coefficient,  $F$ , is given as  $1/2 \rho_f \lambda_{wf} (L/D) Alv$ , where  $D$  = surge line diameter and  $\lambda_{wf}$  is the Darcy friction factor.

$$U_n = M_n C_{v,n} T_g \quad (3.5-123)$$

Using Equation (3.5-123), Equation (3.5-119), the nitrogen energy equation, can be rewritten as

$$M_n C_{v,n} \frac{dT_g}{dt} = -P \frac{dV_D}{dt} + \dot{Q}_D \quad (3.5-124)$$

Differentiating Equation (3.5-122), eliminating the constant term  $M_n R_n$ , and substituting the result into Equation (3.5-124) yields

$$P \left( 1 + \frac{R_n}{C_{v,n}} \right) \frac{dV_D}{dt} + V_D \frac{dP}{dt} = \frac{R_n}{C_{v,n}} \dot{Q}_D \quad (3.5-125)$$

Equations (3.5-121), (3.5-124), and (3.5-125) comprise the system of three differential equations used in the accumulator hydrodynamic model. They are used to numerically advance  $T_D$ ,  $V_D$ , and  $P_D$  in time.

**3.5.7.2 Heat Transfer to the Gas Dome.** In the accumulator, energy transport by convective heat transfer to the gas dome from the walls and fluid surface is modeled using an empirical Newton cooling law formulation

$$Q_i = h_i A_i (T_i - T_g) \quad (3.5-126)$$

where

$i$  = thermal transport surface

$h_i$  = convective heat transfer coefficient

$A_i$  = surface area

$T_i - T_g$  = surface to gas dome temperature difference.

It should be noted that heat and mass transfer in the accumulator discharge line are neglected.

Two turbulent natural convection heat transfer models are used and combined by superposition. First, heat transfer with the cylindrical walls of the tank is considered, using a turbulent natural convection correlation<sup>3.5-9</sup> for heat transfer within a vertical cylinder with closed ends for which

$$h_1 = 0.1 \frac{k_D}{\frac{1}{2} D_{TK}} (GrPr)^{\frac{1}{3}} \frac{L}{\delta} \quad (3.5-127)$$

and

$$A_1 = \pi D_{TK} L \quad (3.5-128)$$

where

$h_1$	=	gas dome to cylinder heat transfer coefficient
$L$	=	gas dome cylinder length
$\delta$	=	gas dome characteristic diameter
$k_n$	=	noncondensable gas thermal conductivity
$D_{TK}$	=	tank diameter
$Gr$	=	gas dome Grashof number
$Pr$	=	gas dome Prandtl number.

Second, heat transfer from the disk-shaped ends of the cylinder is considered, where the top disk is the metal top of the tank and the bottom disk is the liquid-gas interface. For this model, a turbulent natural convection correlation<sup>3.5-9</sup> is used for heat transfer between two horizontal disks separated vertically where, for each disk,

$$h_2 = 0.15 \frac{k_n}{L} (GrPr)^{\frac{1}{3}} \frac{L}{\delta} \quad (3.5-129)$$

and

$$A_2 = \frac{\pi D_{TK}^2}{4} \quad (3.5-130)$$

In the case of a spherical tank, Equation (3.5-127) is used with  $A_1$  replaced by the surface area of the tank in contact with the gas,

$$A_1 = 2\pi LR \quad (3.5-131)$$

where  $L$  is the height of the gas dome and  $R$  is the radius of the sphere. The characteristic diameter of a spherical gas dome is defined as the ratio of volume to surface area. The correlation given by Equation (3.5-129) is not used for a spherical tank, hence  $h_2$  is set equal to zero.

In the correlations given by Equations (3.5-127) and (3.5-129), the product of the Grashof and Prandtl numbers represents the convective thermal circulation in the gas dome, where the Grashof number represents the ratio of circulation potential to viscous stress and the Prandtl number represents the ratio of viscous stress to thermal diffusion. Only the Grashof number is a function of the gas dome dimensions and temperature difference for which

$$Gr = \frac{g\beta_n |T_i - T_n| \delta^3}{v_n^2} \quad (3.5-132)$$

where

$g$  = acceleration due to gravity

$\beta_n$  = noncondensable gas isobaric coefficient of thermal expansion

$T_i - T_n$  = magnitude of the interface, gas dome difference

$v_n$  = noncondensable gas kinematic viscosity

$\delta$  = characteristic overall diameter of the gas dome.

If the Prandtl number is written in terms of the gas dome thermal diffusivity, then

$$Pr = \frac{\mu_n}{\rho_n \alpha_n} \quad (3.5-133)$$

where

$\rho_n$  = noncondensable gas density

$\alpha_n$  = noncondensable gas thermal diffusivity.

The characteristic diameter is defined in terms of the typical volume-to-surface-area ratio as

$$\delta = \frac{4V_D}{A_i} \quad (3.5-134)$$

where  $A_i$  is the combined gas dome cylinder, disk top, and bottom surface areas. In the case of a spherical gas dome,  $A_s = A_1 + A_i$ , where  $A_1$  is given by Equation (3.5-131) and  $A_i$  is the surface area of liquid-gas interface,

$$A_i = \pi L(2R - L) \quad (3.5-135)$$

where  $L$  is the height of the gas dome and  $R$  is the radius of the sphere.

**3.5.7.3 Mass Transfer to the Gas Dome.** When the accumulator is in its stagnant initial condition, the gas dome and liquid are in thermal equilibrium and the gas dome is saturated with water vapor. However, as the accumulator blows down, the gas dome temperature decreases due to expansion, while the liquid remains essentially isothermal. As a result, there is simultaneous vaporization at the liquid-gas interface and condensation in the gas dome. This mechanism transports a large amount of energy to the gas dome as a result of the heat of vaporization of the water.

At the liquid-gas interface, as vaporization occurs, the relatively warm vapor rapidly diffuses due to buoyancy into the gas dome. Assuming that the process can be approximated by a quasi-steady formulation, then for diffusion in a stagnant gas, the mass transfer for the process can be written as

$$\dot{M}_{vap} = -\zeta A_i \frac{dC}{dx} \quad (3.5-136)$$

where

$\dot{M}_{vap}$  = rate of vapor diffusion

$\zeta$  = diffusion coefficient

$A_i$  = surface area of the liquid-gas interface

$\frac{dC}{dx}$  = vapor concentration gradient.

The concentration can be expressed in terms of partial pressure such that

$$C = \frac{P_s}{P} \rho_s \quad (3.5-137)$$

where

$C$  = vapor concentration

$P_s$  = local water vapor partial pressure

$$\rho_s = \text{water vapor density (saturated vapor at } P_s).$$

Hence, at the dome pressure, the concentration gradient can be written as

$$\frac{dC}{dx} = \frac{1}{P} \frac{d(P_s \rho_s)}{dx} \quad (3.5-138)$$

Combining Equations (3.5-136) and (3.5-138) and integrating gives

$$\dot{M}_{vap} L_D = -\frac{\zeta A_i}{P} \left( P_s \int_{x=0}^{x=L_D} d\rho_s + \bar{\rho} \int_{x=0}^{x=L_D} dP_s \right) \quad (3.5-139)$$

where the integration is performed by parts.

Both of the differential terms  $d\rho_s$  and  $dP_s$  can be written in terms of temperature differentials if 100% relative humidity is assumed so that

$$P_s = P^s(T_g) \quad (3.5-140)$$

where  $P^s(T_g)$  is the saturation pressure at the temperature  $T_g$ . Hence, the density differential can be expanded as

$$d\rho_s = \left[ \left( \frac{\partial \rho_s}{\partial P_s} \right)_T \frac{dP_s}{dT} + \left( \frac{\partial \rho_s}{\partial T} \right)_{P_s} \right] dT \quad (3.5-141)$$

where

$$\left( \frac{\partial \rho_s}{\partial P_s} \right)_T = \kappa_s \rho_s \quad (3.5-142)$$

$$\left( \frac{\partial \rho_s}{\partial T} \right)_{P_s} = -\beta_s \rho_s \quad (3.5-143)$$

Combining Equations (3.5-141), (3.5-142), and (3.5-143) and substituting Clapeyron's equation for the  $dP^s/dT$  term gives

$$d\rho_s = \bar{\rho}_g \left[ \kappa_g \left( \frac{h_{fg}}{T_g^s V_{fg}} \right) - \beta_g \right] dT \quad (3.5-144)$$

where Clapeyron's equation is

$$dP^s = \left( \frac{h_{fg}}{T_g v_{fg}} \right) dT \quad (3.5-145)$$

and the term  $(h_{fg}/T_g v_{fg})$  is treated as a constant. Combining Equations (3.5-140), (3.5-144), and (3.5-145), the diffusion equation can be rewritten as

$$\dot{M}_{vap} = \frac{\zeta A_i}{L_D P} \{ \bar{P}_s \bar{p}_s \left[ \kappa_s \left( \frac{h_{fg}}{T_g v_{fg}} \right) - \beta_s \right] + \bar{p}_s \left( \frac{h_{fg}}{T_g v_{fg}} \right) \} (T_f - T_g) \quad (3.5-146)$$

where the dome average terms are evaluated at the dome average temperature,  $T_g$ .

Equation (3.5-146) can be made analogous to a convective equation by expressing the mass transfer coefficient as

$$h_{2s} = \frac{\zeta}{L_D} \quad (3.5-147)$$

where  $h_{2s}$  is the mass transfer coefficient in a stagnant gas. Then, by applying Reynolds analogy, a turbulent natural convection mass transfer coefficient can be derived in terms of the heat transfer coefficient,  $h_2$ , from Equation (3.5-129) such that

$$h_{2s} = h_2 \left( \frac{\zeta}{k_D} \right) \left( \frac{\alpha_D}{\zeta} \right)^{1/3} \quad (3.5-148)$$

where  $\alpha_D$  is the thermal diffusivity in the gas dome.

Equation (3.5-148) can then be substituted in place of  $(\zeta/L)$  in Equation (3.5-146) to give

$$\dot{M}_{vap} = h_2 \left( \frac{\zeta}{k_n} \right) \left( \frac{\alpha_n}{\zeta} \right)^{1/3} \left( \frac{A_i}{P} \right) \{ \bar{P}_s \bar{p}_s \left[ \kappa_s \frac{h_{fg}}{T_g v_{fg}} - \beta_s \right] + \bar{p}_s \left( \frac{h_{fg}}{T_g v_{fg}} \right) \} (T_f - T_g) \quad (3.5-149)$$

which gives the rate at which water vapor is transported into the accumulator gas dome by turbulent diffusion.

Since the energy transported to the gas dome by the vaporization process must come from the liquid and since the energy per unit mass required for vaporization is  $h_{fg}$ , then the rate of energy transport to the gas dome by vaporization is

$$\dot{Q}_{\text{vap}} = \dot{M}_{\text{vap}} h_g(T_f) \quad (3.5-150)$$

where  $\dot{M}_{\text{vap}}$  is the rate of vaporization at the liquid gas interface.

In the gas dome, as the accumulator blows down, the gas temperature decreases and condensation of water vapor occurs. The rate of condensation may be approximated by assuming that the gas dome remains at 100% humidity and by considering simple humidity relationships. The humidity ratio can be written as

$$w = \frac{M_s}{M_n} = \frac{N_s P_s}{N_n P_D} \quad (3.5-151)$$

where

$M_s, M_n$  = water vapor, gas masses, respectively

$N_s, N_n$  = water vapor, gas molecular weights, respectively

Taking the derivative of Equation (3.5-151) gives

$$\frac{dM_s}{dt} = \frac{1}{P} \left( M_n \frac{N_s}{N_n} \frac{dP_s}{dt} - M_s \frac{dP}{dt} \right) \quad (3.5-152)$$

From equal Gibb's free energy, the equilibrium relationship between the vapor and liquid condensate in the dome is

$$v_s(P_s, T_g) \frac{dP_s}{dT_g} - S_s(P_s, T_g) = v_f(P, T_g) \frac{dP}{dT_g} - S_f(P, T_g) \quad (3.5-153)$$

and substituting the relationship

$$\frac{dP}{dt} = \frac{dP}{dT} \frac{dT}{dt} \quad (3.5-154)$$

into Equation (3.5-153) and rearranging gives

$$\frac{dP_s}{dt} = \frac{v_f(P, T_g)}{v_s(P_s, T_g)} \frac{dP}{dt} - \frac{h_g(P_s, T_g) - h_f(P, T_g)}{T_g v_g(P_s, T_g)} \frac{dT_g}{dt} \quad (3.5-155)$$

Combining Equations (3.5-152) and (3.5-151) with Equations (3.5-124) and (3.5-125) gives

$$\frac{dM_s}{dt} = \frac{1}{P} \left( M_n \frac{N_s}{N_n} - M_s \right) \frac{v_f(P, T_g)}{v_s(P_s, T_g)} \frac{1}{V_D} \left[ Q_D \frac{R_n}{C_v} - P \left( 1 + \frac{R_n}{C_v} \right) \frac{dV_D}{dt} \right] + \frac{1}{P N_n} \left( \frac{h_g(P_s, T_g) - h_f(P, T_g)}{T_g v_g(P_s, T_g)} \right) \frac{1}{C_{v,n}} \left( Q_D - P \frac{dV_D}{dt} \right) \quad (3.5-156)$$

and the rate of condensate formation is given as

$$\dot{M}_c = - \frac{dM_s}{dt} + \dot{M}_{vap} \quad (3.5-157)$$

The energy transported by the condensate to the interface is expressed as

$$\dot{Q}_{m_c} = \dot{m}_c h_f^s(T_g) \quad (3.5-158)$$

Also, since the condensation is taking place in the gas dome, the energy given up by the condensation process is given up to the gas dome at the rate expressed as

$$\dot{Q}_{M_c} = \dot{M}_c h_{fg}(T_g) \quad (3.5-159)$$

Finally, since it is assumed that the condensate is transported to the interface at the condensation rate,

$$\dot{m}_c = \dot{M}_c \quad (3.5-160)$$

the net energy given up to the gas dome by the condensation process can be expressed as

$$\dot{Q}_c = \dot{Q}_{M_c} - \dot{Q}_{m_c} = \dot{m}_c (h_{fg}(T_g) - h_f^s(T_g)) \quad (3.5-161)$$

### 3.5.7.4 Energy Transported to the Gas Dome by Combined Heat and Mass Transfer.

The total energy transported to the gas dome can be rewritten by combining Equations (3.5-126), (3.5-127), (3.5-129), (3.5-150), and (3.5-161) and summing to give

$$\dot{Q}_D = (h_1 A_1 + h_2 A_2) (T_w - T_g) + h_2 A_2 (T_f - T_g) + \dot{M}_{vap} h_g^s(T_f) + \dot{m}_c (h_{fg}(T_g) - h_f^s(T_g)) \quad (3.5-162)$$

**3.5.7.5 Numerical Implementation.** The numerical scheme used for the accumulator model includes special features for coupling the solution scheme to the main code in such a way that it is time step independent. This scheme is semi-implicit, and special considerations are employed to preserve the

nitrogen energy and mass. Since a spherical accumulator has a variable cross-sectional area, the momentum equation is generalized to the case of a variable flow area.

The numerical scheme uses finite-difference techniques to solve the differential equations. The momentum equation is formulated by integrating Equation (3.5-121) over space and writing the time variation in difference form as

$$\begin{aligned} & \left[ \rho_f (L_{f_L} + L_{f_{TK}}) \left( \frac{A_L}{A_f} \right) + F_f \Delta t + \rho_g (L_{g_L} + L_{g_{TK}}) \left( \frac{A_L}{A_g} \right) + F_g \Delta t \right] v_{f_L}^{n+1} \\ &= - (P^{n+1} - P_D^{n+1}) \Delta t + \Delta P_z \Delta t + [\rho_f L_{f_L} + L_{f_{TK}} \left( \frac{A_L}{A_f} \right) \\ &+ \rho_g (L_{g_L} + L_{g_{TK}}) \left( \frac{A_L}{A_g} \right)] v_{f_L}^n - \text{CONVF} - \text{CONVG} \end{aligned} \quad (3.5-163)$$

where  $P^{n+1}$  is the pressure downstream from the accumulator junction. The inertia term is represented by

$$\rho_f (L_{f_L} + L_{f_{TK}}) \left( \frac{A_L}{A_f} \right) + \rho_g (L_{g_L} + L_{g_{TK}}) \left( \frac{A_L}{A_g} \right) \quad (3.5-164)$$

where  $L_{f_L}$ ,  $L_{f_{TK}}$ ,  $L_{g_L}$ , and  $L_{g_{TK}}$  are the lengths of the liquid and gas in the discharge line and tank, respectively,  $A_L$  is the area of the discharge line, and  $A_f$  and  $A_g$  are the mean flow areas in the tank and discharge line of the liquid and gas, respectively. In the case of a spherical tank,  $A_g$  used in the gas inertia term is obtained from the relation

$$L_{g_{TK}} A_g = V_{g_{TK}} \quad (3.5-165)$$

and  $A_f$  used in the liquid inertia term is obtained from the relation

$$L_{f_{TK}} A_f = V_{f_{TK}} \quad (3.5-166)$$

where  $V_{g_{TK}}$  and  $V_{f_{TK}}$  are the gas and liquid volumes, respectively. The volume of gas in the tank is

$$V_{g_{TK}} (L_{g_{TK}}) = \frac{\pi}{3} L_{g_{TK}}^2 (3R - L_{g_{TK}}), \quad (3.5-167)$$

and the available volume of liquid in the tank is

$$V_{f_{TK}}(L_{g_{TK}}) = \frac{4\pi}{3}R^3 - V_{g_{TK}} - \frac{\pi}{3}L_{min}^2(3R - L_{min}), \quad (3.5-168)$$

where  $L_{min}$  is the minimum liquid level that is determined by the position of the discharge line which may protrude into the tank. The inertia terms are computed at each time step and vary explicitly with time; as the accumulator blows down, the inertia term changes from a liquid-dominant to a vapor-dominant term.

The liquid and gas friction terms, respectively, are formulated as

$$F_f = \frac{\rho_g}{2} \left( \lambda \frac{L_{fL}}{D_L} + K_L \frac{L_{fL}}{L_L} \right) v_{fL}^n \quad (3.5-169)$$

for the liquid, and

$$F_g = \frac{\rho_g}{2} \left( \lambda \frac{L_{gL}}{D_L} + K_L \frac{L_{gL}}{L_L} \right) v_{gL}^n \quad (3.5-170)$$

for the vapor, where friction is neglected in the tank and the line friction factor is assumed to be the constant turbulent-turbulent Darcy friction factor given as

$$\lambda = \left[ 1.74 - 2 \log_{10} \frac{2\epsilon}{D} \right]^{-2} \quad (3.5-171)$$

The loss factor term,  $K_L$ , is assumed to be distributed over the discharge line length,  $L_L$ . The term  $D_L$  is the surge line hydraulic diameter, and  $\epsilon$  is the discharge line wall roughness. The elevation head term,  $\Delta P_z$ , is formulated as

$$\Delta P_z = - \frac{g \Delta z_{TK} \left( \rho_f L_{f_{TK}} + \frac{1}{2} \rho_g L_{g_{TK}} \right)}{L_{TK}} - \frac{g \Delta z_L \left( \rho_f L_{f_L} + \rho_g L_{g_L} \right)}{L_L} \quad (3.5-172)$$

where  $\Delta z_{TK}$  and  $\Delta z_L$  are the tank and surge line elevation changes, respectively, and  $g$  is the gravitational acceleration. The liquid and vapor momentum flux terms, CONVF and CONVG, respectively are formulated in linear implicit form as

$$CONVF = \frac{1}{2} \rho_f \left[ 1 - \left( \frac{A_L}{A_f} \right)^2 \right] \Delta t v_{fL}^n \left( 2v_{fL}^{n+1} - v_{fL}^n \right) \quad (3.5-173)$$

if there is liquid in the tank,

$$\text{CONVF} = 0.0 \quad (3.5-174)$$

where there is no liquid in the tank,

$$\text{CONVG} = \frac{1}{2} \rho_g \left[ \left( \frac{A_L}{A_f} \right)^2 - \frac{1}{4} \left( \frac{A_L}{A_g} \right)^2 \right] \Delta t v_{g_L}^n \left( 2v_{g_L}^{n+1} - v_{g_L}^n \right) \quad (3.5-175)$$

if there is vapor in the discharge line, and, finally

$$\text{CONVG} = 0 \quad (3.5-176)$$

where there is no vapor in the discharge line. In the case of a spherical tank, the value of  $A_{TK}$  used in CONVF is the flow area at the liquid-gas interface, and the value of  $A_{TK}$  used in CONVG is the mean flow area of the tank. In this formulation, the momentum equation is solved over the pressure gradient from the centroid of the gas dome to the accumulator junction. However, the momentum of the fluid downstream from the accumulator junction is not included. Flow begins when the pressure, gravity, and friction forces result in positive flow out of the accumulator; and flow ceases when these forces result in reverse flow. Also, since fluxing of the gas through the junction is not allowed,

$$v_{g_L}^n = v_{f_L}^n \quad (3.5-177)$$

until the accumulator empties of liquid. The effect of this formulation is that as the accumulator blows down, the liquid-gas interface moves out of the accumulator tank and surge line. Thus, the centroid of the gas dome moves towards the centroid of the combined tank and surge line.

The pressure solution is obtained by combining Equations (3.5-119) and (3.5-123) and multiplying by  $R_n / C_{v,n}$ , which results in

$$M_n R_n \frac{dT}{dt} = - \frac{R_n P dV_D}{C_{v,n} dt} + \frac{R_n}{C_{v,n}} \dot{Q}_D \quad (3.5-178)$$

where  $\dot{Q}_D$  is given by Equation (3.5-162).

Since the liquid is incompressible,

$$\frac{dV_D}{dt} = - \frac{dV_f}{dt} = A_L v_{f_L}; \quad (3.5-179)$$

and substitution into Equation (3.5-125) and expanding in nonconservative finite difference form gives

$$P^n \left( 1 + \frac{R_n}{C_{v,n}} \right) A_L \Delta t v_{f_L}^{n+1} + V_D^n (P^{n+1} - P^n) = \frac{R_n}{C_{v,n}} Q_D^n \Delta t \quad (3.5-180)$$

The energy equation may then be solved directly for the new time gas temperature by combining Equations (3.5-122), (3.5-125), and (3.5-180) and integrating, which gives

$$T_g^{n+1} = T_g^n e^{\left( \frac{R_n}{C_{v,n}} \ln \frac{V_D^n}{V_D^{n+1}} + \Delta t \frac{R_n}{C_{v,n} P^n V_D^n} Q_D^n \right)} \quad (3.5-181)$$

The algorithm used to track the liquid level is based on the tank mass balance which is given by

$$A_L v_{f_L} = -A_{TK} \frac{dL_{g_{TK}}}{dt} \quad (3.5-182)$$

In the case of a spherical tank,  $A_{TK}$  is given by

$$A_{TK} = \pi L_{g_{TK}} (2R - L_{g_{TK}}) \quad (3.5-183)$$

Given  $L_{g_{TK}}^n$  Equation (3.5-182) is solved by explicit numerical integration to obtain  $L_{g_{TK}}^{n+1}$ ,

$$L_{g_{TK}}^{n+1} = L_{g_{TK}}^n - \frac{A_L v_{f_L}^{n+1} \Delta t^{n+1}}{\pi L_{g_{TK}}^n (2R - L_{g_{TK}}^n)} \quad (3.5-184)$$

### 3.5.8 ECC Mixer

In order to calculate the process of mixing of a jet of cold water injected into a two-phase mixture and the resulting steam condensation that follows, as in the case of emergency core cooling (ECC) injection in a PWR, a special component model, called ECCMIX, has been introduced into RELAP5/MOD3.

**3.5.8.1 ECCMIX Component.** An ECC mixing component is a specialized branch that requires three junctions with a certain numbering order. The physical extent of the ECCMIX component is a length of the cold leg pipe centered around the position of the ECC injection location. The length of this segment should be about three times the inside diameter of the cold leg pipe. Junction number one is the ECC connection, junction number two is the cold leg cross section through which flow enters this component in normal reactor operation, and junction number three is the one that leads to the reactor vessel. A schematic vertical cross section of an ECCMIX component is shown in Figure 3.5-24. The geometrical description of the ECCMIX component is very similar to that of the JETMIXER component except for the specification of an angle for the ECC pipe connection.

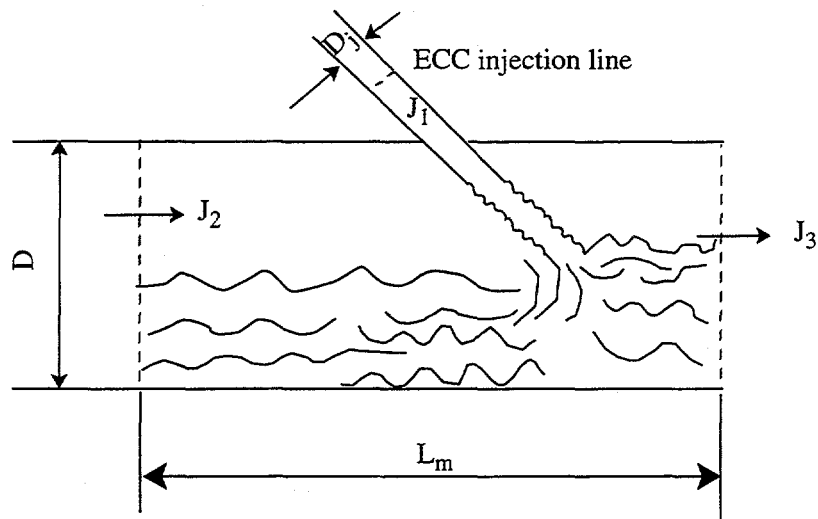


Figure 3.5-24 ECCMIX component.

The computational model for ECCMIX employs a particular flow regime map for condensation and, for each flow pattern, uses a different correlation for interfacial heat transfer to calculate  $h_{if}$ , as described in detail in the following subsections. The ECCMIX component calculations are evoked only if there is subcooled ECC injection and if there is any steam to be condensed in that component. Otherwise, the ECCMIX component is treated as an ordinary BRANCH in the RELAP5 calculations.

**3.5.8.2 Flow Regimes in Condensation.** Prior to the introduction of the ECCMIX component, RELAP5 included three flow regime maps, as described in the RELAP5/MOD2 manual<sup>3.5-10</sup> and in RELAP5/MOD2 models and correlations report.<sup>3.5-11</sup> However, neither of those would apply specifically to the condensation process. A flow regime map for condensation inside horizontal tubes is reported by Tandon et al.,<sup>3.5-12</sup> and it was considered a more suitable basis for interfacial heat transfer calculation in condensation. A detailed description of the resultant ECC mixer volume flow regime map is found in Section 3.3.4 of this volume of the manual.

The variable names that are used in the coding for the coordinates of the condensation flow regime map are

$$\text{voider} = (1.0 - \alpha)/\alpha \quad (3.5-185)$$

$$\text{stargj} = v_g^* = X_f G / [g D \rho_g (\rho_f - \rho_g)]^{1/2} \quad (3.5-186)$$

These variables are also described in more detail in Section 3.3.4.

**3.5.8.3 Vapor Mass Flux and Liquid Velocity in ECCMIX.** Before describing the calculational procedure for any of those patterns, it should be mentioned how the vapor mass flux and liquid velocity inside the ECCMIX component are calculated.

**3.5.8.3.1 Vapor Mass Flux in ECCMIX**--A volume-averaged vapor mass flux ( $X_f G$ ) must be determined before the variable  $v_g^*$  can be calculated.

$$X_f G = (|W_{g2}| + |W_{g3}|)/(2.0A) \quad (3.5-187)$$

where

$$\begin{aligned} W_{g2} &= \text{the total vapor flow rate at junction 2} \\ &= \alpha_{gj2} \rho_{gj2} v_{gj2} A_{j2} \\ W_{g3} &= \text{the total vapor flow rate at junction 3} \\ &= \alpha_{gj3} \rho_{gj3} v_{gj3} A_{j3} \\ A &= \text{cross-sectional area of the ECCMIX component.} \end{aligned}$$

**3.5.8.3.2 Liquid Velocity in ECCMIX**--The liquid velocity that is used for determining the Reynolds number inside the ECCMIX component is calculated on the basis of the smallest of the absolute values of the axial liquid velocity at either end of the ECC mixer and the additional contribution of the liquid jet from the ECC connection line. The impact of the incoming ECC liquid jet is a function of the jet velocity  $v_{jet}$  and the difference between the pressure in the hydraulic cell upstream of the injection port and the pressure in the ECCMIX component,  $\Delta P_{jet}$ .

$$\Delta I_{jet} = 2.0 \Delta P_{jet} / \rho_{fjet} + v_{jet}^2 \quad (3.5-188)$$

and

$$v_{fres} = [\Delta I_{jet} + v_{fim}^2]^{1/2} \quad (3.5-189)$$

where

$$v_{fim} = \min (|v_{fj2}|, |v_{fj3}|).$$

$v_{fres}$  is the resultant liquid velocity that is used to determine the liquid Reynolds number in heat transfer and interfacial friction calculations.

**3.5.8.4 Interfacial Heat Transfer Rates.** The two-fluid model in RELAP5/MOD3 requires formulation of heat exchange between either phase and the interface. These are expressed as

$$Q_{ik} = H_{ik} (T^s - T_k) \quad (3.5-190)$$

where

$k$  = f or g for liquid and vapor, respectively

$H_{ik}$  = volumetric interfacial heat transfer coefficient for phase k

=  $h_{ik} \cdot A_i$

$h_{ik}$  = interfacial heat transfer coefficient for phase k

$A_i$  = interfacial area per unit volume

$T^s$  = saturation temperature

$T_k$  = phasic bulk temperature.

As implied in Equation (3.5-190), the interface is assumed to be at saturation temperature, corresponding to the vapor pressure. In condensation of saturated steam, there is almost no temperature difference between vapor and the interface, while there is a very high rate of heat transfer from the steam to the interface (through mass transfer). For this reason, the volumetric heat transfer coefficient between vapor and the interface is set to a high constant value of  $10^7$  W/m<sup>3</sup>·K.

The limiting factor is the rate of heat transfer to liquid,  $H_{if}$ . According to Equation (3.5-190),  $H_{if}$  varies with the heat transfer coefficient,  $h_{if}$ , and the interfacial area per unit volume,  $A_i$ , both of which depend on the two-phase flow pattern. The interfacial area,  $A_i$ , and the local heat transfer coefficient for the interface-to-fluid,  $h_{if}$ , are calculated with different equations for the six basic flow patterns that are identified in Table 3.3-1.

**3.5.8.4.1 Heat Transfer to Liquid in the Six Basic Flow Patterns**--The basic modes of heat transfer to liquid are designed as:

- $H_{ifb1}$  for wavy flow
- $H_{ifb2}$  for plug flow
- $H_{ifb3}$  for slug flow
- $H_{ifb4}$  for bubbly flow

- $H_{ifb5}$  for annular/annular-mist flow
- $H_{ifb6}$  for dispersed droplet flow.

### Heat Transfer in Wavy Flow

#### Interfacial Area

Wavy flow inside a horizontal tube is regarded as a kind of horizontally stratified flow for the purpose of interfacial contact and exchanges between vapor and liquid. With this assumption, the interfacial (contact) area between the liquid and vapor is calculated from the geometrical dimensions of the ECCMIX component, vapor void fraction, and the diameter of the ECC injection pipe. **Figure 3.5-25** and **Figure 3.5-26** show schematic cross sections of the flow topology inside the ECCMIX component in two vertical planes.

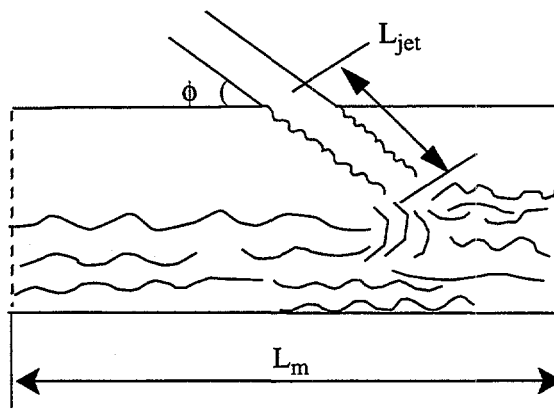


**Figure 3.5-25** Schematic cross section of stratified flow along the ECCMIX component, showing the length of interface,  $L_m$ , and the jet length,  $L_{jet}$ .

The volume-average vapor void fraction,  $\alpha_g$ , is used to determine the width of the liquid surface that is a function of the half-angle,  $\theta$ , facing the free surface. RELAP5 uses a particular function, called HTHETA, to calculate  $\theta$  for a given volume fraction that is bound by  $\theta$ . If the liquid level is above the pipe center ( $\alpha_g < \alpha_f$ ), then HTHETA is called with  $\alpha_g$  as an argument and  $\theta$  is calculated. However, if  $\alpha_g > \alpha_f$ , then  $\alpha_f$  is used as an argument for calculating  $\theta$ . For this reason, care is taken to calculate the length of the liquid jet,  $L_{jet}$ , differently for these cases, as the cylindrical surface of the liquid jet is also a part of the condensation surface. The jet surface area is given by

$$A_{jet} = \pi d_{jet} \cdot L_{jet} \quad (3.5-191)$$

where

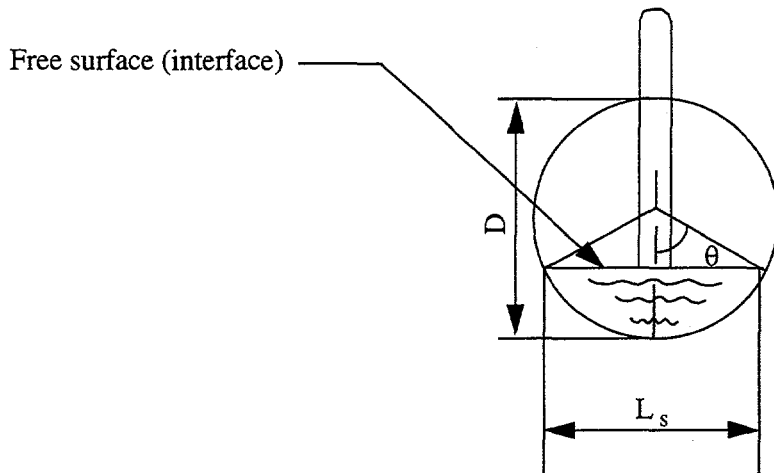


**Figure 3.5-26** Schematic vertical cross section of the ECCMIX component, showing the width of liquid surface,  $L_s$ , and the tending half-angle,  $\theta$ .

$$L_{jet} = 0.5D \frac{(1.0 - \cos \theta)}{\sin \phi} \quad \text{if } \alpha_g < \alpha_f \quad (3.5-192)$$

$$L_{jet} = 0.5D \frac{(1.0 - \cos \theta)}{\sin \phi} \quad \text{if } \alpha_g \geq \alpha_f. \quad (3.5-193)$$

The interfacial contact area per unit volume, in this case, is the sum of the jet surface area and the rectangular horizontal interface area minus the impinging area of the jet, all divided by the component volume.

$$A_{i1} = [A_{jet} + L_m D \sin \theta - (s_{jet} / \sin \phi)] / (A_m L_m) \quad (3.5-194)$$

where

$$s_{jet} = \text{cross-sectional area of the liquid jet.}$$

A minimum value for  $A_{i1}$  that is used in the code is  $1/2 \pi \cdot d_{jet} L_m / (A_m \cdot L_m)$ .

#### Heat Transfer Coefficient

The heat transfer coefficient for wavy flow is calculated according to an experimentally established correlation by Lim, Bankoff, Tankui, and Yuen,<sup>3.5-13</sup> based on their data from condensation in cocurrent flow of vapor and liquid in a horizontally stratified flow situation. The correlation that is taken from Reference 3.5-13 is the one that is recommended for the case of rough liquid surface, namely

$$Nu = 0.0344 (Re_g)^{0.58} (Re_f)^{0.42} (Pr_f)^{0.33} \quad (3.5-195)$$

where

$Nu$  = Nusselt number

$Re$  = Reynolds number

$Pr$  = Prandtl number (see nomenclature).

Using this correlation for Nusselt number, the overall heat transfer coefficient from the interface to liquid, per unit volume, in wavy flow is expressed as

$$H_{ifb1} = A_{i1} Nu \left( \frac{k_{fm}}{D} \right) \quad (3.5-196)$$

### Heat Transfer in Plug Flow

#### Interfacial Area

According to the flow regime map (Figure 3.3-4), this flow pattern exists for vapor void fractions between 0.25 and 0.666. It is assumed that the interfacial area changes from completely stratified at voider = 0.5 ( $\alpha_g = 0.666$ ) to a complete circular cross section of the ECCMIX component at voider = 3.0 (for  $\alpha = 0.25$ ). Hence, the interface area is interpolated between these limits, using the following parameter

$$tv1 = 0.4 (\text{voider} - 0.5) \quad \text{for } 0.5 < \text{voider} < 3.0 \quad (3.5-197)$$

The interfacial area for the stratified flow condition is calculated according to Equation (3.5-194), and the interpolated area for wavy flow is

$$A_{i2} = (1.0 - tv1) A_{i1} + tv1 / L_m \quad (3.5-198)$$

#### Heat Transfer Coefficient

Since plug flow is considered an extension of the wavy flow pattern with interrupting liquid plugs, the same heat transfer coefficient that was used for wavy flow, Equation (3.5-195), has been used for plug flow. Hence, the overall heat transfer coefficient from interface to liquid, per unit volume, in plug flow is

$$H_{ifb2} = A_{i2} Nu \left( \frac{k_{fm}}{D} \right) \quad (3.5-199)$$

in which  $Nu$  is given by Equation (3.5-195).

## Heat Transfer in Slug Flow

### Interfacial Area

Slug flow is assumed to always include some contribution of the bubbly flow pattern; hence, there is a gradual changeover from slug flow to a pure bubbly flow. The degree of this transition depends on vapor void fraction. This approach is used for all volumes in RELAP/MOD3 (see Volume IV). There is only a slight modification in the application of this approach to the ECCMIX component, that is, the lower limit of vapor void fraction is set at  $\alpha_b = 0.20$  and the upper end void fraction is set at  $\alpha_c = 0.666$ . These changes had to be imposed according to the limits specified for slug flow in the modified flow regime map for condensation, as shown in **Figure 3.3-4**.

The interfacial area of slug bubbles (these are called Taylor bubbles in **Reference 3.5-11**) per unit volume is calculated as

$$A_{i3s} = 4.5 \frac{\alpha_s}{D} \quad (3.5-200)$$

where

$$\alpha_s = \frac{(1 - \alpha_g) - \alpha_{bb}}{1 - \alpha_{bb}} \quad (3.5-201)$$

$$\alpha_{bb} = \alpha_b \exp \left\{ - \left[ \frac{6.778}{\alpha_c - \alpha_b} (\alpha_g - \alpha_b) \right] \right\}. \quad (3.5-202)$$

The numerical value of  $\alpha_{bb}$  varies from 0.2 ( $= \alpha_b$ ) when  $\alpha_g = \alpha_b$  to about 0.0002277 when  $\alpha_g = \alpha_c$ . As a result,  $A_{i3s}$  varies from 0.0 at  $\alpha_g = 0.2$  to about  $4.5(1.0 - \alpha_g)/D_c$  for  $\alpha_g = \alpha_c$ .

The variable  $\alpha_{bb}$  is also used to calculate the contribution of the small bubbles to the interfacial area, for both heat and shear transfer calculations. The calculation of bubble flow area, average bubble diameter and hydraulic diameter, as a function of  $\alpha_g$  and  $\alpha_{bb}$ , are performed in a subroutine called FIDIS. This is a part of RELAP5/MOD3 and is documented in Volume IV.

### Heat Transfer Coefficient

For the slug part, the heat transfer coefficient is calculated for the Taylor bubbles moving through liquid. The correlation that is explained in Volume IV, is

$$Nu_{tb} = 1.18942 [Re_{tb}Pr]^{0.5} \quad (3.5-203)$$

where

$$Re_{tb} = \rho_f D \min (|v_g - v_f|, 0.8) / \mu_f \quad (3.5-204)$$

The overall heat transfer coefficient from the interface to the liquid, per unit volume, in slug flow is

$$H_{ifb3} = A_{i3s} N u_{tb} \left( \frac{k_{fm}}{D} \right) + H_{ifb4} \quad (3.5-205)$$

in which  $H_{ifb4}$  is the contribution of the heat transfer by small bubbles in slug flow, and is calculated by consecutive calls to two of the existing subroutines in RELAP5/MOD3, namely FIDIS and HIFBUB, according to the procedure that is described in the following section.

### Heat Transfer in Bubbly Flow

#### Interfacial Area

The interfacial area per unit volume for bubbly flow in the ECCMIX component is calculated in the same manner that is done for all other components in RELAP5/MOD3, as documented in Volume IV. The interfacial area per unit volume for bubbles is

$$A_{i4} = \frac{0.72 \alpha_g \rho_f (v_g - v_f)^2}{\sigma} \quad (3.5-206)$$

The derivation of this equation and the assumptions used in its derivation are given in Volume IV of this manual. Among other things, it is assumed that the average bubble diameter is  $0.5 d_{max}$  and that  $d_{max}$  is determined by using a critical Weber number of  $Wec = 10$ . Computation of  $A_{i4}$  is done by using the FIDIS subroutine in RELAP5.

#### Heat Transfer Coefficient

For the bubbly flow regime, the heat transfer coefficient between the interface and liquid is calculated with a model based on the modified Unal bubble collapse model<sup>3.5-14,3.5-15</sup> and the Lahey model.<sup>3.5-16</sup> This is the same model that is used in non-ECCMIX volumes.

The heat transfer coefficient between the interface and liquid, per unit volume, in bubbly flow that is calculated in the HIFBUB subroutine is according to the following equation:

$$H_{ifb4} = \frac{F_5 \alpha_g h_{fg} \rho_f \rho_g}{\rho_f - \rho_g} \quad (3.5-207)$$

where

$$F_5 = 0.075 \quad \text{for } \alpha_{bub} \geq 0.25 \quad (3.5-208)$$

$$F_5 = 1.8 \phi C \exp(-45\alpha_{bub}) + 0.075 \quad \text{for } \alpha_{bub} < 0.25 \quad (3.5-209)$$

$$C = 65.0 - 5.69 \times 10^{-5} (P - 1.0 \times 10^5) \quad \text{for } P \leq 1.1272 \times 10^6 \quad (3.5-210)$$

$$C = 2.5 \times 10^9 P^{-1.418} \quad \text{for } P > 1.1272 \times 10^6 \quad (3.5-211)$$

$$\phi = 1.0 \quad \text{for } |v_f| \leq 0.61 \text{ m/s} \quad (3.5-212)$$

$$\phi = [1.639344 |v_f|]^{0.47} \quad \text{for } |v_f| > 0.61 \text{ m/s} \quad (3.5-213)$$

$$\alpha_{\text{bub}} = \max(\alpha_g, 10^{-5}). \quad (3.5-214)$$

### Heat Transfer in Annular/Annular-Mist Flow

Heat transfer between interface and liquid in the annular and annular-mist flow regimes is calculated according to the procedures that are used in TRAC-BF1.<sup>3.5-17,3.5-18</sup> According to this model, the interfacial exchanges of heat and momentum at the interface have two components, one at the interface between the vapor core and the liquid film on the walls and another one at the interface between the vapor and the entrained liquid droplets. The contribution of the entrained droplets is minimal at the start of the annular flow, but the entrained liquid fraction increases with increasing vapor velocity and it becomes 100% at the end of the annular flow, that is the start of dispersed droplet (mist) flow. Variations of the entrainment fraction serve as an interpolation mechanism in the calculation of interfacial exchanges between the annular and droplet flows.

#### Liquid Droplet Entrainment Fraction

The fraction of liquid flow entrained as droplets is calculated with the following equation recommended by Andersen et al.<sup>3.5-18,3.5-19</sup>

$$E_f = \frac{X_e - 0.03}{[1.0 + (X_e + 0.1)^2]^{0.5}} \quad (3.5-215)$$

in which

$$X_e = 1.0^{-6} \cdot j_g^{* 2.5} D^{* 1.25} Re_{\text{rel}}^{0.25} \quad (3.5-216)$$

where

$$D^* = D[g(\rho_f - \rho_g)/\sigma]^{1/2} \quad (3.5-217)$$

$$j_g^* = \frac{\alpha_g v_g}{\left[ \frac{\sigma g (\rho_f - \rho_g)}{\rho_g^2} \left( \frac{\rho_g}{\rho_f - \rho_g} \right)^{0.667} \right]^{0.25}} \quad (3.5-218)$$

$$Re_{rel} = \alpha_f \rho_f v_f D / \mu_f \quad (3.5-219)$$

A vapor void fraction for the vapor droplet mixture of the core is calculated as

$$\alpha_{dc} = 1.0 - (1.0 - \alpha_g) E_f \quad (3.5-220)$$

and a vapor void fraction corresponding to the liquid in the film alone is calculated as

$$\alpha_f = 1.0 - (1 - \alpha_g) (1 - E_f) \quad (3.5-221)$$

With these definitions, the two components of interfacial area and heat transfer are calculated in the following way:

#### Film Interfacial Area

The average film thickness is

$$\delta_f = 0.5 D (1.0 - \alpha_f)^{0.5} \quad (3.5-222)$$

A minimum film thickness is calculated as<sup>3.5-18,3.5-19</sup>

$$\delta_{fmin} = \left( \frac{18 \mu_f^2 \sigma}{g^2 \rho_f^3} \right)^{0.2} \quad (3.5-223)$$

The average film thickness is selected as

$$\delta_{fa} = \max(\delta_f, \delta_{fmin}) \quad (3.5-224)$$

A void fraction corresponding to  $\delta_{fmin}$  is calculated as

$$\alpha_{min} = \left( 1.0 - \frac{2\delta_{fmin}}{D} \right)^2 \quad (3.5-225)$$

Since the inside diameter of the liquid film is related to the inside diameter of the channel,  $D_c$ , through  $\alpha_f$  by the relationship  $D_i = D_c(\alpha_f)^{1/2}$ , the interfacial area per unit volume for the liquid film is then

$$A_{isf} = 4.0 \frac{(\alpha_f)^{1/2}}{D} \quad (3.5-226)$$

If  $\alpha_{\min} < \alpha_g$ , then

$$A_{isf} = 4 \frac{(\alpha_f)^{1/2}}{D} \frac{1.0 - \alpha_f}{1.0 - \alpha_{\min}} \quad (3.5-227)$$

### Droplet Interfacial Area

According to **Reference 3.5-19**, an average droplet diameter is calculated based on the total mass flux,  $j_{mt}$

$$j_{mt} = |\alpha_g v_g + (1 - \alpha_g) v_f| \quad (3.5-228)$$

The relative droplet velocity is

$$v_{drop} = 1.414 \left[ \frac{g \sigma \Delta \rho}{\rho_f^2} \right]^{0.25} \quad (3.5-229)$$

However, if

$$j_{mt} > 1.456 \left[ \frac{g \sigma \Delta \rho}{\rho_g^2} \right]^{0.25} \left[ \frac{\mu_g^2}{\sigma \rho_g \sqrt{\sigma / (g \Delta \rho)}} \right]^{-1/12} \quad (3.5-230)$$

then

$$v_{drop} = \frac{3\sigma}{\rho_g} \left[ \frac{(g \Delta \rho)^2}{\mu_g \rho_g} \right]^{0.33} j_{mt}^{-2} \quad (3.5-231)$$

These are based on Ishii's work.<sup>3.5-20</sup> The droplet velocity is used to calculate the average droplet diameter, based on a critical Weber number of 2.7

$$D_{drop} = \frac{2.7\sigma}{\rho_g \cdot \max(v_{drop}^2, j_{mt}^2)} \quad (3.5-232)$$

In order to avoid physically unrealistic values for  $D_{drop}$ , it is compared to some limiting values and adjusted if necessary. These are:

- If  $D_{drop} < 2.0 \times 10^{-4}$  m, then  $D_{drop} = 2.0 \times 10^{-4}$  m

- If  $D_{drop} > 0.25 D_c$ , then  $D_{drop} = 0.25 D_c$ .

Another limit on  $D_{drop}$  is that of no more than  $10^6$  droplets per cubic meter, which gives

$$D_{drop} \leq D_{drop1} = \left[ 6 \frac{1 - \alpha_g}{10^6 \pi + 1} \right]^{0.333} \quad (3.5-233)$$

The adjusted droplet diameter is then used to calculate the droplet interfacial area per unit volume, that is

$$A_{i6} = 6 \frac{1.0 - \alpha_{dc}}{D_{drop}} \quad (3.5-234)$$

#### Film Interfacial Heat Transfer Coefficient

The heat transfer coefficient at the film interface is calculated according to **Reference 3.5-18** with the following equation that is based on Megahed's work.<sup>3.5-21</sup>

$$h_{iff} = \frac{0.0771 C_{pf} \dot{m}_f}{\pi D_{if} (j_{ax} Re_{ff})^{2/3}} \left( \frac{g \rho_f^2}{\mu_f^2} \right)^{1/3} \quad (3.5-235)$$

in which  $\dot{m}_f$  is the film mass flow rate and  $Re_{ff}$  is the Reynolds number based on that flow. These variables and  $j_{ax}$  are given below

$$\dot{m}_f = (1 - E_f) (1 - \alpha_g) \rho_f v_f A_m \quad (3.5-236)$$

$$j_{ax} = \frac{C_{pf} (T^s - T_f)}{h_{fg}} (\rho_f / \rho_g)^{1/2} \quad (3.5-237)$$

$$Re_{ff} = \frac{4 \dot{m}_f}{\mu_f \pi D} \quad (3.5-238)$$

The inside film diameter,  $D_{if}$ , that is used in Equation (3.5-235) is considered to be more relevant to the interface than  $D$  that has been used in TRAC-BF1 coding of this equation.

#### Droplet Interfacial Heat Transfer Coefficient

The heat transfer coefficient for interface to droplets is

$$h_{id} = 1.8 \pi^2 k_f / D_{drop} \quad (3.5-239)$$

This equation is based on the works of Andersen et al.<sup>3.5-22</sup>

Hence, for annular-mist flow, including droplet entrainment, the overall rate of heat transfer to liquid, per unit volume, is

$$H_{ifb5} = A_{i5f} h_{iff} + A_{i6} h_{id} \quad (3.5-240)$$

### Heat Transfer in Dispersed Droplet Flow

The interfacial area per unit volume and the heat transfer coefficient for droplets were described above. The overall heat transfer rate to liquid in this flow regime is

$$H_{ifb6} = A_{i6} h_{id} \quad (3.5-241)$$

where  $A_{i6}$  and  $h_{id}$  are given by Equations (3.5-234) and (3.5-239), respectively.

**3.5.8.4.2 Heat Transfer to Liquid in Transition Zones**--As shown in Table 3.3-1, there are five transition zones in the modified condensation flow regime map. The numerical values of the heat transfer rates,  $H_{if}$ , in the adjacent zones of the basic mode may vary considerably, and a linear interpolation over the boundary zones would not be adequate to produce a smooth transition. For this reason, an exponential interpolation is employed, as detailed in the following.

For transition between wavy and annular-mist flows,

$$H_{ift1} = H_{ifb5}^{(1-van)} H_{ifb1}^{van} \quad (3.5-242)$$

where

$$van = 9 - 8 v_g^* \quad \text{for } 1 \leq v_g^* \leq 1.125.$$

For transition between wavy and slug flows,

$$H_{ift2} = H_{ifb3}^{psw} H_{ifb1}^{(1-psw)} \quad (3.5-243)$$

where

$$psw = 8 \frac{1-\alpha}{\alpha} - 4 \quad \text{for } 0.5 \leq \frac{1-\alpha}{\alpha} \leq 0.625. \quad (3.5-244)$$

For transition between wavy, plug, and slug flows (double interpolation), first an interpolation is made in terms of  $v_g^*$  and then another one in terms of  $(1 - \alpha)/\alpha$ .

$$H_{ift3} = H_{iftsp}^{p2} H_{ifb1}^{(1-p2)} \quad (3.5-245)$$

where

$$H_{iftsp} = H_{ifb2}^{(1-p1)} H_{ifb3}^{p1} \quad (3.5-246)$$

$$p1 = 400v_g^* - 4. \text{ for } 0.01 \leq v_g^* \leq 0.0125 \quad (3.5-247)$$

$$p2 = 8 \frac{1-\alpha}{\alpha} - 4. \text{ for } 0.5 \leq \frac{1-\alpha}{\alpha} \leq 0.625. \quad (3.5-248)$$

For transition between plug and slug flows

$$H_{ift4} = H_{ifb2}^{(1-pp)} H_{ifb3}^{(1-pp)} \quad (3.5-249)$$

where

$$pp = 400v_g^* - 4. \text{ for } 0.01 \leq v_g^* \leq 0.0125. \quad (3.5-250)$$

Finally, for transition between bubbly and plug flows

$$H_{ift5} = H_{ifb4}^{pb} H_{ifb2}^{(1-pb)} \quad (3.5-251)$$

where

$$pb = \frac{1-\alpha}{\alpha} - 3.0 \text{ for } 3.0 \leq \frac{1-\alpha}{\alpha} \leq 4.0. \quad (3.5-252)$$

Computation of the interfacial heat transfer according to these equations is done in the ECCMXV subroutine, that is called within subroutine PHANTV, whenever the ECCMIX component is encountered and specific logical tests indicate that there is some vapor in this component and a flow of subcooled liquid is entering through the ECC injection line. Otherwise, the ECCMIX component is treated just as a regular BRANCH component in the RELAP5/MOD3 calculations.

**3.5.8.5 Effect of Noncondensable Gases.** It is known that the presence of noncondensable gases, such as air or pure nitrogen, reduces the rate of condensation. An experimental study of the effect of noncondensable gases at different partial pressures on the rate of condensation heat transfer is reported by

DeVuono and Christensen.<sup>3.5-23</sup> According to their findings, the degradation in the condensation heat transfer with concentration of air can be correlated with the following:

$$f_r = (1 - y)^{4.31} \text{ for } 0 < y < 0.14 \quad (3.5-253)$$

where

$f_r$  = reduction factor in condensation heat transfer

$y$  = air concentration (air volume at prevailing pressure and time divided by total volume).

The reduction factor,  $f_r$ , of Equation (3.5-253) is applied to  $H_{if}$  as calculated in the ECCMXV subroutine. It should be noted that the actual plots of measured data reported in Reference 3.5-23 indicate a much stronger sensitivity to air concentration as compared to what can be calculated with their correlation.

**3.5.8.6 Interfacial Friction.** Calculation of the interfacial friction for different flow patterns in the ECCMX component is done with the same correlations that are used for similar flow patterns in all other horizontal components in RELAP5/MOD3. The only remarks to be made on the interfacial friction calculations in the ECCMX components are the following:

- Transition between different flow patterns is according to the modified condensation flow regime map.
- Linear interpolation is used between the friction values of the basic pattern around each interpolation zone, employing the same interpolation variables that were used for interfacial heat transfer in those boundary zones.
- For plug flow, it is assumed that the two phases are locked into each other; hence, the interfacial friction factor is set to 1.

Computation of the interfacial friction factors is performed in a separate subroutine called ECCMXJ, whenever the ECCMX component is encountered and specific logical tests indicate that there is some vapor in the ECCMX component and that a flow of subcooled liquid is entering through the ECC injection line. Otherwise, the ECCMX component is treated just as a regular BRANCH in the RELAP5/MOD3 calculations.

**3.5.8.7 Wall Friction.** The two-fluid model of RELAP5/MOD3 requires that each phase should have its own fraction of the wall friction for momentum balance. The distribution of the total wall friction between vapor and liquid varies with flow regimes. Calculations of the fractions of wall friction for each phase in different flow regimes are done according to the same procedures that are used in other components. However, transition between different flow regimes is determined in the same way that is used for the interfacial heat and momentum transfer calculations. The only differences that are introduced for wall friction in the ECCMX component are the following:

- In bubbly flow, 100% of the wall friction is assigned to the liquid phase and nothing to the vapor phase.
- In droplet flow, 100% of the wall friction is assigned to the vapor phase and nothing to the liquid phase.
- Linear interpolation is used for wall friction over the transition zones, employing the same interpolation variables that were defined for the interfacial heat transfer.

Computations of wall friction fractions for vapor and liquid are performed in parallel with the  $H_{if}$  calculations in the ECCMXV subroutine.

### 3.5.9 Annulus

For an annulus component in the annular mist regime for both the junction and volume flow regimes, the code assumes that all the liquid is in the film and that there are no drops. Thus,  $\alpha_{ff} = \alpha_f$  and  $\alpha_{fd} = 0$ . This was based on work by Schneider<sup>3.5-24</sup> on RELAP5/MOD3 calculations for UPTF Test 6, who showed that this was necessary in order to get downcomer penetration following a cold leg break. In addition, the Bharathan<sup>3.5-25</sup> correlation used in RELAP5/MOD2 was replaced by a standard laminar correlation and the modified Wallis<sup>3.5-26</sup> correlation in the turbulent region for the interfacial drag when in the annular mist flow regime (for either an annulus or any other component). Schneider found this was also necessary in order to get downcomer penetration in UPTF Test 6. This interphase drag approach for an annulus component was also used in RELAP5/MOD1.

### 3.5.10 References

- 3.5-1. Y. K. Cheung, V. Parameswaran, and J. C. Shaug, *BWR Refill-Reflood Program Task 4.7-Model Development TRAC-BWR Component Models*, NUREG/CR-2574, EPRI NP-2376, GEAP-22052, April 1983.
- 3.5-2. R. H. Moen, et al., "Advances in Boiling Water Reactor Steam Separator Systems," *ASME-60-WA/NE-5*, November 1969.
- 3.5-3. E. L. Burley, "Performance of Internal Steam Separator System in Boiling Water Reactors," *ASME-69-WA/NE-24*, November 1969.
- 3.5-4. S. Wolf and R. H. Moen, "Advances in Steam-Water Separators for Boiling Water Reactors," *ASME-73-WA/PWR-4*, November 1973.
- 3.5-5. V. H. Ransom et al., *RELAP5/MOD1 Code Manual*, NUREG/CR-4312, EGG-2070, March 1982.
- 3.5-6. EG&G Idaho, Inc., *RELAP4/MOD6: A Computer Program for Transient Thermal-Hydraulic Analysis of Nuclear Reactors and Related Systems, Users Manual*, CDAP-TR-003, May 1978.
- 3.5-7. J. K. Salisbury, *Steam Turbines and Their Cycles*, New York: Kreiger, 1950.

- 3.5-8. J. K. Vennard and R. L. Street, *Elementary Fluid Mechanics*, 6th Edition, New York: John Wiley and Sons, 1982.
- 3.5-9. J. P. Holman, *Heat Transfer*, 4th Edition, New York: McGraw-Hill Book Company, Inc., 1976, pp. 244-245, 280.
- 3.5-10. V. H. Ransom et al., *RELAP5/MOD2 Code Manual*, NUREG/CR-4312, EGG-2396, August 1985.
- 3.5-11. R. A. Dimenna et al., *RELAP5/MOD2 Models and Correlations*, NUREG/CR-5194, August 1988.
- 3.5-12. T. N. Tandon, H. K. Varma, and C. P. Gupta, "A New Flow Regime Map for Condensation Inside Horizontal Tubes," *Journal of Heat Transfer*, 104, November 1982, pp. 763-768.
- 3.5-13. I. S. Lim, S. G. Bankoff, R. S. Tankui, and M. C. Yeun, *Co-current Steam/Water Flow in a Horizontal Channel*, NUREG/CR-2289, August 1981.
- 3.5-14. H. C. Unal, "Maximum Bubble Diameter, Maximum Bubble-Growth Time and Bubble-Growth Rate During the Subcooled Nucleate Flow Boiling of Water up to 17.7 MN/m<sup>2</sup>," *International Journal of Heat Mass Transfer*, 19, 1976, pp. 643-649.
- 3.5-15. R. A. Riemke, "Modification to Unal's Subcooled Flow Boiling Bubble Model," *Nuclear Technology*, 102, 1993, pp. 416-417.
- 3.5-16. R. T. Lahey, "A Mechanistic Subcooled Boiling Model," *Proceedings from Sixth International Heat Transfer Conference, Toronto, Canada, 1978*, Volume 1, pp. 293-297.
- 3.5-17. W. L. Weaver et al., *TRAC-BF1 Manual: Extensions to TRAC-BD1/MOD1*, NUREG/CR-4391, EGG-2417, August 1986.
- 3.5-18. S. Z. Rouhani et al., *TRAC-BF1 Models and Correlations*, NUREG/CR-4391, EGG-2680, August 1992.
- 3.5-19. J. M. G. Andersen, K. H. Chu, and J. C. Shaug, *BWR Refill-Reflood Program, Task 4.7--Model Development, Basic Models for the BWR Version of TRAC*, NUREG/CR-2573, EPRI NP-2375, GEAP-22051, September 1983.
- 3.5-20. M. Ishii, *One-Dimensional Drift-Flux Model and Constitutive Equations for Relative Motion Between Phases in Various Two-Phase Flow Regimes*, ANL-77-47, October 1977.
- 3.5-21. M. M. Megahed, *Interfacial Heat Transfer Countercurrent Flows of Steam and Water*, EGG-RTH-2495, January 1987.
- 3.5-22. J. G. M. Andersen and H. Abel-Larsen, *CORECOOL-Model Description of the Program*, RISO-M-21380, November 1980.

- 3.5-23. A. C. DeVuono and R. N. Christensen, "Experimental Investigation of the Pressure Effect on Film Condensation of Steam-Air Mixture at Pressure Above Atmospheric," *Fundamentals of Phase Change: Boiling and Condensation*, ASME-HTD Vol. 38, 1984, pp. 73-80.
- 3.5-24. K. Schneider, "Siemens Contributions to RCP Modeling and Evaluation of UPTF Test 6," *ICAP Meeting, Bethesda, MD, October 18-20, 1989*.
- 3.5-25. D. Bharathan, G. B. Wallis, and H. T. Richter, *Air-Water Counter-Current Annular Flow*, EPRI NP-1165, 1979.
- 3.5-26. G. B. Wallis, *One-Dimensional Two-Phase Flow*, New York: McGraw-Hill Book Company, 1969.

## 4 HEAT STRUCTURE MODELS

### 4.1 Heat Conduction Numerical Technique

Heat structures provided in RELAP5 permit calculation of the heat transferred across solid boundaries of hydrodynamic volumes. Modeling capabilities of heat structures are general and include fuel pins or plates with nuclear or electrical heating, heat transfer across steam generator tubes, and heat transfer from pipe and vessel walls. Heat structures are assumed to be represented by one-dimensional heat conduction in rectangular, cylindrical, or spherical geometry. Surface multipliers are used to convert the unit surface of the one-dimensional calculation to the actual surface of the heat structure. Temperature-dependent thermal conductivities and volumetric heat capacities are provided in tabular or functional form either from built-in or user-supplied data.

Finite differences are used to advance the heat conduction solutions. Each mesh interval may contain a different mesh spacing, a different material, or both. The spatial dependence of the internal heat source may vary over each mesh interval. The time-dependence of the heat source can be obtained from reactor kinetics, one of several tables of power versus time, or a control system variable. Boundary conditions include symmetry or insulated conditions, a correlation package, tables of surface temperature versus time, heat transfer rate versus time, and heat transfer coefficient versus time or surface temperature. The heat transfer correlation package can be used for heat structure surfaces connected to hydrodynamic volumes, and contains correlations for convective, nucleate boiling, transition boiling, and film boiling heat transfer from the wall to water and reverse transfer from water to wall including condensation.

The following describes the numerical techniques for heat conduction. The integral form of the heat conduction equation is

$$\iiint_V \rho(T, \bar{x}) \frac{\partial T}{\partial t}(\bar{x}, t) dV = \iint_S k(T, \bar{x}) \nabla T(\bar{x}, t) \cdot d\bar{s} + \iiint_V S(\bar{x}, t) dV \quad (4.1-1)$$

where

$k$  = the thermal conductivity

$s$  = the surface

$S$  = the internal heat source

$t$  = time

$T$  = temperature

$V$  = volume

$x$  = the space coordinates

$\rho$  = the volumetric heat capacity.

The boundary conditions applied to the exterior surface have the form

$$A(T)T(t) + B(T)\frac{\partial T(t)}{\partial n} = D(T, t) \quad (4.1-2)$$

The  $n$  denotes the unit normal vector away from the boundary surface. Thus, if the desired boundary condition is that the heat transferred out of the surface equals a heat transfer coefficient,  $h$ , times the difference between the surface temperature,  $T$ , and the sink temperature,  $T_{sk}$ , i.e.,

$$-k\frac{\partial T}{\partial n} = h(T - T_{sk}) \quad (4.1-3)$$

then the correspondence between the above expression and Equation (4.1-2) yields

$$A = h, B = k, \text{ and } D = h T_{sk} \quad (4.1-4)$$

In one-dimensional problems, boundary conditions are applied on the left and right surfaces. In steady-state problems, a valid physical problem requires that  $A$  be nonzero on at least one of the two boundary surfaces. If a transient or steady-state problem has cylindrical or spherical geometry and a zero radius for the left surface (that is, a solid cylinder or sphere), the left boundary condition is normally the symmetry condition,  $\frac{\partial T}{\partial \bar{n}} = 0$ . Under these conditions, if  $B$  is nonzero, the numerical technique forces the symmetry boundary condition, even if it is not specified.

## 4.2 Mesh Point and Thermal Property Layout

**Figure 4.2-1** illustrates the placement of mesh points at which temperatures are to be calculated. The mesh point spacing for a rectangular problem is taken in the positive  $x$  direction. For cylindrical and spherical problems, the mesh point spacing is in the positive radial direction. Mesh points are placed on the external boundaries of the problem, at the interfaces between different materials, and at desired intervals between the interfaces, boundaries, or both.

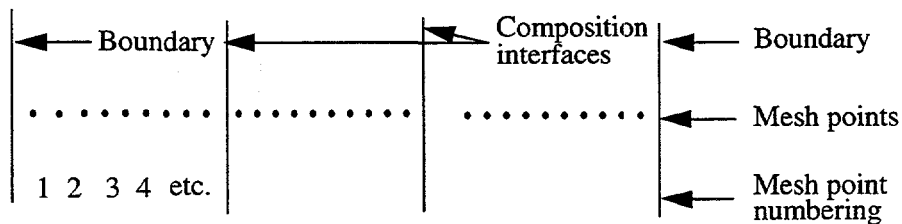


**Figure 4.2-1** Mesh point layout.

**Figure 4.2-2** represents three typical mesh points. The subscripts are space indexes indicating the mesh point number; and 1 and r (if present) designate quantities to the left and right, respectively, of the mesh point. The  $\delta$ 's indicate mesh point spacings that are not necessarily equal. Between mesh points, the thermal properties,  $k$  and  $\rho$ , and the source term,  $S$ , are assumed spatially constant; but  $k_{lm}$  is not necessarily equal to  $k_{rm}$  and similarly for  $\rho$  and  $S$ .

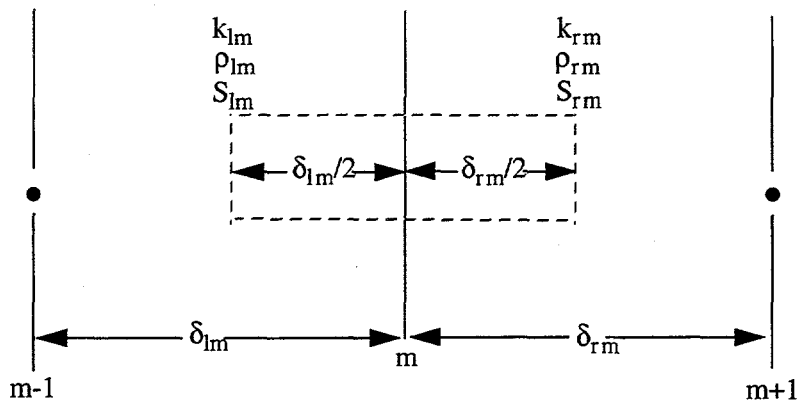


**Figure 4.2-2** Typical mesh points.

To obtain the spatial-difference approximation for the  $m$ -th. interior mesh point, Equation (4.1-1) is applied to the volume and surfaces indicated by the dashed line shown in **Figure 4.2-2**. For the spatial difference approximation at the boundaries, Equations (4.1-1) is applied to the volumes and interior surfaces indicated by the dashed lines shown in **Figure 4.2-3** and Equation (4.1-2) is used to define the gradient along the exterior surfaces. If the coefficient of the gradient in the boundary equation is zero, the surface temperature is given directly from Equation (4.1-2). Since the code is one-dimensional, the dimensions of the volume for other than the  $x$  or  $r$  coordinate are set to one. For rectangular geometry, the volume is a rectangular solid. For cylindrical geometry, the volume is a cylindrical annulus; and for spherical geometry, the volume is a spherical shell.

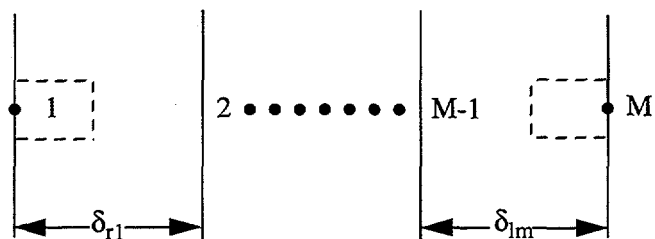


**Figure 4.2-3** Boundary mesh points.

The spatial finite-difference approximations use exact expressions for the space and volume factors and simple differences for the gradient terms. To condense the expressions defining the numerical approximations and to avoid writing expressions unique to each geometry, the following quantities are defined.

For rectangular geometry,

$$\delta_{lm}^v = \frac{\delta_{lm}}{2}, \delta_{rm}^v = \frac{\delta_{rm}}{2}, \delta_{lm}^s = \frac{1}{\delta_{lm}}, \delta_{rm}^s = \frac{1}{\delta_{rm}}, \delta_m^b = 1 \quad (4.2-1)$$

For cylindrical geometry,

$$\begin{aligned} \delta_{lm}^v &= 2\pi \frac{\delta_{lm}}{2} \left( x_m - \frac{\delta_{lm}}{4} \right), \delta_{rm}^v = 2\pi \frac{\delta_{rm}}{2} \left( x_m + \frac{\delta_{rm}}{4} \right), \\ \delta_{lm}^s &= \frac{2\pi}{\delta_{lm}} \left( x_m - \frac{\delta_{lm}}{2} \right), \delta_{rm}^s = \frac{2\pi}{\delta_{rm}} \left( x_m + \frac{\delta_{rm}}{2} \right), \\ \delta_m^b &= 2\pi x_m. \end{aligned} \quad (4.2-2)$$

For spherical geometry,

$$\begin{aligned} \delta_{lm}^v &= \frac{4\pi}{3} \left[ x_m^3 - \left( x_m - \frac{\delta_{lm}}{2} \right)^3 \right], \delta_{rm}^v = \frac{4\pi}{3} \left[ \left( x_m + \frac{\delta_{rm}}{4} \right)^3 - x_m^3 \right], \\ \delta_{lm}^s &= \frac{4\pi}{\delta_{lm}} \left( x_m - \frac{\delta_{lm}}{2} \right)^2, \delta_{rm}^s = \frac{4\pi}{\delta_{rm}} \left( x_m + \frac{\delta_{rm}}{2} \right)^2, \\ \text{and} \\ \delta_m^b &= 4\pi x_m^2. \end{aligned} \quad (4.2-3)$$

For all geometries,

$$G_m = \rho_{lm} \delta_{lm}^v + \rho_{rm} \delta_{rm}^v. \quad (4.2-4)$$

The superscripts, v and s, refer to volume and surface-gradient weights. The  $\delta_m^b$  is a surface weight used at exterior boundaries and in heat transfer rate equations.

### 4.3 Difference Approximation at Internal Mesh Points

Using a forward difference for the time derivative, the first term of Equation (4.1-1) for the volume of Figure 4.2-1 is approximated by

$$\iiint_V \rho(T, \bar{x}) \frac{\partial T}{\partial t}(\bar{x}, t) dV \approx (T_m^{n+1} - T_m^n) \frac{G_m}{\Delta t} . \quad (4.3-1)$$

The superscript  $n$  refers to time; thus,  $T_m^n$  indicates the temperature at mesh point  $m$  at time  $t^n$ , and  $T_m^{n+1}$  indicates the temperature at mesh point  $m$  at time  $t^{n+1} = t^n + \Delta t$ .

The second term of Equation (4.1-1) for the surfaces of **Figure 4.2-2** is approximated by

$$\iint_s k(T, \bar{x}) \nabla T(\bar{x}, t) d\bar{s} \approx (T_{m-1} - T_m) k_{lm} \delta_{lm}^s + (T_{m+1} - T_m) k_{rm} \delta_{rm}^s . \quad (4.3-2)$$

Note that the above expression includes the standard interface conditions of continuity of temperature and heat flow. The surface integral of Equation (4.1-1) is usually evaluated by integrating only along the exterior surfaces of the volume indicated by the dashed line in **Figure 4.2-2**. If, however, the volume is divided into two sub-volumes by the interface line and the surface integrals of these sub-volumes are added, the surface integrals along the common interface cancel because of the continuity of heat flow. The continuity of temperature is implied by use of a single-valued temperature at the interface.

A contact-resistance interface condition cannot be specified directly since the temperature, instead of being continuous at the interface, is given by  $q = h_c \Delta T$ , where  $q$  is the heat transfer rate across the interface,  $h_c$  is the contact conductivity, and  $\Delta T$  is the temperature change across the interface. This condition can be specified by defining a small mesh interval with thermal properties of  $k = h_c \delta$  and  $\rho = 0$ . The size of the mesh interval,  $\delta$ , is arbitrary except in cylindrical or spherical geometry, where the surface and volume weights are dependent on the radius. This mesh interval is usually chosen very small with respect to the dimensions of the problem.

The space and time dependence of the source term in Equation (4.1-1) is assumed to be separable into functions of space and time,

$$S(x, t) = P_f P(t) Q(x) \quad (4.3-3)$$

where  $P_f$  is the factor that relates the reactor power (or power from a table) to the heat generation rate for a particular heat structure;  $P(t)$  is the time varying function and may be reactor power, power from a table, or a control variable; and  $Q(x)$  is the space-dependent function. The value of  $Q(x)$  is assumed constant over a mesh interval, but each interval can have a different value. The third term of Equation (4.1-1) is then approximated as

$$\iiint_V S(\bar{x}, t) dV \approx P_f P(t) (Q_{lm} \delta_{lm}^v + Q_{rm} \delta_{rm}^v) . \quad (4.3-4)$$

Gathering the approximations of terms in Equation (4.1-1), the basic difference equation for the  $m$ -th mesh point is

$$\frac{(T_m^{n+1} - T_m^n) G_m}{\Delta t} = - (T_m - T_{m-1}) k_{lm} \delta_{lm}^s + (T_{m+1} - T_m) k_{rm} \delta_{rm}^s + P_f P(t) (Q_{lm} \delta_{lm}^v + Q_{rm} \delta_{rm}^v) \quad (4.3-5)$$

Using the symbol,  $\zeta_m$ , to represent the right side, Equation (4.3-5) can be written as

$$\frac{(T_m^{n+1} - T_m^n) G_m}{\Delta t} = \zeta_m \quad (4.3-6)$$

Thus far, the time superscripts for  $G_m$  and  $\zeta_m$  have been omitted, and the procedure for approximating the temperature-dependence of the thermal properties has not been mentioned. The procedures for temperature-dependent thermal properties are discussed later. However, superscripts for thermal properties are written here even though their significance is not explained until later. For steady state, the difference approximation becomes

$$\zeta_m = 0 \quad (4.3-7)$$

and no time superscripts are needed. For the time-dependent case, an equation of the type

$$\frac{(T_m^{n+1} - T_m^n) G_m}{\Delta t} = w \zeta_m^{n+1} + (1 - w) \zeta_m^n \quad (4.3-8)$$

is an explicit formula if  $w$  is zero and is an implicit formula when  $w$  is nonzero. RELAP5 uses the implicit formulation with  $w = 1/2$ , sometimes called the Crank-Nickelson method.

Writing Equation (4.3-8) in full, the difference approximation for the  $m$ -th. interior mesh point for transient and steady-state cases is

$$a_m^n T_{m-1}^{n+1} + b_m^n T_m^{n+1} + c_m^{n+1} T_{m+1}^{n+1} = d_m \quad (4.3-9)$$

$$a_m^n = - \frac{k_{lm}^n \delta_{lm}^s \Delta t}{\sigma + 1} \quad (4.3-10)$$

$$b_m^n = \sigma G_m^n - a_m^n - c_m^n \quad (4.3-11)$$

$$c_m^n = - \frac{k_{rm}^n \delta_{rm}^s \Delta t}{\sigma + 1} \quad (4.3-12)$$

$$d_m = -\sigma a_m^n T_{m-1}^n + \sigma (G_m^n + a_m^n + c_m^n) T_m^n - \sigma c_m^n T_{m+1}^n + \Delta t P_f \left( \frac{P^{n+1} + \sigma P^n}{\sigma + 1} \right) (Q_{lm} \delta_{lm}^v + Q_{rm} \delta_{rm}^v); \quad (4.3-13)$$

$\sigma$  is 1 for transient cases, and  $\sigma$  is 0 and  $\Delta t$  is 1.0 for steady-state cases. Separate subroutines are used for steady-state and transient cases, and  $\sigma$  and  $\Delta t$  do not appear in the steady-state coding.

#### 4.4 Difference Approximation at Boundaries

To obtain the difference approximations for the mesh points at the boundaries, Equation (4.1-1) is applied to the volumes of **Figure 4.2-3** with Equation (4.1-2) used to define the gradient at the surface. The second term of Equation (4.1-1) at  $x = x_1$  is approximated by

$$\iint_s k(T, \bar{x}) \nabla T(\bar{x}, t) \cdot d\bar{s} = -\frac{k_{rl}}{B_1} (A_1 T_1 - D_1) \delta_1^b + k_{rl} (T_2 - T_1) \delta_{rl}^s. \quad (4.4-1)$$

The complete basic expression for the left boundary mesh point becomes

$$\frac{(T_1^{n+1} - T_1^n)}{\Delta t} \rho_{rl} \delta_{rl}^v = -\frac{k_{rl}}{B_1} (A_1 T_1 - D_1) \delta_1^b + k_{rl} (T_2 - T_1) \delta_{rl}^s + P_f P(t) Q_{rl} \delta_{rl}^v. \quad (4.4-2)$$

If  $B$  in the boundary condition equation is zero, the above equation is not used, since the boundary condition alone determines the temperature. Also in that case, a divide by zero would be indicated if Equation (4.4-2) were used. Approximations for the boundary at  $x = x_m$  are derived in a similar fashion. These equations for the boundary mesh points are converted to the implicit formulas in the same manner as for the interior mesh points, except that the boundary condition information is evaluated completely at the  $n+1$  time level. Thus, for the left boundary

$$b_1^{n+1} T_1^{n+1} + c_1^{n+1} T_2^{n+1} = d_1 \quad (4.4-3)$$

$$b_1^n = \sigma \rho_{rl}^n \delta_{rl}^v + \frac{k_{rl}^n A_1^n \delta_1^b \Delta t}{B_1^n} - c_1^n \quad (4.4-4)$$

$$c_1^n = -\frac{k_{rl}^n \delta_{rl}^s \Delta t}{\sigma + 1} \quad (4.4-5)$$

$$d_1 = -\sigma c_1^n T_2^n + \sigma (\rho_{rl}^n \delta_{rl}^v + c_1^n) T_1^n + \frac{k_{rl}^n \delta_1^b D_1^n \Delta t}{B_1^n} + P_f \frac{(\sigma P^n + P^{n+1}) Q_{rl} \delta_{rl}^v \Delta t}{\sigma + 1}. \quad (4.4-6)$$

For the right boundary,

$$a_M^{n+1} T_{M-1}^{n+1} + b_M^{n+1} T_M^{n+1} = d_M \quad (4.4-7)$$

$$a_M^n = \frac{-k_{IM}^n \delta_{IM}^s \Delta t}{\sigma + 1} \quad (4.4-8)$$

$$b_M^n = \sigma p_{IM}^n \delta_{IM}^v + \frac{k_{IM}^n A_M^n \delta_M^b \Delta t}{B_M^n} - a_M^n \quad (4.4-9)$$

$$d_M = -\sigma a_M^n T_{M-1}^n + \sigma (p_{IM}^n \delta_{IM}^v + a_M^n) T_M^n + \frac{k_{IM}^n \delta_M^b D_M^n \Delta t}{B_M^n} + P_f \frac{(\sigma P^n + P^{n+1}) Q_{IM} \delta_{IM}^v \Delta t}{\sigma + 1} \quad (4.4-10)$$

## 4.5 Thermal Properties and Boundary Condition Parameters

The thermal conductivity,  $k$ , and the volumetric heat capacity,  $\rho$ , are considered functions of temperature and space. These thermal properties are obtained for each interval by using the average of the mesh point temperatures bounding the interval

$$k_{l,m} = k \left( \frac{T_{m-1} + T_m}{2} \right) = k_{r,m-1} \quad (4.5-1)$$

$$k_{r,m} = k \left( \frac{T_m + T_{m+1}}{2} \right) = k_{l,m+1} \quad (4.5-2)$$

The quantity,  $\rho$ , is treated in the same manner. The boundary condition parameters,  $A$ ,  $B$ , and  $D$ , are considered functions of temperature and time.

## 4.6 RELAP5 Specific Boundary Conditions

The development of the difference equations uses a general form for the boundary conditions and the specific conditions implemented in RELAP5 are expressed in that form. For heat structure boundaries attached to hydrodynamic volumes, a convective package is typically used to define the boundary conditions. In addition, symmetry or insulated conditions are provided, and for special situations, tabular based conditions can be specified.

#### 4.6.1 Correlation Package Conditions

The correlation package partitions the total heat flux at the heat structure surface into heat fluxes from or to the liquid and vapor phases. The heat fluxes are defined using five heat transfer coefficients and four fluid temperatures.

$$q_f = h_{ff}[T_{sr} - T_f] + h_{fT}[T_{sr} - T^s(P)] \quad (4.6-1)$$

$$q_g = h_{gg}[T_{sr} - T_g] + h_{gT}[T_{sr} - T^s(P)] + h_{gp}[T_{sr} - T^s(P_s)] \quad (4.6-2)$$

$$q_b = q_f + q_g \quad (4.6-3)$$

where

$q_f$	=	heat flux to liquid
$q_g$	=	heat flux to vapor
$q_b$	=	total heat flux
$T_{sr}$	=	surface temperature
$T_f$	=	liquid temperature
$T_g$	=	vapor temperature
$h_{ff}$	=	heat transfer coefficient for difference of surface temperature and liquid temperature for heat transfer to liquid
$h_{fT}$	=	heat transfer coefficient for difference of surface temperature and saturation temperature corresponding to total pressure for heat transfer to liquid
$h_{gg}$	=	heat transfer coefficient for difference of surface temperature and vapor temperature for heat transfer to vapor
$h_{gT}$	=	heat transfer coefficient for difference of surface temperature and saturation temperature corresponding to total pressure for heat transfer to vapor
$h_{gp}$	=	heat transfer coefficient for difference of surface temperature and saturation temperature corresponding to partial pressure of water vapor for transfer to vapor

Using first order Taylor series approximations,

$$q_f^{n+1} = q_f^0 + \frac{\partial q_f}{\partial T_{sr}} \Delta T_{sr} + \frac{\partial q_f}{\partial T_f} \Delta T_f + \frac{\partial q_f}{\partial T_T} \Delta T^s (P) \quad (4.6-4)$$

$$q_g^{n+1} = q_g^0 + \frac{\partial q_g}{\partial T_{sr}} \Delta T_{sr} + \frac{\partial q_g}{\partial T_g} \Delta T_g + \frac{\partial q_g}{\partial T^s(P)} \Delta T^s(P) + \frac{\partial q_g}{\partial T^s(P_s)} \Delta T^s(P_s) \quad (4.6-5)$$

where  $\Delta$  is an operator,  $\Delta F = F^{n+1} - F^n$ .

Note that  $q_f^0$  and  $q_g^0$  are not old time values of heat fluxes but instead are the heat fluxes obtained from the correlations using old time surface temperature and fluid conditions. Because only new time boundary condition information is used in the difference equations, the old time heat fluxes do not appear in the difference equations.

Assuming the heat transfer coefficients are constant over a time step,

$$\frac{\partial q_f}{\partial T_{sr}} = h_{ff} + h_{fT} \quad (4.6-6)$$

$$\frac{\partial q_f}{\partial T_f} = -h_{ff} \quad (4.6-7)$$

$$\frac{\partial q_f}{\partial T_T} = -h_{fT} \quad (4.6-8)$$

$$\frac{\partial q_g}{\partial T_{sr}} = h_{gg} + h_{gT} + h_{gp} \quad (4.6-9)$$

$$\frac{\partial q_g}{\partial T_g} = -h_{gg} \quad (4.6-10)$$

$$\frac{\partial q_g}{\partial T_T} = -h_{gT} \quad (4.6-11)$$

$$\frac{\partial q_g}{\partial T_p} = -h_{gp} \quad (4.6-12)$$

Then,

$$q_f^{n+1} = q_f^0 + [h_{ff} + h_{fT}] \Delta T_{sr} - h_{ff} \Delta T_f - h_{fT} \Delta T^s (P) \quad (4.6-13)$$

$$q_g^{n+1} = q_g^0 + [h_{gg} + h_{gT} + h_{gp}] \Delta T_{sr} - h_{gg} \Delta T_g - h_{gT} \Delta T^s (P) - h_{gp} \Delta T^s (P_s) \quad (4.6-14)$$

$$q_b^{n+1} = q_f^0 + q_g^0 + h_b \Delta T_{sr} - h_{ff} \Delta T_f - h_{gg} \Delta T_g - [h_{fT} + h_{gT}] \Delta T^s (P) - h_{gp} \Delta T^s (P_s) \quad (4.6-15)$$

where

$$h_b = h_{ff} + h_{fT} + h_{gg} + h_{gT} + h_{gp} \quad (4.6-16)$$

Expressing Equation (4.6-15) in terms of the general boundary condition,

$$A = -h_b \quad (4.6-17)$$

$$B = -k \quad (4.6-18)$$

$$D = q_f^0 + q_g^0 + h_b \Delta T_{sr} - h_{ff} \Delta T_f - h_{gg} \Delta T_g - [h_{fT} + h_{gT}] \Delta T^s (P) - h_{gp} \Delta T^s (P_s) \quad (4.6-19)$$

#### 4.6.2 Insulated and Tabular Boundary Conditions

The other boundary conditions implemented in RELAP5 are given below. The first two conditions are flux-specified conditions; the first condition is a symmetry or insulated condition and is just a special case of the second condition. The third condition is a convection condition similar to that used with the correlation package except that only a total heat transfer coefficient which is a tabular function of time or surface temperature is used. The last condition directly specifies the surface temperature.

$$-k \frac{\partial T}{\partial x} = 0 \quad (4.6-20)$$

$$-k \frac{\partial T}{\partial x} = q_{TA}(t) \quad (4.6-21)$$

$$-k \frac{\partial T}{\partial x} = h_{TA}(T - T_{TA}) \quad (4.6-22)$$

$$T = T_{TA}(t) \quad (4.6-23)$$

where

$q_{TA}$  = the total heat flux as a function of time obtained from input tables  
 $h_{TA}$  = the total heat transfer coefficient as an input tabular function of either time or surface temperature  
 $T_{TA}$  = either an input tabular function of time or the void fraction weighted average of the liquid and vapor temperatures of the hydrodynamic volume attached to the boundary.

## 4.7 Solution of Simultaneous Equations

The difference approximation for the mesh points [Equations (4.3-9), (4.4-3), and (4.4-7)] lead to a tri-diagonal set of M equations.

$$\begin{bmatrix} b_1 & c_1 & & & & \\ a_2 & b_2 & c_2 & & & \\ \cdot & \cdot & & & & \\ & \cdot & \cdot & \cdot & & \\ & & & & b_{M-1} & c_{M-1} \\ & & & & a_M & b_M \end{bmatrix} \begin{bmatrix} T_1 \\ T_2 \\ \vdots \\ \vdots \\ T_{M-1} \\ T_M \end{bmatrix} = \begin{bmatrix} d_1 \\ d_2 \\ \vdots \\ \vdots \\ d_{M-1} \\ d_M \end{bmatrix} \quad (4.7-1)$$

Equations 1 and M correspond to the left and right boundary mesh points respectively, and equations 2 through M-1 correspond to the interior mesh points. The terms in  $d_2$  through  $d_{M-1}$  do not include any of the fluid or saturation temperatures,  $T_f$ ,  $T_g$ ,  $T^s(P)$ , and  $T^s(P_s)$ . But

$$d_1 = d_{10} + d_{11}\Delta T_{1f} + d_{1g}\Delta T_{1g} + d_{1T}\Delta T_1^s(P) + d_{1p}\Delta T_1^s(P_s) \quad (4.7-2)$$

$$d_M = d_{M10} + d_{Mf}\Delta T_{Mf} + d_{Mg}\Delta T_{Mg} + d_{MT}\Delta T_M^s(P) + d_{Mp}\Delta T_M^s(P_s) \quad (4.7-3)$$

where the first subscript, 1 or M, has been introduced to indicate the left or right boundary. The coefficient matrix is symmetric unless a boundary condition specifies the surface temperature. In that case, the corresponding off-diagonal element is zero and thus symmetry may not exist in the first and/or last rows. The solution to the above equation is obtained by

$$E_1 = \frac{c_1}{b_1} \text{ and } F_1 = \frac{d_1}{b_1} \quad (4.7-4)$$

$$E_j = \frac{c_j}{b_j - a_j E_{j-1}} \text{ and } F_j = \frac{d_j - a_j F_{j-1}}{b_j - a_j E_{j-1}} \text{ for } j = 2, 3, \dots, M-1 \quad (4.7-5)$$

$$g_M = \frac{d_M - a_M F_{M-1}}{b_M - a_M E_{M-1}} \quad (4.7-6)$$

$$g_j = -E_j g_{j+1} + F_j \text{ for } j = M-1, M-2, \dots, 3, 2, 1 \quad (4.7-7)$$

$$T_j^{n+1} = g_j \text{ for all } j \quad (4.7-8)$$

These procedures can be derived by applying the rules for Gaussian elimination. This method of solution introduces little roundoff error if the off-diagonal elements are negative and the diagonal is greater than the sum of the magnitudes of the off-diagonal elements. From the form of the difference equations, these conditions are satisfied for any values of the mesh point spacing, time step, and thermal properties.

Expanding the expression for  $T_j^{n+1}$ ,

$$T_j^{n+1} = g_{j0} + g_{j1f} \Delta T_{1f} + g_{j1g} \Delta T_{1g} + g_{j1T} \Delta T_1^s(P) + g_{j1p} \Delta T_1^s(P_s) + g_{jMf} \Delta T_{Mf} + g_{jMg} \Delta T_{Mg} + g_{jMT} \Delta T_M^s(P) + g_{jMp} \Delta T_M^s(P_s) \quad (4.7-9)$$

For the  $g$  factors, the first subscript indicates the mesh point number, the second subscript indicates the boundary, and the third subscript indicates the particular fluid temperature.

A user option allows an explicit or an implicit coupling between the heat conduction-transfer and hydrodynamic time advancements. With the explicit option, the changes in hydrodynamic temperatures are assumed zero at this point and the new time temperatures are given by the first term of Equation (4.7-9). If the implicit advancement is used, the final temperatures are computed using Equation (4.7-9) after the fluid temperatures are computed.

## 4.8 Computation of Heat Fluxes

When the correlation boundary condition package is used, the new time heat fluxes to the liquid and vapor phases are computed by substituting the Equation (4.7-9) for the surface temperature into the boundary conditions given in Equation (4.6-1) and (4.6-2). The expression for any temperature could involve the fluid temperatures from both the left and right boundary volumes. If only one side of the heat structure is attached to a hydrodynamic volume, that boundary condition would involve only those volume conditions. That fits in well with the numerical approximations in the hydrodynamic solution which assume the conservation equations for each volume include new time values only from that volume. Most heat structures such as fuel pins or plates and piping have only one side connected to a hydrodynamic volume. An important case where the two sides are connected to two different volumes is a heat structure representing heat exchanger tubing. This situation would involve unknown temperatures from more than one volume in the energy equations for each attached volume and thus would not be compatible with the

hydrodynamic advancement scheme. To avoid this problem, the heat flux for one boundary ignores the effects of fluid temperature changes in the other volume. This is a reasonable approximation since the effects of temperature changes of the fluid on one side of the heat structure has a highly attenuated effect on the heat flux on the other side.

Dropping the subscript for the particular surface, the expressions for heat fluxes are

$$q_f^{n+1} = q_f^0 + [h_{ff} + h_{ft}] [g_0 - T_{sr}^n] + [h_{ff} + h_{ft}] [g_f \Delta T_f + g_g \Delta T_g + g_T \Delta T^s(P) + g_p \Delta T^s(P_s)] - h_{ff} \Delta T_f - h_{ft} \Delta T^s(P) = q_{f0} + q_{ff} \Delta T_f + q_{fg} \Delta T_g + q_{ft} \Delta T^s(P) \quad (4.8-1)$$

$$q_g^{n+1} = q_g^0 + [h_{gf} + h_{gt} + h_{gp}] [g_0 - T_{sr}^n] + [h_{gg} + h_{gt} + h_{gp}] [g_f \Delta T_f + g_g \Delta T_g + g_T \Delta T^s(P) + g_p \Delta T^s(P_s)] - h_{gg} \Delta T_g - h_{gt} \Delta T^s(P) - h_{gp} \Delta T^s(P_s) = q_{g0} + q_{gf} \Delta T_f + q_{gg} \Delta T_g + q_{gt} \Delta T^s(P) + q_{gp} \Delta T^s(P_s) \quad (4.8-2)$$

The expression following the second equal sign in the equations above is a convenient gathering of terms for passing heat flux information to the hydrodynamic advancement. The coefficients of the fluid temperature changes are zero if the explicit coupling between the heat conduction-transfer and hydrodynamics is used.

For heat fluxes from boundaries not using the correlation package, a total heat flux is computed and distributed to the liquid and vapor phases in direct proportion to their void fractions. The heat fluxes are returned in  $q_{f0}$  and  $q_{g0}$ , and the coefficients of the fluid temperature changes are set to zero. For flux specified conditions, the total heat flux is given directly by the boundary condition. For a convection boundary, the total heat flux is obtained by substituting in the surface temperature. If the other boundary uses the convective package, the surface temperature is that assuming the fluid temperature changes are zero. For the temperature-specified boundary, the heat flux is computed from the boundary difference equation (even though it was not used to compute the temperature). The expression for the right boundary (the left is similar) is

$$q_M^{n+1} \delta_{1M}^n = \frac{k_{1M}^n}{\sigma + 1} (T_{M-1}^{n+1} - T_M^{n+1}) \delta_{1M}^s + \frac{\sigma k_{1M}^n}{\sigma + 1} (T_{M-1}^n - T_M^n) \delta_{1M}^s + P_f \frac{(\sigma P^n + P^{n+1})}{\sigma + 1} Q_{1M} \delta_{1M}^v - \frac{\sigma \rho_{1M}^n}{\Delta t} (T_M^{n+1} - T_M^n) \delta_{1M}^v \quad (4.8-3)$$

## 4.9 Two-Dimensional Conduction Solution/Reflood

A two-dimensional conduction scheme is used in the reflood model for cylindrical or rectangular heat structures. **Figure 4.9-1** shows an elemental cell around the mesh point. For a cylindrical geometry, the volume elements are

$$V_1 = \pi \delta_t \delta_l (r_i - \delta_l/4)/2 \quad (4.9-1)$$

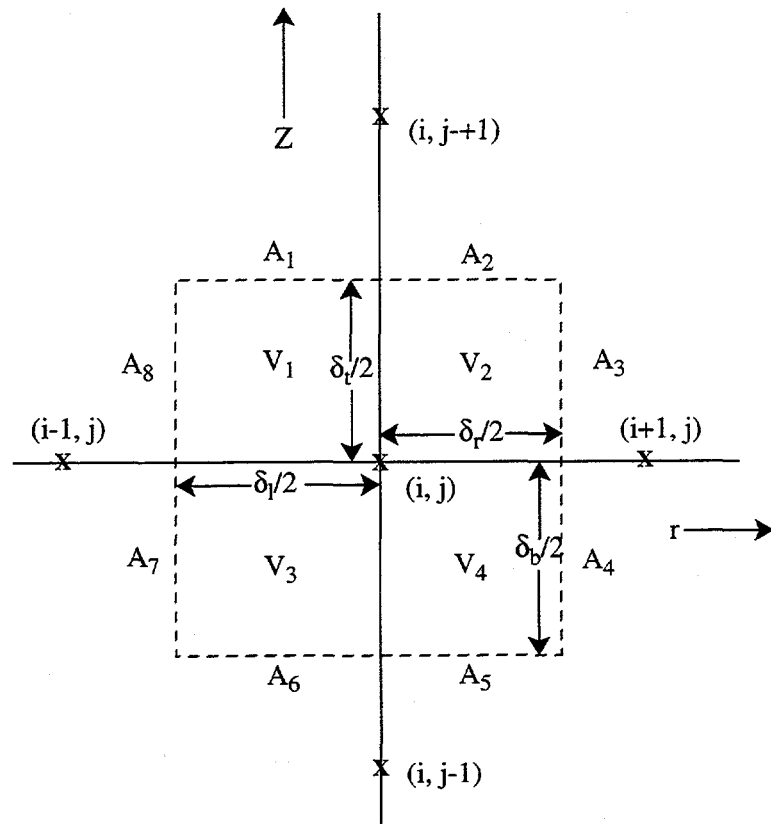


Figure 4.9-1 Volume and surface elements around a mesh point  $(i, j)$ .

$$V_2 = \pi \delta_t \delta_r (r_i + \delta_r/4)/2 \quad (4.9-2)$$

$$V_3 = \pi \delta_b \delta_l (r_i - \delta_l/4)/2 \quad (4.9-3)$$

$$V_4 = \pi \delta_b \delta_r (r_i + \delta_r/4)/2 \quad (4.9-4)$$

and the surface elements are

$$A_1 = \pi \delta_l (r_i - \delta_l/4) \quad (4.9-5)$$

$$A_2 = \pi \delta_r (r_i + \delta_r/4) \quad (4.9-6)$$

$$A_3 = \pi \delta_t (r_i + \delta_r/2) \quad (4.9-7)$$

$$A_4 = \pi \delta_b (r_i + \delta_r/2) \quad (4.9-8)$$

$$A_5 = A_2 \quad (4.9-9)$$

$$A_6 = A_1 \quad (4.9-10)$$

$$A_7 = \pi \delta_b (r_i - \delta_l/2) \quad (4.9-11)$$

$$A_8 = \pi \delta_b (r_i - \delta_l/2) \quad (4.9-12)$$

Integration of the heat conduction Equation (4.1-1) over the elemental cell yields the following form of finite difference equation

$$G_{ij} (T_{i,j}^{n+1} - T_{i,j}^n) / \Delta t = a_{ij}^L T_{i-1,j} + a_{ij}^R T_{i+1,j} + a_{ij}^T T_{i,j+1} + a_{ij}^B T_{i,j-1} - (a_{ij}^L + a_{ij}^R + a_{ij}^B + a_{ij}^T) T_{ij} + S_{ij} \quad (4.9-13)$$

By defining the material properties,  $\rho_{ij}$  and  $k_{ij}$ , at the center of the r-direction interval between mesh points (ij) and (i+1,j), the coefficients  $G_{ij}$ ,  $a_{ij}^R$  and  $a_{ij}^T$  of Equation (4.9-13) can be written as

$$G_{ij} = \rho_{i-1,j} (V_1 + V_3) + \rho_{ij} (V_2 + V_4) \quad (4.9-14)$$

$$a_{ij}^R = k_{ij} (A_3 + A_4) / \delta r \quad (4.9-15)$$

$$a_{ij}^T = [(k_{ij} + k_{i,j+1}) A_2 / 2 + (k_{i-1,j} + k_{i-1,j+1}) A_1 / 2] / \delta t \quad (4.9-16)$$

The other two coefficients,  $a_{ij}^L$  and  $a_{ij}^B$ , are obtained by the symmetry relations

$$a_{ij}^L = a_{i-1,j}^R \quad (4.9-17)$$

$$a_{ij}^B = a_{i,j-1}^T \quad (4.9-18)$$

The space and time dependence of the source term, S, described in Equation (4.3-3) are extended to the two-dimensional cases as

$$S = P_R P(t) Q(r,z) \quad (4.9-19)$$

with the assumption that  $Q$  is independent of  $z$  within a heat structure. Accordingly, the heat source term  $S_{ij}$  of Equation (4.9-13) is

$$S_{ij} = P_R P(t) (Q^T V_1 + Q^B V_3 + Q_r^T V_2 + Q_r^B V_4) . \quad (4.9-20)$$

Here,  $Q_1^T = Q_1^B$  and  $Q_r^T = Q_r^B$  if the entire cell is within the same heat structure.

Equation (4.9-13) is written for an interior point (ij). For a point on the boundary, some of the coefficients  $a_{ij}^L$ ,  $a_{ij}^R$ ,  $a_{ij}^B$ , and  $a_{ij}^T$  should vanish. For example, at the bottom corner,  $a_{ij}^L$  and  $a_{ij}^B$  are zero. Also some of the terms in Equations (4.9-16) and (4.9-20) disappear. Furthermore, the boundary condition must be added. To be consistent with the one-dimensional heat conduction scheme, an assumption is made that no heat is fluxed across the top and bottom ends. For the right and left boundaries, the boundary condition can be represented by one of the forms described in Equations (4.6-1), (4.6-2), and (4.6-20) through (4.6-22). The boundary condition specifying the surface temperature as a function of time, Equation (4.6-23), has been dropped in the two-dimensional scheme for computational efficiency.

The two-dimensional capability currently uses only explicit coupling between the heat conduction-transfer and hydrodynamics.

The difference Equation (4.9-13) is solved using the alternating direction implicit (ADI) method. The scheme is represented by two steps as follows:

#### 1. Column Inversion:

$$(T_{ij}^{n+1/2} - T_{ij}^n) G_{ij} / (\Delta t / 2) = a_{ij}^L T_{i-1,j}^n + a_{ij}^R T_{i+1,j}^n + a_{ij}^B T_{i,j-1}^{n+1/2} + a_{ij}^T T_{i,j+1}^{n+1/2} - (a_{ij}^L + a_{ij}^R) T_{ij}^n - (a_{ij}^T + a_{ij}^B) T_{ij}^{n+1/2} + S_{ij} . \quad (4.9-21)$$

#### 2. Row Inversion:

$$(T_{ij}^{n+1} - T_{ij}^{n+1/2}) G_{ij} / (\Delta t / 2) = a_{ij}^L T_{i-1,j}^{n+1} + a_{ij}^R T_{i+1,j}^{n+1} + a_{ij}^B T_{i,j-1}^{n+1/2} + a_{ij}^T T_{i,j+1}^{n+1/2} - (a_{ij}^L + a_{ij}^R) T_{ij}^{n+1} - (a_{ij}^T + a_{ij}^B) T_{ij}^{n+1/2} + S_{ij} . \quad (4.9-22)$$

Here the superscripts  $n$ ,  $n+1/2$ , and  $n+1$  denote the values at times  $t$ ,  $t+\Delta t/2$ , and  $t+\Delta t$ , respectively.

## 4.10 Fine Mesh Rezoning Scheme

A fine mesh-rezoning scheme is implemented to efficiently use the two-dimensional conduction solution for reflood calculations. The scheme is similar to the one used in COBRA-TF<sup>4.10-1</sup> and is intended to resolve the large axial variation of wall temperatures and heat fluxes. The number of axial nodes in the heat structures is varied in such a way that the fine nodes exist only in the nucleate boiling and transition boiling regions.

A heat-structure geometry, which is composed of 1 to 99 heat structures as specified by users, is selected as an elementary unit for the reflood model. **Figure 4.10-1** shows a typical heat structure geometry with one fluid-control volume connected to each heat structure. The dots are radial mesh points. At the initiation of the reflood model, each heat structure is subdivided into two axial intervals (**Figure 4.10-2**). A two-dimensional array of mesh points is thus formed. Thereafter, the number of axial intervals may be doubled, halved, or unchanged at each time step according to a set of rules to be discussed in the next paragraph. **Figure 4.10-2** also shows an example of a heat structure going through a cycle of axial nodalization variation.

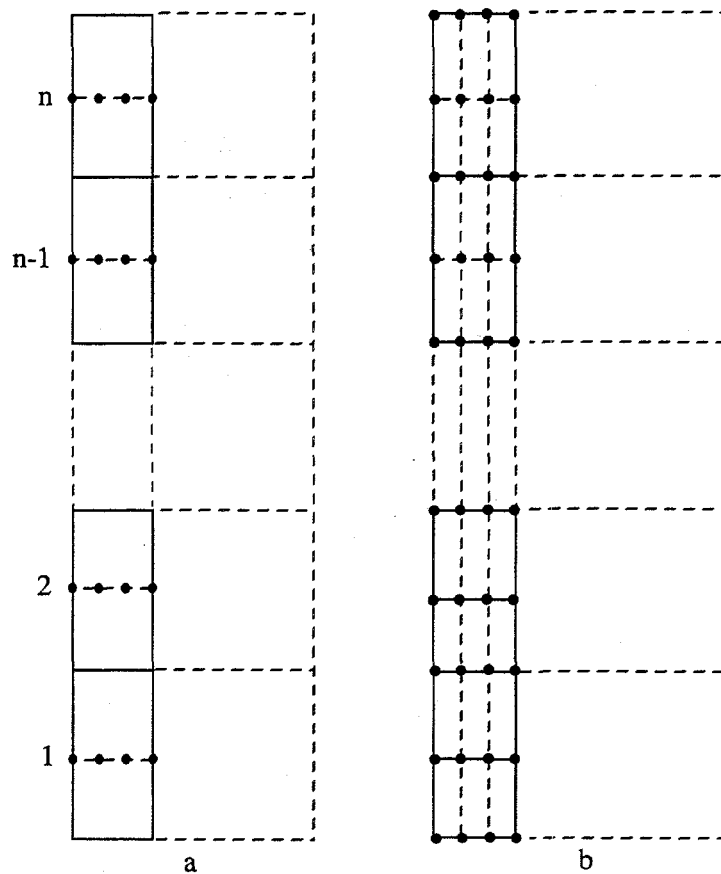


**Figure 4.10-1** An elementary heat structure unit for reflood.

The number of axial mesh intervals in a heat structure depends on the heat-transfer regimes in the heat structures. At each time step, all heat structures in a heat-structure geometry are searched to find the positions of  $T_{CHF}$ , the wall temperature where critical heat flux occurs,  $T_Q$ , the quench or rewetting temperature, and  $T_{IB}$ , the wall temperature at the incipience of boiling. Let us assume that  $T_{IB}$ ,  $T_{CHF}$ , and  $T_Q$  are at the  $i$ -,  $j$ -, and  $k$ -th heat structures and  $k \geq j \geq i$ . Also, let  $N$  be the maximum number of axial mesh intervals specified by the user and  $a_g$  be the void fraction in the connected control volume. The number of axial mesh intervals in a heat structure is determined according to the following rules:

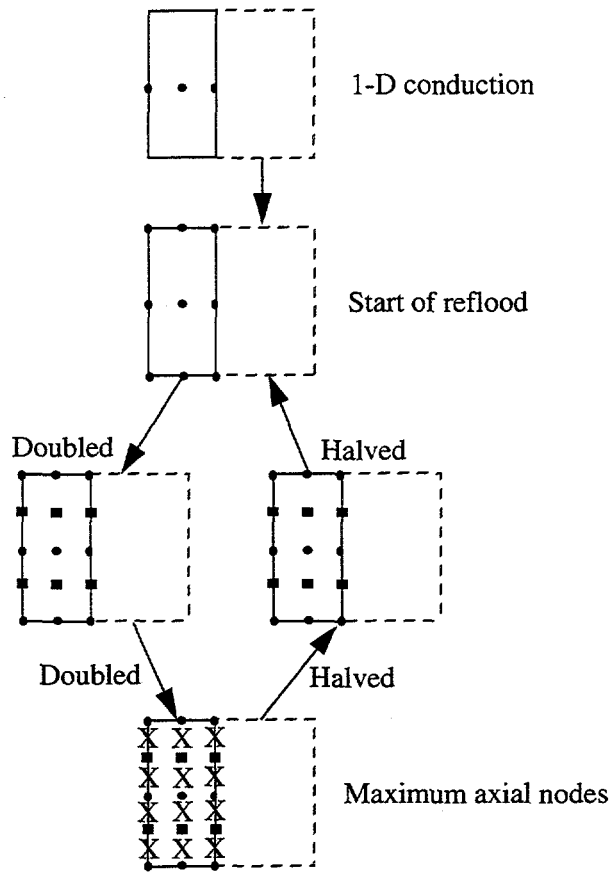


Figure 4.10-2 An example of the fine mesh-rezoning process.

- For  $\alpha_g > 0.999$  or  $\alpha_g = 0$ , the number is halved but not less than 2.
- For the  $(k+1)$ -th heat structure, the number is doubled but not greater than  $N/2$ .
- For the  $(i-1)$ -th heat structure, the number is halved but not less than  $N/2$ .
- The number is doubled up to  $N$  for the heat structures between  $\max(j+1, k)$  and  $\min(j-1, i)$  and in the region of maximum wall temperature gradient.
- For all other heat structures, the number is unchanged.

#### 4.10.1 Reference

4.10-1. J. M. Kelly, "Quench Front Modeling and Reflood Heat Transfer in COBRA-TF," *ASME Winter Annual Meeting, New York, NY, 1979, 79-WA/HT-63.*

## 4.11 Gap Conductance Model

The RELAP5 dynamic gap conductance model defines an effective gap conductivity based on a simplified deformation model generated from FRAP-T6.<sup>4.11-1</sup> The model employs three assumptions as follows: (a) the fuel-to-cladding radiation heat transfer, which only contributes significantly to the gap conductivity under the conditions of cladding ballooning, is neglected unless the cladding deformation model is activated (see Section 4.14); (b) the minimum gap size is limited such that the maximum effective gap conductivity is about the same order as that of metals; (c) the direct contact of the fuel pellet and the cladding is not explicitly considered.

The gap conductance through the gas is inversely proportional to the size of the gap. Since the longitudinal axis of the fuel pellets is usually offset from the longitudinal axis of the cladding, the width of the fuel-cladding gap varies with circumferential position. This variation causes the conductance through the gas in the fuel-cladding gap to vary with circumferential position. The circumferential variation of the conductance is taken into account by dividing the gap into several equal length segments, as shown in **Figure 4.11-1**. The conductance for each segment is calculated and then an average conductance,  $h_g$ , is computed in the FRAP-T6 model by the equation

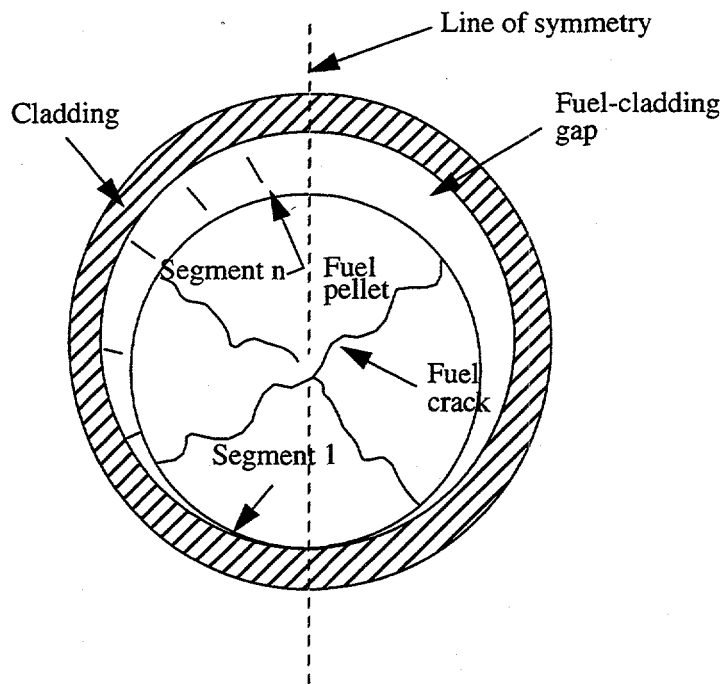


**Figure 4.11-1** Segmentation at the fuel-cladding gap.

$$h_g = \frac{k_g}{N} \sum_{n=1}^N \frac{1}{[t_n + 3.2(R_F + R_c) + (g_1 + g_2)]} \quad (4.11-1)$$

where

$h_g$  = conductance through the gas in the gap (W/m<sup>2</sup>•K)  
 $n$  = number of a circumferential segment  
 $N$  = total number of circumferential segments = 8  
 $k_g$  = thermal conductivity of gas (W/m•K)  
 $t_n$  = width of fuel-cladding gap at the midpoint of the  $n$ -th circumferential segment (m)  
 $R_F$  = surface roughness of the fuel (m)  
 $R_c$  = surface roughness of the cladding (m)  
 $g_1, g_2$  = temperature jump distance terms for fuel and cladding.

The width of the fuel-cladding gap at any given circumferential segment is calculated by the equation

$$t_n = t_g + [-1 + (2n-1)/N] t_0 \quad (4.11-2)$$

where

$t_g$  = circumferentially averaged fuel-cladding gap width (m)  
 $t_0$  = as-fabricated fuel-cladding gap width (m).

The value of  $t_n$  in Equation (4.11-2) is limited between zero and  $2t_g$ .

The temperature jump distance terms account for the temperature discontinuity caused by incomplete thermal accommodation of gas molecules to the surface temperature. The terms also account for the inability of gas molecules leaving the fuel and cladding surfaces to completely exchange their energy with neighboring gas molecules, which produces a nonlinear temperature gradient near the fuel and cladding surfaces. The terms are calculated by

$$g_1 + g_2 = 0.024688k_g T_g^{1/2} / \left( P_g \sum_i f_i a_i M_i^{-1/2} \right) \quad (4.11-3)$$

where

$T_g$  = temperature of gas in the fuel-cladding gap (K)

$P_g$  = gas pressure (Pa)

$f_i$  = mole fractions of  $i$ -th component of gas

$a_i$  = accommodation coefficient of the  $i$ -th component of gas

$M_i$  = molecular weight of the  $i$ -th component of gas.

The accommodation coefficients for helium and xenon are obtained by using curve fits to the data of Ullman:<sup>4.11-2</sup>

$$a_{He} = 0.425 - 2.3 \times 10^{-4} T_g \text{ (helium)} \quad (4.11-4)$$

$$a_{Xe} = 0.740 - 2.5 \times 10^{-4} T_g \text{ (xenon)} \quad (4.11-5)$$

If  $T_g$  is  $> 1000$  K,  $T_g$  is set to 1000 K. The accommodation coefficients for other gases are determined by interpolation and written as

$$a_i = a_{He} + \frac{(M_i - M_{He})}{(M_{Xe} - M_{He})} (a_{Xe} - a_{He}) \quad (4.11-6)$$

The circumferential averaged width of the fuel cladding gap,  $t_g$ , in Equation (4.11-2) is determined by the expression

$$t_g = t_o - u_F + u_C \quad (4.11-7)$$

where

$u_F$  = radial displacement of the fuel pellet surface (m),

$u_C$  = radial displacement of cladding inner surface (m).

The radial displacements,  $u_F$  and  $u_C$ , are primarily due to thermal expansion.

The radial displacement, of the fuel pellet surface,  $u_F$ , is calculated by the equation

$$u_F = u_{TF} + u_r + u_s \quad (4.11-8)$$

where

$u_{TF}$  = radial displacement due to thermal expansion (m)

$u_r$  = radial displacement due to uniform fuel relocation (m)

$u_s$  = radial displacement due to fission gas induced fuel swelling and densification (m).

In the RELAP5 model, the variable  $u_r$  is assumed to be zero. The value of the variable  $u_s$  is supplied by the user. The fuel thermal expansion is obtained from the equation

$$u_{TF} = \sum_{n=2}^N (r_n - r_{n-1}) \epsilon_{TF} (T_{n+1/2}) \quad (4.11-9)$$

where

$n$  = radial mesh point number

$N$  = total number of mesh points in the fuel

$r_n$  = radius of radial mesh point  $n$

$\epsilon_{TF}$  = function defining thermal expansion of fuel as a function of temperature

$T_{n+1/2}$  = average fuel temperature at the center of the node between mesh points  $n$  and  $n+1$ .

The radial displacement of the inner surface of the cladding is calculated by

$$u_c = u_{TC} + u_{cc} + u_e \quad (4.11-10)$$

where

$u_{TC}$  = radial displacement due to thermal expansion (m)

$u_{cc}$  = radial displacement due to cladding creepdown (m)

$u_e$  = radial displacement due to elastic deformation (m).

The value of  $u_{cc}$  must be supplied by the user. For beginning-of-life fuel rods,  $u_{cc}$  is equal to zero. For fuel rods with a significant amount of burnup, a FRAPCON-2<sup>4.11-3</sup> analysis is required to determine the value of  $u_{cc}$ . The thermal expansion,  $u_{TC}$ , is obtained from

$$u_{TC} = r_{cm} \varepsilon_{TC} (T_c) \quad (4.11-11)$$

where

$r_{cm}$  = radius of midplane of cladding (m)  
 $\varepsilon_{TC}$  = function defining thermal expansion of cladding as a function of temperature  
 $T_c$  = temperature of cladding at midplane (K).

The elastic deformation,  $u_e$ , is calculated by

$$u_e = r_{cm} (\sigma_h - v \sigma_z) / E \quad (4.11-12)$$

where

$E$  = Young's modulus for the cladding (Pa)  
 $\sigma_h$  = cladding hoop stress (Pa)  
 $\sigma_z$  = cladding axial stress (Pa)  
 $v$  = Poisson's ratio for the cladding.

The cladding hoop and axial stress are given by

$$\sigma_h = (P_g r_i - P_f r_o) / (r_o - r_i) \quad (4.11-13)$$

$$\sigma_z = (P_g r_i^2 - P_f r_o^2) / (r_o^2 - r_i^2) \quad (4.11-14)$$

where

$P_f$  = coolant pressure (Pa)  
 $r_i$  = inner radius of cladding (m)  
 $r_o$  = outer radius of cladding (m).

The Poisson's ratio used is

$$\nu = 0.3 \quad . \quad (4.11-15)$$

The internal gas pressure  $P_g$  is determined in FRAP-T6<sup>4.11-1</sup> by a detailed plenum model. Since a plenum model is not included in the simplified approach, a static-ideal gas approximation for a fixed-plenum volume is used to calculate  $P_g$ , i.e.,

$$P_g = P_{g,i} (T_f/T_{f,i}) \quad (4.11-16)$$

where

$P_{g,i}$  = initial gas pressure in the gap (Pa)

$T_{f,i}$  = initial coolant temperature at the top of the core (K)

$T_f$  = current coolant temperature at the top of the core (K).

The initial internal gas pressure must be supplied by the user.

The volumetric heat capacity and thermal conductivity of the fuel rod materials, except for the thermal conductivity of the gap gas, must be supplied by the user. For the computation of the gas thermal conductivity, the user is required to provide the gas composition in terms of the mole fractions of seven common gases included in the model. The properties for determining material thermal expansion and elastic deformation are calculated from permanent data within the code, and no user input is needed. The user, however, should be aware that these properties are computed under the assumption that the fuel material is uranium oxide and the cladding material is zircaloy. The properties of  $UO_2$  and zircaloy along with gas conductivity are taken from MATPRO-11 (Revision 2)<sup>4.11-4</sup> and are described below.

The conductivity as a function of temperature for a pure noble or diatomic gas is calculated using

$$k_g = A T_g^B \quad . \quad (4.11-17)$$

The constants A and B for seven common gases are given in Table 4.11-1. The thermal conductivity of a gas mixture is calculated from the expression

Table 4.11-1 Constants used in gas thermal conductivity correlation.

Constant		
Gas	A	B
Helium	$2.639 \times 10^{-3}$	0.7085

**Table 4.11-1** Constants used in gas thermal conductivity correlation. (Continued)

	Constant	
Argon	$2.986 \times 10^{-4}$	0.7724
Krypton	$8.247 \times 10^{-5}$	0.8363
Xenon	$4.351 \times 10^{-5}$	0.8616
$H_2$	$1.097 \times 10^{-3}$	0.8785
$N_2$	$5.314 \times 10^{-4}$	0.6898
$O_2$	$1.853 \times 10^{-4}$	0.8729

$$k_g = \sum_{i=1}^N k_i X_i / \left( X_i + \sum_{j=1}^N \Phi_{ij} X_j \right) \quad (4.11-18)$$

where

$$\Phi_{ij} = [1 + (k_i/k_j)^{1/2} (M_i/M_j)^{1/4}]^2 / [8(1 + M_i/M_j)]^{1/2} \quad (4.11-19)$$

$N$  = number of components in the mixture

$M_i$  = molecular weight of component  $i$

$X_i$  = mole fraction of the component  $i$

$k_i$  = thermal conductivity of the component  $i$  (W/m·K).

The strain function,  $\varepsilon_{TF}$  in Equation (4.11-9), of the  $UO_2$  fuel due to thermal expansion is described by

$$\varepsilon_{TF} = 1.0 \times 10^{-5} T - 3.0 \times 10^{-3} + 4.0 \times 10^{-2} \exp(-6.9 \times 10^{-20}/k_B T) \quad (4.11-20)$$

where

$T$  = fuel pellet temperature

$k_B$  = Boltzmann constant ( $1.38 \times 10^{-23}$  J/K).

The radial strain function,  $\varepsilon_{TC}$  in Equation (4.11-11), for the cladding thermal expansion is given by

$$\varepsilon_{TC} = 1.5985 \times 10^{-3} + 6.721 \times 10^{-6} T \quad (4.11-21)$$

for  $T < 1073.15$  K ( $\alpha$  phase) and

$$\varepsilon_{TC} = -4.150 \times 10^{-3} + 9.7 \times 10^{-6} T \quad (4.11-22)$$

for  $T > 1273.15$  K ( $\beta$  phase), where  $T$  = cladding temperature (K). In the  $\alpha$  to  $\beta$  phase transition zone ( $1073.15 \leq T \leq 1273.15$  K), a table lookup is used. Some selected values are listed in **Table 4.11-2**.

**Table 4.11-2** Radial thermal strain of zircaloy for  $1083 \text{ K} < T < 1273 \text{ K}$ .

Temperature (K)	$\varepsilon_{TC}$
1083.0	$5.22 \times 10^{-3}$
1093.0	$5.25 \times 10^{-3}$
1103.0	$5.28 \times 10^{-3}$
1123.0	$5.24 \times 10^{-3}$
1143.0	$5.15 \times 10^{-3}$
1183.0	$4.45 \times 10^{-3}$
1223.0	$2.97 \times 10^{-3}$
1273.0	$2.90 \times 10^{-3}$

Young's modulus,  $E$ , for zircaloy cladding is approximated by neglecting the effects of oxidation, cold work, and irradiation. Young's modulus is given by

$$E = 1.088 \times 10^{11} - 5.475 \times 10^7 T \quad (4.11-23)$$

for  $T < 1090$  K ( $\alpha$  phase) and

$$E = \max (1.0 \times 10^{10}, 9.21 \times 10^{10} - 4.05 \times 10^7 T) \quad (4.11-24)$$

for  $T > 1240$  K ( $\beta$  phase), where  $T$  is the cladding temperature (K). In the  $\alpha$  to  $\beta$  phase transfer zone,  $1090 \leq T \leq 1240$  K, Young's modulus is given by

$$E = 4.912 \times 10^{10} - 4.827 \times 10^7 (T-1090) \quad (4.11-25)$$

#### 4.11.1 References

- 4.11-1: L. J. Siefken et al., *FRAP-T6: A Computer Code for the Transient Analysis of Oxide Fuel Rods*, EGG-CDAP-5410, April 1981.
- 4.11-2: A. Ullman, R. Acharya and D. R. Olander, "Thermal Accommodation Coefficients of Inert Gases on Stainless Steel and  $UO_2$ ," *Journal of Nuclear Materials*, 51, 1974, pp. 277-279.
- 4.11-3: G. A. Berna et al., *FRAPCON-2 Developmental Assessment*, NUREG/CR-1949, PNL-3849, July 1981.
- 4.11-4: D. L. Hagrman, G. A. Reyman, and R. E. Mason, *MATPRO-Version 11 (Revision 2), A Handbook of Materials Properties for Use in the Analysis of Light Water Reactor Fuel Rod Behavior*, NUREG/CR-0479, TREE-1280, Revision 2, August 1981.

## 4.12 Surface-to-Surface Radiation Model

Several radiation text books (Reference 4.12-1 and Reference 4.12-2) describe the approach used here to compute the rate of radiation exchange between surfaces. The surfaces that have a line-of-sight or a reflection path through which they can communicate with each other are in the same enclosure. The computation method is a lumped-system approximation for gray diffuse surfaces contained in an enclosure. The assumptions of this method are that:

- The fluid in the enclosure neither emits nor absorbs radiant thermal energy.
- Reflectance from a surface is neither a function of incident nor reflected direction nor of radiation frequency.
- Temperature, reflectance, and radiosity are constant over each surface.

The radiosity of a surface is the total radiant energy leaving a surface (i.e., the emitted energy plus the reflected energy). Mathematically this is written for the  $i$ -th surface as:

$$R_i = \epsilon_i \sigma T_i^4 + \rho_i \sum_{j=1}^n R_j F_{ij} \quad (4.12-1)$$

where

$R$  = radiosity

$\epsilon$  = emissivity

$\sigma$  = Stefan-Boltzmann constant

$T$  = temperature

$$\rho = 1 - \varepsilon; \text{reflectivity}$$

$$F_{ij} = \text{view factor from surface } i \text{ to surface } j.$$

The net heat flux,  $Q$ , at surface  $i$  is the difference between the radiosity for  $i$  and the radiosity of all surfaces times their view factor to surface  $i$ :

$$Q_i = R_i - \sum_{j=1}^n R_j F_{ij} . \quad (4.12-2)$$

The above two equations can be combined to yield:

$$Q_i = \frac{\varepsilon_i}{\rho_i} (\sigma T_i^4 - R_i) . \quad (4.12-3)$$

Thus, the only problem in obtaining the heat flux at surface  $i$  is to solve for  $R_i$ . Equation (4.12-3) represents a set of  $n$  simultaneous linear algebraic equations, which can be written in a matrix form as:

$$(\delta_{ij} - \rho_i F_{ij}) R_i = \varepsilon_i \sigma T_i^4 \quad (4.12-4)$$

where the Kronecker delta is defined as

$$\delta_{ij} = 0 \quad i \neq j$$

$$\delta_{ij} = 1 \quad i=j.$$

The solution of Equation (4.12-4) involves a matrix inversion written as:

$$R_i = (\delta_{ij} - \rho_i F_{ij})^{-1} \varepsilon_i \sigma T_i^4 . \quad (4.12-5)$$

Fortunately, the matrix inversion need only be performed once during initialization since it does not involve variables that change with time.

Radiation changes the conduction solution boundary condition to the form:

$$-k \frac{\partial T}{\partial r} \Big|_i = h_i (T_i - T_r) + Q_i \quad (4.12-6)$$

where

$k$	=	surface conductivity
$r$	=	radius
$h$	=	convective heat transfer coefficient
$T_r$	=	reference temperature.

Note that the radiation term is not implicit in surface temperature. This can cause solution instabilities for thin surfaces and large time steps unless convection dominates radiation.

The tedious part of performing a radiation calculation in an enclosure with surfaces having arbitrary shapes is finding the view factors. Text books describe integral, graphical, and mechanical methods of doing this. For many types of surfaces, formulas, tables, or charts are available. Naturally, the view factors from each surface to all other surfaces must sum to 1. Also, to conserve energy, the area times view factor for each surface  $i$  to any other surface  $j$  must equal the area of  $j$  times the view factor from  $j$  to  $i$ . These two restrictions are written as:

$$\sum_{i=1}^n F_{ij} = 1.0 \quad (4.12-7)$$

$$A_i F_{ij} = A_j F_{ji} \quad (4.12-8)$$

This latter restriction is known as the reciprocity rule. RELAP5 has a built in check that if the above two equations are not satisfied within 0.1 percent, a message is printed and the calculation will not go beyond input checking, because energy conservation errors will be too large.

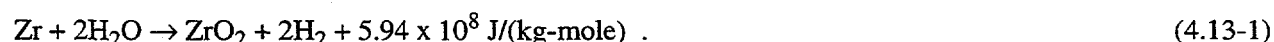
#### 4.12.1 References

- 4.12-1. T. J. Love, *Radiative Heat Transfer*, Merrill Publishing Co., 1968.
- 4.12-2. E. M. Sparrow and R. D. Cess, *Radiation Heat Transfer*, Belmont CA: Brooks-Cole Publishing Co., 1966.

### 4.13 Metal-Water Reaction Model

The reaction of zirconium and steam is treated using the correlation developed by Cathcart.<sup>4.13-1</sup> The metal-water reaction model is coupled with the fuel rod deformation model so that if a rod ruptures, the inside of the cladding can react. The model assumes that there is an unlimited amount of steam available for the metal-water reaction.

The chemical equation being modeled is



The oxide layer thickness on the cladding's outer surface at time point n is given by

$$dr_n = \left[ dr_{n-1}^2 + (K\Delta t) \exp\left(-\frac{A}{RT}\right) \right]^{\frac{1}{2}} \quad (4.13-2)$$

where

$dr_n$  = oxide thickness at time point n (m)

$dr_{n-1}^2$  = oxide thickness at time point n-1 (m)

K =  $2.252 \times 10^{-6} \text{ m}^2/\text{s}$

$\Delta t$  = time step size ( $t^{n+1} - t^n$ ) (sec)

A = 35889 mole/cal

R = 1.987 cal/(K-mole)

T = cladding temperature (K).

The amount of heat added to the cladding's outer surface between time point n and n-1 is given by multiplying the volume of cladding undergoing reaction by the density of zirconium and the reaction heat release:

$$Q = \rho\pi [(r_o - dr_{n-1})^2 - (r_o - dr_n)^2] H/W \quad (4.13-3)$$

where

Q = heat addition per unit length (J/m)

$\rho$  = density of zirconium = 6500 Kg/m<sup>3</sup>

$r_o$  = cladding outer radius (m)

H = reaction heat release =  $5.94 \times 10^8 \text{ J/(kg-mole)}$

W = molecular weight of zirconium = 91.22 kg/(kg-mole).

Similar equations are used for the cladding's inner surface if cladding rupture occurs.

The total hydrogen mass generated by the metal-water reaction is calculated by multiplying the mass of zirconium reacted by the ratio of the molecular weight of 4 hydrogen atoms to 1 zirconium atom.

#### 4.13.1 Reference

4.13-1. J. V. Cathcart et al., *Reaction Rate Studies, IV, Zirconium Metal-Water Oxidation Kinetics*, ORNL/NUREG-17, August 1977.

### 4.14 Cladding Deformation Model

An empirical cladding deformation model from FRAP-T6<sup>4.14-1</sup> has been incorporated into RELAP5. The model may be invoked only in conjunction with the dynamic gap conductance model. The purpose of the model is to allow plastic deformation of the cladding to be accounted for in the calculation of fuel rod's cladding temperature during LOCA simulations; and to inform a user of the possible occurrence of rod rupture and flow blockage and hence the necessity of conducting more detailed simulations of the fuel rods' behavior.

With the deformation model modifications, an additional term is included in the gap conductance [Equation (4.11-1)] to account for radiation across the gap

$$h_r = \sigma F (T_f^2 + T_c^2) (T_f + T_c) \quad (4.14-1)$$

$$F = \frac{1}{\left\{ \frac{1}{\varepsilon_f} + \left[ \frac{R_f}{R_c} \right] \left[ \frac{1}{(\varepsilon_c - 1)} \right] \right\}} \quad (4.14-2)$$

where

$h_r$  = radiation gap conductance

$\sigma$  = Stefan-Boltzmann constant =  $5.67 \times 10^{-8} \text{ W}/(\text{m}^2 \text{ K}^4)$

$F$  = emissivity factor

$\varepsilon_f$  = emissivity of fuel

$\varepsilon_c$  = emissivity of cladding

$R_f$  = outer radius of fuel (m)

$R_c$  = inner radius of cladding (m)

$T_f$  = temperature of fuel's outer surface (K)

$T_c$  = temperature of cladding's inner surface (K).

When the deformation model is active, the total cladding strain is the sum of the thermal strain, the elastic strain, and a plastic strain given by

$$E_p = 0.25 E_{rup} \exp [-0.0153(T_r - T_c)] \quad (4.14-3)$$

where

$E_p$  = plastic hoop strain before rupture

$E_{rup}$  = cladding strain at rupture

$T_r$  = rupture temperature, °C

$T_c$  = average cladding temperature, °C.

The rupture temperature is

$$T_r = 3960 - [20.4S/(1 + H)] - [8.51 \times 10^6 S/(100(1 + H) + 2790S)] \quad (4.14-4)$$

where

$S$  = cladding hoop stress (kpsi)

$H$  =  $\max [(heating\ rate)/(28\ ^\circ C/s), 1.0]$ .

The rupture temperature correlation is depicted in **Figure 4.14-1**.

Plastic strain is calculated only if the average cladding temperature exceeds  $T_{plas}$ , the temperature at which plastic strain begins

$$\begin{aligned} T_{plas} &= T_r - 70 & ; & \quad T_r < 700 \\ &= T_r - 70 - 0.14(T_r - 700); & 700 < T_r < 1300 \\ &= T_r - 155 & ; 1300 < T_r \end{aligned} \quad (4.13-5) \quad (4.14-5)$$

If the average cladding temperature exceeds the value of  $T_{plas}$ , then the rupture temperature is used together with the heating rate to determine the rupture strain  $E_{rup}$ , via a table lookup. When rupture occurs, a similar table lookup is used to obtain the flow blockage. The rupture strain and blockage tables are from

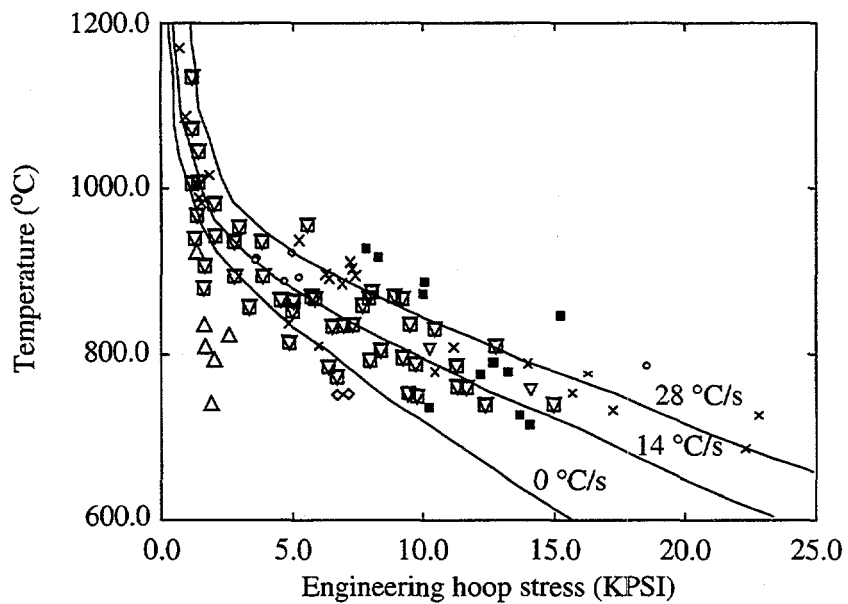


**Figure 4.14-1** ORNL correlation of rupture temperature as a function of engineering hoop stress and temperature-ramp rate with data from internally heated zircaloy cladding in aqueous atmospheres.

**Reference 4.14-2.** The correlations used for cladding strain and rupture are given in **Table 4.14-1** and illustrated in **Figure 4.14-2** through **Figure 4.14-4**.

**Table 4.14-1** Tabulation of cladding correlations.

	Slow-Ramp Correlations ( $\leq 10$ °C/s)		Fast-Ramp Correlations ( $\leq 25$ °C/s)		
	Rupture Temperature (°C)	Burst Strain (%)	Flow Blockage (%)	Burst Strain (%)	Flow Blockage (%)
600	10	6.5	6.5	10	6.5
625	11	7.0	10	6.5	6.5
650	13	8.4	12	7.5	7.5
675	20	13.8	15	10.0	10.0
700	45	33.5	20	13.8	13.8
725	67	52.5	28	20.0	20.0
750	82	65.8	38	27.5	27.5
775	89	71.0	48	35.7	35.7

Table 4.14-1 Tabulation of cladding correlations. (Continued)

Rupture Temperature (°C)	Slow-Ramp Correlations (≤ 10 °C/s)		Fast-Ramp Correlations (≤ 25 °C/s)	
	Burst Strain (%)	Flow Blockage (%)	Burst Strain (%)	Flow Blockage (%)
800	90	71.5	57	43.3
825	89	71.0	60	46.0
850	82	65.8	60	46.0
875	67	52.5	57	43.3
900	48	35.7	45	33.5
925	28	20.0	28	20.0
950	25	18.0	25	18.0
975	28	20.0	28	20.0
1000	33	24.1	35	25.7
1025	35	25.7	48	35.7
1050	33	24.1	77	61.6
1075	25	18.0	80	64.5
1100	14	9.2	77	61.6
1125	11	7.0	39	28.5
1150	10	6.5	26	18.3
1175	10	6.5	26	18.3
1200	10	6.5	36	26.2

If a fuel rod ruptures, the rod's internal pressure is set equal to the external fluid's pressure; metal-water reaction is initiated on the inner surface of the cladding for the structure where rupture occurs if the metal-water reaction model is active; and additional form loss coefficients are (optionally) computed for the junctions just below and just above the rupture location:

$$K_e = (1-B)^2, \text{ expansion loss coefficient} \quad (4.14-6)$$

$$K_c = 0.45(1-B), \text{ contraction loss coefficient} \quad (4.14-7)$$

$$B = (\text{flow area after blockage}/(\text{flow area before blockage})) \quad (4.14-8)$$

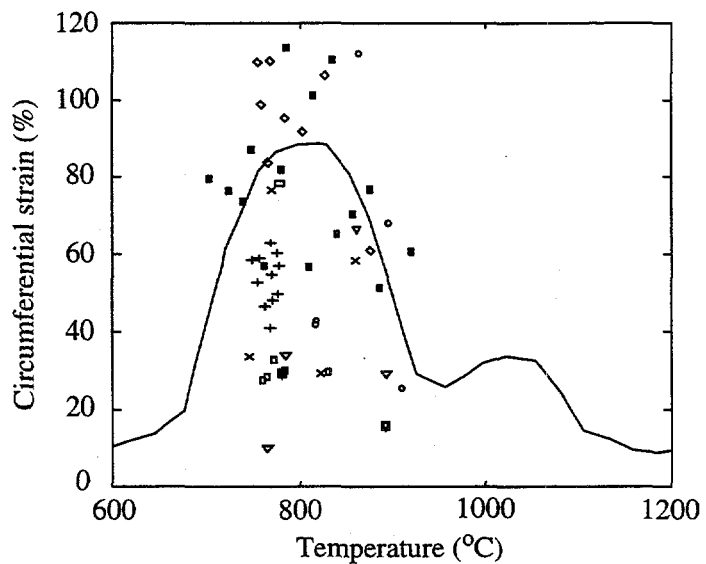


**Figure 4.14-2** Maximum circumferential strain as a function of rupture temperature for internally heated zircaloy cladding in aqueous atmospheres at heating rates less than or equal to 10 °C/s.

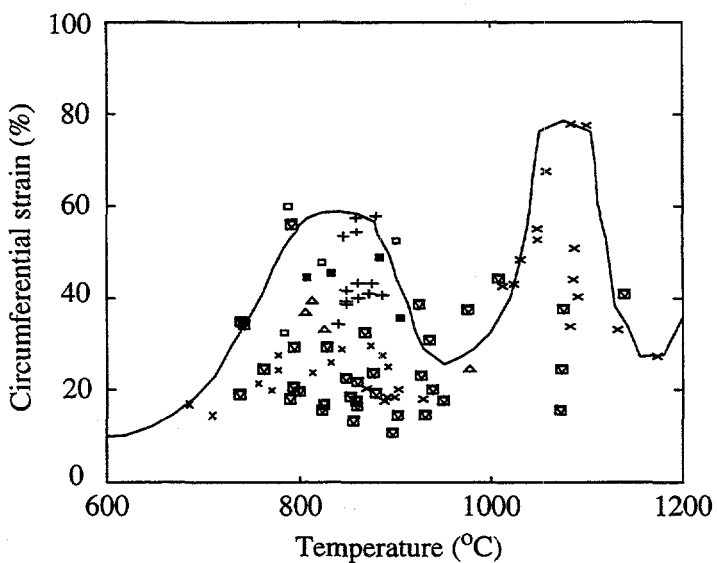


**Figure 4.14-3** Maximum circumferential strain as a function of rupture temperature for internally heated zircaloy cladding in aqueous atmospheres at heating rates greater than or equal to 25 °C/s.

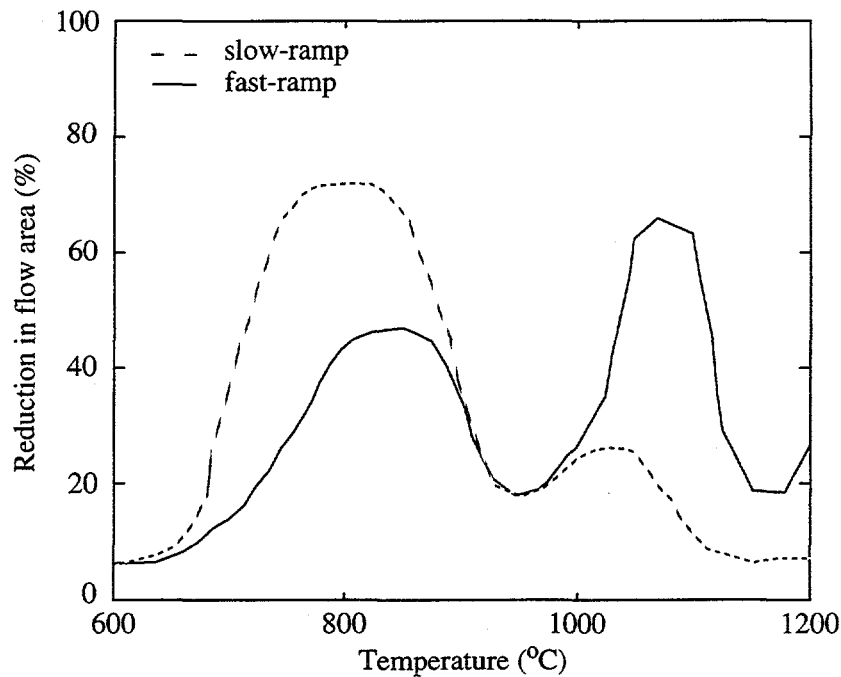


**Figure 4.14-4** Reduction in PWR assembly flow area as a function of rupture temperature and ramp.

The cladding deformation model does not alter any other parameters affecting the RELAP5 hydraulic solution. In particular, it does not alter the flow area of the fluid cell containing a ruptured heat structure. Also, the geometric changes in a heat structure experiencing plastic deformation are not coupled to the geometry seen by the heat structures heat conduction solution. The geometry changes enter the conduction solution only by affecting the value being calculated for gap conductance.

When the reflood fine mesh rezoning algorithm is active, the deformation model sees only the coarse zones. Deformation calculations are not done for each of the fine mesh points in a axial set of heat structures. Rather, the deformation calculation is done once for each of the axial heat structures and all of the fine mesh nodes within a particular heat structure having the same gap conductance value.

#### 4.14.1 References

- 4.14-1. S. C. Resch et al., *FRAP-T6: The Transient Fuel Rod Behavior Code*, NUREG/CR-2950, September 1982.
- 4.14-2. D. A. Powers and R. O. Meyer, *Cladding Swelling and Rupture Models for LOCA Analysis*, NUREG-0630, April 1980.



## 5 TRIP SYSTEM

The trip system consists of the evaluation of logical statements. Each trip statement is a simple logical statement that has a true or false result and an associated variable, TIMEOF. The TIMEOF variable is -1.0 whenever the trip is false, and contains the time the trip was last set true whenever the trip is true. This variable allows for time delays and unit step functions based on events during the transient.

Within the structure of RELAP5, the trip system is considered to be only the evaluation of the logical statements. The decision of what action is needed, based on trip status, resides within other models. For example, valve models are provided that open or close the valve based on trip values; pump models test trip status to determine whether a pump electrical breaker has tripped.

Two types of trip statements are provided--variable and logical trips. Since logical trips involve variable trips and other logical trips, complex logical expressions can be constructed from simple logical statements. Both types of trips can be latched or unlatched. A latched trip, once set true, is no longer tested and remains true for the remainder of the problem or until reset at a restart. An unlatched trip is evaluated every time step.

### 5.1 Variable Trips

A variable trip evaluates the statement

$$T_{ri} = V_1 \text{ OP } (V_2 + C) . \quad (5.1-1)$$

The value  $T_{ri}$  is the  $i$ -th trip variable that may be true or false. Values  $V_1$  and  $V_2$  are quantities from the heat structures, hydrodynamics, reactor kinetics, control systems, or may be a TIMEOF quantity.  $C$  is a constant; OP is one of the arithmetic relational operations: EQ is equal; NE is not equal; GT is greater than; GE is greater than or equal; LT is less than; LE is less than or equal.

Trips are evaluated at the beginning of the overall RELAP5 time advancement and are evaluated in numerical order. Except for TIMEOF variables, all other  $V$  quantities have beginning of time step values; and the results of the trip evaluation are independent of the evaluation order. But when a variable trip statement references TIMEOF ( $T_{rk}$ ), the new value of TIMEOF is used if  $k < i$ .

### 5.2 Logical Trips

A logical trip evaluates

$$T_{ri} = \pm T_{rj} \text{ OP } \pm T_{rl} . \quad (5.2-1)$$

The values  $T_{rj}$  and  $T_{rl}$  are variable or logical trips, and the minus sign, if present, denotes the complement of the trip value. The value OP is one of the logical operations AND, OR (inclusive or), or XOR (exclusive or).

Logical trips are evaluated following the evaluation of variable trips and are evaluated in numerical order. When  $T_{rj}$  (or  $T_{rl}$ ) is a variable trip, new trip values are used; when  $T_{rj}$  is a logical trip used in logical trip expression  $i$ , new values are used when  $j < i$  and old values are used when  $j \geq i$ .

## 6 CONTROL SYSTEM

The control system provides the capability to evaluate simultaneous algebraic and ordinary differential equations. The capability is primarily intended to simulate control systems typically used in hydrodynamic systems, but it can also model other phenomena described by algebraic and ordinary differential equations (see Section 8.4.5 for a description of special controllers for use in steady-state initialization). Another use is to define auxiliary output quantities, such as differential pressures, so they can be printed in major and minor edits and be plotted.

The control system consists of several types of control components. Each component defines a control variable as a specific function of time-advanced quantities. The time-advanced quantities include hydrodynamic volume, junction, pump, valve, heat structure, reactor kinetics, trip quantities, and the control variables themselves (including the control variable being defined). This permits control variables to be developed from components that perform simple, basic operations.

In the following equations that define the control components and associated numerical techniques,  $Y_i$  is the control variable defined by the  $i$ -th control component,  $A_j$ ,  $R$ , and  $S$  are real constants input by the user,  $I$  is an integer constant input by the user,  $V_j$  is a quantity advanced in time by RELAP5 and can include  $Y_i$ ,  $t$  is time, and  $s$  is the Laplace transform variable. Superscripts involving the index  $n$  denote time levels. The name in parentheses to the right of the definition is used in input data to specify the component.

### 6.1 Arithmetic Control Components

#### 6.1.1 Constant

$$Y_i = S \quad (\text{CONSTANT}) \quad (6.1-1)$$

#### 6.1.2 Addition-Subtraction

$$Y = S (A_0 + A_1 V_1 + A_2 V_2 + \dots) \quad (\text{SUM}) \quad (6.1-2)$$

#### 6.1.3 Multiplication

$$Y_i = S V_1 V_2 \dots \quad (\text{MULT}) \quad (6.1-3)$$

#### 6.1.4 Division

$$Y_i = \frac{S}{V_1} \text{ or } Y_i = \frac{S V_2}{V_1} \quad (\text{DIV}) \quad (6.1-4)$$

**6.1.5 Exponentiation**

$$Y_i = S V_1^I \quad (\text{POWERI}) \quad (6.1-5)$$

$$Y_i = S V_1^R \quad (\text{POWERR}) \quad (6.1-6)$$

$$Y_i = S V_1^{V_2} \quad (\text{POWERX}) \quad (6.1-7)$$

**6.1.6 Table Lookup Function**

$$Y_i = S F(V_1) \quad (\text{FUNCTION}) \quad (6.1-8)$$

where  $F$  is a function defined by table lookup and interpolation.

**6.1.7 Standard Functions**

$$Y = S F(V_1, V_2, V_3, \dots) \quad (\text{STDFNCTN}) \quad (6.1-9)$$

where  $F$  can be  $|V_1|$ ,  $\exp(V_1)$ ,  $\ln(V_1)$ ,  $\sin(V_1)$ ,  $\cos(V_1)$ ,  $\tan(V_1)$ ,  $\tan^{-1}(V_1)$ ,  $(V_1)^{1/2}$ ,  $\text{MAX}(V_1, V_2, V_3, \dots)$ , and  $\text{MIN}(V_1, V_2, V_3, \dots)$ . Only  $\text{MAX}$  and  $\text{MIN}$  may have multiple arguments and must have at least two arguments.

**6.1.8 Delay**

$$Y_i = S V_1(t - t_d) \quad (\text{DELAY}) \quad (6.1-10)$$

where  $t_d$  is the delay time. A user input,  $h$ , determines the number of pairs of data used to store past values of  $V_1$ . The maximum number of time-function pairs is  $h+2$ . The delay table time increment is  $t_d/h$ . The delayed function is obtained by linear interpolation using the stored past history. As time is advanced, new time values are added to the table. Once the table fills, new values replace values that are older than the delay time.

**6.1.9 Unit Trip**

$$Y_i = S U (\pm t_r) \quad (\text{TRIPUNIT}) \quad (6.1-11)$$

### 6.1.10 Trip Delay

$$Y_i = S T_r (t_r) \quad (\text{TRIPDISPLAY}) \quad (6.1-12)$$

In the above two trip-related components,  $t_r$  is a trip number and, if negative (TRIPUNIT only), indicates that the complement of the trip is to be used;  $U$  is 0.0 or 1.0, depending on trip  $t_r$  (or its complement if  $t_r$  is negative) being false or true; and  $T_r$  is -1.0 if the trip is false and the time the trip was last set true if the trip is true.

No numerical approximations are involved in evaluating the algebraic components. Evaluation is by simply performing the indicated operations. In the sequence of operations that perform a time advancement of the trip, heat conduction, hydrodynamic, reactor kinetic, and control systems of RELAP5, the control system is processed last. Thus, the end of time step ( $n+1$ ) values for trip variables  $t_r$  and all  $V_i$  variables except control variables  $Y_i$  are available. The control components are evaluated in component number order. As the first control variable  $Y_1$  is being evaluated, only old time values are available for all control component variables. Once  $Y_1$  is evaluated, the new time value for  $Y_1$  is available for the remaining control variable evaluations of  $Y_i$ . In general, while  $Y_i$  is being evaluated, new time values are available for  $Y_k$ ,  $k < i$ , and only old time values are available for  $Y_k$ ,  $k \geq i$ .

In the example,

$$Y_{10}^{n+1} = A_0 + A_1 T^{n+1} + A_2 P^{n+1} + A_3 Y_8^{n+1} + A_4 Y_{10}^n + A_5 Y_{15}^n \quad (6.1-13)$$

$T$  and  $P$ , which represent a temperature and pressure from the heat structure or hydrodynamic systems, are new time values. The value  $Y_8$  is also a new time value because it was advanced before control component 10, and  $Y_{10}$  and  $Y_{15}$  are old time values.

Initialization of the algebraic control components is very similar to a time advancement. At the start of control component initialization, all other time-advanced quantities have been initialized. Control component input includes an initial value and a flag that indicates if initialization is to be performed. The initialization proceeds in the order of component numbers. The initial value entered becomes the initial value if no initialization is specified. If initialization is specified, it is simply the specified computation using the available data. If component  $i$  references  $Y_k$ ,  $k < i$ , the initialized value of  $Y_k$  is used; if  $k \geq i$ , the entered initial value is used.

## 6.2 Integration Control Component

The integration component evaluates

$$Y_i = S \int_{t_1}^t V_i dt \quad (\text{INTEGRAL}) \quad (6.2-1)$$

where  $t_1$  is the simulation time when the component is added to the system, and the initial value at  $t_1$  is the input item regardless of the initialization flag.

The integral is advanced by trapezoidal approximation,

$$Y_1^{n+1} = Y_1^n + S [V_1^n + V_1^{n+1}] \frac{\Delta t}{2} . \quad (6.2-2)$$

Both new time ( $n+1$ ) and old time ( $n$ ) values are available for  $V_1$  except when it is a control variable  $Y_k$ ,  $k > i$ . For the case when  $V_1 = Y_k$ ,  $k \geq i$ , the  $V^n$  and  $V^{n+1}$  are instead  $V^{n-1}$  and  $V^n$ . Use of the integral component when old time values will be used should be avoided. Consider the example

$$a = P_1 - P_2 - BV - kd \quad (6.2-3)$$

$$v = \int a \, dt \quad (6.2-4)$$

$$d = \int v \, dt . \quad (6.2-5)$$

This acceleration-velocity-distance system cannot be advanced without use of old values. As a general rule, it is considered better to use the old value in the algebraic expression and not in the integral expressions.

Thus, using  $Y_1 = a$ ,  $Y_2 = V$ , and  $Y_3 = d$ ,

$$Y_1 = P_1 - P_2 - BY_2 - kY_3 \quad (6.2-6)$$

$$Y_2 = \text{INTEGRAL} (Y_1) \quad (6.2-7)$$

$$Y_3 = \text{INTEGRAL} (Y_2) . \quad (6.2-8)$$

### 6.3 Differentiation Control Components

Two components provide for differentiation

$$Y_i = \frac{dV_1}{dt} . \quad (6.3-1)$$

One component evaluates the derivative by the inverse of the integration technique,

$$Y_i = \frac{2S}{\Delta t} (V_i^{n+1} - V_i^n) - Y_i^n \quad (\text{DIFFERNI}) \quad (6.3-2)$$

This component is not recommended, since it can be unstable, requires an accurate initial value, and does not recover from a bad initial value. Deletion of this component is being considered. The recommended derivative component uses a simple difference expression,

$$Y_i = S \frac{(V_i^{n+1} - V_i^n)}{\Delta t} \quad (\text{DIFFERND}) \quad (6.3-3)$$

Differentiation is a noisy process and should be avoided. Differentiation of control system variables can almost always be avoided. Filtering the result of differentiation of other variables should be considered. Similar to the case of the integral component, old time values are used when advancement of  $Y_i$  involves  $V_i = Y_k$ ,  $k \geq i$ .

## 6.4 Proportional-Integral Component

This component evaluates

$$Y_i = S \left[ A_1 V_i + A_2 \int_{t_i}^t V_i dt \right] \quad (\text{PROP-INT}) \quad (6.4-1)$$

or, in Laplace transform notation,

$$Y_i(s) = S \left[ A_1 + \frac{A_2}{s} \right] V_i(s) \quad (6.4-2)$$

This component is advanced in time by

$$I^{n+1} = I^n + (V_i^n + V_i^{n+1}) \frac{\Delta t}{2} \quad (6.4-3)$$

$$Y_i^{n+1} = S (A_1 V_i^{n+1} + A_2 I^{n+1}) \quad (6.4-4)$$

The comments in the previous section concerning integration with  $V_i = Y_k$  hold for this component. If the initialization flag is off,  $Y^o$  is the entered initial value and

$$I^o = \frac{1}{A_2} \left( \frac{Y_i^o}{S} - A_1 V_i^o \right) \quad (6.4-5)$$

If the initialization flag is on,

$$I^o = 0 \quad (6.4-6)$$

$$Y_i^o = S A_1 V_1^o \quad (6.4-7)$$

## 6.5 Lag Control Component

The lag component is defined in Laplace transform notation as

$$Y_i(s) = S \left( \frac{1}{1 + A_1 s} \right) V_1(s) \quad (\text{LAG}) \quad (6.5-1)$$

Through algebraic rearrangement,

$$Y_i(s) + A_1 s Y_i(s) = S V_1(s) \quad (6.5-2)$$

$$\frac{Y_i(s)}{s} + A_1 Y_i(s) = \frac{S V_1(s)}{s} \quad (6.5-3)$$

$$Y_i(s) = \frac{S V_1(s) - Y_i(s)}{A_1 s} \quad (6.5-4)$$

Transforming to the time domain gives

$$Y_i = \int_0^t \frac{[S V_1 - Y_i] dt}{A_1} \quad (6.5-5)$$

The above expression is advanced numerically by

$$Y_i^{n+1} = Y_i^n + [S (V_1^n + V_1^{n+1}) - Y_i^n - Y_i^{n+1}] \frac{\Delta t}{2A_1} \quad (6.5-6)$$

or

$$Y_i^{n+1} = \frac{Y_i^n \left(1 - \frac{\Delta t}{2A_1}\right) + S(V_1^n + V_1^{n+1}) \frac{\Delta t}{2A_1}}{1 + \frac{\Delta t}{2A_1}} \quad (6.5-7)$$

If the initialization flag is not set,  $Y_i^{\circ}$  is the entered initial value. If it is set,

$$Y_i^{\circ} = SV_1^{\circ} \quad (6.5-8)$$

## 6.6 Lead-Lag Control Component

The lead-lag component is defined in Laplace transform notation as

$$Y_i(s) = S \left( \frac{1 + A_1 s}{1 + A_2 s} \right) V_1(s) \quad (\text{LEAD-LAG}) \quad (6.6-1)$$

Rearranging algebraically, this yields

$$Y_i(s) + A_2 s Y_i(s) = SV_1(s) + A_1 s SV_1(s) \quad (6.6-2)$$

or

$$Y_i(s) = \frac{A_1 SV_1(s)}{A_2} + \frac{SV_1(s) - Y_i(s)}{A_2 s} \quad (6.6-3)$$

Transforming to the time domain gives

$$Y_i = \frac{A_1 SV_1}{A_2} + \int_0^t \left( \frac{SV_1 - Y_i}{A_2} dt \right) \quad (6.6-4)$$

Note that the differentiation implied by the  $sV_1(s)$  term has been avoided. The above expression is advanced numerically by

$$Y_i^{n+1} = \frac{A_1}{A_2} SV_1^{n+1} + I^n + [S(V_1^n + V_1^{n+1}) - Y_i^n - Y_i^{n+1}] \frac{\Delta t}{2A_2} \quad (6.6-5)$$

or

$$Y_i^{n+1} = \frac{\frac{A_1}{A_2} S V_1^{n+1} + I^n + [S(V_1^n + V_1^{n+1}) - Y_1^n] \frac{\Delta t}{2A_2}}{1 + \frac{\Delta t}{2A_2}} \quad (6.6-6)$$

and finally

$$I^{n+1} = I^n + [S(V_1^n + V_1^{n+1}) - Y_i^n - Y_i^{n+1}] \frac{\Delta t}{2A_2} \quad (6.6-7)$$

If no initialization is specified,  $I^0 = 0$  and  $Y_i$  is the entered initial value. If initialization is specified, then

$$Y_i^0 = S V_i^0, I^0 = \left(1 - \frac{A_1}{A_2}\right) S V_i^0 \quad (6.6-8)$$

For both lag and lead-lag components, if  $V_1 = Y_k$ ;  $k = i$  is an error; when  $k < i$ , old and new values are used as indicated; if  $k > i$ ,  $V_1^n$  and  $V_1^{n+1}$  are really  $Y_k^{n-1}$ ,  $Y_k^n$ .

## 6.7 Shaft Component

The shaft component is a special control component that advances the rotational velocity,

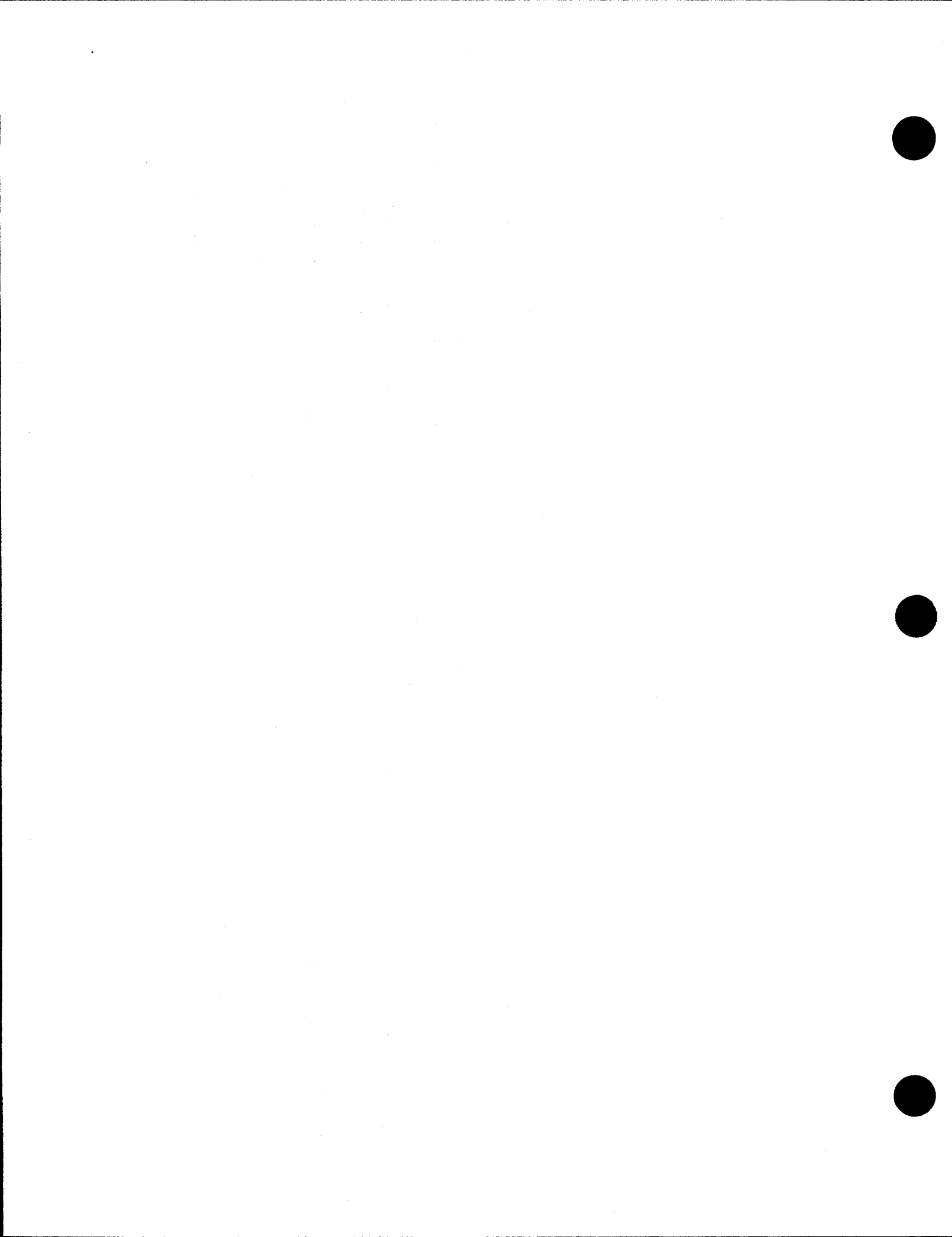
$$\sum_i I_i \frac{d\omega}{dt} = \sum_i \tau_i - \sum_i f_i \omega + \tau_c \quad (\text{SHAFT}) \quad (6.7-1)$$

where  $I_i$  is the moment of inertia from component  $i$ ,  $\tau_i$  is the torque from component  $i$ ,  $f_i$  is the friction from component  $i$ , and  $\tau_c$  is an optional torque from a control component. The summations are over the pump, generator, motor, or turbine components that are connected to the shaft and the shaft itself. The shaft and each associated component contains its own model, data, and storage for inertia, friction, and torque and has storage for its rotational velocity. Each associated component also has a disconnect trip number. If zero (no trip), the component is always connected to the shaft. If a trip is specified, the component is connected when false and disconnected when true. Any disconnected component is advanced separately and thus can have a different rotational velocity than the shaft. All connected components have the same rotational velocity.

The shaft equation is advanced explicitly by

$$\sum_i I_i \frac{(\omega^{n+1} - \omega^n)}{\Delta t} = \sum_i \tau_i^n - \sum_i f_i^n \omega^n + \tau_c \quad (6.7-2)$$

Inertias, torques, and friction are evaluated using old time information. The torque from the control system,  $\tau_c$ , would be in terms of new time values for quantities other than control variables and would use new or old time values for control variables depending on their component numbers relative to the shaft component number. Except when a generator component is involved, the shaft component calculations consist of solving Equation (6.7-2) for  $\omega^{n+1}$  separately for each component disconnected from the shaft (if any) and for the shaft and the connected components as one system. For separated components, the new rotational velocity is stored with the component data, and the summations are only over terms within the component. For the shaft and the connected components, the summations are over the shaft and the connected components; and the new rotational velocity is stored as the shaft's and each connected component's rotational velocity. A tripped generator, attached or connected, is treated as described above. An untripped generator rotates at the input synchronous speed; and, if connected to the shaft, the shaft and all connected components are forced to the synchronous speed.



## 7 POINT REACTOR KINETICS MODEL

The point reactor kinetics model can be used to compute power behavior in a nuclear reactor. The power is computed using the space-independent or point kinetics approximation which assumes that power can be separated into space and time functions. This approximation is adequate for cases in which the space distribution remains nearly constant.

The point reactor kinetics model computes both the immediate fission power and the power from decay of fission products. The immediate power is that released at the time of fission and includes power from kinetic energy of the fission products and neutron moderation. Decay power is generated as the fission products undergo radioactive decay. The user can select the decay power model based on either the American Nuclear Society Proposed Standard ANS 5.1, Decay Energy Release Rates Following Shutdown of Uranium-Fueled Thermal Reactors, revised October 1973, or the American National Standard for Decay Heat Power in Light Water Reactors, ANSI/ANS-5.1-1979.

### 7.1 Point Reactor Kinetics Equations

The point kinetics equations are

$$\frac{d}{dt}\phi(t) = \frac{[\rho(t) - \beta]\phi(t)}{\Lambda} + \sum_{i=1}^{N_d} \lambda_i C_i(t) + S \quad (7.1-1)$$

$$\frac{d}{dt}C_i(t) = \frac{\beta f_i}{\Lambda} \phi(t) - \lambda_i C_i(t) \quad i = 1, 2, \dots, N_d \quad (7.1-2)$$

$$\psi(t) = \sum_i \phi(t) \quad (7.1-3)$$

$$P_f(t) = Q_f \psi(t) \quad (7.1-4)$$

where

$t$  = time

$\phi$  = neutron flux

$C_i$  = number of delayed neutron precursors of group  $i$

$\beta$  = effective delayed neutron fraction

$\Lambda$  = prompt neutron generation time

$\rho$  = reactivity (only the time dependence has been indicated; however, the reactivity is dependent on other variables)

$f_i$	=	fraction of delayed neutrons of group i
$\lambda_i$	=	decay constant of group i
$S$	=	source
$\psi$	=	fission rate in #/s
$\Sigma_f$	=	macroscopic fission cross section
$P_f$	=	immediate fission power in MeV/s
$Q_f$	=	immediate fission energy per fission in MeV.

## 7.2 Fission Product Decay Model

The 1979 standard expresses the power  $P_{s\alpha}(t)$  in MeV/s as a function of time  $t$  resulting from one fission of isotope  $\alpha$  at  $t = 0$  as

$$P_{s\alpha}(t) = \sum_{j=1}^{N_\alpha} a_{\alpha j} \exp(-\lambda_{\alpha j} t) \quad (7.2-1)$$

Data are presented for three isotopes,  $^{235}\text{U}$ ,  $^{238}\text{U}$ , and  $^{239}\text{Pu}$ . The parameters  $a$  and  $\lambda$  were obtained by fitting to fission decay power data. The fitting for each isotope used 23 groups ( $N_\alpha = 23$ ). The above expression is an impulse response to one fission and can be extended to an arbitrary fission rate  $\psi_\alpha(t)$  through the convolution integral

$$P_\alpha(t) = P_{s\alpha}(t) * \psi_\alpha(t) = \sum_{j=1}^{N_\alpha} a_{\alpha j} \exp(-\lambda_{\alpha j} t) * \psi_\alpha(t) \quad (7.2-2)$$

where the convolution operation is defined by

$$A(t) * B(t) = \int_0^t A(t-\tau) B(\tau) d\tau = \int_0^t A(\tau) B(t-\tau) d\tau \quad (7.2-3)$$

Since numerical evaluation of convolution integrals is cumbersome, a set of differential equations equivalent to the convolution integral is derived.

Assume that the power from each group is from radioactive decay of a fission fragment  $i$ . Then

$$P_{\alpha j}(t) = \lambda_{\alpha j} \gamma_{\alpha j}(t) = a_{\alpha j} \exp(-\lambda_{\alpha j} t) \quad (7.2-4)$$

For simplification in the following derivation, the  $\alpha$  and  $j$  subscripts are dropped and the following expressions represent an equation for one group for one isotope. From Equation (7.2-4) we have

$$\gamma(t) = \frac{a}{\lambda} \exp(-\lambda t) \quad (7.2-5)$$

Laplace transforming Equation (7.2-5) gives

$$\gamma(s) = \frac{a}{\lambda(s + \lambda)} \quad (7.2-6)$$

Rearranging Equation (7.2-6) gives

$$s\gamma(s) = \frac{a}{\lambda} - \lambda\gamma(s) \quad (7.2-7)$$

Transforming to real time yields

$$\frac{d}{dt}\gamma(t) = \frac{a}{\lambda}\delta(0) - \lambda\gamma(t) \quad (7.2-8)$$

where  $\delta(0)$  is the impulse function. Applying a time-dependent fission rate  $\psi(t)$  in place of the single fission (impulse response), Equations (7.2-7) and (7.2-8) become

$$s\gamma(s) = \frac{a}{\lambda}\psi(s) - \lambda\gamma(s) \quad (7.2-9)$$

$$\frac{d}{dt}\gamma(t) = \frac{a}{\lambda}\psi(t) - \lambda\gamma(t) \quad (7.2-10)$$

Solution of Equations (7.2-9) or (7.2-10) (remembering that  $P = \lambda\gamma$ ) for an impulse yields Equation (7.2-1) and a similar expression in the standard. Solution of Equations (7.2-9) or (7.2-10) for an arbitrary fission source yields Equation (7.2-2). When specifying

$$\psi(t) = \begin{cases} 1, & 0 \leq t \leq T \\ 0, & t > T \end{cases} \quad (7.2-11)$$

Equations (7.2-9) and (7.2-10) yield another solution given in the standard. (Note that the standard defines  $t$  as starting at 0 after fissioning for  $T$  s.)

A physical model can be attached to the terms in Equation (7.2-10). The first term on the right represents production of the isotope during fission; the last term is the loss of the isotope due to decay. A more mechanistic model would also provide for production of one isotope due to the decay of another (see Section 7.3).

The 1979 ANS standard for decay power can be implemented by advancing the differential equations, which become

$$\frac{d}{dt} \gamma_{\alpha j}(t) = \frac{F_\gamma a_{\alpha j}}{\lambda_{\alpha j}} F_\alpha \psi(t) - \lambda_{\alpha j} \gamma_{\alpha j}(t) \quad j = 1, 2, \dots, N_\alpha \quad \alpha = 1, 2, 3 \quad (7.2-12)$$

$$P'_\gamma(t) = \sum_{\alpha=1}^3 \sum_{j=1}^{N_\alpha} \lambda_{\alpha j} \gamma_{\alpha j}(t) \quad (7.2-13)$$

where  $\psi$  is the fission rate from all isotopes,  $F_\alpha$  is the fraction of fissions from isotope  $\alpha$ , and  $P'_\gamma$  is the uncorrected decay power. Summation of  $F_\alpha$  over  $\alpha$  is 1.0. The value  $F_\gamma$  is a input factor to allow easy specification of a conservative calculation. It is usually 1.0 for best-estimate calculations, and 1.2 was recommended for a conservative calculation with the 1973 data. The 1979 data should allow consistent use of 1.0 for  $F_\gamma$ .

The ANS standard uses a correction factor to the energy from fission product decay to account for the effects of neutron absorption. Both an equation and a table for the correction factor are provided. The table is a maximum value for the  $G$  factor. The equation is

$$G(t) = 1.0 + (3.24 \cdot 10^{-6} + 5.23 \cdot 10^{-10} t) T^{0.4} \psi_g \quad (7.2-14)$$

where  $\psi_g$  is the number of fissions per initial fissile atom,  $T$  is the reactor operating time including any periods of shutdown, and  $t$  is the time since shutdown. Limits on the quantities are  $1.0 \geq \psi_g \geq 3.0$ ,  $T < 1.2614 \cdot 10^8$  s, and  $t < 10^4$  s. The table is used for  $t \geq 10^4$ . Note that there is a discontinuity in  $G(t)$  when switching from the equation to the table. The standard allows the table to be used in place of the equation and the code through user input allows the same. The corrected decay power is given by

$$P_\gamma = G(t) P'_\gamma \quad (7.2-15)$$

The 1973 proposed standard uses one isotope and prescribes data for 11 groups. The 1979 standard lists data for three isotopes,  $^{235}\text{U}$ ,  $^{238}\text{U}$ , and  $^{239}\text{Pu}$ , and uses 23 groups for each isotope. A user option also allows only the 1979 standard data for  $^{235}\text{U}$  to be used. The data for both standards are built into the code as default data, but the user may enter different data.

### 7.3 Actinide Decay Model

The actinide model describes the production of  $^{239}\text{U}$ ,  $^{239}\text{Np}$ , and  $^{239}\text{Pu}$  from neutron capture by  $^{238}\text{U}$ .

$$\frac{d}{dt}\gamma_{\text{U}}(t) = F_{\text{U}}\psi(t) - \lambda_{\text{U}}\gamma_{\text{U}}(t) \quad (7.3-1)$$

$$\frac{d}{dt}\gamma_{\text{N}}(t) = \lambda_{\text{U}}\gamma_{\text{U}}(t) - \lambda_{\text{N}}\gamma_{\text{N}}(t) \quad (7.3-2)$$

$$P_{\alpha}(t) = \eta_{\text{U}}\lambda_{\text{U}}\gamma_{\text{U}}(t) + \eta_{\text{N}}\lambda_{\text{N}}\gamma_{\text{N}}(t) \quad (7.3-3)$$

The quantity  $F_{\text{U}}$  is user-specified and is the number of atoms of  $^{239}\text{U}$  produced by neutron capture in  $^{238}\text{U}$  per fission from all isotopes. A conservative factor if desired should be factored into  $F_{\text{U}}$ . The  $\lambda$  and  $\eta$  values can be user-specified, or default values equal to those stated in the 1979 ANS standard can be used.

The first equation describes the rate of change of atoms of  $^{239}\text{U}$ . The first term on the right represents the production of  $^{239}\text{U}$ ; the last term is the loss of  $^{239}\text{U}$  due to beta decay. The second equation describes the rate of change of  $^{239}\text{Np}$ . The production of  $^{239}\text{Np}$  is from the beta decay of  $^{239}\text{U}$ , and  $^{239}\text{Pu}$  is formed from the decay of  $^{239}\text{Np}$ . Solution of the actinide Equations, (7.3-1) and (7.3-2), for the fission source given in Equation (7.2-11) yields the result quoted in the 1979 standard.

### 7.4 Transformation Of Equations For Solution

The differential equations to be advanced in time are Equations (7.1-1), (7.1-2), (7.2-12), (7.3-1), and (7.3-2). Multiplying by  $\Sigma_f$  and  $X$  which is the conversion factor from MeV/s to watts, the equations become

$$\frac{d}{dt}[X\psi(t)] = \frac{[\rho(t) - \beta]X\psi(t)}{\Lambda} + \sum_{i=1}^{N_d} \lambda_i X \Sigma_f C_i(t) + X \Sigma_f S \quad (7.4-1)$$

$$\frac{d}{dt}[X \Sigma_f C_i(t)] = \frac{\beta f_i X \psi(t)}{\Lambda} - \lambda_i X \Sigma_f C_i(t) \quad (7.4-2)$$

$$\frac{d}{dt}[X \gamma_{\alpha j}(t)] = \frac{F_{\gamma} a_{\alpha j} F_{\alpha} X \psi(t)}{\lambda_{\alpha j}} - \lambda_{\alpha j} X \gamma_{\alpha j}(t) \quad (7.4-3)$$

$$\frac{d}{dt}[X\gamma_U(t)] = F_U X \psi(t) - \lambda_U X \gamma_U(t) \quad (7.4-4)$$

$$\frac{d}{dt}[X\gamma_N(t)] = \lambda_U X \gamma_U(t) - \lambda_N X \gamma_N(t) \quad (7.4-5)$$

The total power  $P_T$  is the sum of immediate fission power, corrected fission product decay, and actinide decay, and now in units of watts is

$$P_T(t) = Q_f X \psi(t) + G(t) \sum_{\alpha=1}^3 \sum_{j=1}^{N_\alpha} \lambda_{\alpha j} X \gamma_{\alpha j}(t) + \eta_U \lambda_U X \gamma_U(t) + \eta_N \lambda_N X \gamma_N(t) \quad (7.4-6)$$

For solution convenience, the following substitutions are made:

$$\rho(t) = \beta r(t) \quad (7.4-7)$$

$$X\psi(t) = \psi'(t) \quad (7.4-8)$$

$$\frac{X \Sigma_f \Lambda S}{\beta} = S' \quad (7.4-9)$$

$$X \Sigma_i C_i(t) = \frac{\beta f_i}{\Lambda \lambda_i} W_i(t) \quad (7.4-10)$$

$$X \gamma_{\alpha j}(t) = \frac{F_\gamma a_{\alpha j} F_\alpha}{\lambda_{\alpha j}^2} Z_{\alpha j}(t) \quad (7.4-11)$$

$$X \gamma_U(t) = \frac{F_U}{\lambda_U} Z_U(t) \quad (7.4-12)$$

$$X \gamma_N(t) = Z_N(t) \quad (7.4-13)$$

The equations to be advanced are now:

$$\frac{d}{dt}\psi'(t) = \frac{\beta}{\Lambda} \left[ [r(t) - 1]\psi'(t) + \sum_{i=1}^{N_d} f_i W_i(t) + S' \right] \quad (7.4-14)$$

$$\frac{d}{dt}W_i(t) = \lambda_i \psi'(t) - \lambda_i W_i(t) \quad (7.4-15)$$

$$\frac{d}{dt}Z_{\alpha j}(t) = \lambda_{\alpha j} \psi'(t) - \lambda_{\alpha j} Z_{\alpha j}(t) \quad (7.4-16)$$

$$\frac{d}{dt}Z_u(t) = \lambda_u \psi'(t) - \lambda_u Z_u(t) \quad (7.4-17)$$

$$\frac{d}{dt}Z_N(t) = F_u Z_u(t) - \lambda_N Z_N(t) \quad (7.4-18)$$

$$P_T(t) = Q_f \psi'(t) + G(t) \sum_{\alpha=1}^3 \sum_{j=1}^{N_{\alpha}} \frac{F_{\gamma} a_{\alpha j} F_{\alpha} Z_{\alpha j}(t)}{\lambda_{\alpha j}} + F_u \eta_u Z_u(t) + \eta_N \lambda_N Z_N(t) \quad (7.4-19)$$

These equations are advanced using the modified Runge-Kutta method described in Section 7.7.

## 7.5 Initialization

Two initialization options are provided. In both options, the fission rate and delayed neutrons are in steady state or equilibrium conditions, that is, their time derivatives are zero. With  $r(0)$  an input quantity,

$$W_i(0) = \psi'(0) \quad i = 1, 2, \dots, N_d \quad (7.5-1)$$

$$S' = -r(0) \psi'(0) \quad (7.5-2)$$

The first option assumes that the fission product decay and actinides are also in equilibrium. This is equivalent to assuming that the reactor has been operating at a constant total power for an infinite period of time. The initial conditions are

$$Z_{\alpha j}(0) = \psi'(0) \quad i=1,2,\dots N_{\alpha} \quad \alpha = 1, 2, 3 \quad (7.5-3)$$

$$Z_u(0) = \psi'(0) \quad (7.5-4)$$

$$Z_N(0) = \frac{F_U}{\lambda_N} \psi'(0) \quad (7.5-5)$$

$$P_T(0) = \left[ Q_f + G(0) \sum_{\alpha=1}^3 \sum_{j=1}^{N_\alpha} \frac{F_\gamma a_{\alpha j} F_\alpha}{\lambda_{\alpha j}} Z_{\alpha j}(0) + F_U \eta_U Z_U(0) + \eta_N \lambda_N Z_N(0) \right] \psi'(0) \quad (7.5-6)$$

$$Q = Q_f + \sum_{\alpha=1}^3 \sum_{j=1}^{N_\alpha} F_\gamma a_{\alpha j} F_\alpha + F_U \eta_U + F_U \eta_N \quad (7.5-7)$$

The quantity  $Q$ , which is the total energy in MeV generated per fission, is either an input value or can be defaulted to 200 MeV. The quantity  $Q_f$  is defined from Equation (7.5-7) and the user-specified or defaulted data, even if the second initialization option is used. The total power is an input quantity, and  $\psi'(0)$  is determined from Equation (7.5-6). The remaining quantities are computed from  $\psi'(0)$  using Equations (7.5-1) through (7.5-5). Depending on a user option, the  $G$  factor is evaluated from Equation (7.2-14) with the reactor operating time  $T$  set to the user input and the operating time  $t$  set to zero or from the first value in the  $G$  factor table in the standard (1.020).

The second option uses a power history to determine the initial values of the fission product and actinide quantities. The power history consists of one or more periods of constant total power. For each period, the input consists of the total power, the time duration at that power, and, in the case of three isotopes, the fraction of power from each isotope. The fission product and actinide differential Equations, (7.4-16), (7.4-17), and (7.4-18), are advanced in time starting with initial values of zero. The fission rate,  $\psi$ , is defined from Equation (7.5-7). Depending on a user option, the  $G$  factor during this advancement is obtained from Equation (7.2-14) with the reactor operating time  $T$  advanced in time and the shutdown time  $t$  equal to zero or using the first value in the  $G$  factor table in the standard (1.020). The fission rate is reset to zero whenever a negative value is computed. This would occur whenever the user-entered total power is less than the current fission product and actinide decay power. Thus, for shutdown periods, the user may conveniently enter zero total power even though significant decay power remains. The fission product and actinide values at the end of the power history become the initial values for the transient. The initial fission rate is computed from Equation (7.5-7), using the total reactor power at the start of the transient (which may be different from the last power history value). If this fission rate is negative or zero, it is reset such that the immediate fission power is  $10^{-12}$  times the decay power.

The differential equations for the power history calculation are advanced using the same numerical technique as for the transient advancement except for a simplified time step control. Time step control consists of starting the advancement of each history period with a time step of 1 second. The time step is doubled after each advancement. When the next advancement would exceed the time duration, the last advancement is with the remaining time. This scheme was selected since, with each different power value, the solution moves toward a new equilibrium condition asymptotically; and the most rapid change is at the beginning of a power change.

## 7.6 Reactivity Feedback

Either separable or tabular models can be selected for reactivity feedback in point reactor kinetics.

### 7.6.1 Separable Feedback Model

The separable model, which is similar to the RELAP4<sup>7.6-1</sup> model, defines reactivity as

$$r(t) = r_o - r_B + \sum_{i=1}^{n_s} r_{si}(t) + \sum_{i=1}^{n_c} V_{ci} + \sum_{i=1}^{n_p} [W_{pi}R_p(p_i(t)) + a_{wi}T_{wi}(t)] + \sum_{i=1}^{n_f} [W_{fi}R_f(T_{fi}(t)) + a_{fi}T_{fi}(t)] . \quad (7.6-1)$$

The quantity  $r_o$  is an input quantity that represents the reactivity corresponding to assumed steady-state reactor power at  $t = 0$ . The quantity  $r_B$  is the bias reactivity which is calculated during input processing such that  $r(0) = r_o$  and is printed in the input level printout. Should the user check the bias reactivity computation using Equation (7.6-1), the temperature used in the  $a_{wi} T_{wi}(t)$  and  $a_{fi} T_{fi}(t)$  terms should use absolute temperature, i.e., Kelvin in SI units and Rankine in British units. The temperature used in the table lookup term  $W_{fi}R_f(T_{fi}(t))$ , however, should still use Kelvin in SI units and Fahrenheit in British units.

The quantities  $r_{si}$  are obtained from input tables defining  $n_s$  reactivity curves as a function of time. The quantities  $V_{ci}$  are  $n_c$  control variables that can be user-defined as reactivity contributions.  $R_p$  is a table defining reactivity as a function of the current density of water  $p_i(t)$  in the hydrodynamic volume  $i$ ;  $W_{pi}$  is the density weighting factor for volume  $i$ ;  $T_{wi}(t)$  is the spatial density averaged temperature of volume  $i$ ;  $a_{wi}$  is the temperature coefficient (not including density changes) for volume  $i$ ; and  $n_p$  is the number of hydrodynamic volumes in the reactor core. The quantity  $R_f$  is a table defining reactivity as a function of the volume average fuel temperature  $T_{fi}(t)$  in heat structure  $i$ ;  $W_{fi}$  and  $a_{fi}$  are the fuel temperature weighting factor and the fuel temperature coefficient, respectively; and  $n_f$  is the number of heat structures in the reactor core.

The model assumes nonlinear feedback effects from moderator density and fuel temperature changes and linear feedback from moderator temperature changes. It is called the separable model because each effect is assumed to be independent of the other effects. Boron feedback is not provided, but a user-defined boron feedback can be implemented with the control system. The separable model can be used if boron changes are quite small and the reactor is near critical about only one state point.

### 7.6.2 Tabular Feedback Model

A postulated BWR anticipated transient without scram (ATWS) accident is an example where the reactor could be nearly critical for two different state points. One point is at normal power operating conditions--high moderator and fuel temperatures, highly voided, and no boron. During accident recovery, the reactor might approach a critical condition with relatively cold moderator and fuel temperatures, with no voids, but with some boron concentration. The reactivity could be nearly critical for both states, but the contributions from the different feedback effects are vastly different. The assumptions of no interactions among the different feedback mechanisms, especially boron, cannot be justified.

The tabular feedback model computes reactivity from multi-dimensional table lookup and linear interpolation. The tabular model overcomes the objections of the separable model since all feedback mechanisms can be nonlinear and interactions among the mechanisms are included. The penalty for the expanded modeling capability is greatly increased input data requirements.

Two different options within the tabular feedback option are available. One option allows two different sets of independent variables. Both sets of variables use a boron related variable as one of the four variables. The second option chooses between three or four independent variables and the boron related variable is omitted when only three variables are used.

### 7.6.2.1 Standard Variables

With standard independent variables, the tabular model defines reactivity as

$$r(t) = r_o - r_B + \sum_{i=1}^{n_c} r_{si} + \sum_{i=1}^{n_c} V_{ci} + R(\bar{p}(t), T_w(t), T_f(t), B(t)) \quad (7.6-2)$$

$$\bar{p}(t) = \sum_{i=1}^{n_p} W_{pi} p_i(t) \quad (7.6-3)$$

$$T_w(t) = \sum_{i=1}^{n_p} W_{pi} \left[ \frac{\alpha_{fi} p_{fi} T_{fi}(t) + \alpha_{gi} p_{gi} T_{gi}(t)}{\alpha_{fi} p_{fi} + \alpha_{gi} p_{gi}} \right] \quad (7.6-4)$$

$$B(t) = \sum_{i=1}^{n_p} W_{pi} B_i(t) \quad (7.6-5)$$

$$T_f(t) = \sum_{i=1}^{n_F} W_{Fi} T_{Fi}(t) \quad (7.6-6)$$

The variables,  $r_o$ ,  $r_B$ ,  $r_{si}$ , and  $V_{ci}$  are the same as for separable feedback,  $p_i$  is the density in volume  $i$  (mass of liquid, vapor, and noncondensable divided by volume of volume),  $T_{fi}$  and  $T_{gi}$  are liquid and vapor temperatures of volume  $i$ ,  $\alpha_{fi}$  and  $\alpha_{gi}$  are liquid and vapor void fractions in volume  $i$ ,  $B_i$  is spatial boron density, and  $T_{Fi}$  is the volume averaged fuel temperature for heat structure  $i$ . The average quantities are obtained with the use of one weighting factor for each hydrodynamic volume  $W_p$  contributing to reactivity feedback and one weighting factor for each heat structure  $W_{Fi}$  contributing to reactivity feedback. The reactivity function  $R$  is defined by a table input by the user. In the Input Requirements, Volume II of these manuals, TABLE3 and TABLE4 options refer to the above set of independent variables; TABLE4 option specifies a four dimensional table, TABLE3 option assumes no boron dependence and the table is then three dimensional.

**7.6.2.2 Alternate Variables.** With alternate independent variables, the tabular model defines reactivity as

$$r(t) = r_o - r_B + \sum_{i=1}^{n_c} r_{si} + \sum_{i=1}^{n_c} V_{ci} + R(\alpha_g(t), T_f(t), T_F(t), B_c(t)) \quad (7.6-7)$$

$$\alpha_g(t) = \sum_{i=1}^{n_p} W_{pi} \alpha_{gi}(t) \quad (7.6-8)$$

$$T_f(t) = \sum_{i=1}^{n_p} W_{pi} T_{fi}(t) \quad (7.6-9)$$

$$B_c(t) = \sum_{i=1}^{n_p} W_{pi} \frac{B_i}{\rho_{fi}}(t) \quad (7.6-10)$$

$$T_F(t) = \sum_{i=1}^{n_F} W_{Fi} T_{Fi}(t) \quad (7.6-11)$$

The quantity  $B_c$  is the boron concentration in parts of boron per parts of liquid water and the other quantities are the same as for the standard variables. Input options TABLE3A and TABLE4A specify the alternate set of independent variables; TABLE4A selects four independent variables and TABLE3A selects only three independent variables with the boron concentration being omitted.

**7.6.2.3 Interpolation Procedures.** The reactivity function  $R$  is evaluated by a direct extension of the one-dimensional table lookup and linear interpolation scheme to multiple dimensions. One-dimensional table lookup and interpolation of the function  $V = F(W)$  uses an ordered set of  $N_w$  independent variable values  $W_i$ , with the corresponding values of the dependent variable  $V_i$ , to determine the value of  $V$  corresponding to a search argument  $W$ . The independent variable is searched such that  $W_i$  and  $W_{i+1}$  bracket  $W$ ; an equation for a straight line is fitted to the points  $W_i, V_i$ , and  $W_{i+1}, V_{i+1}$ ; and the straight line equation is evaluated for the given  $W$ .

Using subscripts 0 and 1 for the bracketing independent values and corresponding dependent values and defining  $w = (W - W_0)/(W_1 - W_0)$  so that  $w$  varies from 0 through 1 as  $W$  varies from  $W_0$  through  $W_1$ , the interpolation equations are

$$V = \sum_{i=0}^1 a_i w^i \quad (7.6-12)$$

$$a_0 = V_0 \quad (7.6-13)$$

$$a_1 = V_1 - V_0 \quad (7.6-14)$$

For two-dimensional interpolation of  $V = F(W, X)$ , two sets of independent variables are used;  $N_w$  values of  $W_i$  and  $N_x$  values of  $X_j$ . A total of  $N_w N_x$  dependent values of  $V_{ij}$  are entered, one value for each combination of variables from the two sets of independent variables. Graphically, the two sets of independent variables form a rectangular grid when the  $W_i$  and  $X_j$  variables are plotted on horizontal and vertical coordinates, respectively. The dependent variables are entered corresponding to the intersections of the mesh lines. The search for bracketing values in each independent set locates a mesh rectangle, and the dependent values at the four corners are used to form an interpolation equation which is the product of two straight line functions, one for each independent variable. Using 0 and 1 subscripts for the bracketing values,

$$V = \sum_{i=0}^1 \sum_{j=0}^1 a_{ij} w^i x^j \quad (7.6-15)$$

$$x = \frac{X - X_0}{X_1 - X_0} \quad (7.6-16)$$

$$a_{00} = V_{00} \quad (7.6-17)$$

$$a_{01} = V_{01} - V_{00} \quad (7.6-18)$$

$$a_{10} = V_{10} - V_{00} \quad (7.6-19)$$

$$a_{11} = V_{11} - V_{01} - V_{10} + V_{00} \quad (7.6-20)$$

This process is simply extended to three and four dimensions. Three sets of independent variables define a three dimensional rectangular grid; and eight dependent quantities corresponding to the corners of a rectangular solid are used to define the interpolation equation, which is the product of three straight line functions. In four dimensions, four sets of independent variables are defined; and 16 dependent values are used to define the interpolation equation, which is the product of four straight line functions.

For three dimensional interpolation,

$$V = F(W, X, Y) \quad (7.6-21)$$

$$y = \frac{Y - Y_0}{Y_1 - Y_0} \quad (7.6-22)$$

$$V = \sum_{i=0}^1 \sum_{j=0}^1 \sum_{k=0}^1 a_{ijk} w^i x^j y^k \quad (7.6-23)$$

$$a_{000} = V_{000} \quad (7.6-24)$$

$$a_{001} = V_{001} - V_{000} \quad (7.6-25)$$

$$a_{010} = V_{010} - V_{000} \quad (7.6-26)$$

$$a_{100} = V_{100} - V_{000} \quad (7.6-27)$$

$$a_{011} = V_{011} - V_{001} - V_{010} + V_{000} \quad (7.6-28)$$

$$a_{101} = V_{101} - V_{001} - V_{100} + V_{000} \quad (7.6-29)$$

$$a_{110} = V_{110} - V_{010} - V_{100} + V_{000} \quad (7.6-30)$$

$$a_{111} = V_{111} - V_{011} - V_{101} - V_{110} + V_{001} + V_{010} + V_{100} - V_{000} \quad (7.6-31)$$

For four dimensional interpolation,

$$V = F(W, X, Y, Z) \quad (7.6-32)$$

$$z = \frac{Z - Z_0}{Z_1 - Z_0} \quad (7.6-33)$$

$$V = \sum_{i=0}^1 \sum_{j=0}^1 \sum_{k=0}^1 \sum_{m=0}^1 a_{ijkm} w^i x^j y^k z^m \quad (7.6-34)$$

$$a_{0000} = V_{0000} \quad (7.6-35)$$

$$a_{0001} = V_{0001} - V_{0000} \quad (7.6-36)$$

$$a_{0010} = V_{0010} - V_{0000} \quad (7.6-37)$$

$$a_{0100} = V_{0100} - V_{0000} \quad (7.6-38)$$

$$a_{1000} = V_{1000} - V_{0000} \quad (7.6-39)$$

$$a_{0011} = V_{0011} - V_{0001} - V_{0010} + V_{0000} \quad (7.6-40)$$

$$a_{0101} = V_{0101} - V_{0001} - V_{0100} + V_{0000} \quad (7.6-41)$$

$$a_{0110} = V_{0110} - V_{0010} - V_{0100} + V_{0000} \quad (7.6-42)$$

$$a_{1001} = V_{1001} - V_{0001} - V_{1000} + V_{0000} \quad (7.6-43)$$

$$a_{1010} = V_{1010} - V_{0010} - V_{1000} + V_{0000} \quad (7.6-44)$$

$$a_{1100} = V_{1100} - V_{0100} - V_{1000} + V_{0000} \quad (7.6-45)$$

$$a_{0111} = V_{0111} - V_{0011} - V_{0101} + V_{0110} + V_{0001} + V_{0010} + V_{0100} - V_{0000} \quad (7.6-46)$$

$$a_{1011} = V_{1011} - V_{0011} - V_{1001} + V_{1010} + V_{0001} + V_{0010} + V_{1000} - V_{0000} \quad (7.6-47)$$

$$a_{1101} = V_{1101} - V_{0101} - V_{1001} + V_{1100} + V_{0001} + V_{0100} + V_{1000} - V_{0000} \quad (7.6-48)$$

$$a_{1110} = V_{1110} - V_{0110} - V_{1010} + V_{1100} + V_{0010} + V_{0100} + V_{1000} - V_{0000} \quad (7.6-49)$$

$$a_{1111} = V_{1111} - V_{0111} - V_{1011} - V_{1101} - V_{1110} + V_{0011} + V_{0101} + V_{0110} + V_{1101} + V_{1001} + V_{1010} + V_{1100} - V_{0001} - V_{0010} - V_{0100} - V_{1000} + V_{0000} \quad (7.6-50)$$

The interpolating equations define a continuous function. There is no discontinuity in the dependent quantity as any one or combination of dependent variables pass to the next bracketing pair of values.

Using  $N_W$ ,  $N_X$ ,  $N_Y$ , and  $N_Z$  as the number of values in the four sets of independent variables, the number of data points for a three dimensional table is  $N_W N_X N_Y$  and is  $N_W N_X N_Y N_Z$  for a four dimensional table. Using only four values for each independent variable, a four dimensional table requires 256 data points.

### 7.6.3 Reference

7.6-1. EG&G Idaho, Inc., *RELAP4/MOD6: A Computer Program for Transient Thermal-Hydraulic Analysis of Nuclear Reactors and Related Systems Users Manual*, CDAP-TR-003, May 1978.

## 7.7 Reactor Kinetics Numerical Procedures

The reactor kinetics equations are advanced in time using the modified Runge-Kutta method of Cohen.<sup>7.7-1</sup> A first order differential equation is written as

$$n(t) = \alpha n(t) + R(n,t) \quad (7.7-1)$$

where  $\alpha$  is constant over the time step, and  $R(n,t)$  contains the remaining terms of the differential equation, including the non constant portion of any coefficient of  $n(t)$ . If the coefficient of  $n(t)$  is  $\beta(n,t)$ ,  $\alpha$  would be  $\beta[n(0),0]$ ; and  $R(n,t)$  would contain a term of the form  $\beta[n(t),t] - \alpha n(t)$ . Multiplying Equation (7.7-1) by an integrating factor and integrating gives

$$n(t) = n(0) e^{\alpha t} + \int_0^t e^{\alpha(t-\lambda)} R(n, \lambda) d\lambda \quad (7.7-2)$$

Since

$$n(0) e^{\alpha t} = n(0) + \int_0^t \alpha n(0) e^{\alpha(t-\lambda)} d\lambda, \quad (7.7-3)$$

$$n(t) = n(0) + \int_0^t [\alpha n(0) + R(n, \lambda)] e^{\alpha(t-\lambda)} d\lambda \quad (7.7-4)$$

Letting  $\lambda = ut$ , then  $d\lambda = tdu$ , and

$$n(t) = n(0) + \int_0^1 [\alpha n(0) + R(n, u)] e^{\alpha t(1-u)} du \quad (7.7-5)$$

The numerical technique for advancing the solution over the time step consists of making approximations to the behavior of  $R(n,u)$  over the time step. For convenience in the following expressions, the following function is defined,

$$C_m(x) = \int_0^1 u^{m-1} e^{x(1-u)} du \quad (7.7-6)$$

Stage 1:

Assume  $R(n,\lambda) = R[n(0),0] = R_0$  and write  $n(0)$  as  $n_0$ ; then compute  $n\left(\frac{h}{2}\right)$  by

$$n_1 = n\left(\frac{h}{2}\right) = n_0 + \frac{h}{2} [\alpha n_0 + R_0] C_1\left(\alpha \frac{h}{2}\right) \quad (7.7-7)$$

Stage 2:

Assume straight line variation of  $R(n, \lambda)$  between  $R_0$  and  $R_1 = R\left(n_1, \frac{h}{2}\right)$  and compute  $n\left(\frac{h}{2}\right)$  by

$$R(n, \lambda) = R_0 + \frac{2(R_1 - R_0)\lambda}{h} \quad (7.7-8)$$

$$R(n, \lambda) = R_0 + (R_1 - R_0)u \quad (7.7-9)$$

$$n_2 = n\left(\frac{h}{2}\right) = n_1 + \frac{h}{2} [R_1 - R_0] C_2\left(\alpha \frac{h}{2}\right) \quad (7.7-10)$$

Stage 3:

Assume straight line variation of  $R(n, \lambda)$  between  $R_0$  and  $R_2 = R\left(n_2, \frac{h}{2}\right)$  and compute  $n(h)$  by

$$R(n, \lambda) = R_0 + \frac{2}{h} [R_2 - R_0] \lambda \quad (7.7-11)$$

$$R(n, u) = R_0 + 2 [R_2 - R_0] u \quad (7.7-12)$$

$$n_3 = n(h) = n_0 + h(\alpha n_0 + R_0) C_1(\alpha h) + 2h(R_2 - R_0) C_2(\alpha h) \quad (7.7-13)$$

Stage 4:

Assume quadratic through points  $R_0$ ,  $R_2$ , and  $R_3 = R(n_3, h)$ , then compute  $n(h)$  by

$$R(n, u) = (2R_0 + 4R_2 + 2R_3) u_2 + (-3R_0 + 4R_2 - R_3) u + R_0 \quad (7.7-14)$$

$$n_4 = n(h) = n_3 + h (R_4 - R_3) [2C_3(\alpha h) - C_2(\alpha h)] \quad (7.7-15)$$

Stage 5:

Assume quadratic through points  $R_0$ ,  $R_2$ , and  $R_4 = R(n_4, h)$ , then compute  $n(h)$  by

$$n_5 = n(h) = n_4 + h (R_4 - R_3) [2C_3(\alpha h) - C_2(\alpha h)] \quad (7.7-16)$$

Third, fourth, and fifth order approximations are obtained by terminating the process at the end of the third, fourth and fifth stages, respectively. RELAP5 uses only the fifth order approximation.

By direct integration, the function  $C_1(x)$  is given by

$$C_1(x) = \frac{e^x - 1}{x} . \quad (7.7-17)$$

Using integration by parts, a recursion relation for  $C_m(x)$  is

$$C_{m+1}(x) = \frac{mC_m(x) - 1}{x} . \quad (7.7-18)$$

During machine calculations of the  $C_m(x)$  functions for  $x \leq 1$ , excessive loss of significance occurs. For this range,  $C_3(x)$  is computed from its MacLaurin series expansion

$$C_3(x) = 2 \left[ \frac{1}{3!} + \frac{x}{4!} + \frac{x^2}{5!} + \frac{x^3}{6!} + \frac{x^4}{7!} + \frac{x^5}{8!} + \frac{x^6}{9!} + \frac{x^7}{10!} \right] . \quad (7.7-19)$$

$C_2$  and  $C_1$  are evaluated by solving Equation (7.7-18) for  $C_m(x)$ .

During the advancement in time of the solution, the time increment is automatically increased or decreased to maintain a specified degree of accuracy. After the calculations for a reactor kinetics time advancement, an empirical formula is used to estimate the error. If the error is excessive, the time increment is halved; and the advancement calculation is redone. If the error is sufficiently small, the time interval is doubled for the next time step. If the estimated error is between limits, the same interval is used for the next time advancement. These procedures for time step control, taken from the AIREK code<sup>7.7-2</sup> are as follows:

$$\omega_1 = \frac{\psi'(0)}{\psi(0)} \quad (7.7-20)$$

$$\omega_3 = \frac{\psi'(h)}{\psi(h)} . \quad (7.7-21)$$

$\bar{\omega}$  is defined by

$$\psi'(h) = \psi'(0) e^{\bar{\omega}h} \quad (7.7-22)$$

$$Q = \frac{hC_2(\alpha h)}{1 + C_1(\alpha h)} [\omega_1 - 2\bar{\omega} + \omega_3] \quad (7.7-23)$$

The  $\alpha$  in Equation (7.7-18) is that of the neutron flux Equation (7.4-14)

$$\delta = \max \left[ \frac{n_{1i} - n_{0i}}{n_{1i}} \right] \quad (7.7-24)$$

The  $Q_L$  and  $Q_H$  appearing below are 0.0001 and 0.001 respectively.

1. If  $\delta < 2^{-15}$  and  $Q \geq Q_L$ , the program continues with the same time step.
2. If  $\delta < 2^{-15}$  and  $Q < Q_L$ , the program doubles the time step for the next advancement.
3. If  $\delta \geq 2^{-15}$  and
  - a.  $Q < Q_L$ , the time step is doubled for the next advancement.
  - b.  $Q \leq Q_H$ , the same time step is used for the next advancement.
  - c.  $Q > Q_H$ , the time advancement is recalculated with half the time step.
4. The time advancement is also recomputed with the time step halved if
  - a.  $\alpha h$  of any equation  $> 88.0$ .
  - b. negative or zero power is computed.

If the coefficient of the neutron flux in Equation (7.4-14) is negative, a subtraction is involved in determination of the derivative and a loss of significant digits can occur. If this coefficient is negative, a check is made of the number of bits lost in the subtraction. If more than nine bits are lost, the value of neutron flux computed by the current stage of the advancement procedure is discarded; instead, neutron flux is determined from the expression obtained by setting the neutron flux derivative to zero

$$\psi(t) = \frac{- \sum_{i=1}^{N_d} f_i W_i(t) - \frac{S\Lambda}{\beta}}{r(t) - 1} \quad (7.7-25)$$

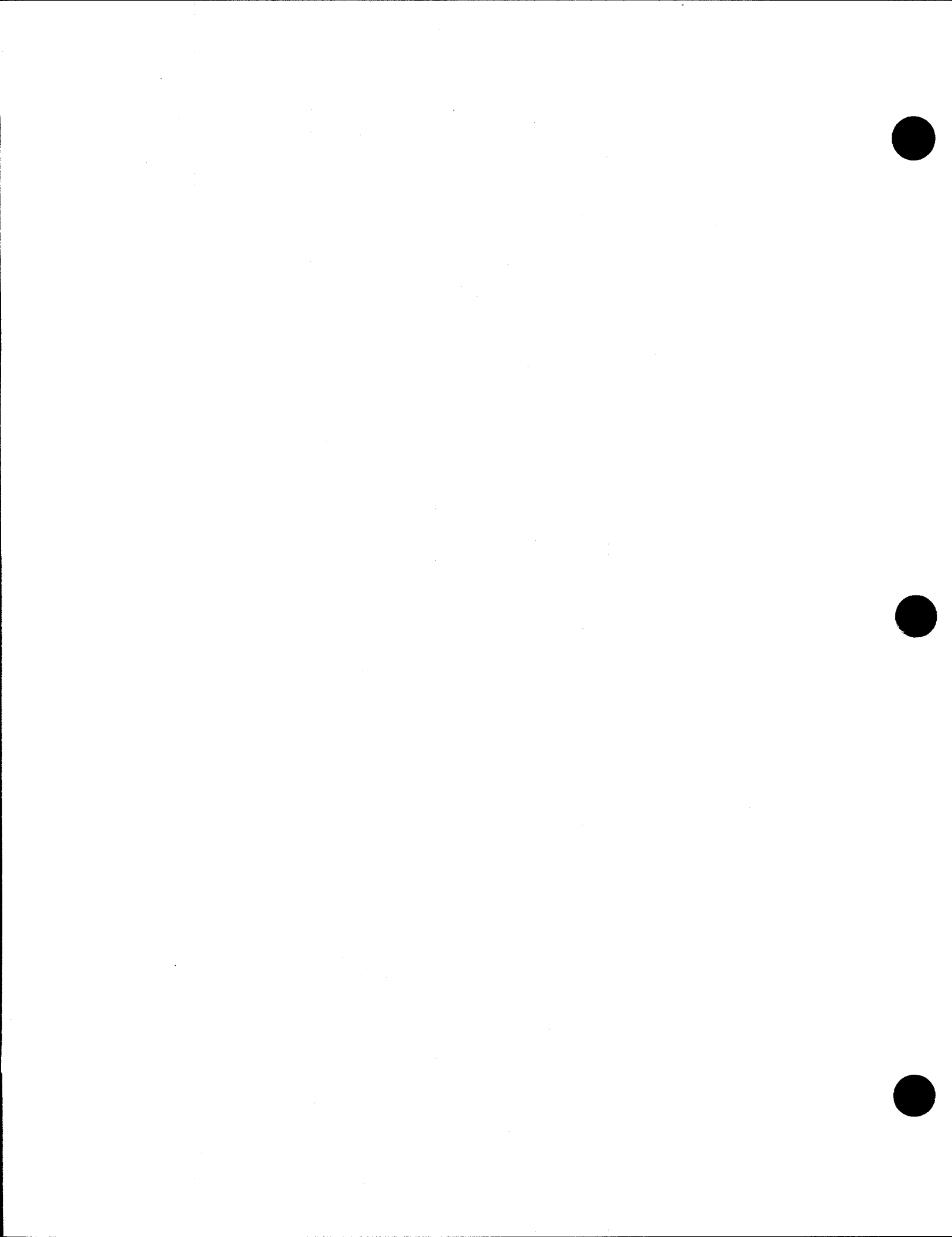
The transfer of information between the reactor kinetics calculation and the other calculations is explicit. Hydrodynamic and heat conduction/transfer calculation precede reactor kinetics, and the control system calculation follows reactor kinetics. The reactor power used in hydrodynamics and heat conduction is the value at the beginning of the time step. The reactivity used as the end of time step value in the

kinetics advancement is computed from end of time step values from hydrodynamics and heat conduction and beginning of time step values from the control system.

The reactor kinetics equations are advanced at the same time step as the hydrodynamics, and reactivity is assumed to vary linearly between time step values. The maximum time step for the reactor kinetics advancement is the hydrodynamic time step. That time step is reduced, if necessary, as described above.

### 7.7.1 References

- 7.7-1. E. R. Cohen, *Some Topics In Reactor Kinetics*, A/CONF, 15, 1958, p 629.
- 7.7-2. A. Schwartz, *Generalized Reactor Kinetics Code AIREK II*, NAA-SR-Memo-4980, 1960.



## 8 SPECIAL TECHNIQUES

The mass from the state relationship is compared to the mass from the continuity equation, and the difference is a measure of the truncation error inherent in the numerical solution. This is the main method used to control the time step and thus control the truncation error.

Special methods are provided in the code for use in obtaining initial conditions. These methods are based on the transient solution algorithm but make use of an accelerated thermal transient solution technique in order to shorten the computer time required to achieve steady state.

### 8.1 Time Step Control

A variety of checks on solution acceptability are used to control the time step. These include material Courant limit checks, mass error checks, phase appearance checks, material properties out of defined ranges, water property errors, or excessive extrapolation of state properties in the metastable regimes.

The material Courant limit check is made before a hydrodynamic advancement takes place. Thus, it may reduce the time step, but it does not cause a time step to be repeated. All of the other checks may cause all or part of the time advancement to be repeated at a smaller time step. The material Courant limit is evaluated for each hydrodynamic volume using the volume mass average velocity i.e.,

$$(\Delta t_c)_i = (\Delta x) \max(\alpha_f^n, \alpha_g^n) / \max(|\alpha_f^n v_f^n|, |\alpha_g^n v_g^n|) \quad i = 1, 2, \dots, N \quad (8.1-1)$$

The N volumes are divided into five subsets, i.e., the 1st, 6th, 11th, ... volumes belong to the first subset, the 2nd, 7th, 12th,... volumes belong to the second subset, etc. The minimum Courant limits for each of the five subsets are rearranged in ascending order, i.e.,

$$\Delta t_c^1 \leq \Delta t_c^2 \leq \Delta t_c^3 \leq \Delta t_c^4 \leq \Delta t_c^5 \quad (8.1-2)$$

Obviously,  $\Delta t_c^1$  is the Courant limit for the entire system. This is the number printed at each major edit under "CRNT. DT =". For the semi-implicit scheme,  $\Delta t_c^2$  is used for limiting the time step size. Thus, partial violation of the material Courant limit is allowed for this scheme. For the nearly implicit scheme, 20 times  $\Delta t_c^2$  is used for limiting the time step size for the transient mode, and 40 times  $\Delta t_c^2$  is used for limiting the time step size for the steady-state mode.

The mass error check is made when the time step solution is nearly complete. If excessive mass error is detected, the time step is repeated at a reduced interval. Two types of mass error measures are computed. The first one is designed to check the validity of the density linearization and is defined as

$$\varepsilon = \max \left( \frac{|\rho_{mi} - \rho_{li}|}{\rho_i} \right) i = 1, N \quad (8.1-3)$$

where  $\rho_{mi}$  is the total density of the  $i$ -th volume obtained from the mass continuity equation, and  $\rho_i$  is the total density of the  $i$ -th volume computed from the state relationship. The second one is a measure of overall system mass error and is given by

$$\epsilon_{rms} = 2 \sum_{i=1}^N [V_i (\rho_i - \rho_{mi})]^2 / \sum_{i=1}^N (V_i \rho_i)^2 . \quad (8.1-4)$$

If either  $\epsilon_m$  or  $\epsilon_{rms}$  is  $> 8 \times 10^{-3}$ , the time step is rejected and repeated with one half of the time step size. Otherwise, the time step is accepted, and the next time step size is doubled if both  $\epsilon_m$  and  $\epsilon_{rms}$  are  $< 8 \times 10^{-4}$ .

At any point in the solution flow, if a material property is found to lie outside the defined range, the time step is halved and repeated. This halving process proceeds until the property is within range or the user-specified minimum time step is reached. If the minimum time step is reached without obtaining a valid solution, the code calculation is terminated; the last time step is repeated with a diagnostic dump printed, and the program stops at the completion of the advancement. This same procedure is applied for all water property or extrapolation failures. The liquid metastable checks used are specific volume less than or equal to 0 and liquid temperature greater than 50 K above saturation temperature. The vapor metastable checks are vapor specific volume less than or equal to 0 and the vapor temperature less than 50 K below saturation temperature.

In addition to the time step control algorithm described above, there is a time step control based on the change in the pressure in a volume during an advancement, which is used whenever noncondensable gas first appears in a volume. This time step control algorithm causes the code to repeat a time step if the change in pressure during a time step exceeds the old time value, the new time value, or 50,000 Pa. This time step control has the effect of allowing the pressure to change by no more than a factor of two during a time step.

## 8.2 Mass/Energy Error Mitigation

The semi-implicit numerical scheme described in Section 3.1.4 and Section 3.1.5 has two calculations of the new time variables  $\alpha_g$ ,  $U_g$ ,  $U_f$ , and  $X_n$ . These variables are first calculated in connection with a linearization of all the product terms involved in the time derivatives and are referred to as tentative new time variables [see Equations (3.1-87) through (3.1-91)]. They are denoted by a tilde in Section 3.1.4 and Section 3.1.5. This first calculation uses a numerically conservative form for all flux calculations of mass and energy, but because the products in the time derivatives are linearized, the quantities  $\alpha_g \rho_g$ ,  $\alpha_f \rho_f$ ,  $\alpha_g \rho_g U_g$ ,  $\alpha_f \rho_f U_f$ , and  $\alpha_g \rho_g X_n$  are not numerically conserved. These tentative new time values are only used to evaluate the interphase heat and mass transfer terms to be used in the second evaluation of the basic equations. In this second evaluation of the basic equations [see Equations (3.1-107), (3.1-109), (3.1-110), (3.1-112), and (3.1-113)], the products appearing in the time derivatives are not linearized. This second step also uses the numerically conservative form for the flux terms. Hence, the final end of time step values have been calculated using a consistent and numerically conservative form of differencing. The truncation errors in the linearization procedure may produce errors in the solution for pressure, phasic energies, and void fraction. Since the state is computed from these basic variables, the resultant density may have some error. This error is used in the time step control presented in Section 8.1.

There are mass and energy errors that the numerically conservative form of differencing cannot remove. The convective terms in the field equations are computed with donor properties determined by the direction of phasic velocities. There are times that the final velocities may differ in directions from the explicit velocities used to define the donor properties. This may result in mass/energy errors due to incorrect properties used in the numerical scheme. The term *velocity flip-flop* refers to the situation in which the final velocities and the explicit velocities differ in sign. In the RELAP5 numerical scheme, the pressures and final velocities are calculated using the donor properties based on the explicit velocities (see Section 3.1.4). The velocity flip-flop implies that inconsistent donor properties were used for the pressure computation and the final mass/energy computation. This may result in bad velocity and energy solutions and large mass errors. Thus, a mitigation scheme is employed to detect errors of this type.

Let  $\alpha_{fj}$ ,  $\tilde{\rho}_{fj}$ ,  $\tilde{U}_{fj}$ ,  $\alpha_{gj}$ ,  $\tilde{\rho}_{gj}$ , and  $\tilde{U}_{gj}$  be the junction liquid fraction, liquid density, liquid energy, void fraction, vapor density, and vapor energy, respectively, based on the explicit velocities, and let  $\tilde{\alpha}_{fj}$ ,  $\tilde{\rho}_{fj}$ ,  $\tilde{U}_{fj}$ ,  $\tilde{\alpha}_{gj}$ ,  $\tilde{\rho}_{gj}$  and  $\tilde{U}_{gj}$  be the same variables based on the final velocities. A velocity flip-flop has occurred when one of the junctions in a system satisfies the following condition:

$$\alpha_{fj}\tilde{\rho}_{fj}\tilde{U}_{fj} + \alpha_{gj}\tilde{\rho}_{gj}\tilde{U}_{gj} - \tilde{\alpha}_{fj}\tilde{\rho}_{fj}\tilde{U}_{fj} - \tilde{\alpha}_{gj}\tilde{\rho}_{gj}\tilde{U}_{gj} > 0.20(\alpha_{fj}\tilde{\rho}_{fj}\tilde{U}_{fj} + \alpha_{gj}\tilde{\rho}_{gj}\tilde{U}_{gj}) \quad (8.2-1)$$

Under such circumstances, the pressures and final velocities are recalculated using the donor properties of the previously calculated final velocities.

Another situation that may cause excessive mass and/or energy errors is when a noncondensable gas first appears in a volume. Because the linearized phasic properties are evaluated at the state existing at the beginning of an advancement, the derivatives of the phasic properties with respect to the noncondensable gas quality will be zero since there is no noncondensable gas in the volume at the beginning of the advancement. The convection of noncondensable gas into the volume during the advancement will result in an inconsistent state at the end of the advancement because the derivatives needed for the computation of a consistent state are identically zero. The inconsistency may be manifested as a large mass error where the noncondensable gas fails to appear in the volume even though the flux of noncondensable gas into the volume is positive. The inconsistency may also be manifested as a unphysically high vapor temperature when noncondensable gas first appears in a volume. This inconsistency is corrected by repeating the advancement when noncondensable gas first appears in a volume. The code checks for this situation at the end of every advancement if the noncondensable gas model has been activated by the user. The situation is detected whenever the noncondensable quality in a volume is zero at the beginning of the advancement and the flux of noncondensable gas into the volume during the advancement is positive. The noncondensable quality and vapor fraction that would result from the flux of noncondensable gas into the volume is estimated from an explicit mass balance on the vapor phase in the volume. The estimated noncondensable gas quality is then used in the computation of the derivatives of the phasic properties. The estimated noncondensable gas quality and vapor fraction are also used in the construction of the linearized conservation equations instead of the beginning of advancement quantities. The modified linearized conservation equations are then used to compute the end of advancement quantities as described previously. The time step size used for the repeated advancement is the same as that used for the original attempted advancement unless the pressure change in the cell is too large. The time step control based on the change in the pressure described previously is activated for volumes in which noncondensable gas is first appearing. The time step control based on pressure may result in multiple time step repeats with smaller and smaller time steps when a noncondensable gas first appears in a volume.

## 8.3 Steady State

A steady-state initialization capability is included in RELAP5. With this capability, the transient solution algorithm is continually monitored to determine the achievement of a steady state. During this process, convergence criteria are calculated and used in the steady-state testing scheme. These convergence criteria are related to an overall calculational precision. This overall precision is the result of combining both the precision of the transient solution algorithm and the standard tolerance of the thermodynamic state algorithm. The following discussion describes the fundamental concepts of tests to detect steady state during transient calculations.

### 8.3.1 Fundamental Concepts for Detecting Hydrodynamic Steady-State During Transient Calculations

The fundamental concept of steady state is that the state of a reactor system being modeled does not change with respect to time. In the hydrodynamic solution scheme, three terms can be monitored whose variation in time include the variation of all of the other terms. These three terms are the thermodynamic density, internal energy, and pressure. Furthermore, these three terms can be combined into a single term, enthalpy. Hence, monitoring the time variation of enthalpy is equivalent to monitoring the time variation of all of the other variables in the solution scheme. For each volume cell in the system model, the enthalpy can be written as

$$V_i \rho_i^n h_i^n = V_i (\rho_i^n U_i^n + P_i^n) \quad (8.3-1)$$

where subscript  $i$  denotes the  $i$ -th volume element,  $h_i$  is the volume element specific enthalpy in units of energy per unit mass, and  $V_i$  is the element volume. Since volume is constant, Equation (8.3-1) can be simplified as

$$\rho_i^n h_i^n = \rho_i^n U_i^n + P_i^n . \quad (8.3-2)$$

The rate of variation with respect to time of Equation (8.3-2) can be expressed numerically as

$$\left( \frac{d(\rho h)}{dt} \right)_i^n = \frac{(\rho_i^{n+1} U_i^{n+1} + P_i^{n+1}) - (\rho_i^n U_i^n + P_i^n)}{\Delta t^n} \quad (8.3-3)$$

Absolute hydrodynamic steady state occurs when Equation (8.3-3) is zero for each of the volume elements in the modeled system.

In order to simplify the task of detecting steady state, a system mean enthalpy can be expressed as

$$\overline{(\rho h)}^n = \frac{\sum_{i=1}^{NVOLS} V_i (\rho_i^n U_i^n + P_i^n)}{\sum_{i=1}^{NVOLS} V_i} \quad (8.3-4)$$

A system mean rate of change can also be formulated as

$$\overline{\frac{d}{dt}(\rho h)}^n = \frac{1}{\Delta t^n} \frac{\sum_{i=1}^{NVOLS} V_i [(\rho_i^{n+1} U_i^{n+1} + P_i^{n+1}) - (\rho_i^n U_i^n + P_i^n)]}{\sum_{i=1}^{NVOLS} V_i} \quad (8.3-5)$$

However, since the rate of change in any volume element can be positive or negative, these terms would tend to cancel. Hence, a better formulation for the mean rate of change is a mean square summation that can be written as

$$\left( \overline{\left( \frac{d}{dt}(\rho h) \right)^2} \right)^n = \frac{1}{(\Delta t^n)^2} \frac{\sum_{i=1}^{NVOLS} V_i^2 [(\rho_i^{n+1} U_i^{n+1} + P_i^{n+1}) - (\rho_i^n U_i^n + P_i^n)]^2}{\sum_{i=1}^{NVOLS} V_i^2} \quad (8.3-6)$$

During the course of the problem solution, Equation (8.3-6) can be used to monitor the system approach to steady state because, as each volume element approaches steady state, its rate of change goes to zero and drops out of the summation. The detection of absolute steady state is therefore relatively simple, since the calculations need only be monitored until Equation (8.3-6) becomes zero. However, another property of Equation (8.3-6) is that it will fluctuate wildly, varying between small and large magnitudes. These fluctuations decrease in magnitude as the calculations proceed toward steady state. Hence, Equation (8.3-6) is not a well-behaved function, and it is therefore difficult to monitor its behavior. However, a well-behaved function can be curve-fitted to the results of Equation (8.3-6) over reasonable time intervals. An exponential function is of this type; and if

$$\left( \overline{\left( \frac{d}{dt}(\rho h) \right)^2} \right)^n = y = e^{\alpha + \beta t^n + \gamma (t^n)^2 + \phi (t^n)^3}, \quad (t_o \leq t^n \leq t) \quad (8.3-7)$$

the coefficients  $\alpha$ ,  $\beta$ ,  $\gamma$ , and  $\phi$  may be computed by the method of least squares over any reasonable time interval greater than four time steps. Equation (8.3-7) has the property that it can increase to large values at small values of time and then decrease to small values as time increases and the system approaches steady state. Equation (8.3-7) represents the time-smoothed root mean square (RMS) rate of change in system enthalpy.

Because the user must provide boundary conditions, controls, or trips to guide the transient solution to steady state, it may not be possible to achieve an absolute steady state. For example, a steam generator water level control may be modeled so that the water level oscillates between high and low set points. In addition, since numerical schemes are inexact, it may only be possible to calculate absolute steady state within a small limit of precision. For this kind of fluctuating average steady state, the RMS ( $dph/dt$ ) will approach a constant, positive, non-zero value. As a result, an additional method must be used to detect an average steady state over limited time intervals.

If the system  $\overline{(\rho h)^n}$  is varying with time over the interval  $t_1 \leq t^n \leq t_2$ , its variation can be expressed approximately in the form of a straight line such that

$$H^n = b + at^n \approx \overline{(\rho h)^n} . \quad (8.3-8)$$

If the system is approaching an absolute steady state, then the line rate of change will be zero and Equation (8.3-8) will give the system time average ( $\overline{\rho h}$ ) such that

$$\overline{(\rho h)} \Big|_{t_1}^{t_2} = b, \quad (t_1 \leq t^n \leq t_2) \quad (8.3-9)$$

where the averaging is over the interval  $t_1 \leq t^n \leq t_2$ .

The second testing method consists of monitoring the system  $(\rho h)^n$  at the completion of each successful time step and, at reasonable time intervals, solving for the straight line coefficients  $a$  and  $b$  using the method of least squares.

In performing the method of least squares, the mean system enthalpy is computed at the successful completion of each time step in the interval  $t_1 \leq t^n \leq t_2$ , and an equation expressing the sum of the squares of the differences between  $\rho h^n$  and Equation (8.3-8) can be written as

$$\xi_{\rho h}^2 \Big|_{t_1}^{t_2} = \sum_{n=n_1}^{n_2} \left( \overline{(\rho h)^n} - b - at^n \right)^2 . \quad (8.3-10)$$

The coefficients  $a$  and  $b$  can then be calculated by the method of least squares.

A measure of the RMS fluctuation of  $(\rho h)^n$  with respect to the line of Equation (8.3-8) can also be computed using the mean square form of Equation (8.3-10), where

$$\overline{(\rho h)}_{\text{RMS}} \Big|_{t_1}^{t_2} = \left[ \frac{1}{(n_2 - n_1)} \xi_{\rho h}^2 \Big|_{t_1}^{t_2} \right]^{1/2} . \quad (8.3-11)$$

The RMS fluctuation then represents a measure of the typical difference between the mean system enthalpy and the line of Equation (8.3-8). However, the coefficients a and b cannot be calculated with any better precision than the overall precision of the solution scheme for the entire system.

### 8.3.2 Calculational Precision and the Steady-State Convergence Criteria

In the RELAPS solution scheme, at the successful completion of calculations over a time step, three fundamental variables are computed for each volume element in the system modeled. These variables are

1.  $\rho_{mi}^{n+1}$ , the thermodynamic density of the volume substance, where subscript m denotes the solution by conservation of mass
2.  $U_i^{n+1}$ , the thermodynamic internal energy of the volume substance resulting from conservation of energy
3.  $P_i^{n+1}$ , the thermodynamic pressure of the volume substance resulting from the combined solution conserving momentum, mass, and energy.

The thermodynamic pressure, phasic internal energies, and vapor volume fraction are used to compute the state using a set of properties tables. In the resulting calculations, a thermodynamic density  $\rho^{n+1}$  is calculated corresponding to the solution results. If the pressure and overall internal energy are preserved, then the precision of the calculations can be defined as

$$\varepsilon_{\rho,i}^{n+1} = \rho_i^{n+1} - \rho_{mi}^{n+1} \quad (8.3-12)$$

for each volume element in the system. If the calculations were exact, then Equation (8.3-12) would be zero. However, the properties tables are limited in precision to a tolerance of  $\pm 1$  in the fifth significant figure. In statistical terminology, the mean expected precision would be approximately  $\pm 5$  in the sixth significant figure. If the mean expected precision is considered to be a *standard* precision, an approximate expression can be written in terms of the properties table density as

$$\varepsilon_{std,\rho,i}^{n+1} \sim \pm (5 \times 10^{-6}) \rho_i^{n+1} \quad (8.3-13)$$

which is approximately  $\pm 5$  in the density sixth significant figure and which represents the best expected precision for the calculational scheme.

In the steady-state testing scheme, the precision of the volume enthalpy can be written as

$$\varepsilon_{ph,i}^{n+1} = (\rho_i^{n+1} U_i^{n+1} + P_i^{n+1}) - (\rho_{mi}^{n+1} U_i^{n+1} + P_i^{n+1}) \quad (8.3-14)$$

or

$$\varepsilon_{\rho h, i}^{n+1} = (\rho_i^{n+1} - \rho_{mi}^{n+1}) U_i^{n+1} \quad (8.3-15)$$

Similarly, the precision of the rate of change in volume enthalpy can be written as

$$\begin{aligned} \varepsilon_{\frac{d}{dt}(\rho h), i}^{n+1} &= \frac{1}{\Delta t^n} \{ [(\rho_i^{n+1} U_i^{n+1} + P_i^{n+1}) - (\rho_i^n U_i^n + P_i^n)] \\ &\quad - [(\rho_{mi}^{n+1} U_i^{n+1} + P_i^{n+1}) - (\rho_{mi}^n U_i^n + P_i^n)] \} \end{aligned} \quad (8.3-16)$$

which simplifies to

$$\varepsilon_{\frac{d}{dt}(\rho h), i}^{n+1} = \frac{1}{\Delta t^n} \varepsilon_{\rho h, i}^{n+1} \quad (8.3-17)$$

For the entire system at the current time step, a statistical precision can be defined where

$$\varepsilon_{\rho h}^{n+1} = \left( \frac{\sum_{i=1}^{NVOLS} V_i^2 [(\rho_i^{n+1} - \rho_{mi}^{n+1}) U_i^{n+1}]^2}{\sum_{i=1}^{NVOLS} V_i^2} \right)^{1/2} \quad (8.3-18)$$

for the system mean enthalpy and where

$$\varepsilon_{\frac{d}{dt}(\rho h)}^{n+1} = \left[ \frac{1}{(\Delta t^n)^2} (\varepsilon_{\rho h}^2)^{n+1} \right]^{1/2} \quad (8.3-19)$$

for the system rate of change in enthalpy.

Simple mean differences for the entire system can also be written as

$$\bar{\delta}_{\rho h}^{n+1} = \frac{\sum_{i=1}^{NVOLS} V_i (\rho_i^{n+1} - \rho_{mi}^{n+1}) U_i^{n+1}}{\sum_{i=1}^{NVOLS} V_i} \quad (8.3-20)$$

for the system mean enthalpy and as

$$\bar{\delta}_{\frac{d}{dt}(\rho h)}^{n+1} = \frac{1}{\Delta t^n} \bar{\delta}_{\rho h}^{n+1} \quad (8.3-21)$$

for the system rate of change in enthalpy.

The relationship between the mean difference and precision terms defines the uncertainty characteristics of the overall solution scheme. From Equations (8.3-18) through (8.3-21), it is obvious that

$$-\varepsilon_\eta \leq \varepsilon_\eta \leq \varepsilon_\eta \quad (8.3-22)$$

where subscript  $\eta$  denotes the particular term,  $\rho h$  or  $\frac{d}{dt}(\rho h)$ , being considered. In particular, if  $\varepsilon_\eta$  is small, it can be concluded that calculations are made with a high degree of precision throughout the entire system modeled. If the mean difference term is such that  $\delta_\eta \sim 0$ , then the overall system solution is said to be unbiased. This means that the overall system mass, energy, and momentum are precisely conserved. However, if  $\delta_\eta \sim \varepsilon_\eta$ , then the overall system solution is said to be biased. This means that if Equation (8.3-22) is true and  $\delta_\eta < 0$ , then the overall system solution behaves as if it were losing mass, energy, or momentum. If  $\delta_\eta > 0$ , then the system solution behaves as if it were gaining mass, energy, or momentum. In RELAP5, the size of the calculational time steps are controlled to maintain a high degree of precision which, in turn, limits the system bias. However, the characteristics just described can have an effect in determining time average steady state.

Since the time average straight line test defined by Equation (8.3-6) is conducted over a time interval, time average precision and mean difference terms must be calculated over the same time interval using the relationships

$$\overline{(\varepsilon_{\rho h})^2} \Big|_{t_1}^{t_2} = \frac{\sum_{n=n_1}^{n_2} \Delta t^n (\varepsilon_{\rho h}^n)^2}{\sum_{n=n_1}^{n_2} \Delta t^n} \quad (8.3-23)$$

$$\left( \overline{\varepsilon_{\frac{d}{dt}(\rho h)}}^2 \right) \Big|_{t_1}^{t_2} = \frac{\sum_{n=n_1}^{n_2} \Delta t^n \left( \left( \overline{\varepsilon_{\frac{d}{dt}(\rho h)}} \right)^2 \right)^n}{\sum_{n=n_1}^{n_2} \Delta t^n} \quad (8.3-24)$$

$$\overline{\delta_{\frac{d}{dt}(\rho h)}} \Big|_{t_1}^{t_2} = \frac{\sum_{n=n_1}^{n_2} \Delta t^n \delta_{\rho h}^n}{\sum_{n=n_1}^{n_2} \Delta t^n} \quad (8.3-25)$$

$$\bar{\delta}_{\frac{d}{dt}(\rho h)} \Big|_{t_1}^{t_2} = \frac{\sum_{n=n_1}^{n_2} \Delta t^n \delta_{\frac{d}{dt}(\rho h)}^n}{\sum_{n=n_1}^{n_2} \Delta t^n} \quad (8.3-26)$$

where the averaging is over the time interval,  $t_2 - t_1$ , and the summation terms  $n_1$  and  $n_2$  denote the number of time steps taken over the interval.

Equations (8.3-23) through (8.3-26) represent the precision of the actual calculations relative to the thermodynamic state algorithm. These equations have the characteristic that if the system approaches absolute steady state, both Equations (8.3-23) and (8.3-24) will become very small. Since the property tables are limited in precision, it is useless in a practical sense to continue calculations if absolute steady state is achieved with a precision better than that for the properties tables. This criterion can be defined by considering equations similar to Equations (8.3-23) and (8.3-24) but written in terms of the properties tables *standard* precision. These equations can be derived by simply substituting Equation (8.3-24) for the density difference term in the equations leading to Equations (8.3-23) and (8.3-24).

The steady-state convergence criteria can then be defined by combining the calculational and standard precisions such that

$$(\varepsilon_{c, \rho h})^2 \Big|_{t_1}^{t_2} = \left\{ \frac{1}{2} \left[ \left( \varepsilon_{std, \rho h} \Big|_{t_1}^{t_2} \right)^2 + \left( \varepsilon_{\rho h} \Big|_{t_1}^{t_2} \right)^2 \right] \right\}^{1/2} \quad (8.3-27)$$

for the system mean enthalpy, and

$$\varepsilon_{c, \frac{d}{dt}(\rho h)} \Big|_{t_2}^{t_2} = \left\{ \frac{1}{2} \left[ \left( \varepsilon_{std, \frac{d}{dt}(\rho h)} \Big|_{t_1}^{t_2} \right)^2 + \left( \varepsilon_{\frac{d}{dt}(\rho h)} \Big|_{t_1}^{t_2} \right)^2 \right] \right\}^{1/2} \quad (8.3-28)$$

for the system rate of change in enthalpy.

Equations (8.3-27) and (8.3-28) represent the steady-state convergence criterion. It can be said that, within the limits of calculational and properties precision, time average steady state is achieved when the mean rate of change in system enthalpy is within the limits of

$$-\varepsilon_{c, \frac{d}{dt}(\rho h)} \Big|_{t_1}^{t_2} \leq a \leq \varepsilon_{c, \frac{d}{dt}(\rho h)} \Big|_{t_2}^{t_2} \quad (8.3-29)$$

where "a" is the mean rate of change in system enthalpy given by Equation (8.3-8). If Equation (8.3-29) is true and if Equation (8.3-7) is such that

$$y \leq \varepsilon_{c, \frac{d}{dt}(\rho h)} \Big|_{t_1}^{t_2} \quad (8.3-30)$$

then absolute steady state is achieved. If Equation (8.3-29) is true and

$$y > \varepsilon_{c, \frac{d}{dt}(\rho h)} \Big|_{t_1}^{t_2} \quad (8.3-31)$$

then the system is fluctuating and time average steady state is achieved.

### 8.3.3 Steady-State Testing Scheme, Time Interval Control, and Output

In the steady-state testing scheme, the concepts discussed for detecting steady state are used, and calculations are performed over time intervals composed of a number of time steps. Because the *nature* of each problem is different, a systematic method of varying the test time intervals is performed.

These tests are performed in two parts. First, the system model overall state and rate of change in state are monitored by evaluating Equations (8.3-1) through (8.3-5) and including these results in the least-square terms for Equation (8.3-6). At time intervals computed internally, Equation (8.3-6) is evaluated; and the current system rate of change is determined. If the rate of change in state is increasing, then a *divergent* condition is indicated. If the rate of change in state is decreasing or zero, then a *convergent* condition is indicated. Second, if a *convergent* condition is indicated, then calculations are performed to determine the system average state and average rate of change in state over the internally computed time intervals. These time averages are formed by obtaining successive overlapping least-square solutions for Equation (8.3-7). These successive time average values are compared, and the achievement or non-achievement of a time average steady state is determined. In performing these tests, the calculational precision is accounted for by using Equations (8.3-12) through (8.3-29).

In the steady-state scheme, each time a solution for Equation (8.3-6) is obtained, the overall-state and steady-state convergence test results are printed. This printout is composed of current time results and time smoothed results integrated over the test time interval. The current time results are (a) the state and rates of change in state resulting from Equations (8.3-4), (8.3-5), and (8.3-6); (b) the current time uncertainties resulting from Equations (8.3-18) through (8.3-21); and (c) the current time mean and root mean square (RMS) mass errors. The time-smoothed results that are printed are the current time evaluation of Equation (8.3-7) and the resultant coefficients of Equation (8.3-7) determined by the least-squares solution over the time interval from  $t_1$  to the current time TIMEHY. The time,  $t_1$ , corresponds to the time at the successful completion of calculations for the first time step after problem initiation. For example, if the problem is a NEW problem, then  $t_1$  corresponds to

$$t_1 = 0 + \Delta t_1 \quad (8.3-32)$$

where  $\Delta t_1$  is the first successful time step. If the problem is a RESTART problem, then  $t_1$  corresponds to

$$t_1 = TREST + \Delta t \quad (8.3-33)$$

where TREST is the time of restart and  $\Delta t$  is the first successful time step after restart. If the results of the overall state tests indicate a *convergent* condition, then time average tests are initiated.

The time average tests consist of approximating the overall state with a set of three straight lines where each test line is fitted to the calculational results over successive test intervals. The time rates of change of these test lines are then monitored to determine time average steady state. In the testing scheme, when the time average tests are initiated, calculations continue until the successive test time interval is exceeded. At this time, the first test line, Line A, is defined and its results are printed. Calculations then continue until the next successive test time interval is exceeded. At this time, the second test line, Line B, is defined for the second test interval and the third test line, Line C, is defined for the combined first and second test intervals. The results for the three test lines are then printed, and tests are performed to determine the achievement of time average steady state. If steady state has not been achieved, then test Line A is reset to Line B, and the process is repeated until steady state is achieved.

In the printed edit for time average steady state tests, the results for each of the three test lines are printed. The test line results are obtained by curve fitting Equation (8.3-8) over each of the line test intervals. The results printed are the endpoints of Equation (8.3-8) evaluated at the test interval start and end times and the time rate of change of Equation (8.3-8). Also printed are the time average uncertainties from Equations (8.3-23) through (8.3-26), the RMS fluctuation of system mean ph about the line from Equation (8.3-11), and the mass error integrated over the line test interval.

In performing both the overall and time average sets of tests, calculations proceed through a logic scheme to perform tests that monitor the solution scheme's approach to steady state. After completing the logic scheme calculations, the steady-state conclusions and next course of action are printed. This printout is composed of statements of the mode of convergence and the state of the system in alphanumeric terms. These statements are defined as the calculations proceed through the logic scheme. To prevent excessive printout during the overall state convergence tests, the first test for overall convergence is not performed until the completion of ten successful time steps. At this time, a current test time interval is initialized as  $\Delta t_c = TIMEHY - t_1$ . If this test indicates a *divergent* condition, then the test time interval is increased and the test procedure is repeated. To increase the test time interval, three tests are performed. First, the current test time interval is halved and the time  $t_2$  is estimated as

$$t_2 = TIMEHY + \frac{1}{2}\Delta t_c . \quad (8.3-34)$$

Then, Equation (8.3-7) is evaluated as  $y(t_2)$ . If  $y(t_2)$  is greater than the current value of  $y$ , then the time  $t_2$  is reset to

$$t_2 = TIMEHY + \Delta t_c \quad (8.3-35)$$

and Equation (8.3-7) is reevaluated, which results in resetting  $y(t_2)$ . If  $y(t_2)$  is again  $> y$ , then the time  $t_2$  is again reset to

$$t_2 = TIMEHY + 2\Delta t_c . \quad (8.3-36)$$

In any case, the test time interval is expanded by either maintaining, halving, or doubling the current test time interval based on a projected estimate of the current time-smoothed convergence function. This test procedure is then successively repeated until a *convergent* condition is calculated.

To provide efficiency for the time average testing scheme, upon the first occurrence of an overall state *convergent* condition, the time average testing scheme is activated and the test time interval is redefined by estimating the time interval over which a 10% change in state will occur. This time interval is approximately

$$\Delta t_c \sim 0.1 \overline{(\rho h)}^n / y . \quad (8.3-37)$$

However, to prevent excessively small or large intervals, the time interval is limited such that  $10 dt \leq \Delta t_c \leq 100 dt$ , where  $dt$  is the current calculational time step. The calculations for the time average scheme then proceed with each successive test time interval specified 10% larger than the time interval just completed. As the calculations progress and approach steady state, the line segments approach a constant value within the steady-state convergence criteria. When this condition is met, the test time interval is doubled. If this condition is recursively maintained for two more successive test intervals, then a final steady state has been achieved and the calculations are terminated. If the line segment tests indicate the solution is diverging from steady state, the results of the time average tests are discarded. When the conditions of Equation (8.3-7) again become true, the time average tests are reinitiated, and the procedure is continued until steady state is achieved.

A user control over termination of advancements toward steady state is available as part of the time step control options. The control can be set to force continued advancements regardless of the steady state termination algorithm up to a specified time, then allow automatic termination during a following time period.

#### 8.3.4 Heat Structure Heat Conductance Scheme for Steady-State

In both the steady-state and transient solution schemes, the same transient heat transfer algorithm is used. However, in the steady-state scheme, the heat structure heat capacity data input by the user are ignored, and this term is evaluated as an artificially small number such that

$$\frac{\rho C_p (\Delta x)^2}{k \Delta t_{hc}} \geq 2 \quad (8.3-38)$$

where  $\rho C_p$  is the volumetric heat capacity,  $\Delta x$  is the heat structure mesh interval,  $k$  is the heat structure thermal conductivity, and  $\Delta t_{hc}$  is the heat conduction scheme calculational time step. Equation (8.3-38) corresponds to the explicit stability criteria for a transient numerical heat conduction scheme.

In a transient solution scheme, the volumetric heat capacity is treated analogously to a *thermal* inertia, and its magnitude determines the characteristic response time of the conduction solution. For example,  $\rho C_p$  is typically quite large, on the order of  $10^5$  or larger. Hence, a large value of  $\rho C_p$  results in a characteristic response time much greater than the hydrodynamic response time. Indeed, hydrodynamic

steady state can be approximately achieved in reasonably short calculational times before large heat structures have even begun to respond.

By making the value of the volumetric heat capacity small, the characteristic response time is made small and on the order of or less than the hydrodynamic calculational time step. The resultant solution would therefore be equivalent to a steady-state solution that is damped and stabilized by a small thermal inertia. Hence, fluctuations of the heat structure rate of change in state are on the order of or less than the fluctuations of its hydrodynamic boundary conditions. As a result, the heat structure solution scheme will achieve time average steady state at approximately the same time as time average hydrodynamic steady state.

### 8.3.5 Interrelationship of Steady-State and Transient Restart/Plot Records

During the course of the calculations, restart/plot records are written at the frequency specified by the user. When the code determines that steady state has been achieved, a restart/plot record is written unconditionally. Subsequent problems can then be run as restarts using any of these restart records. However, the code will treat the restart records differently, depending on the type of problem using the restart record.

If a transient problem is being run by restarting from a steady-state restart record or, conversely, if a steady-state problem is being run restarting from a transient restart record, the restart is treated as a new problem. In this case, only the restart record at which the problem restarts is written and used for initial conditions. The code time step counters, statistics, and problem simulation time are reset to zero, and additional restart/plot records are written as the problem progresses.

If a steady-state problem is being run restarting from a steady-state restart record or, conversely, if a transient problem is being run restarting from a transient restart record, then the restart is treated as a continuation of the problem. In the continuation case, the previous restart/plot records up to the point of restart are preserved; and additional records are written as the problem progresses.

## 8.4 Self-Initialization

### 8.4.1 General Description

Obtaining a desired, steady-state condition for a RELAP5 plant model often requires considerable time and effort on the part of the analyst. Typically, this process involves successive calculations involving a trial-and-error approach in adjusting various input data. While the RELAP5 code can compute a steady-state condition for a particular set of boundary conditions, this steady-state may not match all parameters measured in the plant due to the particular nodalization chosen by the analyst, inherent inaccuracies in code models of the physical processes, inability to model geometric details, etc. The self-initialization option is designed to reduce the time, effort, and cost to achieve a steady-state for a given RELAP5 plant model to more nearly match plant data if necessary.

The strategy of the scheme is to automate the control aspects of the problem and to significantly reduce the computational time needed to reach a steady state. The concept retains the conventional approach of conducting a transient calculation that is driven to a desired steady-state condition.

Automation of plant model control is effected by a generic set of controllers that mimic an actual plant control system. These controllers are control components defined by the user. Four suboptions are

permitted with respect to the definition of independent and dependent plant model parameters. The choice of suboptions affords the user flexibility in meeting particular analysis objectives. Moreover, the overall scheme has been designed such that the user may invoke a standard control package or opt to custom-tailor the new control components to suit a particular plant model.

A reduction in calculational computer time to perform the initialization is accomplished by using the steady-state and nearly implicit solution scheme options (see Section 8.3 and Section 3.1.6, respectively). The steady-state option diminishes thermal capacitance terms to lower stability limits, thereby significantly reducing thermal relaxation of the model. It also monitors for a steady-state condition. The nearly implicit solution scheme permits time steps larger than those implied by the material Courant limit.

The self-initialization option is described for PWR-type models employing either U-tube or once-through steam generators and of single or multiple loop design. However, the principles illustrated can be applied to other systems.

#### 8.4.2 Required Plant Model Characteristics

The option accommodates plant models representing all domestically produced PWR designs, i.e., those of Westinghouse, Combustion Engineering, and Babcock & Wilcox. More specifically, single-loop, two-loop, three-loop, four-loop, and 2 x 4 loop representations are accommodated, using either U-tube or once-through steam generators. Other assumptions and restrictions related to the plant model are as follows:

- The model must have at least one coolant loop consisting of a core region, pump, steam generator, and pressurizer.
- The core power must be constant or it too must be driven by a control system to constant power. The reactor kinetics model may be used and held to constant input power by not entering feedback data. Reactor kinetics data with feedback needed for the transient can be entered at the restart starting the transient.
- User-specified makeup and letdown flow modeling should be suppressed during the null transient. The same applies to pressurizer heater and spray modeling. They may be introduced into the model as a renodalization at transient initiation. Volume and pressure control during the null transient must be effected through a time-dependent volume that serves to replace the pressurizer.
- Self-initialization of the plant model encompasses the primary coolant system and steam generators under the standard approach described subsequently. That is, no provisions have been made to include the balance-of-plant components in the testing for a steady state, though this is possible and is not incompatible with the self-initialization option. However, if the plant model includes a balance-of-plant representation (e.g., turbine, condensers, feedwater pumps, feedwater heaters, etc.), appropriate controllers would have to be supplied by the user to govern the operation of these components.
- The option is executable from either a new problem data deck or the restart of an old problem.

### 8.4.3 Standard Suboptions

Four standard suboptions are available in terms of specifying the independent parameter data set. This flexibility allows the user to select the suboption that best suits the situation at hand. Here it should be noted that the term standard refers to the employment of the control components in a standardized way that will subsequently be described. The nature of the control components, however, allows them to be used in other ways (i.e., with respect to sensed variable and controlled variable).

Recognize that the state of the plant model cannot be totally dictated by the analyst, since this would represent an overspecification of the problem. Certain interdependencies are implied by the plant model geometry and the mathematical models in the code. For example, one cannot simultaneously specify the thermal power, cold leg temperature, primary coolant flow rate, secondary pressure, and coolant level. This is an overspecification, since the overall heat transfer characteristics of the steam generator(s) have been implied by its (their) geometrical description and the heat transfer models in the code. Either the secondary pressure (and temperature) or cold leg temperature would have to be dependent in this example.

Each of the four standard suboptions has a common set of fixed parameters. These, and the remaining independent and dependent parameters for each suboption, are listed in **Table 8.4-1**. These suboptions are derived from the four logical combinations that result from selecting two of four variables, allowing the other two to be dependent. These four are primary flow, reactor coolant pump (RCP) speed, cold leg temperature, and secondary pressure. Each of the suboptions is described below.

**Table 8.4-1** Independent/dependent data set suboptions.

Always fixed	Core thermal power Pressurizer pressure Feedwater temperatures Secondary coolant level	
Suboption	Independent	Dependent
A	Loop flow  Cold leg temperature	RCP speed  Secondary pressure  Secondary flow
B	RCP speed  Cold leg temperature	Loop flow  Secondary pressure  Secondary flow
C	Loop flow  Secondary pressure	RCP speed  Cold leg temperature  Secondary flow
D	RCP speed  Secondary pressure	Loop flow  Cold leg temperature  Secondary flow

**8.4.3.1 Suboption A.** Loop flow and cold leg temperature are specified. (Note that specification of primary flow, core thermal power, and primary pressure fixes the differential temperature across the

vessel.<sup>a</sup>) This suboption requires that the pump speed, secondary pressure, and secondary feedwater flow be dependent variables.

The pump speed (N) is determined based on loop flow ( $\dot{m}$ ), loop pressure drop ( $\Delta P$ ), and the pump characteristics, as determined from pump model input. That is,

$$N = f(\dot{m}, \Delta P) \quad (8.4-1)$$

Here it should be noted that the resulting pump speed may be different than an observed value (in the case of an experimental facility) or the synchronous speed (in the case of a full-scale plant). This merely implies that a mismatch is present in the input data. For example, the user-specified geometry and/or loss coefficients for the primary coolant system (PCS) may be inaccurate, and/or the pump model may be inaccurate. The analyst must resolve such inconsistencies. The code will not alter either the pump model or loss coefficients to arrive at a flow/speed combination that matches facility data.

Analogously, specifying the cold leg temperature (along with power and loop flow) requires that the secondary pressure and flow must be dependent. The secondary pressure dictates the secondary sink temperature and, therefore, the primary-to-secondary heat transfer potential and cold leg temperature. Here again, it should be noted that the resulting secondary pressure may not match that observed in the plant or test facility. This may mean one of two things. Either the plant model representation of the steam generator is inadequate (e.g., inaccurately modeled, improperly nodalized, etc.), or the physical models in the code are imprecise. For example, the failure to match a measured value of secondary pressure might be due to the fact that the tube fouling was not accounted for in the input model.

**8.4.3.2 Suboption B.** RCP speed and cold leg temperature are specified, while loop flow, secondary pressure, and secondary flow are dependent. This suboption is similar to suboption A except that the roles of RCP speed and loop flow as dependent and independent variables are reversed. This suboption would be desirable when modeling a plant for which no data exist but the synchronous pump speed is known.

**8.4.3.3 Suboption C.** Loop flow and secondary pressure are specified, while RCP speed, cold leg temperature, and secondary flow are dependent. This suboption is desirable when secondary pressure matching (to data) would play an important role in the transient.

**8.4.3.4 Suboption D.** RCP speed and secondary pressure are specified, while loop flow, cold leg temperature, and secondary flow are dependent. This suboption is similar to suboption C, except that the independent/dependent roles of loop flow and pump speed are reversed.

#### 8.4.4 Inherent Model Incompatibilities

With such generality possible in defining a plant model with RELAP5, it is clearly possible that a desired steady-state condition is impossible to achieve given the input data supplied. Several types of

---

a. This takes into account the total pump power and heat losses as well.

incompatibilities will not be readily apparent until a null transient is attempted. For example, the overall heat transfer capacity of the steam generator(s) may be insufficient to transfer the total core thermal power without causing the hot leg temperature to exceed  $T_{SAT}$ . Such anomalies will be obvious as the null transient proceeds but cannot be readily identified from the input data stream.

#### 8.4.5 Description of Standard Controllers

To effect overall control of the model during the null transient, three generic control components are available and are used to invoke any one of the four suboptions just described. These control components are identified as PUMPCTL, STEAMCTL, and FEEDCTL. For all suboptions, both STEAMCTL and FEEDCTL are needed; whereas, PUMPCTL is used only for suboptions A and C where loop flow control is desired. The following subsections describe the design and operation of the controllers.

**8.4.5.1 PUMPCTL Controller.** The standard use of the PUMPCTL component is to sense loop flow and control pump speed to achieve the desired flow rate. As is the case with the other controllers, it uses proportional and integral control. Through input, the user specifies (among other things) the desired flow rate, where the flow is to be sensed, and which pump is to be controlled. The mathematical expressions representing the operation of the controller are next described.

An error signal ( $E_1$ ) is generated by subtracting the actual ( $V_2$ ) from desired ( $V_1$ ) flow rate and dividing the result by a user-supplied constant ( $S_1$ ):

$$E_1 = \frac{V_1 - V_2}{S_1} \quad (8.4-2)$$

This error signal is used to compute a new output signal (pump speed =  $Y_1$ ) for the next time advancement in accordance with the relationship:

$$Y_1^{n+1} = G_1 \left( \frac{E_1}{T_1} + \frac{\int_{t_0}^{t_n} E_1 dt}{T_2} \right) + (Y_1)_0 \quad (8.4-3)$$

where  $G_1$  equals the gain,  $T_1$  is a constant applied to the proportional part,  $T_2$  is the time constant for the integral part, and  $(Y_1)_0$  is the initial value of the pump speed.

**8.4.5.2 STEAMCTL Controller.** The standard employment of the STEAMCTL component is to sense either cold leg temperature (suboptions A and B) or secondary pressure (suboptions C and D) and control steam flow (through adjustment of steam valve flow area) to achieve the desired set point. It functions in exactly the same way as the PUMPCTL component just described, except that the definition of sensed and controlled variables is changed. For the STEAMCTL component,

$$E_2 = \frac{V_3 - V_4}{S_j} \quad (8.4-4)$$

where  $V_3$  is the desired temperature (or pressure),  $V_4$  is the actual value, and  $S_j$  is a constant supplied by the user. Likewise, the output signal (normalized steam valve area) for each new advancement is given as

$$Y_2^{n+1} = G_2 \left( \frac{E_2}{T_3} + \frac{\int_{t_0}^{t_n} E_2 dt}{T_4} \right) + (Y_2)_0 \quad (8.4-5)$$

where the terms are analogous to those for the PUMPCTL component.

**8.4.5.3 FEEDCTL Controller.** The standard employment of the FEEDCTL component is to sense steam flow and steam generator secondary coolant level (or coolant mass) and control feedwater flow (through adjustment of feedwater valve flow area) to achieve a match between feedwater flow and steam flow and to achieve the desired coolant level (or mass). It is also a proportional/integral controller but uses a summed error signal made up of the individual flow and level (mass) errors:

$$E_3 = \frac{V_5 - V_6}{S_k} + \frac{V_7 - V_8}{S_m} \quad (8.4-6)$$

where

$V_5$  = desired level (mass)

$V_6$  = actual level (mass)

$S_k$  = user-supplied constant

$V_7$  = actual steam flow

$V_8$  = actual feedwater flow

$S_m$  = user-supplied constant.

The output signal (feedwater valve flow area) is computed analogously to the PUMPCTL and STEAMCTL components:

$$Y_3^{n+1} = G_3 \left( \frac{E_3}{T_5} + \frac{\int_{t_0}^{t_n} E_3 dt}{T_6} \right) + (Y_3)_0 \quad (8.4-7)$$

**8.4.5.4 Pressure and Volume Control.** The self-initialization option requires that a constant pressure boundary condition be imposed on the primary coolant system during the null transient. The user supplies this condition by adding a time-dependent volume as a replacement for the pressurizer. This time-dependent volume should be defined as containing liquid at the desired primary system pressure and at a temperature near that estimated to be the final hot leg temperature. During the null transient, liquid will either flow into or out of the time-dependent volume to accommodate expansion and shrinkage, with no attendant change in primary pressure. When the self-initialization option is invoked, the code will check to determine if the time-dependent volume has been included.

BIBLIOGRAPHIC DATA SHEET

(See instructions on the reverse)

2. TITLE AND SUBTITLE  
RELAP5/MOD3 Code Manual,  
Code Structure, Systems Models, and Solution Methods

1. REPORT NUMBER  
(Assigned by NRC, Add Vol., Supp., Rev.,  
and Addendum Numbers, if any.)

NUREG/CR-5535  
INEL-95/0174 (Formerly  
EGG-2596  
Vol. 1

3. DATE REPORT PUBLISHED  
MONTH                   YEAR

August                   1995

4. FIN OR GRANT NUMBER  
W6238

5. AUTHOR(S)  
The RELAP5 Development Team

6. TYPE OF REPORT  
Technical

7. PERIOD COVERED (Inclusive Dates)

8. PERFORMING ORGANIZATION - NAME AND ADDRESS (If NRC, provide Division, Office or Region, U.S. Nuclear Regulatory Commission, and mailing address; if contractor, provide name and mailing address.)

Idaho National Engineering Laboratory  
Lockheed-Martin Idaho Technologies  
P. O. Box 1625  
Idaho Falls, Idaho 83415

9. SPONSORING ORGANIZATION - NAME AND ADDRESS (If NRC, type "Same as above"; if contractor, provide NRC Division, Office or Region, U.S. Nuclear Regulatory Commission, and mailing address.)

Division of Systems Technology  
Office of Nuclear Regulatory Research  
U. S. Nuclear Regulatory Commission  
Washington, D.C. 20555-0001

10. SUPPLEMENTARY NOTES

11. ABSTRACT (200 words or less) The RELAP5/MOD3 computer code has been developed for best-estimate simulation of light water reactor coolant systems during postulated accidents. The code models the coupled behavior of the reactor coolant system and the core for loss-of-coolant accidents and operational transients such as anticipated transient without scram, loss of offsite power, loss of feedwater, and loss of flow. A generic modeling approach is used that permits simulating a variety of thermal-hydraulic systems. Control system and secondary system components are included to permit modeling of plant controls, turbines, condensers, and secondary feedwater systems.

RELAP5/MOD3 code documentation is divided into seven volumes: Volume I presents modeling theory and associated numerical solution schemes; Volume II details instructions for code application and input data preparation; Volume III presents the results of developmental assessment cases that demonstrate and verify the models used in the code; Volume IV discusses in detail RELAP5 models and correlations; Volume V presents guidelines that have evolved over the past several years through the use of the RELAP5 code; Volume VI discusses the numerical scheme used in RELAP5; and Volume VII presents a collection of independent assessment calculations.

12. KEY WORDS/DESCRIPTIONS (List words or phrases that will assist researchers in locating the report.)

Computer Code, Thermal-hydraulics, Safety analysis, Two-phase flow,  
LWR simulation, LOCA analysis, Transient analysis

13. AVAILABILITY STATEMENT

Unlimited

14. SECURITY CLASSIFICATION

(This Page)

Unclassified

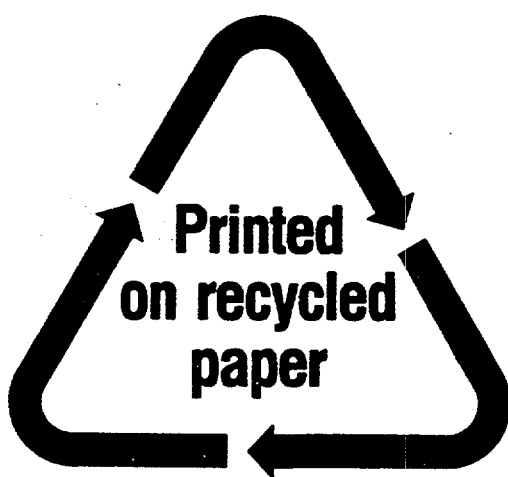
(This Report)

Unclassified

15. NUMBER OF PAGES

16. PRICE

RECEIVED  
SEP 19 1995  
OSTI



Federal Recycling Program